ISSN 0973-3302

JOURNAL OF ACOUSTICAL SOCIETY OF INDIA

Volume 43 Number 1 January 2016

A Quarterly Publication of the JASI

http://www.acousticsindia.org

Journal of Acoustical Society of India

Volume 43 Number 1 January 2016 pp 1-60

JASI

Journal of Acoustical Society of India

The Refereed Journal of the Acoustical Society of India (JASI)

The Journal of Acoustical Society of India is a refereed journal of the Acoustical Society of India **(ASI)**. The **ASI** is a non-profit national society founded in 31st July, 1971. The primary objective of the society is to advance the science of acoustics by creating an organization that is responsive to the needs of scientists and engineers concerned with acoustics problems all around the world.

Manuscripts of articles, technical notes and letter to the editor should be submitted to the Chief Editor. Copies of articles on specific topics listed above should also be submitted to the respective Associate Scientific Editor. Manuscripts are refereed by at least two referees and are reviewed by Publication Committee (all editors) before acceptance. On acceptance, revised articles with the text and figures scanned as separate files on a diskette should be submitted to the Editor by express mail. Manuscripts of articles must be prepared in strict accordance with the author instructions.

All information concerning subscription, new books, journals, conferences, etc. should be submitted to Chief Editor:

B. Chakraborty, CSIR - National Institute of Oceanography, Dona Paula, Goa-403 004,
Tel: +91.832.2450.318, Fax: +91.832.2450.602, e-mail: bishwajit@nio.org

Annual subscription price including mail postage is Rs. 2500/= for institutions, companies and libraries and Rs. 2500/= for individuals who are not **ASI** members. The Journal of Acoustical Society of India will be sent to **ASI** members free of any extra charge. Requests for specimen copies and claims for missing issues as well as address changes should be sent to the Editorial Office:

ASI Secretariat, C/o Acoustics, Ultrasonics & Vibration Section, CSIR-National Physical Laboratory, Dr. KS Krishnan Road, New Delhi 110 012, Tel: +91.11.4560.8317, Fax: +91.11.4560.9310, e-mail: asisecretariat.india@gmail.com

ISSN 0973-3302

Printed at Alpha Printers, WZ-35/C, Naraina, Near Ring Road, New Delhi-110028 Tel.: 9810804196. JASI is sent to ASI members free of charge.

JASI

Journal of Acoustical Society of India (JASI)

A quarterly publication of the Acoustical Society of India

Volume 43, Number 1, January 2016

ARTICLES

INFORMATION

Journal of Acoustical Society of India : Vol. 43, No. 1, 2016 (pp. 1-8)

Free Size Optimization Study for Optimal Thickness Distribution on Engine Foundation

V Ramakrishna[1*], P V S Ganesh Kumar[1], DA Rao[1] and S Ramakrishna[2]
[1]Naval Science and Technological Laboratory, Visakhapatnam-530027, India
[2]G V P College of Engineering, Visakhapatnam-530048, India
e-mail: ramkrishna.v@nstl.drdo.in

[Received:17.12.2015; Revised: 29.03.2016; Accepted: 29.03.2016]

ABSTRACT

Stealth technology plays a vital role for the underwater radiated noise. Machinery, flow and propeller noises are the major sources for the radiated noise. Machinery vibrations are transmitted to the hull through the foundations. Hence foundations are to be designed optimally to reduce the vibration transmission thereby leading to lesser underwater radiated noise. The purpose of this study is to optimize the thickness values of the elements of a Marine engine foundation based on the defined objectives and constraints. The study involves free-size optimization (thickness optimization) of an engine foundation with an objective of minimizing weight with a specified stress constraint. Initially, solid model of existing foundation is generated using CATIA software and static analysis is carried out to find the static strength and deformation of existing engine foundation. Finite element analysis is carried out using Ansys software. Altair Optistruct is used for free-size optimization of the structure with specified constraints and objective function. The free-size optimization would provide basis to make necessary design modifications so as to minimize the weight and stress in foundation. Subsequently, static analysis is performed on modified design of foundation to find the static strength and deformation. Ultimately, the study will be utilized for noise reduction with optimal foundation.

1. INTRODUCTION

Naval Stealth plays significant role in warfare today. Underwater radiated noise is thus an important aspect to be considered in naval stealth studies. This needs in turn vibration reduction from ship structures such as marine engine foundations. Hence, structural optimisation of these foundations is useful for achieving acoustic stealth of ships. Structural optimization has drawn the attention of many researchers for a few decades. Mathematical programming methods used in structural optimization are generally based on two categories. First catagory is based on gradient methods which normally use objective function, derivatives of objective function and constraint functions. The other catagory based on non-gradient methods which use only objective function and constraint functions. A gradient-based method is expected to be more efficient since it requires more information in each analysis. Therefore it needs fewer iterations of structural analysis. Research in structural optimization may be categorized into three main areas namely shape optimization, thickness optimization and topology optimization. Free-size optimization in OptiStruct optimizes the thickness of every element in the design space to generate an optimized thickness distribution in the structure, for the given objective under given constraints. In this paper, study on Free-size optimization of the reference base frame is for given loads with an objective of minimizing weights is discussed.

Zienkiewicz and Campbell [1] discussed the problem of finding the optimum shape of two-dimensional structures known as shape optimization. Chang and Lee *et al.* [2] verified the structural analysis methodology of compressor bracket for the topology optimization with static and dynamic loading condition. The objective function used for the topology optimization was to minimize combined compliance and the constraint was the first natural frequency over 250 Hz. Since then several researchers have contributed in this area such as Choi and Haug [3], Haftka and Grandhi [4] and Lam *et al*. [5] who applied general methods to obtain the optimum structure by varying the shape of an initial structure. In sizing optimisation problems, design variables are cross-sectional areas (beams and trusses) or the thicknesses (plate and shell structures) while the geometric shape of structures remains unchanged. Sang *et al.* [6] proposed nonlinear Response Optimization using Equivalent Loads (NROEL) for nonlinear response structural optimization. A nonlinear response optimization problem is converted to linear response optimization with equivalent loads. The modified NROEL is verified through three examples with contact conditions for shape optimization with stress constraints, size optimization with stress/displacement constraints and topology optimization. Reasonable results are obtained in the optimization process. Lim *et al.* [7] developed a new structural design technology to build a new type of land vehicle in military use. A two-stage design process is proposed employing topology and cross section optimization methods. Overall frame arrangement of the new vehicle structure is obtained by the topology optimization in the first design stage and the detailed dimensions of the frames are obtained by the cross section optimization in the second design stage.

From literature study, it is understood that it is possible to reduce weight of by modification of baseline design using free size structural optimization. The OptiStruct algorithm alters the material distribution of the structure to optimize it for the user defined objective under the given constraints. The free-size optimization in OptiStruct deals with the element thicknesses of the structure within a given design space. It optimizes the thickness values of the elements of a structure based on the user defined objectives and constraints [8].

2. MODELING OF EXISTING MARINE ENGINE FOUNDATION

The dimensions of the existing marine engine foundation are obtained through reverse engineering method. Co-ordinate Measuring Machine (CMM) is used to obtain the exact dimensions of the marine engine foundation. This machine with FARO's Laser Line Probe (LLP) scanning attachment fully integrates with 7-axes measurement arm system, transforming it into the Laser Scan Arm. Unlike other systems, measurements can be carried out with or without direct contact with the object ensuring uninterrupted workflow - eliminating the need for software or hardware adjustments. The Laser Scan Arm is perfectly suited for CAD comparison and reverse engineering. This is directly coupled to data acquisition system to

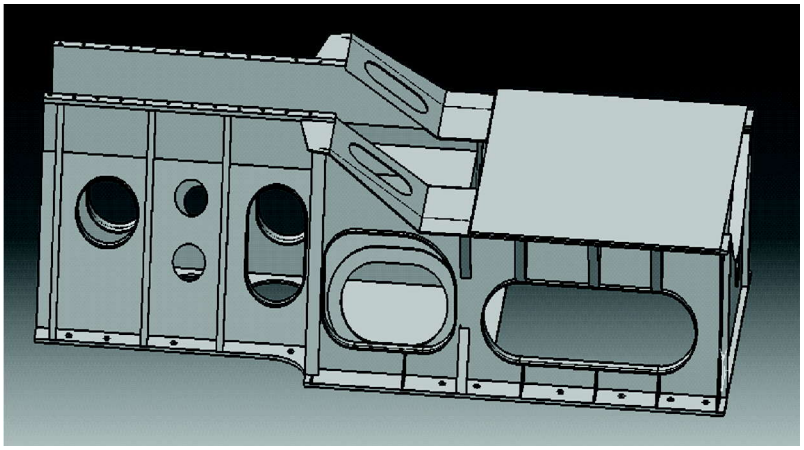

Fig. 1. Solid model of baseline Marine engine foundation generated in CATIA

store the all dimensions and also uses in built software in the data acquisition system to generate solid model. Solid model is generated in CATIA. Fig. 1 shows the solid model of baseline marine engine foundation generated. With the density specified, the overall mass of marine engine foundation in finite element model is 790.5 kg, which compares closely with the measured 787.5 kg of the actual marine engine foundation.

3. FREE SIZE OPTIMIZATION

The free-size optimization in OptiStruct deals with the element thicknesses of the structure within a given design space. It optimizes the thickness values of the elements of a structure based on the user defined objectives and constraints. The geometric surface model of the baseline marine engine foundation is modeled using Computer-Aided Engineering software CATIA V5. These surfaces are generated in the "wire frame and surface" module in CATIA. This geometric model is imported into HyperWorks to generate the Finite Element Model for free size optimization.

The original geometry of the baseline marine engine foundation has many ribs, bosses, fillets and many curved surfaces. The primary fillets, bosses and ribs are generated in the CAD model whenever necessary. The approximate dimensions of the base frame were measured with respect to a reference point. The key dimensions for generating the required curves were also measured using co-ordinate measuring machine. For generating the curved surfaces, these key dimensions are used to generate curves in the "sketcher" module. The final surface model marine engine foundation is shown in Fig. 2.

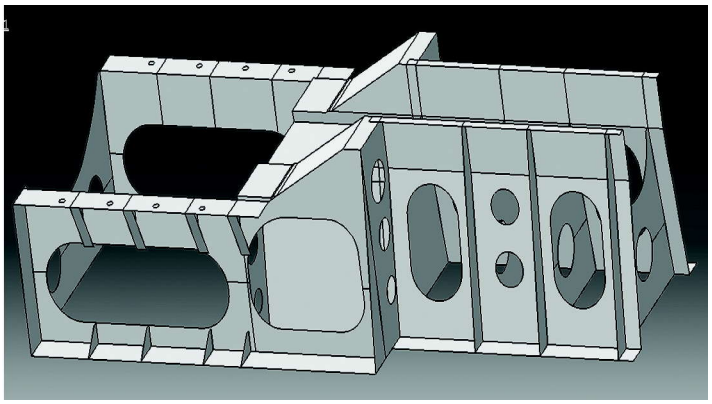

Fig. 2. Surface model of baseline marine engine foundation for free size optimization

The surfaces of the geometric model are meshed in HyperMesh using shell elements of size 15. Four node quadrilateral elements of type CQUAD4 are used to generate the Finite Element mesh of the geometric model. Triangular elements of type CTRIA3 are also present in the mesh. The elements are "cleaned" in order to produce a high quality mesh and the mesh is checked for equivalence and other quality checks like warpage, aspect ratio and skewness. A total of 34, 151 nodes and 33,344 elements are present in the Finite element mesh of the geometric surface model. With the density specified, the overall mass of existing marine engine foundation in finite element model is 790.5 kg, which compares closely with the measured 787.5 kg of the physical reference marine engine foundation. Fig. 3 shows the finite element meshed model of baseline marine engine foundation used for free size optimization respectively.

Free-size optimization in OptiStruct optimizes the thickness of every element in the design space to generate an optimized thickness distribution in the structure, for the given objective under given constraints. Free-size optimization of the reference base frame is done for all the load cases discussed earlier with an objective of minimizing weight. Fig. 4 shows the finite element model of baseline marine engine foundation. For all sub-cases, loads are defined as 31,000 N on engine side and 39,600 N on alternator side and fixed boundary condition is applied on bottom surface of the base frame.

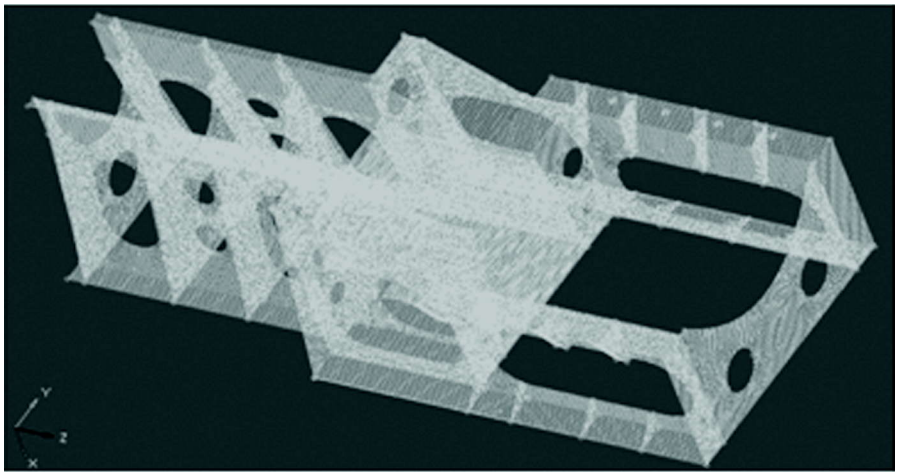

Fig. 3. Meshed surface model of baseline marine engine foundation for free size optimization

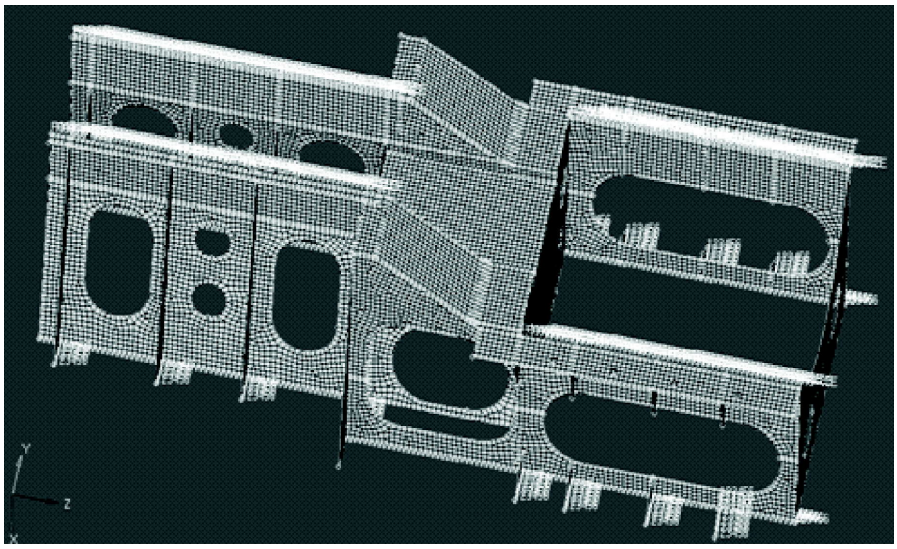

Fig. 4. Finite element model of baseline marine engine foundation for free size optimization

4. RESULTS AND DISCUSSION

Fig. 5 and Fig. 6 shows the contour of total displacement and Von-Mises stresses on surface model of baseline marine engine foundation before free size optimization respectively. From these figures it is observed that the maximum displacement is 0.74 mm and maximum Von-Mises stress is 107.7N/mm^2. The design variable for free-size optimization is the thickness of the shell elements on the surfaces. Thickness is allowed to vary between 3 mm and 20 mm. The lower bound for the thickness is given as 3 mm, which is the smallest thickness that can withstand the given direct loads. The upper bound for the thickness is the thickness of the reference base frame, 20 mm. A stress constraint is applied on the optimization problem such that the stress in the base frame should not exceed the Yield Strength, which is 60 MPa. OptiStruct ignores any artificial stress concentrations present in the structure within a preset tolerance. In this study a displacement constraint is also used to constrain the top most node on the reference frame not to deflect

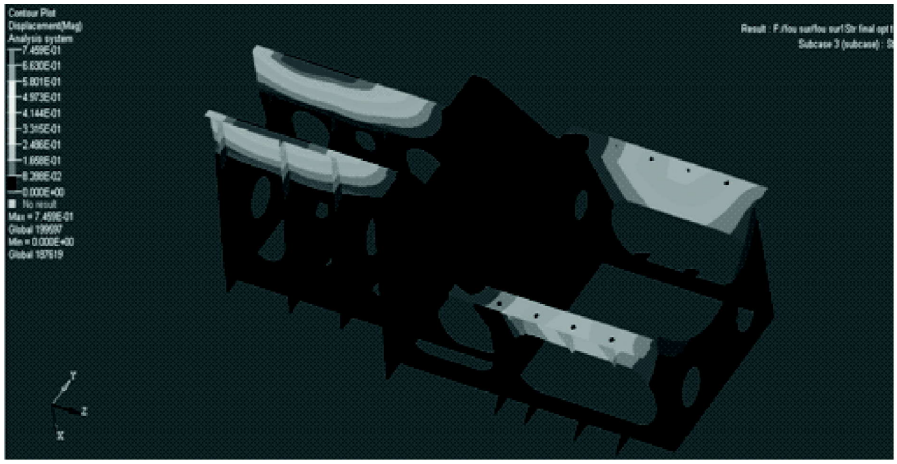

Fig. 5. Contour of total displacement on surface model of baseline marine engine foundation before thickness optimization

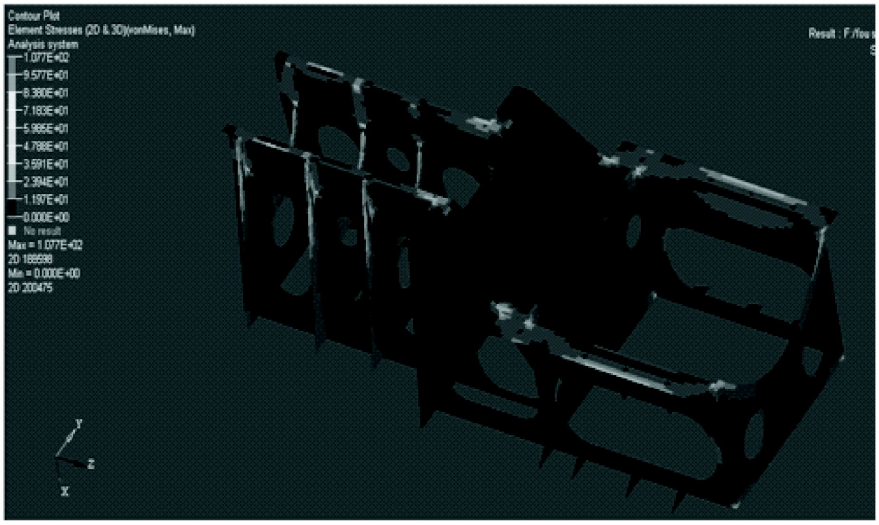

Fig. 6. Contour of Von-Mises stresses on surface model of baseline marine engine foundation before free size optimization

more than 0.14 mm in the direction of applied load. Fig. 7 shows the Optimization setup on surface model of baseline marine engine foundation for free size optimization. OptiStruct automatically optimizes the base frame for all applied loads. Fig. 8 shows the contour of optimum thickness distribution on surface model of baseline marine engine foundation after free size optimization. It shows that the thickness is only 5 mm on all surfaces except the surfaces where load is applied. The thickness of surfaces on which load is applied is 16 mm and 18 mm. The other surfaces showing the combination of different thicknesses is not suitable for fabrication. Instead of changing the thickness the design of the surfaces are changed in the redesigned marine engine foundation in order to reduce the stresses. Fig. 9 and Fig. 10 show the Contour of total displacement and Von-Mises stresses on surface model of baseline marine engine foundation after free size optimization respectively. From these figures it is observed that the maximum displacement is 0.28 mm and maximum Von-Mises stress is 41.5 N/mm^2. The total deformation and Von-Mises stress of baseline marine engine foundation after free size optimization is greatly reduced compared with those

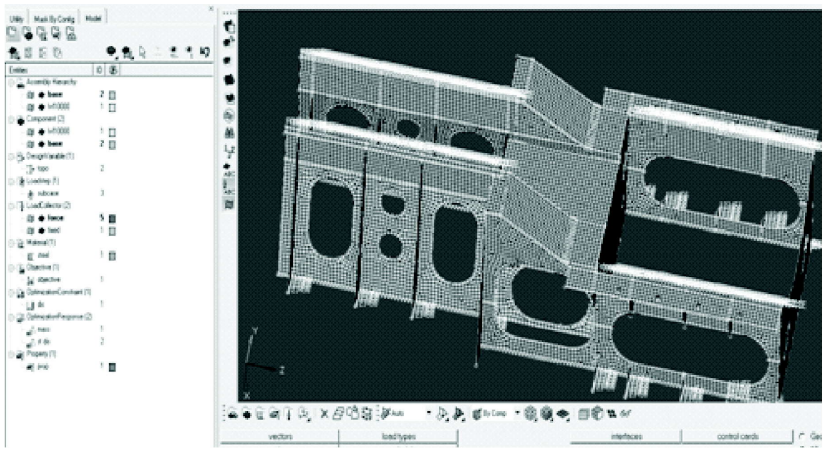

Fig. 7. Optimization setup on surface model of baseline marine engine foundation for free size optimization

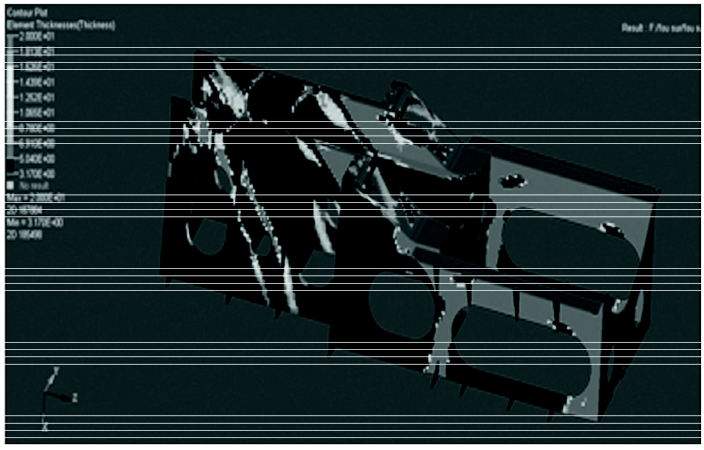

Fig. 8. Contour of optimum material distribution on surface model of baseline marine engine foundation after free size optimization

Fig. 9. Contour of total displacement on surface model of baseline marine engine foundation after free size optimization

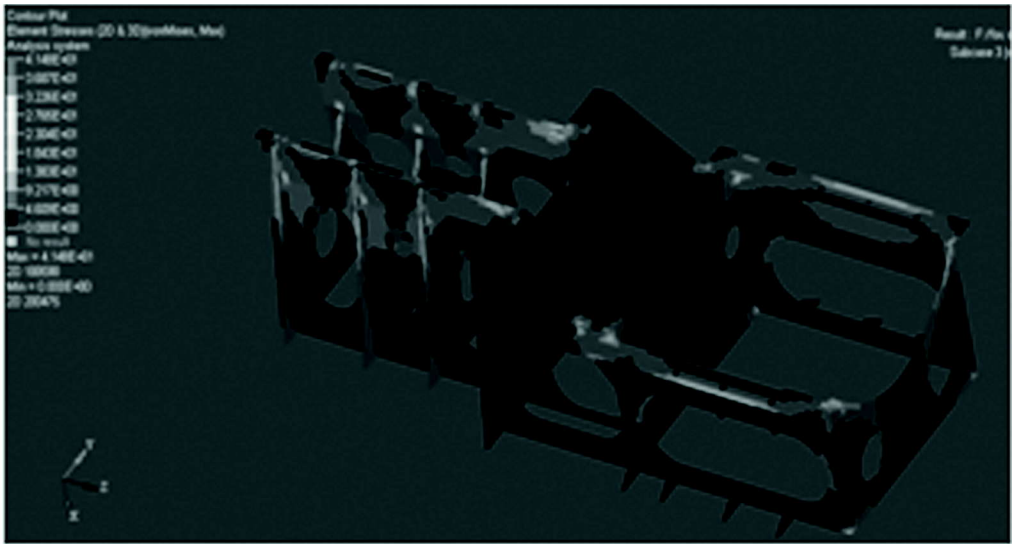

Fig. 10. Contour of Von-Mises stresses on surface model of baseline marine engine foundation after free size optimization

before optimization. With the density specified, the overall mass of marine engine foundation after free size optimization in finite element model is 695 kg, which is 95 Kg less than baseline marine engine foundation.

5. CONCLUSION

(i) A free size optimization procedure was carved out based on 'optistruct' of Altair for optimal structural modification to minimize the weight of a structure.

(ii) Weight of the optimized structure is less than the baseline structure for the same stress constraint.

(iii) It is established that free size optimization can be used effectively to minimize the weight of a structure with specified stress and displacement constraints.

(iv) Experimental validation of the findings of the present study would be undertaken in future for verifying the veracity of the approach.

6. ACKNOWLEDGEMENTS

The authors wish to express their sincere gratitude to Dr CD Malleswar, Outstanding Scientist and Director, NSTL Visakhapatnam for Permitting to publish this paper.

7. REFERENCES

[1] O.C. ZIENKIEWICZ and J. S. CAMPBELL, 1973. Optimum Structural Design, *Shape optimization and sequential linear programming*, Wiley, London.

[2] JEONG WOO CHANG and YOUNG SHIN LEE, 2008. Topology optimization of compressor bracket, *J. Mech. Sci. and Tech.*, **22**(9), 1668-1676.

[3] K. K. CHOI and E. J. HAUG, 1983. Shape design sensitivity analysis of elastic structures, *J. Struc. Mech.*, **11**, 231-269.

[4] R. T. HAFTKA and R. V. GRANDHI, 1982. Structural shape optimization - a survey, *Comp. Meth. Appl. Mech. Engg.*, **30**, 263-284.

[5] Y. C. LAM, D. MANICKARAJAH and A. BERTOLINI, 2000. Performance characteristics of resizing algorithms for thickness optimization of plate structures, *Fin. Elem. Anal. Des.* **34**, 159-174.

[6] SANG-IL YI, HYUN-AH LEE and GYUNG-JIN PARK, 2011. Optimization of a structure with contact conditions using equivalent loads, *J. Mech. Sci. and Tech,* **25**(3), 773-782.

[7] HONG SEOK LIM, YONG WOO KIM, MAN HOI KOO, HAK IN GIMM and HONG HEE YOO, 2010. Two-stage design process of a frame-panel land vehicle structure employing topology and cross section optimization, *J. Mech. Sci. and Tech*, **24**(10), 1963-1967.

[8] Altair Engineering Inc., 2007. OptiStruct 8.0, Users Guide.

Journal of Acoustical Society of India : Vol. 43, No. 1, 2016 (pp. 9-17)

Soundscapes in the shallow waters off Southwest coast of India during pre-monsoon season

M. M. Mahanty*, G. Latha and Edwards Durai P
National Institute of Ocean Technology, Pallikaranai, Chennai-600100, India
**e-mail: mmmahanty@niot.res.in*

[Received: 21.12.2015; Revised: 09.02.2016; Accepted: 09.02.2016]

ABSTRACT

Underwater soundscapes vary due to the geophonic and biophonic sound sources of the region. This paper presents a study on characterising the acoustic environment in the shallow water off southwest coast of India (off Cochin) utilizing time series passive acoustic measurements acquired during the period January to May, 2011. The recorded data were analysed using time/frequency spectrograms analyses method. The temporal variability, frequency distribution, and biological pattern of the soniferous species showed clear differences. The geophonic sound sources such as wind induced noise are dominant in the frequency range of 0.5-5kHz, whereas the rain noise is prevailing in the higher frequency band. The study area exhibited clear biological with its high temporal variability. The onset of Terapontidae chorus appearing after dusk period, is maximal during January to end of March, but ceased down by the month of May. The planktivorous fish chorus spectral maxima are observed around 0.6 kHz before midnight, displaying lunar trend during the period January 22- February 8, 2011. The Eel fish buries under seabed at the day time and produces sound like jackhammer at night, during the month of May. The thematic structure and harmonic sound is produced by humpback whales during the period from mid-January to mid-March, with a peak in February, when the mean SST is ~ 28°C and no presence is recorded after mid-March. This determines the functions of the humpback whale song and their breeding habitat. This study demonstrates that the passive acoustic measurements are the key elements for understanding the acoustic environment as it plays an important role in the ecology of multiple life history stages.

1. INTRODUCTION

Monitoring the soundscape or acoustic environment represents an important part of the ecosystem management [1-2]. They are potential to provide important sensory information to marine species that reflects the changing biological and physical characteristics of the environment[1]. Underwater soundscapes comprise a variety of sounds produced by geophony, biophony and anthrophony [3-4]. The temporal and spatial variation of ambient noise in the sea is generated predominantly by geophonic components including geological and meteorological activities. In the shallow water, the soundscape is particular and influenced by seabed features and bottom topography, and are mostly affected by surface conditions driven by wind, rain and waves [5]. Besides, sounds produced by the biophonic sources corresponding to marine mammals and fishes as they call for breeding, spawning, defend their territories or escapes predators [6-8]. The anthrophony in the ocean has increased in the last few decades through industrial and shipping activities, and can interfere in the animal communication systems [9-10].

Large numbers of marine species are distributed in shallow water environments [11] where anthropogenic activities are most intense [12]. There are relatively fewer studies on soundscapes, and its potential effects on marine species [13]. These species produce and listen to sounds, especially important for marine ecological processes including spawning, navigation, defense and habitat selection [1, 14]. These sounds typically vary on daily, monthly, and seasonal time scales in a high biodiversity coastal habitat. Huijbers *et al.* [15] demonstrated that different types of marine habitats with distinct biological composition have unique soundscapes. However, few studies have observed site-specific and temporal variations in the coastal habitat of the world ocean [16-17]. Recent studies on soundscape ecology are a promising field, and observations of the ambient acoustic environment within ecological marine habitats are important. The present study is intended to understand the biological soundscapes in the shallow water off southwest coast of India by characterising the sound field in terms of spectra.

2. MATERIALS AND METHODS

An automated sub-surface ambient noise measurement system comprising of vertical linear array of omnidirectional hydrophones with data acquisition modules was deployed in shallow water off southwest coast of India during the period from January-May 2011 (Fig.1). The system was deployed at 30 m water depth and VLA (Vertical Linear Array) positioned at the mid water column, so that the noise due to surface and bottom reflections could be measured effectively. The data recorded by first element of the vertical linear array has been considered for the analysis. The omnidirectional hydrophones are configured for measuring underwater sound in the frequency range 0.05-10kHz, with a sampling rate of 50 kHz per channel. The data was recorded at every 3 hour with a sampling duration of 30s. The array of hydrophones sense acoustic pressure fluctuation due to various sources of noise which translates into electrical signals and then logged by the data acquisition system. The recorded voltage values are subsequently converted to pressure units (µPa) by applying pre-amplifier gain and receiving sensitivity (-170 dB) of the hydrophone. Power level computation of the noise spectrum facilitates in detection and classification of signals embedded in the noise. The Welch's averaging periodgram method was used to calculate the noise spectrum level. The multiple spectra are obtained by segmenting data into smaller portions, using a Hamming window and 2048 point FFT with 50% overlap. The resulting spectra are then averaged to obtain the final spectrum.

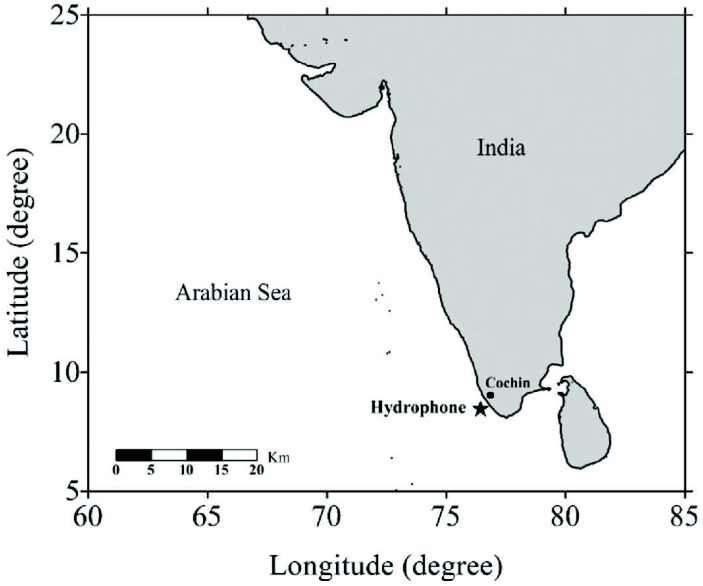

Fig. 1. Geographic location of the moored hydrophone in the shallow water off southwest coast of India. The location of the hydrophone is indicated as ★.

The frequency resolution, determined by the sampling frequency and the number of points in the FFTs in each power spectrum is 24.4 Hz.

3. RESULTS AND DISCUSSION

3.1 Characteristics of sounds produced by geophony sources

The geophonic wind and rain on the sea surface can generate an important natural source of sound. The frequency spectrum of sound generated by the wind has a distinct shape, as compared to that of rain. The slope of the rain spectra is not as steep as wind generated and can be distinguished from each other by observing the slope and shape of the underwater sound spectrum [18]. Fig. 2 shows noise level produced due to rain, and wind at different Beaufort scales within the frequency range of 0.5-5 kHz. The noise level fluctuation is higher in the lower frequency and lower in the higher frequency, whereas the noise level increases due to rain at higher frequencies.

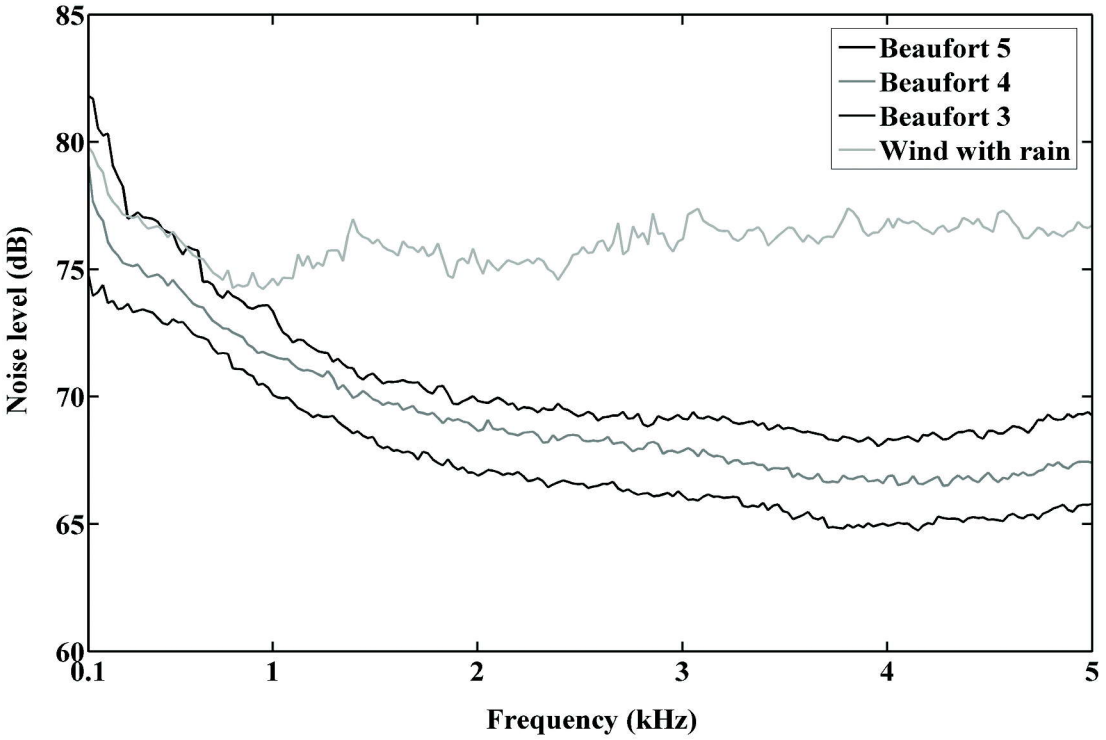

Fig. 2. Noise spectrum level at different Beaufort scale and the noise from rain in shallow water off southwest coast of India.

3.2 Characteristics of sounds produced by biophony sources

3.2.1 Humpback whales :

The spectrographic analyses facilitate the identification of Humpback whale sound pattern. Different sound units are distinguished from one another by the contours in the spectrogram. A sequence of different sound units grouped into a phrase and different phrases constitute a theme. Two theme types are identified, Theme-I and Theme-II (Fig.3).Themes-I and -II were static themes; their phrase structure remained consistent with each consecutive repetition. These are characteristically upsweeps and downsweeps along with harmonics. The significant increase in the acoustic energy in the frequency ranges from 0.11-8.8 kHz and 0.12-4.8 kHz for Theme-I and Theme-II respectively. Upsweep calls display high spectral level as compared

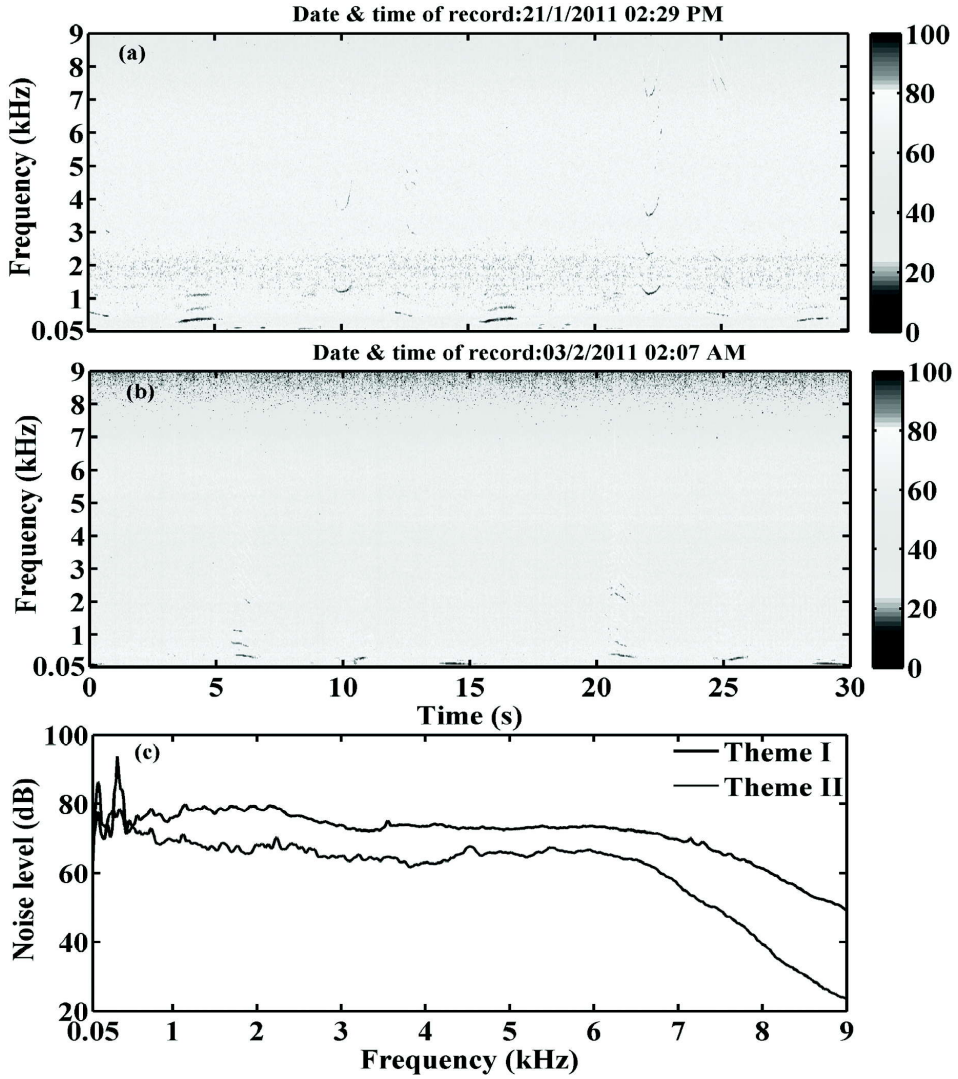

Fig. 3. Spectrogram of humpback whale sounds in the shallow water off southwest coast of India (a) Theme I, (b) Theme II and (c) Corresponding power spectral density of theme I & II.

to the downsweep calls.This thematic structure determines the function of humpback whale song form. The sound produced by humpback whales are mainly dominant during the period mid-January to mid-March, with a peak in February. The mean sea surface temperature (SST) in this study area is ~28°C, and within the range reported in other areas (24-28°C) [19].

3.2.2 Terapontidae :

Sounds produced by more than one species is called en masse and described as sounding like 'trumpet'. The recorded chorus is attributed to the family Terapontidae. The chorus and related features of the call types follow similar characteristics as compared with the published results [16]. The spectrogram and the power spectra of the Terapontidae chorus is depicted in Fig. 4. The occurrences of this high level chorus dominate the ambient sea noise spectra. The variation in trumpet sound exhibits a strong daily pattern during the study period. The chorus was generally seen as peaks in the noise level before dawn and after dusk. The generated sound was higher during hours of dusk than during hours of dawn. The occurrence of

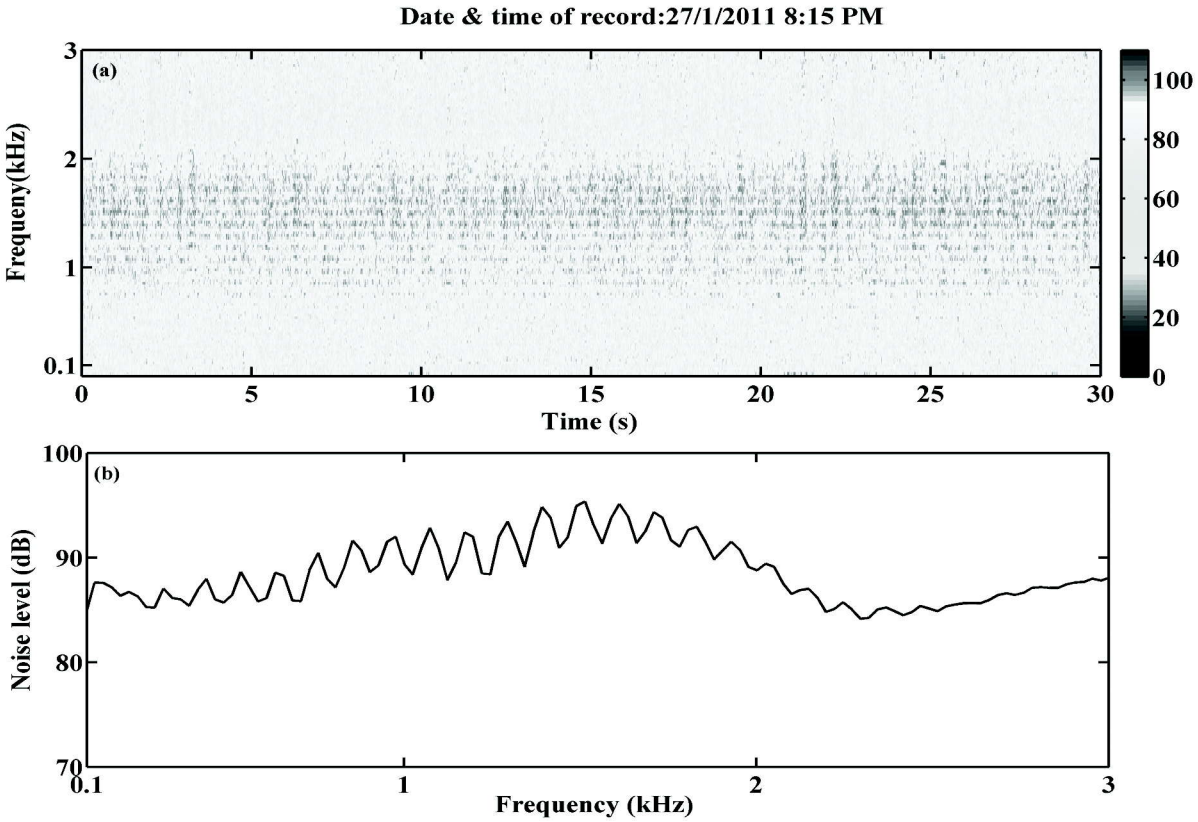

Fig. 4. The spectrogram and the corresponding power spectral density of Terapontidae chorus in the shallow water off southwest coast of India.

chorus was higher in the beginning of January that extends till the end of March, followed by a cease in May. The pulse repetition rate evident in the frequency range 0.1-0.12 kHz can be ascribed to the swimbladder mechanism. The swimbladder resonant spectral peak is normally extended over the frequency range 0.6-1.5kHz.

3.2.3 Planktivorous :

The chorus is attributed to nocturnal planktivorous fishes which are sounding likes 'pop'. The chorus is comprised of a single broad band pulse generated as a result of the swimbladder contraction. McCauley [20] discussed swimbladder sound production mechanism in details. Fig. 5 illustrates the spectrogram and power spectra of the Planktivorous chorus. The spectral maxima are observed around 0.6 kHz before midnight displaying lunar trend during the study period. McCauley [16] had reported that the planktivorous fish chorus is strongly influenced by moon phase, with a longer period of maximum chorus level within the moon period, just after full moon to new moon.

During data acquisition period, two choruses are recorded with distinct characteristic patterns in daily timing, frequency content and call characteristics. As an example, the noise spectra for three consecutive days representing Terapontidae chorus during the dusk and the Planktivorous chorus during the midnight is shown in Fig. 6.

3.2.4 Eel fish :

The sounds produced by eel fish was recorded only during the month of May. The spectrogram and the power spectra of eel sound recorded during this period are illustrated in Fig. 7. The computed average

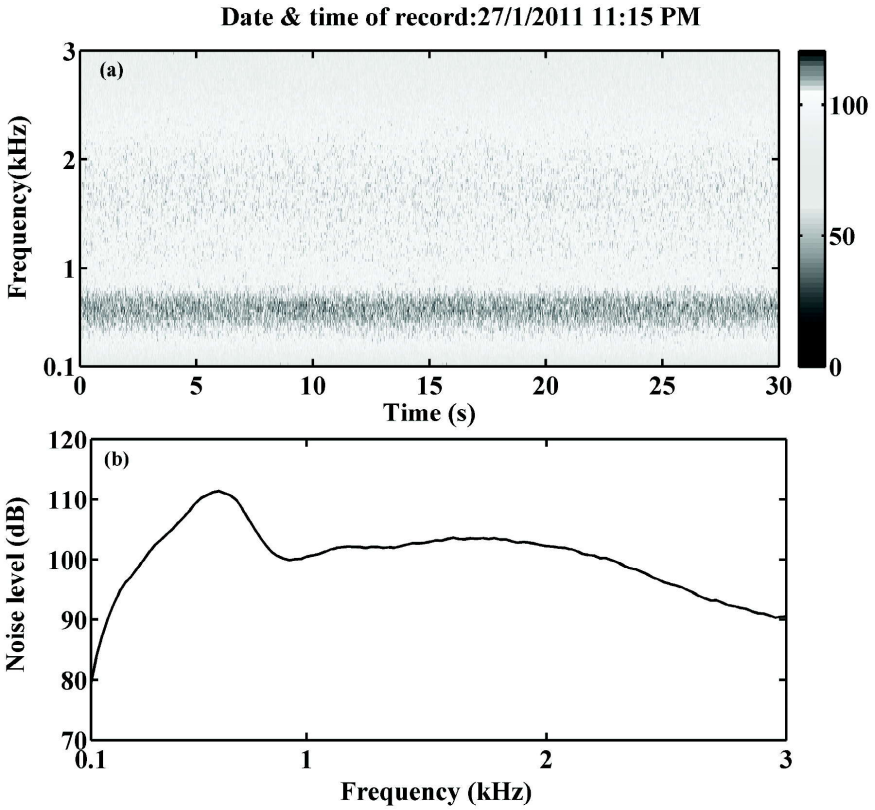

Fig. 5. The spectrogram and the corresponding power spectral density of Planktivorous chorus in the shallow water off southwest coast of India.

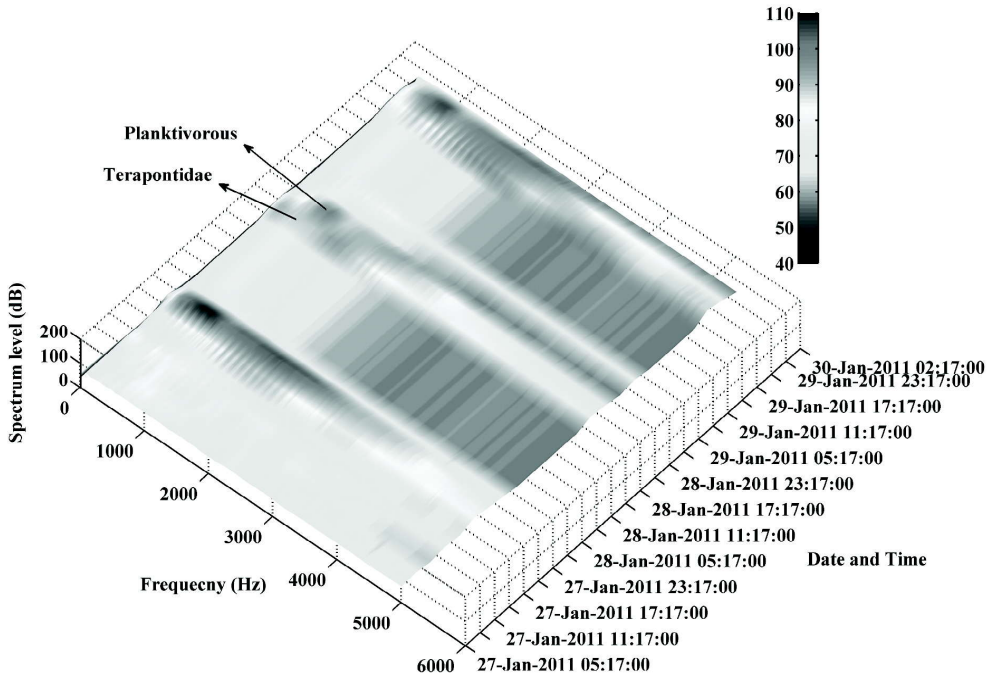

Fig. 6. Diurnal variation of fish chorus recorded in the in shallow water off southwest coast of India.

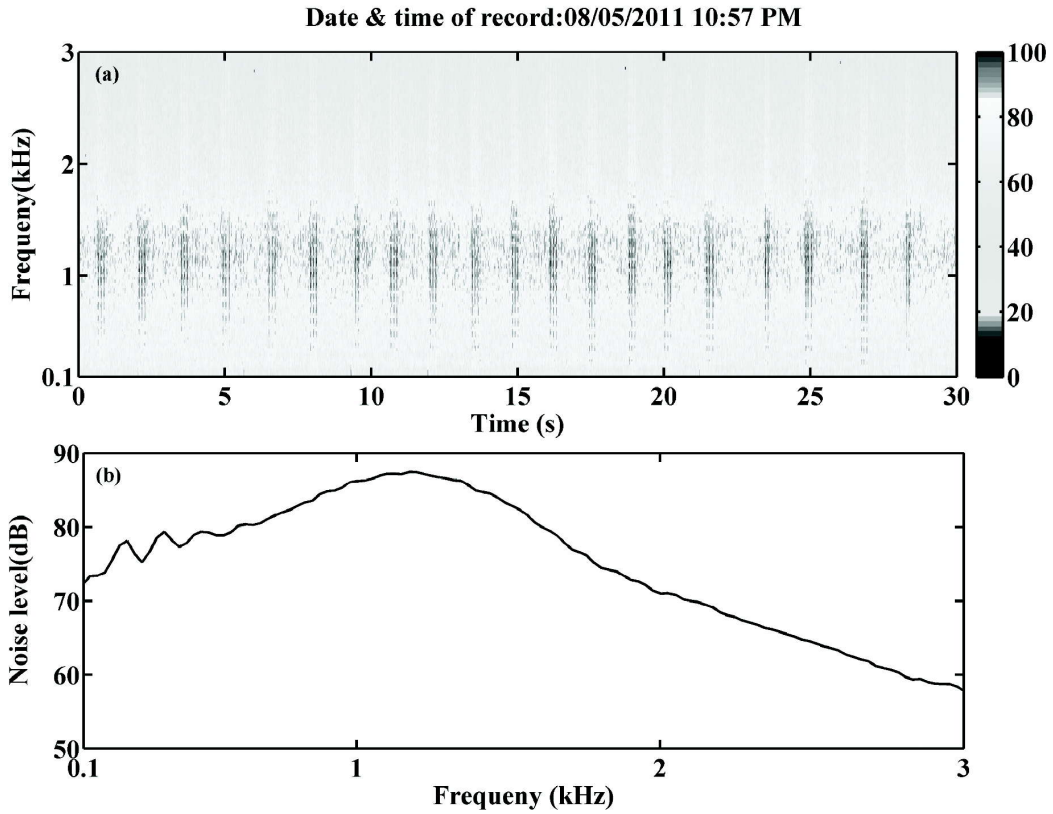

Fig. 7. The spectrogram and the power spectral density of Eel fish sound in the shallow water off southwest coast of India.

power spectra of the eel sound indicate its dominant frequency at 1.21 kHz with a maximum sound level of 89 dB re 1 μPa. Besides, the eel produces sound akin to jackhammer during the night (between 10 PM to 11 PM).

4. CONCLUSION

The present study highlights the first time measurement of soundscape variation in the shallow water off southwest coast of India. The temporal biological soundscape in the study area is diurnal that varies monthly. The Terapontidae chorus appearing before dawn and after dusk, and is maximal during January to end of March, but ceased down by month of May, and the planktivorous chorus produce before midnight displaying lunar trend during the period January 22-February 8. The eel fish produce sound similar to jackhammer at night, during the month of May. Fish chorus has the major influence on ambient noise levels and spectral characteristics of soundscape in shallow water off southwest coast of India. Thematic structure with harmonic sounds produced by humpback whales, illustrating significant increase in acoustic energy in frequencies greater than 8 kHz in the period mid-January to mid-March, and indicates the functions of the humpback whale songs and their breeding habitat. Habitat related soundscapes play an important role in the ecology of shallow water environment, and passive acoustic measurement is key element to understand the acoustic ecology.

5. ACKNOWLEDGEMENTS

The authors are grateful to the Director, NIOT for his support in carrying out this work. The authors gratefully thank A. Thirunavukkarasu, G. Raghuraman, M.Ashokan, R.Kannan, K. Nithyanandam, and C. Dhanaraj

of ocean acoustics group at National Institute of Ocean Technology for their help in measurement of ambient noise. The authors thankfully acknowledge Mrs. A. Malarkodi and Dr. M.C Sanjana for their help in testing and calibration of hydrophones.

7. REFERENCES

[1] A. COTTER, 2008.The soundscape of the sea, underwater navigation, and why we should be listening more. ***In:*** Payne A, Cotter J, Potter T (eds) *Advances in fisheries science: 50 years on from Beverton and Holt.*, John Wiley and Sons.

[2] B.C.PIJANOWSKI, L.J.VILLANUEVA-RIVERA, S.L.DUMYAHN, A. FARINA, B.L.KRAUSE, B.M.NAPOLETANO, S.H. GAGE and N.PIERETTI, 2011. Soundscape ecology: The science of sound in the landscape, *Biosci.*, **61**(3), 203-216.

[3] R.J.URICK, 1983. *Principles of underwater sound*, Peninsula Publishing, New York.

[4] B.L.KRAUSE, 2008. Anatomy of the soundscape: evolving perspectives, *J. Audio Eng. Soc.*, **56**, 73-80.

[5] R.J.URICK, 1984. *Ambient noise in the sea, Report to the Undersea Warfare Technology Office,* Washington, D.C.

[6] R.D.McCAULEY and D.H.CATO, 2000. Patterns of fish calling in a nearshore environment in the Great Barrier Reef, *Philos Trans R Soc. Lond B Biol Sci.,* **355**, 1289-1293.

[7] A.A. MYRBERG and L. A. FUIMAN, 2002. The sensory world of coral reef fishes. ***In:*** P.F.Sale (ed.) *Coral reef fishes: dynamics and diversity in a complex ecosystem*. Elsevier Academic Press, San Diego, CA.

[8] M.M.MADAN, G. LATHA and A.THIRUNAVUKKARASU, 2015. Analysis of humpback whale sounds in shallow waters of the Southeastern Arabian Sea: An indication of breeding habitat. *J.Biosci.,* **40**(2), 407-417.

[9] R.K.ANDREW, B.M.HOWE and J.A.MERCER, 2011. Long-time trends in ship traffic noise for four sites off the North American west coast, *J. Acoust. Soc. Am.*, **129**, 642-651.

[10] C.W.CLARK,W.T. ELLISON, B.L.SOUTHALL, L.HATCH, S.M.VAN PARIJS, A. FRANKEL and D.PONIRAKIS, 2009. Acoustic masking in marine ecosystems: intuitions, analysis, and implication. *Mar. Ecol. Prog. Ser.*, **395**, 201-222.

[11] S.POMPA, P.R. EHRLICH and G. CEBALLOS, 2011. Global distribution and conservation of marine mammals, *Proc. Natl. Acad. Sci.*, **108**, 13600-13605.

[12] S.M. MAXWELL, E.L.HAZEN, S.J.BOGRAD, B.S. HALPERN, G.A.BREED, B.NICKEL, N.M. TEUTSCHEL, L.B.CROWDER, S. BENSON, P.H.DUTTON, H.BAILEY, M.A. KAPPES, C.E.KUHN, M.J.WEISE, B.MATE, S.A.SHAFFER, J.L.HASSRICK, R.W.HENRY, L.IRVINE, B.I.MCDONALD, P.W.ROBINSON, B.A. BLOCK and D.P.COSTA, 2013. Cumulative human impacts on marine predators, Nat. Commun, **4**, 2688.

[13] N.D. MERCHANT, E. PIROTTA, T.R. BARTON and P.M. THOMPSON, 2014. Monitoring ship noise to assess the impact of coastal developments on marine mammals, *Mar. Pollut. Bull*, **78**, 85-95.

[14] A. LILLIS, D.B. EGGLESTON and D.R. BOHNENSTIEHL, 2013. Oyster larvae settle in response to habitat associated underwater sounds, *PLoS ONE*, **8**(10), 79337.

[15] C.M. HUIJBERS, I. NAGELKERKEN, P.A.C. LÖSSBROEK, I.E. SCHULTEN and A. SIEGENTHALER *et al*, 2011. A test of the senses: Fish select novel habitats by responding to multiple cues, *Ecology*, **93**, 46-55.

[16] R.D. McCAULEY, 2012. Fish choruses from the Kimberley, seasonal and lunar links as determined by long-term seanoise monitoring, *Proceedings of Acoustics 2012 Fremantle*, Fremantle, Western Australia, November, 21-13.

[17] M.M. MAHANTY, G. LATHA and A. THIRUNAVUKKARASU, 2015. Fish chorus recorded in the southeastern Arabian Sea: A comparison study with other shallow water environments. 4th National

conference of the Ocean Society of India on Oceanic Processes along the Coasts of India, OSICON-15, NIO, Goa, India.

[18] B. MA.BARRY, A. JEFFREY, NYSTUEN and R.C. LIEN, 2005. Prediction of underwater sound levels from rain and wind, *J. Acoust. Soc. Am.,* **117**(6), 3555-3565.

[19] H. WHITEHEAD and M.J. MOORE, 1982. Distribution and movements of West Indian humpback whales in winter, *Can. J. Zool.* **60**(9), 2203-2211.

[20] R.D. McCAULEY, 2001. Biological sea noise in northern Australia: Patterns of fish calling. PhD. Thesis, James Cook University Library.

Journal of Acoustical Society of India : Vol. 43, No. 1, 2016 (pp. 18-23)

Effect of initial membrane curvature on the performance of piezoelectric micromachined ultrasonic transducers

Ajay Dangi[2*], Dhananjay Deshmukh[1] and Rudra Pratap[1,2]
[1]*Centre for Nano Science and Engineering, Indian Institute of Science, Bangalore-560012*
[2]*Department of Mechanical Engineering, Indian Institute of Science, Bangalore-560012*
**e-mail: ajayd@mecheng.iisc.ernet.in*

[Received: 27.10.2015; Revised: 07.03.2016; Accepted: 07.03.2016]

ABSTRACT

Micromachined Ultrasonic Transducers (MUTs) represent a new paradigm in ultrasonics by significantly reducing size, reducing energy consumption, and simplifying electronic integrability of huge array of sensors on a single silicon chip. A Piezoelectric Micromachined Ultrasonic Transducer (PMUT) is a suspended multi-layered thin plate structure which vibrates in response to input voltage by the means of in-plane piezoelectric stresses and generates acoustic pressure. In this work we study the effect of initial curvature of the suspended plate on the vibration response and acoustic performance of a PMUT. We consider natural frequency, deflection sensitivity, and directivity of PMUT with the motivation of capturing overall impact of curvature on the acoustic pressure output per unit voltage input. We compare the vibrational response of a curved PMUT and an equivalent flat PMUT using analytical and FEM techniques. The FEM analysis is done using multi-layered shell elements in ANSYS. We observe that the natural frequency of the PMUT increases with curvature almost exponentially beyond a minimum curvature. The deflection per unit input voltage of the PMUT first increases with the initial curvature but drops beyond an optimal value of the initial curvature. We have observed in our previous work that change in size of a flat PMUT, for a given layer configuration, does not change the acoustic pressure output of the PMUT transmitter significantly. This is because any improvement in deflection per unit voltage by increasing the radius of the PMUT is countered by decrease in the natural frequency. However, an increase in the initial curvature increases the deflection sensitivity as well as increases the natural frequency of the PMUT. This effect becomes even more dominant as the radius of curvature approaches the radius of the membrane. This analysis predicts significant improvement in the acoustic pressure output and thus the performance of a PMUT by the introduction of initial curvature. The acoustic directivity improves with increase in operational frequency. We also study the difference between acoustic characteristics of an upward curved (convex) PMUT and downward curved (concave) PMUT. The acoustic directivity deteriorates with increase in curvature for convex PMUT, while it improves with increase in curvature for concave PMUT.

1. INTRODUCTION

Ultrasound has been used widely in medicine, microscopy, navigation, underwater networking, etc. Making conventional Ultrasound transducers with high bandwidth, low power consumption and operating at high frequencies is not cost-effective. Application of micro-fabrication processes adopted from semiconductor

industry has led to significant improvements in various transduction techniques. These processes allow us to fabricate very small ultrasonic sensors on silicon wafers, known as Micromachined Ultrasonic Transducers (MUTs). MUTs represent a new paradigm in ultrasonics by significantly reducing size, reducing energy consumption, and simplifying electronic integrability of huge array of sensors on a single silicon chip. Based on the actuation principle MUTs can be of capacitive or piezoelectric type, also known as CMUTs [1] and PMUTs [2] respectively. CMUTs and PMUTs, made by MEMS technology have shown mechanical impedances closely matching to that of the imaging medium.

Piezoelectricity based devices require low power, give large output forces, have a wide range of operational frequencies and provide a good signal to noise ratio. A Piezoelectric Micromachined Ultrasonic Transducer (PMUT) is a suspended multi-layered thin plate structure, wherein at least one layer is of piezoelectric material. PMUTs have been under research for more than a decade now with most of the work focused on planar unimorph configuration [3]. These devices use the bending caused by moment load due to the voltage across the piezoelectric layer. In recent years, efforts have been put into improving the performance of these devices. Some researchers have focused their attention on imparting curvature to the membrane. Curved PMUTs are expected to give better acoustic output as the deflection will occur due to bending load as well as in-plane stresses. D Morris *et.al.* [4] and Fleischman *et.al* [5] have used static pressure to induce curvature in PMUT. Fleischman *et.al.* [5] used PVDF to fabricate the piezoelectric films, and created a near-field focused ultrasonic transducer by backfilling the sphere exterior with epoxy. D Morris *et.al.* [5] have deposited PZT using sol-gel techniques and has given a mathematical model. A Hajati *et.al.* [6] have fabricated a dome-shaped PMUT and studied its acoustic properties. S Akhbari *et.al.* [7] have shown highly responsive, curved PMUTs using AlN, with centre deflection 55 times more than that of a planar device.

In our work we have studied the change in frequency and amplitude with change in curvature of the PMUT. Imparting an initial curvature can change not only the natural frequency but also the acoustic directivity of a PMUT. We have studied how acoustic directivity changes with frequency and with the radius of curvature. We have also studied how acoustic directivity differs depending on whether the membrane is concave or convex.

2. DEVICE ARCHITECTURE

For the analysis, a multi-layered membrane as shown in Fig. 1 is considered. The piezoelectric (PZT) layer lies sandwiched between the top Gold electrode and the bottom Platinum electrode, which enables an electric field to be applied across the piezoelectric layer. This structure sits on top of a Silicon passivation layer. The passive layer causes the centre of piezoelectric stress to be eccentric with respect to the neutral axis, thus causing an overall bending moment in response to the voltage. The radius of the membrane is 100 μm. The radius of gold electrode is 0.8 times the radius of device in order to cause moment load in

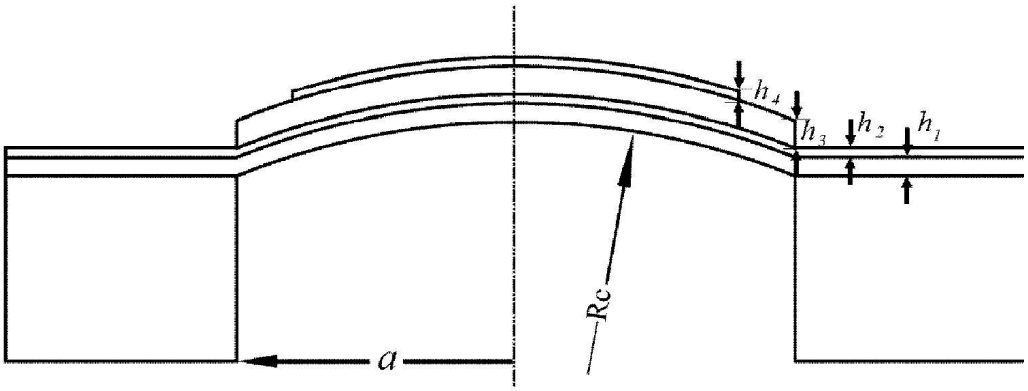

Fig. 1. Cross Section view of a Curved PMUT

Table 1. Material Properties of Layers

Material	Density (kg/m^3)	Poisson's Ratio	Young's Modulus (GPa)	Thickness (nm)
Silicon	ρ_1 = 2330	ν_1 = 0.28	Y_1 = 165	h_1 = 1000
Platinum	ρ_2 = 21450	ν_2 = 0.38	Y_2 = 168	h_2 = 150
PZT	ρ_3 = 7600	ν_3 = 0.3	Y_3 = 115	h_3 = 1000
Gold	ρ_4 = 19280	ν_4 = 0.44	Y_4 = 165	h_4 = 150

optimal location [2]. The thickness of PZT and Silicon are 1000 nm each. Both the electrodes (Gold and Platinum) are 150 nm thick.

Application of voltage across the electrode causes in-plane stress in the piezoelectric layer which results in bending as well as stretching of the PMUT. This generates acoustic pressure output in response to alternating voltage input when PMUT is used as a transmitter. Converse of this phenomenon leads to generation of charge on PMUT receiver.

3. ANALYTICAL SOLUTION

In this section, curved PMUT has been modeled as a multi-layered curved shell with the assumptions of classic shell theory. The equation of motion for vibrations of a curved PMUT with radius of curvature, Rc, in response to harmonic pressure load Pin can be written as [8]:

$$\nabla^6 w + d_1 \nabla^4 w + d_2 \nabla^2 w + d_3 w + d_4 R_c P_{in} = 0 \quad [1]$$

where w is amplitude of vibration ($w^* = w.\, e^{j\omega t}$) and d_1, d_2, and d_3 are as given below.

$$d_1 = \frac{4}{R_c^2} + \frac{\rho_{eq}\omega^2 {h_T}^3}{12 D_{eq}} \quad [2a]$$

$$d_2 = \frac{Y_{eq} h_T}{D_{eq} R_c^2} - \frac{\rho_{eq}\omega^2 h_T}{D_{eq}} \quad [2b]$$

$$d_3 = \frac{2 Y_{eq} h_T}{D_{eq} R_c^4} + (1+3v)\frac{\rho_{eq}\omega^2 h_T}{R_c^2 D_{eq}} - \frac{1}{12}\left(\frac{\rho_{eq}\omega^2 {h_T}^2}{D_{eq}}\right)^2 \quad [2c]$$

$$d_4 = \left[\frac{(1-v)}{D_{eq} R_c^3} + \frac{\rho_{eq}\omega^2 {h_T}^3}{R_c {D_{eq}}^2}\right] \quad [2d]$$

Here, D_{eq} is equivalent flexural rigidity, ρ_{eq} is average density, h_T is total thickness, Y_{eq} is equivalent young's modulus, R_c is radius of curvature, ω is frequency of harmonic input load, and ν is equivalent Poisson's ratio of the multi-layered shell structure [8]. The mode shape of vibration in axisymmetric modes is assumed to be

$$w_\alpha = w_s + A_\alpha P_{l_\alpha}(\cos\phi) + B_\alpha Q_{l_\alpha}(\cos\phi), \quad \alpha = 1,2,3, \quad [3]$$

Here w_s is the specific solution to equation (1) and can be written in simplified form as :

$$w_s = -\frac{d_4 R_c P_{in}}{d_3} \quad [4]$$

The coefficients B_α are set to zero to avoid singularity in the solution. $P_{l\alpha}$ are the Legendre functions of first kind of order l_α which are obtained by solving 3rd order polynomial equation obtained by substituting

the assumed solutions in the equation of motion. The coefficients, A_α are obtained by imposing boundary conditions of zero in-plane and out-of-plane deflection, and zero change in slope at the boundary of the curved PMUT [8]. Natural frequency is obtained by observing maxima in deflection along frequency axis.

4. SIMULATION OF CURVED PMUT

The key figure of merit of an ultrasonic transducer is pressure transmitted per unit voltage input. Pressure output is proportional to volume swept by the membrane during vibration and square of the frequency of operation. Improvement in directivity of an ultrasound transducer while avoiding secondary lobes is also a desirable for imaging type of applications. Considering these factors, we have focused on three parameters for present assessment: first natural frequency, deflection sensitivity, and acoustic directivity.

We have modelled the curved PMUTs in ANSYS using multi-layered shell elements. In order to emulate exact piezoelectric loads we have considered bending loads as well as in-plane loads in the shell model. Acoustic directivity has been observed using an equivalent single layer axisymmetric plate in COMSOL environment.

5. EFFECT OF CURVATURE ON NATURAL FREQUENCY

An almost flat PMUT with 100 μm radius shows the first resonance at 471 KHz for material properties given in Table 1. For small curvatures ($R_c/\alpha > 60$) no significant increase in the natural frequency of PMUT is observed. Any further increase in curvature results in exponential increase in the natural frequency of the PMUT reaching up to 5.3 MHz for almost hemispherical PMUTs.

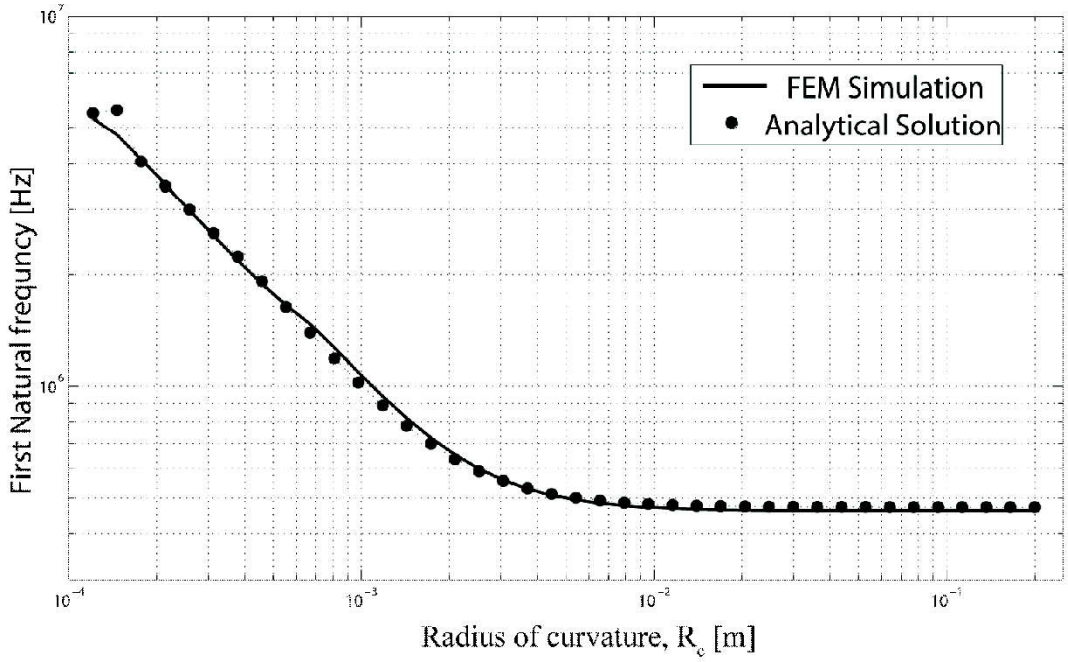

Fig. 2. Dependence of natural frequency on curvature of a PMUT

Higher frequency is generally desirable for ultrasound imaging based applications in order to achieve higher resolution. This can be done by increasing the thickness or reducing the radius or introducing tensile stresses. Reducing radius below 50 μm becomes very difficult due to fabrication constraints, increasing thickness reduces sensitivity of the device and tensile stresses are difficult to control. Introduction of curvature provides a lucrative alternative for increasing the natural frequency of PMUT with only apparent downside of difficulties in fabrication.

6. EFFECT OF CURVATURE ON DEFLECTION SENSITIVITY

We have presented the deflection of a PMUT for a static voltage load in Fig. 3. To represent static deflection we have considered static loading condition instead of dynamic loading condition in order to ignore any effects caused by change in quality factor of the device. Unlike a flat PMUT, deflection in a curved PMUT is caused by piezoelectric moment load as well as in-plane stretching. The ANSYS simulation result suggests that the deflection at the center of the PMUT caused by in-plane stretching and bending moment can compete against each other causing the center of the PMUT to move in one direction for in-plane stress dominated deflection and in the other direction for moment load dominated deflection.

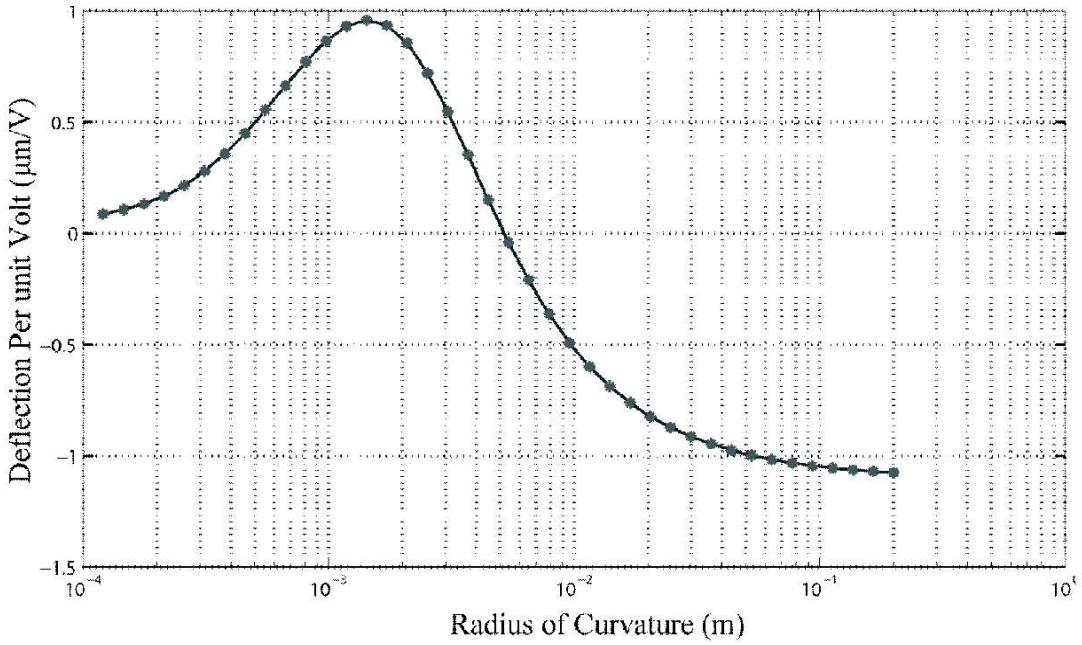

Fig. 3. Static deflection of PMUT vs radius of curvature

7. EFFECT OF CURVATURE ON ACOUSTIC DIRECTIVITY

Acoustic directivity by definition is the ratio of far field sound pressure level at any angle to the sound pressure level at the axis of the transducer. It plays an important role in determining resolution of an

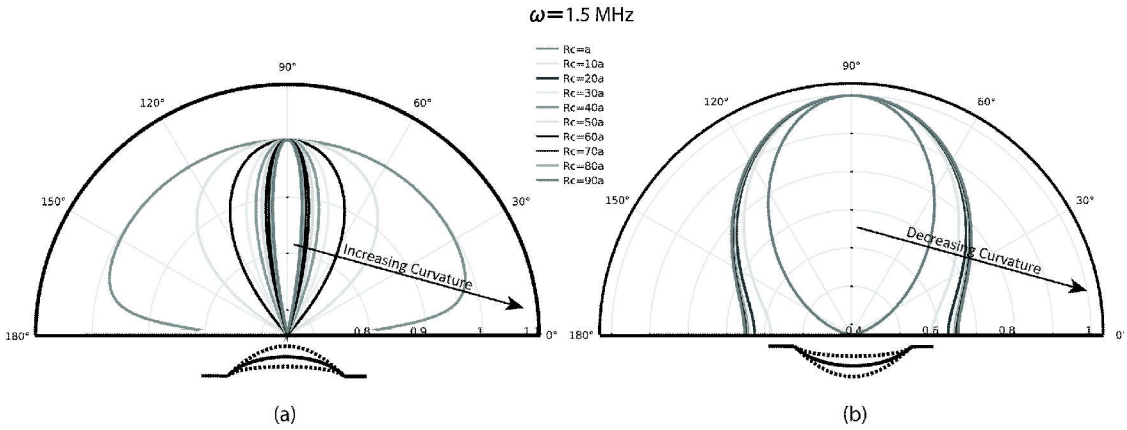

Fig. 4. Directivity of (a) upward curved and (b) downward curved PMUT with varying R_c

arrayed transducer in imaging type applications. Acoustic directivity of a radiator of a given radius, improves as frequency of operation is increased. Since introduction of curvature increases the natural frequency it automatically improves the directionality by improving the wave number. The simulation results shown in Fig. 4, confirms the improvement in directivity because of higher frequency.

These results show that a downward curved (concave) PMUT will radiate more directed sound as compared to an upward curved PMUT (convex).

8. CONCLUSION

Natural frequency of a PMUT of 100 μm radius increases by almost ten times with increase in curvature from a flat to hemi-spherical case. The deflection at the centre of PMUT increases with curvature up to an optimum level, beyond which it starts decreasing. The acoustic directivity improves for a downward curved PMUT as compared to an upward curved PMUT. Overall an improvement in frequency, deflection sensitivity, and directivity is observed by introduction of curvature thus pointing to a possibility of developing better ultrasonic sensors at small scale.

9. REFERENCES

[1] A.S. ERGUN, G.G. YARALIOGLU and B.T. KHURI-YAKUB, 2003. Capacitive Micromachined Ultrasonic Transducers: Theory and Technology, *J. Aerosp. Eng*., **16**(2), 76-84.

[2] S. SHELTON, M.-L. CHAN, H. PARK, D. HORSLEY, B. BOSER, I. IZYUMIN, R. PRZYBYLA, T. FREY, M. JUDY, K. NUNAN, F. SAMMOURA and K. YANG, 2009. CMOS-compatible AlN piezoelectric micromachined ultrasonic transducers, *Proc. IEEE International Ultrasonic Symposium,* 402-405.

[3] RICHARD J. PRZYBYLA, HAO-YENTANG, ANDRÉ GUEDES, STEFON E. SHELTON, DAVID A. HORSLEY and BERNHARD E. BOSER, 2015. 3D Ultrasonic Rangefinder on a Chip, *IEEE Journal of Solid-State Circuits,* **50**(1), 320-334.

[4] DYLAN J. MORRIS, RYAN F. NEED, MICHAEL J. ANDERSON and DAVID F. BAHR, 2010. Enhanced actuation and acoustic transduction by pressurization of micromachined piezoelectric diaphragms, *Sensors and Actuators*, 164-172.

[5] AARON FLEISCHMAN, RUSHABH MODI, ANUJA NAIR, JAMES TALMAN, GEOFFREY LOCKWOOD and SHUVO ROY, 2003. Miniature high frequency focused ultrasonic transducers for minimally invasive imaging procedures, *Sensors and Actuators,* **103**, 76-82.

[6] ARMAN HAJATI, DIMITRE LATEV, DEANE GARDNER, AZADEH HAJATI, DARREN IMAI, MARC TORREY and MARTIN SCHOEPPLER, 2012. Three-dimensional micro electromechanical system piezoelectric ultrasound transducer, *Appl. Phys. Lett.*, 101.

[7] SINA AKHBARI, FIRAS SAMMOURA, STEFON SHELTON, CHEN YANG, DAVID HORSLEY and LIWEI LIN, 2014. Highly Responsive Curved Aluminum Nitride, *PMUT, MEMS 2014, IEEE,* San Francisco.

[8] FIRAS SAMMOURA, SINA AKHBARI and LIWEI LIN, 2014. An Analytical Solution for Curved Piezoelectric Micromachined Ultrasonic Transducers With Spherically Shaped Diaphragms, *IEEE Transactions on Ultrasonics, Ferroelectrics, and Frequency Control,* **61**(9).

Journal of Acoustical Society of India : Vol. 43, No. 1, 2016 (pp. 24-31)

Design and fabrication of single wafer capacitors for MEMS devices

Meera Garud[1*], Jayaprakash Reddy. K[1], Vamsy Godthi[2] and Rudra Pratap[1,2]
[1]*Centre for Nano Science and Engineering, Indian Institute of Science, Bangalore-560012*
[2]*Department of Mechanical Engineering, Indian Institute of Science, Bangalore-560012*
**e-mail: meera.v.garud@gmail.com*

[Received: 27.10.2015; Revised: 09.03.2016; Accepted: 09.03.2016]

ABSTRACT

This paper reports the development of a MEMS (Micro-Electro-Mechanical-Systems) capacitive transducer specifically a microphone using a single wafer process in contrast to the current practice of using multiple wafers and wafer bonding. We consider design challenges mainly present due to squeeze film damping effect, frequency range requirements, and sensitivity. In order to fabricate the device using simple fabrication steps on the SOI wafer, we designed the substrate of the wafer to have openings which ultimately decide the final dimension of the structure. The diaphragm of the microphone is created on the device layer of the SOI wafer and the handle layer acts as the rigid backplate of the microphone. The buried oxide layer acts as the sacrificial layer. We pattern the openings in the backplate using a single photo printed mask and use DRIE (Deep-Reactive-Ion-Etching) process to etch the pattern. We use these openings to facilitate wet etching of the buried oxide. The openings also allow easy escape of trapped air during operation of the device. The initial characterization results suggest that the proposed design and fabrication process is worth exploring.

1. INTRODUCTION

The advent of MEMS (Micro-Electro-Mechanical Systems) technology has paved the way for inexpensive and miniature sensors powering consumer electronics. There are various types of MEMS transducers in market for example electro-mechanical, thermo-electric, chemical, optical transducers. Commercially, electro-mechanical type of transducers are widely used. Capacitive transducer is one such electro-mechanical transducer which converts mechanical quantity such as displacement into electrical voltage. Our work here, focuses on a way of fabricating capacitive transducer for a MEMS microphone. Microphone is a sensor that has benefited from MEMS technology and has been commercially available since the last decade for various applications. Microphones typically consist of a suspended membrane. The deformation of the membrane due to incident sound pressure is sensed either by piezo-electric [1,2], piezo-resistive [1,3], or capacitive methods [1,4,5]. Capacitive MEMS microphones are the most widely used devices due to the relative ease of fabrication and electronic integration [6].

In capacitive sensing, two oppositely charged plates (electrodes) are separated by a distance typically forms a parallel plate capacitor. Usually, in capacitive MEMS devices, one electrode is a vibrating plate and the other is the fixed substrate. In a MEMS microphone the vibrating plate is a structural membrane and the main acoustic pressure sensing element. The membrane deflects in response to any incoming acoustic pressure affects changes in capacitance. This changes the charge on the two electrodes [7]. The capacitance

is given by, $C = \frac{\varepsilon A}{g}$ where, A is the electrode surface area, ε is the permittivity of the medium between the two plates forming capacitor, and g is the gap between the plates. Hence, closely spaced plates with large area cause greater current flow than two distant plates with smaller area.

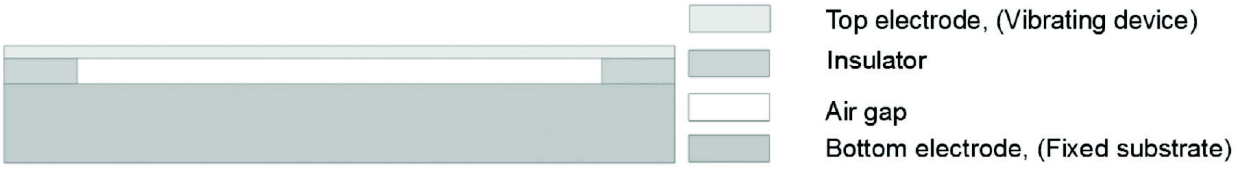

Fig. 1. Figure showing schematic for the cross-section of typical device that uses capacitive sensing.

With micro fabrication, it is relatively easy to realize devices based on capacitive sensing. The electrodes are separated by very small gaps as shown in Fig. 1 (usually a few microns). But we will see that this requirement of small separation between a vibrating structure and a fixed substrate imposes restrictions on the design of MEMS devices.

Majority of existing capacitive MEMS microphone designs are intricate consisting of perforated or slotted diaphragms [8,9], multilevel contacts, and patterned back-plates that involve complex fabrication processes like multilayer deposition and patterning [10] and two wafer bonding. Our work is aimed at exploring simpler designs such that the devices can be realized with the least number of fabrication steps using a single wafer.

2. DESIGN OF CAPACITIVE MEMS MICROPHONE

In-order to have a linear response of the structure to the incident sound pressure in the frequency range of interest (typically audible frequency limit of 20 kHz), we keep the fundamental resonant frequency of the device far above the required range. The natural frequency of the membrane is given [11] as:

$$f_n = \frac{\beta_n}{\rho\pi}\sqrt{\frac{Et^3}{\rho d^4(1-\nu^2)'}} \tag{1}$$

Where, f_n is the natural frequency, E is the Young's modulus, d is the diameter of the membrane (treated as a thin plate here), ν is the Poisson's ratio, ρ the mass density, and β_n is a non-dimensional constant which depends on boundary conditions and it is equal to 11.84 for the first mode of circular plate with clamped edges. We design the radius of the membrane for different natural frequencies of interest as listed in Table 1.

Table 1. Table listing radius of membrane and corresponding natural frequency for Silicon < 100 > with properties as follows; Young's Modulus, E = 160 GPa, Poisson's ratio, ν = 0.28, mass density, ρ = 2328 kg/m^3.

Radius of Membrane (mm)	Natural Frequency (kHz)
1	8.2
0.8	12.8
0.6	22.8

2.1 Challenges in design

Since we have decided to use capacitive sensing, we design our structure considering the following-the gap between the electrodes and the effects of squeeze film. The acoustic sensitivity (S) of a capacitive microphone is the output voltage per unit input acoustic pressure [4] and is given by the expression

$$S = \frac{V}{p} \alpha \frac{1}{g}, \quad [2]$$

where, V is the output voltage, P is the input acoustic pressure, and g is the air gap between the two electrodes. Hence we see that the sensitivity is inversely proportional to the air gap. So, ideally we would like to have as small a gap as can be fabricated. But, when the membrane vibrates, the air in the gap gets squeezed and contributes to added damping and stiffness of the structure. This added damping and stiffness are functions of the frequency of vibration and hence affect the dynamic response of the MEMS devices over a range of frequencies [12]. This squeeze film damping effect reduces sensitivity of the device. Hence, it is necessary to account for and reduce this added damping and stiffness for a successful design of the device. Squeeze film is a common phenomenon and has been well studied in the context of the influence of squeeze film damping on MEMS structures as summarized by Bao and Yang [13] and Pratap *et al.* [14]. The simplest approach to reduce squeeze film effects is to vent the squeezed air by providing openings either on the fixed substrate or on the vibrating structure.

In the case of MEMS microphones, improperly designed openings on the vibrating structure have a deteriorating effect on the acoustic performance of the transducer due to equalization of the sound pressure (called low frequency roll-off) [15]. Hence, we provide openings on the substrate. But on the contrary, we reduce the available electrode area if we increase the openings, which in turn reduces sensitivity. Hence, this is an optimisation between having a large electrode area and having openings to reduce squeeze film. Before going for optimised design, substrate with maximum possible electrode area while still having enough openings to reduce squeeze film effects, just to check the feasibility of the design, we decide the opening area based on limitations in chosen fabrication process as discussed in later section. Several analytical and numerical methods exist to model the squeeze film with holes [15], and we use ANSYS to model squeeze film and to verify that the openings in the substrate adequately vent the squeeze film pressure. Fig. 2(a) shows normalized displacement of diaphragm clamped at periphery subjected to uniformly distributed load and Fig. 2(b) shows normalized squeeze film pressure variation on the same. It is clear that the diaphragm displacement and pressure are out of phase.

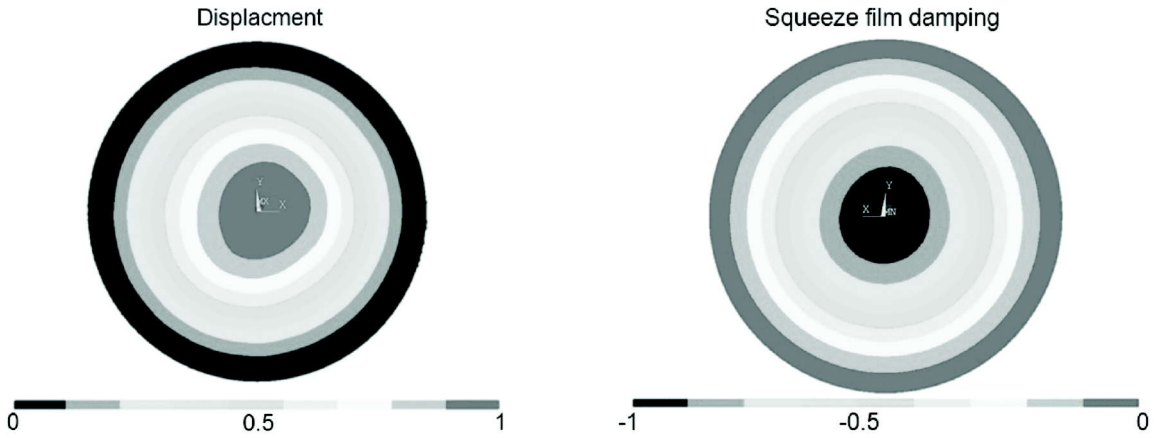

Fig. 2. Figure showing ANSYS results for diaphragm clamped at periphery subjected to uniformly distributed load, where (a) gives normalised displacement plot and (b) gives normalised pressure distribution plot.

3. FABRICATION

We fabricate the device using a single SOI (Silicon-On-Insulator) wafer as depicted in Fig. 3 and a single mask. We print our design on a regular transparent sheet and use it as a mask. This process is much cheaper than conventional mask making process and also reasonably accurate for our design. Our design uses

Fig. 3. Figure showing schematic representation of SOI (Silicon-On-Insulator) wafer and its nomenclature.

buried oxide in SOI as a sacrificial layer. The choice of SOI wafer is decided by the sheet resistance of handle silicon and the device silicon. For our case we choose a wafer with specifications listed in Table 2.

Table 2. Table lists specification for SOI wafer ((100) Orientation).

Property	Value	Unit
Device layer thickness	2	μm
Buried oxide layer thickness	1	μm
Handle silicon thickness	500/±10	μm
Sheet resistivity	0.005 - 0.020	ohm-cm

First we start by cleaning the SOI wafer with piranha solution (1:4 :: H_2O_2:H_2SO_4) for a duration of 10 minutes. Fig. 4(a) shows schematic representation of cleaned SOI wafer. Then we deposit oxide to get 1.5 micron thick oxide layer on top of the handle silicon using PECVD (Plasma Enhanced Chemical Vapor Deposition) process as depicted in Fig. 4(b). This oxide layer is used as a masking material in dry etching process. Next, using photolithography technique we transfer the design pattern printed on the mask, on top of the oxide layer as shown in Fig. 4(c). To get the openings on the substrate, first we etch the oxide layer using RIE (Reactive Ion Etching) process and reach the handle layer silicon. Then we further etch the handle layer using DRIE (Deep Reactive Ion Etching) process. This etching process ends when we reach buried oxide which acts as an etch stopper in DRIE process. Fig. 4(d) shows device after DRIE process. To get the gap between the device layer silicon and the handle layer silicon, we etch the sacrificial layer of

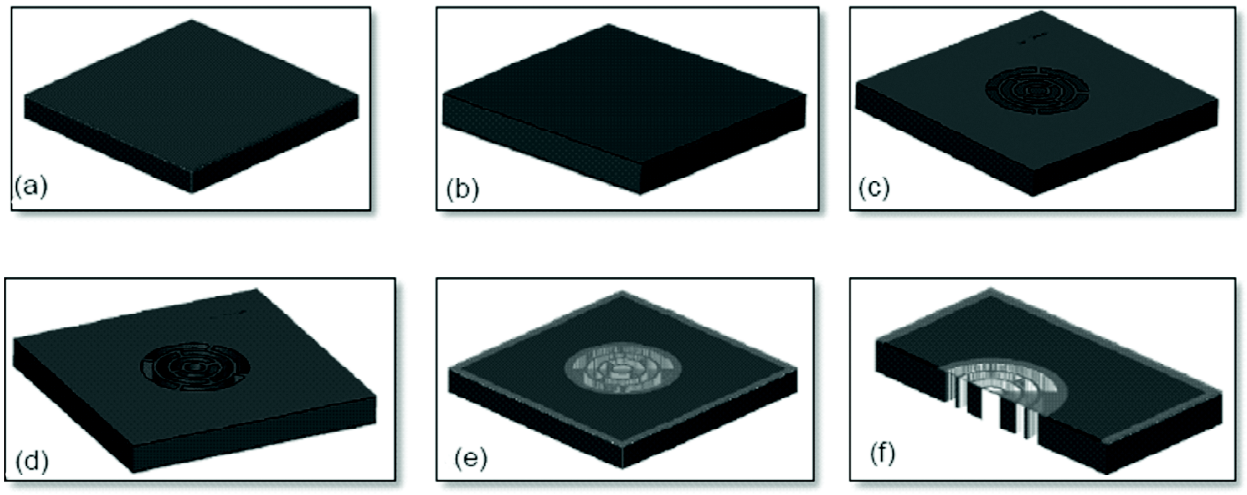

Fig. 4. Figure depicting steps in fabrication process; (a) piranha cleaned SOI wafer, (b) PECVD Oxide deposited on handle silicon, (c) structure mask patterned oxide, (d) DRIE processed handle silicon, (e) device release after sacrificial etch by HF vaporiser, and (f) cross-sectional view of the fabricated microphone.

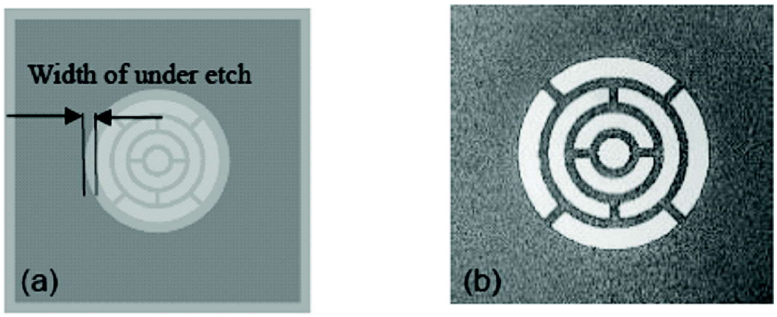

Fig. 5. Figure showing (a) the schematic of top view of a completely realized microphone, it shows under-etching caused by process of wet etching in the step of buried oxide removal, (b) the actual microphone after realization as seen from bottom side.

buried oxide. We etch it using HF (Hydro Fluoric) vaporizer. We get device with released membrane as shown in Fig. 4(e) and the corresponding cross-sectional view is as depicted in Fig. 4(f). Fig. 5(b) shows actual device as seen under microscope. In the process of wet etching by use of HF vaporizer, we control the membrane area by setting duration of the etch process. The width of under-etch and area of diaphragm of realized device is schematically represented in Fig. 5(a). Since we choose an SOI wafer with low resistivity value, silicon can be used as both top electrode and bottom electrode of the microphone.

To overcome the challenges in design as specified in section 2.1, ideally we should have large number of narrow openings in the substrate. This will provide sufficient openings for venting trapped air and thus reducing squeeze film effect along with giving large electrode area. But step of printing of mask using normal photo printing in proposed fabrication process imposes a lower limit on the width of openings. Also because we need to etch 500 micron thick substrate using DRIE, considering lateral etching present in the process, the minimum width possible is 75 micron for realisation of the device. This minimum feature size is the major governing factor in designing the substrate etch pattern as mentioned in Section 2.1.

4. CHARACTERISATION OF FABRICATED DEVICES

4.1 Mechanical characterisation

First, we study the mechanical response of the membrane (to electrostatic actuation) using LDV (Laser Doppler Vibrometer), MSA 500 from Polytech GmbH. We actuate our device by applying electric potential

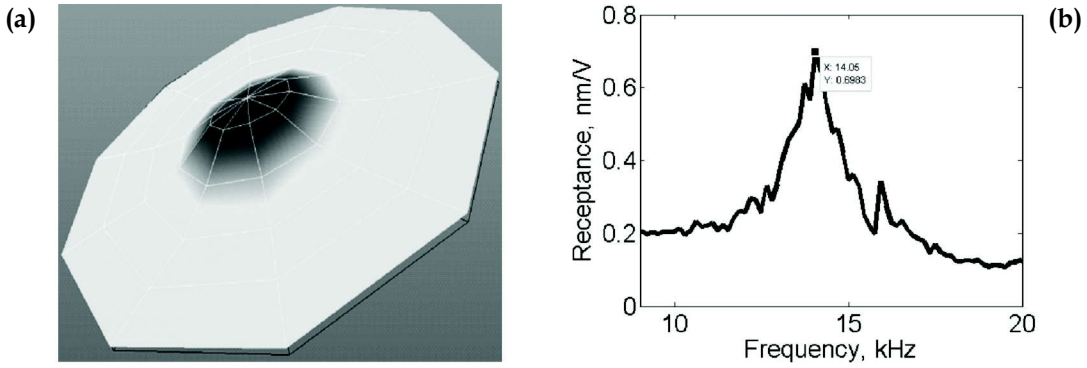

Fig. 6. Figure showing (a) the first mode shape for device membrane when excited by periodic chirp signal with 4 volts AC and 4 volts DC voltage using Laser Doppler Vibrometer, and (b) Receptance of the device as obtained on electrical excitation (displacement value per applied volt).

between the bottom electrode (substrate) and the top electrode (device layer). We use internal signal generator present in the data management system to provide sinusoidally varying voltage. The visualisation of mode shape is obtained using PSV software as shown in Fig. 6(a). It shows the release of the device. The device can be further checked for its function as an electro-acoustic sensor. We use the measured frequency response as shown in Fig. 6(b), to check the resonant frequency and damping of the membrane. Here we get the frequency response for device in terms of deflection of membrane. The deflection is measured at centre of vibrating circular membrane, which is at the point of maximum deflection for fundamental mode the membrane. The deflection can be used further in calculations for device specifications like sensitivity. Also, we get certain geometric information about the device such as electrode area (actual electrode area after fabrication can be calculated from microscopic image of device) and the initial gap between the electrodes (since the membrane is flat as observed under microscope of MSA 500, the initial gap is equal to buried oxide thickness) which is useful in further research and development.

4.2 Electrical characterisation

After visually checking the device and probing its mechanical characteristics, we test it for its electrical characteristics. On DC probe station we connect the electrodes on the device and use device analyser to perform tests. First we check for current against voltage (I-V) characteristics to get the resistance value. This characterization is performed on DC Probe Station 1 (PM5 with Thermal Chuck, Agilent Device Analyzer B1500A). The applied voltage is varied from -5 to +5 volts and corresponding current is measured. Low resistance shows that the device is shorted and not released properly but resistance in the range of a few mega or giga ohms shows that the insulation between the two electrodes is good. Fig. 7(a) shows the I-V plot for the device which indicates that the device is not shorted and also the obtained resistance value which is in giga ohms implies that the two electrodes are well insulated from each other. After I-V check we proceed to get the capacitance against voltage (C-V) characteristics. The capacitance across the top and bottom electrodes of the structure is inversely proportional to the gap, which decreases with increase in the voltage due to the electrostatic force of attraction. Hence for a successfully released device the capacitance increases with increase in the magnitude of the applied voltage irrespective of the polarity while for a partially released structure, the capacitance remains constant. Fig. 7(b) shows the C-V characteristics for the device. The curve shows capacitor variation with change in the voltage as expected and shows that the device is acting as a capacitor.

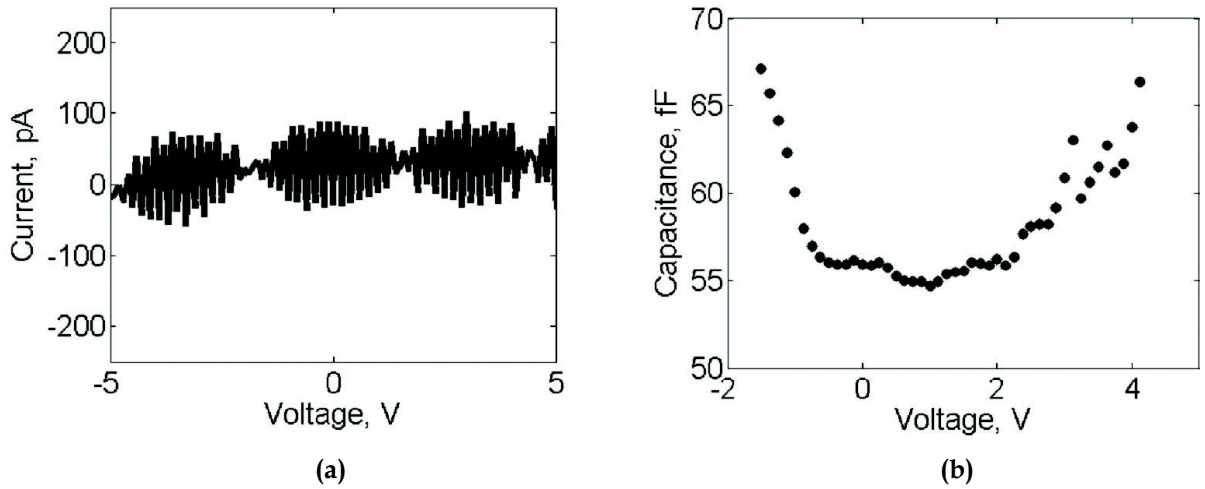

Fig. 7. Figure showing electrical characteristics of the device - (a) plot of current, I vs voltage V, voltage as voltage is swept form -5 volts to 5 volts DC, and (b) plot of capacitance, C vs voltage, V, as voltage is swept from -4 to 4 volts DC with, 0.25 volts of AC component and at 0.2 MHz of frequency.

5. RESULTS

We fabricated devices with diaphragm of 1000 μm radius. From mechanical characterisation as shown in Fig. 6 (b), the fundamental mode is observed at 14 kHz. The electrical characteristics give average resistance value of 14 GΩ. It shows that the two electrodes are not touching each other. Also the I-V curve as shown in Fig. 7(b) confirms that the electrodes are well insulated from each other. C-V curve as shown in Fig. 7(a) shows that the device is working as a capacitor. Also to get base value of capacitance, we carry out measurements using lock-in amplifier. We supply a constant voltage to the device while sweeping the frequency and measure the output current. From the plot of angular frequency against output current, shown in Fig. 8, we get the value of base capacitance as 0.3 pF.

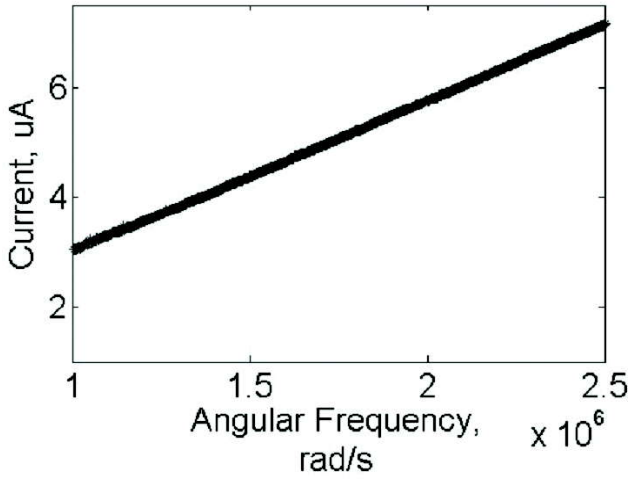

Fig. 8. Figure showing plot of Current for varying frequency at constant voltage of 9 volts Vpp.

6. CONCLUSION

The initial results are encouraging and make us believe that the proposed design will greatly simplify the fabrication of capacitive transducers especially MEMS microphones.

9. REFERENCES

[1] P.R. SCHEEPER, A.G.H. VAN DER DONK, W. OLTHUIS and P. BERGVELD, 1994. A review of silicon microphones, *Sensors and Actuators A*, **44**, 1-11.

[2] SANG CHOON KOA, YONG CHUL KIMB, SEUNG SEOB LEEB, SEUNG HO CHOIC and SANG RYONG KIMD, 2002. Micromachined piezoelectric membrane acoustic devices, 0-7803-7185-2/02 *IEEE.*

[3] R. SCHELLIN and G. HESS, 1992. A silicon subminiature microphone based on piezoresistive polysilicon strain gauges. *Sensors and Actuators A: Physical, Proc of Eurosensors,* **32**(1-3), 555-559,

[4] P.-C. HSU, C. H. MASTRANGELO and K. D., 1998. A high sensitivity polysilicon diaphragm condenser microphone, 0-7803-4412-X/98, *IEEE.*

[5] J. W. WEIGOLD, T. J. BROSNIHAN, J. BERGERON and X. ZHANG, 2006. A MEMS condenser microphone for consumer applications, 10.1109/*MEMSYS.1627742. Proc IEEE 19th Int. Conf. on Micro Electro Mechanical Systems, Istanbul.*

[6] JANUSZ BRYZEK, SHAD ROUNDY, BRIAN BIRCUMSHAW, CHARLES CHUNG, KENNETH CASTELLINO, JOSEPH R. STETTER and MICHAEL VESTEL, 2006. Advanced IC Sensors and Microstructures for High Applications, 8755-3996/06, *IEEE.*

[7] Akustica Microphone Backgrounder, 2011. http://www.akustica.com.

[8] MARK KRETSCHMAR and LION PRECISION, Design and fabrication of a new MEMS capacitive microphone using a perforated aluminium diaphragm, Sensors online.

[9] JIANMIN MIAO, RONGMING LIN, LONGQING CHEN, QUANBO ZOU, SIN YEE LIM and SUAN HEE SEAH, 2000. Design considerations in micromachined silicon microphones, Design, Modeling, and Simulation in Microelectronics. Proc. SPIE, 4228.

[10] R. GRIXTI, I. GRECH, O. CASHA, J.M. DARMANIN, E. GATT and J. MICALLEF, 2004. Feasibility study of a MEMS microphone design using the PolyMUMPs process, *DTIP* 2-4 April 2014, Cannes Côte d'Azur, France.

[11] *Natural frequencies for common systems*, Modal Analysis and Controls Laboratory University of Massachusetts Lowell.

[12] VAMSY GODTHI, JAYAPRAKASH REDDY and RUDRA PRATAP, 2015. A Study of Pressure Dependent Squeeze Film Stiffness as a Resonance Modulator using Static and Dynamic Measurement. *Journal of Micro-eclectro-mechanical systems*, **24**(6), 1-1.

[13] M. BAO and H. YANG, 2007. Squeeze film air damping in MEMS, *Sensors and Actuators, A: Physical,* **136**(1), 3-27.

[14] R. PRATAP, S. MOHITE and A.K. PANDEY, 2007. Squeeze Film Effects in MEMS Device, *Journal of the Indian Institute of Science,* **87**(1), 75-94.

[15] CHARANJEET KAUR MALHI, 2014. *Studies on the Design of Novel MEMS Microphone*, A thesis presented to Indian Institute of Science, for the degree of doctor of philosophy in the faculty of engineering Department of Mechanical Engineering, Bangalore.

Journal of Acoustical Society of India : Vol. 43, No. 1, 2016 (pp. 32-47)

On longitudinal and secondary vertically plane waves propogation at interface between solid-liquid magnetized media presence in initial stress and two thermal relaxation times

S. M. Abo-Dahab[1,2]
[1]*Math. Dept., Faculty of Science, SVU, Qena 83523, Egypt*
[2]*Math. Dept., Faculty of Science, Taif University 888, Saudi Arabia*
**e-mail: sdahb@yahoo.com*

[Received: 28.10.2015; Revised: 01.01.2016; Accepted: 01.01.2016]

ABSTRACT

In this estimation, the effects of magnetized and initial stress on longitudinal (p) and secondary vertically (SV) waves propagation are investigated. We have investigated the problem of reflection and transmission of thermoelastic wave at a solid-liquid interface in presence of initial stress, two thermal relaxation times, and magnetic field. In the context of Green-Lindsay theory of generalized, the problem has been solved. The boundary conditions at the interface for (i) displacement continuity, (ii) Vanishing the tangential displacement, (iii) Continuity of normal force per unit initial area, (iv) Tangential force per unit initial area must vanish, and (v) Continuity of temperature are applied. The appropriate expressions to find the amplitudes ratios for the three incidence waves (P- and SV-wave) have been obtained. The reflection and transmitted coefficients for the incident waves are computed numerically, considering the initial stress and magnetic field effect and presented graphically.

1. INTRODUCTION

During the last five decades, wide spread attention has been given to thermoelasticity theories which consider finite speed for the propagation of thermal signal. Initial stresses develop in the medium due to various reasons, such as the difference of temperature, process of quenching shot pinning and cold working, slow process of creep, differential external forces, and gravity variations. The Earth is under high initial stress and therefore, it is of great interest to study the effect of these stresses on the propagation of elastic waves. A lot of systematic studies have been made on the propagation of elastic waves. Biot[1] showed that the acoustic propagation under initial stresses would be fundamentally different from that under stress free state. Lord and Shulman[2] reported a new theory based on a modified Fourier's law of heat conduction with one relaxation time and subsequently a more rigorous theory of thermoelasticity was formulated by Green and Lindsay[3] introducing two relaxation times. These non-classical theories are often regarded as the generalized dynamic theory of thermoelasticity. Various problems have been investigated and discussed in the light of these two theories and the studies reveal some interesting phenomena. Problem on wave propagation phenomena in coupled or generalized thermoelasticity is discussed by Sinha and Elsibai[4] and Abd-alla and Al-Dawy [5]. Abd-alla et al.[6] investigated the reflection of generalized magneto-thermo-viscoelastic waves at the boundary of a semi-infinite solid considering that the free surface of the solid is

adjacent to vacuum. Sinha and Elsibai[7], investigated the reflection and refraction of thermoelastic waves at an interface of two semi-infinite media with two relaxation times. The representative theories in the range of generalized thermoelasticity are prepared by Hetnarski and Ignaczak[8]. Singh[9] investigated reflection and transmission of plane harmonic waves at an interface between liquid and micropolar viscoelastic solid with stretch. Problem on reflection and refraction in coupled or generalized thermoelasticity have been a topic of research for various authors as Sharma*et al.*[10]. Abd-Alla and Abo-Dahab[11] discussed an influence of the viscosity on reflection and transmitted of plane shear elastic waves in two magnetized semi-infinite media. The generalized magneto-thermoelasticity model with two relaxation times in an isotropic elastic medium under the effect of reference temperature on the modulus of elasticity is pointed out by Othman and Song[12]. Estimation on magnetic field effect in an elastic solid half-space under thermoelastic diffusion is discussed by Abo-Dahab and Singh[13]. The impact of magnetic field, initial pressure, and hydrostatic initial stress on reflection of P and SV waves considering a Green Lindsay (GL) theory is discussed by Abo-Dahab and Mohamed [14]. Abo-Dahab *et al.* [15] studied the rotation and magnetic field effects on P wave reflection from stress-free surface elastic half-space with voids under one thermal relaxation time. Reflection of P and SV waves from stress-free surface elastic half-space under influence of magnetic field and hydrostatic initial stress without energy dissipation is been illustrated by Abo-Dahab [16]. Abo-Dahab *et al.* [17] studied relaxation times and magnetic field sense effects on the reflection of thermoelastic waves phenomena from isothermal and insulated boundaries of a half space. Abo-Dahab and Asad [18] estimated Maxwell's stresses effect on reflection and transmission of plane waves between two thermo-elastic media in the context of GN Model. Chakraborty and Singh [19] studied the problem of reflection and refraction of thermo-elastic wave under normal initial stress at a solid-solid interface under perfect boundary condition. Deswal *et al.* [20] pointed out the reflection and refraction at an interface between two dissimilar thermally conducting viscous liquid half-spaces. Abd-Alla*et al.* [21] studied the radial deformation and the corresponding stresses in a homogeneous annular fin for an isotropic material.

Recently, Abo-Dahab and Singh [22] investigated rotational and voids effects on the reflection of P waves from stress-free surface of an elastic half-space under magnetic field, initial Stress and without energy dissipation. Reflection and refraction of P-, SV- and thermal waves, at an initially stressed solid-liquid interface in generalized thermoelasticity has been discussed by Singh and Chakraborty [23]. Abo-Dahab and Salama [24] discussed a plane thermoelastic waves reflection and transmission between two solid media under perfect boundary condition and initial stress with and without influence of magnetic field. A theoretical study of diurnal shift in reflection height of VLF waves using IRI electron density model is studied by Latha *et al.* [25]. Recently, some new researches with new features on reflection of reflection of waves are dismised in ref. [26]-[29].

In this paper, an attempt is made to investigate waves propagation is investigated under influence of magnetic field and initial stress. The problem of reflection and transmission of thermoelastic wave at a solid-liquid interface in presence of initial stress and magnetic field considering GL theory of generalized has been solved. The boundary conditions at the interface are applied to solve the problem. The appropriate expressions to find the amplitudes ratios for the three incidence waves (P- and SV-wave) have been obtained to calculate the reflection and transmitted coefficients and computed numerically, considering the initial stress and magnetic field effect and presented graphically.

2. FORMALUATION OF THE PROBLEM

We consider a plane interface between two solid half-space homogeneous isotropic elastic with a primary temperature T_0 and magnetic field acts on z-direction. Both of the media under different initial stress and heat source in the two media. A plane SV-wave is incident in medium M at the plane interface which reflection to P-wave (dilatational wave), SV-wave (rotational wave), and thermal wave (dilatational wave). Rest of the wave continues to travel in the other medium M' after refraction, as P-wave, SV-wave and one thermal wave as shown in (Fig. 1).

We assume a Cartesian coordinate system oxyz with origin 'o' on the plane y = 0. Since we consider a two-dimensional problem, we restrict our analysis to plane strain parallel to oxy-plane. Hence all the held

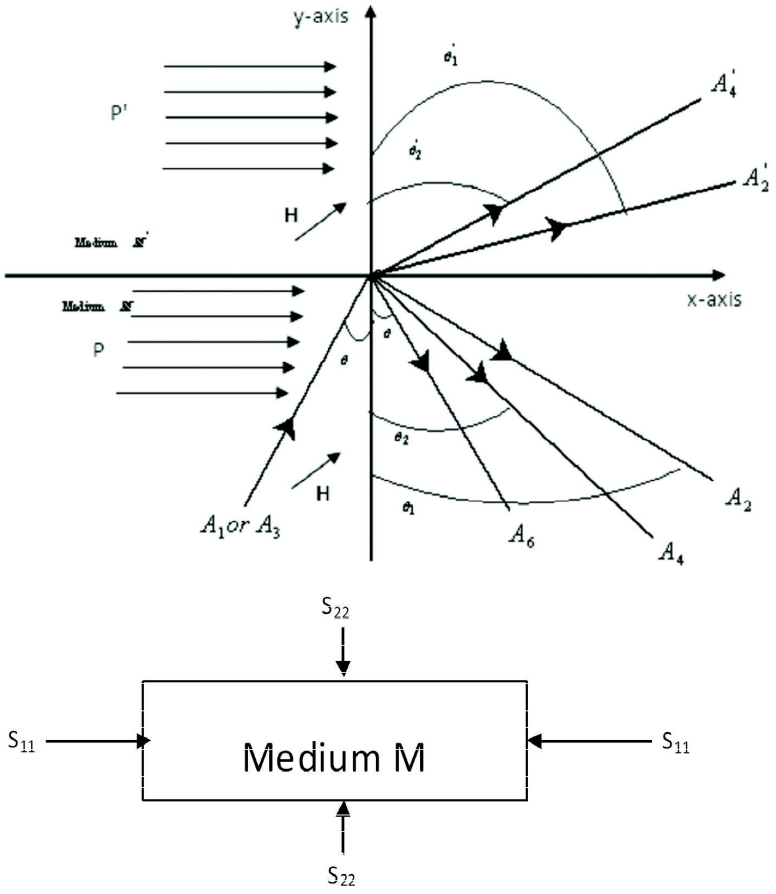

Fig. 1. Geometry of the problem

variables depend only on x, y and time t. For easy reference, we follow a convention: All quantities in medium M are represented unprimed whereas corresponding quantities in medium M' are represented as primed. The initial stress components in medium M are shown in Fig. 1 (See, [24]) where, the initial stress $P = S_{22} - S_{11}$ in the medium M, $P' = S'_{22} - S'_{11}$ in the medium M.

3. BASIC EQUATIONS

1) The dynamical equations of motion the rotating frame of reference for a plane strain under initial stress in absence of heat source, given by Biot [1], taking into account the presence of Lorentz force are :

$$\frac{\partial S_{11}}{\partial x} + \frac{\partial S_{12}}{\partial y} - P\frac{\partial \bar{\omega}}{\partial y} + F_1 = \rho\frac{\partial^2 u}{\partial t^2}$$
$$\frac{\partial S_{12}}{\partial x} + \frac{\partial S_{12}}{\partial y} - P\frac{\partial \bar{\omega}}{\partial x} + F_2 = \rho\frac{\partial^2 v}{\partial t^2} \qquad (1)$$

where, $\bar{\omega} = \frac{1}{2}\left(\frac{\partial v}{\partial x} - \frac{\partial u}{\partial y}\right)$

2) The stress-strain relations with incremental isotropy are given by Biot [1]

$$S_{11} = (\lambda + 2\mu + P)e_{xx} + (\lambda + P)e_{yy} - \gamma\left(T + \tau_1\frac{\partial T}{\partial t}\right)$$
$$S_{22} = \lambda e_{xx} + (\lambda + 2\mu)e_{yy} - \gamma\left(T + \tau_1\frac{\partial T}{\partial t}\right) \qquad (2)$$
$$S_{12} = 2\mu e_{xy}$$

3) The incremental strain- components are given by Biot [1]

$$e_{xx}=\frac{\partial u}{\partial x},\quad e_{yy}=\frac{\partial v}{\partial y},\quad e_{xy}=\frac{1}{2}\left(\frac{\partial u}{\partial y}+\frac{\partial v}{\partial x}\right) \tag{3}$$

4) The modified heat conduction equation is

$$K\nabla^2 T=\rho C_e\left(\frac{\partial T}{\partial t}+\tau_0\frac{\partial^2 T}{\partial t^2}\right)+T_0\gamma\left[\frac{\partial}{\partial t}\left(\frac{\partial u}{\partial x}+\frac{\partial v}{\partial y}\right)+\tau_0\delta_{ij}\frac{\partial^2}{\partial t^2}\left(\frac{\partial u}{\partial x}+\frac{\partial v}{\partial y}\right)\right] \tag{4}$$

where, C_e is specific heat per unit mass, e_{ij} is strain components, K is thermal conductivity, S is entropy per unit mass, P is initial stress, S_{11}, S_{22}, S_{12} is incremental stress components, λ and μ are Lame's constants, T_0 is natural temperature of the medium, λ_{ij} is Kronecker delta, T is absolute temperature of the medium, τ_0 and τ_1 are thermal relaxation times, α_t is coefficient of linear thermal expansion, μ_i is components of the displacement vector, $\bar{\omega}$ is magnitude of local rotation.

5) Taking into account the absence of displacement current, the linearized Maxwell equations governing the electromagnetic fields for a slowly moving solid medium having perfect electrical conductivity are

$$\begin{aligned}&\operatorname{curl}\vec{h}=\vec{J}, &&\operatorname{curl}\vec{E}=-\mu_e\frac{\partial\vec{h}}{\partial t},\\ &\operatorname{div}\vec{h}=0, &&\operatorname{div}\vec{E}=0.\end{aligned} \tag{5}$$

where

$$\vec{h}=\operatorname{curl}(\vec{u}\times\overrightarrow{H}).$$

we have used

$$\overrightarrow{H}=\overrightarrow{H_0}+\vec{h}(x,z,t),\qquad \overrightarrow{H_0}=(0,0,H)$$

then

$$\begin{aligned}F_x&=\mu_e H^2\left(\frac{\partial^2 u}{\partial x^2}+\frac{\partial^2 v}{\partial x\partial y}\right)\\ F_y&=\mu_e H^2\left(\frac{\partial^2 u}{\partial x\partial y}+\frac{\partial^2 v}{\partial y^2}\right)\end{aligned} \tag{6}$$

where, $\vec{B}$ is magnetic induction vector, $\vec{E}$ is electric intensity vector, $\vec{F}$ is Lorentz's body forces vector, $\vec{h}$ is perturbed magnetic field vector, $\vec{H}$ is magnetic field vector, $\vec{H}_0$ is primary constant magnetic field vector, $\vec{J}$ is electric current density vector, μ_e is magnetic permeability,

Again Maxwell's stress equation can be given in the form as

$$\tau_{ij}=\mu_e\left[H_i h_j+H_j h_i-H_k h_k\delta_{ij}\right] \tag{7}$$

which reduces to

$$\tau_{11}=\tau_{22}=\mu_e H^2\left(\frac{\partial u}{\partial x}+\frac{\partial v}{\partial y}\right),\quad \tau_{12}=0$$

where, τ_{ij} is Maxwell's stress tensor.

4. SOLUTION OF THE PROBLEMS

With the help of Eqs. (2), (3) and (7) in Eq. (1), we get,

$$\left(\lambda+2\mu+P+\mu_e H^2\right)\frac{\partial^2 u}{\partial x^2}+\left(\lambda+\frac{P}{2}+\mu+\mu_e H^2\right)\frac{\partial^2 v}{\partial x\partial y}+\left(\mu+\frac{P}{2}\right)\frac{\partial^2 u}{\partial y^2}=\rho\frac{\partial^2 u}{\partial t^2}+\gamma\left(\frac{\partial T}{\partial x}+\tau_1\frac{\partial^2 T}{\partial x\partial t}\right), \tag{8}$$

$$\left(\mu-\tfrac{\mathrm{P}}{2}\right)\frac{\partial^2 \mathrm{v}}{\partial \mathrm{x}^2}+\left(\lambda+\tfrac{\mathrm{P}}{2}+\mu+\mu_{\mathrm{e}}\mathrm{H}^2\right)\frac{\partial^2 \mathrm{u}}{\partial \mathrm{x}\partial \mathrm{y}}+\left(2\mu+\lambda+\mu_{\mathrm{e}}\mathrm{H}^2\right)\frac{\partial^2 \mathrm{v}}{\partial \mathrm{y}^2}=$$
$$\rho\left(\frac{\partial^2 \mathrm{u}}{\partial \mathrm{t}^2}\right)+\gamma\left(\frac{\partial \mathrm{T}}{\partial \mathrm{y}}+\tau_1\frac{\partial^2 \mathrm{T}}{\partial \mathrm{y}\partial \mathrm{t}}\right). \tag{9}$$

To separate the dilatational and rotational components of strain, we introduce displacement potentials Φ and Ψ defined by the following relations:

$$\mathrm{u}=\frac{\partial \Phi}{\partial \mathrm{x}}-\frac{\partial \Psi}{\partial \mathrm{y}},$$
$$\mathrm{v}=\frac{\partial \Phi}{\partial \mathrm{y}}+\frac{\partial \Psi}{\partial \mathrm{x}} \tag{10}$$

From Eqs. (11) and (13), we get the following equations:

$$\nabla^2\Phi=\frac{\rho}{\left(\lambda+2\mu+\mathrm{P}+\mu_{\mathrm{e}}\mathrm{H}^2\right)}\left(\frac{\partial^2 \Phi}{\partial \mathrm{t}^2}\right)+\frac{\gamma}{\left(\lambda+2\mu+\mathrm{P}+\mu_{\mathrm{e}}\mathrm{H}^2\right)}\left(\mathrm{T}+\tau_1\frac{\partial \mathrm{T}}{\partial \mathrm{t}}\right), \tag{11}$$

$$\nabla^2\Psi=\frac{\rho}{\left(\mu+\frac{P}{2}\right)}\left[\frac{\partial^2 \Psi}{\partial t^2}\right]. \tag{12}$$

From Eqs. (11) and (12), we get,

$$\nabla^2\Phi=\frac{\rho}{\left(\lambda+2\mu+\mu_e H^2\right)}\left[\frac{\partial^2 \Phi}{\partial t^2}\right]+\frac{\gamma}{\left(\lambda+2\mu+\mu_e H^2\right)}\left(T+\tau_1\frac{\partial T}{\partial t}\right), \tag{13}$$

$$\nabla^2\Psi=\frac{\rho}{\left(\mu-\frac{P}{2}\right)}\left[\frac{\partial^2 \Psi}{\partial t^2}\right] \tag{14}$$

where, $\nabla^2=\dfrac{\partial^2}{\partial x^2}+\dfrac{\partial^2}{\partial y^2}$

Using Eq. (10) in (4), we get

$$K\nabla^2 T=\rho C_e\left(\frac{\partial T}{\partial t}+\tau_0\frac{\partial^2 T}{\partial t^2}\right)+T_0\gamma\frac{\partial}{\partial t}\left(1+t_0\delta_{ij}\frac{\partial}{\partial t}\right)\nabla^2\Phi \tag{15}$$

5. SOLUTION USING GL MODELS

In Green-Lindsay theory: $\tau_1 \geq \tau_0 > 0$ and $\delta_{ji} = 0$. Eqs. (13) and (14) can be rewritten as,

$$\nabla^2\Phi=\frac{1}{C_1^2\left(1+R_H\right)}\frac{\partial^2 \Phi}{\partial t^2}+\frac{\gamma}{\rho C_1^2\left(1+R_H\right)}\left(T+\tau_1\frac{\partial T}{\partial t}\right) \tag{16}$$

$$\nabla^2\Psi=\frac{1}{C_2^2}\left[\frac{\partial^2 \Psi}{\partial t^2}\right] \tag{17}$$

where, $R_H=\frac{C_A^2}{C_1^2}$, $C_1^2=\frac{\lambda+2\mu+P}{\rho}$, $C_2^2=\frac{\mu-\frac{P}{2}}{\rho}$, $C_A^2=\frac{\mu_e H^2}{\rho}$. Here, R_H, C_A, C_1, C_2 represent the magnetic pressure number, velocities of isothermal dilatational and rotational waves respectively, in medium M.

Using GL theory, Eq. (15) can be written as :

$$K\nabla^2 T = \rho C_e\left(\frac{\partial T}{\partial t} + \tau_0 \frac{\partial^2 T}{\partial t^2}\right) + T_0\gamma \frac{\partial}{\partial t}\left(\nabla^2 \Phi\right) \tag{18}$$

Eliminating from Eqs. (16) and (18), we obtain a fourth order differential equation in terms of Φ as :

$$T = \left(1 + \tau_1 \frac{\partial}{\partial t}\right)^{-1}\left[\frac{\rho C_1^2\left(1 + R_H\right)}{\gamma}\nabla^2\Phi - \frac{\rho}{\gamma}\left(\frac{\partial^2 \Phi}{\partial t^2}\right)\right] \tag{19}$$

$$C_3^2\left(1 + R_H\right)\nabla^4\Phi - \left[\left(1 + R_H + \varepsilon_T\right)\frac{\partial}{\partial t} + \left(\left(1 + R_H\right)\tau_0 + \varepsilon_t\tau_1 + \frac{C_3^2}{C_1^2}\right)\frac{\partial^2}{\partial t^2}\right]\nabla^2\Phi + \frac{1}{C_1^2}\left(1 + \tau_0\frac{\partial}{\partial t}\right)\frac{\partial^3\Phi}{\partial t^3} = 0 \tag{20}$$

where, $C_3^2 = \frac{K}{\rho C_e}$, $\varepsilon_T = \frac{T_0\gamma^2}{\rho^2 C_e C_1^2}$ is thermoelastic coupling constant of the solid medium *M*. We seek the solutions for Φ, Ψ and T in the form

$$\begin{aligned} \Phi &= f(y)\ \exp\ [ik(x - ct)] \\ \Psi &= g(y)\ \exp\ [ik(x - ct)] \\ T &= h(y)\ \exp\ [ik(x - ct)] \end{aligned} \tag{21}$$

where, k is wave number, ω is frequency, υ is phase speed, $C = \frac{\omega}{k}$.

Since Eq. (21) is a solution of Eq. (20), it must satisfy Eq. (21).

Putting Eq. (21) in (20), we get,

$$\begin{aligned} C_3^2\left(1 + R_H\right)\left[-k^4 f + \tfrac{d^4 f}{dy^4} - 2k^2\tfrac{d^2 f}{dy^2}\right] - \left[\left(1 + R_H + \varepsilon_T\right) + \left(ik^3 cf(y) - ikc\tfrac{d^2 f}{dy^2}\right) + \left(\left(1 + R_H\right)\tau_0 + \varepsilon_t\tau_1 + \tfrac{C_3^2}{C_1^2}\right)\right. \\ \left. + \left(k^4 c^2 f(y) - k^2 c^2\tfrac{d^2 f}{dy^2}\right)\right] + \tfrac{1}{C_1^2}\left(\left(f(y)ik^3c^3\right) + \tau_0\left(f(y)k^4c^4\right)\right) = 0 \end{aligned} \tag{22}$$

$$\begin{aligned} &\left(1 + R_H\right)\tfrac{d^4 f}{dy^4} + \left[-2k^2\left(1 + R_H\right) + ikc\frac{\left(1 + R_H + \varepsilon_T\right)}{C_3^2} + k^2c^2\frac{\left(\left(1 + R_H\right)\tau_0 + \varepsilon_t\tau_1 + \tfrac{C_3^2}{C_1^2}\right)}{C_3^2}\right]\tfrac{d^2 f}{dy^2} + \\ &+ \left[k^4\left(1 + R_H\right) - ik^3 c\frac{\left(1 + R_H + \varepsilon_T\right)}{C_3^2} - k^4c^2\frac{\left(\left(1 + R_H\right)\tau_0 + \varepsilon_t\tau_1 + \tfrac{C_3^2}{C_1^2}\right)}{C_3^2} + \tfrac{ik^3c^3}{C_1^2C_1^2}\left(\left(1 - i\tau_0 kc\right) - \tfrac{C_1^2}{C^2}\left(1 + R_H + \varepsilon_T\right)\right)\right] f(y) = 0 \end{aligned} \tag{23}$$

Eq. (23) being a fourth order differential equation in f(y), the solution gives four values of f(y) and Eq. (21) becomes

$$\Phi = \begin{bmatrix} \left(A_1\exp\left(ikm_1 y\right) + A_2\exp\left(-ikm_1 y\right)\right) + \\ \left(A_3\exp\left(ikm_2 y\right) + A_4\exp\left(-ikm_2 y\right)\right) \end{bmatrix}\exp\left[ik(x - ct)\right] \tag{24}$$

where, $m_1 = \sqrt{q^2c^2 - 1}$, $m_2 = \sqrt{p^2c^2 - 1}$

$$p^2, q^2 = \tfrac{1}{2c_1^2c_3^2}\left[\left\{c_1^2\left(\tau_0\left(1 + R_h\right) + \varepsilon_T\tau_1\right) + c_3^2 + \tfrac{i\left(1 + R_H + \varepsilon_T\right)c_1^2}{\omega}\right\} \pm \sqrt{N}\right] \tag{25}$$

$$N=\left[c_1^2\left(\tau_0\left(1+R_h\right)+\varepsilon_T\tau_1\right)+c_3^2+\frac{i\left(1+R_H+\varepsilon_T\right)c_1^2}{\omega}\right]^2-\frac{4i\left(1+R_H\right)\left(1-i\omega\tau_0\right)c_1^2c_3^2}{\omega}. \tag{26}$$

Using Eq. (20) in (17), we get

$$\frac{d^2g}{dy^2}+k^2\left(\frac{c^2}{c_2^2}-1\right)g=0 \tag{27}$$

Eq. (27) suggests that the solution yields two values of g(y), and Eq. (20) can be written as :

$$\Psi=\left[A_5\exp\left(ikm_3y\right)+A_6\exp\left(-ikm_3y\right)\right]\exp\left[ik\left(x-ct\right)\right] \tag{28}$$

where

$$m_3=\sqrt{\frac{c^2}{c_2^2}-1}.$$

The constants A_i (i = 1, 2, 3, 4, 5, 6) in pairs represent the amplitudes of incident and reflected thermal, P- and SV-waves respectively.

Substituting from Eqs. (24) in Eq. (11), we get the value of *h(y)* and using that value of *h(y)*, Eq. (19) becomes

$$T=\frac{\rho}{\gamma\tau}\begin{bmatrix}b_1\left(A_1\exp\left(ikm_1y\right)+A_2\exp\left(-ikm_1y\right)\right)\\ b_2\left(A_3\exp\left(ikm_2y\right)+A_4\exp\left(-ikm_2y\right)\right)\end{bmatrix}\exp\left[ik\left(x-ct\right)\right] \tag{29}$$

where

$$\tau=\left(1-i\omega\tau_1\right),\ b_1=\omega^2\left(1-\left(1+R_H\right)q^2c_1^2\right),\ b_2=\omega^2\left(1-\left(1+R_H\right)p^2c_1^2\right)$$

Setting $\mu = P = 0$ in Eqs. (1) - (4) we obtain the basic equations for a non-viscous liquid medium in absence of body forces and using them, we get displacement equations and temperature field equation, valid for the liquid medium M'. The equations are as follows :

$$\left(\lambda'+\mu_eH^2\right)\frac{\partial^2u'}{\partial x^2}+\left(\lambda'+\mu_eH^2\right)\frac{\partial^2v'}{\partial x\partial y}=\rho'\frac{\partial^2u'}{\partial t^2}+\gamma'\left(\frac{\partial T'}{\partial x}+\tau_1'\frac{\partial^2T'}{\partial x\partial t}\right) \tag{30}$$

$$k'\nabla^2T'=\rho'C_e'\left(\frac{\partial T'}{\partial t}+\tau_0'\frac{\partial^2T'}{\partial t^2}\right)+T_0'\gamma'\frac{\partial}{\partial t}\left(\nabla^2\Phi'\right) \tag{31}$$

The primes have been used to designate the corresponding quantities in the liquid medium M' as already been defined in case of solid medium M.

Taking

$$u=\frac{\partial\Phi'}{\partial x},\quad v=\frac{\partial\Phi'}{\partial y} \tag{32}$$

we get

$$\nabla^2\Phi=\frac{1}{C_1'^2\left(1+R_H'\right)}\frac{\partial^2\Phi}{\partial t^2}+\frac{\gamma'}{\rho'C_1'^2\left(1+R_H'\right)}\left(1+\tau_1'\frac{\partial}{\partial t}\right)T' \tag{33}$$

$$K'\nabla^2T'=\rho'C_e'\left(\frac{\partial T'}{\partial t}+\tau_0'\frac{\partial^2T'}{\partial t^2}\right)+T_0'\gamma'\frac{\partial}{\partial t}\left(\nabla^2\Phi'\right) \tag{34}$$

where $c_1'^2 = \frac{\lambda'}{\rho'}$

Solving Eqs. (33) and (34) and proceeding exactly in a similar way as in solid medium *M*, we get the appropriate solution for Φ' and Ψ' as :

$$\Phi' = \left[A_2' \exp\left(ikm_1' y\right) + + A_4' \exp\left(ikm_2' y\right)\right] \exp\left[ik\left(x - ct\right)\right] \tag{35}$$

$$\Psi' = \left[A_5' \exp\left(ikm_3' y\right) + A_6' \exp\left(-ik' m_3 y\right)\right] \exp\left[ik\left(x - ct\right)\right] \tag{36}$$

$$T' = \frac{\rho'}{\gamma' \tau'}\left[b_1' A_2' \exp\left(ikm_1' y\right) + b_2' A_4' \exp\left(ikm_2' y\right)\right] \exp\left[ik\left(x - ct\right)\right] \tag{37}$$

where

$$\tau' = \left(1 - i\omega t_1'\right), b_1' = \omega^2\left(1 - \left(1 + R_H'\right) q'^2 c_1'^2\right), b_2' = \omega^2\left(1 - \left(1 + R_H'\right) P'^2 c_1'^2\right)$$

The constants A_2' and A_4' represent the amplitudes of refracted thermal and P-waves, respectively.

6. BOUNDARY CONDITIONS

1) Normal displacement is continuous at the interface, *i.e.* ν = ν′. This leads to :

$$\frac{\partial \phi}{\partial y} + \frac{\partial \Psi}{\partial x} = \frac{\partial \phi'}{\partial y} + \frac{\partial \Psi'}{\partial x} \tag{38}$$

Using Eqs. (24), (28), (35) and (36) in the above continuity relation, we get,

$$m_1 A_1 - m_1 A_2 + m_2 A_3 - m_2 A_4 + A_5 + A_6 - m_1' A_2' - m_2' A_4' = 0 \tag{39}$$

2) Tangential displacement must vanish at the interface i.e. μ = 0.

This leads to $\frac{\partial \phi}{\partial x} - \frac{\partial \Psi}{\partial y} = 0$. Using Eqs. (24) and (28) in the above boundary condition, we get

$$A_1 + A_2 + A_3 + A_4 - m_3 A_5 + m_3 A_6 = 0 \tag{40}$$

3) Normal force per unit initial area must be continuous at the interface *i.e.* $\Delta f_y = \Delta f'_y$

This leads to $s_{22} + \tau_{22} = 0$

where, $$\tau_{ij} = \mu_e\left[H_i h_j + H_j h_i - (\vec{H}.\vec{h})\delta_{ij}\right],\ i, j = 1,2,3$$

Using Eqs. (2) and (7) for medium M and their corresponding equations for medium *M*′ we get, with the help of Eqs. (13) and (33),

$$\begin{aligned} &\left(\lambda + \mu_e H^2\right)\left(\frac{\partial^2 \Phi}{\partial x^2} + \frac{\partial^2 \Phi}{\partial y^2}\right) + 2\mu\left(\frac{\partial^2 \Phi}{\partial y^2} + \frac{\partial \Psi}{\partial x \partial y}\right) - \gamma\left(T + \tau_1 \frac{\partial T}{\partial t}\right) \\ &= \left(\lambda` + \mu_e' H^2\right)\left(\frac{\partial^2 \Phi`}{\partial x^2} + \frac{\partial^2 \Phi`}{\partial y^2}\right) - \gamma\left(T + \tau_1 \frac{\partial T}{\partial t}\right) \end{aligned} \tag{41}$$

Substituting Eqs. (14), (17), (19), (28) and (29) in the above equation, we get,

$$\begin{aligned} &\left[-\left(2 + \beta\right) + c^2\left(\frac{1}{c_2^2} - \beta q^2\right)\right]\left(A_1 + A_2\right) + \left[-\left(2 + \beta\right) + c^2\left(\frac{1}{c_2^2} - \beta p^2\right)\right]\left(A_3 + A_4\right) + \\ &\left(2 + \beta\right) m_3\left(A_5 - A_6\right) - \rho^*\left(1 + m_3^2\right)\left(A_2' + A_4'\right) = 0 \end{aligned} \tag{42}$$

where, $\rho^* = \frac{\rho}{\rho}$ and $\beta = \frac{p}{\rho c_2^2}$

4) Tangential force per unit initial area must vanish at the interface *i.e.* $\Delta f_x = 0$

This leads to $s_{12} + Pe_{xy} + \tau_{12} = 0$

Using Eqs. (2), (3), (6), (14) and (17) in the above equation, we get,

$$m_1(A_1 - A_2) + m_2(A_3 - A_4) - \frac{1}{2}(m_3^2 - 1)(A_5 + A_6) = 0 \tag{43}$$

5) Temperature must be continuous at the interface *i.e.* $T = T'$.

Using Eqs. (19) and (28) and simplifying, we get

$$\begin{aligned}&\left(1-(1+R_H)q^2c_1^2\right)(A_1+A_2)+\left(1-(1+R_H)p^2c_1^2\right)(A_3+A_4)-\\&-\frac{\rho^*}{\gamma^*\tau^*}\left[\left(1-\left(1+R_H^{'}\right)q^{'2}c_1^{'2}\right)A_2^{'}+\left(1-\left(1+R_H^{'}\right)p^{'2}c_1^{'2}\right)A_4^{'}\right]=0\end{aligned} \tag{44}$$

where, $\gamma^* = \frac{\gamma^{'}}{\gamma}$ and $\tau^* = \frac{\tau^{'}}{\tau}$.

7. EQUATIONS FOR THE REFLECTION AND REFRACTION COEDDICIENTS

To consider the reflection and refraction of a thermoelastic plane wave which is incident at the solid-liquid interface at $y = 0$ making an angle θ with the *y-axis*, we have three different cases.

Case I: For P-wave incidence, we put $C = p^{-1}$ and $A_1 = A_5 = 0$.

Case II: For SV-wave incidence, we put $C = C_2$ cosec θ and $A_1 = A_3 = 0$.

Generalizing, we get a system of five non-homogeneous equations for a thermoelastic plane wave incident,

$$\sum_{i=1}^{5} a_{ij} Z_j = y_i, \ (j = 1,2,...5) \tag{45}$$

where,

$$\begin{aligned}&a_{11} = -m_1, \ a_{12} = -m_2, \ a_{13} = 1, a_{14} = -m_1^{`}, a_{15} = -m_2^{`}, a_{22} = a_{21} = 1, a_{23} = m_3\\&a_{24} = a_{25} = 0, \quad a_{31} = \left[-(2+\beta) + C^2\left(\tfrac{1}{C_2^2} - \beta q^2\right)\right], \quad a_{32=}\left[-(2+\beta) + C^2\left(\tfrac{1}{C_2^2} - \beta q^2\right)\right]\\&a_{24} = a_{25} = 0, \quad a_{31} = \left[-(2+\beta) + C^2\left(\tfrac{1}{C_2^2} - \beta q^2\right)\right], \quad a_{32=}\left[-(2+\beta) + C^2\left(\tfrac{1}{C_2^2} - \beta q^2\right)\right]\\&a_{33} = -(2+\beta)m_3, a_{34} = a_{35} = -\rho^*\left(1+m_3^2\right), a_{41} = -m_1, a_{42} = -m_2, a_{43} = -0.5\left(m_3^2 - 1\right), \text{ where,}\\&a_{44} = a_{45} = 0, \ a_{51} = \left(1-(1+R_H)q^2c_1^2\right), a_{52} = \left(1-(1+R_H)p^2c_1^2\right),\\&a_{53} = 0, a_{54} = -\tfrac{\rho^*}{\gamma^*\tau^*}\left(1-\left(1+R_H^{'}\right)q^{'2}c_1^{'2}\right), a_{55} = -\tfrac{\rho^*}{\gamma^*\tau^*}\left(1-\left(1+R_H^{'}\right)p^{'2}c_1^{'2}\right)\end{aligned}$$

Z_j ($J = 1, 2, ...5$) are the ratios of amplitudes of reflected thermal, P-, SV-waves and refracted thermal, P-waves to that of incident wave respectively.

For the three particular cases, we get,

(I) For incident P-wave :

$$\begin{aligned}&y_1 = a_{12}, \ y_2 = -a_{22}, \ y_3 = -a_{32}, \ y_4 = a_{42}, \ y_5 = -a_{52},\\&Z_1 = \tfrac{A_2}{A_3}, \ Z_2 = \tfrac{A_4}{A_3}, \ Z_3 = \tfrac{A_6}{A_3}, \ Z_4 = \tfrac{A_2^{'}}{A_3}, \ Z_5 = \tfrac{A_4^{'}}{A_3}\end{aligned}$$

(II) For incident SV-wave :

$$y_1 = -a_{13},\ \ y_2 = a_{23},\ \ y_3 = a_{33},\ \ y_4 = -a_{43},\ \ y_5 = a_{53},$$

$$Z_1 = \frac{A_2}{A_5},\ \ Z_2 = \frac{A_4}{A_5},\ \ Z_3 = \frac{A_6}{A_5},\ \ Z_4 = \frac{A_2'}{A_5},\ \ Z_5 = \frac{A_4'}{A_5}$$

Eq. (45) constitute a matrix equation as

$$AZ = Y$$

8. NUMERICAL RESULTS AND DISCUSSION

For a view to illustrate the numerical analysis of the expressions of the reflection and refraction coefficients, we have used the data for crust as solid medium following Choi and Gurnis [27] and water as liquid medium.

For solid medium (*M* crust)

$$\lambda = \mu = 3\times10^{9}\, Nm^{-2}, \qquad \alpha = 1.0667\times10^{-5}\, k^{-1},$$
$$C_e = 1100\, J kg^{-1}k^{-1}, \qquad \rho = 2900\, kg\, m^{-3}, \qquad k = 3 Wm^{-1}k^{-1}$$

For liquid medium (M′ water)

$$\lambda' = \mu' = 20.4\times10^{9}\, Nm^{-2}, \qquad \alpha' = 69\times10^{-6}\, k^{-1},$$
$$C_e' = 4187\, J kg^{-1}k^{-1}, \qquad \rho' = 1000\, kg\, m^{-3}, \qquad k' = 0.6\, Wm^{-1}k^{-1}$$

Taking into consideration $\tau_0 = \frac{3k}{\rho C_e C_1^2}$, $\tau_0' = \frac{3k'}{\rho' C_e' C_1'^2}$, while τ_1, τ_1' have been taken to be of the same order (about 1.5 times) of τ_0 and τ_0', $\omega = 7.5\times10^{13}\, s^{-1}$, $T_0 = 300\, k$. [28].

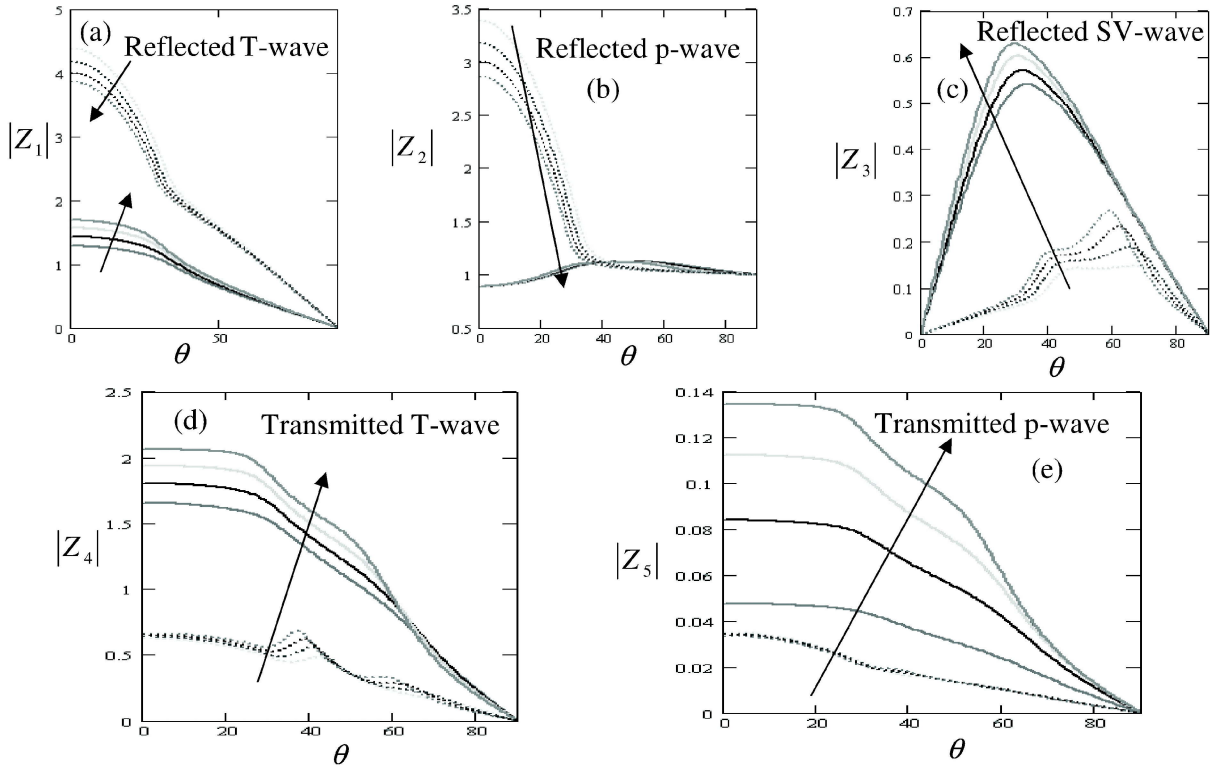

Fig. 2. Variation of the amplitudes z_i (i=1,2,…,5) with the angle of incidence of p-wave for variation of magnetic field: H=0.1, 0.2, 0.3, 0.4, P=1.1(10)^{11} ——, P=0 …….

Figs. 2-4 and 5-7 show the amplitudes ratios variation with the angle of incident p- and SV-wave, respectively. We used (solid ———for presence of initial stress, dot …. for absence of initial stress)

Figs. 2 and 4 display the variation of the amplitudes ratios Z_i (i=1,2,…,5) with the angle of incidence of p-wave for variation of magnetic field with and without initial stress. It is appear that the amplitudes of the reflected T-wave, refracted T- and p-waves start from their maximum values and decreases to tend zero at θ = 90°, amplitude ratio of reflected p-wave tends to the unity, on the other hand, the reflection coefficient for the reflected SV-wave equal zero at θ = {0°, 90°}, increases to arrive to its maximum value and then decreases with the increasing of angle of incidence.

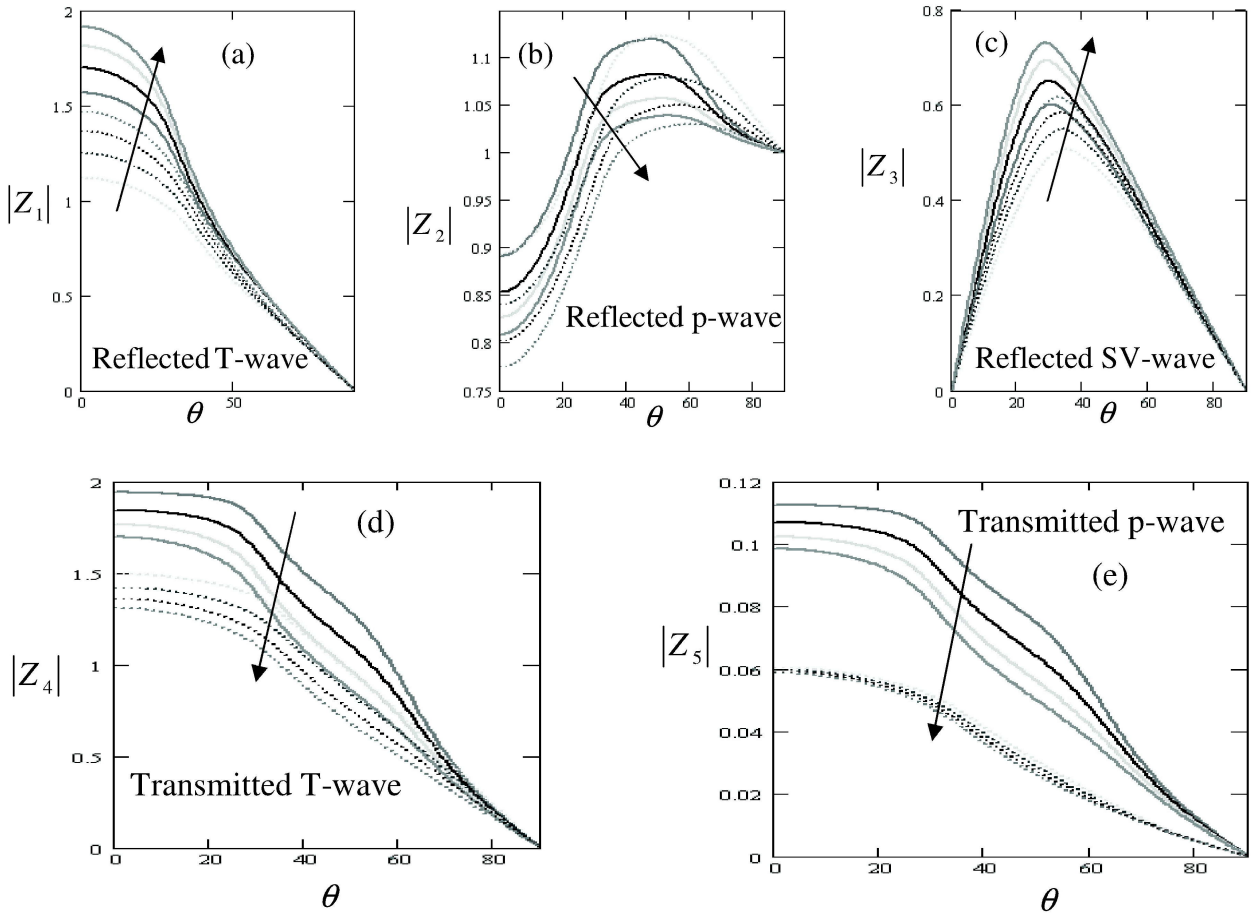

Fig. 3. Variation of the amplitudes z_i (i=1,2,…,5) with the angle of incidence of P-wave for variation of initial stress: P =(1.1, 1.2, 1.3, 1.4) $(10)^{11}$, H=0.3——, H=0 …….

Physically, we concluded that the reflected and transmitted p- waves start from their maximum values and tend to zero but reflected p-wave arrives to unity for the maximum angle of incidence, also, the reflected SV-wave starts and arrives to zero at the minimum and maximum values of θ that indicate to the creating of the reflection coefficient if θ = 0° and interrupted at θ = 90°.

With the variation of the magnetic field in the presence or absence of initial stress, it is seen that $|Z_2|$ decrease with an increasing of the magnetic field parameter but $|Z_3|$, $|Z_4|$, and $|Z_5|$ increase, $|Z_1|$ increase with the increasing of magnetic field in the presence of initial stress but decreases if the initial stress absence. It is shown that if the initial stress is absence, $|Z_1|$, $|Z_2|$ and $|Z_5|$ larger than the correspondence in the presence of initial stress, vice versa in $|Z_3|$ and $|Z_4|$.

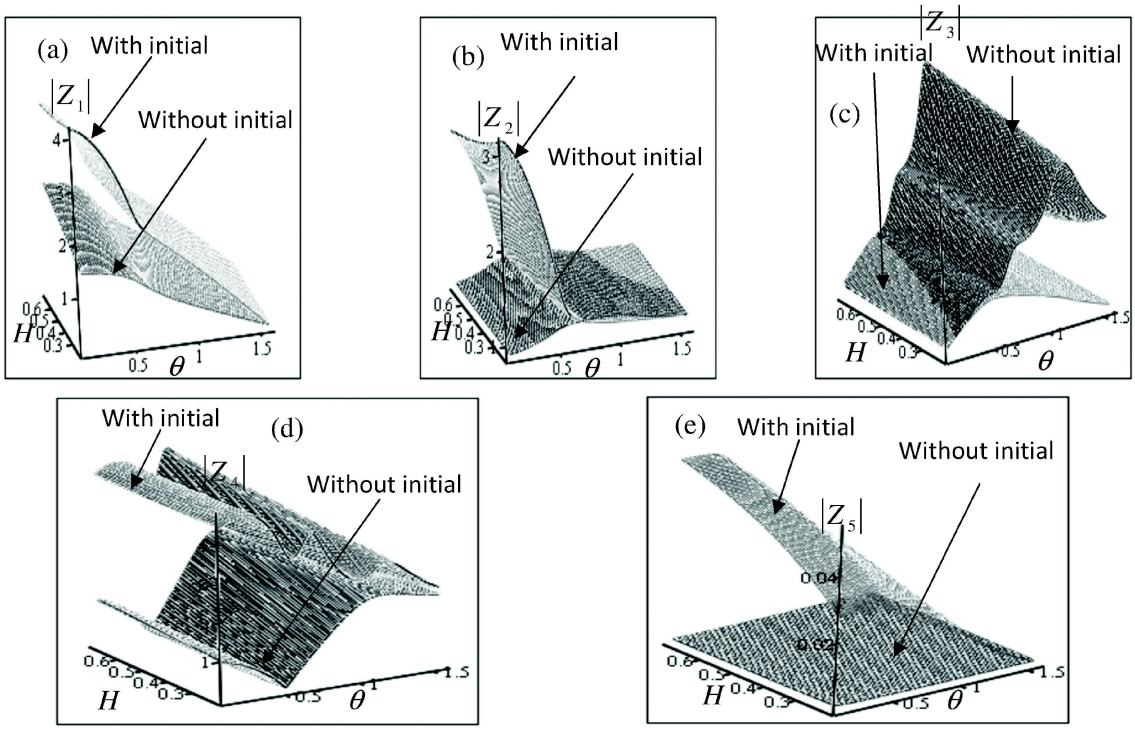

Fig. 4. Variation of the amplitudes zi (i=1,2,…,5) with respect to (θ, H) of P-wave with and without variation of initial stress

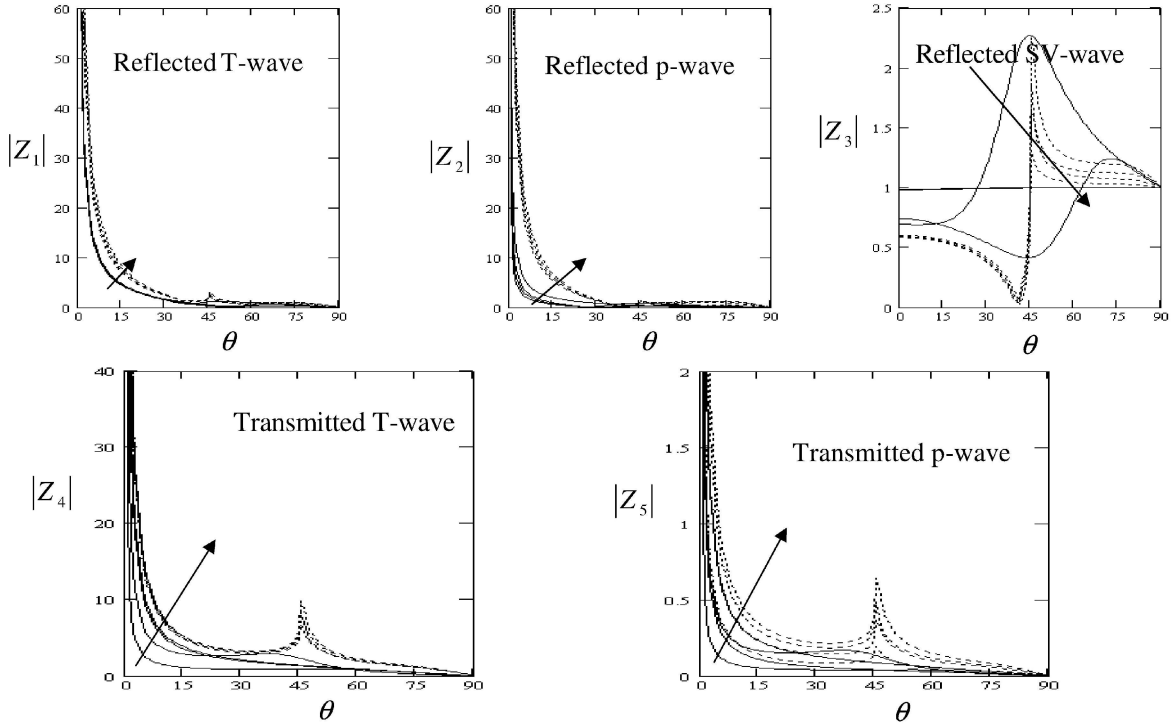

Fig. 5. Variation of the amplitudes z_i (i=1,2,…,5) with the angle of incidence of SV-wave for variation of magnetic field: H=0.1, 0.2, 0.3, 0.4, P=1.1(10)^{11} ———, P=0 …….

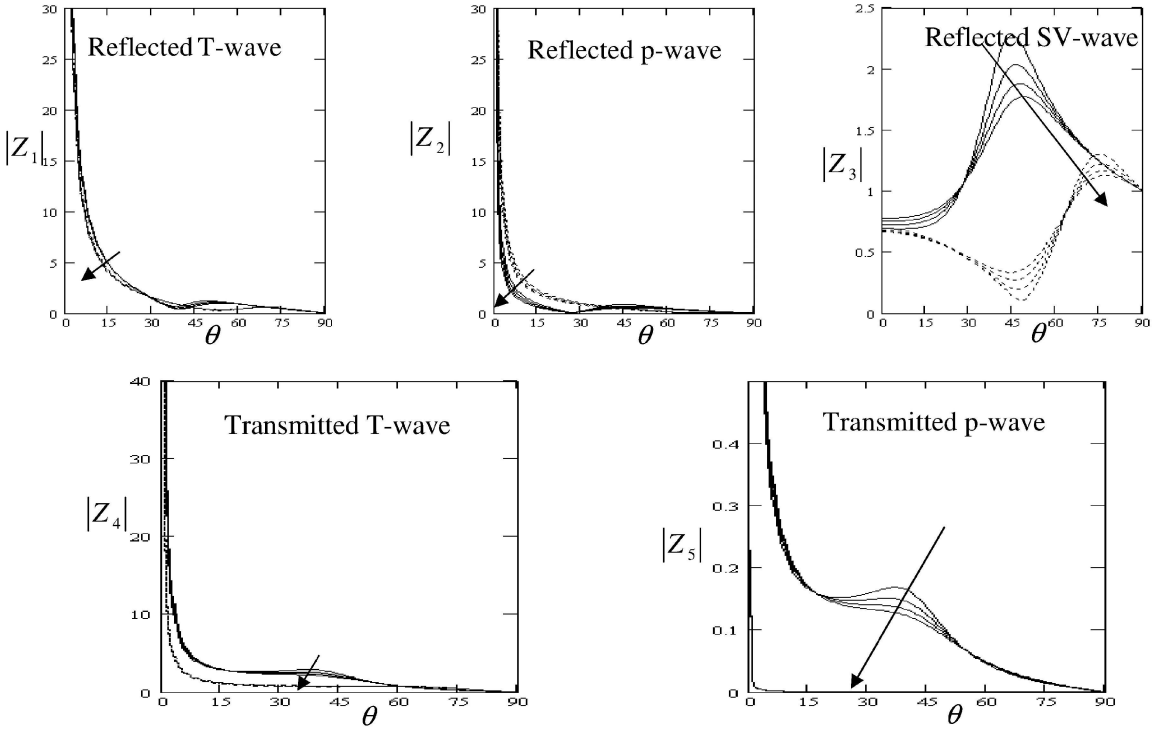

Fig. 6. Variation of the amplitudes z_i (i=1,2,…,5) with the angle of incidence of SV-wave for variation of initial stress: P =(1.1, 1.2, 1.3, 1.4) (10)[11], R_H = 0.3 ———, R_H = 0 …….

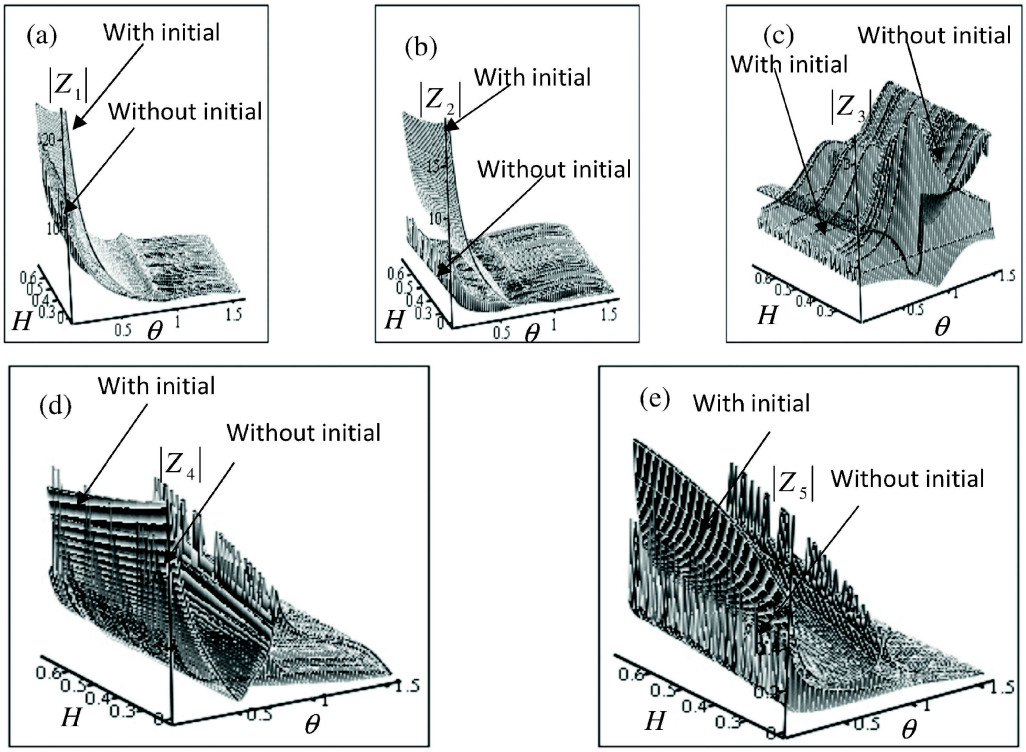

Fig. 7. Variation of the amplitudes z_i (i=1,2,…,5) with respect to (θ, H) of SV-wave

Fig. 3 plots the amplitudes ratios with the angle of incidence and variation of the initial stress in the presence or absence of the magnetic field. It is obvious that $|Z_1|$ and $|Z_3|$ increase with the increased values of the initial stress but $|Z_2|$, $|Z_4|$ and $|Z_5|$ decrease, also, we concluded that the absence of the magnetic field make small interruption on $|Z_1|$, $|Z_2|$, $|Z_3|$, and $|Z_4|$ but additional factor on $|Z_5|$.

Fig. 5 and 7 show the variation of the amplitudes ratios $|Z_1|$, $|Z_2|$ and $|Z_3|$of reflected T-, p-, and SV-waves, $|Z_4|$ of transmission of T-wave and $|Z_5|$ of transmitted p-wave with respect of the angle of incidence of SV-wave for different values of the sensitive part of the magnetic field with initial stress and without initial stress. The reflected T-wave and reflected p-wave increase with increasing sensitive part of the magnetic field, while they decrease with an increasing of angle of incidence. The reflected SV-wave decreases with increasing sensitive part of the magnetic field, while the reflected SV-wave has oscillatory behavior in the whole range of the _-axis, as well the transmission of T-wave and of transmitted p-wave increase with an increasing of the sensitive part of the magnetic field, while it decreases with increasing of angle of incidence. It is shown that $|Z_1|$, $|Z_2|$, $|Z_4|$, and $|Z_5|$ start from their maximum values arriving to their minimum values at. It is noticed that if the initial stress is neglected, the absolute values of the amplitude ratios take large values compared with the corresponding values in the presence of initial stress except $|Z_3|$.

Fig 6 displays and variation of the amplitude ratios $|Z_1|$, $|Z_2|$ and $|Z_3|$ of reflected T-p- and SV-waves, $|Z_4|$of transmission of T-wave, and $|Z_5|$ of transmitted p-wave with respect to the angle of incidence of SV-wave for different values of initial stress P with magnetic field and without magnetic field. The reflected T-, p-, and SV-waves decrease with increasing initial stress, while they decrease with increasing angle of incidence. The reflected SV wave has oscillatory behavior in the whole range of the _-axis as well the transmission of T-wave and of transmitted p-wave decrease with increasing initial stress, while it decreases with increasing angle of incidence. It is shown that $|Z_1|$, $|Z_2|$, $|Z_4|$, and $|Z_5|$ start from their maximum values arriving to their minimum values at. It is noticed that if the magnetic field is neglected, the absolute values of the amplitude ratios take small values compared with the corresponding values in the presence of a magnetic field except $|Z_2|$.

9. CONCLUSION

We model the effect of initial stress, and magnetic field on reflection and refraction of a plane waves at a solid-liquid interface under perfect boundary conditions. The waves amplitudes ratios with initial stress and magnetic field with the angle of incidence are obtained in the framework of GL theory discussed numerically and illustrated graphically.

The following conclusions can be made

1. The reflected and refracted amplitudes depend on the angle of incidence, initial stress and magnetic field, the nature of this dependence is different for different reflected waves.
2. The initial stress and magnetic field play a significant role and the effect has the inverse trend for the reflected and transmitted waves.

Finally, it is observed that the reflection and refraction coefficient is strongly appear in the phenomena that has a lot of applications, especially, in Seismic waves, Earthquakes, Volcanoes, and acoustics.

10. REFERENCES

[1] M. A. BIOT, 1965. *Mechanics of Incremental Deformations*, John Wiley and Sons, Inc., New York.

[2] H.W. LORD and Y. SHULMAN, 1967. A generalized dynamical theory of thermoelasticity, *J. Mech. Phys. Solids,* **15**(5), 299-309.

[3] A.E. GREEN and K.A. LINDSAY, 1972. Thermoelasticity. *J. Elasticity*, **2**(1), 1-7.

[4] S.B. SINHA and K.A. ELSIBAI, 1996. Reflection of thermoelastic waves at a solid half-space with two thermal relaxation times, *J. Therm. Stresses*, **19**, 763-777.

[5] A.N. ABD-ALLA and A.A.S. AL-DAWY, 2000. The reflection phenomena of SV waves in a generalized thermoelastic medium, *Int. J. Math. Math. Sci.,* **23**(8), 529-546.

[6] AN ABD-ALLA, AA YAHIA and SM ABO-DAHAB, 2003. On the reflection of the generalized magneto-thermo-viscoelastic plane waves, *Chaos, Solitons & Fractals,* **16**(2), 211-231.

[7] S.B. SINHA and K.A. ELSIBAI, 1997. Reflection and refraction of thermoelastic waves at an interface of two semi-infinite media with two thermal relaxation times, *J. Therm. Stresses,* **20**(2), 129-146.

[8] RB HETNARSKI and J IGNACZAK, Generalized thermoelasticity, 1999. *J. Therm. Stresses*, **22**, 451-476.

[9] B. SINGH, 2000. Reflection and transmission of plane harmonic waves at an interface between liquid and micropolar viscoelastic solid with stretch, *Sadhana*, **25**(6), 589-600.

[10] J.N. SHARMA, V. KUMAR and D. CHAND, 2003. Reflection of generalized thermoelastic waves from the boundary of a half-space, *J. Therm. Stresses,* **26**(10), 925-942.

[11] AN ABD-ALLA and SM ABO-DAHAB, 2008. The influence of the viscosity and the magnetic field on reflection and transmission of waves at interface between magneto-viscoelastic materials, *Meccanica*, **43**(2), 437-448.

[12] MI OTHMAN and Y SONG, 2008. Reflection of magneto-thermoelastic waves with two relaxation times and temperature dependent elastic moduli, *Appl. Math. Model.,* **32**(4), 483-500.

[13] SM ABO-DAHAB and B SINGH, 2009. Influences of magnetic field on wave propagation in generalized thermoelastic solid with diffusion, *Arch. Mech.*, **61**(2), 121-136.

[14] SM ABO-DAHAB and RA MOHAMED, 2010. Influence of magnetic field and hydrostatic initial stress on wave reflection from a generalized thermoelastic solid half-space, *J. Vib. & Control*, **16**(5), 685-699.

[15] SM ABO-DAHAB, RA MOHAMED and BALJEET SINGH, 2011. Rotation and magnetic field effects on P wave reflection from a stress-free surface of elastic half-space with voids under one thermal relaxation time, *J. Vib. & Control,* **17**(12), 1827-1839.

[16] SM ABO-DAHAB, 2011. Reflection of P and SV waves from a stress-free surface thermoelastic half-space under the influence of a magnetic field and hydrostatic initial stress without energy dissipation, *J. Vib. & Control,* **17**(14), 2213-2221.

[17] SM ABO-DAHAB, RA MOHAMED and AM ABD-ALLA, 2011. Magnetic Field and Relaxation Times Effects on the Propagation of Thermoelastic Waves from Isothermal or Insulated Boundaries of a Half Space, *Int. Review of Physics,* **5**(6), 389-401.

[18] SM ABO-DAHAB and AJ ASAD, 2011. Maxwell's stresses effect on reflection and transmission of plane waves between two thermo-elastic media under GN Model, *Int. Review of Physics* **5**(5), 2286-2999.

[19] N CHAKRABORTY and MC SINGH, 2011, Reflection and refraction of a plane thermoelastic wave at a solid-solid interface under perfect boundary condition, in presence of normal initial stress, *Appl. Math. Model.,* **35**(11), 5286-5301.

[20] S DESWAL, L SINGH and B SINGH, 2011. Reflection and refraction at an interface between two dissimilar thermally conducting viscous liquid half-spaces, *Int. J. Pure & Appl. Math.*, **70**(6). 807-824.

[21] AM ABD-ALLA, SR MAHMOUD and SM ABO-DAHAB, 2012, On problem of transient coupled thermoelasticity of an annular fin, *Meccanica,* **47**(2), 1295-1305.

[22] SM ABO-DAHAB and B SINGH, 2013. Rotational and voids effect on the reflection of P waves from stress-free surface of an elastic half-space under magnetic field and initial stress without energy dissipation, *Appl. Math. Model,* **37**(20), 8999-9011.

[23] MC SINGH and N CHAKRABORTY, 2013. Reflection and refraction of P-, SV-and thermal wave, at an initially stressed solid-liquid interface in generalized thermoelasticity, *Appl. Math. Model.,* **37**(1), 463-475.

[24] S. M. ABO-DAHAB and MOUSTAFA M. SALAMA, 2014. A plane magneto thermo elastic waves reflection and transmission between two solid media with external heat sources and initial stress, *J. Thermal Stresses*, **37**, 1124-1151.

[25] T MADHAVI LATHA, P PEDDI NAIDU, DN MADHUSUDHANA RAO and M INDIRA DEVI, 2012. A theoretical study of diurnal shift in reflection height of VLF waves using IRI electron density model, *Indian J. Phys,* **86**(11), 947-950.

[26] S. M. ABO-DAHAB and A. KILICMAN, 2015. On reflection and transmission of p- and SV-waves phenomena at the interface between solid-liquid media with magnetic field and two thermal relaxation times, *J. Therm. Stresses,* **38**, 447-467.

[27] S. M. ABO-DAHAB, 2015. Propagation of p-, T- and SV-waves at the interface between two solid-liquid media with magnetic field and initial stress in the context of two thermoelastic theory, *Canadian Journal of Physics*, **93**, 1-17.

[28] S. M. ABO-DAHAB, 2015. Magnetic field effect on three plane waves propagation at interface between solid-liquid media placed under initial stress in the context of GL Model, *Appl. Mathematics and Information Science* **9**(6), 3119-3131.

[29] S. M. ABO-DAHAB, A.M. ABD-ALLA and A. KILICMAN, 2015. Propagation of p- and T-waves at interface between magnetized solid-liquid media with initial stress in the context of CT theory, *J. Mechanical Science and Technology*, **29**(2), 579-591.

[30] E. CHOI and M. GURNIS, 2008. Thermally-induced brittle deformation in mid-ocean ridge systems, *Earth Planet. Sci. Lett.,* **269**(1-2), 259-270.

[31] A NAYFEH and SN NASSER, 1971, Thermoelastic waves in solids with thermal relaxation, *Acta Mech.,* **12**(1), 53-69.

Journal of Acoustical Society of India : Vol. 43, No. 1, 2016 (pp. 48-53)

Performance Comparison of Beamforming Algorithms for Buried Object Detection

Dhilsha Rajapan*, Sayanti Bardhan, D.S. Sreedev, Shijo Zacharia, Mahimol Eldhose, Shibu Jacob and M.A. Atmanand

Marine Sensors Systems Group

National Institute of Ocean Technology, Pallikaranai, Chennai-600100, India

**e-mail: krd@niot.res.in*

[Received: 11.11.2015; Revised: 19.12.2015; Accepted: 20.12.2015]

ABSTRACT

Even though advanced systems for acoustic detection of buried objects are available in developed countries, it remains a challenge for developing countries. National Institute of Ocean Technology, Chennai (NIOT) has indigenously developed a Buried Object Detection Sonar (BODS), for the detection of buried objects in shallow waters. The important features of BODS are operation in 2-24 kHz frequency band, hydrophone arrays with high receiving sensitivity (-160 dB re 1V/µPa) and real-time image processing. In this paper, we demonstrate effectiveness of BODS to detect buried objects on 27th May 2015 in shallow water (5-10 m depth) of the Royapuram harbour, Chennai. The result from the experiments show that BODS system detected concrete blocks buried at 0.3 m below the seabed in real-time. In this paper, the data collected from the field trial is also compared in offline processing with Minimum Variance Distortionless Response (MVDR) beamforming and Delay and Sum (DAS) beamforming. The improvement in Peak Signal to Noise Ratio (PSNR) and Signal to Noise Ratio (SNR) in the image obtained with DAS Beamforming compared to MVDR Beamforming is estimated to be 10.7 dB and 8.4 dB respectively.

1. INTRODUCTION

In the past few decades sonar system for underwater imaging of buried objects has been studied by Schock *et.al.*[1-2], but it remains a challenge in India. In an attempt toward solving this challenge, an indigenously developed active sonar system, capable of detecting buried object, is being developed by National Institute of Ocean Technology (NIOT), Chennai, for shallow water applications[3-4]. This Buried Object Detection Sonar (BODS) system is capable of imaging targets like metal plate, concrete blocks buried under the seabed. The BODS system uses an indigenous, light weight (~20 kg), wide band (2-24 kHz), transmitter[5] developed at NIOT and a computer based real-time signal processing technique to detect buried objects.

In the signal processing unit of the BODS system, space-time processing is required to effectively fuse data collected at hydrophone outputs. The approach adopted for carrying out space-time processing of data sampled at the hydrophone output is beamforming. A beamformer is a spatial filter that operates on the output of an array of sensors in order to enhance the amplitude of a signal relative to background noise and directional interference[6-8]. The two beamformers studied in this research article are Delay and Sum (DAS) and Minimum Variance Distortionless Response (MVDR).

DAS beamformer works on the principle to delay each sensor output by appropriate time to synchronize signal from a source, across all sensors[9-12]. Upon summation of the delayed signals, the desired signal

components are reinforced and the noise is suppressed. The conventional method of frequency wavenumber power spectral density estimation uses a fixed wavenumber windowing with its resolution being determined by the beampattern of the array of sensors. MVDR is a high-resolution method of estimation which employs a wavenumber window whose shape changes and is a function of the wavenumber at which an estimate is obtained[13].

In this research article, result from the experiment conducted at the Royapuram harbour in the Bay of Bengal [Lat. 13.13°N, Lon. 80.30°E] with concrete blocks buried 0.3 m below seabed is described. This paper also presents an offline comparative study of the Minimum Variance Distortionless Response (MVDR) beamformer and Delay and Sum (DAS) beamformer with the Royapuram sea trial results.

2. MATERIALS AND METHODS

2.1 System Overview

The block diagram of a BODS system is shown in Fig. 1. The system comprises of a tow body and a deck system. The towed body has a wide band acoustic transmitter, receiver hydrophone arrays and two water tight electronic bottles for accommodating transmitter and receiver electronics. It also houses motion sensor and GPS receiver. Data is collected from two linear hydrophone arrays that consist of eight sensor elements on each, placed along the track .They form 16 channel hydrophone arrays with inter-element spacing of 0.0625 m. However, the fabrication of the modular tow body is in such a way the array arrangement can be extended upto 4 hydrophone arrays, *i.e.* 32 hydrophone elements. Electronic cases of tow body are water tightened with O-ring.

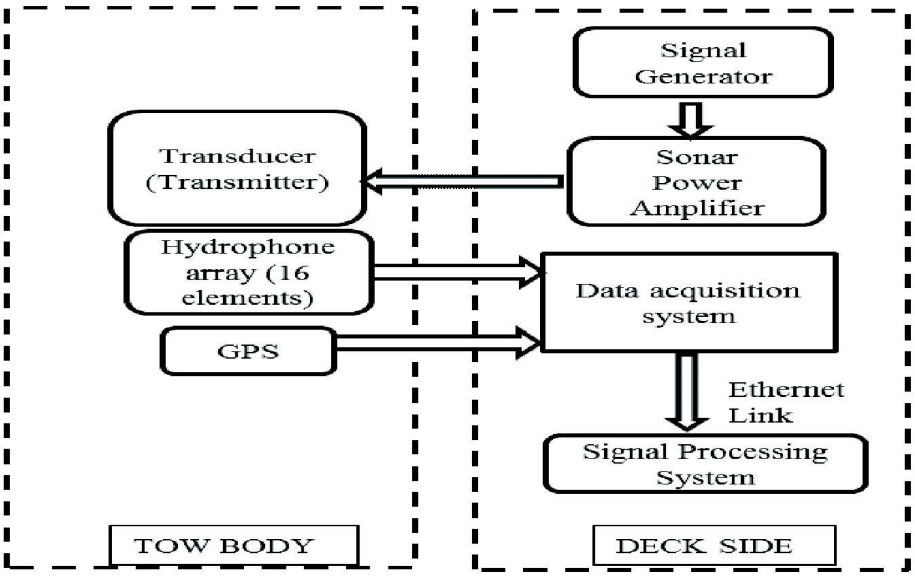

Fig. 1. Block diagram of the sonar system

The acoustic transmitter sends a 2-24 kHz frequency modulated chirp signal at a rate of 4 pings per second. In the deck system each hydrophone output is sampled by an Analog-to-Digital Convertor (ADC) at 100 kHz with a resolution of 16 bits. The data acquisition system is configured with National Instrument (NI) compact RIO-9082. There are 8 NI 9223 series analog input module each of four channels configured into 32 channels of data acquisition. The backscattered signal received from the data acquisition system is filtered with band-pass filter with pass band of 2 kHz to 24 kHz. The filtered data is processed to give real-time images and also stored for facilitating post-processing of the data. The stored data is post-processed for performance comparison between the beamformers.

2.2 Delay and Sum Beamformer

Delay and Sum Beamformer uses delays between each array element that compensate for differences in propagation delay of the desired signal across the array. Signals originating from a desired direction are summed in phase, while other signals undergo destructive interference[14]. The delay and sum beamformer output[15] is given by

$$y(k) = \sum_{L=0}^{J} \sum_{p=0}^{k-1} w_{L,p}^{n} \chi_{L}(k-p) \tag{1}$$

Where y(k) is the output at any time k, K-1 is the number of delays for J sensor channels and w*represents the conjugate of the weights applied to each element. The wideband signal data is transformed at each sensor into frequency domain. After beamforming of the signal at each frequency bin, inverse Fourier transform produces the output time series.

2.3 MVDR Beamformer

MVDR Beamformer is proposed by Capon[13]. The MVDR beamformer is obtained by minimizing the variance of interference and noise at the output of the adaptive beamformer, while ensuring the distortionless response of the beamformer towards the direction of the desired source. Hence, MVDR Beamformer attempts to minimize the power received from noise and any signal coming from directions other than look direction, θ, while maintaining a fixed gain in the look direction. The optimization problem[16] can be expressed mathematically as

$$\min_{w} P \tag{2}$$

$$\text{subject to } \mathrm{w^H\, a}(\theta) = 1 \tag{3}$$

Where P is defined as the output power, w is the weighting vector and $a(\theta)$ is the steering vector. The symbol $(.)^H$ denotes complex conjugate and transpose (Hermite). The optimal weighting vector, w in Eq. (3) can be found using, for instance, the technique of Lagrange multipliers [16]. The computed weight gives the spatial spectrum as[16]

$$P_{(CAP)}(\theta) = \frac{1}{a^{H}(\theta)\hat{R}^{-1}a(\theta)} \tag{4}$$

where R is the spatial covariance matrix. MVDR beamformer attempts to minimize the power contributed by noise and any signals coming from other directions than θ, while maintaining a fixed gain in the look direction θ.

3. EXPERIMENTAL DETAILS

The BODS system was tested in the field on 27th May 2015 at Royapuram Harbour, Chennai [Lat. 13.07°N, Lon. 80.18°E] at 5 m - 5.5 m water column depth. During the experiments the electronic subsystems of BODS were kept in the deck side, as shown in Fig. 1. However, in subsequent experiments the electronic subsystems will be integrated within the electronic bottle in tow body. The sediment type at the experiment site is clay and sand mixture. Concrete blocks were buried at the test site. Nine concrete blocks were arranged in three rows and three columns and buried at about 0.3 m below the seabed. Each block has a dimension of 0.3 m × 0.3 m × 0.03 m.

4. RESULTS AND DISCUSSIONS

The buried concrete block was detected by the BODS system at the Royapuram Harbour. BODS system detected the concrete blocks in real time as the backscattered energy received from the seabed is processed on the deck-side signal processing system in a calm sea state. Fig. 2 shows the real-time images of the detected concrete blocks buried in the seabed. The Y-axis in the Fig. 2 corresponds to depth in metres. The Ping number 350-500 corresponds to the buried concrete blocks in Fig. 2. The beamformer used is DAS

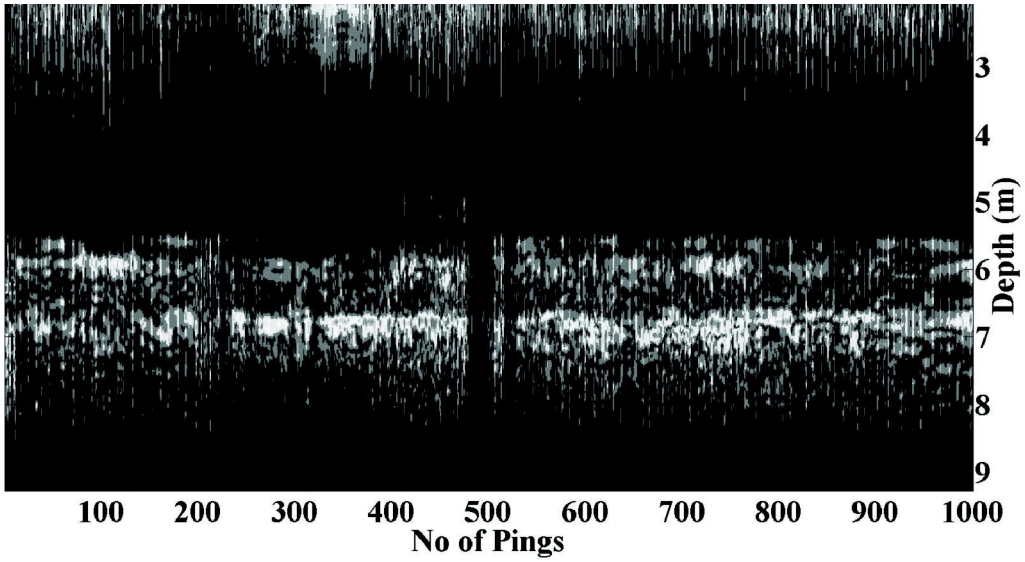

Fig. 2. Real time images of the buried Concrete blocks detected with BODS

Beamformer. The figure shows detection of the seabed at a depth of 6 metres.

Comparison of beamformers was carried out in the post processing of data. Fig. 3 shows the image obtained by delay and sum beamformer. Fig. 4 shows the image obtained by MVDR Beamformer. In both the figures X-axis corresponds to the pings and Y-axis corresponds to depth in metres. In both the cases, the signal processing steps are same with beamforming followed by matched filtering and Hilbert transform.

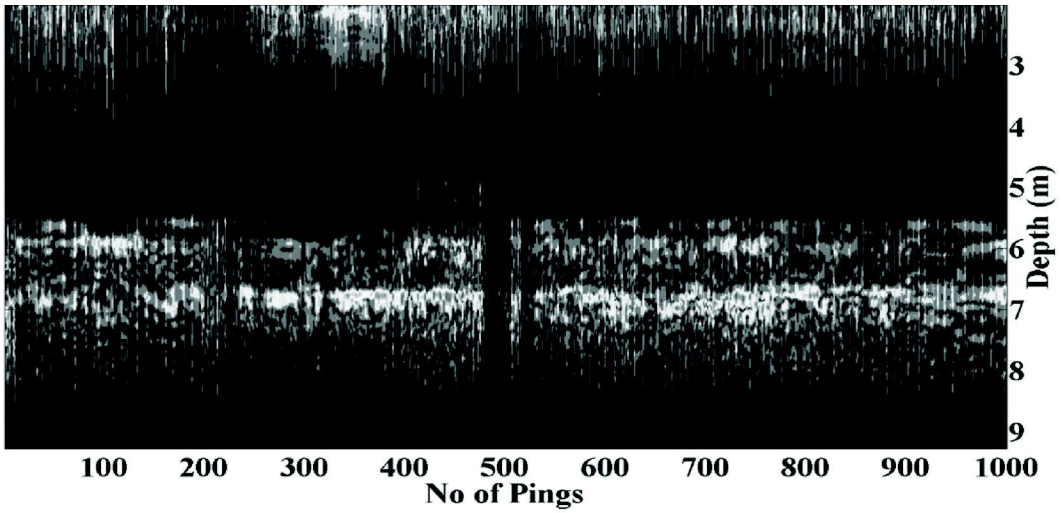

Fig. 3. Image with Time and Delay Beamformer processing

In both the cases, 1000 pings were considered for generating the image. Upon comparison, it is observed that with DAS Beamformer, the concrete blocks are distinctly visible from the seabed whereas with the MVDR Beamformer the image is noisy and objects can't be distinguished. Fig. 3 showed an improvement in Peak Signal to Noise Ratio (PSNR) as 10.7 dB in comparison to Fig. 4. Also an improvement of 8.4 dB in Signal to Noise Ratio (SNR) was calculated in Fig. 3 in comparison to Fig. 4. Further work is being done

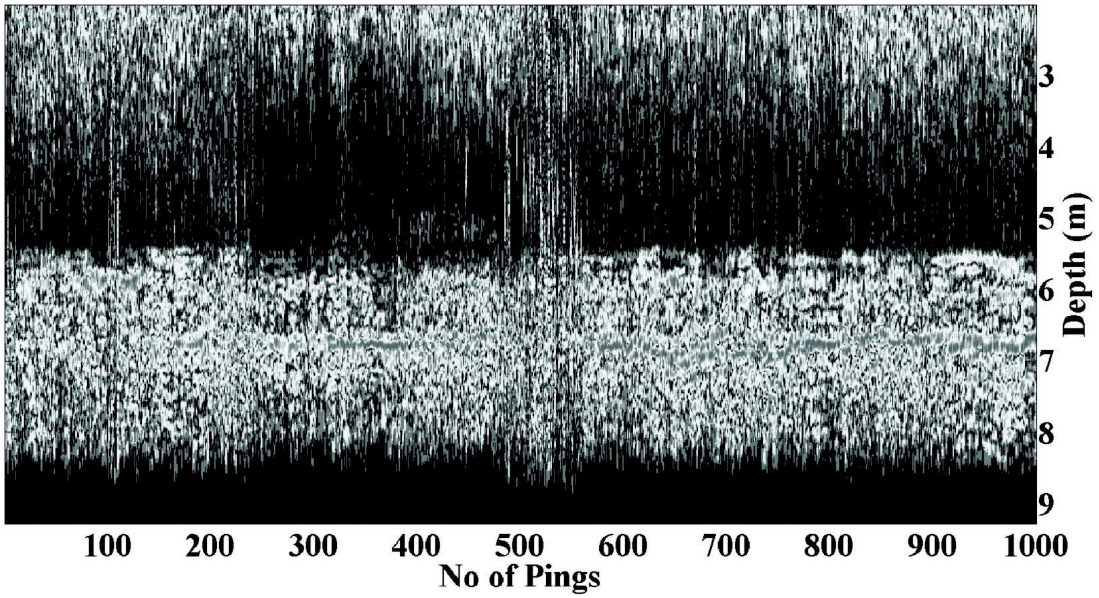

Fig. 4. Image with MVDR Beamformer processing

towards colour quantization for reducing the number of colours required to represent the image from 256 to 8 and will be reported in forthcoming articles.

5. CONCLUSION

Buried Object Detection SONAR (BODS) is an indigenously developed system with a wide bandwidth (2-24 kHz), light weight projector ~ 20 Kg. The hydrophone arrays, tow body and the signal processing software are developed in-house. BODS system has been tested with buried objects like concrete blocks in sea environment. It is observed from the real-time image obtained that BODS system is capable of detecting the concrete blocks buried at a depth of 0.3m. The performance comparison of MVDR and DAS Beamformer on the post processed image shows that Time Delay Beamformer gave an image with an increased PSNR of 10.7 dB and SNR of 8.4 dB.

6. ACKNOWLEDGEMENT

The authors would like to acknowledge all members of the Marine Sensors System Group who was involved in carrying out the experiments successfully. Special thanks are due to Mr. C. Kannan, for his contribution in the tow body development and encapsulation of transducers. The authors would also like to thank Dr. Bishwajit Chakraborty, CSIR-NIO Goa, for fruitful discussions and his encouragement. This work is funded completely by National Institute of Ocean Technology (ESSO-NIOT), Ministry of Earth Sciences, Govt. of India.

10. REFERENCES

[1] STEVEN G. SCHOCK, ARNAUD TELLIER, JIM WULF, JASON SARA and MARK ERICKSEN, 2001. Buried Object Scanning Sonar, *IEEE Journal of Oceanic Engineering*, **26**(4), 677-689.

[2] S. SCHOCK and J. WULF, 2003. Buried Object Scanning Sonar for AUV's, *Oceans,* San Diego, 22-26.

[3] DHILSHA RAJAPAN, 2013. Acoustical Imaging Techniques and its Applications, Proc. of the International symposium on Acoustics, *Acoustics,* NPL, New Delhi, India

[4] S. BARDHAN, DHILSHA RAJAPAN, SHIJO ZACHARIA, MAHIMOL ELDHOSE, P.M. RAJESHWARI, D.S. SREEDEV, KANNAN C, SHIBU JACOB and M.A. ATMANAND, 2015. Detection

of Buried Objects using Active Sonar, Proc. of the International Symposium on Underwater Technology, *IEEE-UT 15*, Chennai, India.

[5] DHILSHA RAJAPAN, 2002. Performance of a low-frequency, multi-resonant broadband Tonpilz transducer, *J. Acoust. Scoc. Am.,* **111**(4), 1692-1694.

[6] VAN VEEN B.D. and BUCKLEY K.M., 1988. Beamforming: A versatile approach to spatial filtering, *IEEE ASSP Magazine,* **2**(5), 4-24.

[7] J. E. PIPER, 2011. Beamforming narrowband and broadband signals, Sonar Systems, InTech Publishing.

[8] H. KRIM and M. VIBERG, 1996. Two decades of array signal processing research: the parametric approach, *IEEE Signal Processing Magazine*, **4**(13), 67-94.

[9] S.A. SCHELKUNOFF, 1943. A mathematical theory of linear arrays, *Bell Syst. Tech. J.*, **22**(1), 80-107.

[10] D. E. Dudgeon, 1977. Fundamentals of digital array processing, *Proc. IEEE*, **65**(6), 898-904.

[11] J. L. FLANAGAN, J. D. JOHNSON, R. ZAHN and G. W. ELKO, 1985. Computer steered microphone arrays for sound transduction in large rooms, *J. Acoust. Soc. Amer.,* **78**(5), 1508-1518.

[12] M. BRANDSTEIN and D. B. WARD, 2001. *Microphone Arrays: Signal Processing Techniques and Applications*, Springer.

[13] J. CAPON, 1969. High-Resolution Frequency-Wavenumber Spectrum Analysis, *Proc. IEEE,* **57**(8), 1408-1418.

[14] J. BENESTY, M. M. SONDHI and Y. HUANG, 2007. *Springer Handbook of Speech Processing*, Springer.

[15] BARRY D. VAN VEEN and KEVIN BUCKLEY, 1988. Beamforming: A Versatile Approach to Spatial Filtering, *IEEE ASSP Magazine,* **5**(2), 4-24.

[16] H. KRIM and M. VIDBERG, 1995. Sensor array signal processing: two decades later, *Laboratory for Information and Decision Systems*, Massachusetts Institute of Technology, LIDS P-2282.

Journal of Acoustical Society of India : Vol. 43, No. 1, 2016 (pp. 54-60)

Short Term Shallow Water Ambient Noise Variability off Kakinada During Northeast Monsoon

R. Kannan[1], G. Latha[1] and M. Prashanthi Devi[2]
[1]*National Institute of Ocean Technology, Pallikaranai, Chennai-600 100, India*
[2]*Bharathidasan University, Palkalaiperur, Tiruchirappalli-620 024, India*
**e-mail: rkannan@niot.res.in*

[Received: 21.12.2015; Revised: 02.03.2016; Accepted: 02.03.2016]

ABSTRACT

This study examine the variations of ambient noise attributed to wind and vessel traffic using the time series measurements collected off Kakinada during November 2014 by an autonomous ambient noise system developed by National Institute of Ocean Technology (NIOT). The study focus on the fluctuation and variability in ambient noise over 12 hour periods that starts at midnight (Period I) and noon (Period II) respectively. The data was recorded once in every three hours and segmented into corresponding 12 hour periods. The concurrent wind speed measurements were also segmented. In each 12 hour period, the data was segregated and analyzed as two sets in the presence and absence of vessel noise. In the absence of vessel traffic, the average ambient noise level and the standard deviation were apparently higher during the period II, indicating prominent sea breeze effect. In the presence of vessel traffic, the average ambient noise level was noticeably higher during period II with an increase in the average noise level up to 12 dB owing to prominent shipping activities. The wind speed dependence on the noise variability was examined, resulting decrease in the standard deviation with an increase in the Beaufort scale. The fluctuation spectra corresponding to both the periods were computed from the time series noise at frequencies ranging between 0.5 to 5 kHz with an increment of 0.5 kHz. The resulting absolute power spectrum levels during period I and period II vary between 61-87 dB and 50-85 dB, 66-98 dB and 53-86 dB at 1 and 5 kHz respectively. Thus, from the study, the greater variability with time and the higher average noise level is evident in period II.

1. INTRODUCTION

The underwater ambient noise variability is dominated by the wind over a significant frequency range as compared to other noise sources namely ship, rain, biological and human activities. In shallow water, particularly in the absence of local shipping and biological activity, the wind generated noise dominates the spectra of distant shipping over the entire frequency range[1]. The ship traffic is an important source of noise, and its noise level is normally observed to be 11 dB above the ambient noise[2]. The soundscape exhibits spatio-temporal variability in the shallow water environment[3]. In order to provide vital data for theoretical analysis, it is imperative to reveal the source of noise fluctuation. The time variability of the ambient noise encompass a wide scale from very fast (transients of breaking waves) to very slow (long-term changes of ship traffic or long-term changes in weather and climate) reflecting the variability of the sources of noise that can be conveniently expressed as fluctuation spectra.

In a site identified in the southern North Atlantic Ocean, Hecht and Mole found a standard deviation value of only 1-1/2 dB for 90% of both 10-sec and 10-min samples[4] which shows the sparse distant ship traffic and the remaining 10% shows the occasional ship traffic[4]. The noise due to shipping varies more rapidly with time than the noise due to the wind. This was demonstrated by Perrone and King by analyzing the data collected off Bermuda and the Grand Banks[5]. Observations of acquired noise over one-year periods employing hydrophones at Bermuda, Wenz and Perrone were successful in throwing light on the long-term variability of noise at a single location[6, 7]. The related interpretations were associated with diurnal sound level variation of 1.5 - 5.0 dB evident at midnight local time regularly throughout the year including daily changes of 10-20 dB during the summer solstice (maximum solar declination) with subtle changes in the winter solstice.

The soundscape of the shallow water marine environment display spatio-temporal variability. The marine environment near to shore and busy harbors are the dynamic locations with rapid changes in the ambient noise. In this work, an attempt has been made to study the variation of ambient noise in the shallow waters of the Bay of Bengal. The daily recorded data (within the frequency range of 0.5-5 kHz) were segmented to corresponding 12 hour periods, and analyzed particularly in the presence and absence of ship noise to differentiate relative contribution of anthropogenic noise.

2. DATA COLLECTION

In the month of November 2014, an automated subsurface ambient noise recording system developed by NIOT was deployed at 20 m water depth for time series measurements of ambient noise off the Kakinada coast in the Bay of Bengal. Location of the study area is shown in Fig. 1. The omni-directional hydrophones array system can record ambient noise in the frequency range of 0.01-25 kHz with a receiving sensitivity of -160 dB. The ambient noise data were acquired once in every three hours with a sampling frequency of 50 kHz for 30 s recording duration. In addition to recording ambient noise, concurrent wind speed measurements from the study location were also collected.

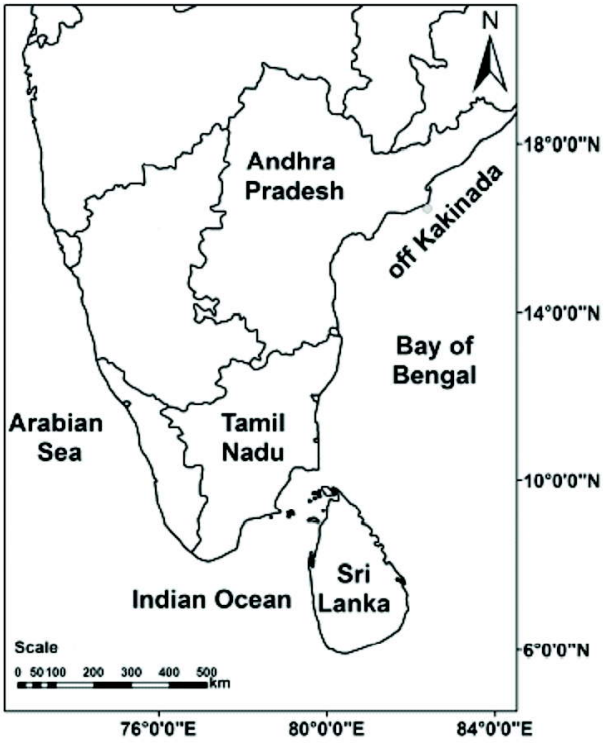

Fig. 1. Location of the study area off Kakinada.

3. METHODOLOGY

Spatial variability of wind dominated ambient noise in the shallow water marine environment had been investigated by researchers ascribing to ocean bottom properties, water depth and sound speed variation in the water column[3,8]. The characteristics of wind and ship traffic generated noise and the corresponding classification were accomplished using traditional statistical techniques[5]. The variability of wind dependent ambient noise in the shallow waters of the Bay of Bengal was studied earlier by correlating with the magnitude of measured atmospheric wind velocity and direction[9]. Besides, the fluctuation and variability of ambient noise was studied in two shallow water sites by evaluating the relative contribution of wind and vessel traffic at the respective sites[10, 11]. In this work, an alternative approach to examine the ambient noise data for the fluctuation studies related to wind and vessel traffic noise is established. The daily recorded ambient noise data along with synchronized wind speed measurements were segmented to corresponding 12 hour periods starting at midnight and noon of the day respectively. In each 12 hour period, the data was analyzed as two sets specifically in the presence and absence of vessel noise to differentiate relative contribution in the ambient noise spectrum. The rose plot representing the magnitude and direction of the atmospheric wind measurements is plotted to substantiate the results of the fluctuation studies during the period.

4. RESULTS AND DISCUSSION

In the first case, the data corresponding to 12 hour periods were examined in the absence of vessel traffic. It is apparent in Fig. 2a that the difference in average vessel noise level around 1 kHz was almost 10 dB higher during period II as compared to period I with a decreasing trend to 2 dB around 2.5 kHz frequency. The standard deviation of the data was higher during period II as illustrated in Fig. 2b. The increase in number of data occurrence evident in Fig. 2c is conspicuous in the lower noise level band during period I, whereas the distribution of number of occurrence is sparsely distributed over a wide range as depicted in Fig. 2d. The results depicted in Fig. 2 also display a clear evidence of local sea breeze effect on the ambient noise variability during period II.

In the second case, the segmented data corresponding to 12 hour periods were analyzed particularly in the presence of vessel traffic. It is evident in Fig. 3a that the difference in average vessel noise level around 1 kHz was almost 12 dB higher during period II as compared to period I, maintaining 5 dB noise level up

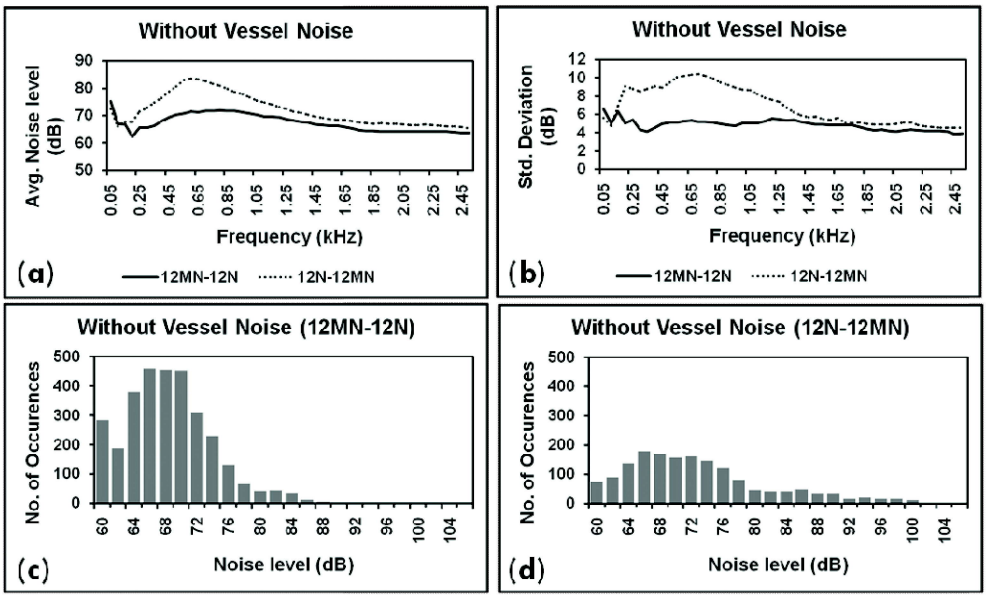

Fig. 2. Characteristics of ambient noise in the absence of vessel noise during 12 hour periods.

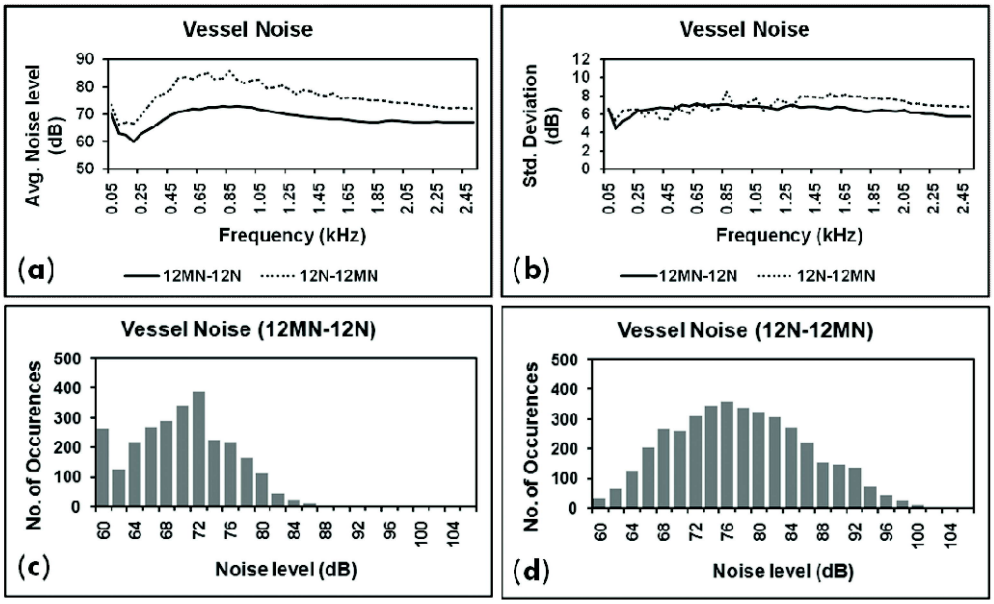

Fig. 3. Characteristics of ambient noise in the presence of vessel noise during 12 hour periods.

to 2.5 kHz frequency band. The corresponding standard deviation of the data exhibit meager variation as the vessel generated noise varies rapidly over a period of time (Fig. 3b). During period I, the higher number of data occurrence (as displayed in Fig. 3c) is noticeable in the lower noise level band, whereas the distribution of data occurrence dominantly shift towards the higher noise level band (Fig. 3d). The results illustrated in Fig. 3 further highlight the characteristics of vessel traffic on the ambient noise fluctuation during period II.

The wind speed dependence on the ambient noise variability was also examined for the entire dataset as shown in Fig. 4. It is obvious in Fig. 4a that the average noise level increases linearly with the Beaufort scale, whereas the corresponding standard deviation decreases with an increase in the Beaufort scale (Fig. 4b).

The fluctuation spectra corresponding to periods I and II were subsequently computed from the time series noise at frequencies ranging between 0.5 to 5 kHz with an increment of 0.5 kHz. The observed noise spectrum level during period I vary between 61-87 dB and 50-35 dB at 1 and 5 kHz respectively (Fig. 5). On the other hand, the observed noise spectrum level during period II vary between 66-98 dB and 53-86 dB at 1 and 5 kHz respectively (Fig. 6). By examining Fig. 5 and 6, the greater variability with time and the higher

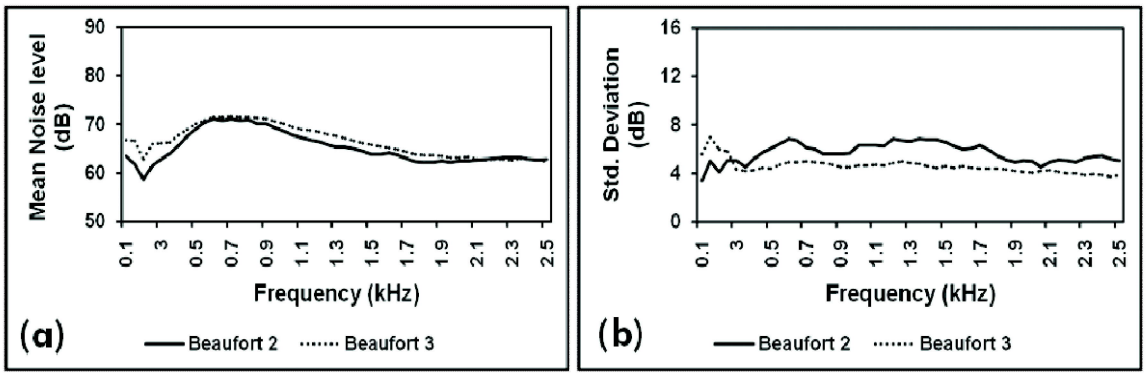

Fig. 4. Observed noise level fluctuation at Beaufort scale 2 and 3.

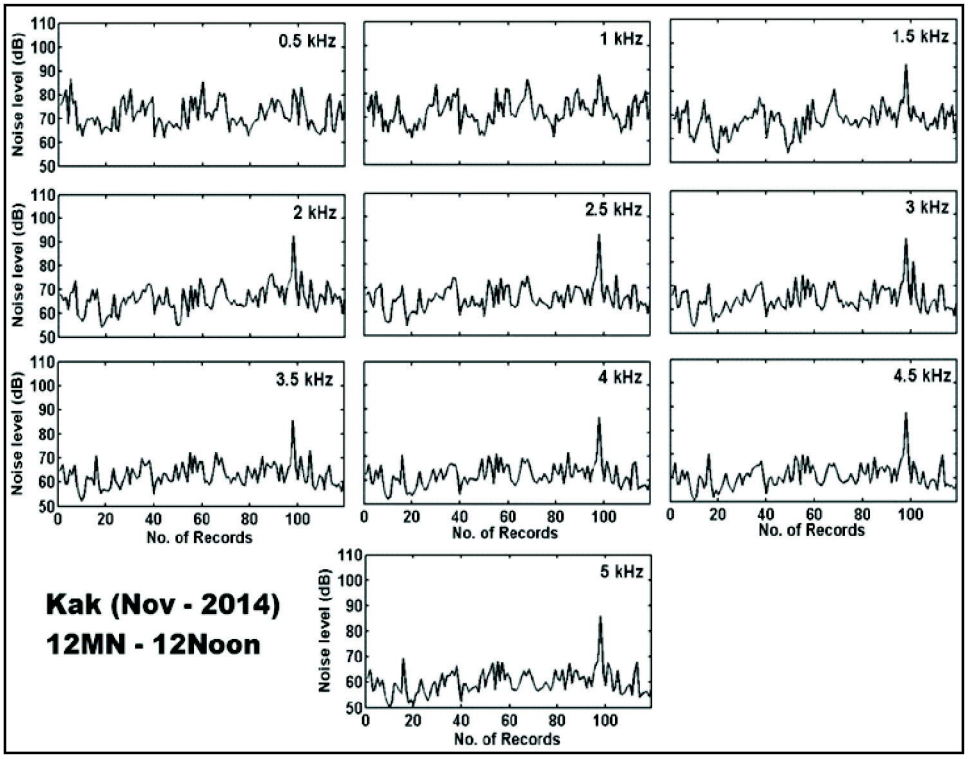

Fig. 5. Fluctuation spectrum during 12 hour midnight to noon time

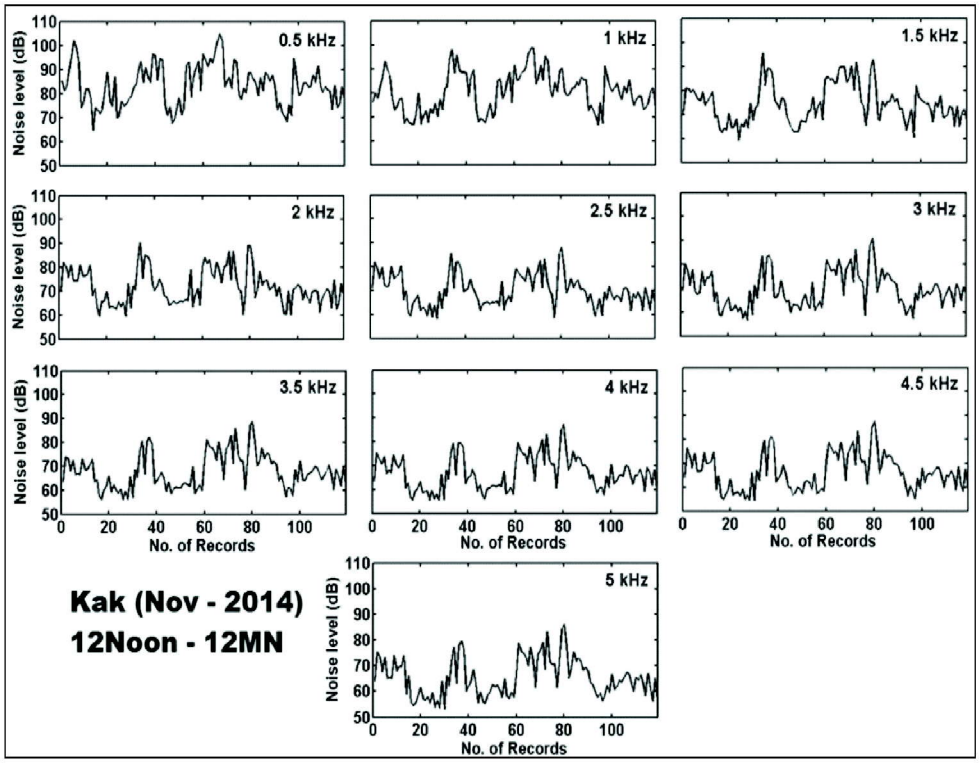

Fig. 6. Resulting fluctuation spectrum during 12 hour noon time to midnight.

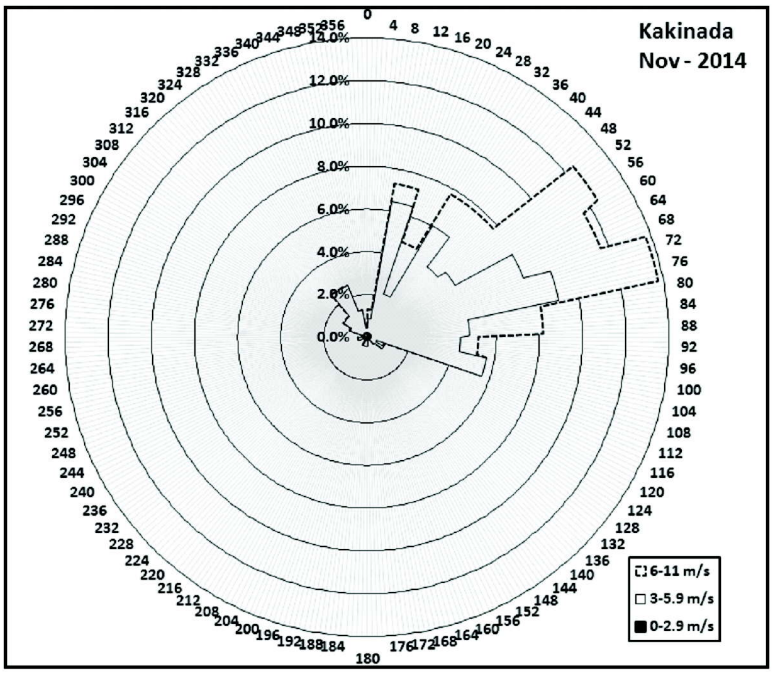

Fig. 7. Wind direction off Kakinada during November 2014.

average noise level is evident during period II. The increase in the average noise level up to 12 dB observed during period II can be attributed to vessel traffic related activity together with the sea breeze effect. The obtained results are in good corroboration with the typical characteristics of noise data recorded in the coastal region with moderate shipping activity.

5. CONCLUSION

Most of the reported studies on ambient noise fluctuation analysis were concerning the entire day. Here, in this study, the fluctuation of ambient noise in two 12 hour periods and also the ambient noise variability during the presence and absence of vessel noise in each period were reported. In the absence of vessel noise, the ambient noise fluctuation was higher during period II and it was because of local sea breeze effect. Whereas in the presence of vessel noise, an increase of 12 dB was observed during period II and it is found to be the vessel movement, since the deployed position of the ambient noise system was in the vicinity of vessel activity region. Wind speed dependence on noise variability revealed that the ambient noise level increases with increase in Beaufort scale.

Thus the present investigations lead us to conclude that the ambient noise variability off Kakinada during northeast monsoon month of November 2014 was examined to be higher in the 12 hour period that starts at noon and was found to be due to the vessel traffic activity jointly with the sea breeze effect.

6. ACKNOWLEDGMENTS

The authors thank Director, National Institute of Ocean Technology for providing all the support to carry out this study. We also thank all our colleagues in the Ocean Acoustics Group who assisted during various aspects of this work.

7. REFERENCES

[1] R J. URICK., 1984. *Ambient Noise in the Sea,* Published by Undersea Warfare Technology Office, Naval Sea Systems Command, Washington, D.C. 20362.

[2] T.M. BROCHER and B.T. IWATAKE, 1982. Sources of Low-Frequency Ambient Seafloor Noise on a Continental Shelf, *Bull. Seismol. Soc. Am.*, **72**, 1129-1142.

[3] T.C. YANG and K. YOO, 1997. Modelling the environmental influence on the vertical directionality of ambient noise in shallow waters, *JASA.,* **101**(5), 2541-54.

[4] R. J. HECHT and L. A. MOLE, 1978. Acoustic Signal Processing Extensions, *JASA.*, **64**, 1206.

[5] A. J. PERRONE and L.A. KING, 1975. Analysis Technique for Classifying Wind and Ship-generated noise characteristics, *JASA.*, **58**, 1186.

[6] G. M. WENZ, 1969. Low-frequency deep-water ambient noise along the Pacific Coast of the United States, *Jounral of Underwater Acoustics.,* **19**, 423-444.

[7] A. J. PERRONE, 1976. Summary of a One-year Ambient Noise Measurement Program off Bermuda, *Naval Underwater Systems Center Tech.* Rep., 4979.

[8] F. INGENITO and S. N. WOLF, 1989. Site dependence of wind dominated ambient noise in shallow water, *JASA.,* **85**, 141-145.

[9] S. RAMJI, G. LATHA, V. RAJENDRAN and S. RAMAKRISHNAN, 2008. Wind dependence of ambient noise in shallow water of Bay of Bengal, *Appl. Acoust.,* **69**, 1294-1298.

[10] M. C. SANJANA, G. LATHA, A. THIRUNAVUKKARASU and V. RAJENDRAN, 2010. Fluctuation and variability of shallow water ambient noise from time series measurements, *Fluctuation and Noise Letters.*, **9**(2), 193-202.

[11] R. KANNAN, M. C. SANJANA and G. LATHA, 2015. Passive Acoustic Recognition of Fishing Vessel Activity in the Shallow Waters of the Arabian Sea: A Statistical Approach, *Fluctuation and Noise Letters.,* **14**(4), 1550035.

INFORMATION FOR AUTHORS

ARTICLES

The Journal of Acoustical Society of India (JASI) is a refereed publication published quarterly by the Acoustical Society of India (ASI). JASI includes refereed articles, technical notes, letters-to-the-editor, book review and announcements of general interest to readers.

Articles may be theoretical or experimental in nature. But those which combine theoretical and experimental approaches to solve acoustics problems are particularly welcome. Technical notes, letters-to-the-editor and announcements may also be submitted. Articles must not have been published previously in other engineering or scientific journals. Articles in the following are particularly encouraged: applied acoustics, acoustical materials, active noise & vibration control, bioacoustics, communication acoustics including speech, computational acoustics, electro-acoustics and audio engineering, environmental acoustics, musical acoustics, non-linear acoustics, noise, physical acoustics, physiological and psychological acoustics, quieter technologies, room and building acoustics, structural acoustics and vibration, ultrasonics, underwater acoustics.

Authors whose articles are accepted for publication must transfer copyright of their articles to the ASI. This transfer involves publication only and does not in any way alter the author's traditional right regarding his/her articles.

PREPARATION OF MANUSCRIPTS

All m

Manusc

mail on a disc. JASI maintains a high standard in the reviewing process and only accept papers of high quality. On acceptance, revised articles of all authors should be submitted to the Chief Editor by e-mail or by express mail.

Text of the manuscript should be double-spaced on A4 size paper, subdivided by main headings-typed in upper and lower case flush centre, with one line of space above and below and sub-headings within a section-typed in upper and lower case understood, flush left, followed by a period. Sub-sub headings should be italic. Articles should be written so that readers in different fields of acoustics can understand them easily. Manuscripts are only published if not normally exceeding twenty double-spaced text pages. If figures and illustrations are included then normally they should be restricted to no more than twelve-fifteen.

The fi

addresses of authors in upper and lowers case. Do not include the author's title, position or degrees. Give an adequate post office address including pin or other postal code and the name of the city. An abstract of not more than 200 words should be included with each article. References should be numbered consecutively throughout the article with the number appearing as a superscript at the end of the sentence unless such placement causes ambiguity. The references should be grouped together, double spaced at the end of the article on a separate page. Footnotes are discouraged. Abbreviations and special terms must be defined if used.

EQUATIONS

Mathematical expressions should be typewritten as completely as possible. Equation should be numbered consecutively throughout the body of the article at the right hand margin in parentheses. Use letters and numbers for any equations in an appendix: Appendix A: (A1, (A2), etc. Equation numbers in the running text should be enclosed in parentheses, i.e., Eq. (1), Eqs. (1a) and (2a). Figures should be referred to as Fig. 1, Fig. 2, etc. Reference to table is in full: Table 1, Table 2, etc. Metric units should be used: the preferred from of metric unit is the System International (SI).

REFERENCES

The order and style of information differs slightly between periodical and book references and between published and unpublished references, depending on the available publication entries. A few examples are shown below.

Periodicals:

[1] S.R. Pride and M.W. Haartsen, 1996. Electroseismic wave properties, *J. Acoust. Soc. Am.*, **100** (3), 1301-1315.

[2] S.-H. Kim and I. Lee, 1996. Aeroelastic analysis of a flexible airfoil with free play non-linearity, *J. Sound Vib.*, **193** (4), 823-846.

Books:

[1] E.S. Skudzryk, 1968. *Simple and Comlex Vibratory Systems*, the Pennsylvania State University Press, London.

[2] E.H. Dowell, 1975. *Aeroelasticity of plates and shells*, Nordhoff, Leyden.

Others:

[1] J.N. Yang and A. Akbarpour, 1987. Technical Report NCEER-87-0007, Instantaneous Optimal Control Law For Tall Buildings Under Seismic Excitations.

SUMISSIONS

All materials from authors should be submitted in electronic form to the JASI Chief Editor: B. Chakraborty, CSIR - National Institute of Oceanography, Dona Paula, Goa-403 004, Tel: +91.832.2450.318, Fax: +91.832.2450.602,(e-mail: bishwajit@nio.org) For the item to be published in a given issue of a journal, the manuscript must reach the Chief Editor at least twelve week before the publication date.

SUMISSION OF ACCEPTED MANUSCRIPT

On acceptance, revised articles should be submitted in electronic form to the JASI Chief Editor (bishwajit@nio.org)

ISSN 0973-3302

JOURNAL OF ACOUSTICAL SOCIETY OF INDIA

Volume 43 Number 2 April 2016

A Quarterly Publication of the JASI

http://www.acousticsindia.org

Journal of Acoustical Society of India Volume 43 Number 2 April 2016 pp 61-132

JASI

Journal of Acoustical Society of India

The Refereed Journal of the Acoustical Society of India (JASI)

The Journal of Acoustical Society of India is a refereed journal of the Acoustical Society of India **(ASI)**. The **ASI** is a non-profit national society founded in 31st July, 1971. The primary objective of the society is to advance the science of acoustics by creating an organization that is responsive to the needs of scientists and engineers concerned with acoustics problems all around the world.

Manuscripts of articles, technical notes and letter to the editor should be submitted to the Chief Editor. Copies of articles on specific topics listed above should also be submitted to the respective Associate Scientific Editor. Manuscripts are refereed by at least two referees and are reviewed by Publication Committee (all editors) before acceptance. On acceptance, revised articles with the text and figures scanned as separate files on a diskette should be submitted to the Editor by express mail. Manuscripts of articles must be prepared in strict accordance with the author instructions.

All information concerning subscription, new books, journals, conferences, etc. should be submitted to Chief Editor:

B. Chakraborty, CSIR - National Institute of Oceanography, Dona Paula, Goa-403 004,
Tel: +91.832.2450.318, Fax: +91.832.2450.602, e-mail: bishwajit@nio.org

Annual subscription price including mail postage is Rs. 2500/= for institutions, companies and libraries and Rs. 2500/= for individuals who are not **ASI** members. The Journal of Acoustical Society of India will be sent to **ASI** members free of any extra charge. Requests for specimen copies and claims for missing issues as well as address changes should be sent to the Editorial Office:

ASI Secretariat, C/o Acoustics, Ultrasonics & Vibration Section, CSIR-National Physical Laboratory, Dr. KS Krishnan Road, New Delhi 110 012, Tel: +91.11.4560.8317, Fax: +91.11.4560.9310, e-mail: asisecretariat.india@gmail.com

ISSN 0973-3302

Printed at Alpha Printers, WZ-35/C, Naraina, Near Ring Road, New Delhi-110028 Tel.: 9810804196. JASI is sent to ASI members free of charge.

JASI

Journal of Acoustical Society of India (JASI)

A quarterly publication of the Acoustical Society of India

Volume 43, Number 2, April 2016

ARTICLES

INFORMATION

EDITORIAL

Human verbal communication is achieved through the speech production and hearing mechanisms. Any impairment in these mechanisms will result in a variety of communication disorders. Profession of Audiology and Speech language Pathology deals with diagnosis, assessment and management of these disorders as well as rehabilitation of persons with these impairments. Speech processing and analysis play a crucial role in this profession, as it helps in proper diagnosis, accurate assessment and effective rehabilitation.

A session on "Speech and Sound Perception" was included in the National Symposium on Acoustics 2015 held at CSIR-NIO, Goa. As many as 29 papers covering different aspects such as speech perception, speech signal processing, speaker recognition etc were presented in this session. The editorial team of JASI selected eight of these papers to be brought out as a special issue on "Acoustic analysis and signal processing for communication disorders". After careful reviews from experts in respective fields, these papers were organized into three groups and included in this special issue. The intention of the special issue is to stimulate and guide development of innovative and improved strategy for research in the application of state-of-the-art techniques of speech processing and analysis in the field of communication disorders.

The first group on sound processing in hearing aids includes a paper by Geetha, Rajarajan & Kishore Tanniru which is an investigation on the benefit of directionality and DNR of binaural WDRC wireless technology hearing aids on speech intelligibility in a noisy environment.

Four papers in the second group, focus on various aspects of speech production or speech perception by normal persons or by persons with communication disorders. In the first paper of this group, Savithri S.R, Sreedevi N, Soumya K and Sushma S have attempted to relate the type and development of rhythm with two parameters - Fundamental frequency (F0) and Intensity (I0) measurements. Results showed that the type of rhythm varied with F0 or I0. The second paper in this group by Prawin Kumar, Geetha C and Manjunatha Y N concludes that the children using hearing aids showed prolonged latency and reduced amplitude for waves P1 and N2. The 3rd paper in this group is by Vineetha C.V. and Sujeet Kumar Sinha, is aimed to investigate correlation of speech signal encoding between cochlea, brainstem and cortical auditory processing in normal young adults and middle aged individuals. The 4th paper is from Shweta Bansal and Agrawal S S which analyzes the differences in nasality formant frequency and pronunciation of Hindi phonemes spoken by the native Hindi speaker and Punjabi and Nepali speakers.

In the third group, three papers are included which deal with speech recognition and speaker recognition. The paper by Arjun M S and Rajasudhakar R reports the study conducted to develop a benchmark for speaker identification suing LPC on vowels preceding nasal continuants in Kannada. The second paper, a pilot study by Akshay M M, Sangeetha Mahesh and Fathima Mohyadeen, provided some proof to examine the efficiency of semiautomatic annotation of read speech using speech recognition. The third paper is a study of nonlinear properties of vocal tract and its effectiveness in speaker modeling by Sunil Kumar R K. Muraleedharan K M, Vivek P and Lajish V L.

As I conclude this overview, I would like to thank Dr. Biswajit Chakraborty, Chief Editor of JASI for his kind support throughout the preparation of this special issue. Our sincere gratitude to the reviewers listed below for sparing their valuable time and for all the inputs in ensuring the quality of the selected papers. I would also like to acknowledge Dr. S.R. Savithri, Director, All India Institute of Speech and Hearing, Mysuru for her support and guidance in bringing out this special issue.

Dr. Ajish K Abraham
Guest Editor
Professor of Electronics and Acoustics & Head, Dept. of Electronics,
All India Institute of Speech & Hearing,
Manasagangothri, Mysore - 570006, India

List of Reviewers

1. Dr. T.V. Ananthapadmanabha
2. Dr. C.S. Vanaja
3. Dr. Animesh Barman
4. Dr. Ananthakrishna Chintanpally
5. Dr. Ajish K Abraham

Journal of Acoustical Society of India : Vol. 43, No. 2, 2016 (pp. 61-72)

Speech rhythm in Kannada speaking children aged 3-4 years

S.R. Savithri, N. Sreedevi, K. Sowmya and S. Sushma
All India Institute of Speech and Hearing,
University of Mysore, Mysore- 570006
e-mail: savithri486@gmail.com

[Received: 18-04-2016; Revised: 10-05-2016; Accepted: 16-08-2016]

ABSTRACT

Speech rhythm, a prosodic feature, refers to an event repeated regularly over a period of time. It differs based on language and the types of syllables used in a language. Rhythm of several languages, as evident in adults' spoken speech, has been classified as syllable-, mora-, and stress-timed. The current study is an attempt to explore the type and development of rhythm in typically developing Kannada speaking children in the age range of 3-4 years using fundamental frequency (F0) and Intensity (I0) measurements. With respect to F0 measure, vocalic and intervocalic pair-wise variability indices (PVIs) showed syllable-timed rhythm. As regards to I0 measure, PVIs indicated the use of mora-timed rhythm. Hence, the rhythm type varied with the parameter in question (F0 or I0). The results can be used to assess and rehabilitate children with communication disorders as they may have problems associated with prosodic aspects of speech.

1. INTRODUCTION

Rhythm is the systematic patterning of timing, accent and grouping in sequences of events. Spoken languages differ in characteristic rhythm [1,2] and, with respect to adult speakers, have been organized as stress-timed, syllable-timed or mora-timed, based on the Rhythm Class Hypothesis. The Rhythm Class Hypothesis states that each language belongs to one of the prototypical rhythm classes as stated earlier. If a language has simple syllabic structure, for *e.g.* CV or CCV ('V' - vowel; C- consonant), the durational difference between the simplest and most complicated syllable is not large. It is possible to generalize and say that the duration of any syllable is less than 330 ms. Under these circumstances, one can use a fast syllable-timed rhythm. If the syllable structure is still simpler, for example V or CV, then the durational difference between syllables is negligible in which case the rhythm of the language can be described as being mora-timed. If a language has complex syllables, for *e.g.* V and CCCVCC, the difference between syllables can be very large. For example, the duration of syllable V (/a/) can be 60 ms and that of CCCVCC (*e.g.* /strength/) can be 600 ms. In these languages, one has to use a slow stress-timed rhythm.

The development of the concept on rhythm measurement began with the idea of isochrony - i.e. each syllable has equal duration. The first attempt to test Rhythm Class Hypothesis was made by [2] using the ***average syllable duration***, but was not found to be effective in classifying rhythm types. Roach[3] used ***inter-stress interval*** which could not classify speech rhythm in languages. The existence of two rhythmic categories-stress and syllable timing-has been the basis of phonetic research on rhythm. Ramus and colleagues[4] measured and found that ***vocalic duration*** (% V) and ***Standard Deviation of consonant intervals*** (ΔC) provided best acoustic correlates of rhythm classes. The ***Pair-wise Variability Index (PVI)***

Table 1. Classification of rhythm based on PVIs

	Intervocalic Interval (IV)	**Vocalic Interval (V)**
Stress-timed	High	High
Syllable-timed	High	Low
Mora-timed	Low	Low

was developed by Low [5] for rhythmic analyses, which is a quantitative measure of acoustic correlates of speech rhythm. It calculates the patterning of successive vocalic and intervocalic intervals. The normalized Pairwise Variability Index (nPVI) and raw Pairwise Variability Index (rPVI) were developed by Low *et al* [6] and are used for rhythmic analyses of vocalic and intervocalic durations, respectively. Later on, Delwo[15] who was concerned about speech rhythm being susceptible to variable speech rate, devised a variation coefficient for ΔC called the Varco C. However, the PVIs are the most widely used rhythm metrics and the classification of rhythm in languages is based on the following pattern. Table 1 shows the classification of rhythm based on PVIs.

In the Indian scenario, there have been attempts at examining rhythm manifestations [7,8,13] and also attempts at development of speech rhythm in young children. Savithri *et al* [7] investigated the rhythm of two etymologically unrelated languages - Hindi (Indo-Aryan) and Kannada (Dravidian) and reported Hindi to be a syllable-timed language (high rPVI and low nPVI) and Kannada to be a mora-timed language (low rPVI and nPVI). Further, Savithri *et al* [8] investigated speech rhythm in 12 Indian languages and reported mora-timed rhythm in Assamese, Punjabi, Telugu, Marathi and Oriya; syllable-timed rhythm in Bengali, Kodava, Malayalam, Tamil and Kashmiri; but, Rajasthani and Gujarathi could not be classified. Savithri *et al* [13] investigated development of speech rhythm in Kannada speaking children in the age range of 3-12 years using durational PVIs of vocalic and intervocalic intervals. The results indicated a developmental trend in speech rhythm. An increasing trend, though not linearly, in the PVIs with age has been noted.

It must be remembered that, even though PVIs were widely used to calculate durational difference between successive vocalic and intervocalic intervals, it is a completely general concept. The application can be extended to other phonetic units such as feet (*sing.* 'foot'- one stressed syllable followed by at least one unstressed syllable), fundamental frequency (F0) and intensity (I0). *For example,* [22] criticised the excessive calculation of PVIs on duration citing that rhythm of a complex signal such as speech cannot be solely reliant on duration alone. In their study, they explored rhythm in Estonian, English, Mexican and Castillian Spanish (two dialects of Spanish) at the level of the foot, their speculation being that, rhythm at the level of foot and syllables may be coexisting yet independent, thus raising the possibility of rhythm being an orthogonal dimension. Normalised syllable and foot PVIs were computed for all languages. In terms of nSPVI (normalised syllable PVI), English stood apart with the highest value of 59.06, while Mexican Spanish had the highest nFPVI (normalised Foot PVI) of 44.47. Results revealed that while there was a stark difference between English and Estonian in terms of nSPVI (English-59.06 (1.41), Estonian-43.93 (1.29)), the nFPVI for the two were nearly the same [English-33.91 (3.65), Estonian-33.92 (0.83). This could give rise to the possibility of the two languages having different yet same rhythm. The authors hence speculated that timing at the level of syllable and foot could vary orthogonally which contradicts with the uni-dimensional concept of rhythm.

Also, literature documenting rhythm research is filled with inconsistencies. While [4] conclude that %V and ΔC are the best metrics to classify rhythm of a language, [12] showed that the PVIs offered different classification for the same language. *For example*, PVIs classified Thai to have stress-timed rhythm while %V and ΔC classified it to have syllable-timed rhythm. While %V-ΔC classify Japanese distinctly as having mora-timed rhythm, PVI scores show Japanese as being syllable-timed. It has also been shown that durational metrics are vulnerable to method of elicitation of speech samples (for *e.g.,* spontaneous speech, read text and read sentences) and kind of material used [23]. These discrepancies might lead one contemplate the

role of intensity (I0) and fundamental frequency (F0) which also contribute to perception of prosodic prominence. Hence, analyzing duration alone as a measure of rhythm may not truly reflect rhythm of a language.

Certain languages are known to use F0 and I0 in varying extent to produce lexical stress and sentence accent. In a study on acoustic and perceptual correlates of stress in Kannada language, [24] reported lengthened word duration, shortening of stressed word, prolongation of the stressed word, extra effort in production, pause before or after stressed word, raising or falling intonation in stressed word and articulation as perceptual correlates and lengthening of duration, increase in fundamental frequency and intensity as acoustic correlates. Thus, changes in duration, pitch and loudness were observed to be major cues for perception of stress. In another study, [25] investigated relative importance of F0, intensity and duration in the identification of word stress in Kannada language. The results indicated that increments in duration were a major cue, followed by increments in F0 and intensity. Likewise, [26] studied acoustic correlates of stress in WH and Y-N interrogatives in Kannada and found that F0, intensity and duration played an important role in stress perception. A study by [27], on stress perception in normals and patients with cerebro-vascular accidents also revealed similar findings although duration seemed to the most important cue. That, the role of markers of prosodic prominences such as F0 and intensity need to be investigated to advance our understanding of rhythm has been emphasized by [28, 29, 30, 31].

Since prominence is a central concept in the definition of rhythm, and as F0 serves as a powerful cue in the production of prominent syllables, it needs to be investigated in order to advance our understanding of rhythm [9]. In this context, the present study uses fundamental frequency (F0) and intensity (I0) to measure PVIs in typically developing Kannada speaking children in the age range of 3-4 years. The results of the current study are compared with a parallel study on rhythm development in 3-4 year old children that considered duration as the identifying parameter of rhythm [13]. As the latter study reported significant gender difference, and as it is known that girls perform better than boys in almost all aspects of speech and language [21], the data of the present study were also compared between boys and girls to evaluate for the same.

2. METHOD

2.1 Material

Simple picture naming cards from the fluency test developed by [10] was used to elicit five minute speech sample.

2.2 Participants

Thirty native Kannada speaking, typically developing children in the age range of 3-4 years (15 girls and 15 boys) participated in the study. All participants were screened informally to rule out any deficits in oral mechanism and function, speech, language, and hearing.

2.3 Procedure

A five-minute speech sample of each child was elicited. The children were tested individually and were instructed to see the pictures carefully and speak about them. Prompting was used at times when the child did not respond.

2.4 Instrumentation

The speech samples were audio-recorded using Olympus Digital Voice Recorder at a sampling frequency of 44,100 Hz. The audio recorder comprised of two internal 90 degree directional stereo condenser microphones. The speech samples were transferred onto the computer memory and zoomed using the PRAAT 5.1.14 software [11].

2.5 Analyses

The maximum fundamental frequency (F0) and intensity (I0) for each vocalic and intervocalic interval were extracted and noted using the Excel sheet of Microsoft. These data were used to calculate pair-wise variability index (PVI). Figure 1 illustrates the maximum F0 and I0 measurement at vocalic (V) and intervocalic (IV) segments.

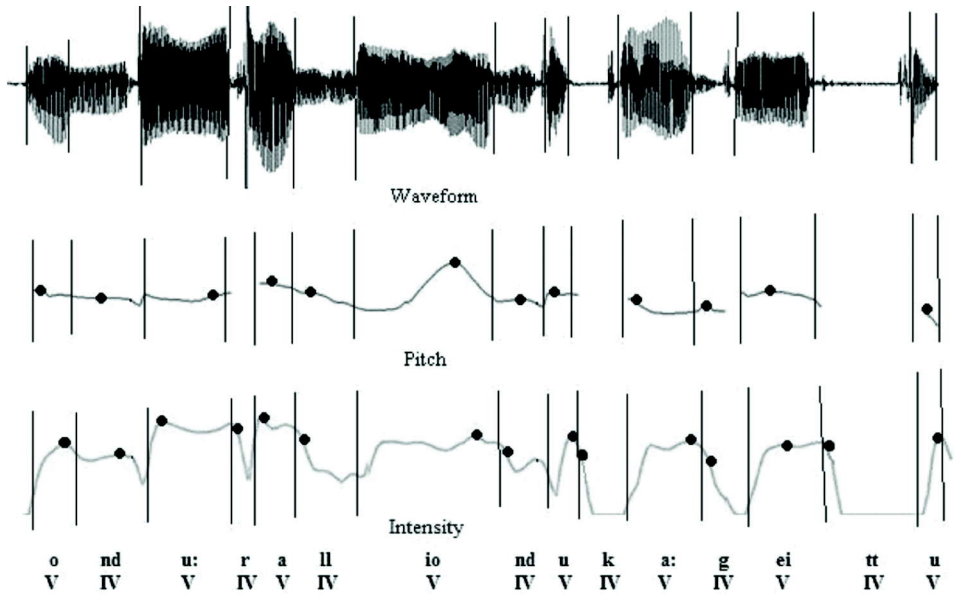

Fig. 1. Illustration of Frequency (F0) or pitch and intensity (I0) measurement of vocalic (V) and intervocalic (IV) segments in the sentence [ondu:ralli ondu ka:ge ittu].

On obtaining the maximum F0 and I0 measures, the difference between each successive vocalic and intervocalic segments was calculated and averaged to obtain PVIs. Pairwise Va-riability Index [12] was used as a measure of rhythm. PVIs were calculated using the formulae given by Grabe and Low (2000) as follows:

$$PVI = \left[\sum_{k=1}^{m-1} \left|\frac{f_k - f_{k+1}}{(f_k + f_{k+1})/2}\right| /(m-1)\right] \quad (1)$$

and

$$PVI = \left[\sum_{k=1}^{m-1} \left|\frac{i_k - i_{k+1}}{(i_k + i_{k+1})/2}\right| /(m-1)\right] \quad (2)$$

where 'm' is the number of vocalic/ intervocalic intervals and 'f' and 'i' are frequency and intensity, respectively at the kth interval.

3. RESULTS

3.1 PVIs for F0

The vocalic PVI ranged between 0.021 to 0.082 with a mean of 0.062 and the intervocalic PVI ranged from 0.036 to 0.165 with a mean of 0.095. The results showed intervocalic PVIs to be higher than vocalic PVIs thereby reflecting syllable-timed rhythm type. Table 2 shows PVIs of all thirty participants (15 boys and 15

girls) of age 3-4 years. Figure 2 shows mean PVIs for F0 in 3-4 years old boys and girls. Girls had higher F0PVIs compared to boys. Vocalic and intervocalic F0 PVI variations were greater in girls compared to boys. Intervocalic F0 PVIs were greater than vocalic F0 PVIs

Table 2. Vocalic PVIs and Intervocalic PVIs for F0

Sl.No.	Vocalic PVI		Intervocalic PVI	
	Boys	Girls	Boys	Girls
1.	0.056	0.072	0.076	0.106
2.	0.055	0.112	0.093	0.165
3.	0.045	0.061	0.077	0.143
4.	0.050	0.066	0.082	0.071
5.	0.039	0.068	0.087	0.102
6.	0.082	0.069	0.157	0.100
7.	0.070	0.056	0.080	0.111
8.	0.055	0.058	0.098	0.124
9.	0.050	0.057	0.091	0.064
10.	0.057	0.040	0.077	0.036
11.	0.068	0.048	0.119	0.081
12.	0.045	0.062	0.065	0.091
13.	0.021	0.080	0.055	0.131
14.	0.045	0.067	0.091	0.107
15.	0.036	0.072	0.066	0.125
Avg.	0.05	0.066	0.088	0.104
SD	0.014	0.065	0.024	0.102

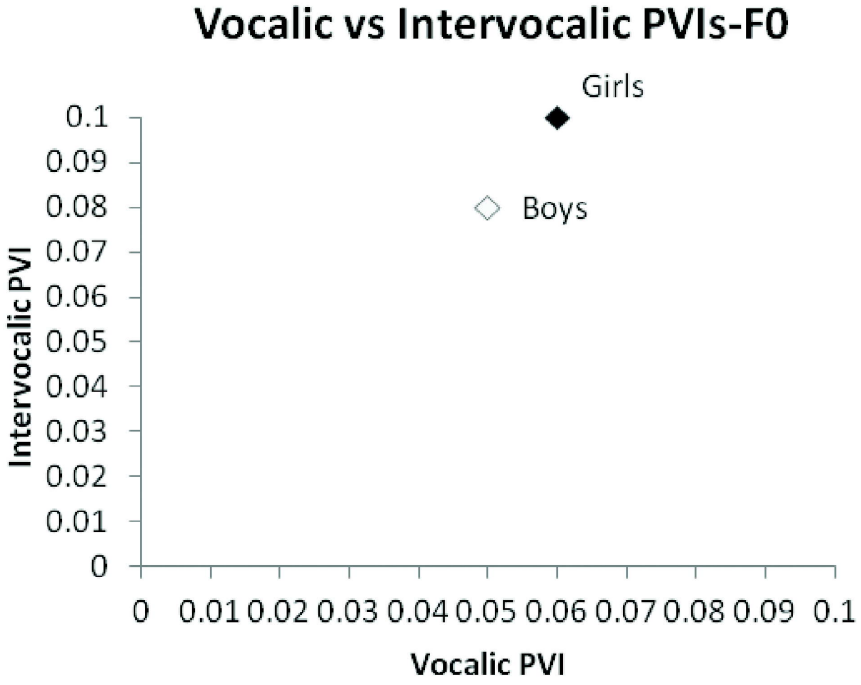

Fig. 2. Mean Vocalic and Intervocalic PVI for F0 in boys and girls

3.2 PVIs for I0

The vocalic PVI for I0 ranged from 0.013 to 0.033 with a mean of 0.023 and intervocalic PVI ranged from 0.018 to 0.063 with the mean of 0.04. This data revealed that both vocalic and intervocalic PVIs were low, indicating mora-timed rhythm. Table 3 shows PVIs of all 30 participants. Mean PVIs in 3-4 years old boys and girls is represented in figure 3. Girls had higher I0PVIs compared to boys. Vocalic and intervocalic 0 PVI variations were greater in girls compared to boys. Intervocalic I0 PVIs were greater than vocalic I0 PVIs.

3.3 Comparison between PVIs of F0 and I0

Results of Mixed ANOVA showed main effect of parameters {vocalic PVIs [$F(1,25) = 263.687$; $p< 0.05$] intervocalic PVIs [$F (1, 25) = 79.744$; $p<0.05$]}.Main effect of gender was also observed for vocalic [$F(1,25) = 10.199$; $p<0.05$] and intervocalic PVI [$F (1,25) =6.897$; $p<0.05$]. Results also revealed interaction effect for F0 on vocalic PVI {vocalic PVI * gender [$F (1,25) = 9.488$; $P< 0.05$} and no interaction effect for I0 { PVI * gender [$F (1,25) = 2.364$; $P> 0.05$}. Results indicated significantly higher intervocalic PVI compared to vocalic PVI. Also girls had significantly higher vocalic and intervocalic PVIs compared to boys.

Spoken Kannada language inherently is said to be of mora-timed rhythm as judged by [7]. In the literature, it has been reported that PVI(IV) < PVI(V) based on duration as a parameter. However, the opposite trend is seen, *i.e.*, PVI(IV)>PVI(V) when F0 and I0 are used as parameters to measure rhythm.

Table 3. Vocalic PVIs and Intervocalic PVIs for I0

Sl.No.	Vocalic PVI		Intervocalic PVI	
	Boys	Girls	Boys	Girls
1.	0.021	0.030	0.029	0.038
2.	0.031	0.031	0.041	0.039
3.	0.023	0.019	0.035	0.031
4.	0.015	0.023	0.033	0.029
5.	0.013	0.027	0.018	0.026
6.	0.020	0.033	0.030	0.041
7.	0.026	0.021	0.035	0.035
8.	0.014	0.027	0.022	0.050
9.	0.017	0.025	0.027	0.054
10.	0.027	0.020	0.045	0.049
11.	0.027	0.019	0.058	0.04
12.	0.021	0.023	0.059	0.048
13.	0.019	0.024	0.053	0.048
14.	0.031	0.021	0.049	0.037
15.	0.023	0.024	0.063	0.054
Avg.	0.022	0.0249	0.037	0.042
SD	0.006	0.025	0.014	0.041

4. DISCUSSION

The results of the present study reflected several salient findings. First, with respect to PVI for F0, it was observed that children used syllable-timed rhythm. Rhythm class hypothesis [2], states that a language can be classified to have stress-timed rhythm, when PVIs are high, mora-timed when PVIs are low, and syllable-timed when intervocalic PVI is high , vocalic PVI is low. On an NPVI-vocalic/intervocalic plane, data

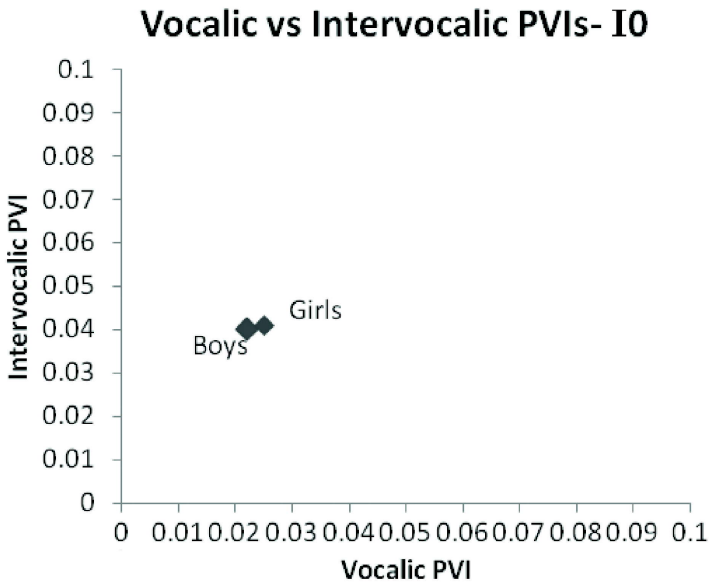

Fig. 3. Mean Vocalic and Intervocalic PVI for I0 in boys and girls

points falling close to 1 were considered to reflect high PVIs, while those falling less than 0.5 were considered to reflect low PVIs.

As the children showed relatively higher intervocalic PVI as compared to vocalic PVI, we can assume that, according to F0, the children had syllable-timed rhythm.

Second, as regards to I0, mora-timed rhythm was used. Previous study [13] based on duration parameter reported low vocalic and intervocalic PVIs in 3-4 year old children which indicated mora-timed rhythm. The vocalic PVI ranged between 0.087 to 0.322 with a mean of 0.164 and the intervocalic PVI (IV PVI) ranged from 0.087 to 0.287 with a mean of 0.163. Therefore, there was a variation in the results when measured by different parameters. This can be because when we are measuring PVIs using F0 or I0 or duration (D0), we compute the relative measure of that parameter. When we compare relative measures of F0, I0 and D0, F0 shows the greatest amount of variation. As a result, PVIs for F0s showed syllable timed rhythm and PVI for I0 and D0 showed mora-timed rhythm.

Third, the study also revealed gender effect for PVI for F0 and I0 where, girls had higher PVIs than boys for both the parameters. This could be attributed to the use of better intonation patterns by girls than boys. As we calculate the difference between each successive vocalic and intervocalic segment to obtain PVIs, a wider difference yielded higher PVIs. Figure 4 illustrates the VPVIs for F0 in boys and girls.

Comparison of VPVIs in boys and girls showed that scattering of PVIs on F0 was wider in boys compared to girls indicating high variations in the usage of F0 within boys. Results of the study [17] in boys and girls (average age in boys = 12.11, average age in girls = 13.0) also indicated higher SD on F0 in boys (43.8) compared to girls (16.1) in a reading task and counting task (boys = 39.8; girls = 19.6).

Fourth, PVIs for F0 was significantly higher compared to those for I0. Fant [16] opined that contrastive to large changes in F0 in connected speech, human speech covers an intensity range of 30 dB. Vowel that carry main stress have a sound pressure level of approximately 65 dB at one meter conversational difference and the unvoiced consonants are on an average 20 dB weaker. However, the natural range of variation for non-nasal voiced sounds produced by average male subjects is around 60-240 Hz. Females on an average have one octave higher fundamental pitch. In case of children, the individual spread is even large. It has been showed that spectrum envelopes fell at an approximate rate of 12 dB/octave and that the rate of fall at higher pitch ranges is greater for lower voice effort because of less abrupt transitions from closed to open

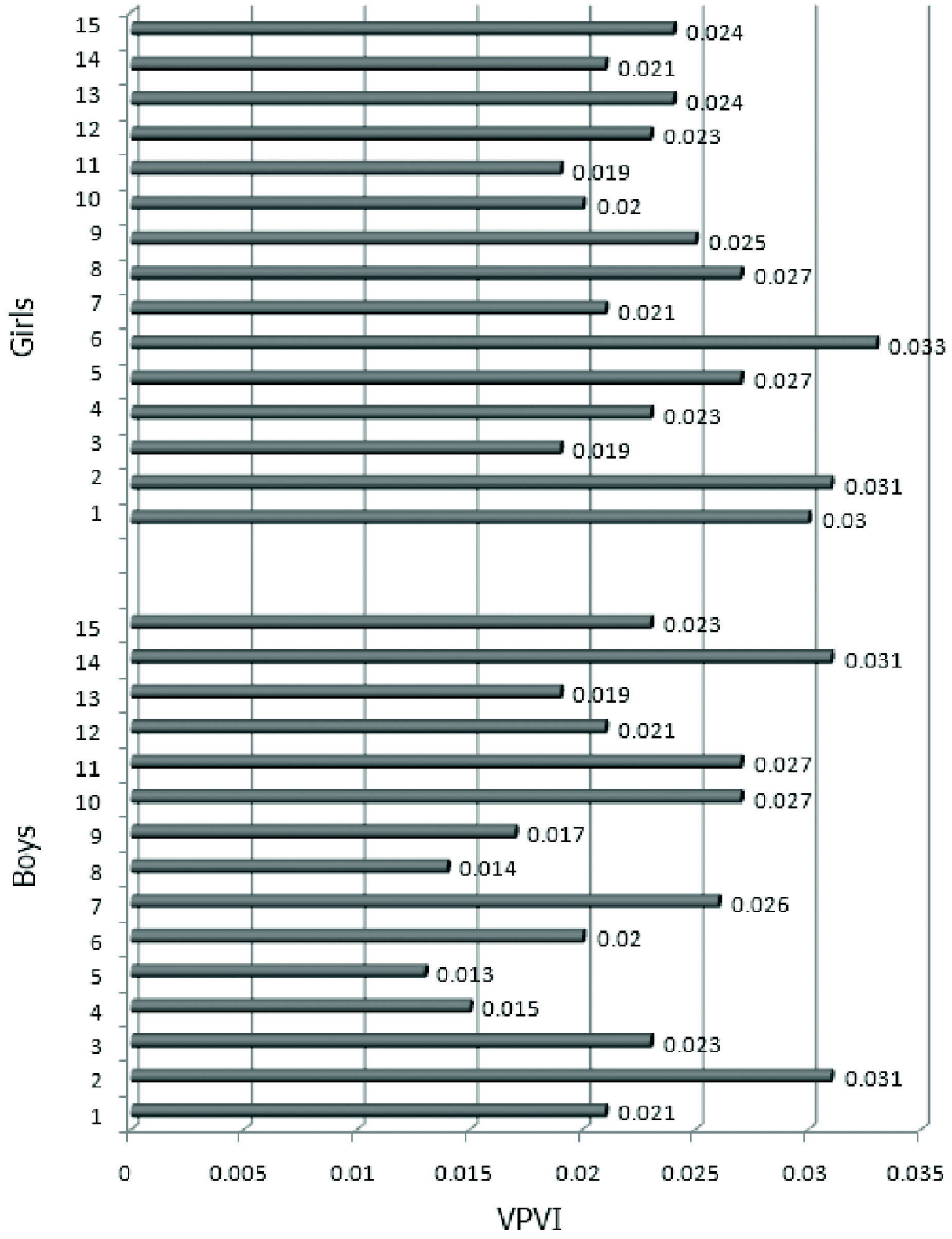

Fig. 4. Individual data VPVIs for F0

phase and vice versa. "As a rule of thumb, a change of voice level at constant pitch which causes the level of the first formant to increase 10 db will cause an increase of 4 dB in the level of voice fundamental. Similar relations hold from the shift from a medium to a low voice effort" [16].

The results of the present study were compared with those of the study by Savithri and colleagues [13] on PVIs for duration. It was observed that PVIs on duration were significantly higher than those on F0 and I0. Results of study by Nataraja and Savithri [18] indicate that the F0 range in speech was 304 Hz (adult females) and intensity range was 22 dB. Compared to duration, F0 and intensity do not change much. Pepiot[19] reported an F0 range of 90 Hz and 41 Hz, respectively in adult female and male American English speakers and an F0 range of 74 Hz in females and 40 Hz in male French speakers. A longitudinal study [20] on children aged between 8-11 years old reported that the 8-, 9- 10- and 11- year olds exhibited an F0 range of 204-270 Hz, 198-264 Hz, 208-259 Hz and 195-259 Hz respectively. Also, while calculating nPVIs in duration, the difference between successive intervals roughly equalled the average of two successive intervals, thereby yielding higher nPVIs, which was unlikely in case of F0 and I0.

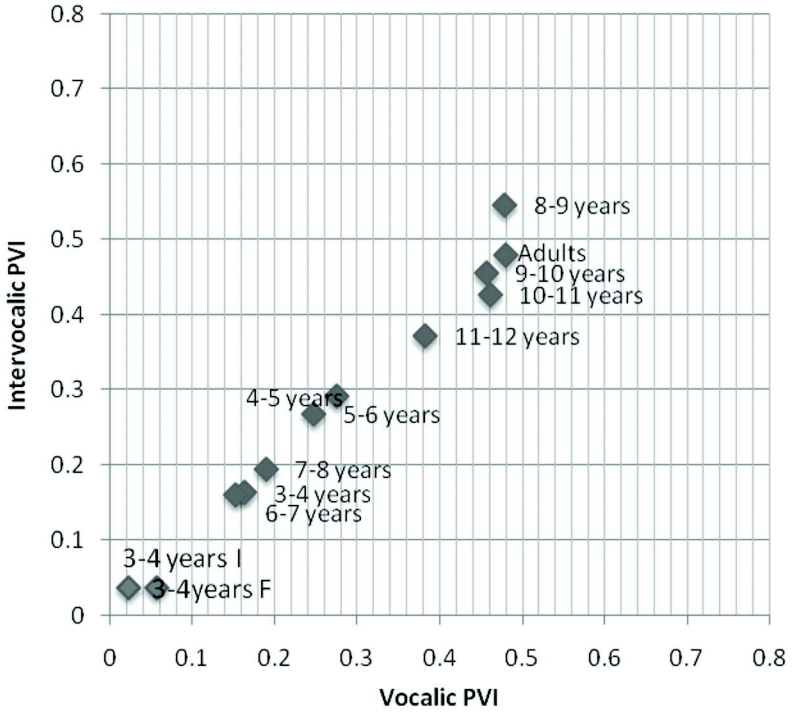

Fig. 5. PVIs for duration in children (blue colour) and adults speaking Kannada and PVI for F0 and I0 (red colour).

Results of study by Savithri and colleagues[7] in adults speaking Kannada revealed higher vocalic PVI compared to intervocalic PVI. However, in the present study the intervocalic PVI was higher than vocalic PVI for F0 and I0. Figure 5 shows a comparison of the result of the present study with that of Savithri and colleagues [7].

The study also sought to compare the findings with those of Grabe and Low[12] in order to study the rhythm of Kannada in relation to other languages of the world. These authors [12] extracted vocalic and intervocalic PVIs of different languages of the world and reported stress-timed rhythm in British English, German, Dutch and Thai; syllable-timed rhythm in Tamil, Spanish, French, and Singapore English; mora-timed rhythm in Japanese and mixed rhythm in Polish and Catalan. Figure 6 was prepared based on the data given by Grabe and Low [12] in their article on Durational Variability in Speech and the Rhythm Class Hypothesis and the data of the present study along with that by Savithri and colleagues [13] on

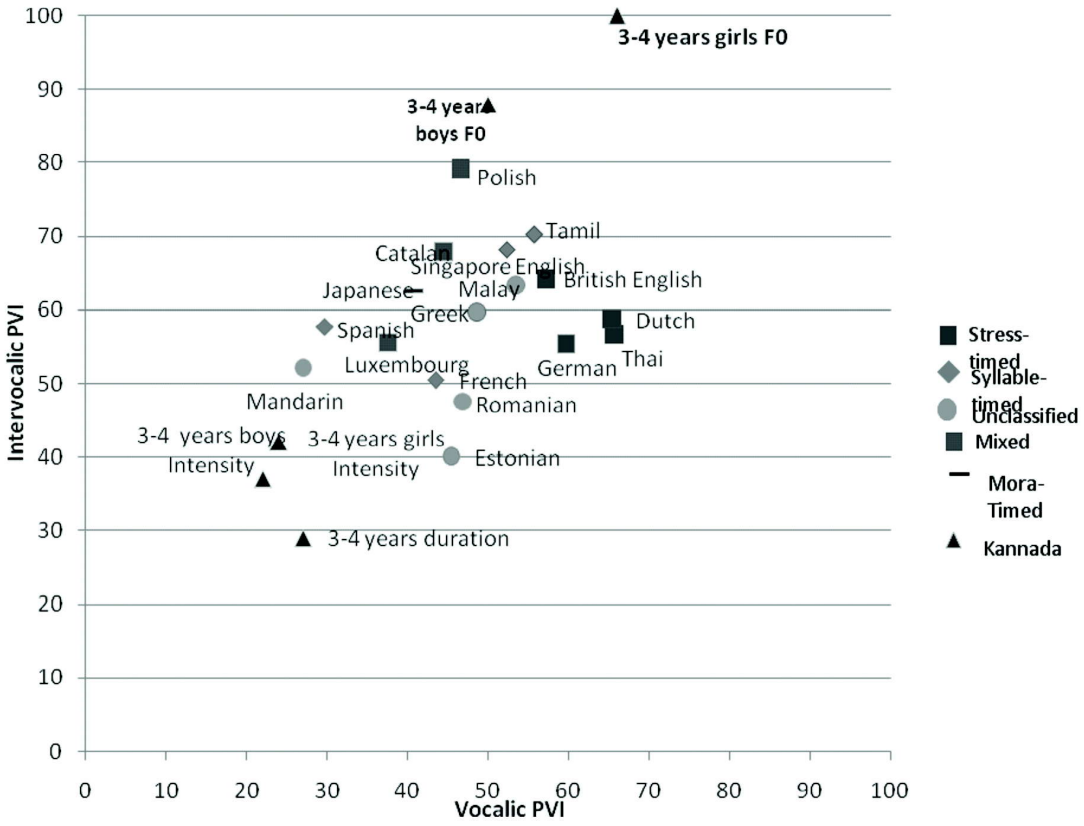

Fig. 6. Vocalic and intervocalic PVIs in Kannada (F0, I0) and other languages (duration) of the world.

duration was inserted on the figure for a comparison. In the present study and in the study by Savithri and colleagues [13] all normalized values varied in the range of 0 to 1. Hence all these normalized values were multiplied by 1000 for the sake of comparison.

Overall, we can observe that the children in the current study did exhibit certain characteristics of syllable-timed rhythm. By default, it is reported that children in the earlier stages of language acquisition produce speech in a syllable-timed rhythm irrespective of the inherent rhythm of the native language [14].

That the possibility of a language having two kinds of rhythm based on the parameter under question (for e.g., whether duration or foot) has been described by [22]. The current study targets a fairly young age group of 3-4 years. The fact that they are still in developmetal stages of speech production could have resulted in subtle variation in rhythm realisation. Whether Kannada truly exhibits two kinds of rhythm needs to be examined only after studying the same in older children and adults.

5. CONCLUSION

The present study investigated the type of speech rhythm in normally developing Kannada speaking children aged 3-4years by measuring vocalic and intervocalic frequency and intensities. PVIs measured using F0 revealed syllable-timed rhythm and PVIs with respect to I0 indicated the use of mora-timed rhythm. However, study by Savithri and col-leagues [13] reported that children used mora-timed rhythm at the age of 3-4years. These measures are helpful in correlating the speech rhythm types in different languages and in different age groups.

6. ACKNOWLEDGEMENT

We express our heartfelt gratitude to the tiny tots who were a part of the study. We also express our thankfulness to the Department of Science and Technology, India for providing us the grants for the study. Thanks are also due to Dr. Vasanthalakshmi M.S., Reader in Biostatistics, AISH, Mysore for assisting with the statistical analyses of the data.

7. REFERENCES

[1] K.A. BEAUCHAINE, M.P. GORGA, J.K. REILAND and L.L. LARSON, 1986. Application of ABRs to the hearing aid selection process: Preliminary data. *Journal of Speech and Hearing Research*, **29**(1),120-128.

[1] K.L. PIKE, 1945. *The intonation of American English*. Ann Arbor: The University of Michigan Press

[2] D. ABERCROMBIE, 1967. *Elements of General Phonetics*. Chicago: Aldine Pub. Co.

[3] P. ROACH, 1982. *On the distinction between 'Stress-timed' and 'Syllable-timed' languages*. In D. Crystal, 1986. Linguistic Controversies, 73-79. London: Arnold.

[4] F. RAMUS, M. NESPOR and J. MEHLER, 1999. Correlates of Linguistic Rhythm in the Speech Signal. *Cognition,* **72**, 1-28.

[5] E. L. LOW. 1998. *Prosodic Prominence in Singapore English*. Unpublished Ph.D.Thesis, University of Cambridge.

[6] E.L. LOW, E. GRABE and F. NOLAN, 2000. Quantitative Characterizations of Speech Rhythm 'Syllable timing' in Singapore English. *Lang Speech,* **43**, 377 - 401.

[7] S.R. SAVITHRI, M.JAYARAM, D. KEDARNATH and S. GOSWAMI, 2006. Speech rhythm in Indo Aryan and Dravidian languages. *Proceedings of the International Symposium on Frontiers of Research on Speech and Music*, 31-35.

[8] S.R. SAVITHRI, S. GOSWAMI, MAHARANI and D. DEEPA, 2007. *Speech Rhythm in Indian Languages. Project report funded by AIISH, Mysore.*

[9] J.K. KOHLER, 2009. Rhythm in Speech and Language. A New Research Paradigm. *Phonetica*. **66**, 29-45.

[10] M.N. NAGAPOORNIMA, 1990. Dysfluencies in children: 3-4 years. M. Jayaram, & S.R. Savithri (Eds.). Dissertation abstract: Research at AIISH, **2**, 171-173.

[11] BOERSMA and WEENIK, 2009. *PRAAT 5.1.14 software.*

[12] E. GRABE and E.L. LOW, 2002. *Durational variability in speech and the rhythm class hypothesis*. In Gussenhoven, C., & Warner, N., 2006. Lab Phon, **7**, 515-546. Berlin:Mouton de Gruyter.

[13] S.R. SAVITHRI and N. SREEDEVI, 2012. Development of speech Rhythm in Kannada Speaking Children. *Report of DST funded Project.*

[14] G.D. ALLEN and S. HAWKINS, 1980. The development of phonological rhythm. In M.A. Redford (Ed.). *The Handbook of Speech Production*, 158-172. West Sussex: Wiley Blackwell.

[15] V. Dellwo, 2006. Rhythm and Speech Rate: A Variation Coefficient for deltaC. In P. I.S. Karnowski (Ed.). *Language and language-processing,* 231-241. Frankfurt am Main: Peter Lang.

[16] G. Fant, 1960. *Acoustic theory of speech production: with calculations based on X-ray studies of Russian articulations*. Mouton & Company.

[17] E.C. WILLIS and D.T. KENNY, 2007. *Variability in speaking fundamental frequency in the adolescent voice*. The Inaugural International Conference on Music Communication Science 5-7. Retrieved from http://www.academia.edu/3485951/Variability_in_speaking_fundamental_frequency_in_the_adolescent_voice.

[18] N.P. NATARAJA and S.R. SAVITHRI, 1990. Voice evaluation: Clinical aspects. *Indian Speech, Language and Hearing Tests - The ISHA Battery,* 176-195.

[19] E. PEPIOT, 2014. Male and female speech: a study of mean f0, f0 range, phonation type and speech rate in Parisian French and American English speakers. *Speech Prosody*, **7**, 305-330.

[20] S. BENNET, 1983. A 3-year longitudinal study of school-aged children's fundamental fre-quencies. *Journal of Speech and Hearing Research,* **26**, 137-142.

[21] M. ERIKSSON, P. B. MARSCHIK and T. TULVISTE, 2011. Differences between girl and boys in emerging language skills: Evidence from 10 language communities, *Br J Dev Psychol,* **30**, 326-343.

[22] F. NOLAN and E. ASU, 2009. T he pairwise variability index and coexisting rhythms in language. *Phonetica*, **66**(1-2), 64-77.

[23] A. ARVANITI, T. ROSS and N. FERJAN (2008). On the reliability of rhythm metrics. *J. Acoust. Soc. Am,* 124, 2495.

[24] S.R. SAVITHRI, 1987. Some acoustic & perceptual cues of stress in Kannada. *Journal of Acoustic Society of India*, 209.

[25] S.R. SAVITHRI, 1999. Perception of word stress. *Proceedings of the Fifth Technical Sessions of the MIRC of the Acoustical Society of America*, 110-113.

[26] R. MANJULA, 1997. Aspects of Kannada Intonation in Discourse. An Unpublished Thesis submitted to the University of Mysore, Mysore.

[27] J.K. KOHLER, 2009. Rhythm in Speech and Language. A New Research Paradigm. *Phonetica*, **66,** 29-45.

[28] A. ARVANITI, 2009. Rhythm, Timing and the Timing of Rhythm. Phonetica, **66**, 46-63.

[29] R. CUMMING, 2011. The effect of dynamic fundamental frequency on the perception of duration. *Journal of Phonetics,* **39**, 375-38.

[30] R. FUCHS, 2014. Towards a perceptual model of speech rhythm: Integrating the influence of f0 on perceived duration. *Proceedings from Interspeech 2014, Singapore,* 1949-1953.

Journal of Acoustical Society of India : Vol. 43, No. 2, 2016 (pp. 73-81)

Detection of speech stimuli at cortex in children using hearing Aids: An evidence from speech evoked cortical potential

Prawin Kumar, C Geetha and Y N Manjunatha
Department of Audiology, All India Institute of Speech and Hearing, Manasagangothri, Mysore-570006
e-mail: prawin_audio@rediffmail.com

[Received: 22-04-2016; Revised: 07-06-2016; Accepted: 10-08-2016]

ABSTRACT

The present study aimed was to check speech evoked cortical potentials latencies and amplitude measures at different intensity levels (75 dB SPL, 65 dB SPL& 55 dB SPL) using different speech stimuli (/m/, /t/ & /g/) in children using hearing aids and compared with age-matched typically developing children. There were 44 children (17 children with normal hearing and 27 children using hearing aids) in the age range of 2 to 5 years participated in the present study. The recorded cortical auditory evoked potentials were marked for the two major peaks (P1 & N2) for each stimulus and at each intensity level in both the groups. The results showed that in general the mean latency measures at each speech stimulus and at each intensity level were prolonged (poorer) in children using hearing aids in comparison to typically developing children. Similarly, mean amplitude measures at each intensity for each speech stimulus was reduced (poorer) in children using hearing aids compared to typically developing children. However, there were no statistically significant effects of speech stimuli (/m/, /t/, & /g/) noticed at each intensity level for both latency as well as amplitude measures (P1 & N2) in children using hearing aids and typically developing children. In addition, it was observed in the present study that the CAEP responses were reduced in hearing aid users as the intensity level was reduced from 75 to 55 dB SPL. To conclude, hearing aid users showed prolonged latency and reduced amplitude for wave P1 and N2 in comparison to age-matched typically developing children. The above finding probably indicates that hearing aid users are able to detect the different speech stimulus at each intensity level which indicates stimulation of different frequency regions at cortex.

1. INTRODUCTION

It is always challenging to assess hearing aid effectiveness using behavioural techniques in very young children. There was considerable interest in using the auditory brainstem response (ABR) to assess hearing aid effectiveness during the 1980[1, 2]. However, there were some issues with the use of ABR to assess utility of amplification devices. Stimuli like clicks and brief tone bursts suitable for ABR recordings may be too brief to activate a hearing aid's compression circuitry[3]. A hearing aid activated by the stimuli typically used for ABR testing may perform differently than it would for a speech stimulus. Cortical auditory evoked potentials are an emerging tool for hearing aid fitting evaluation in young children who cannot provide reliable behavioural feedback[4]. They suggested that the presence or absence of CAEPs can provide some indication of the audibility of a speech sound for children with sensorineural hearing loss. Findings have

been suggested that the CAEPs can be used as an objective tool to evaluate whether amplified speech sounds are audible in infants and children fitted with hearing aids[5-7]. It was concluded that the presence or absence of CAEP responses was effective in showing whether increased sensation levels provided by amplification were sufficient to reach the auditory cortex. This was clearly apparent from the significant increase in cortical detection when comparing with unaided testing [8]. They found that the higher sensation level led to a greater number of present CAEP responses being detected. CAEPs can be elicited using both tonal and speech stimuli. Speech stimuli have better face validity for hearing aid evaluation but unfortunately are not available in most clinical evoked potential systems. CAEPs can be reliably recorded in young infants and therefore provide a useful tool for objectively evaluating hearing aid success in this population and in children who are difficult to test behaviourally[9].

Reduced auditory input early in life has an impact on the development of the central auditory functions reflected by the specific pattern of CAEPs[10]. The interaction and the combination of at least two factors, delay in maturation and deficit in central auditory system, could contribute to the pattern of result obtained in children with hearing impairment. The measurements on the cortical responses of babies with normal hearing has shown that cortical responses to /m/, /t/ and /g/ can always be detected, provided the babies are awake, alert and be physically active. The shape of the cortical responses varies markedly with age (Golding, Pearce, Seymour, Cooper, Ching, & Dillon, 2007). The detailed shape and magnitude of the cortical responses also varies from person to person, and from time to time within the same person, depending on the alertness or drowsiness of the person.

The aided CAEPs testing in hearing aid benefit assessment of children showed enhancement of the physiologic activity of the auditory cortex paralleled the enhancement in the psychophysical tests (Hassaan, 2011). It could be a solution to the difficulties encountered in the assessment of hearing aids benefit in infants and very young children. In spite of sporadic existence of literature on cortical auditory evoked potentials to measure the brain's response in hearing aid users, there is a dearth of information to highlights the hearing aid benefit using speech evoked CAEPs. Hence, present study aimed to investigate the effect of different speech stimuli (/m/, /t/ and /g/) at different intensity (75dB SPL, 65dBSPL and 55dBSPL) levels on the aided cortical auditory evoked potentials and comparison with the age-matched typically developing children.

2. METHOD

There were 44 children, out of which 17 children (8 males & 9 females) with normal hearing (control group) and 27 children (11 males & 16 females) with severe to profound sensorineural hearing impairment (experimental group) using own hearing aids in the age range of 2 to 5 years participated in the study. Experimental group were using their own hearing aids with appropriate amplification as prescribed by qualified Audiologists. Control group participants had hearing sensitivity within 15dB HL for octave frequencies between 250 and 8000Hz.They had A/As type tympanogram with reflexes present in both ears which indicated normal middle ear functioning based on Immittance evaluation. All the typically developing children had normal outer hair cell function, based on transient evoked otoacoustic emissions. Experimental group had severe-to-profound sensorineural hearing loss based on conditioned pure tone audiometry/ click evoked auditory brainstem responses, normal middle ear functioning based on Immittance evaluation, and outer hair cell dysfunction based on transient evoked otoacoustic emission. They were using their own digital BTE hearing aids and aided audiograms were well within the speech spectrum at least up to 2 kHz. All behavioural and electrophysiological testing were carried out in a well illuminated and sound treated room.

CAEPs recording were done using the HEARLab instrument, Aided Cortical Assessment (ACA) software module with default setting. The speech stimuli (/m/, /g/ and /t/) of 30 ms duration with band pass filter of 1-30 Hz at 1.1/s repetition rate used for aided CAEPs. The speech stimulus was presented using loudspeaker in sound field. The children were made to sit comfortably on a reclining chain. Silent movies and cartoons were played and visual distracters like toys, puppets were used to reduce the movement of the child and to make sure that the child is awake. The electrode sites Cz (non-inverting), upper forehead

(inverting) and mastoid (ground) were cleaned with the help of NUprep gel and the button electrodes were placed on the prepared site. The loudspeaker was placed one metre away from the subject at the level of ear at an angle of 0° azimuths. The above method was approved by the Ethical Committee of AIISH and written consents were obtained from all the participant's parents or caregiver.

The cortical potential system i.e. HEARLab used in present study judges presence or absence of cortical responses based on a derived statistical techniques i.e. Hotelling T^2 method along with p-value in a separate window on the screen. Hotelling's T^2 uses the averaged responses, which calculates the probability (p) by comparing the mean value of any linear combination of variables, which are significantly different from zero. The resultant p-value is represented graphically, which are colour coded for different speech stimuli. A p-value of less than 0.05 indicated presence of responses for each speech stimulus at each intensity level (Figure 1).

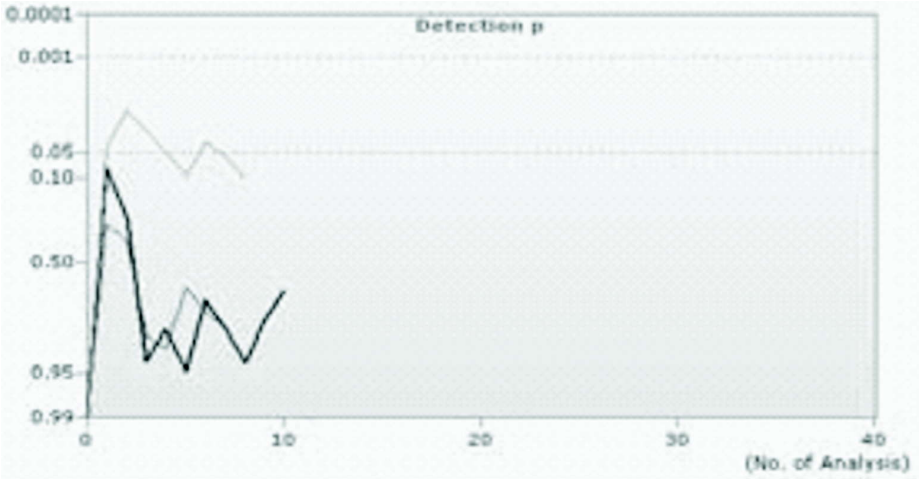

Fig. 1. Hotelling's T^2 technique for the statistical detection of the responses.

AEP responses were Statistically analyzed using SPSS (version 18). Mean and standard deviations (SD) were obtained using descriptive statistics for latencies and amplitudes of P1 and N2. Since the data was not normally distributed based on Shiparo-Wilk test, non-parametric test was performed. Non-parametric test includes Friedman test for within group comparison i.e. to compare latency as well as amplitude measures for different speech stimuli (/m/, t/ and /g/) at 75dBSPL, 65dBSPL and 55dBSPLin each group. Further, comparison between groups was done using Mann Whitney U tests for different speech stimuli at each intensity level.

3. RESULTS

The CAEPs were detected at three intensity levels and for three different speech stimuli in both the groups. In typically developing children, the detection of P1 and N2 peaks of CAEP responses were observed at each intensity for /m/, /g/ and /t/ speech stimuli i.e. 100% detection rate. However, in children with severe to profound hearing impairment using hearing aids, shows 100% detection rate at 75 dB SPL for /m/, /g/, /t/ sounds and at 65 dB SPL for /m/ and /g/ sounds only. However, the detection rate was 89% at 65 dB SPL for /t/ sound. Further, at 55 dB SPL the detection rate was 68% for /m/ sound, 54% for /g/ sound and 49% for /t/ sound in children using hearing aids. The detection rate was lowest at 55 dB SPL compared to 75 dB SPL and 65 dB SPL in hearing aid users. The mean and standard deviation (SD) of cortical potentials latency and amplitude measures at different intensity for each speech stimulus in typically developing children and children using hearing aids are mentioned in table 1 and 2 respectively.

From the table 1 and 2, it is observed that the latency of the peaks P1 and N2of cortical potentials for different speech stimuli were prolonged (poorer) in hearing aid users in comparison to typically developing

Table 1. Mean and standard deviation (SD) of latency and amplitude of P1 and N2 at 75dBSPL, 65dBSPL and 55dB SPL, for the stimuli /m/, /t/ and /g/ for the control group.

CAEP		Latency measures (millisecond)					
		75 dB SPL		65 dB SPL		55 dB SPL	
		Mean	SD	Mean	SD	Mean	SD
/m/	P1	105.93	29.94	104.03	33.22	102.70	32.42
	N2	207.86	40.79	203.32	53.28	207.55	61.25
/t/	P1	103.14	32.54	99.50	31.71	95.60	31.44
	N2	206.92	52.67	186.78	46.16	176.82	42.32
/g/	P1	94.35	28.40	95.32	29.88	90.85	22.47
	N2	204.10	44.45	187.57	46.26	188.07	52.64
		Amplitude measures (microvolt)					
/m/	P1	5.39	4.80	4.66	4.86	5.50	3.74
	N2	-7.41	4.10	-7.20	5.16	-5.22	4.58
/t/	P1	4.91	3.96	3.54	2.15	4.45	3.55
	N2	-7.50	5.04	-6.65	4.03	-4.28	5.33
/g/	P1	6.70	4.84	5.70	4.81	5.44	3.99
	N2	-5.52	4.55	-4.89	3.91	-4.60	3.05

Table 2. Mean and standard deviation of latency and amplitude of P1 and N2 at 75dBSPL, 65dBSPL and 55dB SPL, for the stimuli /m/, /t/ and /g/ for the experimental group.

CAEP		Latency measures (millisecond)					
		75 dB SPL		65 dB SPL		55 dB SPL	
		Mean	SD	Mean	SD	Mean	SD
/m/	P1	125.43	30.30	126.96	37.23	122.11	25.64
	N2	242.31	60.25	240.61	47.69	229.50	30.90
/t/	P1	127.06	39.83	123.11	28.01	122.45	25.21
	N2	244.32	59.91	237.30	50.57	206.55	37.64
/g/	P1	149.73	175.43	120.19	25.10	114.29	13.83
	N2	227.67	58.75	229.58	46.52	207.29	28.31
		Amplitude measures (microvolt)					
/m/	P1	2.93	3.59	2.13	1.86	2.44	1.06
	N2	-4.47	3.91	-4.44	3.81	-3.64	2.65
/t/	P1	2.97	2.59	2.51	2.33	1.84	2.62
	N2	-3.79	3.59	-4.65	4.41	-3.63	3.87
/g/	P1	2.96	2.17	2.77	1.68	2.07	1.51
	N2	-4.88	3.10	-3.67	2.90	-4.37	3.76

children. Similarly, amplitude of peaks P1 and N2 were reduced (poorer) in hearing aid users in comparison to typically developing children. In addition, standard deviation of latency for N2 is larger than that for the P1 in both the groups. Similar trend was observed for the amplitude in both the groups at each intensity level.

A sample waveform is mentioned in figure 2 and 3, which shows the better morphology of CAEP responses obtained from typically developing children with normal hearing in comparison to children using hearing aids at different intensity levels. In figure 2 and 3, in the left panel, the automatic detection of the presence or absence of responses is mentioned as screen shot. The different colour represents different speech stimuli i.e. red colour for /m/, green colour for /g/ and blue colour for /t/ speech sound and right hand side there are three boxes which represents presence or absence of cortical responses at different intensity levels *i.e.* 75 dB SPL, 65 dB SPL, and 55 dB SPL.

For within group comparison at each intensity level for different speech stimuli, Friedman test was done. The result shows no statistically significant differences between different speech stimuli at each intensity level i.e. at 75 dB SPL, 65 dB SPL, and 55 dB SPL for both P1 and N2 latency and amplitude measures in each group. The Friedman test indicates that in each group i.e. children with normal hearing and children using aids did not shows any effect of speech stimuli in terms of latency and amplitude measures of P1 and N2 peaks of CAEP. There were alike CAEP responses using these speech stimuli in

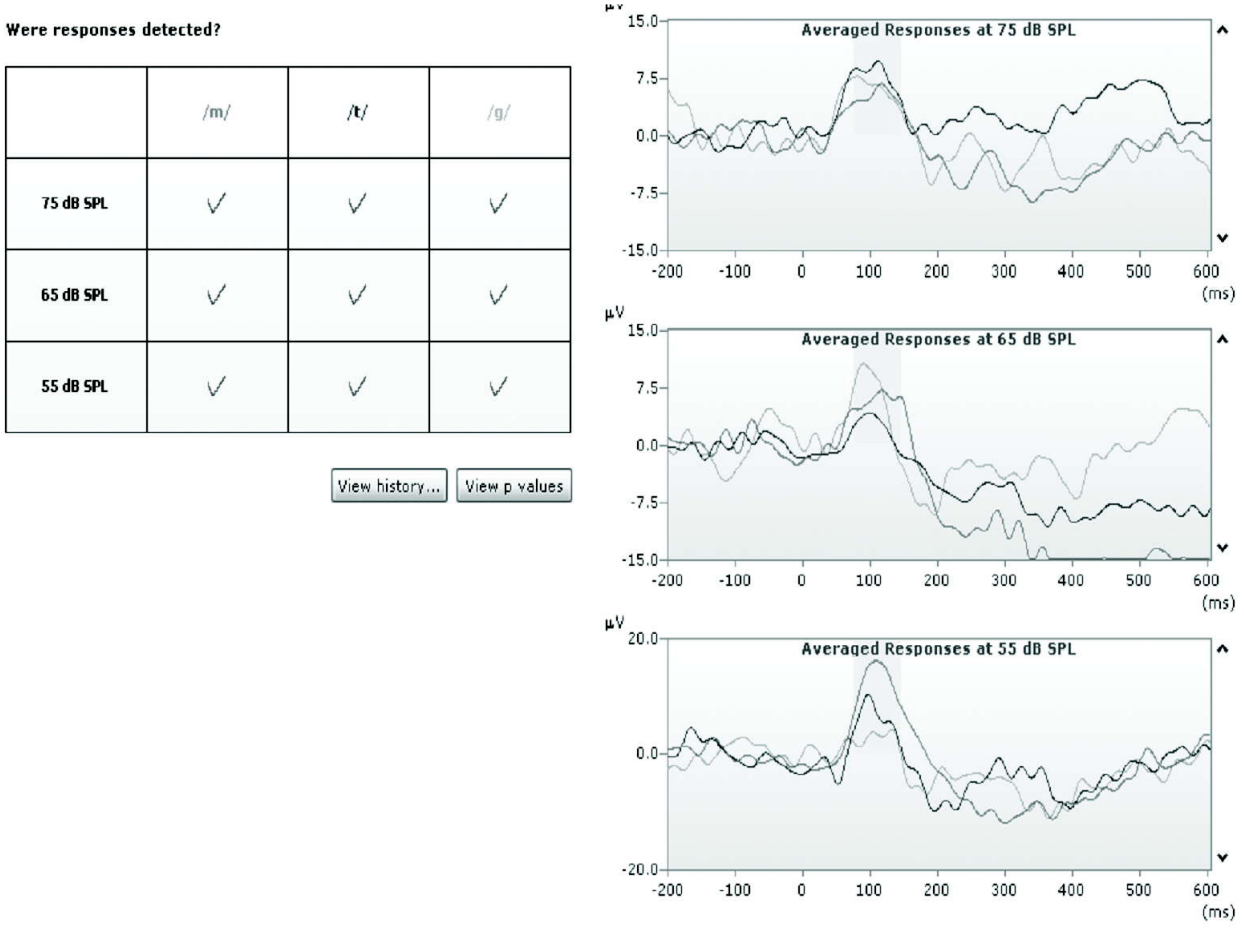

Fig. 2. A sample waveform and detection response screen of the cortical evoked potential using HEARLab system from a participant having normal hearing [Dark Gray line- /m/; Dark Black line-/g/; Light gray line-/t/ sound].

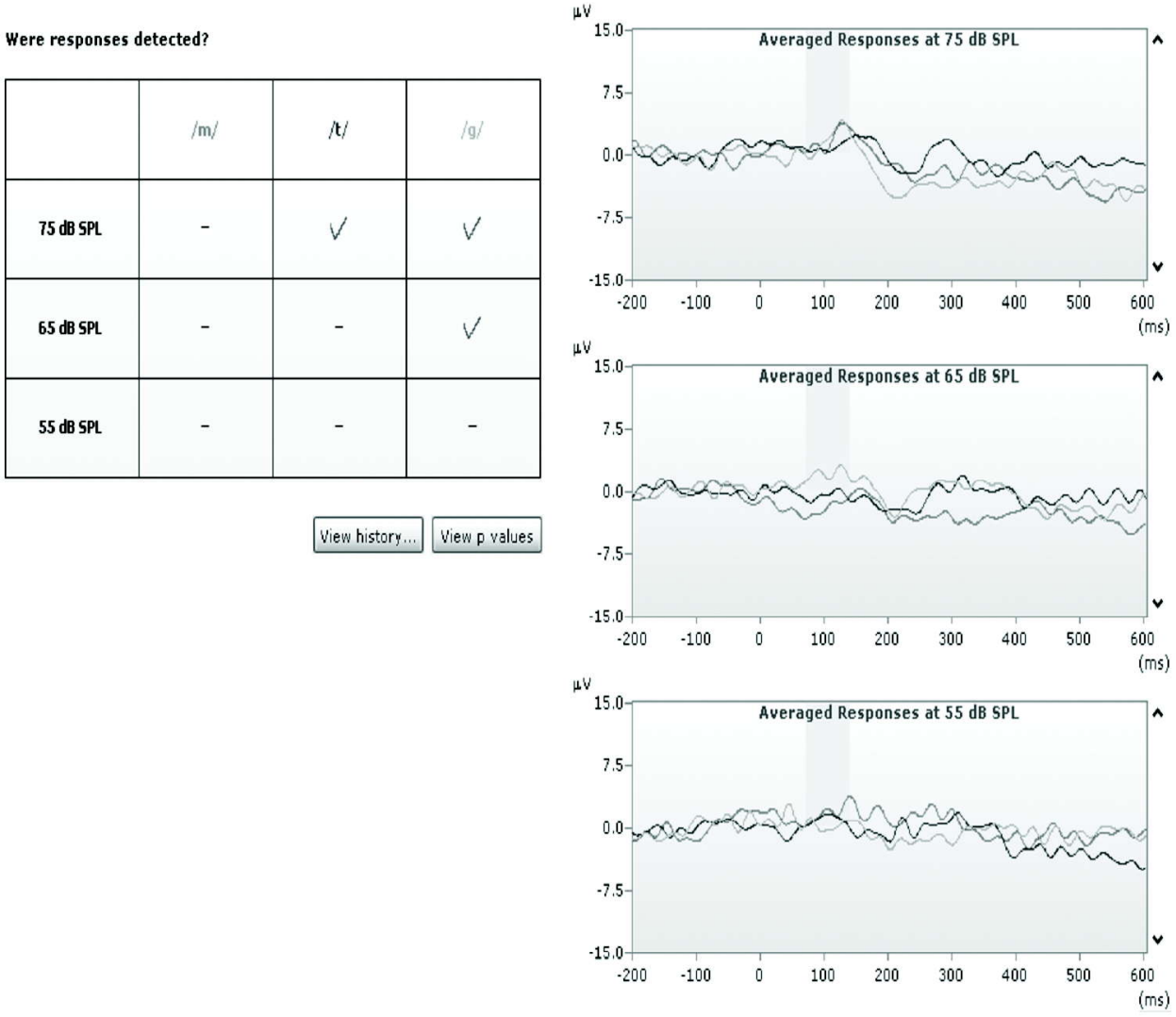

Fig. 3. A sample waveform and detection response screen of cortical aided potential using HEARLab system from a hearing aid user [Dark Gray line- /m/; Dark Black line-/g/; Light gray line-/t/ sound].

each group. However, both the groups could able to detect these different speech stimuli which represent different frequency regions at the cortical level.

Between group comparisons at each intensity level was done using Mann Whitney U test. The result shows there were statistically significant differences between two groups for latency and amplitude measures of peak P1 and N2 at 75 dB SPL except P1 amplitude of /t/ and N2 amplitude of /g/ speech sound. Similarly at 65 dB SPL, there were significant differences between two groups for both latency and amplitude measures of peak P1 and N2 except P1 latency of /m/ sound, N2 amplitude of /m/ and /t/ sound as well as P1 amplitude of /g/ sound. Further at 55 dB SPL, there were significant differences between two groups only for amplitude measures of P1 and N2 except N2 peak of /t/ and /g/ sound. The latency measures of peak P1 and N2 did not show significant differences between two groups at 55 dB SPL for any speech stimulus (Table 3).

Table 3. Comparison between control and experimental groups for latency and amplitude measures at each intensity level (Mann Whitney U test outcomes)

Intensity Levels (dB SPL)	CAEP	Speech Stimuli	Latency measures		Amplitude measures	
			/Z/	p-value	/Z/	p-value
75 dB SPL	P1	/m/	-2.74	0.00	-3.16	0.00
	N2		-2.77	0.00	-2.54	0.01
	P1	/t/	-2.16	0.03	-0.87	0.38#
	N2		-3.94	0.00	-2.58	0.01
	P1	/g/	-2.33	0.02	-2.26	0.02
	N2		-1.99	0.04	-1.82	0.06#
65 dB SPL	P1	/m/	-1.67	0.09#	-4.25	0.00
	N2		-3.35	0.00	-1.83	0.06#
	P1	/t/	-3.52	0.00	-3.42	0.00
	N2		-3.06	0.00	-0.97	0.33#
	P1	/g/	-2.60	0.00	-1.67	0.09#
	N2		-2.28	0.02	-2.07	0.03
55 dB SPL	P1	/m/	-1.11	0.26#	-3.72	0.00
	N2		-0.59	0.55#	-2.01	0.04
	P1	/t/	-1.46	0.14#	-3.26	0.00
	N2		-0.23	0.81#	-0.67	0.49#
	P1	/g/	-0.60	0.54#	-2.88	0.00
	N2		-0.14	0.88#	-1.10	0.26#

*p<0.05; #p>0.05

4. DISCUSSION

In the present study, the CAEPs were detected in all the typically developing normal hearing children at three intensity levels for the speech stimuli /m/, /t/ and /g/ and it was found that the normal hearing children obtained shorter latency, higher amplitude and better morphology as compared to their age matched children with severe to profound hearing loss who were using own digital hearing aids. The presence of CAEP responses in the children using hearing aids gives some evidence that the speech stimuli is being detected at the level of auditory cortex. In addition, findings from different studies do suggested that the cortical auditory evoked potentials can be used as an objective tool to evaluate whether amplified speech sounds are detectable at the level of auditory cortex in infants and children fitted with hearing aids [5-7].

Within group comparison, present study showed that there were no significant differences across different speech stimuli at each intensity level for latencies and amplitude measures of peaks P1 and N2. The above finding is supported by a study done by Dun *et al.,* 2012 [4], tried to evaluate relationship between the sensation level of speech sounds and the detection sensitivity of CAEPs in infants with sensorineural hearing impairment in the age range of 8 months to 30 months. They used different speech stimuli i.e. [m], [g], and [t] using HEARLab evoked system for recording CAEP responses. The results revealed that there were no significant differences between three different speech stimuli for both amplitudes and latencies of CAEPs in these infant fitted with hearing aids. Similarly, Kumar et al., in 2015 also reported no significant difference between /m/, /g/ and /t/ (latency and amplitude) for children (5-7 years) as

well as adults (17-24 years) [13]. In contrast, Golding *et al.* (2006) [7] reported difference in CAEP responses with presentation of different speech stimuli. They reported larger amplitude and earlier latency response with /t/ sound compared to other two speech sounds *i.e.* /m/ and /g/ sound. However, Golding *et al* assessed CAEP only at 65 dB SPL while present study estimated at three different intensity levels i.e. 75 dB SPL, 65 dB SPL, and 55 dB SPL [7]. In addition, even study done by Purdy *et al* in 2004 found that the differences in amplitudes existed for the speech stimuli pair [m] & [t] and [t] & [g] in the infants using hearing aids [14]. Studies in literature do demonstrated that the aided responses for the stimuli [m] were better than for the [t] and [g] [5-7]. The reason for obtaining such results can be due to the fact that the different speech stimulus are having different frequency content in it such as speech stimulus [m] represents low frequency, [t] represents high frequency and [g] represents mid frequency syllable. Chang *et al* in 2012 found that the CAEP responses were better for the speech stimuli [t] and [g], than for [m], in the infants who were fitted with hearing aids [8]. However present study, in contrary to the above studies and in accordance with Dun *et al* 2012, observed that there was no significant effect of speech stimulus on the latency and amplitudes of CAEPs [4]. The significant differences observed for the effect of stimulus on the latency and amplitude measures at few intensity levels could be attributed as chance factors, since there was no clear trends noticed in the present study.

When comparison were done between children using hearing aids and typically developing children, hearing aid users showed prolonged latency and diminished amplitudes (poorer responses) for each speech stimulus [m, g, t] at 75 dB SPL and 65 dB SPL. However at 55 dB SPL, significant differences were only noticed in terms of amplitude measures between two groups. The latency measures of P1 and N2 were alike in both the groups at 55 dB SPL. The prolonged latency in case of children using hearing aids can be due to multiple reasons. It is suggested that the presence of CAEPs provide some indication of the audibility of a speech sound in children with sensorineural hearing loss [4]. The detection of a CAEP might provide confidence, to a degree commensurate with the detection probability, that the children is detecting that sound at the level presented.

It is also observed in present study that, for few children using hearing aids, despite being prescribed with hearing aids, the CAEP responses were absent at lower level *i.e.* at 55 dB SPL which indicate the different speech stimuli were not detected using these hearing aids at presented intensity level. However, detection ability was much better at 75 dB SPL and 65 dB SPL.As suggested the CAEPs become more detectable as the intensity level is higher and also more CAEP waveforms were detected in aided condition than in the unaided condition for the children with hearing loss [8].It could be a solution for the difficulties faced by the Audiologists in aiding the difficult to test population and the young infants. Thus, the auditory evoked potentials provide an objective measure of the brain's response to sound and can be considered as a tool that can be used to assess aided as well as unaided auditory function in children with hearing impairment.

The larger standard deviations in the latencies and amplitudes of the P1 and N2 can be due to age differences and the maturational factors of the children since the CAEPs are greatly affected by age and maturation. Presence of peak P1 and N2 for any of these stimuli is considered as the stimulus is being coded in the auditory cortex. When the peaks were observed for /m/, /t/ and /g/, it can be said that, the low, mid and high frequency information have been coded in the auditory cortex. In those cases where there is no cortical response, there is a need to pay attention to such children. Though the hearing aids were prescribed with standardized prescriptive formulas, it is not an indication that the child is benefitting from the hearing aid. Hence, there is a need of using speech evoked CAEPs for assessing hearing aid benefit in hearing aid users.

5. CONCLUSION

The study focussed on how the CAEP responses being affected by the change in intensity for the stimuli /m/, /t/ and /g/, which constitutes different frequency regions (low, mid and high) in hearing aid users. However, there were no significant differences noticed in the present study across different speech stimuli at each intensity level in children using hearing aids. But present study showed detection of these stimuli at

each intensity level. Overall, aided CAEPs showed prolonged latencies and reduced amplitude in hearing aid users as compared to age matched normal children. This can be partially attributed to the fact that in spite of compensating hearing impairment by using hearing aids which compensate for audibility, processing deficit may be a contributing factor in children with hearing impairment.

6. ACKNOWLEDGEMENT

Authors would like to thank Director, AIISH, Mysore for providing infrastructure to carry out present study. Authors also thank HOD-Audiology and all the participants for their co-operation.

7. REFERENCES

[1] K.A. BEAUCHAINE, M.P. GORGA, J.K. REILAND and L.L. LARSON, 1986. Application of ABRs to the hearing aid selection process: Preliminary data. *Journal of Speech and Hearing Research*, **29**(1),120-128.

[2] B.M. BERGMAN, K.L. BEAUCHAINE and M.P. GORGA, 1992. Application of the auditory brainstem response in pediatric audiology. *Hearing Journal*, **4**, 19-21, 24-25.

[3] E. BROWN, A.J. KLEIN and K.A. SNYDEE, 1999. Hearing aid- processed tone pips: Electroacoustic and ABR characteristics. *Journal of the American Academy ofAudiology,* **10**, 190-197.

[4] B.V. DUN, L. CARTER and H. DILLON, 2012. Sensitivity of cortical auditory evoked potential detection for hearing-impaired infants in response to short speech sounds. *Audiology Research,* **2**, e13.

[5] J.S. GRAVEL, D. KURTZBERG, D.R. STAPELLS, H.G. VAUGHAN and I.F. WALLACE, 1989. Case studies. *Seminars in Hearing,* **10**(3), 272-287.

[6] A. SHARMA, K. MARTIN, P. ROLAND, P. BAUER and M.H. SWEENEY, 2005. P1 latency as a biomarker for central auditory development in children with hearing impairment. *Journal of the American Academy of Audiology,* **16**, 564 - 573.

[7] M. GOLDING, H. DILLON, J. SEYMOUR, S. PURDY and R. KATSCH, 2006. Obligatory cortical auditory evoked potentials (CAEPs) in infants: A five year review.*National Acoustic Laboratories Research & Development Annual Report*, 2005/2006, 15-19.

[8] H.W. CHANG , H. DILLON, L. CARTER, B.V. DUN and S.T. YOUNG, 2012. The relationship between cortical auditory evoked potential (CAEP) detection and estimated audibility in infants with sensorineural hearing loss. *International Journal of Audiology.* **51**, 663-670

[9] S.C. PURDY and A.S. KELLY, 2001. Cortical auditory evoked potential testing in infants and young children. *The New Zealand Audiological Society Bulletin*, **11**(3), 16-24.

[10] A. KORAVAND, B. JUTRAS and M. LASSONDE, 2012. Cortical Auditory Evoked Potentials in Children with a Hearing Loss: A Pilot Study. *International Journal of Paediatrics*, 250-254.

[11] M. GOLDING, W. PEARCE, J. SEYMOUR, A. COOPER, T. CHING and H. DILLON, 2007. The Relationship between Obligatory Cortical Auditory Evoked Potentials (CAEPs) and Functional Measures in Young Infants. *Journal of the American Academy of Audiology,* **18**,117-125.

[12] M.R. HASSAAN, 2011. Aided evoked cortical potential: An objective validation tool for hearing aid benefit, Egyptian Journal of Ear, Nose, *Throat and Allied Sciences,* **12**, 155-161.

[13] P. KUMAR, H.K. SANJU, V. BOHRA and A. KHANNA, 2015. Speech evoked cortical potentials in normal hearing children and adults using three phonemes. *Journal of Hearing Science,* **5**, 9-15.

[14] S.C. PURDY, R. KATSCH, H. DILLON, L. STOREY, M. SHARMA and K. AGUNG, 2004. *Aided cortical auditory evoked potentials for hearing instrument evaluation in infants*. In book: A Sound Foundation through Early Amplification. Chicago, Illinois, 115-127.

Journal of Acoustical Society of India : Vol. 43, No. 2, 2016 (pp. 82-88)

Effect of ageing on encoding of speech signal in the auditory system

C. V. Vineetha[1] and Sujeet Kumar Sinha[2]
[1]Audiologist District Hospital ,Chamarajanagara
[2]Department of Audiology, All India Institute of Speech and Hearing, Manasagangothri, Mysore-570006
e-mail: cvvineetha.91@gmail.com

[Received: 21-06-2016; Revised: 30-06-2016; Accepted: 12-08-2016]

ABSTRACT

Composite signal such as speech processing in auditory system is one of the major processes that get influenced by systematic effect of ageing on auditory system. Even with the normal audiometric thresholds middle-aged listeners report difficulty in conversing in social environment which could be attributed to influence of ageing in throughout auditory system from cochlea, brainstem and at the central system. The current study aimed to investigate correlation of speech signal encoding between cochlea, brainstem and cortical auditory processing in normal young adults and middle aged individuals. Two groups of participants were included in the study. Group 1 (younger adults) included of 15 subjects (15 ears) age ranged between 18 to 30 years (Mean age range =25.7) .Group 2 (Middle aged adults) included of 15 subjects (15 ears) aged ranged between 45 to 60 years (Mean age range =54.2). All the participants in two groups had normal hearing sensitivity, normal middle ear function, no history of exposure to noise and no otological and neurological problems. All the participants first went through routine audiological evaluations such as pure tone audiometry, tympanometry & Reflexometry to confirm the candidacy. Later for all the participants in two groups, Speech evoked ABR and Speech evoked late latency responses were recorded. Results revealed a reduction in encoding of fundamental frequency and first formant frequency encoded at brainstem level in middle aged listeners compare to the younger participants. There was also a prolonged latency of P1 and increased amplitude at N1 in the auditory late latency responses in middle aged group. Thus, the results of the study indicate, that processing of composite signal such as speech get influenced by the ageing which needs routine evaluations in middle aged individuals.

1. INTRODUCTION

Hearing loss associated with older individuals in one of the main complaint among these subjects. The hearing loss associated with presbycusis often results in significant changes in speech perception abilities of individual even when these individuals do not have a significant hearing loss with increase in age. Several anatomical, physiological and cognitive changes take place in these individuals and these changes might lead to hearing and speech perception related difficulties.

Effect of age-related changes (40-50 years) in auditory system reflects changes in both peripheral and central auditory systems (Geal-Dor *et al.,* 2006). Even with the normal audiometric thresholds middle-aged listeners report difficulty in conversing in social environment (Helfer& Wilber, 1990; Dubno *et al,* 2002). Studies have reported poor performance in task such as speech perception in noise (Ewertsen & Birk-

Nielsen, 1971; Plomp & Mimpen,1979; Era *et al*., 1986; Gelfand *et al*., 1986) or in reverberation (Nabelek & Robinson, 1982), auditory event-related potential (Geal-Dor *et al*., 2006) and gap detection ability (Helfer *et al*., 2009).

Changes in cochlea with respect to age related changes is based on the anatomical changes that involves sensory, neural, metabolic and mechanical active process, which results in decreased number of OHCs, effect on afferent and efferent system, degeneration of stria vascularis, stiffness of basilar membrane, spiral ligament and other structures are responsible for loss of sensitivity respectively, which might effect on OAE generation (Scholtz *et al*., 2001). Loss of both inner and outer hair cells has been reported after the age of 45 years (Engstorm *et al*. 1987), whereas for the subjects above the age of 60 years, degeneration was widespread along all the cochlear turns (Scholtz *et al*. 2001). TEOAEs may provide information about the changes occurring in the outer hair cells in middle aged individuals and hence there is a need to study TEOAEs in middle aged individuals.

The study aimed to investigate correlation between cochlea, brainstem and cortical auditory processing in normal young adults and middle aged individuals.

2. METHOD

Two groups of participants were included in the study. Group 1 (younger adults) included of 15 subjects age ranged between 18 to 30 years (Mean age range =25.7) .Group 2 (Middle aged adults) included of 15 subjects aged ranged between 45 to 60 years (Mean age range = 54.2). All the participants had hearing sensitivity within normal limits (≤15 dBHL thresholds) at octave frequencies from 250 Hz to 8000 Hz for air conduction and from 250 Hz to 4000 Hz for bone conduction. 'A' type tympanogram on immitance evaluation and presence of both ipsilateral as well as contralateral reflexes at 500 Hz, 1000 Hz, 2000 Hz and 4000 Hz indicative of normal middle ear functioning. Participants didn't have any history/presence of relevant otological and neurological dysfunction and also didn't have any exposure to occupational noise and usage of ototoxic drugs. None of the participants had history/presence of systematic medical illness (Diabetes/ hypertension). All participants had presence of TEOAEs with a criteria of signal to noise ration of >6dB in baseline averaged response of TEOAES. Participants having SPIN scores of ≥60% at 0dB SNR were taken into the study. No evidences of any abnormality on click evoked auditory brainstem responses in all the participants indicative of absence of retro cochlear pathology.

2.1 Procedure

The Stimulus for Speech evoked auditory brainstem and auditory cortical response used synthesized speech syllable /da/ stimulus of 40 msec .The time domain waveform of the stimulus is depicted in the figure 1.

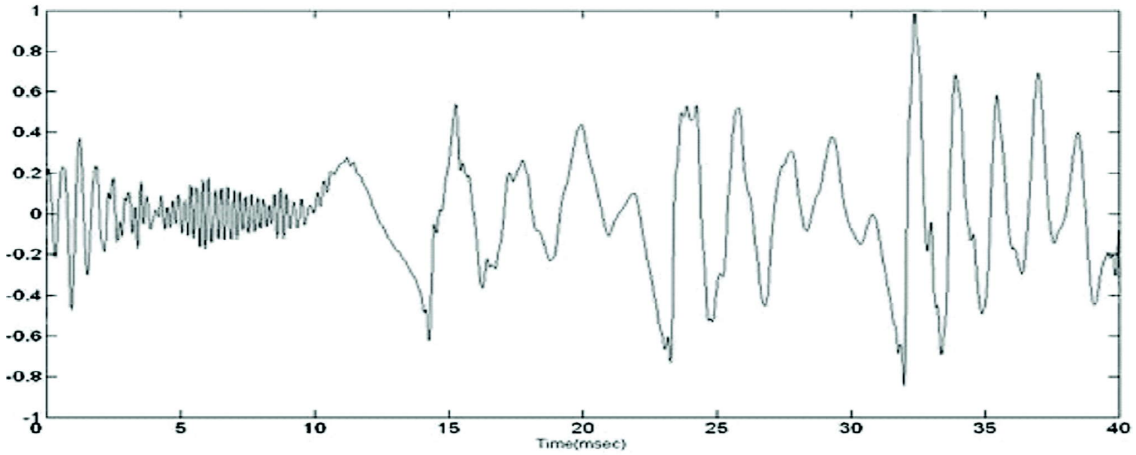

Fig. 1. Time domain waveform of the 40 ms /da/ stimulus.

The stimulus was produced using KLATT synthesizer (Klatt, 1980), which is available with BIOLOGIC NAVIGATOR PRO instrument in the BIOMARK protocol. The fundamental frequency (F0) of the/da/ stimulus with voicing beginning at 5 ms and an onset noise burst during the first 10 msec linearly rises from 103 to 125 Hz .The first formant (F1) rises from 220 to 720 Hz, while the second formant (F2) decreases from 1700 to 1240 Hz over the duration of the stimulus. The third formant (F3) falls slightly from 2580 to 2500 Hz, while the fourth (F4) and fifth formants (F5) remain constant at 3600 and 4500 Hz, respectively.

The stimulus was presented with alternating polarity, at 10.1 per second repetition rate. The responses were recorded for 70 msec stimulus period along with 10 msec pre-stimulus period. The recorded responses were then amplified one lakh times and bands pass filtered between 100 Hz to 3000 Hz. The responses were averaged for 2000 stimuli. The speech evoked auditory late latency response was recorded in single channel, using 40 msec/da/speech stimuli at 80 dBSPL. The stimulus was presented with alternating polarity, at 1.1 per second repetition rate. The responses were recorded for 433 msec stimulus period along with 30 msec pre-stimulus period. The recorded response was then amplified fifty thousand times and band pass filtered between 1 Hz to 30 Hz. The responses were averaged for 200 stimuli.

3. RESULTS

The all the participant had the presence of Speech evoked ABR and Speech evoked LLR responses. The data obtained for both the groups were subjected to statistical analysis. Following statistical analyses were carried out using SPSS Version 20.

3.1 Effect of age on speech evoked on Speech evoked ABR

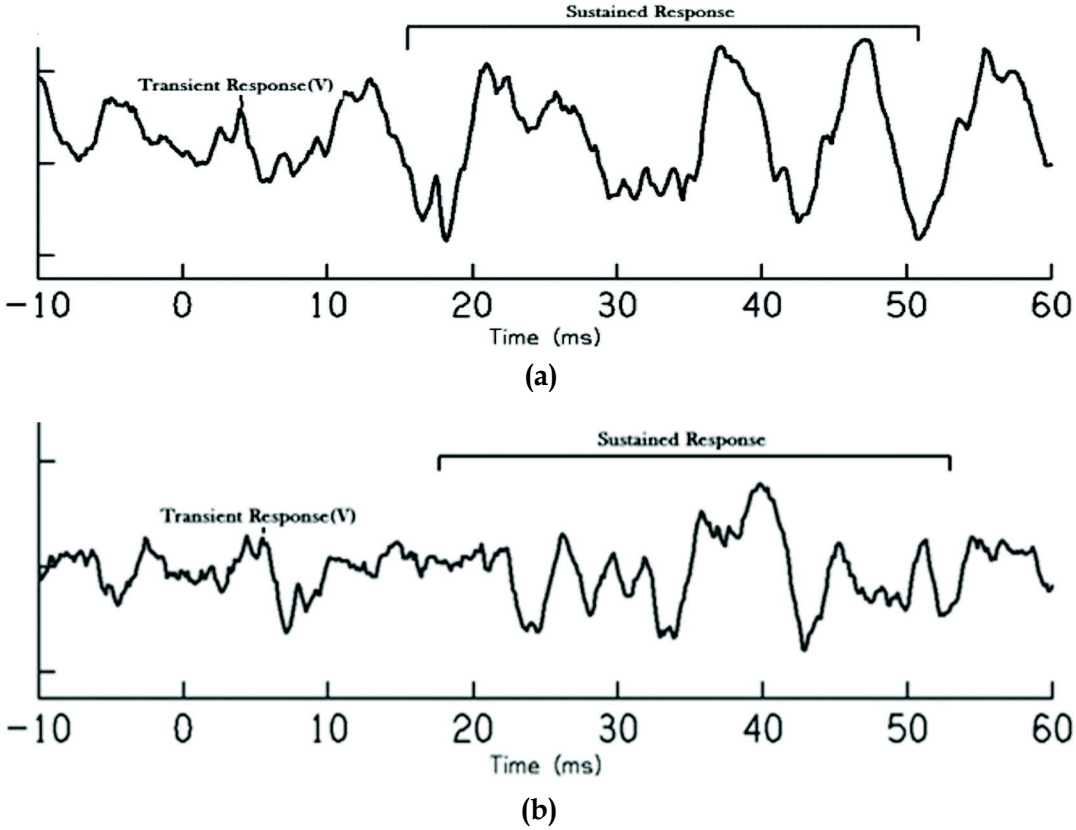

Fig. 2. The grand average wave form of Speech evoked ABR
(a) in younger adults and (b) middle aged individual

The latency of wave V was calculated for both the groups. Descriptive statistics was done to find out the mean and standard deviation for the wave V latency for both the groups. Table 3-1 shows the mean and standard deviation of wave V latency for both the groups.

It can be seen from Table-3.1 that wave V latency was more for middle aged individuals compared to the younger counterparts. As the age had an influence on wave V latency, a repeated measure ANOVA was administered to see the significant main effect of age and also significant interaction across variable on wave V latency. It revealed a no significant main effect for wave V latency [$F(1,28)=2.91, p>0.05$] but a significant main effect on groups for wave V latency [$F(1,28)=14.16$, $p<0.05$]. It also revealed significant interaction effect between wave V latency and groups [$F(1, 28)=16.265$, $p<0.05$].

Table 3.1. Latency of wave v in young and middle aged individuals in both groups.

Groups	Mean (msec)	Standard deviation
Young adults	6.806	0.4891
Middle aged	7.090	0.842

Further, Multivariate analysis of variance revealed significant main effect for wave V latency [$F(1, 28)=1.37$, $p>0.05$]. Further to understand the significant difference between two groups for wave V latency an Independent sample 't' test was done. It revealed no significant difference [$t(28)=-1.170, p>0.05$] between two groups .

Descriptive statistics was done to find out the mean and standard deviation for the fundamental frequency (F0), first formant frequency (F1) and second formant frequency (F2) for both the groups. Table-3.2 shows the mean and standard deviation of fundamental frequency (F0), first formant frequency (F1) and second formant frequency (F2) for both the groups.

Table 3.2. Mean and standard deviation of fundamental frequency (F0), first formant frequency (F1) and second formant frequency (F2).

Groups	Amplitude of F0		Amplitude of F1		Amplitude of F2	
	MEAN (μv)	SD (μv)	MEAN (μv)	SD	MEAN (μv)	SD
Young adults	11.54	0.10	1.12	0.37	0.42	0.10
Middle aged	4.85	0.11	0.51	0.31	0.10	0.11

It can be seen from Table-3.2 that the mean amplitude of fundamental frequency (F0), first formant frequency (F1) and second formant frequency (F2) higher for the younger group compared to the middle aged group. As the age had an influence on F0,F1 and F2 amplitude, a Repeated measure ANOVA was administered to see the significant main effect of age and also significant interaction F0,F1 and F2 amplitude and groups. It revealed a significant main effect of age on amplitude of sustained responses [$F(2,56)=81.943, p<0.001$] and a significant main effect of group of amplitude of sustained portion [$F(1,28)=18.618, p<0.000$]. However, It did not reveal any significant between amplitude of F0, F1 and F2 and groups [$F(2,56)=14.039, p<0.001$].

Multivariate analysis of variance was done to see the age effect on amplitude of F0,F1 and F2 amplitude. It revealed significant main effect of age on F0 [$F(1,28)=15.521, p<0.001$]. MANOVA also revealed significant main effect of age on F1 amplitude [$F(1,28)=28.816, p<0.001$] . However, no significant main effect of age on F2 amplitude [$F(1,28)=2.348$, $p>0.05$].

Further to understand the significant difference between two groups for F0, F1 and F2 amplitude, an Independent sample 't' test was done. It revealed significant difference between two groups for F0

[t(28)=3.940, p<0.001], F1 [t(28)=5.368, p<0.001], and but failed to show a significance difference for F2 formant frequency. [t(28)=1.532, p>0.05] between the two groups.

3.2 Effect of age on speech evoked on Speech evoked LLR

Long latency response (LLR) for speech stimulus such as /da/ were present in all the individuals in both groups .Latency and amplitude of P1,N1 and P2 peaks were calculated for both groups. The following graph 4.9 and 4.10 represents the Speech evoked ABR waveform containing both the transient and sustained response in younger and middle aged adults respectively.

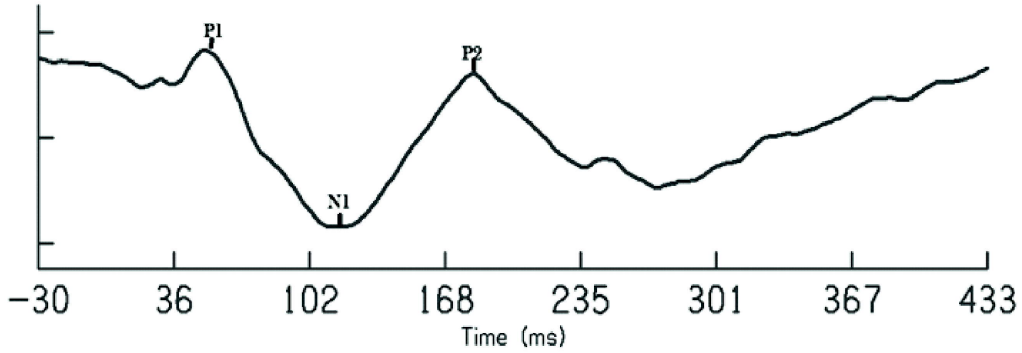

Fig. 3. Grand average waveform of Speech evoked LLR in younger adults.

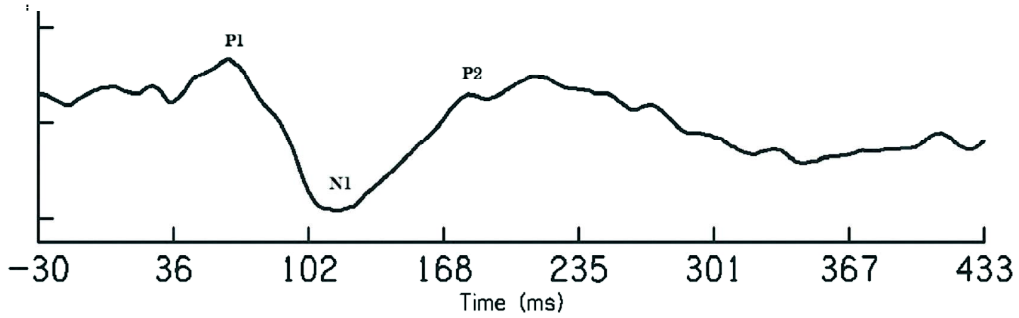

Fig. 4. Grand average waveform of Speech evoked LLR in middle aged group.

Effect of age on latency and amplitude of P1,N1 and P2 peaks

Descriptive statistics was done to find out the mean and standard deviation for the P1, N1 and P2 latencies for both the groups. Table-3.3 shows the mean and standard deviation P1, N1 and P2 latencies for both the groups.

It can be seen from Table-3.3 that middle-aged individuals have prolonged latency compared to the younger individual at all the peaks. As the age had an influence on latency of P1, N1 and P2, a Repeated

Table 3.3. Mean and standard deviation of Latency of P1, N1 and P2 in both groups.

Groups	Latency of P1		Latency of N1		Latency of P2	
	MEAN (ms)	SD (μv)	MEAN (ms)	SD	MEAN (ms)	SD
Young adults	52.9	9.81	108.26	23.64	170.04	36.68
Middle aged	66.02	8.91	121.4	12.95	187.74	22.32

measure ANOVA with group as between subject factor was administered to see the significant main effect of age and also significant interaction between latency of P1, N1 and P2 and groups. It revealed significant main effect of age on LLR latency of [F (1, 28) =1296.017, $p<0.001$], and a significant main effect of age on the groups [F(1,28)=5.644, $p<0.05$]. However, failed to show any significant interaction between group and the LLR latency [F (1, 28) =3.861, $p>0.05$].

Since the groups showed a main effect on latency of P1, N1 and P2, Multivariate analysis of variance was done to see the age effect on latency of P1, N1 and P2. MANOVA revealed significant main effect of age on P1 latency [F (1, 28) =14.533, $p<0.05$]. However did not show any significant main effect of age on N1 latency [F(1,28)=3.589, $p>0.05$], and P2 peaks [F(1,28)=2.529, $p>0.05$].

Additional to understand the significant difference between two groups for latency of P1, N1 and P2 Independent sample't' test was done. It revealed significant difference for P1 latency [t(28)=3.812, $p<0.05$] and no significance for N1 [t(28)=1.895, $p>0.05$] and P2 [t(28)=1.590, $p>0.05$) latencies.

As the age had an influence on amplitude of P1, N1 and P2, Repeated measure ANOVA was administered to see the significant main effect of age and also significant interaction across variable on amplitude of P1, N1 and P2. It revealed significant main effect for LLR amplitude [F(1,28)=1296.017, $p<0.001$], and a significant main effect of group on LLR amplitude [F(1,28)=5.644,$p<0.05$] . However there was no significance interaction between group and the amplitude of LLR peaks [F(1,28)=3.861, $p>0.05$].

Since the groups showed a main effect on amplitude of P1, N1 and P2, Multivariate analysis of variance was done to see the age effect on amplitude of P1, N1 and P2. It revealed significant main effect of age on N1 amplitude [F(1,28)=4.808, $p<0.05$] and no significant main effect of age on amplitude of P1 and P2 peaks [F(1,28)=0.175, $p>0.05$], [F(1,28)=1.425, $p>0.05$] respectively.

4. DISCUSSION

In Speech ABR significant reduction in amplitude of F0 in middle aged could be due to the reduced phase locking ability in these individuals. This also could be due to changes in neural synchrony of the peripheral auditory nerves (Clinard *et al.* 2010).These alteration in neural synchrony may arises due to age related variation in metabolic activity of the cochlea or may be due to the reduction in number of auditory nuclei (Mills *et al.* 2006). These reduction in ability of inner hair cells may leads to the damage to synapse between inner hair cells and the auditory nerve (Moser *et al.* 2006).

LLR results conclude that normal P1 outcomes in these studies assisted as a confirmation that the auditory cortex was being adequately stimulated and indicated inadequate auditory stimulation that led to abnormal auditory central pathway maturation. Thus, from the result of the present study it can be concluded that probably P1 can be used to know the central auditory degeneration in older population. The delay in latency of P1in older participants might indicate an inadequate stimulation of the auditory cortical system in these participants and thus a significant delay in latency was obtained.

Also, the amplitude of N1 was higher in the middle aged participants compared to the younger participants. The current study is in correlation with study by Amenedo and Diaz (1999) who reported enhanced N1 peak amplitude in older adults compared to younger adults. Whereas several studies indicated the age-related differences in the waveform of auditory evoked N1 and P2 components during selective attention tasks have shown inconsistent findings. In contrast others do not find such differences (Brown *et al*. 1983; Picton *et al*. 1984; Barrett *et al*. 1987; Woods 1992; Iragui *et al*. 1993). The same inconsistency can be found concerning the P2 component. Whereas some authors found increased peak amplitudes in older adults (Anderer *et al*. 1998; Friedman *et al*. 1993; Pfefferbaum *et al*. 1984).

5. SUMMARY AND CONCLUSION

Ageing is the biological process that alters the structural and physiological process of the auditory system. This age related change represents changes in both peripheral and central auditory systems (Geal-Dor et al., 2006). The changes can be noticed at cochlea which is based on the anatomical changes that involves

sensory, neural, metabolic and mechanical active process. Similarly changes at the higher system such as brainstem and cortical structures also undergo the both structural and physiological changes that results in reduced neuronal function.

The complex stimuli such as speech stimuli reflect neural detection of transient and sustained measures of temporal cues are necessary for speech perception (Russo et al., 2004). The age related alterations are more adverse at age of above >60 years ,however these variations with the normal audio logical threshold could be noticed in middle aged adults (40-60 years),which further gets worsened above with advances in ageing.

6. REFERENCES

[1] M. GEAL-DOR, A. GOLDSTEIN, Y. KAMENIR and H. BABKOFF, 2006. The effect of aging on event-related potentials and behavioral responses: comparison of tonal, phonologic and semantic targets. *Clinical Neurophysiology,* **117**, 1974-1989.

[2] K.S. Helfer and L.A. Wilber, 1990. Hearing loss, age and speech perception in reverberation and noise. *Journal of Speech and Hearing Research*, **33**, 149-155.

[3] J.R.Dubno, A.R. Horwitz and J.B. Ahlstrom, 2002. Benefit of modulated maskers for speech recognition by younger and older adults with normal hearing. *Journal of Acoustical Society of America,* **111**, 2897-2907.

[4] H.W. Ewertsen, and H.B. Birk-Nielson, 1971. A comparative analysis of the audiovisual, auditive and visual perception of speech. *Acta Otolaryngologica,* **72**, 201-205.

[5] R. Plomp and A.M. Mimpen, 1979. Speech-reception threshold for sentences as a function of age and noise level. *Journal of the Acoustical Society of America,* **66**, 1333-1342.

[6] S.A. Gelfand, N. Piper and S. Silman 1986. Consonant recognition in quiet and in noise with aging among normal hearing listeners. *Journal of the Acoustical Society of America,* **80**, 1589-1598.

[7] P. Era, J. Jokela, Y. Qvarnberg and E. Heikkinen, 1986. Pure-tone thresholds, speech understanding, and their correlates in samples of men of different ages. *Audiology,* **25**, 338-352.

[8] A. Nabelek 1988. Identification of vowels in quiet, noise, and reverberation: Relationships with age and hearing loss. *Journal of the Acoustical Society of America*, **84**, 476-484.

[9] A.W. Scholtz, K. Kammen-jolly, E. Felder, S. Kristen, 2001. Selective aspects of human pathology in high-tone hering loss of ageing in inner ear. *Hearing Research,* **157**(1-2), 77-86.

[10] Engström, B., Hillerdal, M., Laurell, G., & Bagger-Sjöbäck, D. (1987). Selected pathological findings in the human cochlea. *Acta-otolaryngologica*, **436**, 110- 116.

[12] J.F. Willot, 1991. Central physiological correlates of ageing and presbycusis in mice. *Acta otolaryngologica,* **111**, 153-156.

[13] C.G. Clinard, K.L. Tremblay and A.R. Krishnan, 2010. Aging alters the perception and physiological representation of frequency: Evidence from human frequency following responses recordings. *Hearing research*, **264**, 48-55

[14] E. Amenedo and F. Diaz, 1998. Aging related changes in processing of non target and target stimuli during an auditory odd ball task. *Biological Psychology,* **48**, 235-267.

Journal of Acoustical Society of India : Vol. 43, No. 2, 2016 (pp. 89-96)

A comparative acoustic – Phonetics Study of Hindi

Shweta Bansal[1], S.S. Agrawal[2] and Atul Kumar[3]
[1,2]KIIT College of Engineering, Gurgaon
[3]Ansal University, Gurgaon
e-mail: bansalshwe@gmail.com

[Received: 06-05-2016; Revised: 30-06-2016; Accepted: 07-09-2016]

ABSTRACT

Accent features of an individual speaker are influenced by native accent while speaking a non-native language In this paper we present a study to compare the acoustic phonetic features of Hindi phonemes (vowels as well as consonants) spoken both by the native Hindi and Non Native speakers of Punjabi and Nepali. The study concentrates on analyzing the differences in various acoustic parameters such as nasality, formant frequency and spectral characteristics of the speech sounds when they are pronounced by the Non Native Speakers compared to Native speakers. A phonetically rich data base of 150 sentences was created from a corpus of 50,000 words spoken by 10 male and 10 female speakers of Hindi as well as of Punjabi and Nepali. The phonemes of Hindi speech were segmented and annotated for further study. Signal processing tools such as PRAAT and Cool Edit were used to analyze the Acoustic characteristics of phonemic segments. The result shows that there is a significant influence of one's Native language as observed in the spectral details and also through perception of these sounds. Some sounds are influenced more significantly compared to other sounds. The results may play an important role in spoken language identification and speech recognition in multi lingual context.

1. INTRODUCTION

Regional dialectal accent is always reflected as a speaker profile characteristic, which is one of the important features used to provide clues in the course of a forensic investigation through recorded speech. As a part of research on these characteristic features of regional dialectal accent, experiments have been conducted on the native accent of Hindi speakers as compared to the accent features of Punjabi and Nepali speakers. If recorded speech is available as evidence in the event where suspected culprits are not available, dialect accent of an individual plays an important role in the course of crime investigation.[1, 2]

The study presents:

1. Acoustic Measurement of Nasality in Hindi Punjabi and Nepali
2. Formant analysis of phonemes
3. Durational Analysis of phonemes

1.1 Gurmukhi and Devnagari Script

Gurmukhi, meaning "from the mouth of the Guru" is the most commonly used script in India for writing in Punjabi. Gurmukhi has 38 consonants, 10 vowels alphabets (Independent vowels), 9 vowel symbols (Dependent vowels), 2 symbols for nasal sounds and 1 symbol that duplicates the sound of consonants.

Whereas Devnagari script is used for writing in Nepali and Hindi. Devanagri has 65 consonants, 18 full vowel alphabets, 17 vowel symbols, 2 symbols for nasal sounds. Hindi uses only 11 vowel alphabets. In Hindi, there are thirty four consonantal syllables and thirteen vowels. Except minor differences, most of the alphabets are same in both the scripts. [3]

Table 1. Articulatory Classification of Hindi and Punjabi Consonants

Articulatory Classification of Hindi and English Consonants

POA / MOA		Bilabials		Dentals: Labio Dentals		Dentals: Lingua Dental		Alveolar		Retroflex		Palatal/ Paleto Alveolar		Velar		Glottal	
Stop & Affricates	UvUa	p	प				त	t			ट	ʧ	च	k	क़ क		
	VoUa	b	ब ब़				द	d			ड ड़	ʤ	ज	g	ग ग़		
	UvAs		फ़				थ				ठ		छ		ख ख़		
	VoAs		भ				ध				ढ ढ़		झ		घ		
Fricative	Uv	फ़		f		θ		s	स		ष श	ʃ	श	ख़		h	ह ग
	Vo			v		ð		z				ʒ ज़		ग़			
Vowel like(Approximant)		w	व					r l	र ल		ड़ ळ	Y	य				
Nasal		m	म					n	न		ण		ञ	ŋ	ङ		

MOA=Manner of Articulation
VoUa=Voiced Unaspiration
POA=Place of Articulation

UvUa=Unvoiced Unaspirated
VoAs=Voiced Aspirated
UvAs=Unvoiced Aspirated

2. DATABASE COLLECTION

For this study we have prepared phonemically balanced Hindi text database of 50000 words. Out of these words, we have created 150 phonetically rich Hindi sentences which cover all the phonemes. These sentences have been recorded by 10 (5 males and 5 females) native Hindi and non native Punjabi and Nepali speakers each. All the speakers have educational background in the native language at least up to senior schooling. Speakers were provided with the sentences in the Hindi script and were instructed to speak in their own way of pronouncing the words. All these utterances were recorded using an electret microphone in a partially sound treated room with "PRAAT" software using sampling rate of 16 kHz/16 bit in a quite environment to avoid echo effect. The distance between lips and microphone was kept nearly 30 cm.

3. ACOUSTIC MEASUREMENT OF NASALITY IN HINDI, PUNJABI AND NEPALI

An acoustic comparison is done by measuring the vowel nasality in three languages: Hindi Punjabi and Nepali. The nasal and oral vowels of three languages are compared. The production of nasalized vowels introduces nasal resonances and anti resonances. Many acoustic parameters have been found in nasalization, including a reduction in amplitude of first formant (A1) and the difference between A1 and P0 and the difference between A1 and P1. Acoustic analysis of nasalized vowels in the frequency domain indicates the presence of extra peaks: one between the first two formants with amplitude P1 and one at lower frequencies, often below the first formant, with amplitude P0[1]. A study has been done to measure the nasality in different vowels of different languages. Equal number of nasalized and oral vowels were selected from the speech corpora uttered by the native and non native speakers. The maximum and minimum range of A1-P0 for low and mid vowels and A1-P1 for high vowels for three languages is represented in Table 2.

Table 2. Range of A1-P0 low & mid vowels, A1-P1 for High vowels

Max-Min Range of A1-P0							
		Hindi		Nepali		Punjabi	
Vowels		Oral	Nasal	Oral	Nasal	Oral	Nasal
Low	आ	2.4-10.8	1.8-13.2	6.5-13.6	4.1-8.3	9.6-18.8	3.8-12.7
Mid	ए,ऐ	22.6-27.4	10-18.6	6.2-32.5	0.8-27.4	5-12.3	3.1-9.1
	ओ	2.1-14.1	1.7-5.7	6.40-11.1	2.1-8.0	9.3-11.1	6.4-.4
Max-Min Range of A1-P1							
		Hindi		Nepali		Punjabi	
Vowels		Oral	Nasal	Oral	Nasal	Oral	Nasal
HIGH	इ,ई	27.5-41.4	19.3-30.7	17.1-35.9	18.8-30.7	32.5	20.3-30
	उ,ऊ	23.9-33.4	10.2-25.4	23.1-34.4	20.9-32.5	27.8-31.3	10.8-21.0

It has been observed that there is a wide difference in the maximum and minimum values of the A1-P1 of the Nepali language where as this difference is very small in Hindi native speakers.

In Hindi Language all vowels can be nasalized. Nasalization is indicated by either the symbol "ं" or by the symbol "ँ". The former symbol is called *bindu*("dot"), and the latter symbol is called *chandrabindu* ("moon and dot").The spectrum of the nasalized low mid vowel 'आ' /a:/ for native and nonnative speakers , is shown in figure 1, indicating A1 and P0 values in frequency domain

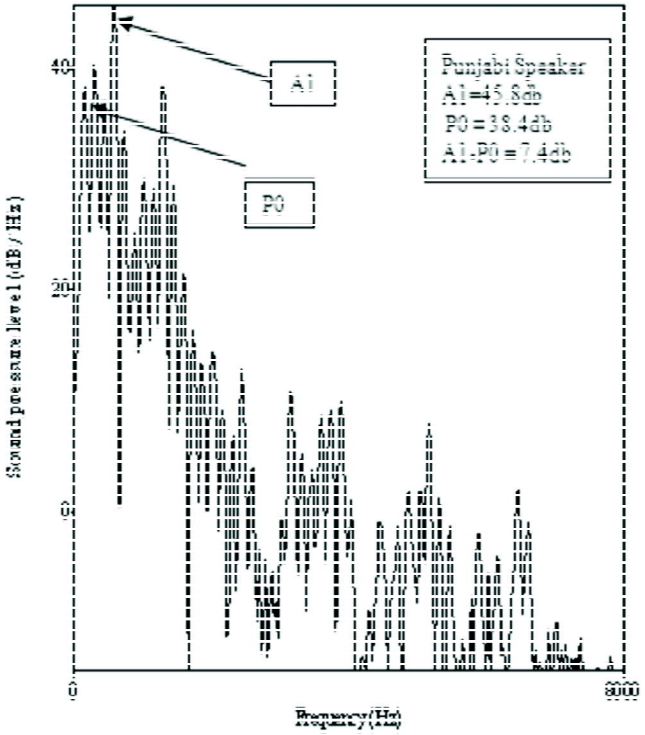

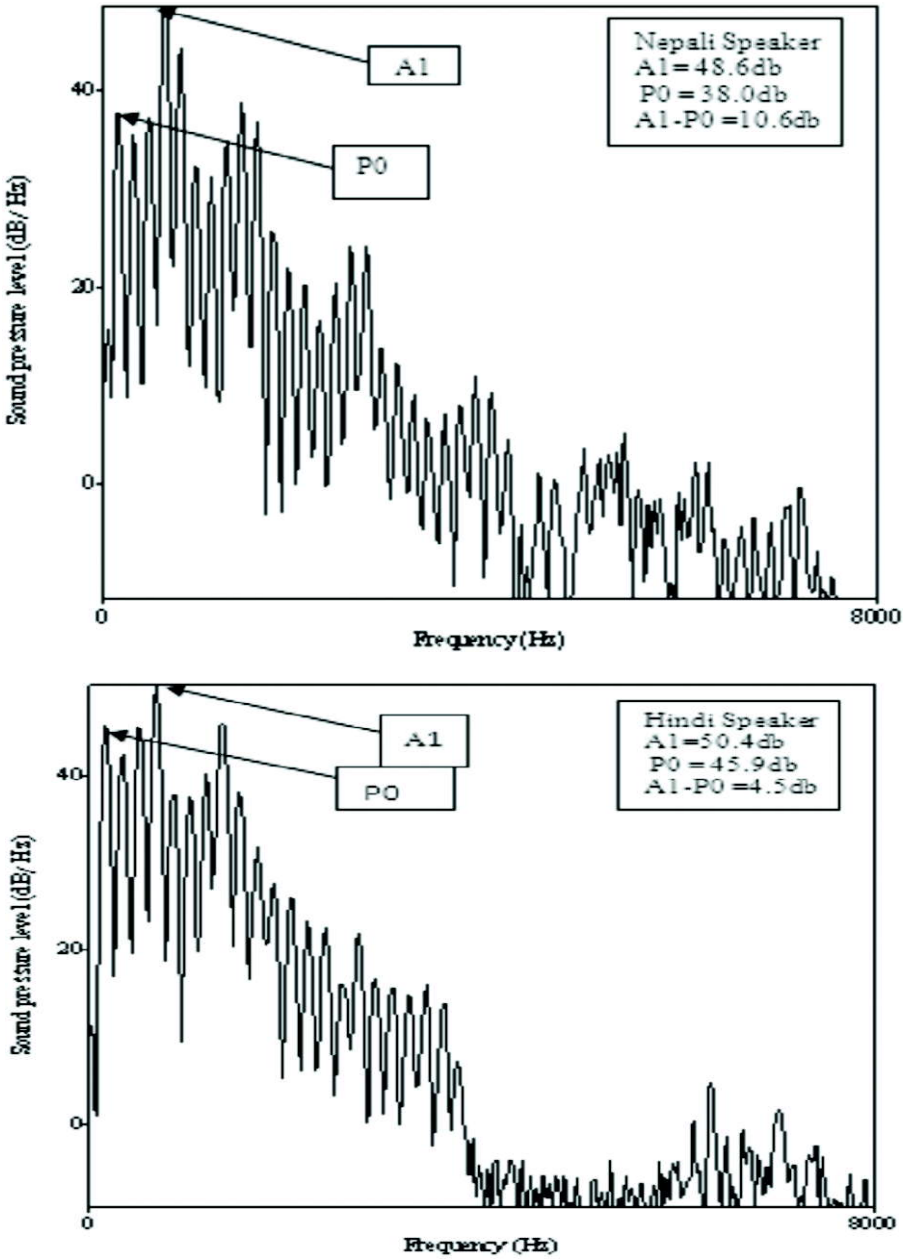

Fig. 1. Frequency spectrum of nasalized 'आ'/a:/ uttered by Punjabi, Nepali and Hindi speakers

It has been observed that presence of spectral peak in the vicinity of first formant is more in Punjabi and Hindi speakers than the Nepali speakers for the same nasalized vowel. This result shows that the nasalization in vowel 'आ'/a:/ is more in Hindi and Punjabi than Nepali. Same differences have been found for other vowels also as mentioned in the table 2.

Figure 2 represents the comparison of A1-P0 value of oral vowels of Hindi native speakers and A1-P0 values of nasalized vowels of non native speakers *i.e.* Punjabi and Nepali speakers. It has been observed that the degree of nasality is more in Punjabi native speakers for vowels /u/, /i:/ and / □:/ than the Hindi native speakers and Nepali native speakers .

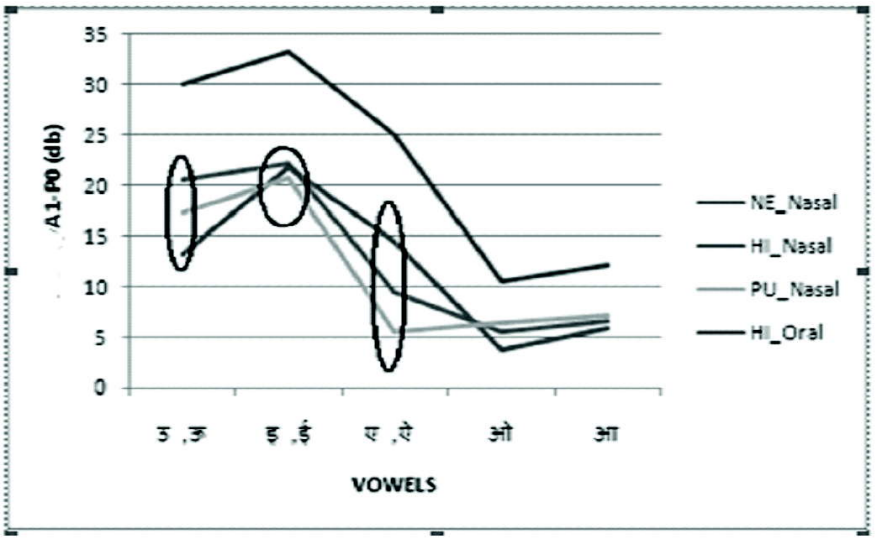

Fig. 2. Comparison of A1-P0 value of oral vowels of Hindi with A1-P0 values of nasalized vowels of Punjabi and Nepali speakers

4. FORMANT ANALYSIS

The formant frequencies are considered to be important parameters to distinguish the speech sounds. We have compared the spectrum of the perceived phonemes with the intended sounds. In several cases it has been found that the spectrum (formant frequencies and the noise spectrum) of the perceived sound is closer to the similar sound available in the vocabulary and not with the intended sound. For example 'घ' (g^h) of Hindi perceived as 'ग' (g) when it is uttered by Punjabi speakers. It has been observed that the sound of some phonemes changed according to the positions of phoneme by Punjabi speakers when they uttered Hindi. For example 'घ' is heard as 'घ' only when it is in initial position of word whereas sound as 'ग' in middle and final positions. Similarly 'भ' /b^h/ of Hindi sound as 'प' /p/ in initial position whereas 'ब'/b/ in middle and final positions. Following table 3 shows the difference in sounds uttered by native Hindi speakers and non native Punjabi speakers. The spectral comparison of these sounds are shown in figure 3 and 4.

Table 3. Difference in sounds uttered by native Hindi speakers and non native Punjabi speakers

Actual Phonemes of Hindi	Phonemes as Uttered by Punjabi Speakers
घ (g^h)	ग (g) at middle and final positions
	ब (b) at middle and final
भ (b^h)	प (p) at initial
य(j)	ज (dʒ)
ध (d^h)	ट(t)
त्र (tr)	(तर) (tər)
प्	प(p)
त्	त (t)

From the table 1 and 2, it is observed that the latency of the peaks P1 and N2 of cortical potentials for different speech stimuli were prolonged (poorer) in hearing aid users in comparison to typically developing children. Similarly, amplitude of peaks P1 and N2 were reduced (poorer) in hearing aid users in comparison to typically developing children. In addition, standard deviation of latency for N2 is larger than that for the P1 in both the groups. Similar trend was observed for the amplitude in both the groups at each intensity level.

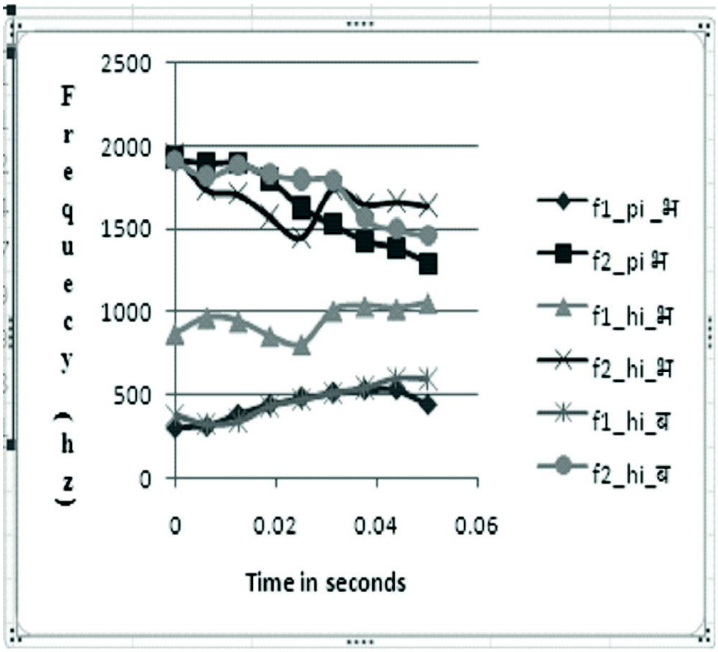

Fig. 2. Formant analysis of 'भ'/b^h/ and 'ब'/b/ for native and non native speakers

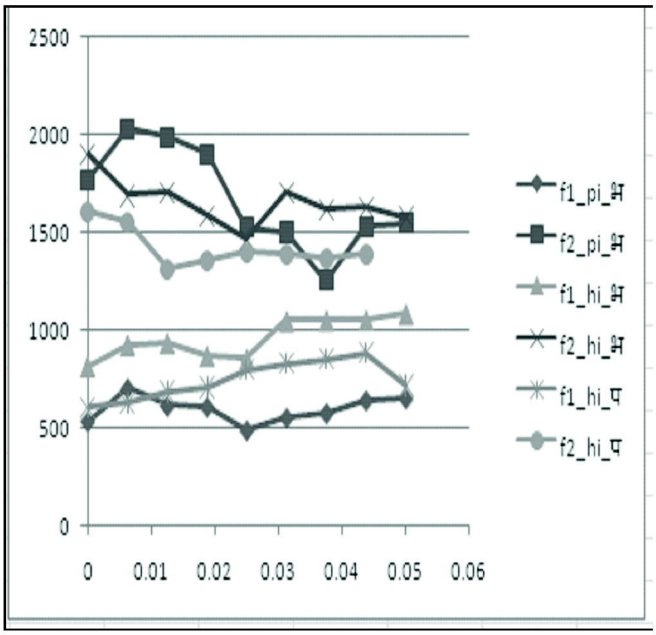

Fig. 3. Formant analysis of 'भ'/b^h/ and ''प''/p/ for native and non native speakers

In Nepali, the differences are found in following phonemes of Hindi. It is also been observed that some nasal vowels of Hindi sounds as oral vowel when uttered by Nepali speakers an viceversa. It has been found that the phonemes क्ष(k□), ष(□), श(ʃ), श्र(ʃrə) of Hindi uttered as स (sə) by Nepali speakers where as nasal vowel in Hindi like 'ऑ' uttered as 'आ' by Nepalese. These differences are represented in following table:

Table 4. Difference in Phonemes of Hindi uttered by Nepali speakers

Actual Phonemes in Hindi	Phonemes as Uttered by Nepali Speakers
क्ष(kʂ), ष(ʂ),श(ʃ),श्र(ʃrə)	स (sə)
ज (dʒ)	ज़ (z)
व (ʋ)	ब (b)
ऑ (ã:)	आ (a:)
ओ (õ)	ओ (o)

The spectral comparison of these sounds are shown in figure 4

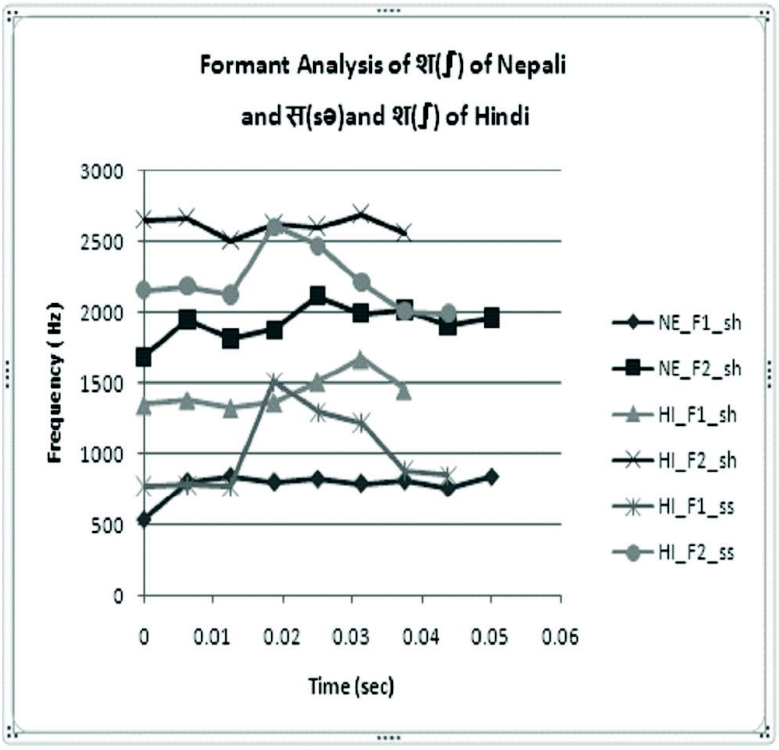

Fig. 4. Formant analysis of 'श(ʃ)' and 'स (sə)' for native and non native speakers

5. CONCLUSION

In this paper, preliminary results of a comparative acoustic-phonetics study of Hindi spoken by native and non native speakers have been presented. It has been observed that the non natives shows variations in the pronunciation of many sounds which are influenced by the sounds of their native languages. These results are important for considering development of multilingual grapheme to phoneme conversion systems. The present study is a part of the project to study the phonological and prosodic variations in Hindi that appear in different dialects and multilingual context and will provide more insight into the diachronic and synchronic variations in Hindi.

6. ACKNOWLEDGEMENT

The authors would like to acknowledge the help received from Mr. A.K. Dhamija and Mr. Gautam Kumar in recording and analysis of the speech samples collected from speakers of different linguistic backgrounds. Our special thanks to Dr. Harsh Vardhan Kamrah and Dr. Neelima Kamrah for their support and encouragement. We also thank to SAG, DRDO for providing partial financial support for conducting these studies.

7. REFERENCES

[1] M.Y. CHEN, 1997. Acoustic correlates of English and French nasalized vowels. *J. Acoust. Soc. Am.* **102**, 2360- 2370.

[2] P. BHASKARARAO, 2011. "Salient phonetic features of Indian languages in speech technology" *Sadhna* **36**(5).

[3] KARUNESH ARORA, SUNITA ARORA, SOMI RAM SINGLA and SHYAM SUNDER AGRAWAL, 2007 "SAMPA for Hindi and Punjabi based on their Acoustic and Phonetic Characteristics" OCOCOSDA, Vietnam.

[4] J.J. GUMPERZ, "Phonological differences in three Hindi dialects" Language, **34**(2), 212-224.

[5] M. OHALA, "Aspects of Hindi phonology" *Motilal Banarsidass, Delhi.*

[6] P. LADEFOGED, 1971 "Preliminaries to linguistic phonetics" *Univ. of Chicago Press, Chicago*.

[7] ADAMS, CORINNE and MUNRO, 1978 . "In search of the acoustic correlates of stress: Fundamental frequency, amplitude, and duration in the connected utterances of some native and nonnative speakers of English" *Phonetica* **35**,125-156.

[8] SUNITA ARORA, KARUNESH ARORA, AMAN SUNEJA and S.S AGRAWAL, 2003 . "Statistical Analysis of Text and Speech Sounds from Parallel Corpus of Indian Languages" OCOCOSDA, Singapore.

[9] S. ARORA, KARUNESH ARORA, AMBARISH DWIVEDI and S.S AGRAWAL, 2005 "Analysis of Intonation Patterns of Hindi Speech" OCOCOSDA, Indonesia.

[10] ARCHANA BALYAN, S.S. AGRAWAL and AMITA DEV, 2011. "Phonetic Segmentation Based on HMM of Hindi Speech" OCOCOSDA, Nepal.

[11] S.S AGRAWAL, K.K. ARORA, S. ARORA and K.K. GOSWAMI. "Phonology, Phonetics and Orthography of Hindi" in computer processing of Asian languages; Ed. S.Itahashi and Chin-yu Tseng.

[12] B TIWARI, "Hindi Bhasha ki Dhwani Samrachna (Sound Structure of Hindi Language)" *Sahkar Publications, Delhi, India*.

Journal of Acoustical Society of India : Vol. 43, No. 2, 2016 (pp. 97-107)

Benchmark for Speaker Identification using Linear Prediction Coding (LPC) on Vowels Preceding Nasal Continuants in Kannada

M.S. Arjun and R. Rajasudhakar
Department of Speech-Language Sciences, All India Institute of Speech and Hearing, Manasagangothri, Mysuru-570006, Karnataka State, India
e-mail: arjun.aiish@gmail.com

[Received: 25-04-2016; Revised: 31-05-2016; Accepted: 11-08-2016]

ABSTRACT

The aim of the present study was to obtain the percentage of speaker identification using vowels preceding nasal continuants in Kannada speaking individuals using semi-automatic method. The participants were twenty Kannada speaking adult males in the age range of 21-32 years. The material was meaningful Kannada words containing long vowels */a:/, /i:/ and /u:/* preceding nasal continuants */m/ and /n/* embedded in Kannada sentences. The participants read the material four times each under two conditions (a) live recording and (b) mobile network recording. The target words were truncated using the PRAAT software. Each vowel preceding nasal was subjected for LPC using Speech Science lab workbench for Semi-automatic speaker recognition software. The study was compared under three conditions: (a) Live vs live recording, (b) Mobile network vs mobile network recording and (c) Live vs mobile network recoding. The results of the present study indicated relatively high percent of correct speaker identification using LPC in Live vs Live and Mobile network vs Mobile network conditions compared to Live vs mobile network condition. Thus, the present study provided some proof to examine the efficiency of semi-automatic method using LPC which helps in speaker identification. The obtained results would serve as potential measure in the forensic scenario for Speaker Identification using vowel preceding nasal continuants in Kannada.

1. INTRODUCTION

Biometrics refers to the identification of a person's identity based on his/her traits. Such traits may vary from simple factors such as height, weight, build, facial complexion, colour of the eyes, etc to the more sophisticated factors such as finger prints, DNA *etc.* With the merging of telephony and computers, and with the extensive use of speech in man-machine communications, the need to recognize a person by his or her voice is constantly increasing. Applications of speaker recognition are wide ranging, including computer access control, telephone voice authentication for banking access, intelligent answering machines and law enforcement (Forensic speaker identification)[20],[29].

The crime rates of all sorts are increasing at a world-wide scale. The usage of mobile phones has increased exponentially and the rate of its usage in committing crimes has also dramatically increased. When a crime is committed through telecommunication, voice is the only evidence available for analysis. Therefore, there is a pressing need on the part of police and the magistrate for establishment of legal proof of identity from measurements of voice.

Vowels, nasals and fricatives (in decreasing order) are generally suggested for voice recognition because they are relatively easy to identify in speech signals and their spectra contain features that reliably distinguish speakers. Nasals have been of particular interest because the nasal cavities of different speakers are distinctive and not easily modified (except via colds)[34]. One study found nasal co articulation between */m/ and an* ensuing vowel to be more useful than spectra during nasals themselves [37]. The nasalization of the acoustic signal applies not only to the nasal consonants but also to certain surrounding sounds, particularly vowels. In general, vowels preceding or following nasal consonants tend to be nasalized to some degree. The present study is focused on bilabial *(/m/)* and dental *(/n/)* place of articulation and the vowels *(/a:/, /i:/ & /u:/)* preceding nasal continuants which fall under the category of structured consonants of the Kannada script. The mean percentage and standard deviation of frequency of occurrence of vowels */a/, /i/ and /u/* is 14.6% (1.3), 6.7% (0.44) and 4.3% (0.47), respectively, and frequency of occurrence of phonemes */m/ and /n/* is 2.8% (0.26) and 7.6% (0.31), respectively in Mysuru dialect of conversional Kannada [35].

In the legal process, forensic speaker identification is seeking an expert opinion to take a decision as to whether two or more speech recordings are of same person (Rose, 2002). Identification of speaker in forensic perspective is generally about comparing voices. Speaker identification is deciding if a speaker belongs to group of known speaker population. Speaker verification is verifying the identity claim of the speaker. If the system is forced to choose one of the enrolled speakers then it is called a closed set identification system. If the system has the flexibility to make a choice 'none from the specified group' then it is called an open set identification system. Based on the content used for speaker identification or verification, the tasks can further be classified as text dependent, where the speaker's identity is dependent on the text uttered, and text independent, where no constraints are placed on the text uttered [21]. Furthermore, the speech samples used for speaker identification or verification can be contemporary (recordings from same time period) and non-contemporary (recordings from different time period).

The task of speaker recognition or speaker identification becomes very important in our digital world. Most of the law enforcement organizations use either automatic or manual speaker identification tools for investigation processes. In any case, before carrying out the identification analysis, they usually need to record a voice sample from the suspect either for one to one comparison or to fill in the database. So, the effect of recording media or voice sample recording for forensic speaker identification is very imperative [5].

The present study is focused on semi-automatic speaker identification (SAUSI)where the examiner selects unknown and known samples (similar phonemes, syllables, words and phrase) from speech samples, which have to be compared, here the computer process these samples, extracts parameters and analyse them according to a particular program. The interpretation is made by the examiner, especially to decide whether samples are good enough or affected by factor such as noise, co-articulation, rate of speech etc. to select comparable parts of speech samples for computerized acoustic analysis and to evaluate the results that the computer provides. This is typically encountered in for forensic where an interaction of computer and investigator takes place. Computer automatically extracts comparable data from forensic samples after they have been selected by the investigator[19].

Effects on influence of co-articulation can be of three types; (a) forward effect, (b) backward effect or (c) both. There are anticipatory and/or carryover co-articulatory effects of vowel on the production acoustic realization of a neighbouring consonant[10]. The majority of the studies have found greater backward effect than forward effect [31]. Thus, the nasal phonemes have been identified as being more reliable as a speaker cue because nasal cavity is both speaker specific and fixed so as its volume and shape cannot be changed [1]. The power spectra of nasal consonants [17] and co-articulated nasal spectra [37] provide strong cues for the automatic speaker identification by machines. An acoustic measurement of nasal co-articulation in a consonant or vowel context was obtained by measuring spectral differences between the mean square spectrum of nasal consonants followed by a front vowel and that of the same consonant followed by a back vowel[4]. One more study reported results that there was greater nasalization for pre-nasal vowels than post nasal vowels[25]. Linear Predictive Coding (LPC) parameter and Mel Frequency Cepstral Coefficients (MFCCs) were used for speaker identification [26] whereas the text-dependent recognition rate of 50 speakers

increased from 42% to 80% and the text-independent recognition rate of 50 speakers increased from 60% to 72%. Researchers have used formant frequencies, fundamental frequency, Fo contour, Linear Prediction Coding[3], [22], Cepstral Coefficients [23], [27], [36]and Mel Frequency Cepstral coefficients [2],[11], [12],[18], [30], [33], [38], [39], [40]to identify speaker. However, the Linear Predictive Cepstral Coefficients and the Mel Frequency Cepstral Coefficients have been found to be more effective in speaker identification compared to other features. A comparative study [7] of LPC (94%) and MFCCs (89%) features was conducted for the recognition of Assamese phonemes - under the same environmental condition, when different set of speakers were used for training and testing the system and LPC was considered to be the best and beneficial in a minimal noise environment whereas MFCCs were considered to be the best and beneficial in a noisy situation.The effectiveness of MFCCs in speaker recognition has been conducted [2]. Hence, the present study is focusing on usefulness of linear prediction coding (LPC) in speaker recognition.The review provided the usefulness and the effectiveness of co-articulation of nasal continuants on preceding vowels in the field of speaker identification. There is no empirical data to establish the benchmark for vowels preceding nasal continuants in Kannada using LPC. To prove that the suspect is the criminal, it needs to be verified beyond reasonable doubt that the voice of the criminal and the voice of the suspect are the same. So in order to overcome this problem, a semi-automatic and reliable speaker identification system is desired. In this context the present study was planned.The aim of the present study was to establish the benchmarking in speaker identification using LPC on Vowels Preceding Nasal Continuants in Kannada. The objectives of the study were to establish speaker identification scores using LPC on vowels preceding nasal continuants in Kannada in live recording, mobile network recording and comparison between them.

2. METHOD

2.1 Participants

Twenty Kannada speaking neuro-typical adult males constituted were chosen to participate in the study. The participants were in the age range of 21-32 years (Mean age = 25 years, SD= 3.4) and were graduates with Kannada as one of the subject and all the participants belonged to the Mysuru dialect of Kannada and were drawn from the work/residential place in and around Mysuru, Karnataka, India. Participants were included in the study only on fulfilling certain criteria. The inclusion criteria of subjects were - no history of speech, language, hearing and communication problems, normal oral structures, no other associated social or psychological or neurological problems and reasonably free from cold or other respiratory illness at the time of recording.Written consent was taken from all the participants after explaining about the aim and objectives of the study. Hearing was screened using Ling's sound test. Kannada Diagnostic Picture Articulation Test (KDPAT) [13] was administered by a Speech Language Pathologist to rule out any misarticulations in speech.

2.2 Materials

The material used was thirty commonly occurring, meaningful Kannada words (Target words) containing the nasal continuant */m/ (Bilabial) and /n/* (Dental) and embedded in seventeen sentences (text-independent). These sentences consisted of words with three basic vowels *(/a:/, /i:/, /u:/)* preceding to the two places of nasal consonants *(/m/ and /n/)* and were embedded in 3-6 word meaningful sentences to maintain the naturalness of speech. The vowels preceding nasals continuants were added in the initial and medial positions. There were five occurrences for each vowel preceding nasal continuants *(/a:m/, /i:m/, / u:m/, /a:n/ , /i:n/ and /u:n/)*.

2.3 Recording Procedure

Speech samples of participants were recorded individually. The participants were asked to repeat each sentence four times at habitual pitch, loudness and rate. Sentences were written on a card that was presented to the participants visually for familiarization (Training the participants). They were specifically instructed not to adopt a strict reading style, instead asked to adopt a casual conversational style while reading out

the sentences under live and mobile network recordings. Mobile network recording was done first and the network used for making the calls was Airtel on a NOKIA 101 handset and the receiving network was Vodafone on a Gionee S5.5 mobile phone. A participant participating in an experiment was given a NOKIA 101 handset (Airtel network). A call was made from the participants' handset to the experimenters' handset (Vodafone network) with recording option held by the experimenter. Speech signal was recorded as the participant uttered the test sentences. All the mobile network recordings were done at different places (College campus and Cafeteria) according to the participant's convenience with some amount of ambient noise (40db - 60db) in a natural setting. The recordings at the receiving end were saved by the experimenter in a microchip or memory SD card of that mobile phone. Later, the recorded sentences were uploaded to a computer memory for further analysis. The live recordings were carried out after two weeks using Computerized Speech Lab (CSL) in a laboratory and the files were stored in ***.wav format***. The distance between the mouth and the dynamic microphone was kept constant at approximately 10 cm. Of the four recordings, the first recording was not analysed as the material was novel to the subject and the second and third recordings of all the twenty participants were considered and were subjected to analysis which in turn were used for comparison throughout the study. If any of the second/third recordings were not well-spoken, then the fourth recording was used. The recorded samples were transferred to computer memory. SSL Workbench version 2.1 software employs sampling frequency of 8 kHz and hence all the live and mobile network recordings were opened in PRAAT software and down sampled to 8 kHz. All the recorded speech samples were stored separately for each speaker onto the computer memory at mono channel, 16 bit format having sampling frequency of 8 kHz and was segmented (approximately 300ms) manually using PRAAT software [8]to obtain the vowels preceding nasal continuants in initial and medial positions of the target words.

2.4 Analyses

SSL Workbench for Semi-Automatic vocabulary dependent speaker recognition (Voice and Speech Systems, Bangalore, India) software was used for analyses. Two repetitions and five occurrences for each vowel preceding nasal continuants were randomized by the software and considered as test set and training set

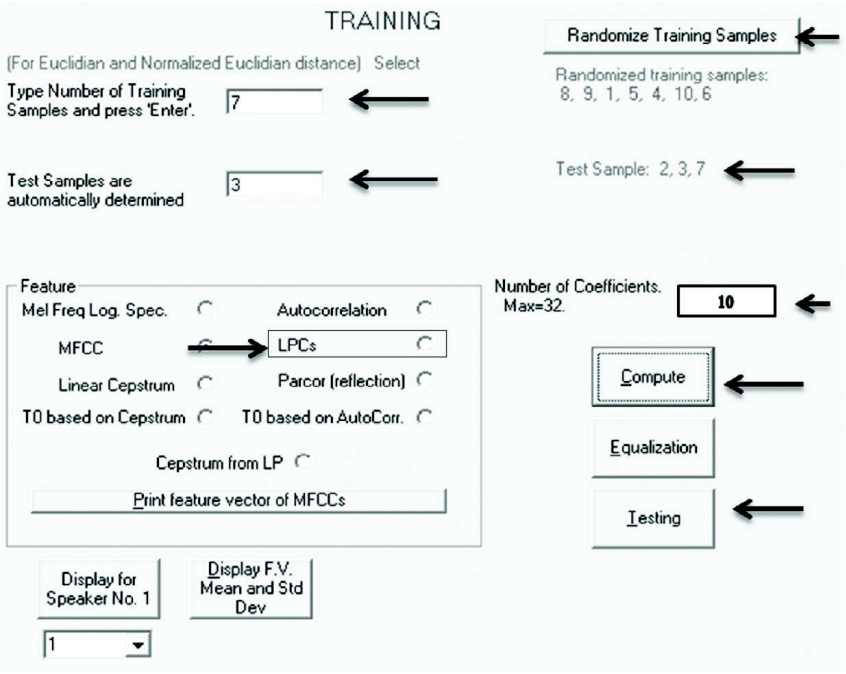

Fig. 1. Training frame of SSL Workbench software depicting LPC analyses.

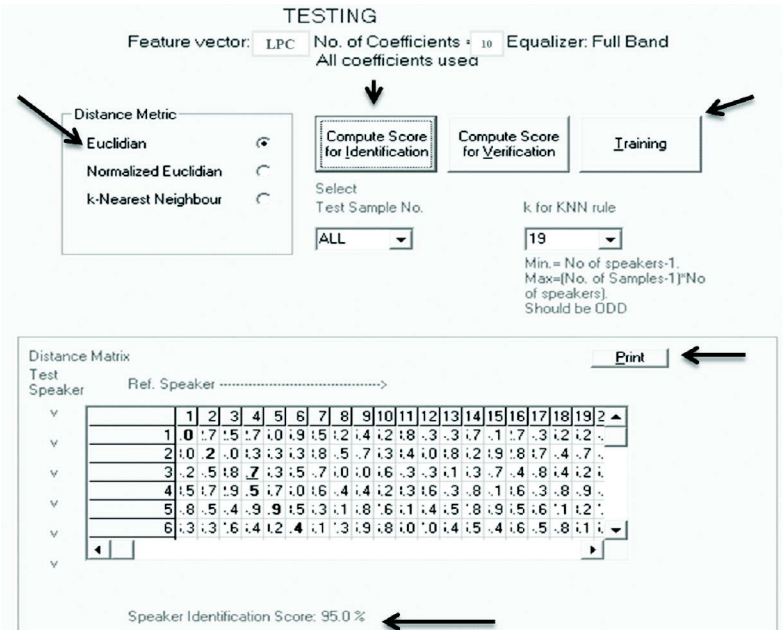

Fig. 2. Testing frame depicting speaker identification score using LPC.

on the ratio of 3:7 (Fig. 1). The file was specified initially using a notepad and .dbs file (extension of notepad file) was created automatically. Followed by this samples for analysis were segmented. As soon as all files were segmented the software opens another window to train the samples randomly. After training, LPC were selected and the sample for identification was tested. Finally the software automatically generated the speaker identification threshold in terms of Euclidian Distance. This data was stored and the same procedure was repeated at least for 10 times by randomizing the training samples and the speaker identification thresholds were noted for the highest score and the lowest score. LPC derived from the vowels preceding nasal continuants were used to compute the Euclidian distance between the test and reference samples. For the present study, the feature vector chosen was LPC with 10 coefficients (Fig. 1). Upon choosing the feature vector, the system computes a measure of distance (Euclidian distance) and displays the summarized distance matrix for the selected test and reference sample. From the distance matrix, the total percentage of correct speaker identification score was displayed (Fig. 2). In this study, the speech samples were contemporary and non-contemporary. Closed set speaker identification tasks were performed, in which the examiner was aware that the 'unknown speaker' is one among the 'known' speakers.

AEP responses were Statistical analysis was done using SPSS (version 18). Mean and standard deviations (SD) were obtained using descriptive statistics for latencies and amplitudes of P1 and N2. Since the data was not normally distributed based on Shiparo-Wilk test, non-parametric test was performed. Non-parametric test includes Friedman test for within group comparison i.e. to compare latency as well as amplitude measures for different speech stimuli *(/m/, t/ and /g/)* at 75dBSPL, 65dBSPL and 55 dBSPL in each group. Further, comparison between groups was done using Mann Whitney U tests for different speech stimuli at each intensity level.

3. RESULTS AND DISCUSSION

The results obtained from this study revealed several interesting points of interest;

First, the percentage of correct speaker identification scores ranged from 70% to 90% when live recording was compared with live recording for the vowels preceding nasal continuants */a:m/, /i:m/, /u:m/, /a:n/, /i:n/*

Table 1. Average (AVG) speaker identification percentage along with test samples for twenty speakers in condition I.

Live Vs Live							
Trial	**Test Sample**	**Percentage**					
		/a:m/	*/i:m/*	*/u:m/*	*/a:n/*	*/i:n/*	*/u:n/*
1	2,3,7	90	70	85	90	65	85
2	2,4,10	70	65	85	90	75	85
3	4,5,9	80	65	75	95	80	75
4	5,7,8	90	75	90	90	80	90
5	3,9,10	90	70	85	90	65	85
6	2,6,8	85	75	85	85	75	85
7	2,3,4	85	70	85	90	75	85
8	7,8,9	80	65	85	95	80	85
9	1,8,9	90	70	90	85	70	90
10	3,6,10	90	75	85	90	85	85
	Average	**85**	**70**	**85**	**90**	**75**	**85**

and /u:n/ and can be stated that these scores were drawn for contemporary speech samples (Table 1). Vowel */a:/* preceding nasal continuant */n/* with 90% had the highest correct identification scores. Table 4 shows the benchmark of highest speaker identification percentage. This result is compatible with those of the other previous studies. A study says nasalization effect stays for 100ms preceding and following the nasal continuant leading to maintenance of nasal characteristics for a longer duration than any other speech sounds[32]. One of the Indian study reported similar results on speaker identification in Malayalam speaking individuals and results of her study indicated above 80% and above 90% correct identification for all vowels preceding nasals using cepstral coefficients and MFCCs, respectively[24].

Table 2. Average (AVG) speaker identification percentage along with test samples for twenty speakers in condition II.

Mobile Network Vs Mobile Network							
Trial	**Test Sample**	**Percentage**					
		/a:m/	*/i:m/*	*/u:m/*	*/a:n/*	*/i:n/*	*/u:n/*
1	2,3,7	65	55	50	65	40	60
2	2,4,10	75	55	50	70	45	55
3	4,5,9	80	60	50	65	45	65
4	5,7,8	75	55	45	55	50	60
5	3,9,10	75	45	55	65	45	55
6	2,6,8	80	55	45	75	40	65
7	2,3,4	65	55	50	65	45	55
8	7,8,9	75	60	55	60	45	60
9	1,8,9	80	55	50	65	45	60
10	3,6,10	80	55	50	65	50	65
	Average	**75**	**55**	**50**	**65**	**45**	**60**

Second, the percentage of speaker identification scores ranged from 45% to 75% when mobile network recording was compared with mobile network recording for the vowels preceding nasal continuants */a:m/ , /i:m/, /u:m/, /a:n/, /i:n/ and /u:n/* and can be stated that these scores were drawn for contemporary speech samples. Vowel */a:/* preceding nasal continuant */m/* with 75% had highest correct identification scores (Table 2). The results showed that the percentage of speaker identification for mobile network recording was drastically lowered compared to live recording. For this condition, speaker identification scores were not as good as scores obtained for live recording because of the recording characteristics of mobile network. GSM (Global System for Mobile Communications) is the pan-European cellular mobile standard. Speech coding algorithms that are part of GSM compress speech signal before transmission, reducing the number of bits in digital representation but at the same time, maintain acceptable quality. Since this process modifies the speech signal, it can have an influence on speaker recognition performance along with perturbations introduced by the mobile cellular network (channel errors, background noise) [6]. During transmission of voice signals through communication channels, the signals are reproduced with errors caused by distortions from the microphone and channel, and acoustical, electromagnetic interferences and noises affecting the transmitting signal.

Third, the percentage of speaker identification scores for twenty speakers ranged from 35% to 45% when mobile network recording was compared with live recording for the vowels preceding nasal continuants */a:m/, /i:m/, /u:m/, /a:n/, /i:n/ and /u:n/* and can be stated that these scores were drawn for non-contemporary speech samples (Table 3). The obtained percent correct identification scores for vowels preceding nasal continuants were lesser than the chance factor (<50%). Mobile network recordings were done initially and the live recordings were done after two weeks. The test speakers were chosen from mobile network recordings and the reference speakers were chosen from live recordings. Scores were poorer because speaker's emotional state during mobile network recording and live recording plays an important role and can affect speaker identification scores. Speaker's emotional state cannot be same during mobile network recording and live recording after two weeks whereas this is the condition in most of the forensic cases. The crime sample will be obtained from mobile whereas the suspect's (reference) sample will be extracted after a week or so in a police station or a recording room and the criminal's emotional state will not be the same under both the circumstances. Also, the environment in which both the recordings were done was considered. Mobile network recording was done in a natural field condition and the live recording

Table 3. Average (AVG) speaker identification percentage along with test samples for twenty speakers in condition III.

		Mobile Network Vs Live					
Trial	**Test Sample**	**Percentage**					
		/a:m/	*/i:m/*	*/u:m/*	*/a:n/*	*/i:n/*	*/u:n/*
1	2,3,7	55	25	70	60	40	60
2	2,4,10	70	30	50	55	45	55
3	4,5,9	40	45	45	75	25	55
4	5,7,8	25	55	40	20	40	40
5	3,9,10	30	35	45	35	35	35
6	2,6,8	35	40	30	30	30	45
7	2,3,4	30	50	30	35	45	35
8	7,8,9	15	20	35	20	25	50
9	1,8,9	25	25	35	35	35	40
10	3,6,10	25	25	20	35	30	35
	Average	**35**	**35**	**40**	**40**	**35**	**45**

was done in a laboratory (noise free) condition. A study reported that when emotions alter the human voice, the performances of the speaker recognition system decrease significantly[16]. One more study reported that when the emotional state of speaker differs in the testing phase the recognition rate decreased drastically and the outcome showed that the accuracy rate of speaker recognition has been significantly increased when compared to the recognition rate where emotional state of the speaker was not considered[14]. Another study was conducted to examine the characteristics of speech transmitted over a mobile network[6]. They concluded that the non-linearity of the GSM channel's frequency response in the range 750-2000 Hz might cause a change in the energy distribution and affect 2nd and 3rd formants (F2 and F3). They also reported a fall-off in the channel's frequency response at 3500 Hz which led to the shifting of the fourth formant (F4). Nasal murmur is typically present below 400 Hz. This information might have been lost due to the transmission characteristics of the mobile network. This could have led to poorer scores in the mobile network condition in comparison with live recording.Characteristically the presentation of a text- independent speaker verification system is poorer than a text-dependent system[9], [15] whereas in the present study, text independent procedure was established.

Table 4. Benchmark for speaker identification using LPC on vowels preceding nasal continuants in Kannada.

Speaker Identification Percentage for 20 Speakers						
	/m/			*/n/*		
	/a:/	*/i:/*	*/u:/*	*/a:/*	*/i:/*	*/u:/*
Live Vs Live (Condition I)	***85***	***70***	***85***	***90***	***75***	***85***
Mobile Network Vs Mobile Network (Condition II)	***75***	***55***	***50***	***65***	***45***	***60***
Mobile Network Vs Live (Condition III)	***35***	***35***	***40***	***40***	***35***	***45***

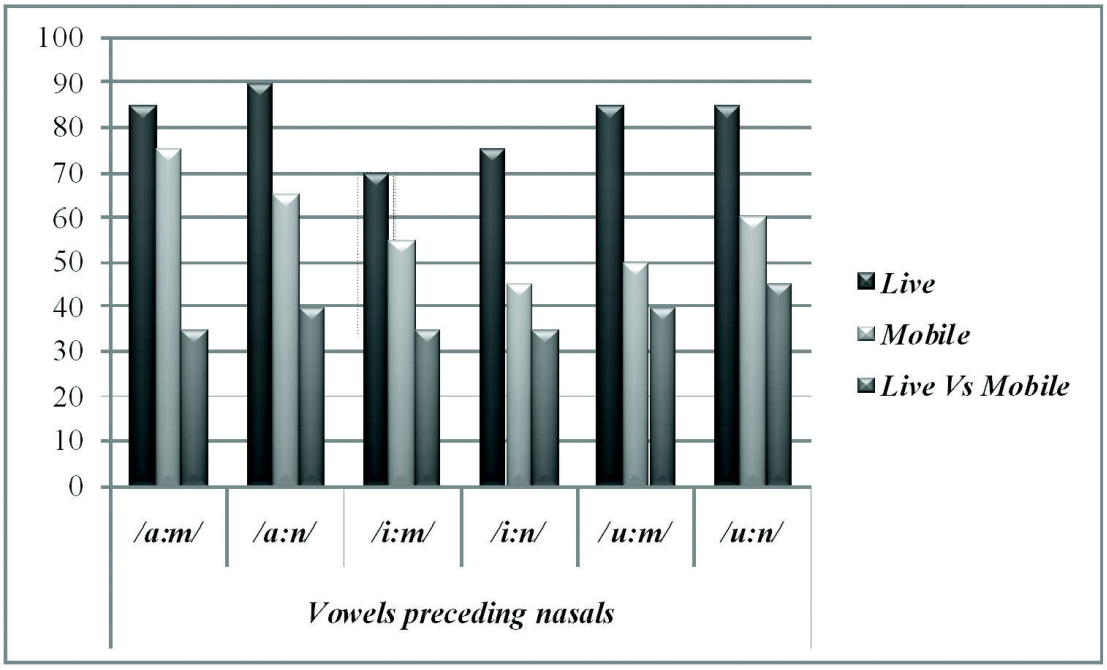

Fig. 3. Graphical representation of speaker identification scores using LPC for vowels preceding nasal continuants in Kannada.

The results of the present study were in agreement with the findings of the power spectra of nasal consonants [17] and co-articulated nasal spectra [37] provide strong cues for the machine matching of speakers. Results of the present study were consistent with the studies conducted by Larson and Hamlet [25] in which they investigated on the phonetic contextual details of nasal co-articulation using nasal voice amplitude ratio instrumentations. Results revealed greater nasalization for pre-nasal vowels than post nasal vowels. The results of present study can be compared with that of Mili [28] which indicated strong anticipatory co-articulation compared to carry over co-articulation. Also, most of the studies have found greater backward effect than forward effect [31]. Also, this study can be compared with a similar study [39] in which vowels following nasals were considered. The present study focused on backward effect *i.e.,* effect of nasals on preceding vowels thus providing good speaker identification scores. Fig. 3 depicts graphical representation of speaker identification scores using LPC for vowels preceding nasal continuants.

4. CONCLUSION

Finally, based on three conditions, vowel */a:/* preceding the two nasals */m/ and /n/* was reliable for speaker identification compared to other vowels. Henceforth, it would enable for the better identification for a particular situation as crime samples can be from any of the conditions. The poor identification scores between mobile network recording and live recording conditions possibly will be attributed to the transmission characteristics of the network. The current study was a text-independent study conducted in a natural environment with background noise and these factors could have contributed to further reduction in accuracy of speaker identification scores. The current study indicated benchmarking for speaker identification using LPC on vowels preceding nasal continuants in Kannada and this outcome can be utilized in forensic speaker identification task. In general, it could be accomplished that vowels preceding nasal continuants also add good percent of correct identification among Kannada speakers on semi-automatic machine procedure of analysis in Forensic Sciences.The obtained outcomes would aid as potential measure in the forensic scenario for Speaker Identification using vowel preceding nasal continuants in Kannada.Further investigation is necessary in the area of semi-automatic and automatic methods by bearing in mind other forensic situations like distortion, disguises, and so on.

5. ACKNOWLEDGEMENT

The authors would like to thank Dr. S. R. Savithri, Director, All India Institute of Speech and Hearing, Mysuru for permitting us to carry out the research. The authors also thank Dr. N. Sreedevi, HOD, Department of Speech-Language Sciences, AIISH for permitting to avail the lab facility and our special thanks to all the participants of the study without whose contribution we could not have accomplished this project.

6. REFERENCES

[1] T. ARAI, K. AMINO and T. SUGAWARA, 2006. Idiosyncrasy of nasal sounds in human speaker identification and their acoustic properties, *Acoustic Science and Technology,* **27**(4).233-235.

[2] M.S. ARJUN, 2015. *Benchmark for Speaker Identification using Mel-Frequency Cepstral Coefficients on vowels preceding nasal continuants in Kannada*. Unpublished project of Post Graduate Diploma in Forensic Speech Science and Technology submitted to University of Mysore, Mysuru.

[3] B.S. ATAL, 1974. Effectiveness of linear prediction characteristics of the speech wave for automatic speaker identification and verification. *The Journal of the Acoustical Society of America*, **55**(6), 1304-1312.

[4] B.S. ATAL, 1976). Automatic recognition of speakers from their voices. *Proceedings of the IEEE*, **64**(4), 460-475.

[5] A. BARINOV, 2010. Voice samples recording and speech quality assessment for forensic and automatic speaker identification. **In** *Audio Engineering Society Convention* 129. Audio Engineering Society.

[6] A. BARINOV, S. KOVAL, P. IGNATOV and M. STOLBOV, 2010. Channel compensation for forensic

speaker identification using inverse processing. **In** *Proceedings of Audio Engineering Society 39th International Conference*. 53-58.

[7] U. BHATTACHARJEE, 2013. A comparative study of LPC and MFCC features for the recognition of Assamese Phonemes. *International Journal of Engineering Research & Technology*, **2**(1), 2278-0181.

[8] BOERSMA and D. WEENINK, 2009. PRAAT S.1.14 software, restricted from http://www.goofull.com /au/program/14235/speedytunes.html.

[9] L. BOVES and E. DEN OS, 1998. Speaker recognition in telecom applications.In *Proceedings IEEE* IVTTA-98, Torino, 203-208.

[10] P.J. Carney and K.L. Moll, 1971. A cinefluorographic investigation of fricative consonant-vowel coarticulation. *Phonetica,* **23**(4), 193-202.

[11] CHANDRIKA, 2010. *The influence of handsets and cellular networks on the performance of a speaker verification system*. Unpublished project of Post Graduate Diploma in Forensic Speech Science and Technology submitted to University of Mysore, Mysuru.

[12] CHANDRIKA, 2015. *Benchmark for Speaker Identification using nasal continuants in Kannada in direct mobile and network recording*. Unpublished project of Post Graduate Diploma in Forensic Speech Science and Technology submitted to University of Mysore, Mysuru.

[13] A. DEEPA, 2010. *Re-standardization of Kannada Articulation Test*. A Dissertation submitted in part fulfillment of final year M.Sc Speech-Language Pathology, University of Mysore, Mysuru.

[14] J. S. DEVI, Y. SRINIVAS and S. P. NANDYALA, 2014. Automatic Speech Emotion and Speaker Recognition based on Hybrid GMM and FFBNN. *International Journal on Computational Sciences & Applications (IJCSA),* **4**(1), 35-42.

[15] G. DODDINGTON, 1998. Speaker recognition evaluation methodology- an overview and perspective. **In** *Proceedings for RLA2C Workshop on Speaker Recognition and its Commercial and Forensic Applications, Avignon, France,* 60-66.

[16] M.V. Ghiurcau, C. Rusu, and J. Astola, 2011. Speaker recognition in an emotional environment. *Proceedings of Signal Processing and Applied Mathematics for Electronics and Communications*, 81-84.

[17] J. W. Glenn and N. Kleiner, 1968. Speaker identification based on nasal phonation. *The Journal of the Acoustical Society of America,* **43**(2), 368-372.

[18] M.R. Hasan, M. Jamil, and M. G. R. M. S. Rahman, 2004. Speaker identification using Mel frequency cepstral coefficients. *Variations*, 1, 4.

[19] M. H. L. Hecker, 1971. Speaker recognition: An interpretive survey of the literature. No.16, USA, ASHA Monographs.

[20] A. Higgins, L. Bahler and J. Porter, 1991. Speaker verification using randomized phrase prompting.*Digital Signal Process*, 1, 89-106.

[21] H. Hollien, 2002. *Forensic Voice Identification*. San Diego, CA: Academic Press.

[22] B. Imperl, Z. Kacic and B. Horvat, 1997. A study of harmonic features for the speaker recognition. *Speech communication*, **22**, 385-402.

[23] S. S. Jakkar, 2009. *Benchmark for speaker identification using Cepstrum*. Unpublished project of Post Graduate Diploma in Forensic Speech Science and Technology submitted to University of Mysore, Mysuru.

[24] JYOTSNA, 2011. Speaker Identification using Cepstral Coefficients and Mel-Frequency Cepstral Coefficients in Malayalam Nasal Co-articulation. Unpublished project of Post Graduate Diploma in Forensic Speech Science and Technology submitted to University of Mysore, Mysuru

[25] P. L. LARSON and S. L. HAMLET, 1987. Coarticulation effects on the nasalization of vowels using nasal/voice amplitude ratio instrumentation. *The Cleft palate journal,* **24**(4), 286-290.

[26] D. MAO, H. CAO, H. MURAT and Q. TONG, 2006. Speaker identification based on Mel frequency cepstrum coefficient and complexity measure. *Sheng wuyixue gong chengxuezazhi= Journal of biomedical engineering= Shengwuyixuegongchengxuezazhi,* **23**(4), 882-886.

[27] S. MEDHA, 2010. *Benchmark for speaker identification by cepstral measurement using text-independent data*. Unpublished project of Post Graduate Diploma in Forensic Speech Science and Technology submitted to University of Mysore, Mysuru.

[28] C.S. MILI, 2003. Labial coarticulation in Malayalam. Unpublished dissertation of Master of Science in Speech Language Pathology submitted to University of Mysore, Mysuru

[29] J. M. NAIK, and G. R. DODDINGTON, 1987. Speaker verification over long distance telephone lines. *ICASSP*, 5243-527.

[30] NITHYA, 2015. *Benchmark for Speaker Identification using Mel-Frequency Cepstral Coefficients in Tamil Nasal Continunats*. Unpublished project of Post Graduate Diploma in Forensic Speech Science and Technology submitted to University of Mysore, Mysuru.

[31] R. N. OHDE and D. J. SHARF, 1975. Coarticulatory effects of voiced stops on the reduction of acoustic vowel targets. *The Journal of the Acoustical Society of America*, **58**(4), 923-927.

[32] J. M. PICKETT, 1980. The sounds of speech communication. *Baltimore, MD: University Park*.

[33] M. D. PLUMPE, T. F. QUATIERI and D. REYNOLDS, 1999. Modeling of the glottal flow derivative waveform with application to speaker identification. *Speech and Audio Processing, IEEE Transactions on*, **7**(5), 569-586.

[34] F. ROSE, 2002. *Forensic Speaker Identification*. London, Taylor and Francis.

[35] N. SREEDEVI and M. D. VIKAS, 2012. *Frequency of occurrence of Phonemes in Kannada*. Project funded by AIISH Research Fund (ARF).

[36] M.S. SREEVIDYA, 2010. *Speaker Identification using Cepstrum in Kannada Language.* Unpublished project of Post Graduate Diploma in Forensic Speech Science and Technology submitted to University of Mysore, Mysuru.

[37] L.S. SU, K.P. LI and K.S. FU, 1974. Identification of speakers by use of nasal coarticulation. *The Journal of the Acoustical Society of America,* **56**(6), 1876-1883.

[38] SUMAN SURESH, 2015. *Benchmark for Speaker Identification using Mel-Frequency Cepstral Coefficients on vowels following nasal continuants in Kannada*. Unpublished project of Post Graduate Diploma in Forensic Speech Science and Technology submitted to University of Mysore, Mysuru.

[39] SUMAN SURESH, 2015. Benchmark for Speaker Identification using LPC on vowels following nasal continuants in Kannada. *Proceedings of National Symposium on Acoustics* (NSA), 64.

[40] R. TIWARI, A. MEHRA, M. KUMAWAT, R. RANJAN, B. PANDEY, S. RANJAN and A. SHUKLA, 2010. Expert system for speaker identification using lip features with PCA. In *Intelligent Systems and Applications (ISA), 2010 2nd International Workshop on* (pp. 1-4). IEEE.

Journal of Acoustical Society of India : Vol. 43, No. 2, 2016 (pp. 108-115)

Application of Automatic Speech Recognition in Communication Sciences and Disorders

Akshay Mendhakar, Sangeetha Mahesh* and Rakshith S.
Department of Clinical Services, All India Institute of Speech & Hearing, Manasagangothri, Mysore 570006
e-mail: smahesh64@gmail.com

[Received: 22-06-2016; Revised: 30-06-2016; Accepted: 06-09-2016]

ABSTRACT

Communication Sciences and Disorders encompass scientific understanding of communication in both typically-developing and communication-disordered population. During this process Speech language pathologists should incorporate new strategies and technologies for diagnosis and rehabilitation. One such Technology is Systematic Analysis of Language Transcripts (SALT) that manages the process of eliciting, transcribing, and analyzing language samples. However, the process seems to be time consuming and sophisticated. In the field of Speech Language Pathology automatic detection of the speech would enable the clinicians for quick decision making. Hence, a speaker adapted automatic speech recognition tool was developed using Sphinx and incorporated Structured Query Language (SQL). The participants in the control group included 30 subjects (15 males and 15 females) within the age range of 18-30 years. The clinical group included 15 participants with 3 clinical conditions such as stuttering, voice disorder, and dysarthria. Participants were instructed to read the passage into the microphone connected to the computer with the designed tool in an acoustic treated room. The data was further analyzed for the automatic speech recognition score. Word recognition accuracy was found to be around 75%. The study concluded that the tool can be further refined and can assist Speech Language pathologists in clinical practice.

1. INTRODUCTION

Speech language pathologists are concerned with identification, assessment and management of speech, language and swallowing disorders. Speech disorder is considered to be an impairment of articulation of sound, fluency or voice. Stuttering as the deviation in the ongoing fluency of speech, an inability to maintain the connected rhythms of speech[1]. A voice disorder exist when the pitch, quality, and loudness differs from the voices of others of similar age, gender or cultural group. Dysarthria refers to imperfect articulation of speech sounds caused by central nervous system damage and exhibit resonatory, respiratory, phonatory and articulation problems.

The Speech-Language professionals use both formal (standardised) and informal (non standardised) tests to deal with communication deficits. The use of state of the art technology in speech language pathology has been identified with increased implications. In recent times advancements has been possible with improved in technology of computers and statistics. Diagnostic formulation has been restricted to quantization of nasalence, intensity of the sustained vowel and other spectral characteristics[2]. Several transcript programs have been used for analysis. One such is the Systematic Analysis of Language Transcripts (SALT) that manages the process of eliciting, transcribing, and analyzing language samples. However, the

process seems to be time consuming and sophisticated. Hence, speech processing methods have gained popularity recently to determine the speech intelligibility[3]. One such technology that has influenced the field of speech language sciences and disorders is Automatic Speech Recognition-ASR[4].

ASR is traditionally been considered as a process of converting speech into a sequence of words with the help of an algorithm implemented on to a personal computer[5]. The early speech recognition software was too cumbersome to handle, too slow and was undependable. ASR systems were introduced way back in 1950's but very not found to be effective initially and the performance was limited to single word/digit recognition which was needed to be modified further[6]. In the recent decades greater advancements in the field of signal processing, computer technology and information statistics ASR has enormous applications. The contribution of ASR are in almost all the fields such as health care (American recovery reinvestment act, 2009), military aviation[7] entertainment[8], banking[9], transport[10], medical sector[11] and few other general purposes such as dictation and translational purposes. ASR technology is bound to replace the traditional interface between man and the machine.

ASR systems can be classified by the types of utterances such as individual words, connected words, speech in terms of both connected and continuous. Similarly they can be classified based on the factors affecting the signal and its recognition i.e. speaker dependent and independent. Issues or factors affecting ASR include environmental factors (different types of noises), transducers (microphone quality, distortion echo), styles in speaking, tone of voice (quiet, normal or loud), speech production (isolated words or speech in terms of continuous or connected), rate of speech (fast, normal, slow) and vocabulary (large, medium or small)[12].

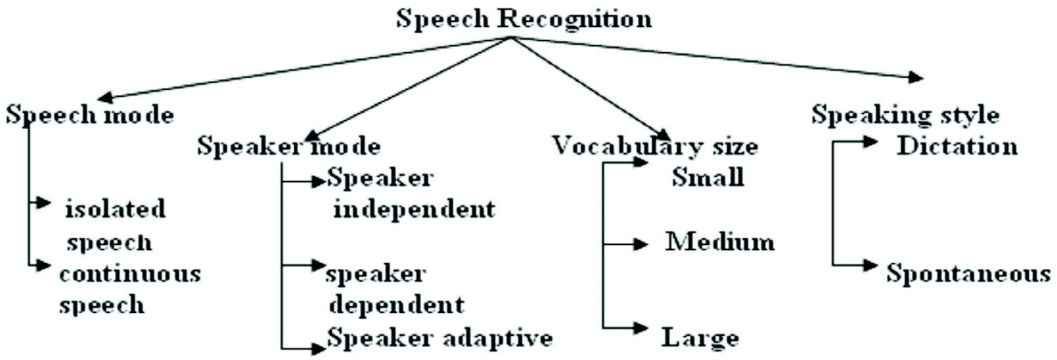

Fig. 1. Factors affecting Automatic Speech Recognition
(Adapted from Speech recognition by machine: A review[5])

Functioning of a typical ASR system can be understood in different steps. Firstly the speech signal which is a acoustic form is transformed into a varying electric current by the microphone. After the signal is adjusted to a constant volume, the electric signal is filtered for noise and other unwanted signals and aliasing. Later ,analogue to digital conversion takes place (Sampling frequencies varies from 8 to 25 kHz) and framed by overlapping and Hamming windows with a frame rate varying from 50 to 100 Hz is applied for a window length of 16 to 32ms sample. The resulting signals are acoustically analysed based on auditory perceptual functions. These functions may be coded with Mel Frequency Cepstral Coefficient (MFCC) or Perceptual Linear Prediction Coefficients (PLPC) .Vocal tract length normalization (VTLN) function is applied to normalise the first and second order derivatives. Feature extraction produces frames that are categorised according to their spatial qualities and coded to reduce data size for subsequent pattern matching and recognition process. The obtained speech frames are compared with the speech frames from the training

corpus of with the help of Gaussian mixture model (GMM) which are implemented in Hidden Markov Model (HMM). A similarity measure or matching distance is utilised to calculate the probability of certain feature vectors given as a set of HMMs. The best matches are selected as candidates to form speech phonics (Sounds).By analogical-statistical methods phones are concatenated to form words and sentences. These processing steps depend much on adequate language models(phoneme, word and sentence level).Language models may be either linguistically or statistically grounded.

The effectiveness of an ASR system is usually expressed in terms of accuracy and speed[5]. Speech recognition accuracy is generally expressed in terms of Word error Rate (WER) or Command Success Rate (CSR). By analogy ASR Systems never produce 100% results. The WER is computed from Levenshtein distance, which works at the word level instead of phoneme level.

Word error rate can be computed as,

$$WER = \frac{S + D + I}{N} \quad \text{... Eq. (1)}$$

Where " S " represents Number of substutions, " D" represents the number of delitions, "I" represents the number of insertions and " N" represents the total words in the reference.

In a routine clinical setup Speech language pathologists tend to follow perceptual judgements which are less time consuming. However, perceptual judgements made even by expert professionals might lack reliability. Hence, it is feasible for the Speech language pathologists to use the best possible, modern, ethical, effectively proven assessment and management protocols for communication disorders. Attempts have been reported to quantify speech and voice but are restricted to assessment of nasalence in text passages, spectral characteristics and intensity of voice in sustained vowels. The application of ASR in voice, speech and language assessment and therapy are important concern to many professionals. Efforts have been made to determine the accuracy of ASR for speech or language disorders[13]. Speech intelligibility assessments using the speech processing methods are receiving increased attention in the current decades.

1.1 Aim of the study

The present study aims to throw light on the accuracy of a custom made ASR system and its accuracy in the field of speech language sciences and pathology.

The specific objectives of the study are as follows,

(1) To investigate the accuracy of ASR system (speech recognition score) for normal adult speakers
(2) To compare the speech recognition scores for normal adult male and female speakers
(3) To investigate the speech recognition score for 3 clinical conditions
(4) To compare the speech recognition scores for normal and clinical population
(5) To evaluate the effects of interaction between the experimenter and clinical condition

2. METHOD

2.1 Participants

A total of 30 normal subjects (15 males and 15 females) within the age range of 15-30 years participated in the study. The clinical group consisted of 15 subjects with various communication disorders such as voice disorders, stuttering, and dysarthria. Each clinical condition constituted a total number of 5 participants. The participants were evaluated for the speech deficits at All India Institute of Speech and Hearing and were diagnosed to have moderate to mild degree of severity. All the above participants were able to read the standardized Rainbow passage[14].A written consent was taken from the participants in the study.

2.2 Material

The Rainbow Passage from is one among the few standard reading passages which is utilised in the field of communication disorders for the purpose of assessment. Speech language pathologists also use the passage to Study accent variations, reading comprehension, and even as a speech exercise. It has also been used in testing language recognition software. It contains almost all phonemes of English except □ and glottal stops.

2.3 Instrumentation

An interactive database system approach was utilised, where the ASR system accepts voice as the input and produces the corresponding text as the output. It is a speaker adaptable ASR system. It takes in voice input as Structured Query Language (SQL) or NO-SQL commands and then converts them into text.Sphinx4 is the tool which is used to execute this module . It is based on HMM (Hidden Markov Models) a type of statistical model. Sphinx4 helps to identify the speech of the user and detects the presence of noise in the speech signal, if present it will be discarded & provides the essential string for further dispensation.

The speech of the users is stored as wave file and is taken as the input for further processing. Here we need to consider the configuration file for processing the user voice input. The configuration file contains the required details for processing a wav file; the sampling rate for processing the speech signal is stored in the configuration file. Sphinx4 plays a vital role and it has an in-built recognizer, decoder, feature extractor in it; it checks with the linguist for any rule violations. When an acoustic model is being generated, the speech signals are initially altered to series of vectors to represent the signal characteristics. Front end is used to produce these vectors and are present inside the recognizer. These features extracted from the speech signals are present in the acoustic model of Sphinx4 which has a dictionary to store it.

In order to represent the grammar used in speech recognition, Uni-gram language model was used. Microphone has the sampling rate of 16 kHz and 16bit mono track. The tool uses windower and MFCC as feature extractors (Mel-frequency cepstral coefficients). Input recognized prior is converted into a standard text format later. Each line of the text is compared within the database with the help of the configuration file and provides the output in terms of accuracy of the system.

$$WR\ [\%] = \frac{C}{R} * 100 \qquad \text{... Eq. (2)}$$

Where "C" is the correctly recognised words and "R" is the total number of words in reference and WRR is the word recognition rate (in percentage).

2.4 Recording protocol

The participants were instructed to read the standardized rainbow passage into the microphone connected to the computer with the designed tool in an acoustic treated room. Adverse factors that might affect the accuracy of the ASR system were taken into consideration such as noise and speaking rate. Further the speech sample was analysed by the tool to provide word recognition accuracy in terms of correctly recognised words and percentage correct words.

3. RESULTS

3.1 Accuracy of ASR system for normal adult speakers

For normal age group (NAG) with a sample size of 30 (N=30), the mean accuracy of speech recognition scores were found to be 73.77% (SD = 5.62). Among the group of 30 participants, minimum and maximum speech recognition scores were found to be 62.55 % and 85.47% respectively. Fig 2 illustrates the overall variation of mean scores for the NAG group. The results suggest that the accuracy of speech recognition scores did differ for the normal participants.

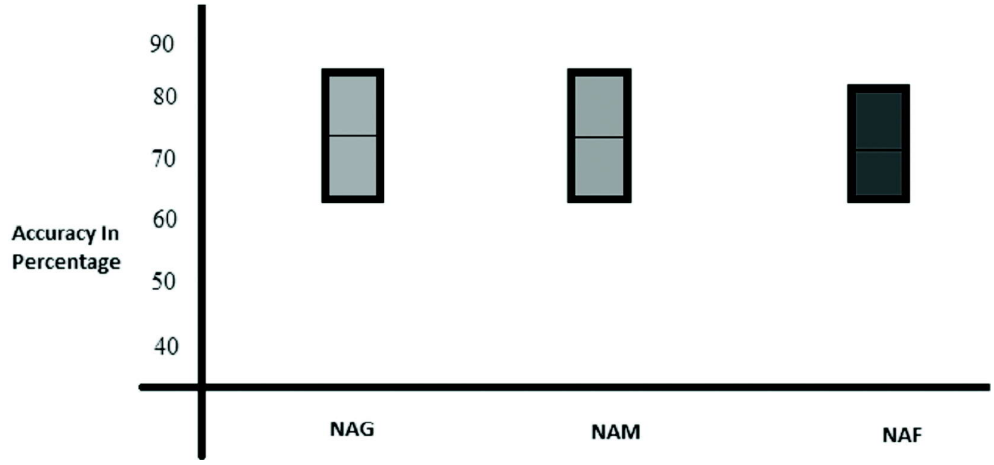

Fig. 2. Showing the mean accuracy scores and standard deviations for NAG, NAM and NAF Groups

3.2 Comparison of speech recognition scores across normal adult male and female speakers

Similarly the analysis was performed and the scores were computed across gender among the normal participants. The mean accuracy for speech recognition in a normal adult male group (NAM) were found to be 74.67 (SD= 6.02) with a range of 62.75 to 85.47. On the similar lines, the mean accuracy for speech recognition in a normal adult female group (NAF) were found to be 72.86 (SD= 5.25) with a range of 62.55 to 81.96. The mean accuracy scores and standard deviations for both the groups are displayed in Fig 2. Independent "t" test was performed to find the significant difference in mean accuracy scores between NAM and NAF groups. Results revealed no significant difference between the groups. Sample size within both the groups i.e. NAM and NAF were kept constant (N=15). The results revealed that the recognition of words by the ASR system, newly developed tool was similar for both the gender groups.

3.3 Accuracy of ASR system across clinical conditions

The clinical group constituted 3 groups, specifically Voice disorder (VD), Dysarthria (DY) and Stuttering (ST). Fig 3 illustrates the mean accuracy scores for the clinical group which included the sample size of 5 in

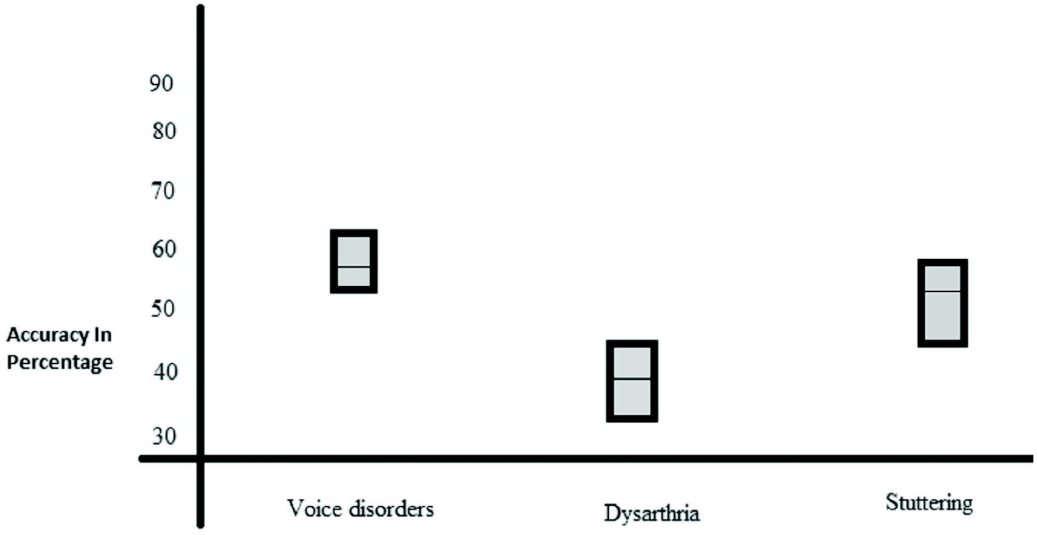

Fig. 3. Mean accuracy scores for the clinical group

each of the subgroup of clinical condition. The mean accuracy for speech recognition for VD, DY, ST were found to be 56.66 (SD = 3.86), 40.2 (SD=3.76), 53.8 (SD= 5.12) respectively. Table 1 represents mean accuracy speech recognition scores across the 3 clinical conditions such as Voice disorder, Dysarthria and Stuttering.

Table 1. Mean accuracy scores of VD, DY and ST groups

Groups	N	Mean	SD
Voice disorder (VD)	5	56.66	3.86
Dysarthria (DY)	5	40.26	3.76
Stuttering (ST)	5	53.81	5.12

Kruskal-Wallis Test was performed to determine the significant difference across clinical groups. The results indicated a significant difference between the clinical groups. The Chi-Square value showed 30.480, $p < 0.001$. Therefore, Mann-Whitney test was employed for further analysis to find pair wise significant variation across the groups. Table 2 summarizes the values of $|z|$ and the level of significance for all the groups. The comparison revealed a significant difference between all the groups except VD and ST clinical group.

Table 2. Level of significance across groups.

Groups	$\|z\|$	p value
Group 1 and 2	3.53	0.00*
Group 1 and 3	3.53	0.00*
Group 1 and 4	3.53	0.00*
Group 2 and 3	2.61	0.00*
Group 2 and 4	0.83	0.40
Group 3 and 4	2.61	0.00*

*Indicates statistical significance at 0.001 level; Group 1 = Normal (NAG); Group 2 = Voice disorder (VD); Group 3 = Dysarthria (DY); Group 4 = Stuttering (ST)

3.4 Comparison of Automatic speech recognition scores for normal and clinical population

On comparing the mean accuracy speech recognition scores for normal and clinical group Mann-Whitney Test results revealed a significant difference. Further a significant value of $|z| = 5.41$ at 0.001 level was noted between the control and clinical group. The results suggested that the overall mean recognition score for clinical group was lower compared to control group. The data revealed that the speech for normal were recognized approximately 70% of the time whereas for the clinical group it was only around 50%.

3.5 To evaluate the effects of interaction between the experimenter and clinical condition

The mean accuracy of speech recognition scores for the experimenter was around 75.37 (SD = 6.08) and for the clinical condition the mean value was 56.17 (SD= 11.02). Wilcoxon Signed Ranks Test was used to test the effects of interaction between the experimenter and clinical condition. The results revealed $|z|$ value to be 2.70, significant at 0.05 levels and Asymp. Sig. (2-tailed) .007 revealing good interactional ability of the ASR system.

4. DISCUSSION

The word recognition scores of around 73.77± 5.62 was observed in the control group . The percentage of correctly identified words (74% approximately) by the newly developed tool is an acceptable score. The speech recognition score by other standard commercially available speech recognition software such as dragon naturally speaking[15] probably might provide a score greater than 70%. However, the difference between score obtained in the present study might be lesser only by 10 - 20 %. The possible reasons for this being the effects of speaking rate, accent variations, influence of language models, no. of specific training protocol used (as the tool was developed as a speaker adaptable ASR system).

The results of the clinical population revealed better speech recognition scores for VD, ST and DY respectively. The clinical conditions are labelled in a descending order of accurate recognition scores. It was noted that the DY subgroup had poor WR when compared to the other subgroups. The obtained results are in accordance with previous research work[16], [17], [18]. The authors reported that the speech recognition score was considerably poor for individuals with dysarthria when compared to individuals without dysarthria.. Specifically,[19] found 75% mean accuracy score for normal and reduction to 57% for dysarthrics.

The results of our tool are the percentage of correctly recognised words (WRR). For clinical purpose the tool is implemented onto a Personal computer with a sound card .The calculation of WRR is quickly performed in less than real time, making it a time and manpower saving procedure. Thus, the above tool can be used in everyday purpose for clinical use.

Normally, ASR systems are used to recognise speech as accurately as possible .we used the technique of ASR to quantify the influence of altered speech on recognition abilities of the ASR system. The assessment of quality of recognition allows in assessing the quality of speech signal. In order to exclude the influence of other factors a standard text with a stable recording setup was used.. The tool might be applicable to other kinds of communication disorders such as aphasia, hearing impairment etc. However, the standardization of the tool with age, gender, diagnostic condition related matched norms must be established before use. The tool should be used on a larger population to quantify the results.

5. CONCLUSIONS

ASR systems can not only produce text from speech, but can also be used to score the speech performance of an individual. This being possible only because recognition process being a sort of mathematical comparison resulting in a measure of distance between the actual performance and the model. The newly developed tool presents an objective, low effort and cost friendly procedure to assist the speech language pathologist. It assists the clinician in assessment, diagnostic formulation, report writing and also function as a self monitoring system. Further, the new ASR system would aid in bridging the gap between other objective procedures and perceptual evaluation for individuals with communication impairment. Henceforth it can be concluded that Speech evaluation using ASR system is a valuable mean for clinical and research purposes in order of determining the global function outcome of speech domain of an individual.

6. REFERENCES

[1] VAN RIPER, CHARLES, 1982. *The Nature of Stuttering*. 2nd edition. Englewood Cliffs, N.J.: Prentice-Hall.

[2] P.H. DEJONCKERE, P. BRADLEY, P. CLEMENTE, G. CORNUT , L. CREVIER-BUCHMAN and G. FRIEDRICH, 2001. A basic protocol for functional assessment of voice pathology, specially for investigating the efficacy of (phonosurgical) treatments and evaluating new assessment techniques. Guideline elaborated by the Committee on Phoniatrics of the European Laryngological Society (ELS). *European Archives of Otorhinolaryngology*, **258**(2), 77-82.

[3] P. KITZING, A. MAIER and V.L ÅHLANDER, 2009. Automatic speech recognition (ASR) and its use

as a tool for assessment or therapy of voice, speech, and language disorders. *Logopedics Phoniatrics Vocology*, **34**, 91-96.

[4] A MAIER, E. N¨OTH, A. BATLINER, E. NKENKE and M. SCHUSTER, 2006. Fully automatic assessment of speech of children with cleft lip and palate. *Informatica*, **30**(4), 477-482.

[5] M.A. ANUSUYA and S.K. KATTI, 2009. Speech Recognition by Machine: A Review (IJCSIS). *International Journal of Computer Science and Information Security*, **6**(3), 181-205

[6] F. JELINEK, 1976. Internet banking adoption among mature customers: early majority or laggards? Continuous speech recognition by statistical methods. *IEEE Proceedings*. **64**, 532-556.

[7] C. BARBER and J. NOYES, 1996. Automatic speech recognition in adverse environments. *Human Factors,* **38**, 142-156.

[8] S.R. FOURNIER, 1996. Developments in voice-input technology. *Journal of Education for business,* **71**, 241-245.

[9] M. MATTILA, H. KARJALUOTO and T. PENTO, 2003. Internet banking adoption among mature customers: Early majority or laggards? *Journal of Services Marketing,* **17**(5), 514-528.

[10] A. OWEN, 1995. Nonparametric Likelihood Confidence Bands for a Distribution Function, *J. Am. Stat. Assoc.* 516-521.

[11] R. PARENTE, N. KOCK and J. SONSINI, 2007. An analysis of the implementation and impact of speech- recognition technology in the healthcare sector Perspectives in health information management/AHIMA, American Health information Management association, **1**, 5.

[12] V. ZUE, R. COLE and W. WARD, 1996. Speech Recognition. Survey of the State of the Art in Human Language Technology. Kauii, Hawaii, USA.

[13] THOMAS-STONELL, A. KOTLER, H. LEEPERand P. DOYLE, 1998. Computerized speech recognition: Influence of intelligibility and perceptual consistency on recognition accuracy. *AAC: Augmentative and Alternative Communication,* **14**(1), 51-56.

[14] G. FAIRBANKS, 1960. Voice and articulation drill book, 2nd edition. New York: Harper & Row. 124-139.

[15] SARNATARO and VALERIE, 2012. Dragon Naturally Speaking (DNS) 12 Review. Technology guide.com. Technology Guide. Retrieved 2013-07-25.

[16] A.L. KOTLER and C. TAM, 2002. Effectiveness of using discrete utterance speech recognition software. *Augmentative and Alternative Communication,* **18**, 137-146.

[17] P. RAGHAVENDRA, E. ROSENGREN and S. HUNNICUTT, 2001. An investigation of different degrees of dysarthric speech as input to speaker-adaptive and speaker-dependent recognition systems. *Augmentative and Alternative Communication,* **17**(4), 265-275.

[18] B. BLANEY and J. WILSON, 2000. Acoustic variability in dysarthria and computer speech recognition. *Clinical Linguistics & Phonetics,* **14**(4), 307-327.

Journal of Acoustical Society of India : Vol. 43, No. 2, 2016 (pp. 116-124)

Study of nonlinear properties of vocal tract and its effectiveness in speaker modeling

R.K. Sunil Kumar[1], K.M. Muraleedharan[2], P. Vivek[3] and V.L. Lajish[4]
[1,2]Department of Physics, Govt. College Madappally, Kerala - 673 102
[3,4]Department of Computer Science, University of Calicut, Kerala - 673635
e-mail: seuron74@gmail.com

[Received: 09-05-2016; Revised: 02-06-2016; Accepted: 22-08-2016]

ABSTRACT

This paper introduces a combined feature method for speaker modelling using the nonlinear properties of the human vocal tract. Speech generation has classically been modelled as a linear system, which provides a convenient and simple mathematical formulation. However a number of nonlinear effects are present in the physical process which limits the effectiveness of the linear model. We have analysed Capacity Dimension (CD), Correlation Dimension (CRD), Kolmogorov Entropy (KE) and Largest Lyapunov Exponent (LLE) of selected phoneme from different speakers. Eigen values of the Reconstructed Phase Space (EV-RPS) and Spectral Decay Coefficients (SDC) are also extracted for speaker modelling. We have experimentally verified the effectiveness of the proposed speaker identification system based on the combination of nonlinear features using Feed Forward Multilayer Perceptron Classifier (FFMLP) simulated using the error back propagation learning algorithm. The results indicate that the human vocal tract shows the properties of a deterministic chaotic system and the proposed nonlinear features can be effectively used for improved speaker identification.

1. INTRODUCTION

Speaker modelling is one of the major task in the speaker recognition problem. The basic objective of speaker modelling is to be identified the speech of an individual speaker from all other unique speakers. Recognising a speaker involves extracting features that characterise the speaker from their speech signal, and modelling them using speaker models. It was Lawrence Kersta who made the first major step towards speaker identification by computers as he developed spectrographic voice identification at Bell Labs in the early 1960s. His identification procedure was based on visual comparison of the spectrogram, which was generated by a complicated electro-mechanical device [1]. Although the visual comparison method cannot cope with the physical and linguistic variation in speech, his work encouraged the introduction of automatic speaker recognition. The global shape of the DFT magnitude spectrum, known as spectral envelope, contains information about the resonance properties of the vocal tract and has been found out to be the most informative part of the spectrum in speaker recognition [2].

In the subsequent four decades, speaker recognition research has advanced a lot. Speech production has been assumed to be linear in the past, and the parameters such as the Mel frequency cepstral coefficients (MFCCs) and linear predictive cepstral coefficients (LPCCs) are used in speech recognition system. Nowadays this linear model has been challenged, and the importance of the nonlinearities emphasised[3]. Nonlinearity is routinely included in attempts to model the physical process of vocal cord vibration, which

have focused on two or more mass models [4].Observation of glottal waveform reinforce this evidence, where it has been shown that this wave form can change shape at different amplitudes. Such change would not be possible in a strictly linear system where the wave form shape is unaffected by the amplitude changes. Nonlinear signal processing techniques have several potential advantages over traditional linear signal processing methodologies [5-13]. They are capable of recovering the nonlinear dynamics of signals of interest possibly preserving natural information. In this context we have analysed Capacity Dimension, Correlation Dimension, Kolmogorov Entropy, Largest Lyapunov Exponent, Eigen values of the Reconstructed Phase Space and Spectral Decay Coefficients of selected phoneme for fifty different speakers. Lyapunov exponents related with a trajectory which gives a measure of the average rates of convergence and divergence of nearby trajectories [14]. Fractal dimensions (capacity dimension and correlation dimension) quantify the number of degrees of freedom and the extent of self-similarity in the attractor's structure [15]. Kolmogorov entropy measures the rate of information loss or gain over the trajectory. These measures search for a signature of chaos in the observed time series [16].Eigen values are special set of scalars obtained when an operator operates on a time series. These scalars can be used to characterize the nature of the operator [17]. Since these measures quantify the structure of the underlying nonlinear dynamical system, they are prime candidates for feature extraction of a signal with strong nonlinearities.

Finally, we analysed the speaker identity based on the non-linear properties of the power spectral measures of the speech samples which are normally not considered in any of the conventional feature extraction methods. The power spectra measures of the speech sample show interesting similarities with the theoretical chaotic models. The source and system are separated by cepstral method and power spectral measures are carried out. It is observed that, there exits an exponential decay in the power spectrum of the speech samples similarly as seen in the case of Lorenz and Rossler chaotic dynamical system models [16]. Spectral Decay Coefficients are then extracted from the power spectrum of the speech data. Different features are combined to model each unique speaker. The speaker identification experiments are conducted based on the proposed SDC features using Feed Forward Multilayer Perceptron Classifier (FFMLP) simulated using the error back propagation learning algorithm. The rest of this paper is organized as follows. Section1presents various nonlinear features used for speaker modelling. The simulation experiment and results are presented in Section 2 and Section 3 concludes the work.

2. NONLINEAR FEATURES USED FOR SPEAKER MODELING

There is strong theoretical and experimental evidence for the existence of important nonlinear 3D fluid dynamics phenomena during the speech production that cannot be accounted by the linear models. Examples of such phenomena include modulations of the speech airflow and turbulence. Teager and Teager present several physical measures that show turbulences in the airflow [17]. We can view the linear model only as a first order approximation to the true speech acoustics, which also contain second-order and nonlinear structures.

To study the nonlinear properties of the system it is necessary to reconstruct a phase space from the time series. The dynamics of a system can be studied by extracting invariant parameters from the experimental time series data. The process of reconstructing the system's attractor is referred to as embedding[7]. The simplest method to embed scalar data is the method of delays. In this method, the pseudo phase-space is reconstructed from a scalar time series, by using delayed copies of the original time series as components of the Reconstructed Phase Space (RPS). According to Takens' embedding theorem a reconstructed phase space can be produced for a measured state variable x_n, where n = 1, 2, 3, 4… N, via the method of delays by creating vectors given by

$$X_n = \left[X_n X_{n+\tau} \; X_{n+2\tau} \; \ldots \; X_{n+(d-1)\tau} \right] \tag{1}$$

Where d is the embedding dimension and τ is the chosen time delay value. The row vector, X_n, defines the single point in the RPS. The row vectors then can be compiled into a matrix called a trajectory matrix to completely define the dynamics of the system and create a reconstructed phase space as :

$$X_d = \begin{bmatrix} X_1 & X_{1+r} & X_{1+2r} & \dots & X_{1+(d-1)r} \\ X_2 & X_{2+r} & X_{2+2r} & \dots & X_{2+(d-1)r} \\ X_3 & X_{3+r} & X_{3+2r} & \dots & X_{3+(d-1)r} \\ . & . & . & \dots & . \\ . & . & . & \dots & . \\ . & . & . & \dots & . \\ X_N & X_{N+r} & X_{N+2r} & \dots & X_{N+(d-1)r} \end{bmatrix} \quad (2)$$

RPS for vowel /a/ spoken by four different speakers *(d=3)* is shown in Fig. 1. There are several ways to generalize dimension to the fractional case, like correlation dimension, Lyapunov dimension *etc.* The following section explains various RPS based nonlinear features used in this study.

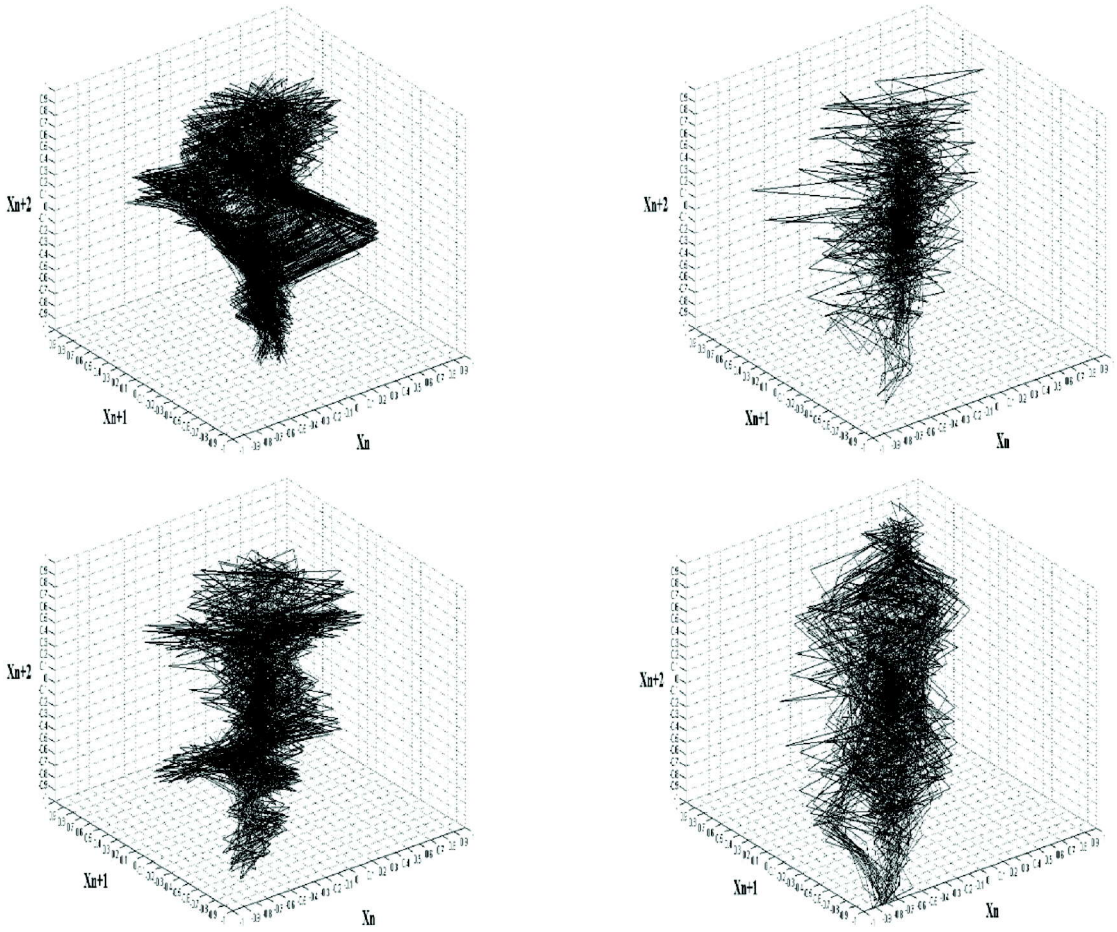

Fig. 1. Reconstructed Phase Space (RPS) for vowel /a/ spoken by four different speakers (d=3)

2.1 Lyapunov Exponents

The analysis of separation in time of two trajectories with infinitesimally close initial points is measured by Lyapunov exponents [14]. For a system whose evolution function is defined by a function *f*, we need to analyse the time evolution of the trajectory in phase space using the relation,

$$\Delta x(t) \approx \Delta x(0)\frac{d}{dx}\left(f^N\right)x(0) \tag{3}$$

Where $\Delta x(t)$ is the variation from true value $x(t)$ at time t and $\Delta x(0)$ is the variation from the true value $x(0)$ at time t=0.

To quantify this separation, we assume that the rate of growth (or decay) of the separation between the trajectories is exponential in time. Hence we define the exponents, λi as :

$$\lambda i = \lim_{n\to\infty}\frac{1}{n}\ln\left(e_i g_i \prod_{p=0}^{n} J(p)\right) \tag{4}$$

Where, J is the Jacobian of the system as the point p moves around the attractor. These exponents are invariant characteristics of the system and are called Lyapunov exponents, and can be computed by applying the above equation to points on the reconstructed attractor. The exponents read from a reconstructed attractor measure the rate of separation of nearby trajectories averaged over the entire attractor. Largest Lyapunov Exponent (LLE) can be used as a feature value for uniquely modelling the speaker. Here we used the method of Rosenstein provided by the TISEAN toolbox for the computation of LLE. The method returns two-column vector with the number of iterations in the first column and the logarithmic stretching factor in the second column. The slope of the semilogarithmic plot of the stretching factor over the iteration is an estimator of the maximal positive Lyapunov exponent. Fig. 2 shows the Lyapunov exponent of the vowel /a/.

2.2 Capacity dimension

There are different ways to define the dimension, $d(A)$, of a set A. One approach is the capacity dimension dB. For a one dimensional figure such as straight line or curve of length L, it can be covered by $N(\varepsilon)$ one dimensional boxes of size ε. The capacity dimension is defined as,

$$dB \approx \frac{\log\ (\varepsilon)}{\log\ \left(\frac{1}{\varepsilon}\right)} \tag{5}$$

To compute the box counting dimension, break up the embedding space into a grid of boxes of size ε. Then count the number of boxes $N(\varepsilon)$, inside which , at least one point of the attractor lies.

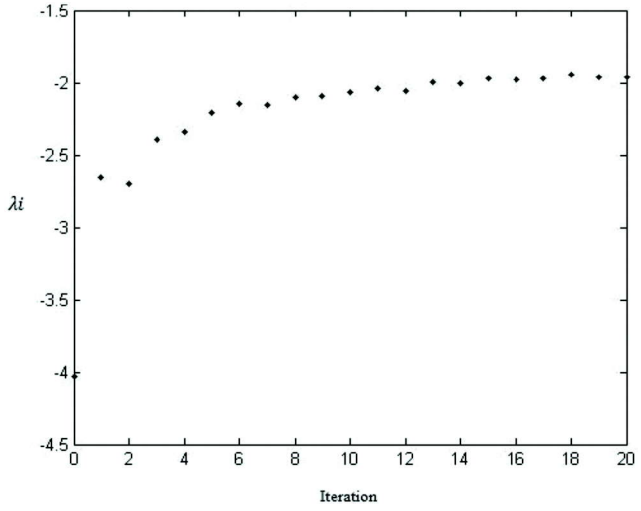

Fig. 2. Lyapunov exponent of the vowel /a/.

2.3 Correlation dimension

Fractals are objects which are self-similar at various resolutions. Self-similarity in a geometrical structure is a strong signature of a fractal object. Correlation dimension is a popular choice for numerically estimating the fractal dimension of the attractor [16]. Suppose that many points are scattered over a set. The typical number of neighbours of a given point will vary more rapidly with distance from that point if the set has high dimension than otherwise. Correlation dimension d_C measures the variation of average fraction of neighbouring points with distance. The correlation integral $C_d(R)$ in d dimensional space is given by

$$Cd(R) = \lim_{N\to\infty}\left[1/N^2\sum_{i,j=1}^{N} H(R-|Xi-Xj|)\right] \tag{6}$$

Where Xi and Xj are points on attractor, $H(y)$ is the Heaviside function, N is the number of point randomly chosen from the data set. The Correlation dimension d_C is the variation of $C_d(R)$ with R.

$$d_c = \lim_{R\to 0} \log \frac{[C_d(R)}{\log\ R} \tag{7}$$

2.4 Kolmogorov entropy

Entropy is a well-known measure used to quantify the amount of disorder in a system. It has also been associated with the amount of information stored in general probability distributions. Numerically, the Kolmogorov entropy can be estimated as the second order Kolmogorov entropy (K_2) and can be related to the correlation integral of the reconstructed attractor as [16]:

$$C_d(\in) \sim \lim_{\substack{S\to 0 \\ d\to\infty}} \in^D \exp(-\tau d K_2) \tag{8}$$

Where D is the fractal dimension of the system's attractor, d is the embedding dimension and τ is the time-delay used for attractor reconstruction. This leads to the relation:

$$K_2 \sim \frac{1}{\tau}\lim_{\substack{\tau\to 0 \\ d\to\infty}} \ln\frac{C_d(\varepsilon)}{C_{d+1}(\in)} \tag{9}$$

In a practical situation, the values of ε and d are restricted by the resolution of the attractor and the length of the time series.

2.5 Eigen value of reconstructed phase space

Eigen values are a special set of scalars associated with a linear system of equations that are sometimes also known as characteristic roots, characteristic values, proper values, or latent roots [18]. Let A be a linear transformation represented by a matrix. If there is a vector $X \in R \neq 0$ such that

$$AX = \lambda X \tag{10}$$

For some scalar λ, then λ is called the eigen value of A with corresponding (right) eigenvector X. The Eigen values can be used for dimensionality reduction [20]. We have calculated eigen values of Reconstructed Phase Space (RPS-EV) for different d values. A detailed analysis of eigen values obtained in different dimensions of RPS had conducted to identify the optimum d value.

2.6 Speaker modelling using chaotic properties of the power spectrum

The power spectrum of a chaotic system exhibits an exponential decay at high frequencies and the decay constant characterizes the system. It is also evident that the speech producing system is chaotic in nature. In this context, we studied the power spectrum of speech signal for extracting certain nonlinear features for speaker modelling.

The power spectrum of the speech signals is computed and compared against each speaker. For further examination, we smoothed the power spectrum using Linear Predictive Coding *(LPC)* based smoothing

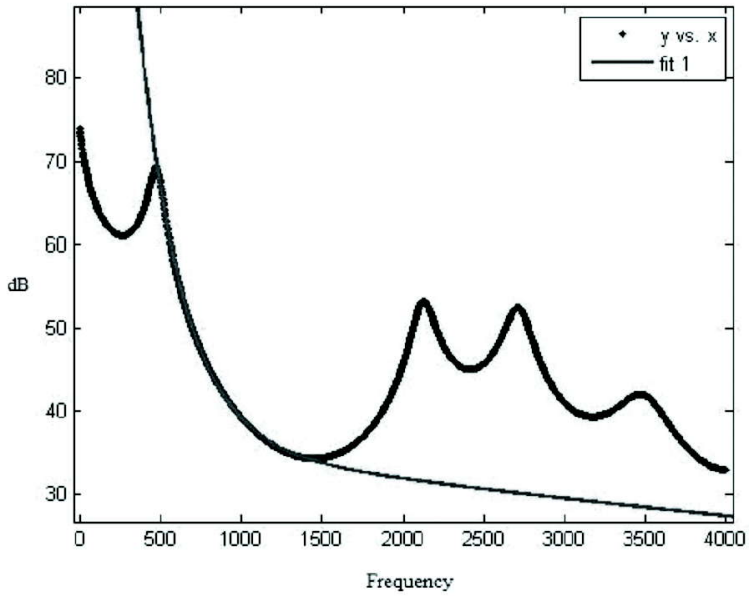

Fig. 3. Exponential fit over the LPC smoothed power spectrum for vowel /a/.

Technique. An *LPC* smoothes using a speech-appropriate vocal tract-like function (based on a simple source filter model of speech), so it is generally well-suited to the analysis of speech and facilitates finding formants[19]. The *LPC* smoothed power spectrum and the corresponding exponential fit extracted for the vowel /a/ are shown in Fig. 3. Further the Spectral Decay Coefficients *(SDC)* are extracted and used as feature for speaker recognition.

3. SIMULATION EXPERIMENT AND RESULTS

The speech database consists of five English vowels *(/a/, /e/, /i/, /o/ and /u/)* uttered by 50 different speakers (20 utterances of each vowel from every speaker) is constructed. We extracted Capacity Dimension *(CD)*, the Correlation Dimension *(CRD)*, Kolmogorov Entropy *(KE)*, Largest Lyapunov Exponent *(LLE)* and Eigen values of the Reconstructed Phase Space *(EV-RPS)* for five vowels uttered by 50 different speakers of same age group. The Reconstructed Phase Space *(RPS)* plots over different dimensions and the eigen values obtained from it are thoroughly analysed and found that optimum result is obtained at d=5. The speaker identification capabilities of the proposed Spectral Decay Coefficient *(SDC)* parameters are investigated. The *SDCs* are extracted from speech samples of five vowels taken from the database.

Here we used the database consisting of 250 samples of five vowels collected from fifty different speaker for training and a disjoint set of vowels of same size from the database for recognition purpose. Further, the FFMLP is simulated with the back propagation learning algorithm. A constant learning rate 0.01, is used (value of I was found to be optimum as 0.01 by trial and error method). The initial weights are obtained by generating random numbers ranging from 0.1 to 1. The number of input layer is fixed according to the feature vector size and the five output nodes representing five vowels. The recognition experiment is repeated by changing the number of hidden layers and number of nodes in each hidden layer for obtaining the successful architecture.

The network is trained using *SDC* feature and *RPC- EV* features extracted from the vowel samples of 50 speakers. Here we used a set of 50 samples each of five vowels spoken by different speakers for iteratively computing the final weight matrix and disjoint set of vowels of same size from the database for identification purpose. The experiment is repeated by adding capacity dimension, the correlation dimension, Kolmogorov entropy and Lyapunov exponent along with the above mentioned parameters. The block diagram of feature extraction techniques is illustrated in Fig. 4.

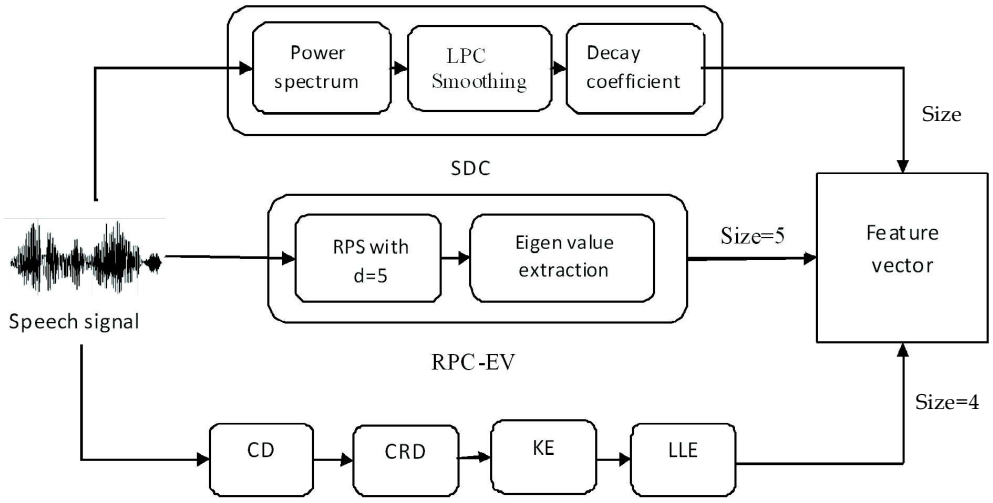

Fig. 4. Block diagram of feature extraction technique

The recognition accuracy obtained for fifty different speakers based on above said features extracted from each of the five vowels using FFMLP classifier are tabulated in table 1. The graphical representation of the recognition result is showed in Fig. 5. The experimental results indicate that the combined feature approach gives better speaker identification accuracy.

Table 1. Speaker Identification Results

Parameters used	Size of the parameter	Speaker identification accuracy (%) (foreachvowel)					Average (%)
		//a/	//e/	//i/	/o/	/u/	
SDC	4	71.12	59.80	64.00	54.74	69.00	63.73
SDC + RPC- EV	9	86.66	63.45	71.00	67.00	77.74	71.17
SDC+RPC-EV+LLE+ CD+CRD+KE	13	88.00	66.00	74.00	70.00	82.00	73.00

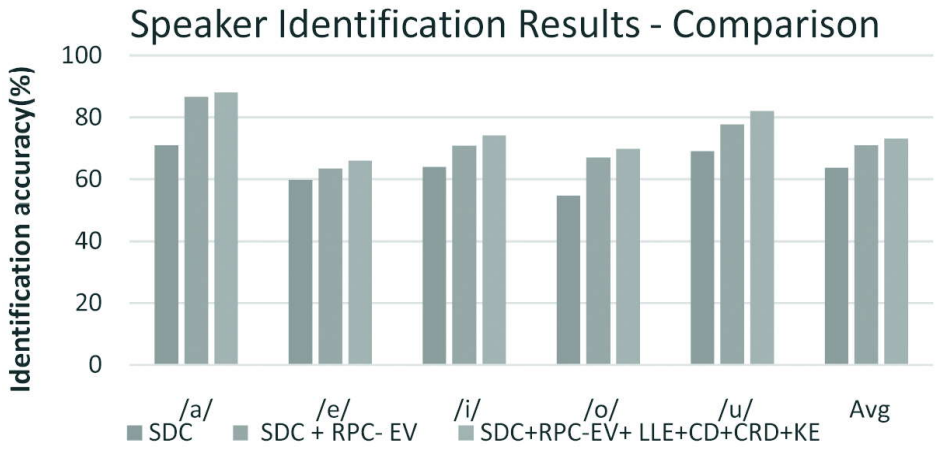

Fig. 5. Comparison of Speaker Identification Results

4. CONCLUSION

In this work, we modelled the speaker identity based on the non-linear properties of the speech samples with invariant features or characteristics of the system for the purpose of identification.

We have analysed the largest positive Lyapunov Exponent, Capacity Dimension, Correlation Dimension, Kolmogorov Entropy, Eigen Values of the Reconstructed Phase Space and Spectral Decay Coefficientsof selected phoneme for fifty different speakers. The speaker recognition experiment is conducted using Multilayer Feed Forward Neural Networks using combined nonlinear features. The experimental results indicate that the proposed SDC approach by itself is still below (63.72%) that of conventional features. The results further shows that the combined approach in which the SDC features, when used with RPC-EV, LLE, CD, CRD and KE, offers enormous improvement in speaker identification (on an average of 73.0%) accuracy.

5. REFERENCES

[1] L.G. KERSTA, 1962. Voiceprint Identification. *Nature,* **196**, 1253-1257.

[2] J. HARRINGTON and S. CASSIDY, 2000. Techniques in speech acoustics. *Computational Linguistics*, **26**(2), 294-295.

[3] T.F. QUATIERI, 2002. *Discrete-time Speech Signal Processing principles and practice*, Prentice Hall.

[4] H. TEAGER, 1980. Some observations on oral air flow during phonation, *IEEE Trans. on Acoustics, Speech, and Signal Processing,* **28**(5), 599-601.

[5] P. MARAGOS, T.F. QUATIERI and J.F. KAISER, 1991. Speech nonlinearities, modulations, and energy operators, *IEEE Int. Conf. on Acoustics, Speech, and Signal Processing*, **1**, 421-424.

[6] C. LINDGREN, M.T. JOHNSON and R.J. POVINELLI, 2003. Speech recognition using phase space features, *Proc. IEEE Int. Conf. on Acoustics, Speech, and Signal Processing*, China, **1**, I-60.

[7] M.T. JOHNSON, A.C. LINDGREN, R.J. POVINELLI and X. YUAN, 2003. Performance of nonlinear speech enhancement using phase space reconstruction, *Proc. IEEE Int. Conf. on Acoustics, Speech, and Signal Processing*, Hong Kong, China **1**, I-920.

[8] PETRY, D. AUGUSTO and C. BARONE, 2002. Speaker Identification using nonlinear dynamical features, *Chaos, Solitons and Fractals*, **13**, 221-231.

[9] V. PITSIKALIS and P. MARAGOS, 2002. Speech analysis and feature extraction using chaotic models, *Proc. IEEE Int. Conf. on Acoustics, Speech, and Signal Processing,* Orlando, Florida, **1**, I-533.

[10] M. BANBROOK, S. MCLAUGHLIN and I. MANN,1999. Speech characterization and synthesis by nonlinear methods, *Proc. IEEE Trans. on Speech and Audio Processing*, **7**, 1-17.

[11] KUMAR and S.K. MULLICK, 1996. Nonlinear dynamical analysis of speech, *Journal of the Acoustical Society of America,* **100**, 615-629.

[12] N. TISHBY, 1990. A dynamical system approach to speech processing, *Proc. Int. Conf. Acoustics, Speech and signal processing*, Albuquerque, 289-292

[13] H. TONG, 1990. *Non-linear time series. A dynamical system approach*. Oxford Statistical Science Series, Oxford: Clarendon Press.

[14] J.P. ECKMANN and D. RUELLE, ERGODIC, 1985. Theory of Chaos and Strange Attractors, *Reviews of Modern Physics*, **57**, 617-656.

[15] H. Kantz and T. Schreiber, 1997, *Nonlinear time series analysis*, Cambridge University Press, Cambridge

[16] M.C. VALSAKUMAR, S.V.M. SATYANARAYANA and V. SRIDHAR, 1997. Signature of chaos in power spectrum, *PRAMANA*, **48**(1), 69-85.

[17] H.M. TEAGER and S.M. TEAGER, 1989. Evidence for nonlinear sound production mechanisms in the vocal tract, *Speech Production and Speech Modelling, W. J. Hardcastle and A. Marchal, Eds.*, **55**, 241-261.

[18] D.S. GURU, B.H. SHEKAR and P. NAGABHUSHAN, 2004. A simple and robust line detection algorithm based on small eigen value analysis. *Pattern Recognition Letters,* **25**(1), 1-13.

[19] R.K. SUNIL KUMAR, V.L. LAJISH and P. VIVEK, 2013. Power spectrum analysis of speech signals (focused on chaotic properties) for speaker identification. *ACOUSTIS 2013*, New Delhi, India, 10-15.

[20] P. VIVEK, V.L. LAJISH and R.K. SUNIL KUMAR, 2015, Improved Vowel Phoneme Classification Over Eigenvalues of the Reconstructed Phase Space Using ANN, *Proc. Conf on Indian Language Computing (NCILC2015)*, **1**, 25-28.

Journal of Acoustical Society of India : Vol. 43, No. 2, 2016 (pp. 125-131)

Evaluation of digital signal processing algorithms in hearing aids with ear to ear synchronization

C. Geetha, R. Rajarajan and Kishore Tanniru
Department of Audiology, All India Institute of Speech and Hearing, Manasagangothri, Mysore-570006
e-mail: geethamysore.cs@gmail.com

[Received: 25-04-2016; Revised: 30-05-2016; Accepted: 02-09-2016]

ABSTRACT

The aim of the present study was to check the benefit of directionality and DNR algorithms of binaural WDRC wireless technology hearing aids on speech intelligibility in a noisy environment. The study had included 14 participants (between 27-55 years of age) with bilateral mild to moderate flat sensorineural hearing loss. Two hearing aids with wireless technology were programmed and fitted. SNR-50 was obtained using sentences in the conditions with and without wireless option, directionality and DNR algorithms. The sentences were played through a speaker at a fixed angle of 0°. Calibrated speech babble was used as noise and the babble was routed through speakers in 0°, 90°, 270° and in both 90° and 270° at a fixed presentation level of 70 dB SPL. The level of speech was varied till SNR-50 was achieved. The mean SNR-50 ranged from + 3.0 dB to + 7.5 dB. Friedman test and Wilcoxon signed rank test were carried out for statistical analysis. Results revealed that there was a significant improvement in SNR-50 using the wireless synchronization hearing aids when compared to deactivation of wireless synchronization option. Activation of directionality and DNR together, and activation of only directionality significantly further improved the speech perception in noise.

1. INTRODUCTION

Digital hearing aids have noise reduction techniques to improve speech perception in noise in individuals with hearing loss. The digital noise reduction algorithm (DNR) and directionality in digital hearing aids analyze the incoming signal based on its acoustical characteristics and the direction and categorize whether the incoming signal is noise or speech. Ear to ear synchronization or wireless synchronization technology is a modern technology added to some of the current digital hearing aids. These hearing aids communicate with each other and give binaural information to the brain. It is important that these algorithms coordinate between the two ears so that the brain identifies the correct sound source and speech even in a complex environment. These advanced digital signal processing algorithms in hearing aids with wireless synchronization technology work by sharing information between the two ears[1]. This has been said to improve the binaural cues, which in turn improves the speech perception in noise. This technology, reportedly, significantly improves speech comprehension, particularly in loud environments. There are a few research studies evaluating the performance of the hearing aids with wireless communication [1][2][3][4]. Most of them report of superior performance of the wireless synchronization technology. Nevertheless, these studies have evaluated the effect of either only the wide dynamic range compression (WRDC) on speech perception in noise [1] or all the digital signal processing algorithms (*i.e.*, WDRC, Directionality and DNR) activated together [4]. There are no published reports, to our knowledge, evaluating each of the

advanced features systematically. The working of the algorithms in wireless hearing aids may or may not be better than that in hearing aids without wireless technology. It is, hence, important to present evidence to see the use directionality and DNR algorithms with wireless communication facility in order to justify the higher cost of the hearing aids with wireless technology.

2. AIM

The current study aimed to check the benefit of directionality and noise reduction algorithms of binaural WDRC wireless synchronization technology hearing aids on speech intelligibility in a noisy environment.

3. OBJECTIVE OF THE STUDY

The objective of the current study was to compare the speech recognition ability in noise in the aided conditions with and without wireless synchronization, directionality and DNR, in individuals with hearing impairment, using binaural wireless synchronization technology hearing aids.

4. METHOD

4.1 Participants

Fourteen participants (10 males and 4 females) with bilateral sensorineural hearing loss, in the age range of 27-55 years (mean age = 39 years) participated in the study. All the participants had mild to moderate flat symmetrical sensorineural hearing loss. They were native speakers of Kannada language. Routine audiological evaluation was carried out prior to testing.

4.2 Equipment / Material

Two digital wireless transmission WDRC hearing aids of same model with fitting range from mild to moderately severe degree of hearing loss were used. These had an option of enabling or disabling the directionality, DNR algorithms and wireless transmission. A computer attached to NOAH link was used for programming the hearing aids using NAL-NL1 prescriptive formula, with appropriate cables and appropriate software. Adequate gain was provided with fine tuning to both ears independently after applying first fit with NAL-NL1. Bruel and Kjaer Hand held sound level meter was used with a ½ inch free-field microphone for the calibration of stimuli. Eight Genelec 8020B speakers mounted on Iso-Pod™ (Isolation position/decoupler™) vibration insulating stand located at 0°, 90°, 90° & 270° azimuth were used for the speech in noise experiment. A personal laptop connected to the Maico MA-52 audiometer's auxiliary input was used to present the stimuli.

4.3 Procedure

Speech intelligibility in noise was assessed using the sentence test in Kannada language developed by Geetha *et al* [5]. This test has 25 equivalent lists with ten sentences each. Each list has 40 key words. The sentences were delivered through the speaker kept at 0°. Eight talker Kannada speech babble was used as noise. The sentences in Kannada language was presented in a) Quiet situation, b) Noise from the front (0° angle), c) Noise from the right (90° angle), d) Noise from the left (270° angle) and e) Noise from both 90° and 270° angle speakers. The speech babble was presented at a constant noise level of 70 dB SPL and the intensity of the speech stimuli was varied in 2 dB steps to find out the SNR at which atleast 50% of the key words were repeated. The difference in the level of noise and speech was noted down as the SNR-50. Before the actual test started, a practice session was given. The test conditions were randomized to reduce the order effect. Each sentence lists was used only once in order to avoid practice effect.

5. RESULTS

The data were subjected to statistical analysis using the SPSS (Statistical package for social science) software version 20. The mean and standard deviation (SD) of SNR-50 in all the eight conditions are given in Table 1.

Table 1. Mean and SD of SNR-50 in all the conditions and in all degrees (n = 14).

S.no	Conditions\Speaker Azimuth	0°		90°		270°		90° & 270°	
		Mean	SD	Mean	SD	Mean	SD	Mean	SD
1	Wireless On All On	3.5	1.15	3.0	1.03	3.0	1.03	3.4	0.93
2	Wireless On Directionality On	4.0	1.10	3.4	0.93	4.0	0.78	5.4	0.93
3	Wireless On DNR On	4.5	0.93	4.5	1.22	4.5	0.93	5.4	0.93
4	Wireless On All Off	4.8	1.02	4.5	0.93	4.7	0.99	6.4	0.85
5	Wireless Off Directionality On	5.1	1.02	5.0	1.03	5.1	1.02	6.0	0.02
6	Wireless Off DNR On	5.0	1.03	5.2	0.99	5.2	0.99	6.2	0.72
7	Wireless Off All On	5.5	1.39	5.2	0.99	5.2	0.99	6.1	0.53
8	Wireless Off All Off	5.7	1.06	6.2	0.72	6.2	0.72	7.5	0.85

Note: Wireless = Wireless synchronization between the right and left hearing aids; All on = DNR and Directionality On; All off = DNR and Directionality off.

From the Table 1, it can be observed that the mean SNR-50 value ranged from + 3.0 dB to + 7.5 dB. A lesser SNR-50 value indicates better performance and a larger SNR-50 indicates poorer performance. The data were assessed for normality. The results showed no normal distribution and hence, non-parametric test, Friedman test and Wilcoxon signed rank test were done. The results of Friedman test revealed a significant effect seen in 0 degree ($x^2(7) = 34.5$), in 90 degree ($x^2(7) = 64.2$), in 270 degree ($x^2(7) = 66.3$) and in both 90 & 270 degree Azimuth ($x^2(7) = 74.9$) at 0.001 level of significance. In order to find out which of the

Table 2. Results of Wilcoxon signed rank test at 0° azimuth condition

Conditions	Wireless On All On	Wireless On Direc-tionality On	Wireless On DNR On	Wireless On All Off	Wireless Off Direc-tion ality On	Wireless Off DNR On	Wireless Off All On	Wireless Off All Off
Wireless On All On								
Wireless On Directionality On	0.180							
Wireless On DNR On	0.008	0.046						
Wireless On All Off	0.007	0.034	0.157					
Wireless Off Directionality On	0.013	0.046	0.206	0.527				
Wireless Off DNR On	0.004*	0.020	0.257	0.739	0.739			
Wireless Off All On	0.002*	0.005*	0.035	0.132	0.366	0.206		
Wireless Off All Off	0.001**	0.001**	0.011	0.058	0.206	0.059	0.763	

Note: Wireless = Wireless synchronization between the right and left hearing aids; All on = DNR and Directionality On; All off = DNR and Directionality off; Significant effects are in bold; **p<0.005, ***p<=0.001.

Table 3. Results of Wilcoxon signed rank test at 90° condition

Conditions	Wireless On All On	Wireless On Directionality On	Wireless On DNR On	Wireless On All Off	Wireless Off Directionality On	Wireless Off DNR On	Wireless Off All On	Wireless Off All Off
Wireless On All On								
Wireless On Directionality On	0.180							
Wireless On DNR On	0.002*	0.005*						
Wireless On All Off	0.005*	0.005*	1.000					
Wireless Off Directionality On	0.002*	0.001**	0.083	0.083				
Wireless Off DNR On	0.003*	0.002*	0.059	0.025	0.317			
Wireless Off All On	0.001**	0.002*	0.096	0.025	0.317	1.000		
Wireless Off All Off	0.001**	0.001**	0.003*	0.001**	0.003*	0.008	0.008	

Note: Wireless synchronization between the right and left hearing aids; All on = DNR and Directionality On; All off = DNR and Directionality off; Significant effects are in bold; **p<0.005, ***p<=0.001.

Table 4. Results of Wilcoxon signed rank test at 270° condition

Conditions	Wireless On All On	Wireless On Directionality On	Wireless On DNR On	Wireless On All Off	Wireless Off Directionality On	Wireless Off DNR On	Wireless Off All On	Wireless Off All Off
Wireless On All On								
Wireless On Directionality On	0.008							
Wireless On DNR On	0.002*	0.046						
Wireless On All Off	0.001**	0.025	0.317					
Wireless Off Directionality On	0.001**	0.005*	0.046	0.083				
Wireless Off DNR On	0.001**	0.003*	0.025	0.046	0.564			
Wireless Off All On	0.000**	0.003*	0.025	0.046	0.655	1.000		
Wireless Off All Off	0.001**	0.001**	0.001**	0.001**	0.005*	0.005*	0.008	

Note: Wireless synchronization between the right and left hearing aids; All on = DNR and Directionality On; All off = DNR and Directionality off; Significant effects are in bold; **p<0.005, ***p<=0.001.

conditions differed from each other, Wilcoxon signed rank test was done. The results of this are presented in Table 2.

As it can be viewed from the Table 2 that, when the speech babble and the speech were given from the same direction (0°), only the 'all algorithms (DNR + Directionality) ON and wireless synchronization ON' condition was significantly ($p<0.01$) better than the 'all algorithms OFF and wireless synchronization OFF' condition. There was no significant difference between other conditions.

From the Table 3 and Table 4, it can be observed that the results were similar in 90° and 270° azimuth conditions. That is, in both the noise conditions, the presence of wireless synchronization lead to significantly better SNR-50 ($p<0.05$) when compared to the conditions where the wireless synchronization was OFF. Further, when wireless synchronization was ON, activation of both directionality and DNR resulted in significantly better SNR-50 ($p<0.01$) followed by directionality when compared to the conditions where wireless synchronization was OFF. However, the performance with DNR alone was comparable in both wireless ON and wireless OFF conditions ($p<0.01$).

Table 5. Results of Wilcoxon signed rank test at 90° & 270° condition

Conditions	Wireless On All On	Wireless On Directionality On	Wireless On DNR On	Wireless On All Off	Wireless Off Directionality On	Wireless Off DNR On	Wireless Off All On	Wireless Off All Off
Wireless On All On								
Wireless On Directionality On	0.000**							
Wireless On DNR On	0.001**	1.000						
Wireless On All Off	0.001**	0.020	0.008					
Wireless Off Directionality On	0.001**	0.046	0.046	0.083				
Wireless Off DNR On	0.001**	0.014	0.014	0.564	0.157			
Wireless Off All On	0.001**	0.025	0.025	0.317	0.317	0.317		
Wireless Off All Off	0.001**	0.001**	0.000**	0.005*	0.001**	0.003*	0.002*	

Note: Wireless = Wireless synchronization between the right and left hearing aids; All on = DNR and Directionality On; All off = DNR and Directionality off; Significant effects are in bold; **$p<0.005$, ***$p<0.001$.

It can be observed from the Table 5 that, when the speech babble was given from both 90° and 270° angles simultaneously, only the 'all algorithms ON and wireless synchronization ON' condition was significantly ($p<0.01$) better than all the other conditions, and the 'all algorithms OFF and wireless synchronization OFF' condition was significantly poorer than all the other conditions.

6. DISCUSSION

The present study evaluated the effect of directionality and DNR algorithms of binaural wireless technology hearing aids on speech intelligibility in noise. From the results, it can be viewed that the wireless

synchronization significantly helps the individuals to hear and understand speech better in competing noise situations compared to without it. These results or in concurrence with Kreisman et al [1] study, where they reported that they found a significantly higher performance with the wireless synchronization when tested with QuickSIN test and HINT test. However, Iman et al [4] reported that they did not find any significant difference in QuickSIN test. The reason could be that, in Iman et al's study, the participants included in their study were older population and age related cognitive deficits may have influenced the performance with hearing aid.

It can be also observed that when speech and noise are from the same azimuth (0°), there was not much of difference found in speech perception across different aided conditions, except that wireless on condition was significantly different from wireless off conditions. Directionality and DNR did not play much role when the speech signal and noise was from the same direction. Studies have reported that, it is difficult to perceive speech when it is originating from the same direction as of noise, because there is no spatial separation between the speech and noise signal and it is difficult for the DSP features to separate these signals due to lack of spatial cues [6][7]. Further, the DNR algorithm did not significantly improve performance at 0, 90 and 270° azimuths. The reason for this could be that the background noise used was speech babble. Speech babble has similar temporal modulations like speech. This might have made it difficult for DNR algorithm to differentiate between speech and noise. In spite of this, as it can be seen from our results, binaural wireless synchronization technology did improve speech perception in noisy situation to some extent due to the preservation of binaural cues [1] [4]. When the noise and speech are from different speakers, that is, 90° condition and 270° condition, there was a significant difference when wireless on along with the DSP features on condition compared to all other condition. Further, directionality also played a significant role in speech perception along with this wireless synchronization when speech (0°) and noise (90°) (270°) arises from different direction. It can be also observed that there is significant improvement in speech perception when wireless synchronization was on compared to the conditions without it. There is a very good improvement in speech perception at these conditions because of spatial separation between the speech signal and the interfering noise. The results also indicate that there is an exchange of information happening between both the hearing aids using wireless synchronization and hence, binaural cues are maintained along with spatial cues which lead to better speech perception [4]. Further, the directionality was fixed to a particular direction. In the present study, since the speech and noise were also fixed, the directionality might have resulted in a very good improvement in binaural cues.

However, when noise was given from both speakers (90° & 270°) simultaneously, directionality and DNR did not yield significant benefit. The same was even observed in Iman et al's study. However, the reason for this was not given. It could be assumed that presenting noise from both the sides could not preserve the binaural cues as much as when noise is presented from only one side.

7. CONCLUSION

The present study attempted to evaluate the effect of directionality and DNR algorithms of binaural WDRC wireless technology hearing aids on speech intelligibility in noise. It can be concluded that there was a significant improvement in understanding speech in noise using the wireless synchronization hearing aids when compared to deactivation of wireless synchronization option. Activation of directionality and DNR together, and activation of only directionality significantly further improved the speech perception in noise. However, the DNR alone did not bring about much difference. In addition, it is also evident that the working of these algorithms depended on the direction of background noise.

8. REFERENCES

[1] B.M. KREISMAN, A.G. MAZEVSKI, D.J. SCHUM and R. SOCKALINGAM, 2010. Improvements in Speech Understanding with Wireless Binaural Broadband Digital Hearing Instruments in Adults with Sensorineural Hearing Loss. *Trends in Ampli.,* **14**(1), 3-11.

[2] P. SMITH, A. DAVIS, J. DAY, S. UNWIN, G. DAY and J. CHALUPPER, 2008. Real-world preferences for linked bilateral processing. *Hear J.,* **61**, 33-8.

[3] R. SOCKALINGAM, K. ENEROTH, M. HOLMBERG and M. SHULTE, 2009. Binaural hearing aid communication shown to improve sound quality and localization. *Hear J.*, **62**, 46-7.

[4] I. IMAN, P. VIJAY, M. EWAN and C. MARGARET, 2013. Evaluation of speech intelligibility and sound localization abilities with hearing aids using binaural wireless technology. *Audiol Research*, **3** e1.

[5] C. GEETHA, K.S.S. KUMAR, P. MANJULA and P. MAHADEVAIAH, 2014. Development and standardization of the sentence identification test in the Kannada language. *J. Hear Sci.,* **4**(1), 18-26.

[6] M. RYCHTARIKOVA, T. BOGAERT, G. VERMEIR and J. WOUTERS, 2011. Perceptual validation of virtual room acoustics: Sound localisation and speech understanding. *Applied Acous*., **72**, 196-204.

[7] M. L. HAWLEY, R. Y. LITOVSKY and H. S. COLBURN, 1999. Speech intelligibility and localization in complex environments. *J. Acoust Soc Am.,* **105**, 3436-48.

INFORMATION FOR AUTHORS

ARTICLES

The Journal of Acoustical Society of India (JASI) is a refereed publication published quarterly by the Acoustical Society of India (ASI). JASI includes refereed articles, technical notes, letters-to-the-editor, book review and announcements of general interest to readers.

Articles may be theoretical or experimental in nature. But those which combine theoretical and experimental approaches to solve acoustics problems are particularly welcome. Technical notes, letters-to-the-editor and announcements may also be submitted. Articles must not have been published previously in other engineering or scientific journals. Articles in the following are particularly encouraged: applied acoustics, acoustical materials, active noise & vibration control, bioacoustics, communication acoustics including speech, computational acoustics, electro-acoustics and audio engineering, environmental acoustics, musical acoustics, non-linear acoustics, noise, physical acoustics, physiological and psychological acoustics, quieter technologies, room and building acoustics, structural acoustics and vibration, ultrasonics, underwater acoustics.

Authors whose articles are accepted for publication must transfer copyright of their articles to the ASI. This transfer involves publication only and does not in any way alter the author's traditional right regarding his/her articles.

PREPARATION OF MANUSCRIPTS

All manuscripts are refereed by at least two referees and are reviewed by the Publication Committee (all editors) before acceptance. Manuscripts of articles and technical notes should be submitted for review electronically to the Chief Editor by e-mail or by express mail on a disc. JASI maintains a high standard in the reviewing process and only accept papers of high quality. On acceptance, revised articles of all authors should be submitted to the Chief Editor by e-mail or by express mail.

Text of the manuscript should be double-spaced on A4 size paper, subdivided by main headings-typed in upper and lower case flush centre, with one line of space above and below and sub-headings within a section-typed in upper and lower case understood, flush left, followed by a period. Sub-sub headings should be italic. Articles should be written so that readers in different fields of acoustics can understand them easily. Manuscripts are only published if not normally exceeding twenty double-spaced text pages. If figures and illustrations are included then normally they should be restricted to no more than twelve-fifteen.

The first page of manuscripts should include on separate lines, the title of article, the names, of authors, affiliations and mailing addresses of authors in upper and lowers case. Do not include the author's title, position or degrees. Give an adequate post office address including pin or other postal code and the name of the city. An abstract of not more than 200 words should be included with each article. References should be numbered consecutively throughout the article with the number appearing as a superscript at the end of the sentence unless such placement causes ambiguity. The references should be grouped together, double spaced at the end of the article on a separate page. Footnotes are discouraged. Abbreviations and special terms must be defined if used.

EQUATIONS

Mathematical expressions should be typewritten as completely as possible. Equation should be numbered consecutively throughout the body of the article at the right hand margin in parentheses. Use letters and numbers for any equations in an appendix: Appendix A: (A1, (A2), etc. Equation numbers in the running text should be enclosed in parentheses, i.e., Eq. (1), Eqs. (1a) and (2a). Figures should be referred to as Fig. 1, Fig. 2, etc. Reference to table is in full: Table 1, Table 2, etc. Metric units should be used: the preferred from of metric unit is the System International (SI).

REFERENCES

The order and style of information differs slightly between periodical and book references and between published and unpublished references, depending on the available publication entries. A few examples are shown below.

Periodicals:

[1] S.R. Pride and M.W. Haartsen, 1996. Electroseismic wave properties, *J. Acoust. Soc. Am.*, **100** (3), 1301-1315.

[2] S.-H. Kim and I. Lee, 1996. Aeroelastic analysis of a flexible airfoil with free play non-linearity, *J. Sound Vib.*, **193** (4), 823-846.

Books:

[1] E.S. Skudzryk, 1968. *Simple and Comlex Vibratory Systems*, the Pennsylvania State University Press, London.

[2] E.H. Dowell, 1975. *Aeroelasticity of plates and shells*, Nordhoff, Leyden.

Others:

[1] J.N. Yang and A. Akbarpour, 1987. Technical Report NCEER-87-0007, Instantaneous Optimal Control Law For Tall Buildings Under Seismic Excitations.

SUMISSIONS

All materials from authors should be submitted in electronic form to the JASI Chief Editor: B. Chakraborty, CSIR - National Institute of Oceanography, Dona Paula, Goa-403 004, Tel: +91.832.2450.318, Fax: +91.832.2450.602,(e-mail: bishwajit@nio.org) For the item to be published in a given issue of a journal, the manuscript must reach the Chief Editor at least twelve week before the publication date.

SUMISSION OF ACCEPTED MANUSCRIPT

On acceptance, revised articles should be submitted in electronic form to the JASI Chief Editor (bishwajit@nio.org)

ISSN 0973-3302

JOURNAL OF ACOUSTICAL SOCIETY OF INDIA

Volume 43 Number 3 July 2016

A Quarterly Publication of the JASI

http://www.acousticsindia.org

Journal of Acoustical Society of India

Volume 43 Number 3 July 2016 pp 133-176

JASI

Journal of Acoustical Society of India

The Refereed Journal of the Acoustical Society of India (JASI)

The Journal of Acoustical Society of India is a refereed journal of the Acoustical Society of India **(ASI)**. The **ASI** is a non-profit national society founded in 31st July, 1971. The primary objective of the society is to advance the science of acoustics by creating an organization that is responsive to the needs of scientists and engineers concerned with acoustics problems all around the world.

Manuscripts of articles, technical notes and letter to the editor should be submitted to the Chief Editor. Copies of articles on specific topics listed above should also be submitted to the respective Associate Scientific Editor. Manuscripts are refereed by at least two referees and are reviewed by Publication Committee (all editors) before acceptance. On acceptance, revised articles with the text and figures scanned as separate files on a diskette should be submitted to the Editor by express mail. Manuscripts of articles must be prepared in strict accordance with the author instructions.

All information concerning subscription, new books, journals, conferences, etc. should be submitted to Chief Editor:

B. Chakraborty, CSIR - National Institute of Oceanography, Dona Paula, Goa-403 004,
Tel: +91.832.2450.318, Fax: +91.832.2450.602, e-mail: bishwajit@nio.org

Annual subscription price including mail postage is Rs. 2500/= for institutions, companies and libraries and Rs. 2500/= for individuals who are not **ASI** members. The Journal of Acoustical Society of India will be sent to **ASI** members free of any extra charge. Requests for specimen copies and claims for missing issues as well as address changes should be sent to the Editorial Office:

ASI Secretariat, C/o Acoustics, Ultrasonics & Vibration Section, CSIR-National Physical Laboratory, Dr. KS Krishnan Road, New Delhi 110 012, Tel: +91.11.4560.8317, Fax: +91.11.4560.9310, e-mail: asisecretariat.india@gmail.com

ISSN 0973-3302

Printed at Alpha Printers, WZ-35/C, Naraina, Near Ring Road, New Delhi-110028 Tel.: 9810804196. JASI is sent to ASI members free of charge.

JASI

Journal of Acoustical Society of India (JASI)

A quarterly publication of the Acoustical Society of India

Volume 43, Number 3, July 2016

ARTICLES

INFORMATION

EDITORIAL

I am very happy to write Guest Editorial Note on "Special Issue on Physical Acoustics and Ultrasonics of Journal of Acoustical Society of India". Dr. Bishwajit Chakraborty, Chief Editor of JASI has requested for my help to edit this issue and carry out review process. However, we both have worked hard to bring this issue in time. He sent me relevant papers presented during NSA-2015 which held at CSIR-NIO, Goa on October 7-9, 2015. Most appropriate papers were selected and authors were asked to submit extended papers within stipulated time.

The extended papers, after assessing their suitability, were sent to reviewers (at least two reviewers for each paper). The reviewers have been very co-operative in sending the reports on time. We are thankful to them. Out of 9 papers, only six papers have been found suitable for publication in this special issue of JASI.

While we were looking for papers on technology, devices, materials development and new measurement applications, only velocity measurement papers (except one from NPL) were available and had to be accommodated. We have selected best available research for this special issue. During the process of the selection of the articles (through previous JASI and Proc. NSA 2015) as well as review, we realized that the most of the articles are of routine type. Only limited groups in the country, are involved in the Physical Acoustics and Ultrasonic research field. We expect in future, this trend will change towards the better direction where calibration of the measurements and material development should include in depth investigations.

In the present issue, one paper is on ultrasonic transducer characterisation while other five are on acoustic/ ultrasonic study along with other parameters of liquids, liquid mixtures, chemicals (amino, pyridine and aniline, binary mixtures, etc.), and composites etc studied at particular temperatures.

The authors and reviewers are thanked again. I give special thanks to our Chief Editor, Dr. Bishwajit Chakraborty, for taking up the task in a very successful manner.

Dr. V.R. Singh
Guest Editor
Special Issue on Physical Acoustics and Ultrasonics of JASI

Journal of Acoustical Society of India : Vol. 43, No. 3, 2016 (pp. 133-137)

Characterization of ultrasonic transducer by acoustic power measurement using vertical float system

Yudhisther Kumar Yadav and Reeta Gupta
CSIR - National Physical Laboratory, Dr. K. S. Krishnan Road, New Delhi (India)
e-mail: ykyadav@nplindia.org

[Received: 19-08-2016; Revised: 04-10-2016; Accepted: 05-10-2016]

ABSTRACT

Acoustic has wide range of industrial and biomedical applications. In medical science ultrasound is used for diagnosis, therapeutic use, kidney stone disintegration, bone density evaluation, *etc.* Knowledge of ultrasonic power output levels used in therapeutic ultrasound equipment has become increasingly important. Accuracy, precision and repeatability of acoustic power measurement assures the quality of measurements and patient safety by giving the exact exposure levels in case where potential risks exist. There are number of techniques used for ultrasonic power measurement such as radiation force balance, torsion balance, planar scanning, pressure measurement, calorimeter, thermocouple, light diffraction etc. In the present paper acoustic power is measured using radiation force vertical float system. Vertical Float system, indigenously developed at NPL, is used for higher acoustic power measurement in the range of 1 to 20 W in frequency range 1 to 5 MHz in degassed water. Acoustic power of an ultrasonic transducer excited by an ultrasonic therapy unit at different voltages and duty cycles (9 to 30 Volts at 25%, 35% and 45% duty cycles) is measured. Results are reported in the paper to optimize the performance of the therapy unit under design with an uncertainty of ± 8.5%.

1. INTRODUCTION

Acoustic power is an important parameter and specifies the characteristics of an ultrasonic transducer used for biomedical and industrial applications. There are number of techniques used for ultrasonic power measurement [1- 5] such as by using radiation force balance, torsion balance, planner scanning, pressure measurement, calorimetric, using thermocouple, light diffraction etc. In the present paper acoustic power of an ultrasonic applicator and an ultrasonic power transducer is measured using radiation force vertical float system. National Physical Laboratory, India (NPLI) maintains Radiation Force Balance (RFB) system for total Acoustic power measurement [1-9] in frequency range 1 MHz to 15 MHz . The Primary Standard RFB with digital microbalance has measuring range from 10 mW to 1 W in the frequency range of 1-15 MHz with an associated measurement uncertainty of ±4.5 %. The Vertical Float System of Acoustic Power Measurement has measuring range from 1 to 20 W in frequency range 0.5 to 5 MHz with an uncertainty of ±8.5 %. Results of the measurements will be helpful in characterisation of the transducers used in the therapy unit or any industrial unit for particular use.

2. VERTICAL FLOAT SYSTEM AND POWER MEASUREMENT

Vertical float system is an indigenously developed system consisting of the water tank with specially designed acoustic absorbers to make the tank anechoic[1-3]. It has specially designed conical hollow vertical Float, a U-shape glass tube and a hollow pipe attached with the height gauge (Fig. 1 and 2).

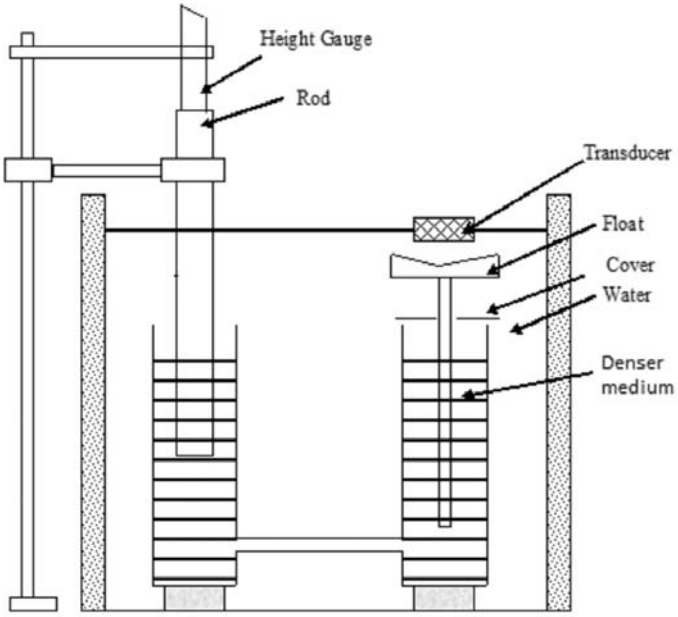

Fig. 1. Block diagram of Vertical Float Setup for acoustic power measurement

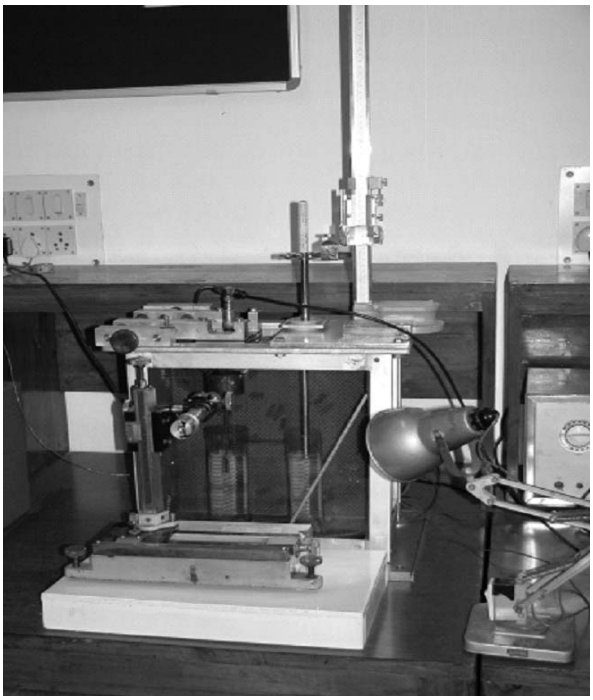

Fig. 2. Photograph of Vertical Float set up for acoustic power measurement

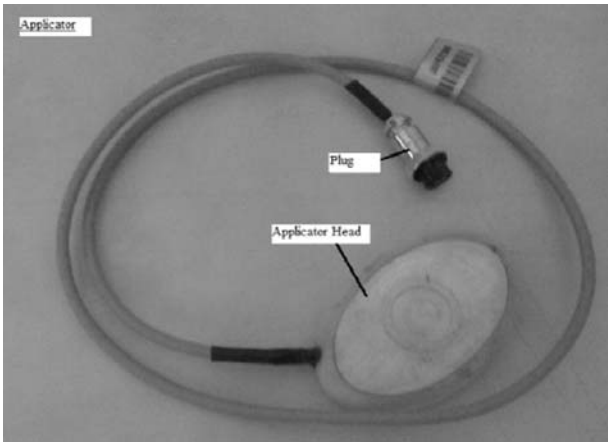

Fig. 3. Ultrasonic Applicator

For measurement of acoustic power, the ultrasonic transducer or ultrasonic applicator (Fig. 3) is adjusted on the vertical float such that the vertical float floats in U-Tube having denser medium and is submerged in the liquid (water) filled in the tank. As the transducer is excited, ultrasonic radiation pressure moves the float downwards. The float is brought back to its original position by the additional displacement of heavier liquid. The heavier liquid, filled in twin tubes, is made to rise by the movement of a steel rod downwards at other end of the U-tube. The distance moved by the rod is calibrated with standard masses and directly linked to evaluate the ultrasonic power.

The measurement is related to a set of calibrated masses. When some mass is placed over the float, the float moves downwards proportionate to the value of weight in water. Ratio of the mass to the distance moved by the rod is evaluated. Equivalent mass is calculated against the distance moved by the rod due to ultrasonic power.

When the distance moved by the rod due to ultrasonic power P is *'l'*, from the ratio of the mass to distance, equivalent mass *'m'* corresponding to distance *'l'* is calculated. Ultrasonic power (in watt) is then calculated from the following relation.

$$P = \frac{mgc}{2\cos^2\theta}$$

Where *m* is mass in kilogram and *g* is acceleration due to gravity in meter per second square and *c* is ultrasonic velocity in water in meter per second at particular temperature of water used. θ = angle between beam direction and normal to reflecting surface.

3. RESULTS AND DISCUSSION

Acoustic power of an Ultrasonic Applicator with the Therapy Unit is measured and results are given in Table 1. Ultrasound Therapy Unit was under design by M/s I-Trace Nanotech Pvt Ltd. and the results are helpful to upgrade the performance of unit. The total output power of the applicator with given excitation range is from 217 to 885 mili watt (Table 1.) which is very less as the power of a therapy unit requires to be in around 10 watts at higher side.

In other experiment acoustic power of a power transducer is measured at the resonance frequency having maximum power at certain voltage. For determining resonance frequency power output was measured with varying frequency at a fixed voltage. The ultrasonic total power of the transducer varies from few mili watts to 5 watts for peak to peak voltage range from 20 V to 150 V (Figure 4). rf voltage is achieved by using ENI Power amplifier and Wavetek function generator. The transducer can be used as a standard source of ultrasonic power for higher frequencies.

Table 1. Ultrasonic power of Applicator at 1.00 MHz (Uncertainty U_n is ± 8.5%).

Sr No	Voltage	Duty cycle	Intensity	Power (mW) at 40 mm of water with plane wave correction	Power at face of transducer (mW)
1	9	25	Low	217.0	217.4
2	9	35	Medium	227.4	227.8
3	9	45	High	222.9	223.2
4	12	25	Low	233.2	233.6
5	12	35	Medium	235.3	235.7
6	12	45	High	241.5	241.9
7	15	25	Low	247.5	247.9
8	15	35	Medium	251.8	252.3
9	15	45	High	253.7	254.1
10	18	25	Low	253.5	254.0
11	18	35	Medium	259.7	260.2
12	18	45	High	275.5	276.0
13	21	25	Low	272.5	273.0
14	21	35	Medium	285.8	286.3
15	21	45	High	358.9	359.6
16	24	25	Low	317.9	318.5
17	24	35	Medium	344.0	344.7
18	24	45	High	497.6	498.5
19	30	25	Low	477.5	478.4
20	30	35	Medium	618.2	619.4
21	30	45	High	883.2	884.8

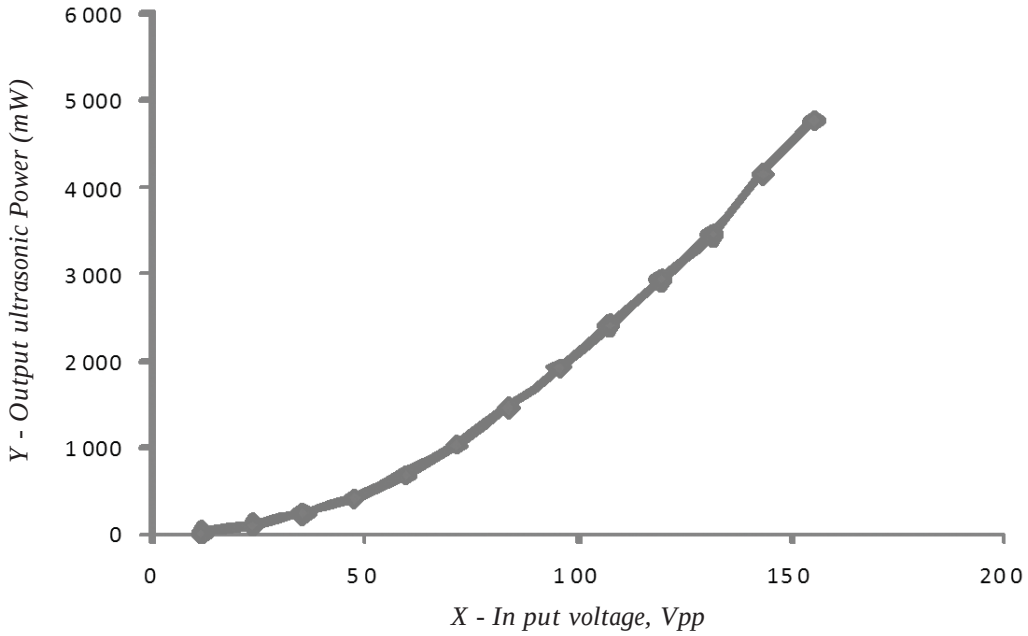

Fig. 4. Ultrasonic power with varying input voltage to the Ultrasonic Power transducer at 1.235 MHz.

4. CONCLUSION

Vertical Float System as Radiation Force Balance used for quality check for output power of a therapy system and ultrasonic power transducer in the range of few mille watt to 5 watt with an measurement uncertainty ± 8.5%. Acoustic power of Power Transducer measured is in the range 1 mW to more than 5 Watt at a frequency of 1.235 MHz for various input peak to peak voltage ranging from 20 Vpp to 150Vpp. Transducer can be used a standard source of ultrasonic power. Acoustic power of Applicator with therapy unit measured is helpful for up-gradation of the Therapy Unit for desired power.

5. ACKNOWLEDGEMENT

Authors are thankful to the Dr P K Dubey and Mr. Ravinder Kumar NPL for their kind support and to the M/s I -Trace Nanotech Pvt Ltd for using their Ultrasonic Therapy Unit for making the measurements.

6. REFERENCES

[1] YUDHISTHER KUMAR YADAV and ASHOK KUMAR, 2011. Ultrasonic Power Measurement and its Biomedical Necessities, *New Dimensions of Physics*, (Crescent Publishers Allahabad) pp. 22-26

[2] V.N. BINDAL and ASHOK KUMAR, 1980. Measurement of ultrasonic power with a fixed path radiation pressure float method, *Acustica,* **46**, 223-225.

[3] V.N. BINDAL, ASHOK KUMAR and R.C. CHIVERS, 1983. On the float method of measuring ultrasonic output, *Acustica,* **53** , 219-23.

[4] K. BRENDEL and K. BEISSNER, 1983. Output measurement of ultrasonic therapeutic equipment, *J. Pure Appl. Ultrason*. **5**, 76-80.

[5] IEC 61161 (1998-05), Ultrasonic power measurement in liquids in the frequency range 0.5 MHz to 25 MHz

[6] K. BEISSNER, 1999. Primary measurement of ultrasonic power and dissemination of ultrasonic power reference values by means of standard transducers, *Metrologia,* **36**, 313-20.

[7] K. BEISSNER, 1984. Minimum target size in radiation force measurements, *J. Acoust. Soc. Amer.*, **76**, 1505-1510.

[8] R.T. HEKKENBERG, K. BEISSNER, B. ZEQIRI, R.A. BEZEMER and M. HODNETT, 2001. Validated ultrasonic power measurements up to 20 W, *Ultrasound in Med. & Biol.*, **27**, 427-438.

[9] J. LUBBERS and R. GRAAFF, 1998, A simple and accurate formula for the sound velocity in water, *Ultrasound in Med. & Biol.* **24**, 1065-68.

Journal of Acoustical Society of India : Vol. 43, No. 3, 2016 (pp. 138-145)

Determination of compatible solvent concentration for dewaxing of crude oil using ultrasonic technique

A. Tripathy[1], G. Nath[2] and R. Paikaray[3]
[1]Department of Applied Science and Humanities, ABES Engg. College, UP
[2]Department of Physics, Veer Surendra Sai University of Technology, Odisha
[3]Department of Physics, Ravenshaw University, Odisha
e-mail: tripathyamita21@gmail.com

[Received: 20-08-2016; Revised: 20-09-2016; Accepted: 02-10-2016]

ABSTRACT

Wax Precipitation is one of the most important flow assurance problems in the transportation of waxy crude oil along horizontal pipeline. This makes the oil industry to spend an extra energy and money. The present work is to study the determination of approximate solvent concentration for dewaxing in crude oil by propagation of ultrasonic wave in a compatible solvent mixture. The compatibility of the solvent mixture of n-heptane and acetone was well studied with the help of acoustic parameters and computed from the ultrasonic velocity and density data. The ultrasonic velocity and density was determined at temperature 20°C. The different acoustic parameters like compressibility, intermolecular free length, acoustic impedance and their deviated values were calculated. Each concentration of solvent mixture was treated with the crude oil in different ratios (1:1, 2:1, 3:1). The variation of acoustic parameters were used to determine the proper solvent concentration for dewaxing process in terms of intermolecular interaction. The yield point of the wax was calculated from the wax recovered after the treatment of it with solvent mixture. The result gave an insight of increasing trend of dewaxing process with the increase in concentration of solvent. The highest amount of wax was produced with 150 gm of the crude oil with the ratio 3:1 of solvent mixture, within two hours of the experimental procedure.

1. INTRODUCTION

The presence of paraffin wax in crude oil presents a multitude of problems to the producers. The problems associated with their presence range from minor to severe; depending on their quantity and composition[1-7]. Petroleum production may be significantly affected by deposition of paraffin wax during crude production, with devastating economic consequences. Hence, predicting wax problems within the flow lines is essential in optimizing production and calculating operating efficiency[8]. Paraffin wax generally consist of straight and branched chain hydrocarbons that precipitates out of crude oil when there is a slight change in equilibrium conditions, causing a loss of solubility of the wax in the crude oil. A decrease in temperature is the most common cause of paraffin wax precipitation; though many other factors could affect the process. However, the solubility of paraffin wax is not only sensitive to temperature variation, but also an integration of physiochemical properties of the crude oil and other operation factors in production system. Thus, accurate knowledge of physiochemical properties of solvent mixture is vital in the quest for finding solution for handling waxy crude. The main goal of this work was to study different physiochemical properties of solvent mixture in presence of high frequency ultrasonic wave and to predict the optimal

concentration of solvent mixture to oil ratio for removal of wax deposition using experimental methodology to simulate wax deposition in the laboratory.

2. MATERIALS

High purity and analytical grade samples of acetone 99% (GC) and n-heptane 99.0% (GC) were procured from CDH fine chemicals Pvt.Ltd., India. The entire chemical used in the study were purified by standard procedure and redistilled before use[9-11]. To minimize the contact of the deliquescent regent with moist air, the product was kept in sealed bottles in desiccators. The purities of the sample were confirmed by GLC. Binary mixtures were prepared by mass in air tight bottles. The mass measurements were performed on high precession digital balance with an accuracy of $\pm$ 1 mg. The densities of pure liquids and their mixture were determined by using double arm pyknometer with accuracy of the order of $\pm$ 0.01 kg / m^3.

3. EXPERIMENTAL METHOD

The ultrasonic velocity was determined using multi frequency ultrasonic interferometer operating at a frequency 2 MHz (Mittal Enterprises, New Delhi, Model-MX-3) at temperature 20°C. The accuracy in the measurement of ultrasonic velocity was within $\pm$ 0.01 ms^{-1}. The density of the mixture was determined with the help of specific gravity bottle. The temperature of the solution was controlled by circulating water at a desired temperature through the jacket of double walled cell within $\pm$ 0.01 K using a constant temperature bath. Each concentration of solvent mixture was treated with the crude oil in different ratios (1:1, 2:1, 3:1). The variation in the acoustic parameters, as observed, were used to determine the proper solvent concentration for dewaxing, interpreting the results in terms of intermolecular interaction[12-13]. The yield point of the wax was calculated from the recovered wax after its treatment with solvent mixture by using the relation.

$$Y = \frac{W_e}{W_o} \times 100$$

Where Y is the yield as a percentage of the total weight of the sample; W_e is the weight of the extract and W_o is the weight of the crude oil sample. The total wax content of the crude oil sample recovered in this study was 25.7% or 1.3 g per 5 g of crude oil sample. After determining the optimum concentration of solvent mixture from the analysis of the different acoustical parameters for the solvent dewaxing process, analysis of the sample was conducted to determine the overall effectiveness of the process.

4. THEORY: CALCULATION OF ACOUSTIC PARAMETERS

The experimental measured values of ultrasonic velocity and computed values of density were used to compute acoustic parameters such as intermolecular free length (L_f), isentropic compressibility (β_S), acoustic impedance (Z), and their deviated values. The above acoustic parameters were determined with the help of the following relations[14-15].

$$\text{Isentropic compressibility } (\beta_S) = \frac{1}{\rho C^2} \quad (1)$$

$$\text{Intermolecular free length } (L_f) = K\beta^{\frac{1}{2}} \quad (2)$$

$$\text{Acoustic impedance } (Z) = pC \quad (3)$$

$$\text{and their deviated values were calculated as } Y^E = Y_{mix} - (X_A Y_A + X_B Y_B) \quad (4)$$

where the constant K is temperature dependent which is given as [93.875 + (0.375T)] $\times 10^{-8}$ [16] and T being the temperature.

5. RESULT AND DISCUSSION

Fig.1 shows the variation of acoustic velocity with the increasing concentration of solvent mixture. The

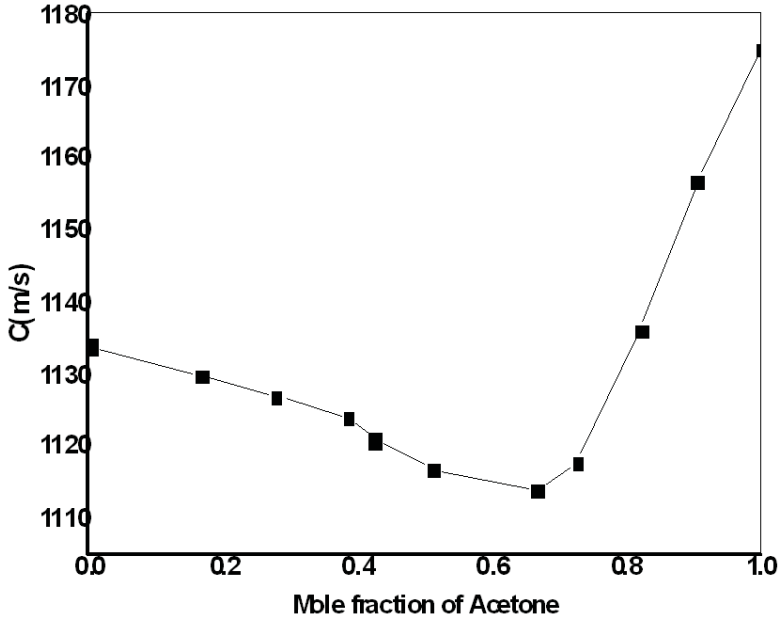

Fig. 1. Variation of ultrasonic velocity

acoustic velocity decreases up to 0.70 mole fraction of solvent mixture *i.e.* when it contains 7.0 g of acetone and 3.0 g of n-heptane by weight, suggesting that the interaction between the components of solvent mixture is more. As a result, the motion of the molecules in the solvent mixture decreases reducing the acoustic velocity. Further, it increases in acetone rich region attributing to the fact of strong hydrogen bonding between the long carbon chain of n-heptane and carbonyl group of acetone and the dispersive force is high between the similar molecules[17].

In fig. 2 the trend in deviated acoustic velocity (ΔC) was negative for entire mole fractions of acetone. It suggests the presence of weak intermolecular interaction within the component molecules. Again, as the chain length has good impact on variation of acoustic velocity, the velocity decreases with the increase in

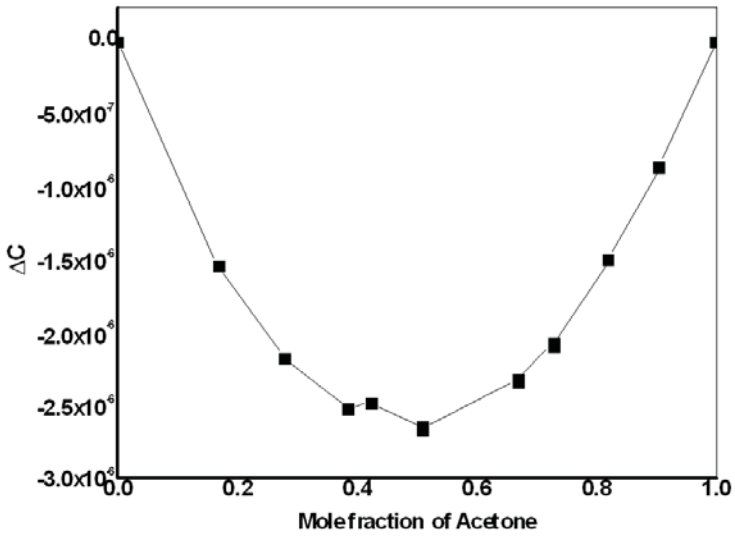

Fig. 2. Variation of deviated ultrasonic velocity

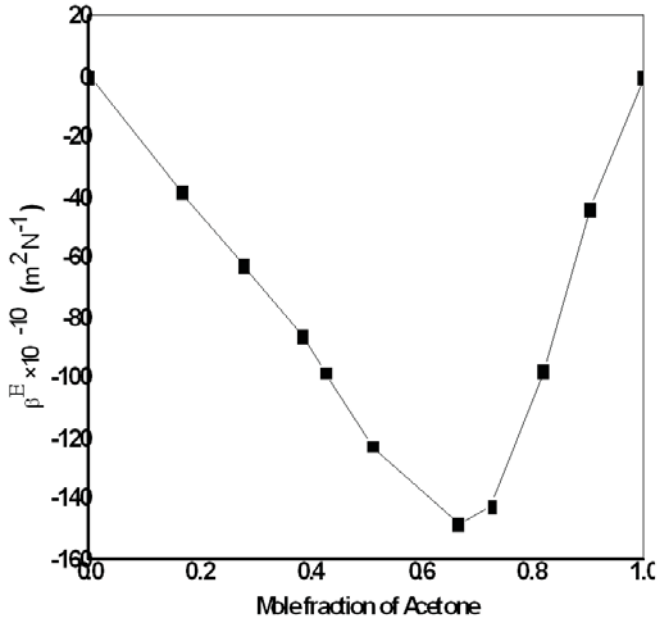

Fig. 3. Variation of deviated isentropic compressibility

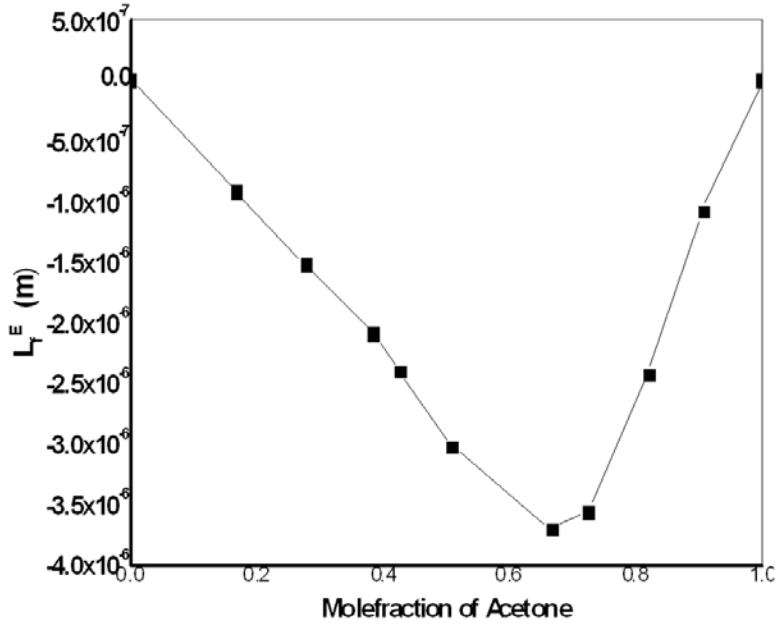

Fig. 4. Variation of deviated intermolecular free length

the concentration of unlike molecules. The variation of deviated adiabatic compressibility and free length in fig. 3 and fig. 4 reaspectively were found to be negative for all mole fractions of acetone, indicating the strong interaction between acetone and n-heptane. This may be due to the more likelihood of formation of hydrogen bond in mixture as compared to that of pure liquids of acetone and n-heptane. Graph showing negative value of β^E depicts that liquid mixture may be highly compressed which is possible when unlike molecules are tightly bound or interaction is high. Negative value of excess L_f^E reflects strong interaction which may be due to the association of molecules.

Acoustic impedance is the opposition offered by the medium for the propagation of sound energy. In fig.5 positive deviation of excess acoustic impedance, which is maximum at 0.75 mole fraction of acetone, signifies strong interaction between polar and non-polar molecules. However, the magnitude of molecular association decreases as component of acetone (polar molecules) increases. The interaction parameter (χ) decreases with the increase in acetone indicating association between solute and solvent, as shown in fig. 6. From fig. 7, it was observed that with the increase in the addition of solvent *i.e.* with the ratio of acetone / n-heptane from 1:1, 2:1, 3:1 to the crude oil, the recovery of wax increased[18]. Maximum wax yield was under the optimum conditions of acetone / n-heptane at ratio 3:1.

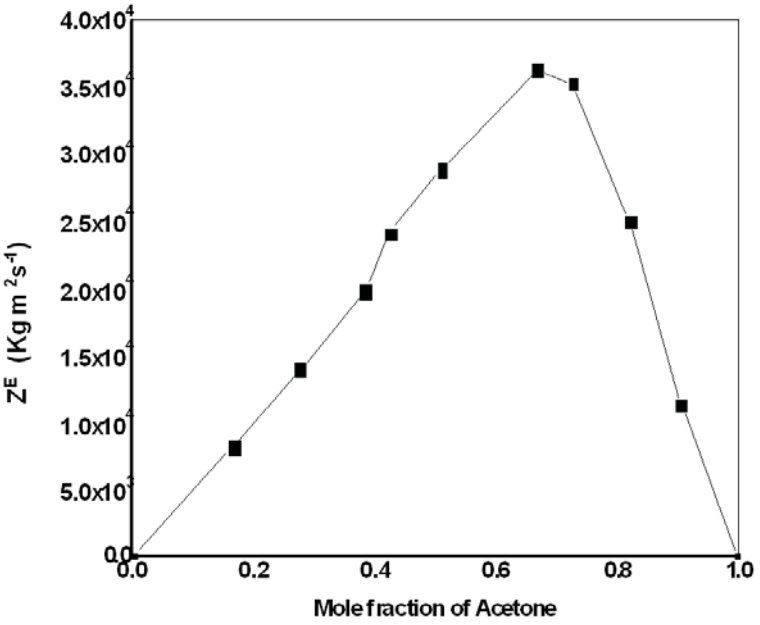

Fig. 5. Variation of deviated acoustic impedance

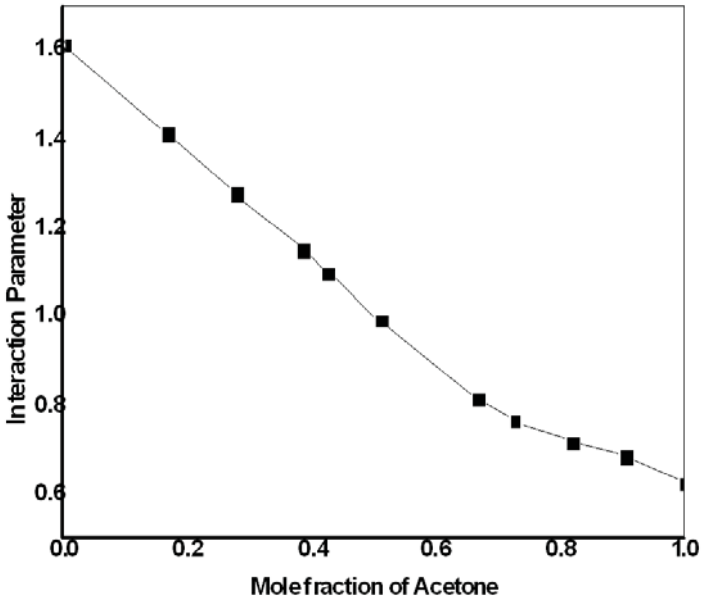

Fig. 6. Variation of interaction parameter

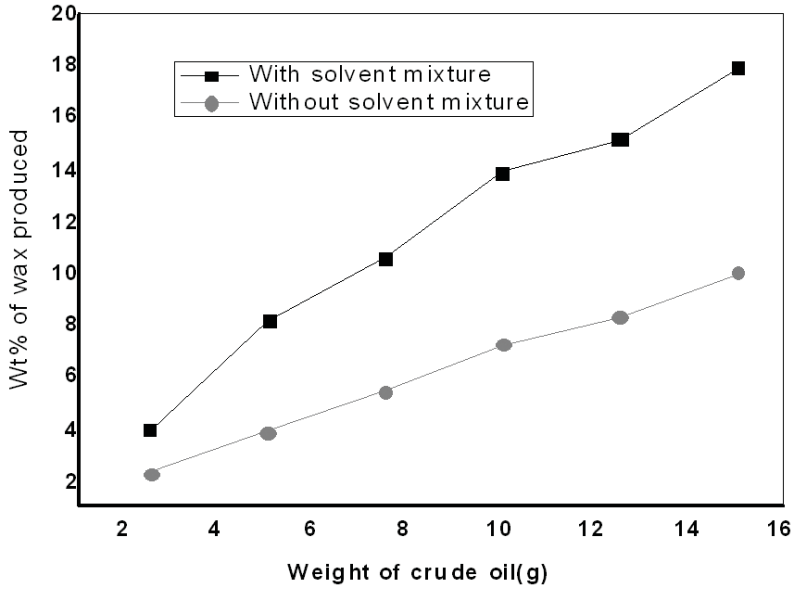

Fig. 7. Variation of wax produced with and without treatment of solvent mixture

It was observed that an increase in initial weight of crude oil from 5g to 15g, increases the amount of wax removal from 2.5 g to 17.8 g. This may be ascribed that with the increase in the amount of crude oil, the amount of paraffinic wax removal also increased. Thus the produced wax after separation and filtration increased. Again, with the help of a light microscope (Metzer 5000 BM having resolving power 40X-1000X, with camera 3 Megapixel CMOS SENSOR) analysis was done to observe the wax content before treatment and after treatment of solvent mixture. Figs. 8 and 9 show crystals of wax appear in crude oil before and after treatment of solvent mixture (weight, ratio of solvent) at best operating conditions (20° C, 2 hr, ratio 3:1). It was observed that the amount of wax minimized after removal of the wax from the crude sample.

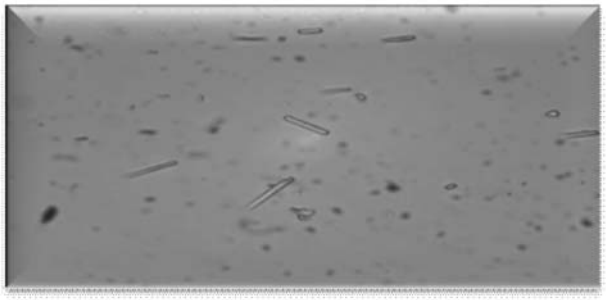

Fig. 8. Wax appearance in crude before treatment with solvent mixture

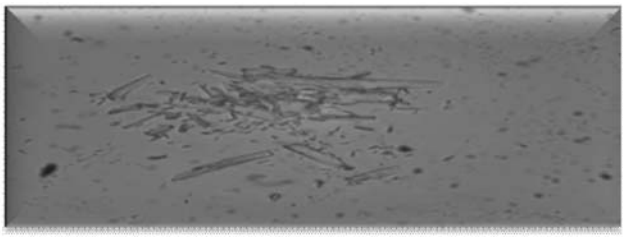

Fig. 9. Wax appearance in crude after treatment with solvent mixture

6. CONCLUSION

From the experimental data, variation of acoustic parameters with solvent mixture indicated the presence of strong interaction for entire range of mole fraction of acetone. It was also predicted that interaction was affected by the length of carbon chain. The variation of acoustic parameters with the concentration indicate the interaction strength and the treatment at each concentration of solvent mixture(with the ratio of acetone / n-heptane from 1:1, 2:1, 3:1) with the crude oil produced more and more wax[19]. From the experimental work, it was concluded that the amount of wax produced increased if the initial weight of the crude oil was increased along with the increase in solvent ratio[20]. It may be revealed that although the extraction performance was similar for 2:1 and 3:1 solvent ratios, the maximum wax extraction was achieved at a solvent to oil ratio of 3:1 or may be greater. More over, the greater ratio of solvent to oil may have a greater solubility preference for the oil than that of the wax which can serve to improve the dewaxing process. This was reflected by the high wax yield obtained from mixtures with 3:1 solvent ratios from the microscopic image.

7. REFERENCES

[1] A. NAGAR, V.K. MANGLA, S.P SINGH and J. KACHARI, 2006. Paraffin Deposition Problems of Mumbai High.

[2] J.C.M. ESCOBAR-REMOLINA, 2006. Prediction of Characteristics of Wax Precipitation in Synthetic Mixtures and Fluids of Petroleum: A New Model. *Fluid Phase Equilib*. **240**,197-203.

[3] B. KEN, 2003. Understanding Paraffin and Asphaltene Problems in Oil and Gas Wells.

[4] P. CLAUDY, J.M. LETOFFE, B. CHAGUE and J. ORRIT, 1988.Crude oils and their distillates: characterization by differential scanning calorimetry, *Fuel,* **67**,58-61.

[5] P. CLAUDY, J.M. LETOFFE, B. NEFF and B. DAMIN,1986. Wax crystallization from distillate fuels, *Fuel,* **65**, 861-864.

[6] A.A. NIMER, A.A. MOHAMED and A.R.ALI, 2014. Determination of Wax Content in Egyptian Crude Oils. *International Journal of Engineering Trends and Technology*, **8**(2) 598-603.

[7] D. SREE LAKSHMI, R.C. PUROHIT, S.P. SRIVASTAVA, S.P. NAUTIYAL, G.B. TIWARI, M. RAMA KRISHNA, M.VENKATESWARA RAO and M.B. RAO, 1997. Low temperature flow characteristics of some waxy crude oils in relation to their composition, *Petroleum Science And Technology,* **15**, 685-697.

[8] S. QU. TUNIO, A.H. TUNIO, N.A. GHIRANO and Z, M. EL ADAWY, 2011. Comparison of different enhanced oil recovery techniques for better oil productivity, *Int. J. Appl., Sci. Technol*. **1**, 5.

[9] A.I. VOGEL, 1937. Text Book of practical organic chemistry, Third Edition, Longmans, London

[10] J.A. RIDDICK and W.B. BUNGER, 1970. Organic Solvents, Third Edition, Wiley - Inter-Science, NY.

[11] A. WEISBERGER, 1955. Techniques of organic chemistry, Vol-III, Interscience, NY.

[12] F.A. EVEREST, 2000. Master handbook of acoustics (Mc Graw Hill, New York).

[13] N.J. DAVID, 2002. Fundamentals and applications of ultrasonic waves (RC press, New York).

[14] G. NATH, S. SAHU and R. PAIKARAY, 2009. Effect of frequency on acoustic parameters in a binary mixture of polar liquids, *Indian Journal of Physics*, **83**(11), 1567-1574.

[15] G. NATH, S. SAHU and R. PAIKARAY, 2008. Acoustical investigation of molecular interaction in binary mixture of acetone and xylene a different frequencies, *Journal of acoustical society of India* **35**, 115-120.

[16] R.J. FORT and W.R. MOORE, 1965. Trans Faradays, *Soc*, **61**, 2102.

[17] H.F. KRISHNA, H.F. RAGHAVENDRA, B.N. KIRASUR, S.H. IMRAN and R.S. JAGADISH, 2015. Molecular interaction studies in binary liquid mixtures of anisole with n-hexane and n-heptane using

ultrasonic technique for 3 MHz at temperature 303K, *World Journal of Pharmaceutical Research*, **4**(4), 1967-1975.

[18] R.M. ROEHNER and F.V. HANSON, 2004.Determination of wax precipitation temperature and amount of precipitated solid wax versus temperature for crude oils using FT-IR spectroscopy. *Energy Fuels:* 15-63.

[19] A.M. AS'AD, A.M. YENENEH and E.O. OBANIJESU, 2015. Solvent Dewaxing of Heavy Crude Oil with Methyl Ethyl Ketone, *Petroleum & Environmental Biotechnology*, **6**(2) 1-5.

[20] A.A. NIMER, A.A. MOHAMED and Ali A. RABAH, 2010. Nile blend crude oil: wax separation using MEK- Toluene mixture" *The Arabian Journal for Science and Engineering*, **35**(2B), 17-24.

Journal of Acoustical Society of India : Vol. 43, No. 3, 2016 (pp. 146-151)

Synthesis, Thermal conductivity and Characterization of alpha- Alumina (α-Al_2O_3) nano particles by Non-destructive Ultrasonic technique

N.R. Pawar[1]*, O.P. Chimankar[2], S.J. Dhoble[2] and R.D. Chavhan[2]

[1]Department of Physics, Arts, Commerce and Science College, Maregaon - 445 303, India

[2]Department of Physics, RTM Nagpur University, Nagpur- 440 033, India

e-mail: pawarsir1@gmail.com

[Received: 10-07-2016; Revised: 10-08-2016; Accepted: 14-08-2016]

ABSTRACT

α-Al_2O_3 is one of the most widely used oxide ceramic material. α-Al_2O_3 nanoparticles were synthesized through alkoxide route using sol-gel method. Aluminum isopropoxide Al $(OC_3H_7)_3$, and aluminum nitrate nanohydrate Al $(NO_3)_3$ 9 H_2O were used for preparing alumina solution. Sodium dodecylbenzene sulfonate (SDBS) was used as the surfactant stabilizing agent. The prepared solution was stirred for 48 hours at 60°C. The sample was characterized by X- ray diffraction (XRD) and scanning electron microscopy (SEM). Average particle size has been estimated by using Debye-Scherrer formula. It was found to be 30 nm. Thermal conductivity related to the surface of nanoparticles and nanoparticle surfactant interactions. Material characterization of α-Al_2O_3 nanosuspension was studied by non-destructive technique at various molar concentrations, temperatures and frequencies.

1. INTRODUCTION

α-Al_2O_3 is one of the most widely used oxide ceramic material. It is used in a variety of plastics, rubber, ceramics, and refractory products. As the α-phase ultrafine Al_2O_3 is a high performance material of far infrared emission, it is used in fibre fabric products and high pressure sodium lamp as far-infrared emission and thermal insulation materials. In addition, α-phase nano-Al_2O_3 with high resistivity and good insulation property, it is widely used as the main components for YGA laser crystal and integrated circuit substrates. Recently, advances in manufacturing technology have permitted the production of particles in the 10 nm to 100 nm range.

In the present investigation the synthesis of α-Al_2O_3 nanoparticles by sol-gel method is discussed. Ultrasonic velocity measurement together with density and viscosity helps in finding out many thermo acoustic parameters and thermal conductivity all these are related to the surface of nanoparticle and nanoparticles surfactant interactions[1-3]. α-Al_2O_3 nanoparticles with surface areas 30 nm have been prepared, their thermal conductivities and characterization have been investigated.

2. EXPERIMENTAL

2.1 Materials

The liquids used were of BDH analar grade and were redistilled in the laboratory. In this study the

measurements have been made in the temperature range 298 K-313 K. The temperature of the liquid mixture was kept constant by the use of thermostat U-10 with ± 0.01 K accuracy. Density measurement was carried out by using hydrostatic sinker method with an accuracy ±0.01%. A monopan electrical balance of least count as 0.0001 gm was used to record change in plunger weight dipped in the solutions correct to fourth place of decimal. Ultrasonic measurements were carried out by an ultrasonic multifrequency interferometer (Mittal enterprises, New Delhi) at frequency 4 MHz with an accuracy of ±0.1%. The time of descent of the liquids between the viscometer marks was measured using an electronic digital timer with least count 0.01 sec. The viscosity was measured in Ostwald's viscometer with an accuracy 0.001 cP.

2.2 Methods

2.1.1 Preparation of Samples

Nanoparticles of alpha alumina (α-Al_2O_3) was prepared by sol-gel method[4-9] from Aluminum isopropoxide [Al $(OC_3H_7)_3$] and aluminum nitrate. Starting solution was prepared by adding aluminum isopropoxide [Al $(OC_3H_7)_3$] gradually in 0.2M aluminum nitrate and solution continuously stirred for 48 hours. Later, Sodium dodecylbenzen sulfonate (SDBS) was added and stirred for one hour. Now this solution were heated up to 60°C and stirred constantly for evaporation process. Now the paste so obtained was heated at 90°C for 8 hours, we get nanoparticles of alpha alumina (α-Al_2O_3) in powder form.

The prepared sample were characterized for their phase purity and crystallinity by X-ray powder diffraction (XRD) using PAN-analytical diffractometer (Cu-Ka radiation) at a scanning step of 0.01°, continue time 20 s, in the 2h range from 10° to 120°. Formation of the compound confirmed by XRD pattern matched with the standard data available in JCPDS file. From this study, average particle size α-Al_2O_3 has been estimated by using Debye-Scherrer formula.

$$D = \frac{0.9\lambda}{W Cos\theta} \tag{1}$$

Where 'λ' is the wavelength of X-ray (0.15460 nm), 'W' is FWHM (full width at half maximum), 'θ' is the diffraction angle and 'D' is particle diameter (size). The estimate size of α-Al_2O_3 nano particles is found to be 30 nm. The prepared α-Al_2O_3 nano particles were suspended in ethanol.

3. RESULT AND DISCUSSION

Fig. 1 represents XRD pattern of α-Al_2O_3 nano particles. Fig. 2(A) and Fig. 2(B) represents SEM images of α-Al_2O_3 nano particles. XRD and SEM helps for the confirmation of particle size.

Fig. 3 shows the variation of ultrasonic velocity versus molar concentration of α-Al_2O_3 nanoparticle suspension in ethanol. The variation in ultrasonic propagation shows analogous behavior with increase in concentration of α-Al_2O_3 nanoparticles in ethanol. The non linear variation of ultrasonic velocity versus molar concentration of α-Al_2O_3 nanoparticle suspension in ethanol shows strong interaction between the constituents[10-12]. It is observed that as concentration of α-Al_2O_3 nano particle suspension in ethanol increases heteromolecular interactions in the constituents becomes stronger. The ultrasonic velocity decreases with increase in temperature because α-Al_2O_3 nanoparticles and thermo-elastic loss arises due to the Brownian motion of nanoparticles. Peak at molar concentration 0.06 indicates strong aggregation of nano suspension.

Fig. 4 shows the variation of density with molar concentration of α-Al_2O_3 nanoparticles in ethanol. Density of α-Al_2O_3 nano suspension increases with increase in molar concentration of α-Al_2O_3 nanoparticles in ethanol. This indicates the close packing between the constituents in the ethanol base fluid suspension.

Fig. 5 shows the variation of adiabatic compressibility with molar concentration of α-Al_2O_3 nanoparticles in ethanol. The adiabatic compressibility of nanosuspension is a thermodynamic parameter of fundamental significance. It enables direct access to the nanosuspension structure in terms of the particle packing density and the inter particle forces. The adiabatic compressibility of a nanosuspension is related to its density and ultrasonic velocity. The adiabatic compressibility shows the reverse trends as that of ultrasonic velocity

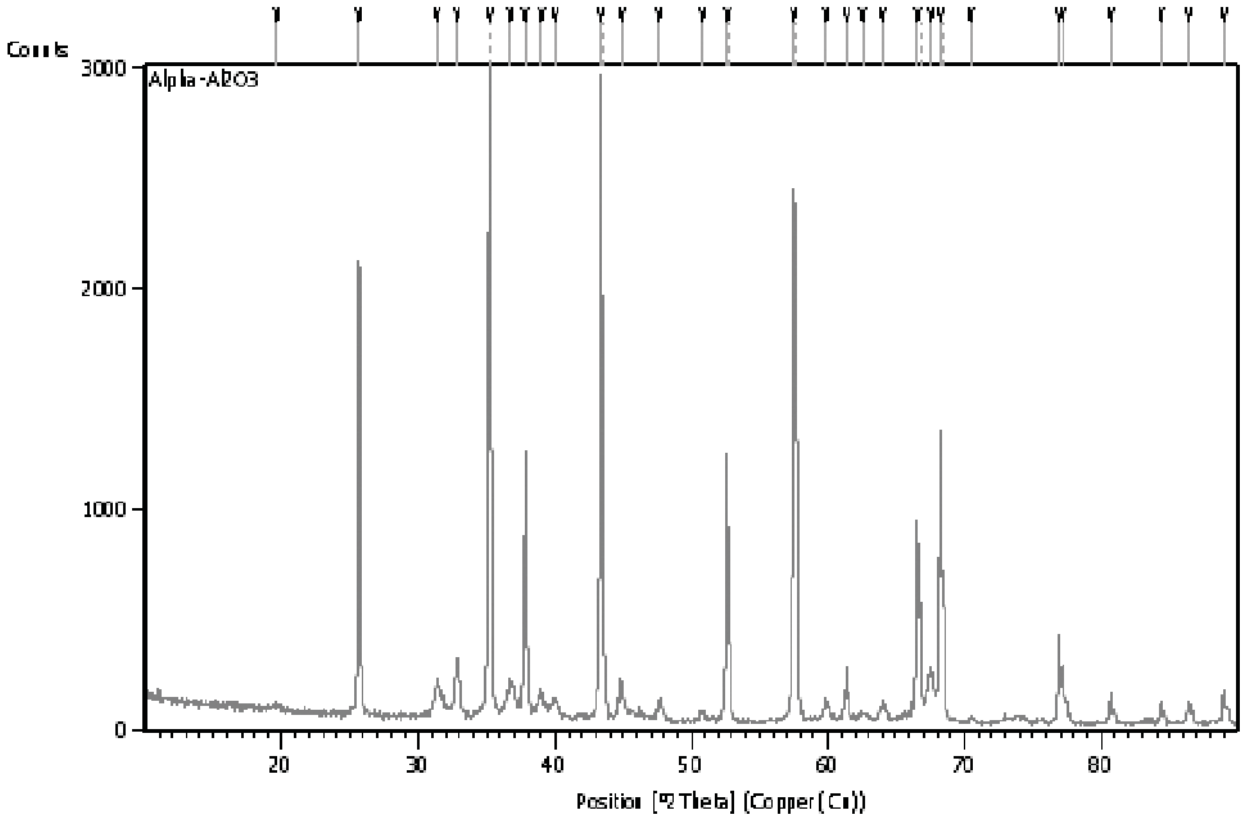

Fig. 1. XRD pattern of α-Al_2O_3 nanoparticles.

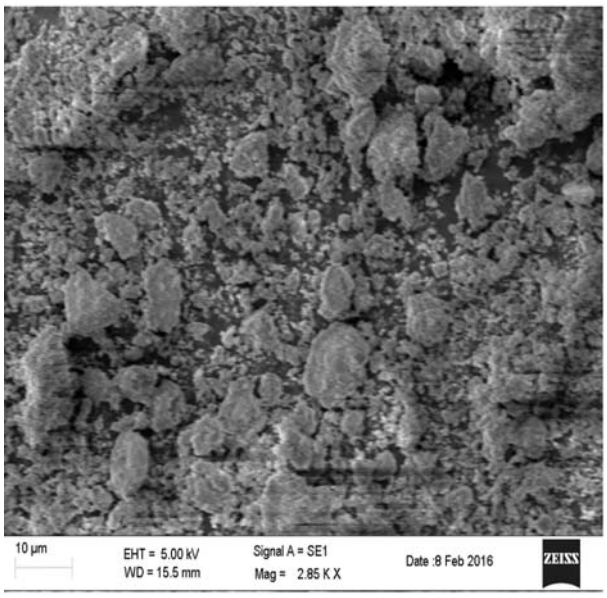

Fig. 2. (A) SEM image of α-Al_2O_3 Nanoparticles.

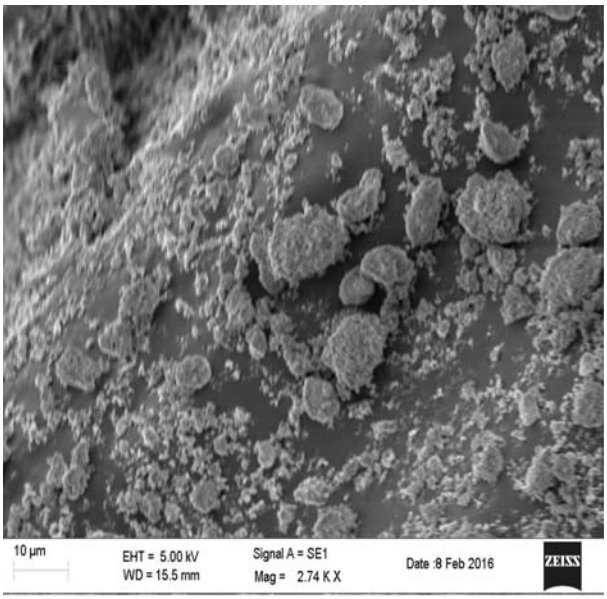

Fig. 2. (B) SEM image of α-Al_2O_3 Nanoparticles.

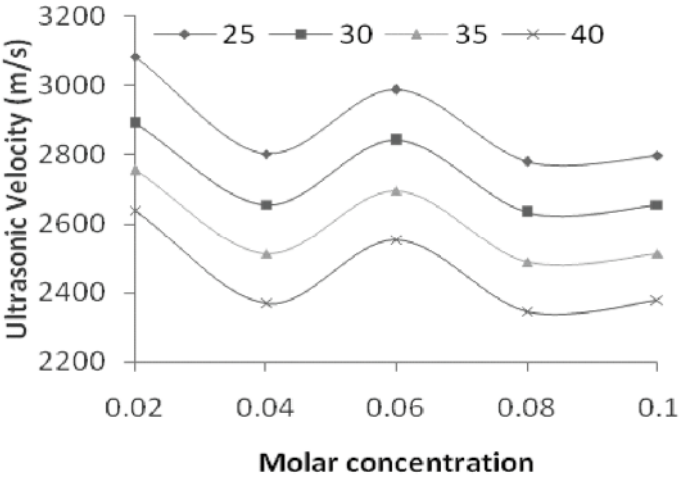

Fig. 3. Ultrasonic velocity vs. molar conc. of α-Al_2O_3 nano particles in ethanol.

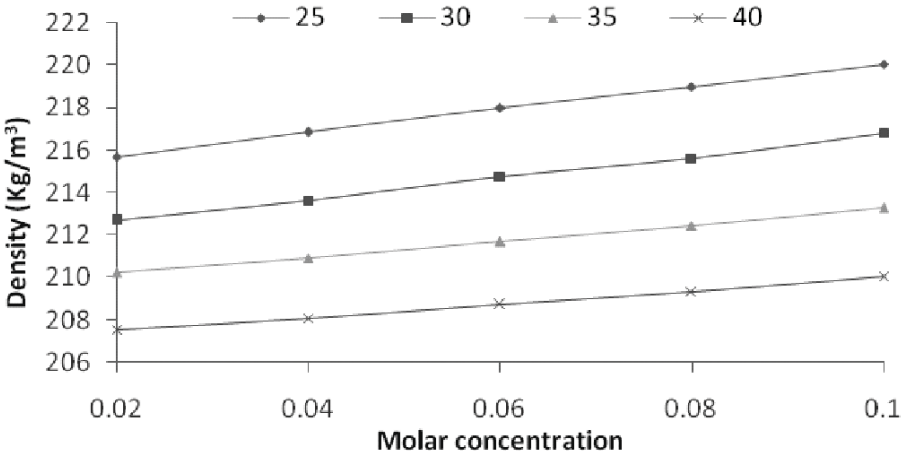

Fig. 4. Density vs. molar conc. of α-Al_2O_3 nano particles in ethanol.

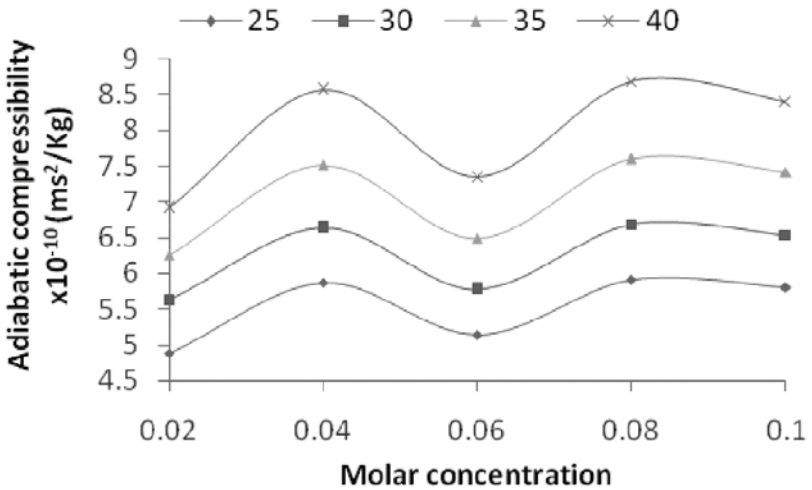

Fig. 5. Adiabatic compressibility vs. molar conc. of α-Al_2O_3 nano particles in ethanol.

which is theoretically accepted. The non-linear variation of adiabatic compressibility with molar concentration indicates the presence of phase separation in nano suspension.

Fig.6 shows the variation of acoustic impedance with molar concentration of α-Al_2O_3 nanoparticles. Acoustic impedance shows similar trends as that of ultrasonic velocity which is theoretically accepted. Peak at 0.06 is due to the aggregation of nanosuspension in ethanol base fluid.

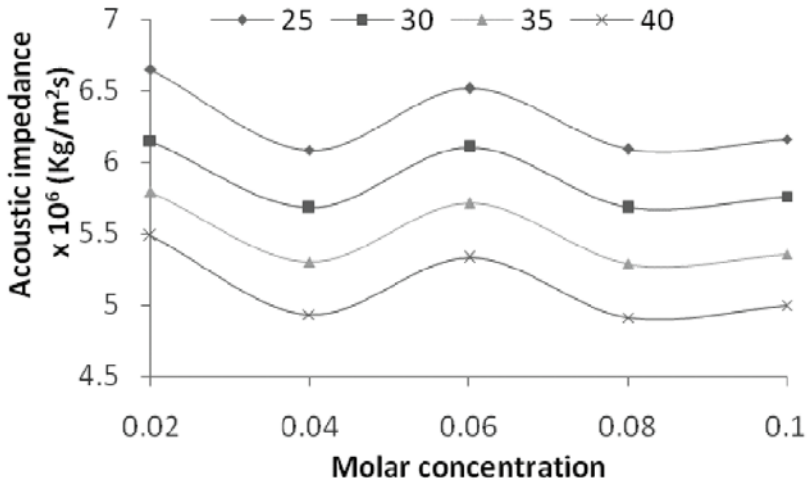

Fig. 6. Acoustic impedance vs. molar conc. of α-Al_2O_3 nanoparticles in ethanol.

Fig.7 shows the variation of thermal conductivity with molar concentration of α-Al_2O_3 nanoparticles in ethanol. The results clearly show that the effective thermal conductivity of α-Al_2O_3 decreases with temperature. The thermal conductivity of α-Al_2O_3 nanoparticles in ethanol has been investigated. Nanoparticle suspensions, at molar concentration 0.06 of α-Al_2O_3 in ethanol, have substantially higher thermal conductivity. The thermal conductivity enhancements are highly dependent on specific surface area (SSA) of nanoparticle, with an optimal SSA for the highest thermal conductivity. The results of Kumar *et al.* and Koo and Kleinstreuer show the strong relationship between Brownian motion and temperature of nanosuspension. Furthermore, the effect of temperature on thermal conductivity is not very well understood and documented. Indeed, only a few papers discuss this important parameter. Due to lack of experimental

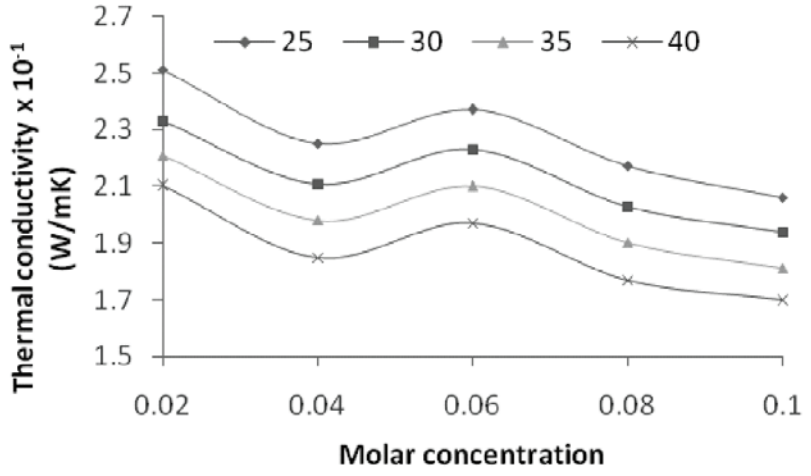

Fig. 7. Thermal conductivity vs molar conc. of α-Al_2O_3 nano particles in ethanol

data, theoretical expressions of the thermal conductivity of nanofluids are generally not accurate and not versatile. The conclusions of theoretical studies clearly express the need of more experimental data.

4. CONCLUSION

1. The ultrasonic velocity increases with an increase of the concentration of nanoparticles. It is due to association of α-Al_2O_3 nanoparticles in ethanol based nano suspension indicating strong interaction between the constituents.
2. Ultrasonic velocity decreases with increase in temperature, this is due to Brownian motion of nanoparticles in ethanol based nano suspension and thermal agitation.
3. It is confirmed that aggregation of nano particles in nano colloids play a key role for association and hence enhancement of ultrasonic velocity.

5. REFERENCES

[1] D.H. KUMAR, H.E. PATEL, V.R.R. KUMAR, T. SUNDARARAJAN, T. PRADEEP and S.K. DAS, 2004. Model for heat conduction of nanofluids, *Physical Review Letters,* **94**(14), 1-3.

[2] S. RAJAGOPALAN, S. J. SHARMA and V.Y. NANOTKAR, 2005. Ultrasonic Characterization of Silver Nanoparticles, *Journal of Metastable and Nanocrystalline Materials,* **23,** 271-274.

[3] Z. GAN, G. NING, Y. LIN and Y. CONG, 2007. Morphological control of mesoporous alumina nanostructures via template-free solvothermal synthesis. *Mater Lett*. **61**(31), 3758-3761.

[4] X. ZHAN, M. HONKANEN and E. LEVA, 2008. Transition alumina nanoparticles and nanorods from boehmite nanoflakes. *J Crystal Growth.* **310**(30), 3674-3679.

[5] Y.K. PARK, E.H. TADD, M. ZUBRIS and R. TANNENBAUM, 2005. Size controlled synthesis of alumina nanoparticles from aluminum alkoxides, *Materials Reasearch Bulletin*, **40**(9), 1512.

[6] D.G. WANG, F. GUO, J.F. CHEN, H. LIU and Z. ZHAG, 2006. Preparation of nano aluminium trihydroxide by high gravity reactive precipitation, Chemical Engineering Journal, **121**(2-3), 109-114.

[7] R. AGHABABAZADEH, A.R. MIRHABIBI, J. POURASAD, A. BROWN, A. BRYDSON and N. AMERI MAHABAD, 2007. Economical synthesis of Nanocrystalline alumina using an environmentally low-cost binder, *Journal of Surface Science*. **601**(13), 2864-2867.

[8] P. CHRISTIAN and M. BROMFIELD, 2010. Preparation of small silver, gold and copper nanoparticles which disperse in both polar and non-polar solvents, *J. Mater. Chem*. **20**, 1135-1139.

[9] R. ROGOJAN, E. ANDRONESCU, C. GHITULICA and B. STEFAN, 2011. Synthesis and characterization of alumina nano-powder by sol-gel method. *UPB Sci Bull Ser B.* **73**(2, 27), 67-76.

[10] V. Bhalla, R. Kumar, S. Tripathi and D. Sing, 2013. Mechanical and thermal properties of praseodymium nanoparticles: an ultrasonic study, *Int. J. Mod. Phys. B*, **27**, 1350116.

[11] N.R. Pawar, 2014. Ph.D thesis Summary on Investigation of Ultrasonic wave absorption in some Bio-liquids. *J Pure and Appl Ultrasonic*. **36**, 69.

[12] N.R. Pawar and O.P. Chimankar, 2015. Comparative Study ultrasonic absorption and relaxation behavior of polar solute and non-polar solvent, *Pure and Appl Ultrasonic*, **37**, 11.

Journal of Acoustical Society of India : Vol. 43, No. 3, 2016 (pp. 152-159)

Confirmation of ultrasonic parameters using FTIR analyse for binary mixture of methyl Benzoate + 2-Ethoxy ethanol and methyl Benzoate + 2-Butoxy ethanol

A.J. Clement Lourduraj* and S. Edwin Jerald
St. Joseph's College (Autonomous), Tiruchirappalli - 620002
**e-mail: ajeevaclement @ gmail.com*

[Received: 19-07-2016; Revised: 25-09-2016; Accepted: 28-09-2016]

ABSTRACT

The binary mixtures of Methyl Benzoate + 2-Ethoxy Ethanol and Methyl Benzoate + 2-Butoxy Ethanol has been measured extensively from the view point of their macroscopic properties at 303.15K, 308.15K and 313.15K for the entire range of mole fraction. Experimental values of density, viscosity and speed of sound are used for the calculation of excess volume (VE). Experimental and computed results are used to study the type and nature of inter and intra molecular interactions between the mixing components. Even though these types of studies exist in the literature there is no confirmation for the observed excess properties through other non-ultrasonic techniques. For the confirmation of the excess properties FTIR spectra have been taken in the regions and also for the participating pure liquid components. FTIR spectra were taken for the liquid mixtures in a FTIR spectrum photometer by using the KBr pellet method.

1. INTRODUCTION

The present work is a continuation of our earlier studies of thermodynamic and physico-chemical properties of non-aqueous binary and ternary liquid mixtures. The present investigation is concerned with the study of the binary system Methyl Benzoate + 2-Ethoxy Ethanol and Methyl Benzoate + 2-Butoxy Ethanol for their entire composition range. A deeper knowledge of mixing properties of such multicomponent liquid system is essential in many industrial applications, such as design calculation, mass transfer, fluid flow etc. The present work reports densities, viscosities and speeds of sound for the system measured at 303.15K, 308.15K and 313.15K. From these data excess volume VE, have been calculated. FTIR spectra have been taken for entire ranges of mole fractions of liquid mixtures and pure liquids.

2. EXPERIMENTAL MATERIALS

High - purity spectroscopic and HPLC grade chemicals of Methyl Benzoate, 2-Ethoxy Ethanol and 2-Butoxy Ethanol were obtained from Merck Co. Their purities were 99.5% or better and no further purification was done. The chemicals were stored over molecular sieves. The verification of the purity of the chemicals was realized by ascertaining the consistency of the values of density, viscosity and ultrasonic velocity at 298.15K which was reasonably in accordance with the values found in the literature.

3. MEASUREMENTS

Densities of liquids and their mixtures were measured at 303.15K, 308.15K and 313.15K with specific gravity bottle method. The results of density are accurate to ± 0.0002 gcm^{-3}. An electronic digital balance is used to measure the mass of the liquids within an accuracy of ± 0.001g. The viscosities of the pure liquids and their mixtures were measured using an Ostwald's viscometer. The flow times are measured within an accuracy of ± 0.01sec. The speed of sound in the mixture has been measured by an ultrasonic interferometer of frequency 2MHz. The speed of sound values is accurate to ± 2$m.s^{-1}$. The measurements have been carried out in a constant temperature bath at 303.15K and 308.15K within an accuracy of ± 0.01K. FTIR spectra were taken for the liquid mixtures in a FTIR spectrum photometer (Perklin Elmer Co. model 1605) by using the KBr pellet method.

Table 1. Determination of mole fraction, velocity, viscosity and density for binary system Methyl Benzoate + 2-Ethoxy Ethanol 303.15K

Mole Fraction (Methyl Benzoate + 2-Ethoxy Ethanol)	AT 303.15K		
	Viscosity (10^{-3} N.s/m^2)	Velocity (m/sec)	Density (10^{-3} kg/m^3)
1+0	1.673	1392	1.0788
0.9+0.1	1.6908	1383	1.06348
0.8+0.2	1.7086	1374	1.04816
0.7+0.3	1.7264	1365	1.03284
0.6+0.4	1.7442	1356	1.01752
0.5+0.5	1.762	1347	1.0022
0.4+0.6	1.7798	1338	0.98688
0.3+0.7	1.7976	1329	0.97156
0.2+0.8	1.8154	1320	0.95624
0.1+0.9	1.8332	1311	0.94092
0+1	1.851	1308	0.9256

Table 2. Determination of mole fraction, velocity, viscosity and density for binary system Methyl Benzoate + 2- Butoxy Ethanol at 303.15K

Mole Fraction (Methyl Benzoate + 2- Butoxy Ethanol)	AT 303.15K		
	Viscosity (10^{-3} N.s/m^2)	Velocity (m/sec)	Density (10^{-3} kg/m^3)
1+0	1.673	1392	1.0788
0.9+0.1	1.61614	1392.9	1.0705
0.8+0.2	1.55928	1392.8	1.0622
0.7+0.3	1.50242	1394.6	1.0539
0.6+0.4	1.44556	1394.4	1.0456
0.5+0.5	1.3887	1396.8	1.0373
0.4+0.6	1.33184	1396.4	1.029
0.3+0.7	1.27498	1398.3	1.0207
0.2+0.8	1.21812	1398.1	1.0124
0.1+0.9	1.16126	1400.3	1.0041
0+1	1.1044	1402	0.9951

3. RESULT AND DISCUSSION

The Excess Volume (V^E) of the binary system Methyl Benzoate + 2-Ethoxy Ethanol and Methyl Benzoate + 2-Ethoxy Ethanol mixtures are maximum negative and positive which shows the presence of interstitial accommodation of one type of molecule into other. The experimental data collected in the literature up to the present provide strong evidence that for mixtures in which strong attractive interactions (*e.g.* dipole-dipole, dipole-induced dipole interactions or hydrogen bonding) are likely to occur between the components (complexation), the excess volume is negative while for mixtures with only weak interactions between the components excess volume is positive. For the present binary mixtures the dipole-dipole and dipole - induced dipole interactions play a role. So, the dipole-dipole interaction contributes to the positive excess volume and dipole-induced dipole interaction contributes to the negative excess volume. The maximum positive

Table 3. Determination of mole fraction, velocity, viscosity and density for binary system Methyl Benzoate + 2-Ethoxy Ethanol at 308.15K.

Mole Fraction (Methyl Benzoate + 2-Ethoxy Ethanol)	AT 308.15K		
	Viscosity (10^{-3} N.s/m^2)	Velocity (m/sec)	Density (10^{-3} kg/m^3)
1+0	1.51	1381	1.074
0.9+0.1	1.5278	1372	1.05868
0.8+0.2	1.5456	1363	1.04336
0.7+0.3	1.5634	1354	1.02804
0.6+0.4	1.5812	1345	1.01272
0.5+0.5	1.599	1336	0.9974
0.4+0.6	1.6168	1327	0.98208
0.3+0.7	1.6346	1318	0.96676
0.2+0.8	1.6524	1309	0.95144
0.1+0.9	1.6702	1300	0.93612
0+1	1.688	1297	0.9208

Table 4. Determination of mole fraction, velocity, viscosity and density for binary system Methyl Benzoate + 2-Butoxy Ethanol at 308.15K

Mole Fraction (Methyl Benzoate + 2-Butoxy Ethanol)	AT 308.15K		
	Viscosity (10^{-3} N.s/m^2)	Velocity (m/sec)	Density (10^{-3} kg/m^3)
1+0	1.51	1381	1.074
0.9+0.1	1.45314	1381.8	1.0658
0.8+0.2	1.39628	1381.6	1.0576
0.7+0.3	1.33942	1383.4	1.0494
0.6+0.4	1.28256	1383.2	1.0412
0.5+0.5	1.2257	1384	1.033
0.4+0.6	1.16884	1385.8	1.0248
0.3+0.7	1.11198	1385.6	1.0166
0.2+0.8	1.05512	1387.4	1.0084
0.1+0.9	0.99826	1388.2	1.0002
0+1	0.9414	1389	0.992

Table 5. Determination of mole fraction, velocity, viscosity and density for binary system Methyl Benzoate + 2-Ethoxy Ethanol at 313.15K

Mole Fraction (Methyl Benzoate + 2-Ethoxy Ethanol)	AT 313.15K		
	Viscosity (10^{-3} N.s/m^2)	Velocity (m/sec)	Density (10^{-3} kg/m^3)
1+0	1.365	1372	1.069
0.9+0.1	1.3828	1363	1.05368
0.8+0.2	1.4006	1354	1.03836
0.7+0.3	1.4184	1345	1.02304
0.6+0.4	1.4362	1336	1.00772
0.5+0.5	1.454	1327	0.9924
0.4+0.6	1.4718	1318	0.97708
0.3+0.7	1.4896	1309	0.96176
0.2+0.8	1.5074	1300	0.94644
0.1+0.9	1.5252	1291	0.93112
0+1	1.543	1288	0.9158

Table 6. Determination of mole fraction, velocity, viscosity and density for binary system Methyl Benzoate + 2-Butoxy Ethanol at 313.15K.

Mole Fraction (Methyl Benzoate + 2-Butoxy Ethanol)	AT 313.15K		
	Viscosity (10^{-3} N.s/m^2)	Velocity (m/sec)	Density (10^{-3} kg/m^3)
1+0	1.365	1372	1.069
0.9+0.1	1.30814	1372.9	1.0613
0.8+0.2	1.25128	1372.5	1.0534
0.7+0.3	1.19442	1373.7	1.0455
0.6+0.4	1.13756	1373.2	1.0376
0.5+0.5	1.0807	1374.1	1.0297
0.4+0.6	1.02384	1374.4	1.0218
0.3+0.7	0.96698	1374.8	1.0139
0.2+0.8	0.91012	1375.9	1.006
0.1+0.9	0.85326	1375.6	0.9981
0+1	0.7964	1376	0.9902

and negative in excess volume which shows the presence of dispersion type interaction which has also been supported by earlier researchers. It is also due to the interstitial accommodation of one type of molecule into other. The FTIR spectrum taken shows a drastic change in the frequency values for the composition of 0.3 mole fraction of Methyl Benzoate and 0.7 mole fraction of 2-Ethoxy Ethanol in the negative region and for in the case of Methyl Benzoate+2-Butoxy Ethanol the frequency values for the composition of 0.6 mole fraction of Methyl Benzoate and 0.4 mole fraction of 2-Butoxy Ethanol in the negative region.

So, the observation from the V^E study has been confirmed by the FTIR spectrum measurement.

The shift in the frequency values of FTIR spectrum measurement is generally due to following observed factors: Interstitial accommodation and Strong interactions (dipole - induced dipole and dipole - dipole).

Table 7. Determination of mole fraction, Excess Volume for binary system Methyl Benzoate + 2-Ethoxy Ethanol at 303.15K.

Mole Fraction (Methyl Benzoate + 2-Ethoxy Ethanol)	Excess Volume (10^6 m^3)
1+0	0
0.9+0.1	-0.0012
0.8+0.2	-0.0021
0.7+0.3	-0.0029
0.6+0.4	-0.0036
0.5+0.5	-0.0044
0.4+0.6	-0.0051
0.3+0.7	-0.0053
0.2+0.8	-0.0045
0.1+0.9	-0.0029
0+1	0

Table 8. Determination of mole fraction, Excess Volume for binary system Methyl Benzoate + 2-Butoxy Ethanol at 303.15K.

Mole Fraction (Methyl Benzoate + 2-Butoxy Ethanol)	Excess Volume (10^6 m^3)
1+0	0
0.9+0.1	-0.356
0.8+0.2	-0.6166
0.7+0.3	-0.7769
0.6+0.4	-0.8321
0.5+0.5	-0.7769
0.4+0.6	-0.6855
0.3+0.7	-0.6009
0.2+0.8	-0.5003
0.1+0.9	-0.3582
0+1	0

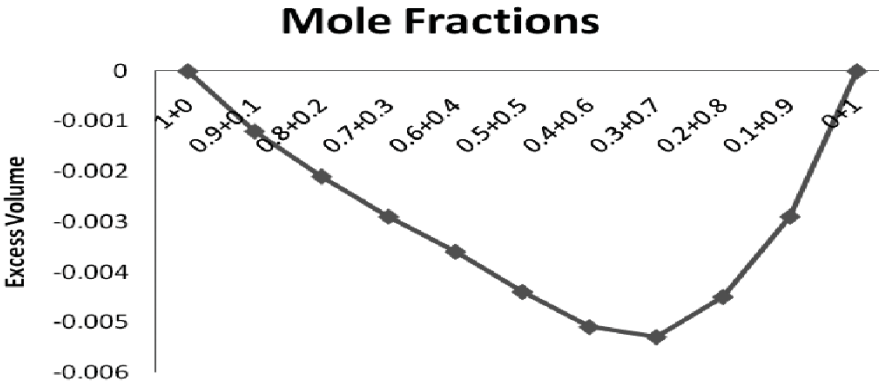

Fig. 1. Excess Volume for the binary system Methyl Benzoate + 2-Ethoxy Ethanol

Table 9. Observations of FTIR Spectrum of the binary system Methyl Benzoate + 2-Ethoxy Ethanol.

0.9 MB + 0.1 2EE cm^{-1}	**0.8 MB + 0.2 2EE cm^{-1}**	**0.7 MB + 0.3 2EE cm^{-1}**	**0.6 MB + 0.4 2EE cm^{-1}**	**0.5 MB + 0.5 2EE cm^{-1}**	**0.4 MB + 0.6 2EE cm^{-1}**	***0.3 MB + 0.7 2EE cm^{-1}**	**0.2 MB + 0.8 2EE cm^{-1}**	**0.1 MB + 0.9 2EE cm^{-1}**
3907.09	3924.14	3921.79	3909.05	3916.36	3922.35	**3919.96**	1039.17	3930.50
3794.70	3434.64	3788.29	3787.99	3791.08	3794.01	**3790.17**	951.46	3789.22
3397.82	3066.75	3422.81	3426.95	3432.46	3430.38	**3435.40**	826.77	3430.04
3059.42	2828.59	3069.58	3059.66	3059.07	3010.71	**3001.95**	750.02	3001.69
2823.01	2743.73	2916.08	2825.73	2914.07	2915.64	**2913.80**	690.35	2916.97
2737.83	2604.24	2822.74	2741.20	2825.07	2829.17	**2827.77**	2746.89	2341.80
1991.24	2337.18	2740.94	2340.32	2741.24	2742.63	**2743.29**	2332.44	2124.07
1914.80	1706.36	2611.82	1998.65	2333.16	2338.18	**2330.60**	2107.16	1654.93
1828.09	1602.03	2502.02	1831.16	1995.96	2000.07	**2102.18**	1999.44	1422.43
1698.86	1443.98	2338.33	1695.65	1831.26	1832.35	**1997.25**	1686.37	1314.93
1599.91	1306.21	1988.46	1605.80	1696.35	1693.91	**1693.73**	1422.23	1206.64
1447.40	1209.95	1914.55	1423.94	1599.49	1423.50	**1601.28**	1313.15	1032.65
1303.48	1043.27	1830.65	1304.41	1424.00	1309.87	**1422.01**	1199.23	952.74
1195.11	942.37	1696.97	1192.38	1309.86	1198.91	**1311.23**	1036.74	694.28
1040.46	830.91	1600.77	1036.85	1201.41	1037.01	**1201.83**	954.69	
824.65	751.19	1415.09	948.44	1038.72	953.58	**1039.17**	823.06	
746.36	673.29	1307.52	821.51	950.94	823.80	**951.46**	683.89	
679.64	451.39	1202.13	745.82	826.56	745.97	**826.77**		
451.32		1032.90	676.39	748.97	682.29	**750.02**		
		950.12	462.30	688.82		**690.35**		
		824.03		456.23				
		747.52						
		690.38						
		457.16						

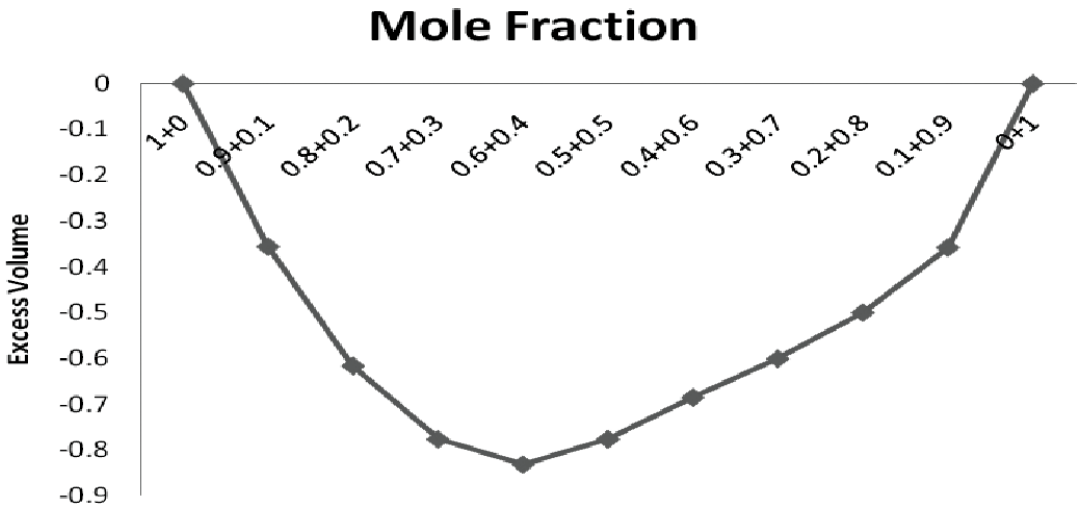

Fig. 2. Excess Volume for the binary system Methyl Benzoate + 2-Butoxy Ethanol

Table 10. Observations of FTIR Spectrum of the binary system Methyl Benzoate + 2-Butoxy Ethanol

0.9 MB + 0.1 2BE cm^{-1}	0.8 MB + 0.2 2BE cm^{-1}	0.7 MB + 0.3 2BE cm^{-1}	0.6 MB + 0.4 2BE cm^{-1}	0.5 MB + 0.5 2BE cm^{-1}	0.4 MB + 0.6 2BE cm^{-1}	*0.3 MB + 0.7 2BE cm^{-1}	0.2 MB + 0.8 2BE cm^{-1}	0.1 MB + 0.9 2BE cm^{-1}
3911	3910	3910	3757	3776	3763	3435	3431	3428
3764	3764	3772	3440	3437	3439	3067	3067	2965
3435	3540	3442	3066	3066	3066	2934	2936	2934
3066	3434	3950	2955	2955	2953	2957	2870	2870
2999	3066	2871	2870	2870	2870	2870	2366	2366
2871	3000	2371	2367	2371	2369	2367	2096	2097
2598	2953	2091	2340	2089	2092	2340	1933	1958
2472	2872	1926	2097	2045	1926	2095	1723	1640
2372	2598	1723	1927	2002	1723	1929	1618	1603
2339	2471	1598	1724	1927	1650	1725	1603	1458
2250	2371	1445	1641	1724	1600	1634	1456	1361
2085	2338	1361	1451	1641	1498	1602	1363	1280
1971	2084	1280	1438	1601	1362	1488	1280	1211
1925	1925	1182	1359	1451	1280	1455	1119	1070
1724	1723	1113	1314	1361	1181	1360	1070	977
1642	1642	1070	1280	1280	1280	1315	973	890
1443	1599	968	1178	1178	1181	1280	890	714
1280	1432	889	1113	1141	1116	1177	822	677
1111	1280	821	1070	1070	1069	1116	714	552
1070	1110	712	1027	1028	969	1070	550	
1027	1027	966	967	890	1030			
966	966	890	890	821	970			
890	890	822	713	714	890			
820	820	712	549	551	850			
712	712	483	822					
618	618	714						
482	482	688						
548								

* Maximum shift in the frequency has been observed.

4. ACKNOWLEDGEMENT

One of the authors Dr. A.J. Clement Lourduraj is thankful to UGC, New Delhi, India for providing financial assistance under Minor Research Project.

5. REFERENCES

Periodicals:

[1] A.J. CLEMENT LOURDURAJ and I. JOHNSON, 2008. Ultrasonic and spectroscopic studies of binary mixtures of cyclohexanone with hexane and heptane. *Journal of Pure and Applied Ultrasonics.* **30**(2), 69-73.

[2] I. JOHNSON, M. KALIDOSS and R. SRINIVASAMOORTHY, 2001. Acoustical investigation of some binary and ternary liquid mixtures. *Proceedings of the 17th International congress on Acoustics (ROME),* Physical Acoustics-Part B. **1**, 12-13.

[3] J.D. PANDEY and ASHOK KUMAR, 1994. Ultrasonic velocity in pure liquids, *Journal of Pure and Applied Ultrasonics*. **16**, 63-68.

[4] S. VISWANATHAN and M. ANAND RAO, 2000. *Journal of Chem. Eng. Data.* **45**, 764-770.

[5] A. MUKHERJEE and S. KAMILA *et al.*, 1999. *Acoustics Letters (U.K).* **23**, 17-24.

[6] M. KALIDOSS, I. JOHNSON and R. SRINIVASAMOORTHY, 1999. *J. Acoust. Soc. Ind.* **27**, 319.

[7] M. KALIDOSS and R. SRINIVASAMOORTHY, 1997. *J. Pure Appl. Ultrason*. **19**, 9.

[8] C.V. SURYANARAYANA and S. KUPPUSAMY, 1979. *J. Acous. Soc. Ind.* **7**, 131.

[9] R.J. FORT and W.R. MOORE, 1965. *Trans. Faraday society*. **61**, 2102-2107.

[10] E. ZOREBSKI and A. ZAK -Z., 1999. *Physikalische chemie.Bd.* **210**, S.223-233.

Books:

[1] J.A. RIDDICK, W.B. BUNGER and T.K. SANAKO, 1986. Organic solvents. Physical properties and methods of purification (Techniques of Chemistry) 4th ed, Wiley-Interscience, New York.

[2] WEISSBERGER, 1955, Technique of Organic Chemistry, Vol. VII, Organic solvents. Physical properties and methods of purification, 2nded, Inter-science publisher, New York.

[3] WILLIAM KEMP, 1991, Organic Spectroscopy 3rd ed, Palgrave, New York.

[4] ROBERT M. SILVERSTEIN and FRANCIS X. WEBSTER, 1998. Spectrometric identification of organic compounds, John Wiley & Sons, Singapore.

Journal of Acoustical Society of India : Vol. 43, No. 3, 2016 (pp. 160-168)

Ultrasonic study in binary mixture of an aprotic liquid with diethyl ether

Ashok Kumar Dash[1*] and Rita Paikaray[2]
[1]Department of Physics,L.N College.Patkura.Kendrapara. Odisha, India
[2]Department of Physics, Ravenshaw University Cuttack, Odisha. India
**e-mail: ashok.phy@rediffmail.com*

[Received: 19-08-2016; Revised: 21-09-2016; Accepted: 28-09-2016]

ABSTRACT

The experimental density (ρ) and ultrasonic velocity (U) of binary mixture of an aprotic liquid dimethyl acetamide (DAMC) and diethyl ether at different frequencies have been measured at temperature 308 K. These data have been used to compute thermo acoustic parameters (adiabatic compressibility, intermolecular free length, molar volume, acoustic impedance, available volume, surface tension), constant parameters (molar sound velocity, molar compressibility and Lennard Jones potential repulsive term exponent), and excess values of some of the above parameters for entire range of mole fraction and are interpreted to explain molecular interaction occurring in the liquid mixture. The negative excess values of L_f^E and β^E are due to charge transfer, dipole-dipole, dipole-induced dipole interactions, interstitial accommodation and orientational ordering which predict the existence of strong molecular interactions in the binary liquid mixture. The increase in Lennard Jones potential repulsive term exponent with the increase in mole fraction of DAMC indicates the increasing dominance of attractive forces over repulsive forces in the binary liquid mixture.

1. INTRODUCTION

The ultrasonic study in liquid systems plays remarkable role in explaining the nature and strength of molecular interactions. A large number of investigations have been made on the molecular interaction in liquid mixtures by ultrasonic methods[1-3]. Recently, ultrasonic method has become a powerful tool to provide information regarding the physiochemical properties of liquid system. The study of DMAC is important because of its utilization in industry and medicine. It is a dipolar aprotic liquid and used as solvent for the production of acrylic fibres, elasthane fibres, polymide resins and various pharmaceuticals[4]. Diethyl ether is a non-polar liquid and used in the production of cellulose plastics[5]. Literature survey reveals that less work has been done on the molecular interactions in the mixtures of dimethyl acetamide. The present investigation deals with the ultrasonic study in binary liquid mixture of dimethyl acetamide (DMAC) with diethyl ether at different frequencies at constant temperature 308K and to check the extraction efficiency of DMAC in the presence of diluent or modifier diethyl ether in solvent extraction process.

Deviation from linearity in the velocity versus concentration in liquid mixture of DMAC is taken as an indication of the existence of interaction between different liquid molecules. The physical and chemical properties of liquid mixture is studied by nonlinear variation of ultrasonic velocity, adiabatic compressibility and other related parameters with structural changes occurring in a liquid and the liquid mixture.

2. METHODS AND MEASUREMENTS

The liquid mixtures of various concentrations in mole fraction were prepared by taking chemicals of analytical reagent (AR) and spectroscopic reagent (SR) grades with minimum assay of 99.9% (E-Merck Ltd, India) which were used as such without further purification. Liquid mixtures of different mole fractions were prepared on concentration scale with a precision 0.0001 g using an electronic digital balance. The density of liquid mixture was determined by a specific gravity bottle of 10 ml capacity. The specific gravity bottle with the liquid mixture was immersed in a temperature controlled water bath. The velocity of ultrasonic waves in the binary liquid mixture was measured by using a multi frequency interferometer (Model M-82 S) with a high degree of accuracy operating at different frequencies supplied by Mittal Enterprises, New Delhi[6]. The measuring cell of the interferometer is a specially designed double walled vessel with provision for constant temperature.

3. THEORY

Using the measured data the acoustical parameters such as adiabatic compressibility (β) intermolecular free length L_f, acoustic Impedance (Z), molar volume V_m and available volume V_a have been computed from the following equations[7-9].

$$\beta = \frac{1}{U^2\rho} \tag{1}$$

$$L_f = k\sqrt{\beta} \tag{2}$$

$$Z = \rho U \tag{3}$$

$$V_m = \frac{M}{\rho} \tag{4}$$

$$V_a = \left(\frac{M}{\rho}\right)\left[1-\frac{U}{U_\infty}\right] \tag{5}$$

Where *k* is a temperature dependent constant, M is the molecular mass of the liquid mixture and U_∞ =1600 m / s.

Their excess values have been calculated from the following relation[10].

$$A^E = A_{exp} - (X_1A_1 + X_2A_2) \tag{6}$$

Where X_1 and X_2 are mole fractions of DMAC and diethyl ether respectively and A is any acoustical parameter.

Molar sound velocity (R), molar compressibility (B), Lennard Jones potential repulsive term exponent (n), surface tension (S) have been calculated from the following relations[11-15].

$$R = \frac{M}{\rho}U^{\frac{1}{3}} \tag{7}$$

$$B = \frac{M}{\rho}\beta^{\frac{-1}{7}} \tag{8}$$

$$n = \frac{6v_m}{V_a} - 13 \tag{9}$$

$$S = 6.3 \times 10^{-4}\rho U^{\frac{3}{2}} \tag{10}$$

3. RESULT AND DISCUSSION

The experimental values of density (ρ) and ultrasonic velocity (U) at 308K for frequencies 2 MHz, 4 MHz, 6 MHz and 8 MHz for the binary liquid mixture are presented in Figs-1 and 2 respectively. These values have been used to calculate the acoustical parameters and the relevant data are displayed graphically in Figs. 3 to 18.

Fig-1 shows that density ρ increases with the increase in mole fraction of DMAC. The increase in density indicates the presence of solvent-solvent interactions in the binary mixture[16]. Fig-2 shows that ultrasonic velocity U in the binary mixture increases with the increase in mole fraction of DMAC. The increase in ultrasonic velocity at a particular frequency indicates the presence of dipole-induced dipole interactions in the liquid mixture. DMAC is a polar molecule and when it is associated with non-polar solvent diethyl ether, the diethyl ether molecule tends to break the DMAC- DMAC dipolar association and releases several DMAC dipoles. The free DMAC dipoles would induce moments in the neighboring diethyl ether molecules resulting dipole-induced dipole interactions in the liquid mixture. Consequently the binary liquid mixture has dipole-dipole interactions between DMAC molecules as well as dipole-induced dipole interactions between DMAC and diethyl ether molecules. This leads to contraction in volume and it causes decrease in adiabatic compressibility and intermolecular free length L_f with the increasing molar concentration of DMAC which are evident from Figs-3 & 4 respectively. This is in agreement with the Eyring Kincaid model for sound propagation[17]. According to this model ultrasonic velocity decreases with the increase in intermolecular free length in the liquid mixture and *vice versa*. Therefore, intermolecular free length is one predominating factor for deciding the nature of variation in ultrasonic parameters in the liquid mixture. In

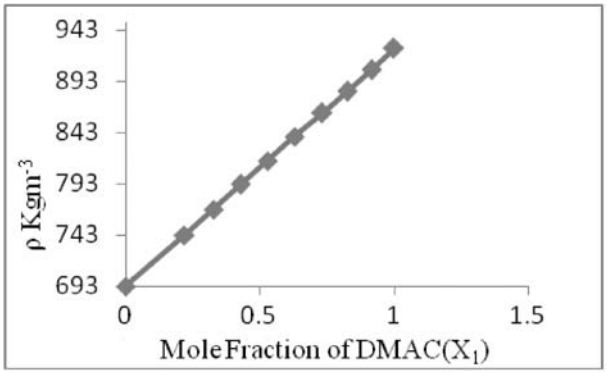

Fig. 1. Variation of ρ Versus X_1

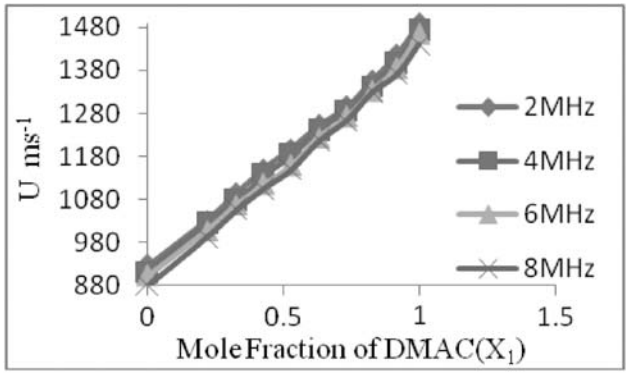

Fig. 2. Variation of U Versus X_1

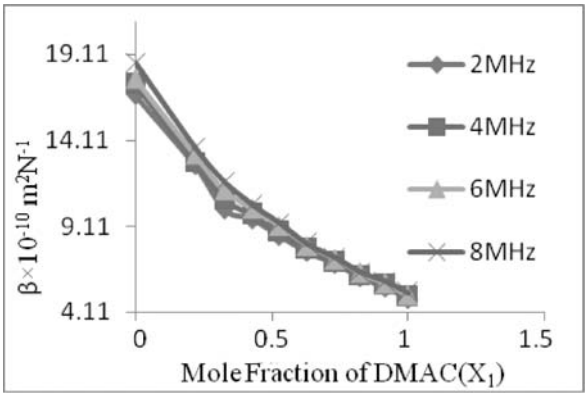

Fig. 3. Variation of β Versus X_1

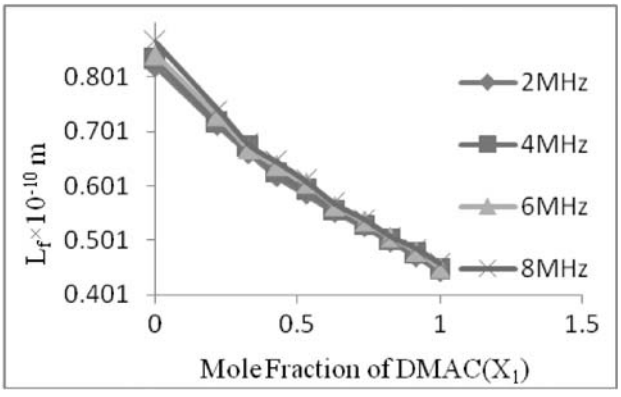

Fig. 4. Variation of L_f Versus X_1

the present study, the decrease in the intermolecular free length causes decrease in the adiabatic compressibility and increase in density and acoustic impedance as the concentration of DMAC increases in the liquid mixture. The variations of molar volume V_m, acoustic impedance Z and available volume V_a with the molar concentration of DMAC are shown in Figs-5 to 7. The decrease in molar volume and available volume while increase in acoustic impedance with the increase in molar concentration of DMAC indicate the close association of molecules and possibility of specific interactions in the binary liquid mixture.

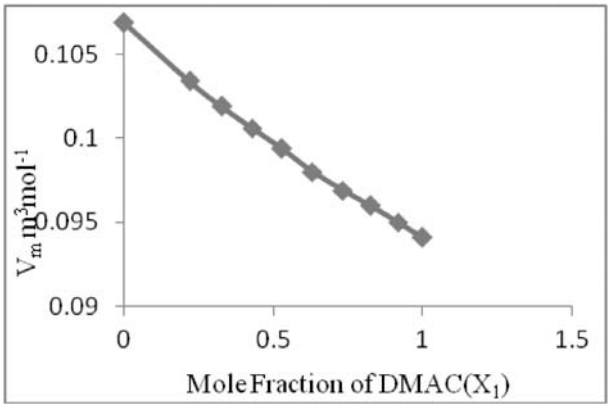

Fig. 5. Variation of V_m Versus X_1

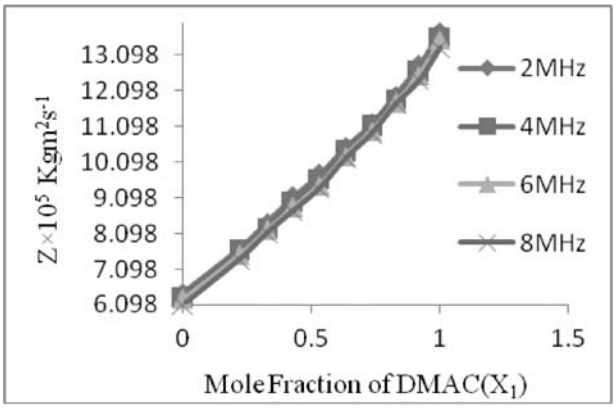

Fig. 6. Variation of Z Versus X_1

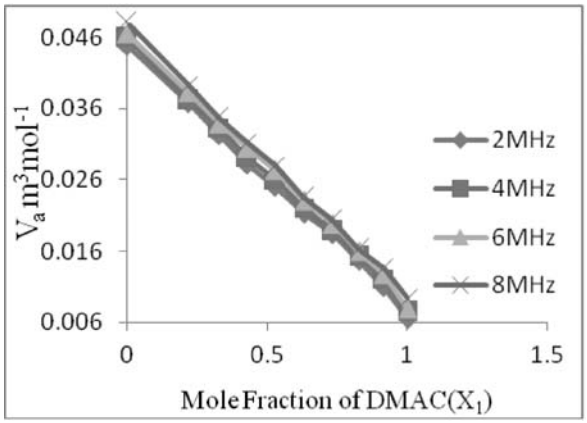

Fig. 7. Variation of V_a Versus X_1

The ultrasonic velocity decreases at a particular concentration of DMAC with the increase in frequency from 2 MHz, to 8 MHz. This decrease in ultrasonic velocity is perhaps due to the decrease in molecular interaction in the binary liquid mixture with the increase in frequency. Consequently the adiabatic compressibility, the intermolecular free length and the available volume increase and the acoustic impedance decreases with the increase in frequency for a particular mole fraction of DMAC.

It is interesting to explain the nature of interactions between the component molecules of the binary liquid mixture in terms of the excess values of acoustical parameters rather than their actual values. It is learnt that the dispersion forces lead to positive contributions to β^E, L_f^E, V_m^E and V_a^E and negative contributions to U^E and Z^E. The attractive forces due to charge transfer, dipole-dipole, dipole-induced dipole interactions, interstitial accommodation and orientational ordering lead to negative contributions to β^E, L_f^E, V_m^E and V_a^E and positive contributions to U^E and Z^E.

Fig-8 shows that the values of excess velocity U^E are negative for the entire range of mole fraction of DMAC for all frequencies. The negative values of U^Z indicate the presence dispersive forces between unlike molecules in the binary liquid mixture. The zigzag nature in the negative variations of U^E suggests the presence of steric hindrance for the formation of H- bonds between unlike molecules in the liquid mixture.

The values of β^E are negative as shown in Fig-9 for the entire range of mole fraction of DMAC for all frequencies. The negative value of β^E is associated with a structure forming tendency and existence of strong molecular interactions in the binary liquid mixture.

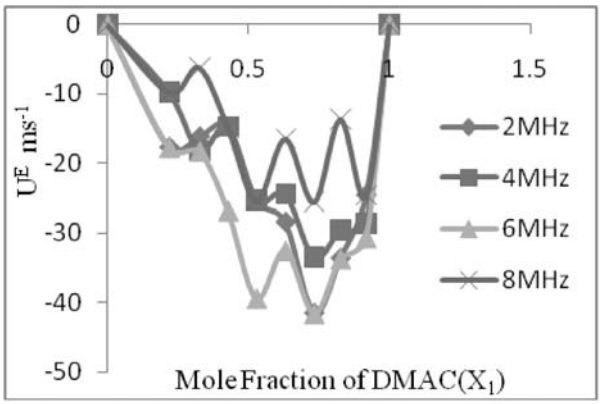

Fig. 8. Variation of U^E Versus X_1

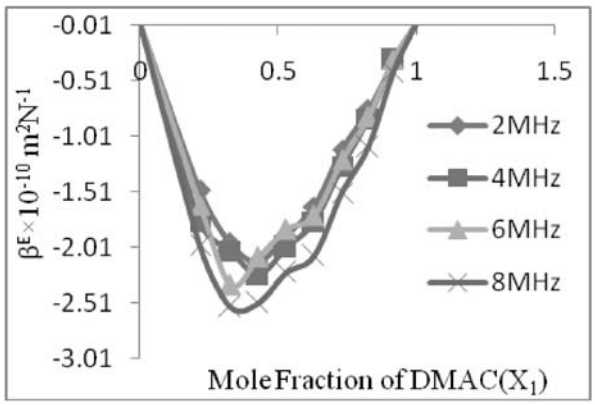

Fig. 9. Variation of β^E Versus X_1

Fig-10 shows that the values of L_f^E are negative for the entire range of mole fraction of DMAC for all frequencies. The negative excess values of L_f^E are due to charge transfer, dipole-dipole, dipole-induced dipole interactions, interstitial accommodation and orientational ordering which predict the existence of strong molecular interactions in the binary liquid mixture.

The values of excess molar volume V_m^E are negative for the entire range of mole fraction of DMAC as shown in Fig-11. The negative values of V_m^E indicate the presence of dipole-dipole and dipole-induced dipole interactions in the binary liquid mixture[18].

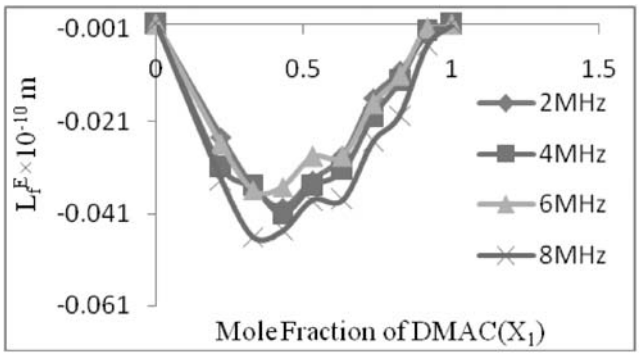

Fig. 10. Variation of L_f^E Versus X_1

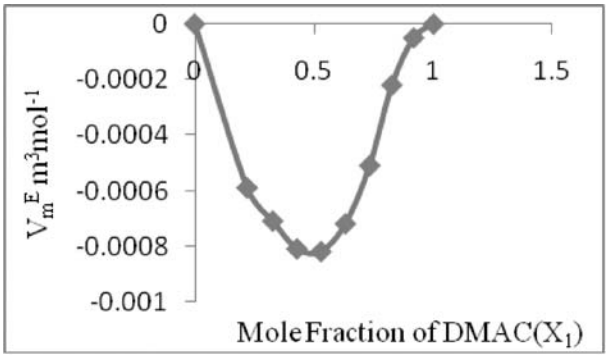

Fig. 11. Variation of V_m^E Versus X_1

The values of Z^E are negative for the entire range of mole fraction of DMAC as shown in Fig-12 for frequencies 2 MHz, 4 MHz, 6 MHz and 8 MHz. The negative values of Z^E indicate the presence of dispersive forces between unlike molecules in the binary liquid mixture.

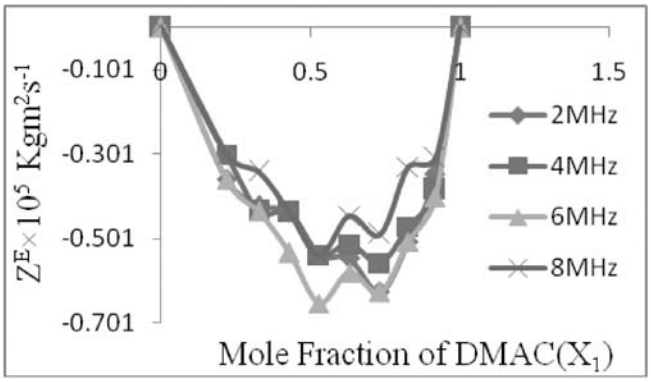

Fig. 12. Variation of Z^E Versus X_1

The values of excess available volume V_a^E as shown in Fig-13 are positive or negative within equimolar concentration region of DMAC which indicate the presence of strong interactions and dispersive forces. The values of excess available volume are positive for the higher concentration region of DMAC for all frequencies which indicate the presence of dispersive forces in the binary liquid mixture.

The excess values of adiabatic compressibility, free length and molar volume are more negative at equimolar region of the mixture which indicate that the dipole-induced dipole interaction is predominant in this region. At lower and higher concentration regions of DMAC there exists dipole-dipole interaction among unlike molecules in the binary liquid mixture.

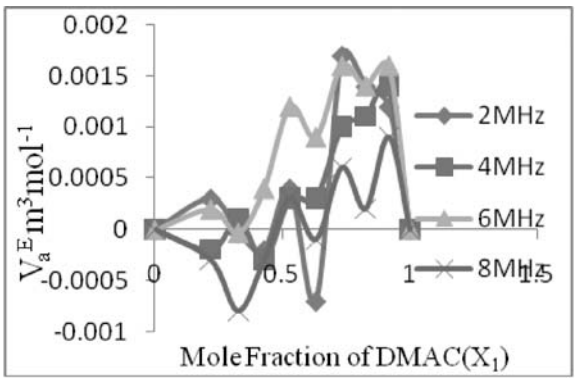

Fig. 13. Variation of V_a^E Versus X_1

The excess values of velocity, adiabatic compressibility, free length acoustic impedance and available volume are changed with the increase in frequency due to the decrease in ultrasonic velocity in the binary liquid mixture.

Figs-14 and 15 show that the values of molar sound velocity R and molar compressibility B increase nonlinearly with the increase in mole fraction of DMAC for a particular frequency. The nonlinear increase in molar sound velocity and molar compressibility indicates the increase in molecular interactions in the binary liquid mixture. The values of R and B decrease with the increase in frequency at a particular concentration of DMAC. This decrease in R and B also supports the reduction in molecular interaction with the increase in frequency in the binary liquid mixture.

Lennard-Jones potential ?(r) is given by the relation.

$$\varphi(r) = -Ar^{-6} + Dr^{-n} \quad (11)$$

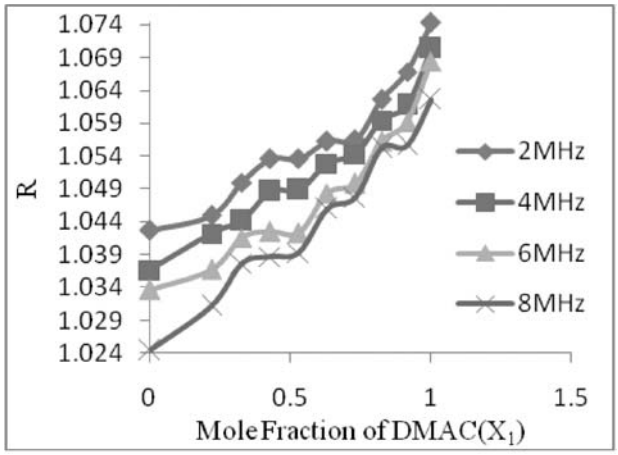

Fig. 14. Variation of R Versus X_1

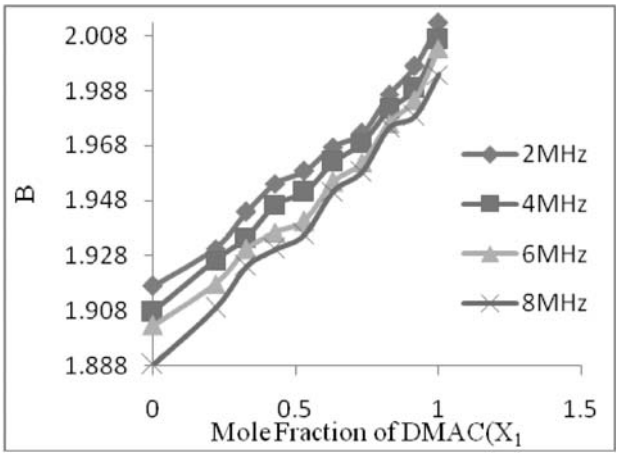

Fig. 15. Variation of B Versus X_1

Where *r* and *n* are intermolecular distance and Lennard-Jones potential repulsive term exponent respectively. *A* and *D* are constants. The first term is the contribution of attractive forces while the second term is the contribution of repulsive forces. Thus large value of n indicates the dominance of attractive forces over repulsive forces. The values of n increase with the increase in mole fraction of DMAC as shown in Fig-16 for a fixed frequency. The increase in n indicates the increasing dominance of attractive force over repulsive forces in the binary liquid mixture. Further, *n* decreases with the increase in frequency for a particular concentration which indicates the increase in repulsive forces due to decrease in molecular interaction in the binary liquid mixture[19-21].

Fig-17 shows that surface tension *S* increases with the increase in mole fraction of DMAC for a particular frequency in the binary liquid mixture which indicates that the liquid system becomes more compact[22, 23]. Further surface tension *S* decreases with the increase in frequency for a particular mole fraction of DMAC in the binary liquid mixture which reveals that molecular interaction is weaker at higher frequencies.

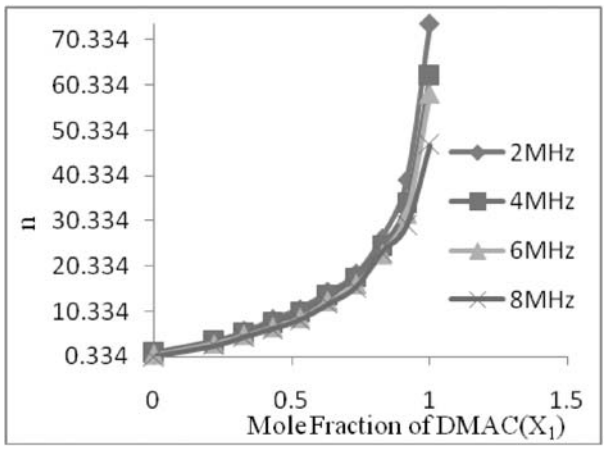

Fig. 16. Variation of n Versus X_1

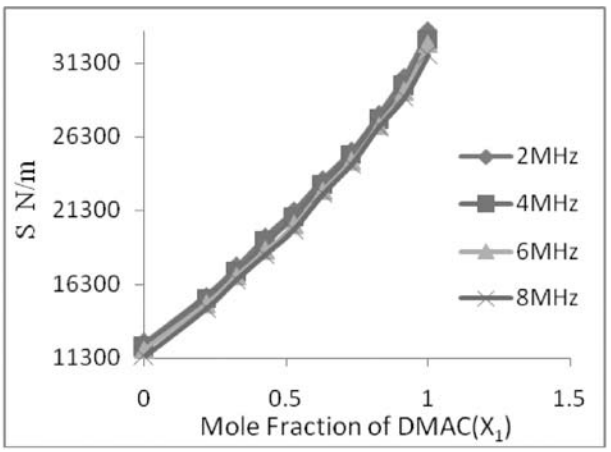

Fig. 17. Variation of S Versus X_1

4. CONCLUSION

On the basis of the experimental values of density, ultrasonic velocity, related acoustical parameters and some of their excess values for the binary liquid mixture it is concluded that there exists molecular

interactions in the binary mixture of DMAC and diethyl ether. The negative excess values of excess adiabatic compressibility β^E and excess free length L_f^E are due to charge transfer, dipole-dipole, dipole-induced dipole interactions, interstitial accommodation and orientational ordering which predict the existence of strong molecular interactions in the binary liquid mixture. The negative values of excess acoustic impedance Z^E indicate the presence of dispersive forces between unlike molecules in the binary liquid mixture. The increase in Lennard Jones potential repulsive term exponent with the increase in mole fraction of DAMC indicates the increasing dominance of attractive forces over repulsive forces in the binary liquid mixture. Further, it is concluded that the molecular interaction decreases with the increase in frequency for a fixed concentration of DMAC in the binary mixture. The binary liquid mixture of DMAC and diethyl ether at equimolar region may be used as a better solvent in the presence of the above prominent molecular interactions.

5. ACKNOWLEDGEMENT

The author Ashok Kumar Dash is thankful to the University Grants Commission (ERO), Kolkata, India for providing financial assistance in the form of M R P grant.

6. REFERENCES

[1] V. Kanappan and R Jaya Santhi, 2005. Ultrasonic study of induced dipole-dipole interactions in binary liquid mixtures, *Indian Journal of Pure & Applied Physics*, **43**, 750-754.

[2] M.K. Gangwar and A.K. Saxena, 2013. Ultrasonic study of molecular interactions in binary mixtures of isopropylbenzene (Cumene) with Benzene, Toluene and Acetone at 303K, *Research Journal of Chemical Sciences*, **3**(2), 27-30

[3] J.N. Ramteke, 2012. Ultrsonic Study on Molecular Interaction in Binary liquid Mixture containing _-picolin in ethanol at 301.15K, *Pelagia Research Library*, **3**(3), 1832-1835.

[4] A.K. Dash and R. Paikaray, 2013. Acoustical study on ternary mixture of dimethyl acetamide (DMAC) in diethyl ether and isobutyl methyl ketone at different frequencies, *Physics and Chemistry of Liquids*, **51**(6), 749-763.

[5] A.K. Dash and R. Paikaray, 2014. Study of Molecular Interaction in Binary Mixture of Dimethyl Acetamidewith Diethyl ether using Ultrasonic and Viscosity Probes, *Research Journal of Chemical Sciences*, **4**(3),45-53.

[6] R. Paikaray and N. Mohanty, 2015. Study of Thermodynamical Acoustic Parameters of Binary Mixture of DBP with O-Xylene at 308k and at different frequencies, *International Journal of Science and Research*, ISU, 171-176.

[7] R. Paikaray and N. Mohanty, 2013. Evaluation of Thermodynamical Acoustic Parameters of Binary mixture of DBP with Toluene at 308K and at different frequencies, *Research Journal of Chemical Sciences*, **3**(5), 71-82

[8] A.K. Dash and R. Paikaray, 2014. Acoustical study in binary liquid mixture containing dimethyl acetamide using ultrasonic and viscosity probes, *Der Chemica Sinica*, **5**(1), 81-88.

[9] R. Uvarani and J. Sivapragasam, 2012. Intermolecular interaction studies on ternary liquid mixtures at 303 K, *Journal of Chemical and Pharmaceutical Research*, **4**(1), 653-655.

[10] A.K. Dash and R. Paikaray, 2014. Ultrasonic Studies on Molecular Interaction in Ternary Liquid Mixture of Dimethyl Acetamide at Different Frequencies, *International Journal of Advanced Science and Technology*, **66**, 89-104.

[11] A.K. Dash and R. Paikaray, 2015. Molecular interaction studies in ternary liquid mixture of dimethylacetamide using ultrasonictechnique at 308 K. *Physics and Chemistry of Liquids*, **53**(2), 230-241.

[12] A.K. Dash and R. Paikaray, 2014. Studies on Acoustic Parameters of Ternary Mixture of Dimethyl Acetamide in Acetone and Isobutyl Methyl Ketone using Ultrasonic and Viscosity Probes, International *Journal of Chemical and Physical Science,* **3**(4), 69-79.

[13] R. Kubendram, F. Liakat Ali Khan, J. Asghar, M Aravinthraj and J. Udayaseelan, 2011. Ultrasonic studies of N, Ndimethylacetamide and N-methylacetamide with alkoxyethanols in carbon tetrachloride at different temperatures, *Scholars Research Library,* **3**(2), 568-576.

[14] A.K. Dash and R. Paikaray, 2015. Visco Metric, Volumetric and Acoustic Studies in Ternary Mixture of Dimethyl Acetamide and Diethyl Ether in an Aprotic Solvent, *International Journal of Science and Research,* ISU, 5-9.

[15] M.K. Praharaj and S. Mishra, 2014. Theoretical evalution of ultrasonic velocity in certain ternary liquid mixtures at different temperatures and concentrations and their comparision with the experimental values, studied through percentage deviation and interaction parameters, *Elixir Ultrasonics,* **76**, 28252-28259.

[16] R. Natrajan and P. Ramesh, 2011. Ultrasonic velocity determination in binary liquid mixtures, *J. Pure appl. And Ind. Phys,* **1**(4), 252-258.

[17] H. Eyring and J.F. Kincaid, 1938. Free volumes and free angle ratios of molecules in liquids, *J. Chem. Physics,* **6**, 620.

[18] S. Thirumaran and M. Rajeswari, 2011. Acoustical studies on binary liquid mixtures of some aromatic hydrocarbons with dimethylsulphooxide (DMSO) at 303.15 K, *Scholars Research Library,* **2**(2), 149-156.

[19] A.K. Gupta, Krishna Kumar and B.K Karn, 2009. Acoustical studies on binary liquid mixtures of some aromatic hydrocarbons with dimethylsulphooxide (DMSO) at 303.15 K, *J. Ind. Council Chem.* **26**, 77-81.

[20] A.K. Dash and R. Paikaray, 2013. Ultrasonic Study on Ternary Mixture of Dimethyl Acetamide (DMAC) in Diethyl ether and Acetone, *Research Journal of Physical Sciences,* **1**(3), 12-20.

[21] A.K. Dash and R. Paikaray, 2013. Study of molecular interaction in binary liquid mixture of dimethyl acetamide and acetone using ultrasonic probe, *Advances in Applied Science Research,* **4**(3), 130-139.

[22] S. Mishra and R. Paikaray, 2013. Acoustical properties of Ternary Mixture of di-(2-ethyl-hexyl) Phosphoric acid in Cyclohexane and Ethanol mixed Solvent at various temperatures, *Research Journal of Physical Sciences,* **1**(4), 15-21.

[23] G.A. Mathana and J. Poongodi, 2015. Interrelationship between Surface Tension and Sound Velocity & Thermodynamical studies of binary liquid mixtures, *International Journal of Research in Pure and Applied Physics,* **5**(1), 1-6.

Journal of Acoustical Society of India : Vol. 43, No. 3, 2016 (pp. 169-176)

Inter-molecular interactions in the binary mixture of pyridine and aniline at different temperatures by ultrasonic investigations

Prashant Dabrase[1]*, B.M. Suryavanshi[2] and R.A. Patil[3]
[1]Bhalerao Science College, Saoner, Dist. Nagpur (M.S.), 441107, India
[2]Department of Physics, Government Institute of Science, Nagpur (M.S.) 440001, India
[3]SSSKR Innani College, Karanja (lad), Dist. Washim (M.S.), 444105, India
**e-mail: prashantdabrase@gmail.com*

[Received: 19-07-2016; Revised: 29-09-2016; Accepted: 06-10-2016]

ABSTRACT

The advancements in ultrasonic measurement technique makes it easy to determine the interactions in liquids and the liquid mixtures. The technique comprises the measurements of Ultrasonic velocity (υ), density (ρ) and coefficient of viscosity (η) of the binary system at different temperatures.Here we reported the values of density, ultrasonic velocity and coefficient of viscosity of the binary mixture of pyridine and aniline. The derived parameters compressibility, free length, free volume have found to decreases with the increase in the concentration of the aniline in the mixture whereas these values increases with temperature of the system. The values of acoustical impedance and internal pressure are changing with composition as well as with temperature. The results are presented graphically and the curves indicates the existence of intermolecular interactions in the mixture. The excess values of velocity υ^E, adiabatic compressibility $\beta_\alpha{}^E$, free length $L_f{}^E$, acoustical impedance Z^E, free volume $V_f{}^E$ and internal pressure $\pi_i{}^E$ have been evaluated and presented graphically.

1. INTRODUCTION

Ultrasonic measurements on various systems provide important molecular information. This method is unique which makes it useful in various fields such as biological, automobile, pharmaceutical, chemical, industrial and other areas of research.It is well known fact that the Ultrasonic methodof measurement have played an important role in the study of liquids and liquid mixtures. Ultrasonic velocity provides the knowledge about various parameters related to physical interactions occurring in the liquids. The study of the different liquids and liquid mixtures consisting of polar or non-polar components is very important in understanding the physical nature and strength of molecular interaction in the liquids and liquid mixtures[1-5].

The aniline and pyridine have used in the present study. Since pyridine is used in the extraction process of coal and in manufacture of vitamin B6 and other drugs[6-9]. Similarly the Aniline is also used in many applications such as bio-medical, chemical and pharmaceutical industries. Aniline molecule is polar and self-associated through hydrogen bonding. It is used in the manufacturing of synthetic dyes, drugs, *etc.*[10]. These liquids and their mixtures are of interest to organic chemists to know about the type of bond and the complexes.

In order to understand the nature of aniline and pyridine and their liquid mixtures. The different ultrasonic parameters are determined from ultrasonic velocity, density and coefficient of viscosity. The excess values are also calculated in order to understand the nature of molecular interaction[11-13]. The investigations are carried out to determine the interactions in the above system.

2. METHODS AND MEASUREMENTS

The chemicals Pyridine and Aniline with purity of 99.5% of AR grade have obtained commercially and were used without further purification.The binary mixtures were prepared with aniline and pyridine for different mole fraction of aniline and the prepared solutions were kept in air tight volumetric flasks to avoid air contact.All the prepared mixtures were utilized within the 24 hours of its preparation.The Ultrasonic velocity (υ) measurements ofpure liquids and their mixture for different concentrations were carried out by using Ultrasonic Interferometer at 1 MHz (Mittal enterprises- model M-81). The temperature of the liquid in the liquid cell was kept constant by water circulation using electronically controlled thermostat. The temperature was kept constant by thermostat within the accuracy of ± 0.1°C. The accuracy in the measurement of ultrasonic velocity was ± 0.1m/s. The densities were measured using specific gravity bottle on sensitive K-Roy (K-12, Classic) mono pan balance. The coefficients of viscosities were measured using the suspended level Ubelohde three limb viscometer. The accuracy in density measurement was ± 0.0001 Kg/m^3 and that in viscosity measurement was ± 0.001 Ns/m^2.

The experimental measurement of density (ρ), ultrasonic velocity (υ) and coefficient of viscosity (η) have been used to determine the following ultrasonic parameters[14, 15].

Adiabatic Compressibility (β_α), $$\beta_\alpha = 1/\rho\upsilon^2 \quad (1)$$

Intermolecular free length (L_f) $$L_f = K\,\beta_\alpha^{1/2} \quad (2)$$

Acoustical Impedance (Z) $$Z = \rho\,\upsilon \quad (3)$$

Free volume (V_f), $$V_f = \left[\frac{M_{eff}\,v}{n\,k}\right]^{\frac{3}{2}} \quad (4)$$

The internal pressure (π_i), $$\pi_i = bRT\left(\frac{kn}{v}\right)^{1/2}\left(\frac{\rho^{2/3}}{M_{eff}^{7/6}}\right) \quad (5)$$

Where, the symbol K -is temperature dependent constant[16] $K=(93.875 + 0.375\ T)\ x10^{-8}$,

M_{eff}-is the effective molecular weight, ($M_{eff} = \Sigma m_i X_i$),

k -is temperature independent constant which is equal to $4.28\ X\ 10^9$ for all liquids,

T-is the absolute temperature,

b-is a constant equal to 2 for the liquid

The excess values of all the parameters are determined by using the relation

$$A^E = A_{exp} \sum_{i=1}^{n} A_i X_i \quad (6)$$

Where, A^E - excess value of any acoustic parameters,

A_{exp}- experimentally determined ultrasonic parameters,

A_i-is any acoustical parameter and X_i - the mole fraction of liquid component.

3. RESULT AND DISCUSSION

The binary solutions of aniline and pyridine have been prepared by relative change of the component of the mixture. The variation in concentration have been quoted in terms of the molar fraction of aniline. The ultrasonic velocity (υ) increases with the increase in concentration of aniline in the mixture. The adiabatic compressibility (β_α), intermolecular free length (L_f) decreases with the concentration of aniline in the binary

mixture. It is also observed here that the values of acoustical impedance (Z) are increasing with the increase in concentration of aniline.

The plots of the values of free length and free volume with increasing concentration of aniline shows non-linear nature indicates there is significant interaction between the two liquids[17-18]. The increase in impedance means the opposition of the passage of the ultrasonic wave increases in the medium. The plot of acoustic impedance and concentration is non-linear thus confirms the existence of interaction between the components of the mixture[19-20].

The extent of change and sign of excess values in thermo-dynamical parameter depends on the strength of intermolecular interaction between the molecules of the mixture[21, 22]. The plots of excess values of different thermo-dynamical parameters for varying concentration of binary mixture have been given in fig. 2(a) to 2(g), show the large change in excess values at 2:8 ratio of the mixture corresponding to associative nature in the mixture. The excess values of velocity seen to be negative and maximum change is at 2:8 ratio of the mixture which may be related to the making and breaking of the structure. The relation of temperature with the excess value confirms decrease in the strength of interaction at higher temperature. The values of coefficient of viscosity (η) also increase with concentration of aniline. It is observed herethat the values of acoustical impedance (Z) and internal pressure (π_i) are increasing with the increase in concentration of aniline in the mixture.

The increasing coefficient of viscosity is the indication of existence of frictional resistive forces that may be due to molecular motions occurring in the mixture. The liquid aniline,when added with the pyridine,mayadjust intermolecular spacing in the binary mixture. It is clear that intermolecular free length depends upon size of the components in the mixture and attractive and repulsive forces. The decrease in free length means there is increase in attractive forces between the components of the mixture andhence the intermolecular spacing decreases. The decrease in free length is responsible for the decrease in free volume which ultimatelyincreases ininternal pressure of the system. These resultsconfirmed from the plots of different parameters given in fig. 1(a)-1(g).

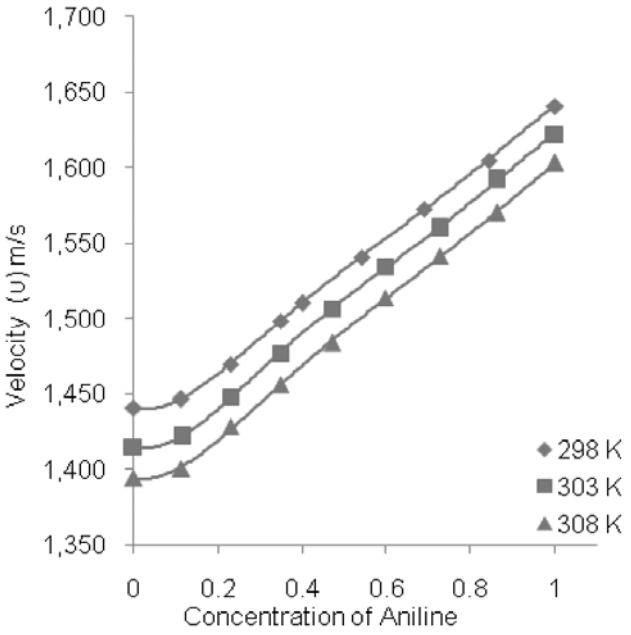

Fig. 1(a)

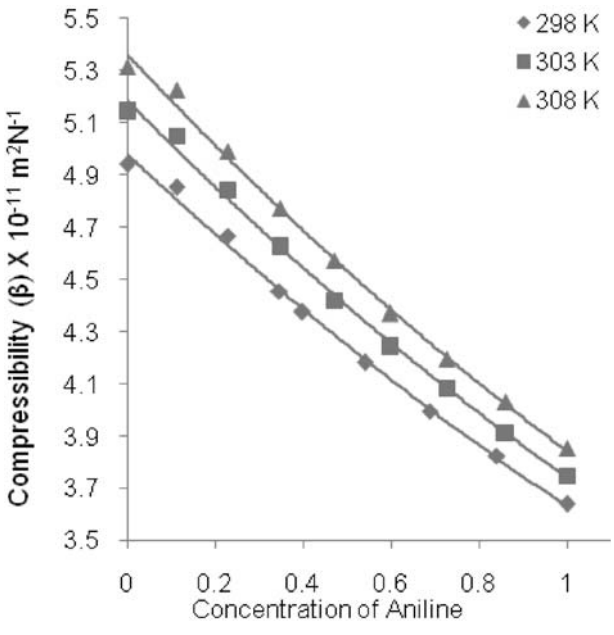

Fig. 1(b)

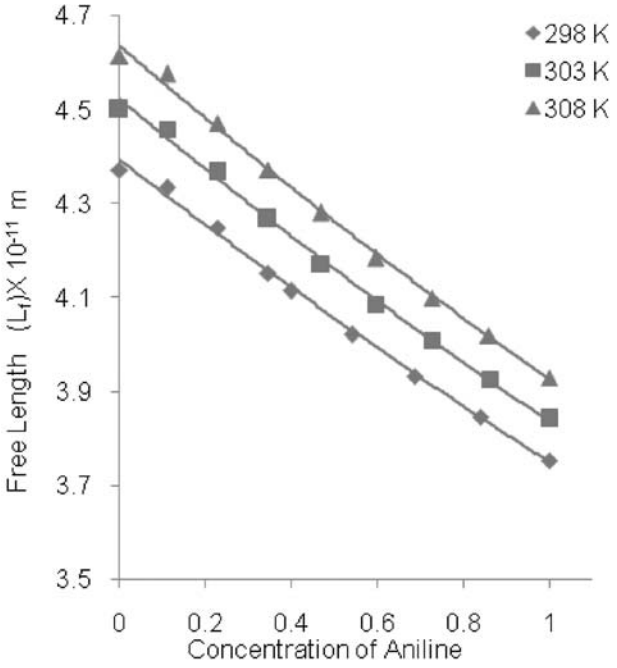

Fig. 1(c)

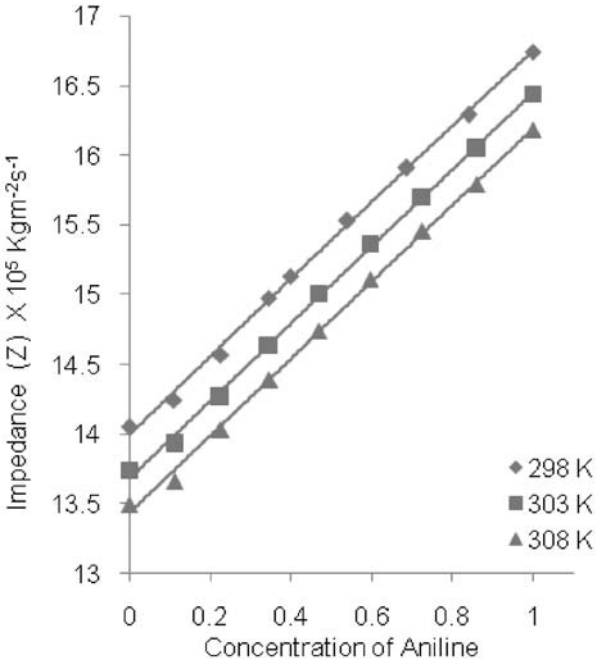

Fig. 1(d)

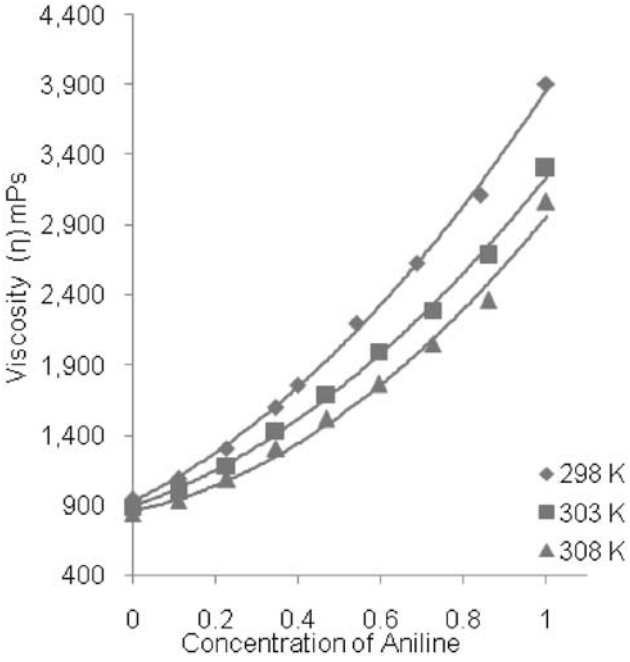

Fig. 1(e)

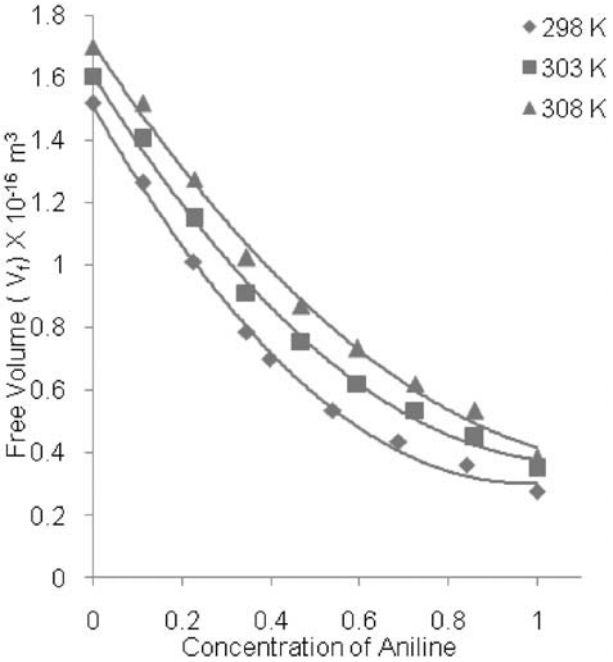

Fig. 1(f)

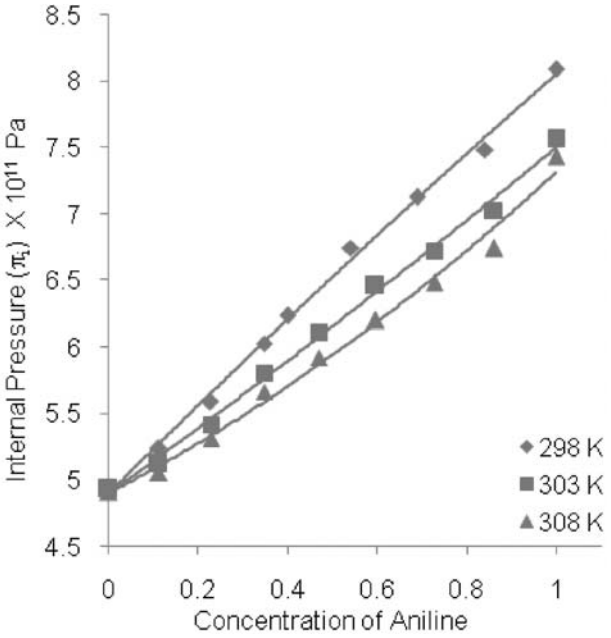

Fig. 1(g)

Fig. 01: (e) to (g) Plots of ultrasonic viscosity, adiabatic comprecsibility, free length, acoustical impedance, coefficient of viscosity, free volume and internal pressure for varying concentration of aniline at 298, 303 and 308 K temperatures.

The excess values of coefficient of viscosity and the internal pressure with concentration have been presented in the fig. 2(b) and 2(g). The maximum change in excess values of coefficient of viscosity and free volume fig. 2(b) and fig. 2(f), is observed at around 1:1 ratio of the components of the mixture and the sign is negative which corresponds to weak associative forces. Whereas the excess values of internal pressure

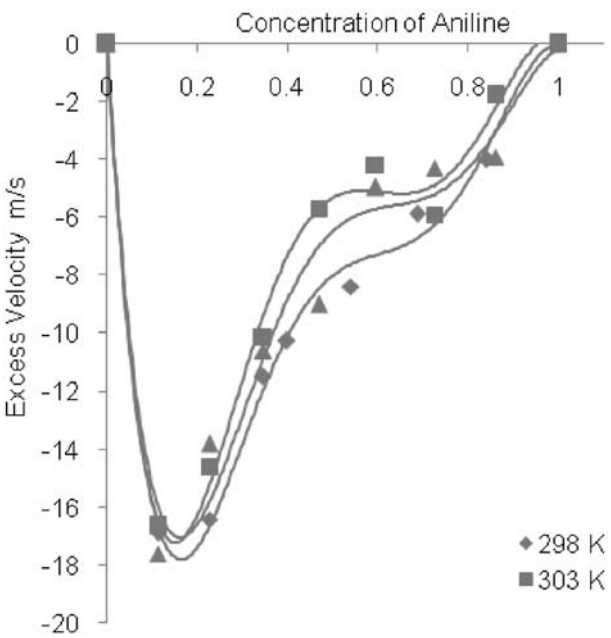

Fig. 2(a)

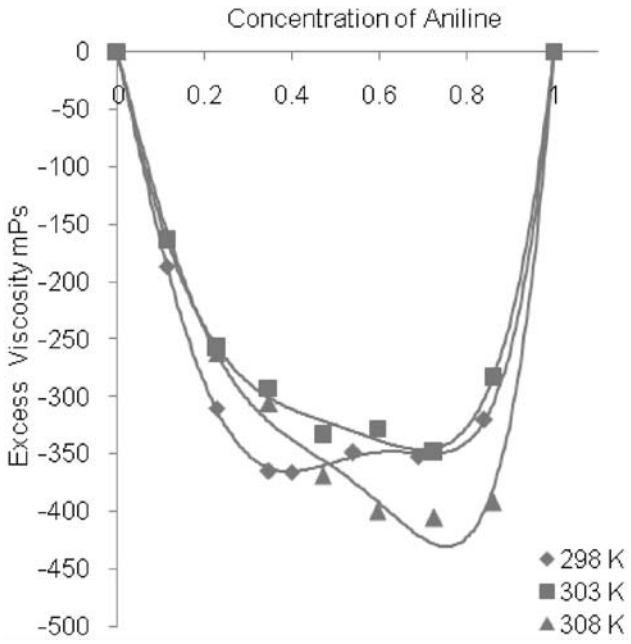

Fig. 2(b)

Fig. 02: (a) and (b) -Plots of excess values of ultrasonic velocity, coefficient of viscosity for varying concentration of aniline at 298, 303 and 308 K temperatures.

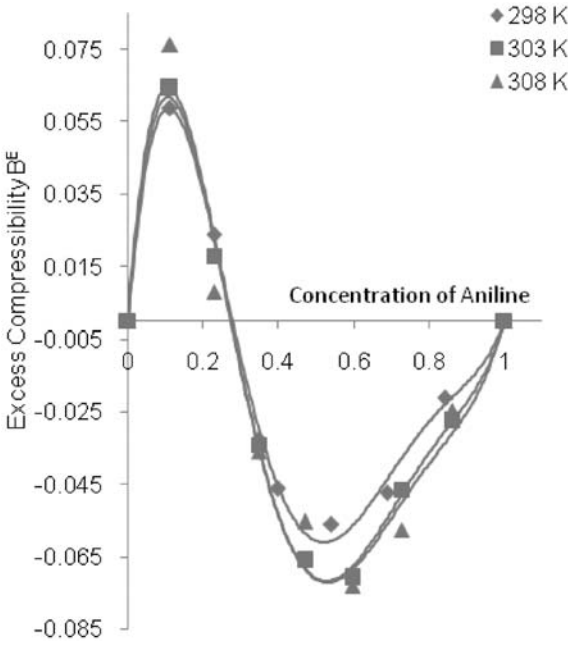

Fig. 2(c)

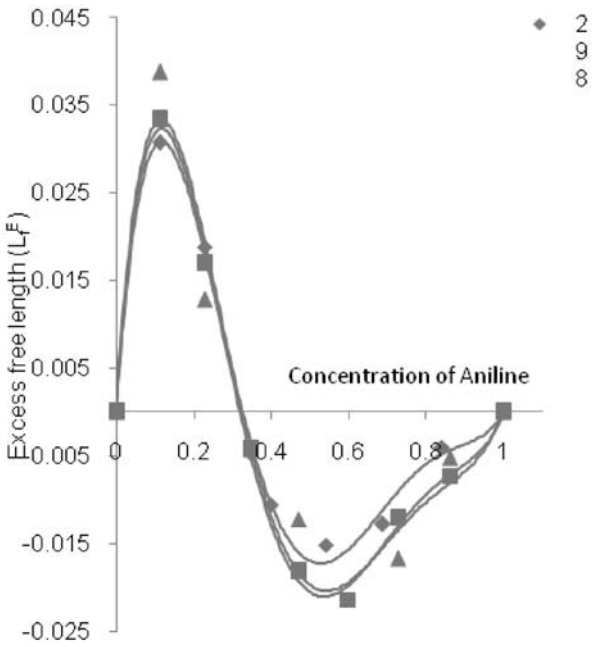

Fig. 2(d)

Fig. 02: (c) and (d) -Plots of excess values of adiabatic compressibility, free length for varying concentration of aniline at 298, 303 and 308 K temperatures.

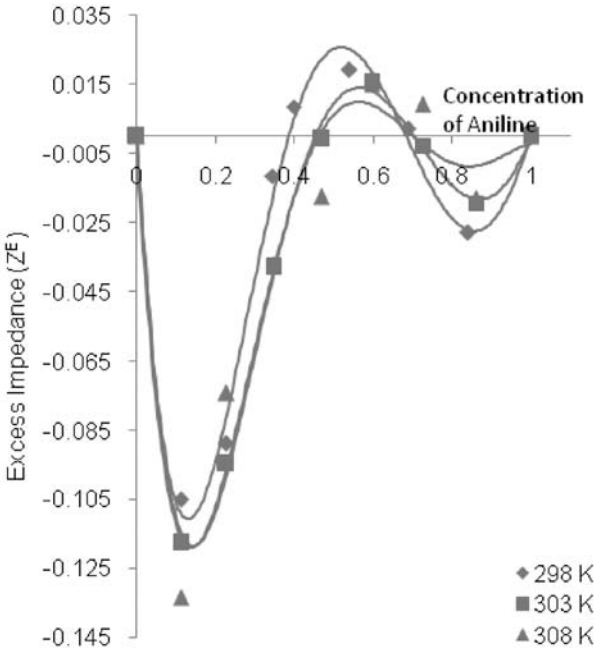

Fig. 2(e)

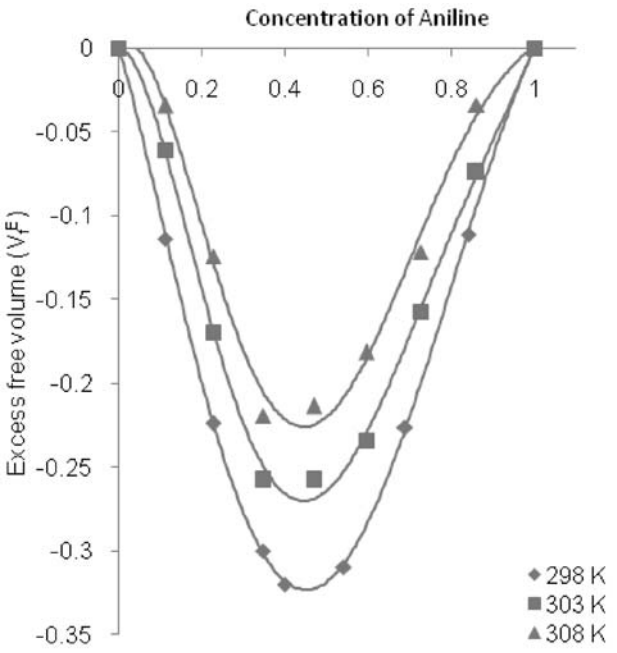

Fig. 2(f)

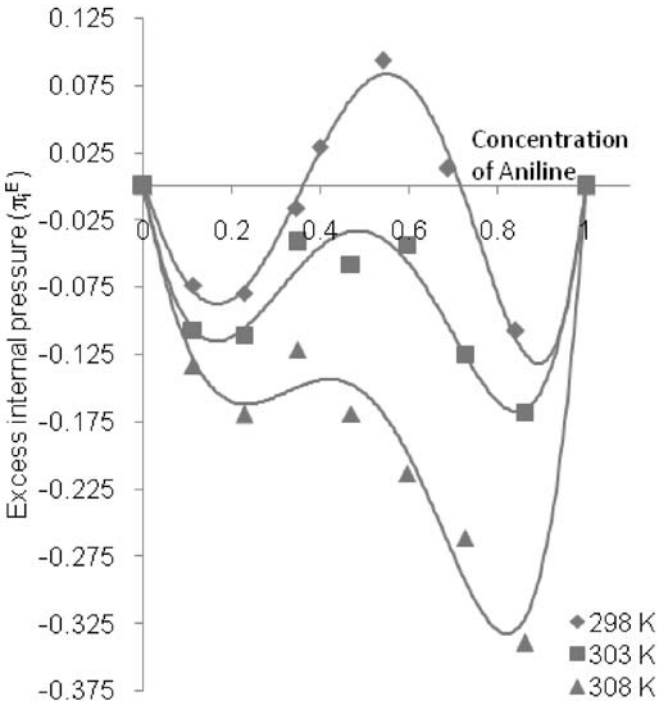

Fig. 2(d)

Fig. 02: (e) to (g)-Plots of excess values of ultrasonic viscosity, coefficient of viscosity, adiabatic comprecsibility, free length, acoustical impedance, free volume and internal pressure for vary concentration of aniline at 298, 303 and 308 K temperatures.

with concentration of aniline in the mixture, fig. 2(g), indicates change at around 2:8, 1:1 and 8:2 and is random in variation may corresponds to weak interaction between the components of the mixture.The sign of excess free length plays a vital role in assessing compactness due to molecular interaction through dipole-dipole interaction[23,24]. The increase in compactness enhances structure making and excess free length tends to negative. It has been observed that Excess compressibility and free length are negative after the 0.3 mole fraction of aniline in the binary mixture. This clearly indicates the weak and strong interactions are prevailing in the binary mixture.

4. CONCLUSION

The ultrasonic velocity, density and coefficient of viscosity of binary liquid mixture of the aniline and pyridine with varying concentration at three different temperatureswere measured for the determination of ultrasonic parameters like, adiabatic compressibility, free length, acoustical impedance, free volume and internal pressure. The decrease in adiabatic compressibility, intermolecular free length with the increase in concentration of aniline in the mixture confirms the existence of intermolecular interaction between the different components of the mixture. The increase in the density and ultrasonic velocity of the binary mixture with the concentration of aniline indicates the interaction exists between the molecules of the mixture.

The values of excess parameters of ultrasonic velocity (η^E), free volume (V_f^E) compressibility (β_α^E) and free length (L_f^E) are negative after the 0.3 molar concentration of aniline in the mixture. Also the excess values of coefficient of viscosity (η^E) and internal pressure (π_i^E) are non-linear but negative at three different temperatures 298, 303, 308 K confirms the presence of strong dispersive interaction between the components of molecules. The nature of plots ofvarious parameters indicates a non-linear behavior with the concentration of the aniline in the mixture. This suggests a significant interaction between the binary molecules. The excess values of the ultrasonic parameters of the binary mixture show large change for particular concentration. Thus the ultrasonic studies of aniline and pyridine mixture is indicative of formation of structure in the binary system.

5. REFERENCES

[1] V. SRINIVASULU and P.R. NAIDU, 1995. *J. Pure and Appl. Ultrasonic.* **17**, 14-28.

[2] K. SWAIN and P. PRIYADARSHANI, 2010. *Indian J.Pure and Appl. Phys.* **48**, 539-542.

[3] H. EYRING and J.F. KINCAID, 1938. *J. Chem, Phys,* **6**, 220-229.

[4] K.S. PITZER, Thermodynamics, 1995. 3rd edition, *McGraw-Hill book Co, NY.*

[5] A.N. KANNAPAN, S. THIRUMAM and R. PALANI, 2009. *J. Phys. Science.* **20**(2), 97-108.

[6] S. THIRUMARAN and K. INDHU, 2009. *Rasayan J. Chem*., ISSN: 0974-1496, **2**(3), 760-768.

[7] A.N. KANNAPPAN, R. KESAVASAMY and V. PONNUSWAMY, 2008. *ARPN Journal of Engineering and Applied Sciences*, ISSN 1819-6608, **3**(4), 41-45.

[8] B.S. FURNISS, A.J. HANNAFORD, P.W.G. SMITH and A.R. TATCHELL, 1941. *Vogal's Text book of practical organic chemistry*. 5th Ed. Addison Wesley Longman Ltd. p. 1442.

[9] R.T. MORRISON and B.R. NELSON, 2001. *Organic Chemistry*. Prentice Hall of India Pvt. Ltd., New Delhi. 6th Ed. p. 1071.

[10] P. Vasantharani, L. Balu, R. Ezhil Pavai and S. SHAILAJHA, 2009. *Global Journal of Molecular Sciences,* ISSN 1990-9241, **4**(1): 42-48.

[11] V.A. TABHANE, S. GHOSH and S. AGRAWAL, 1900. *J. Pure and Appl. Ultrasonic*, **21**, 122.

[12] P.K. GUPTA and F.B. STUMP, 2010. *Indian J pure and Appl. Phys*., **48**, 326-333.

[13] G. ARUL and L. PALANIAPPAN,2005. *Indian J pure and Appl. Phys*. **43**, 755-758.

[14] A. ALI and A.K. NAIN, 2002. *Pramana*, **58**, 695-701.

[15] N. SUDHARAM and L. PALANIAPPAN, 2012. *Current Res. in Physics,* ISSN 2154-3119, 1-6.

[16] JACOBSON and B. ULTRA, 1952. Velo. of liquids and liquid mixt. *J. Chem. Phys.*, **20**, 927-928.

[17] K. RAJGOPAL and S. CHENTHILNATH, 1981. *Indian J.Pure and Appl. Phys.*, **19**, 358.

[18] T .S. BANIPAL, A.F. TOOR and V.K. RATTAN, 2000. *Indian J Chem.* **39A**, 809.

[19] P.S. NAIDU and K. RAVINDRA PRASAD, 2002. *Indian J.Pure and Appl. Phys.*, **40**, 264.

[20] G. ARUL and L. PALANIAPPAN, 2001. *Indian J pure and Appl. Phys*. **39**, 561.

[21] A.N. KANNAPPAN and V. RAJENDRAN, 1999. *Indian J. Pure and Appl. Phys.* **73B**, 531.

[22] A.S RAO, B. VIJAY KUMAR NAIDU and CHAWDOJI RAO, 2000. *J Acoust Soc India*, **28**, 303.

[23] O. REDLICH and A.T. KISTER, 1948. *Ind. Eng. Chem.*, **40**, 345.

[24] A. ALI and A.K. NAIN, 1999. Int. Conf. and Exhi. on Ultrsonics (ICEU-99), Dec-2, New Delhi.

[25] D. ANBANANTHAN, 1979. *Jou Acost Soc of India*, **7**, 123.

[26] NISHA SHARMA and B.P. SINGH, 2010. *Acta Ciencia India*, XXXIV P(3), 375.

[27] M.K. PRAHARAJ *et al.*, 2012. *Journ. Chemical and Pharma. Research*, **4**(4), 1910-1920.

[28] P.B. DABRASE, R.A. PATIL, B.M. SURYAVANSHI, 2013. *Journal of Acoustical Society of India*, **40**(2), 137-142.

[29] P.B. DABRASE, R.A PATIL and B.M. SURYAVANSHI, 2012. *Int. Journal of Research in Pure and Applied Physics*; **2**(4), 49-54.

INFORMATION FOR AUTHORS

ARTICLES

The Journal of Acoustical Society of India (JASI) is a refereed publication published quarterly by the Acoustical Society of India (ASI). JASI includes refereed articles, technical notes, letters-to-the-editor, book review and announcements of general interest to readers.

Articles may be theoretical or experimental in nature. But those which combine theoretical and experimental approaches to solve acoustics problems are particularly welcome. Technical notes, letters-to-the-editor and announcements may also be submitted. Articles must not have been published previously in other engineering or scientific journals. Articles in the following are particularly encouraged: applied acoustics, acoustical materials, active noise & vibration control, bioacoustics, communication acoustics including speech, computational acoustics, electro-acoustics and audio engineering, environmental acoustics, musical acoustics, non-linear acoustics, noise, physical acoustics, physiological and psychological acoustics, quieter technologies, room and building acoustics, structural acoustics and vibration, ultrasonics, underwater acoustics.

Authors whose articles are accepted for publication must transfer copyright of their articles to the ASI. This transfer involves publication only and does not in any way alter the author's traditional right regarding his/her articles.

PREPARATION OF MANUSCRIPTS

All manuscripts are refereed by at least two referees and are reviewed by the Publication Committee (all editors) before acceptance. Manuscripts of articles and technical notes should be submitted for review electronically to the Chief Editor by e-mail or by express mail on a disc. JASI maintains a high standard in the reviewing process and only accept papers of high quality. On acceptance, revised articles of all authors should be submitted to the Chief Editor by e-mail or by express mail.

Text of the manuscript should be double-spaced on A4 size paper, subdivided by main headings-typed in upper and lower case flush centre, with one line of space above and below and sub-headings within a section-typed in upper and lower case understood, flush left, followed by a period. Sub-sub headings should be italic. Articles should be written so that readers in different fields of acoustics can understand them easily. Manuscripts are only published if not normally exceeding twenty double-spaced text pages. If figures and illustrations are included then normally they should be restricted to no more than twelve-fifteen.

The first page of manuscripts should include on separate lines, the title of article, the names, of authors, affiliations and mailing addresses of authors in upper and lowers case. Do not include the author's title, position or degrees. Give an adequate post office address including pin or other postal code and the name of the city. An abstract of not more than 200 words should be included with each article. References should be numbered consecutively throughout the article with the number appearing as a superscript at the end of the sentence unless such placement causes ambiguity. The references should be grouped together, double spaced at the end of the article on a separate page. Footnotes are discouraged. Abbreviations and special terms must be defined if used.

EQUATIONS

Mathematical expressions should be typewritten as completely as possible. Equation should be numbered consecutively throughout the body of the article at the right hand margin in parentheses. Use letters and numbers for any equations in an appendix: Appendix A: (A1, (A2), etc. Equation numbers in the running text should be enclosed in parentheses, i.e., Eq. (1), Eqs. (1a) and (2a). Figures should be referred to as Fig. 1, Fig. 2, etc. Reference to table is in full: Table 1, Table 2, etc. Metric units should be used: the preferred from of metric unit is the System International (SI).

REFERENCES

The order and style of information differs slightly between periodical and book references and between published and unpublished references, depending on the available publication entries. A few examples are shown below.

Periodicals:

[1] S.R. Pride and M.W. Haartsen, 1996. Electroseismic wave properties, *J. Acoust. Soc. Am.*, **100** (3), 1301-1315.

[2] S.-H. Kim and I. Lee, 1996. Aeroelastic analysis of a flexible airfoil with free play non-linearity, *J. Sound Vib.*, **193** (4), 823-846.

Books:

[1] E.S. Skudzryk, 1968. *Simple and Comlex Vibratory Systems*, the Pennsylvania State University Press, London.

[2] E.H. Dowell, 1975. *Aeroelasticity of plates and shells*, Nordhoff, Leyden.

Others:

[1] J.N. Yang and A. Akbarpour, 1987. Technical Report NCEER-87-0007, Instantaneous Optimal Control Law For Tall Buildings Under Seismic Excitations.

SUMISSIONS

All materials from authors should be submitted in electronic form to the JASI Chief Editor: B. Chakraborty, CSIR - National Institute of Oceanography, Dona Paula, Goa-403 004, Tel: +91.832.2450.318, Fax: +91.832.2450.602,(e-mail: bishwajit@nio.org) For the item to be published in a given issue of a journal, the manuscript must reach the Chief Editor at least twelve week before the publication date.

SUMISSION OF ACCEPTED MANUSCRIPT

On acceptance, revised articles should be submitted in electronic form to the JASI Chief Editor (bishwajit@nio.org)

ISSN 0973-3302

JOURNAL OF ACOUSTICAL SOCIETY OF INDIA

Volume 43 Number 4 October 2016

A Quarterly Publication of the JASI

http://www.acousticsindia.org

Journal of Acoustical Society of India

Volume 43 Number 4 October 2016 pp 177-246

JASI

Journal of Acoustical Society of India

The Refereed Journal of the Acoustical Society of India (JASI)

The Journal of Acoustical Society of India is a refereed journal of the Acoustical Society of India **(ASI)**. The **ASI** is a non-profit national society founded in 31st July, 1971. The primary objective of the society is to advance the science of acoustics by creating an organization that is responsive to the needs of scientists and engineers concerned with acoustics problems all around the world.

Manuscripts of articles, technical notes and letter to the editor should be submitted to the Chief Editor. Copies of articles on specific topics listed above should also be submitted to the respective Associate Scientific Editor. Manuscripts are refereed by at least two referees and are reviewed by Publication Committee (all editors) before acceptance. On acceptance, revised articles with the text and figures scanned as separate files on a diskette should be submitted to the Editor by express mail. Manuscripts of articles must be prepared in strict accordance with the author instructions.

All information concerning subscription, new books, journals, conferences, etc. should be submitted to Chief Editor:

B. Chakraborty, CSIR - National Institute of Oceanography, Dona Paula, Goa-403 004,
Tel: +91.832.2450.318, Fax: +91.832.2450.602, e-mail: bishwajit@nio.org

Annual subscription price including mail postage is Rs. 2500/= for institutions, companies and libraries and Rs. 2500/= for individuals who are not **ASI** members. The Journal of Acoustical Society of India will be sent to **ASI** members free of any extra charge. Requests for specimen copies and claims for missing issues as well as address changes should be sent to the Editorial Office:

ASI Secretariat, C/o Acoustics, Ultrasonics & Vibration Section, CSIR-National Physical Laboratory, Dr. KS Krishnan Road, New Delhi 110 012, Tel: +91.11.4560.8317, Fax: +91.11.4560.9310, e-mail: asisecretariat.india@gmail.com

ISSN 0973-3302

Printed at Alpha Printers, WZ-35/C, Naraina, Near Ring Road, New Delhi-110028 Tel.: 9810804196. JASI is sent to ASI members free of charge.

JASI

Journal of Acoustical Society of India

The Refereed Journal of the Acoustical Society of India (JASI)

The Journal of Acoustical Society of India is a refereed journal of the Acoustical Society of India **(ASI)**. The **ASI** is a non-profit national society founded in 31st July, 1971. The primary objective of the society is to advance the science of acoustics by creating an organization that is responsive to the needs of scientists and engineers concerned with acoustics problems all around the world.

Manuscripts of articles, technical notes and letter to the editor should be submitted to the Chief Editor. Copies of articles on specific topics listed above should also be submitted to the respective Associate Scientific Editor. Manuscripts are refereed by at least two referees and are reviewed by Publication Committee (all editors) before acceptance. On acceptance, revised articles with the text and figures scanned as separate files on a diskette should be submitted to the Editor by express mail. Manuscripts of articles must be prepared in strict accordance with the author instructions.

All information concerning subscription, new books, journals, conferences, etc. should be submitted to Chief Editor:

B. Chakraborty, CSIR - National Institute of Oceanography, Dona Paula, Goa-403 004,
Tel: +91.832.2450.318, Fax: +91.832.2450.602, e-mail: bishwajit@nio.org

Annual subscription price including mail postage is Rs. 2500/- for institutions, companies and libraries and Rs. 2500/- for individuals who are not **ASI** members. The Journal of Acoustical Society of India will be sent to **ASI** members free of any extra charge. Requests for specimen copies and claims for missing issues as well as address changes should be sent to the Editorial Office:

ASI Secretariat, C/o Acoustics, Ultrasonics & Vibration Section, CSIR-National Physical Laboratory, Dr. KS Krishnan Road, New Delhi 110 012, Tel: +91.11.4560.8317, Fax: +91.11.4560.9310, e-mail: asisecretariat.india@gmail.com

ISSN 0973-3302

Printed at Alpha Printers, WZ-35/C, Naraina, Near Ring Road, New Delhi-110028 Tel.: 9810804196. JASI is sent to ASI members free of charge.

JASI

Journal of Acoustical Society of India (JASI)

A quarterly publication of the Acoustical Society of India

Volume 43, Number 4, October 2016

ARTICLES

INFORMATION

EDITORIAL

Guest Editors' Introduction to the Special Issue on Sonar

Ships and helicopters use active sonar systems in an effort to detect submarines even though they give away their position when they transmit sound. This is because their position is relatively easily determined by using radar. Submarines usually travel more slowly than ships and use passive sonar to detect their targets as their own positions cannot be easily found using radar. Passive sonars comprise an array of underwater transducers, reception electronics, beam formers, signal processors and displays. Active sonars have, in addition, transmission signal generators, power amplifiers, and, in submarines, another array of transducers.

In this special issue on sonar - the first such issue in JASI - there are papers on some of the technologies that are used in active and passive sonar systems. Other technologies will be covered in another special issue. All the authors of papers in this issue are from Naval Physical and Oceanographic Laboratory, DRDO, Kochi. NPOL is the only Indian organization that designs and delivers sonar systems for defence applications; and its sonars are used by the Indian Navy and by other countries.

In this issue, there are nine papers: four on sonar transducers, one on sonar domes, one on sonar power amplifiers, one on passive detection, and two on passive tracking. These papers contain interesting information about some sub-systems of sonars but, quite expectedly, make no mention of others.

In sonar, as in any other system that is used to detect, the importance of frequency-dependent signal to noise ratio cannot be over-emphasized. In passive sonar, the system designer has no control over either the signal or the noise. In active sonar, the system designer has control over the transmitted sound and some control over reverberation noise but not over the echo or the other noises. The noise generated by the platform on which the sonar is mounted and the noise due to flow over the array can be critical factors. Thus the designers of the system and the sub-systems have to be prepared for a variety of signal and noise scenarios and many disciplines have to be mastered to make a sonar system that can actually detect, track, and classify a silent threat. India is one of the few countries that make sonar systems and many inter-disciplinary areas still pose challenges. It is our hope that this issue will draw the attention of experts in acoustics and other fields to sonar.

Dr. D.D. Ebenezer
Naval Physical and Oceanographic Lab, DRDO, Kochi

Prof. Rajendar Bahl
Indian Institute of Technology Delhi, Delhi

Prof. S.K. Bhattacharyya
Indian Institute of Technology Madras, Chennai

FOREWORD

Naval Physical and Oceanographic Laboratory's Sonars

Naval Physical and Oceanographic Laboratory (NPOL) has celebrated success at sea several times, organized two International Conferences on Sonar, and seen its work published in many leading journals; but this is the first time that an entire special issue of a journal is devoted to its sonars.

Though acoustics is a well established field, its specialized version, namely underwater acoustics, and in particular the field of sonar, is not familiar to those outside its limited circle of practitioners. The only form of energy that propagates underwater, without much attenuation for long distances, is sound and the whole domain of underwater surveillance and communication makes use of sound waves. The underwater living species also make use of sound energy extensively.

This special issue will provide an opportunity for our scientists to share the complexities and challenges in this area with the wider acoustic community and hopefully generate a larger community of researchers interested in taking up the unique problems encountered in this niche area.

Over the years, NPOL has designed and developed several different types of sonars. The journey started with its first active-cum-passive sonar, APSOH (Advanced Panoramic Sonar Hull mounted), installed on the Anti-Submarine Warfare frigate INS Himagiri in the mid 1980s replacing an imported sonar. The excellent performance of the sonar led to installation of APSOH and its variant HUMVAD on 10 ships.

NPOL continued to develop expertise in all the sonar-related fields and was ready with the next generation ship sonar in the early 1990s. HUMSA (Hull Mounted Sonar Advanced) is also an active-cum-passive sonar and is used to hunt for submarines. In addition to a larger array and lower frequencies, new technologies and techniques were used in HUMSA. A large number of frigates and destroyers, both imported and indigenous, were fitted with HUMSA.

Meanwhile, NPOL developed different types of active and passive sonars for submarines. Panchendriya, NPOL's first submarine sonar suite, was fitted and proved on INS Karanj in the mid 1990s. The experience gained from the first submarine sonar has been invaluable. All the tests that are done in acoustic tanks and elsewhere are essential but even special test facilities cannot be used to simulate all the propagation and noise conditions that are encountered on-board a submarine. Therefore, the methods used to detect faint signals when ocean acoustic noise and the own-platform noise are significant are fine-tuned after operating the sonar in various conditions at sea.

The performance of the submarine-sonar emboldened the Indian Navy to replace the sonars in its front-line submarines with NPOL's sonar-suite. USHUS is now being used by many submarines and an advanced version will soon be fitted on other submarines in the class. Another, more advanced, sonar-suite is operational on an indigenously built submarine.

HUMSA-NG and the compact sonar Abhay are NPOL's most recent ship sonars. The Indian Navy's frontline ships are being fitted with the HUMSA-NG system with a bow-mounted sonar array. The state-of-the-art Near-field Acoustic Characterization System (NACS) has been successfully used to find the far-field characteristics of the sonar in a bow-mounted ship and will soon be fitted on many other ships.

NPOL has continued to learn about other types of sonar and has gained vast experience in towed array sonars, torpedo defence and decoy systems, dunking sonar operated from helicopters, and underwater communication systems. These systems are in various stages of induction by the Indian Navy. NPOL has today mastered this difficult technology and also enabled India to become one of the very few countries that have exported sonar systems.

S. Kedarnath Shenoy
Director
Naval Physical and Oceanographic Laboratory
Defence Research and Development Organisation
Ministry of Defence
Kochi, Kerala 682021

Journal of Acoustical Society of India : Vol. 43, No. 4, 2016 (pp. 177-185)

Free flooded ring transducers for deep sea applications

M.R. Subash Chandrabose*, Shan Victor Pereira,
N. Praveen Kumar and D. D. Ebenezer
Naval Physical and Oceanographic Laboratory, DRDO, Kochi-682021, India
e-mail: subashbos@gmail.com

[Received: 19-09-2016; Revised: 10-10-2016; Accepted: 17-10-2016]

ABSTRACT

The unlimited depth capability, broadband response as well as the ease of manufacture make free flooded ring transducers preferable for deep sea applications.Watertight integrity of free flooded ring transducers can be achieved by direct over moulding of polyurethane (PU) or assembling the ceramic ring in an oil filled rubber boot. Direct rubber moulding over the ceramic is not preferred due to high temperature and pressure the PZTwill be subjected to during the moulding process. It is reported in literature that for deep sea applications, compared to polyurethane moulding, an oil filled encapsulation provides better coupling with the medium and higher source level. In this study, ATILA, a finite element package for the design of underwater transducers, is used for modelling the two types of transducers, namely, free flooded PU moulded and oil filled transducer in a rubber boot. The transducers modelled are manufactured and tested in an open acoustic tank as well as under pressure upto 50 bar to study the effect of depth on their acoustic performance. The transducers are also subjected to 90 bar to test their pressure withstanding capability. The test characteristics of these transducers like Transmitting Voltage Response, Receiving Sensitivity are reported. Index Terms- Free Flooded Ring Transducer, Encapsulation, ATILA.

1. INTRODUCTION

The unlimited depth capability, broadband response as well as the ease of manufacture make free flooded ring transducers preferable for deep sea applications.These transducers are used in submarine sonars, dunking sonars, acoustic modems, underwater communication devices and underwater acoustic beacons of aircrafts. The transducer can be manufactured from radially polarised ceramic cylinders (RPC), segmented ceramic wedges or ceramic slab and metal wedge combination. RPCs can be used as the active material for frequencies 4 kHz and above[1].

Watertight integrity of free flooded ring transducers is achieved through direct overmoulding of polyurethane (PU) or by assembling the ceramic ring in an oil filled rubber boot. The PZT will be subjected to high temperature and pressure, during the moulding process and this makes the direct rubber moulding over the ceramic undesirable. The chances for failure of the transducer during the rubber moulding process are high and which in turn leads to low yield in manufacture. An oil filled rubber encapsulation provides better coupling with the medium and higher source level required for deep sea applications, compared to polyurethane moulding over the ceramic. Lipper and Borden reported source level reduction of 3 to 8.5 dB for a polyurethane moulded transducer compared to oil filled transducer in the frequency band of 7 to 15 kHz[2]. The bandwidth and efficiency of oil filled, fibre glass wound segmented ring transducer is enhanced by close coupling of the cavity and hoop mode resonances[3,4]. The fill fluids need to meet varied requirements like acoustic, electric, material compatibility, long term stability, toxicity, cost *etc*.[5]. Silicone oil, Isopar L,

transformer oil and castor oil are widely used as fill fluids. However, these fluids provide almost identical acoustic characteristics[6].

2. OBJECTIVE OF THE STUDY

In the current study, performance of free flooded ring transducers made of RPC with direct PU moulding and RPC assembled in a rubber boot filled with silicone oil are compared. The schematic of the transducer assemblies with dimensions are as shown in Figures 1 and 2. These transducers were modelled using the FEM package, ATILA[7]. The transducers modelled were then manufactured and tested. Initial testing was conducted in an open acoustic tank at a depth of 10 m. Subsequently these transducers were also tested in a pressure chamber upto 50 bar.

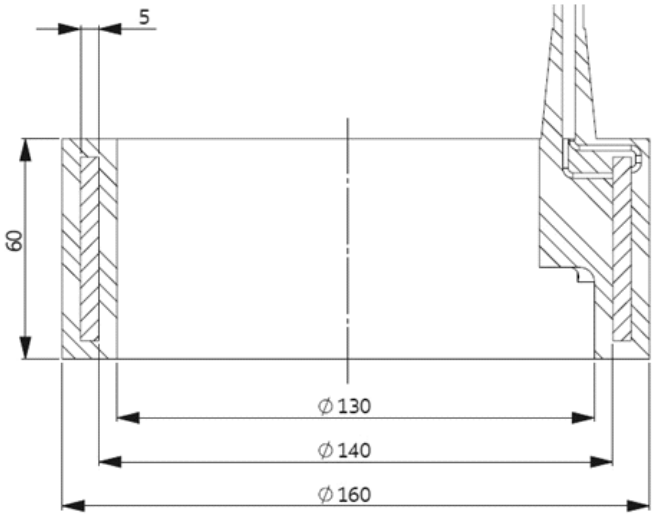

Fig. 1. Schematic of the transducer with PU.

Parameters such as resonance frequency, Transmitting Voltage Response (TVR), Receiving Sensitivity (RS) were measured and compared with the model for both the versions of transducers. The transducers were also subjected to 90 bar for two hours to test the pressure withstanding capability.

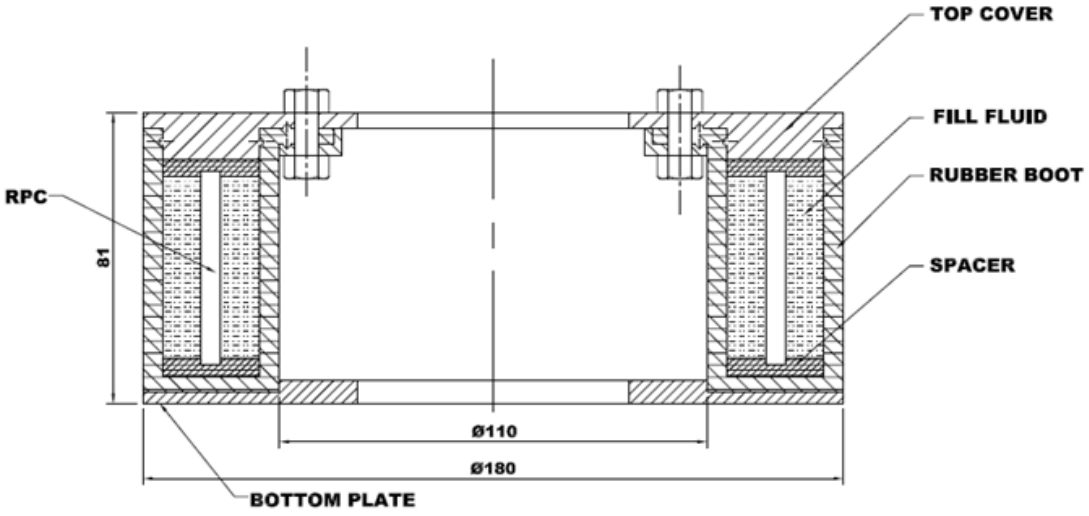

Fig. 2. Schematic of the transducer with oil filled rubber boot.

3. DESCRIPTION OF THE TRANSDUCER AND THE MODEL

A radially polarised piezoceramic ring made of PZT4 material with an outside diameter (OD) of 150 mm, inside diameter (ID) of 140 mm and height of 50 mm is used in the study. In the first case, the transducer has PU moulding over the ceramic ring with an encapsulation thickness of 5 mm all around. In the next case, the transducer is positioned in a rubber casing with locating spacers and the cavity around the ceramic is filled with silicone oil. Since the transducer is axisymmetric with respect to X axis and symmetric with respect to Y axis, only half of the cross section is modelled. Eight noded quadrilateral elements are used to model the piezoelectric, elastic, fill fluid, and water surrounding the transducer. FE mesh of the transducer model used in the study of oil filled transducer is as shown in Fig. 3.

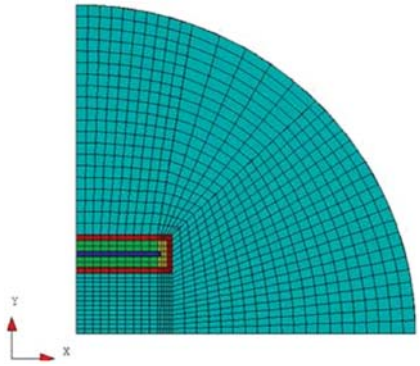

Fig. 3. 2D Axisymmetric model of the oil filled transducer

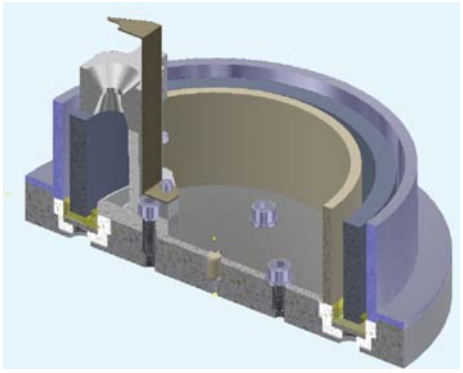

Fig. 4. Cross section of the PU mould.

4. TRANSDUCER MANUFACTURE AND ASSEMBLY

The manufacture of the modelled transducers requires mould for PU and rubber boot moulding. The PU moulding was carried out using a commercially available PU resin, a two-part rigid urethane casting compound. The fully cured PU has a Shore D hardness of 65 and is white in colour[8]. Two stage moulding is required for the PU moulding. In the first stage moulding,a base with groove for the RPC was moulded and then the RPC was positioned in the groove. Then second stage moulding was carried out. Even though the curing time specified is less than an hour, the transducer is generally deployed in water only after 3 to 4 days. The PU mould and the moulded transducer are as shown in Figures 4 and 5.

Fig. 5. PU moulded transducer.

Fig. 6. Transducer with oil filled rubber boot.

The rubber boot is moulded using a specially made rubber composition which can withstand oil and sea water environment for long duration. RPC is positioned inside the moulded rubber boot using a rubber spacer with seating groove. Top of the ring is also located using a similar rubber spacer. A top cover made

of 316L steel material is used to close the transducer. Outer diameter of the boot is clamped to the top cover using a metallic bellyband. Inner diameter of the boot has flange and it is bolted between a metallic plate and top cover. A bottom plate, bolted to the top cover plate, prevent the loading of the rubber boot due to the ceramic and fill fluid weight. There are two holes on the cover plate for oil filling and air release during oil filling. Two core shielded cable is used for electrical connection. Water ingress through the cable outer diameter is prevented using cable glands with metallic and rubber washers. The two threaded holes provided on the top plate aid the mounting of the transducer to the test fixture for measurement in the tank and pressure chamber.The transducer assembled is as shown in Figure 6.

5. EXPERIMENTS CONDUCTED AND THE FACILITIES USED

The transducers manufactured were tested in an open tank of 50 m length, 20 m width and 18 m depth. The test facility has an overhead crane, positioning platforms, and necessary instruments for all acoustic measurements as shown in Fig. 7[9]. The transducer is positioned at a depth of 10 m and parameters like resonance frequency, Transmitting Voltage Response (TVR) and Receiving Sensitivity (RS) are measured. The measurements are then repeated in the pressurised test chamber shown in Fig. 8. The pressure chamber has a length of 8 m and inner diameter of 3 m. The pressure inside the chamber can be fixed as per requirement and the tests are carried out in steps of 10 bar from 10 to 50 bar.

Fig. 7. Open acoustic tank [9].

Fig. 8. Pressurised acoustic test chamber [9].

6. RESULTS AND DISCUSSIONS

The effect of encapsulation is studied for both polyurethane moulded and oil filled transducers. Results of TVR and RS for the model and experiment conducted in an open tank at 10 m depth are shown in Figures 9 to 12. Modelled results shows almost similar trend for TVR for both the transducers except near resonances.

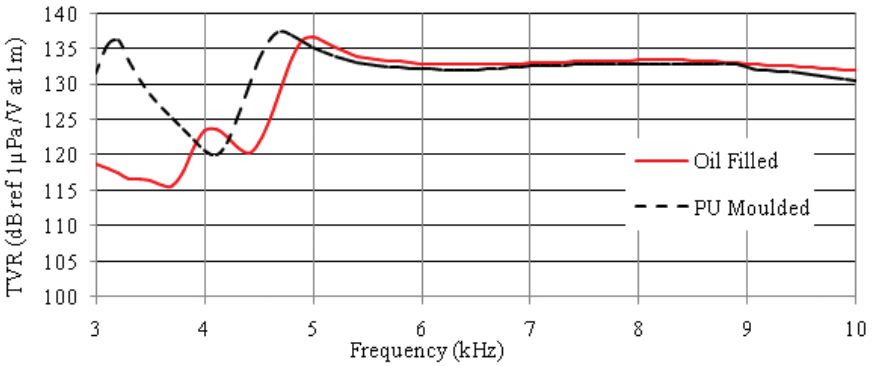

Fig. 9. Model results of TVR.

Measured results from the open tank tests shows that the resonance frequency of oil filled transducer is about 300 Hz lower than the PU moulded transducer. Except near the resonance of oil filled transducer, PU moulded transducer has a higher TVR of 1 to 5 dB in the frequency band of 5 to 10 kHz.

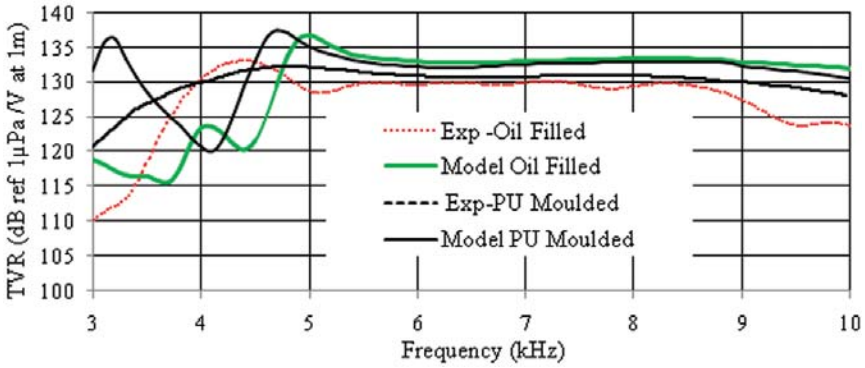

Fig. 10. Model and experimental results of TVR in open tank for PU and oil filled transducers.

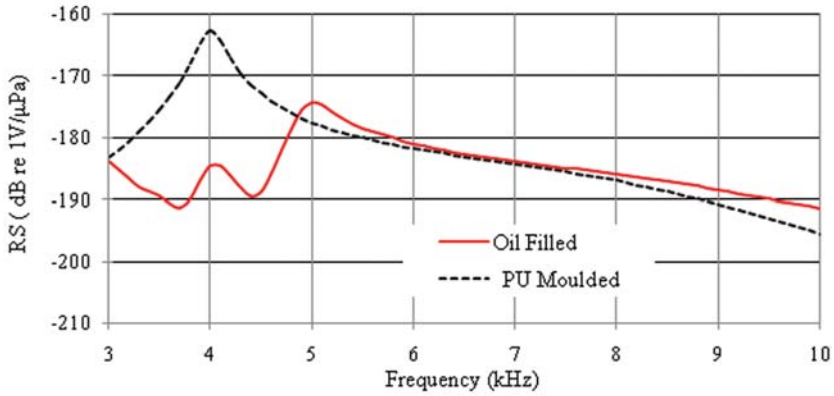

Fig. 11. Model results of Receiving Sensitivity.

Even though the model results show that Receiving Sensitivity of oil filled transducer has slight edge over PU moulded one in the frequency band of 5 to 10 kHz, tank measurements indicate that the Receiving Sensitivity of PU moulded transducer has slightly higher values around resonance and beyond 8 kHz as shown in Figures 11 and 12.

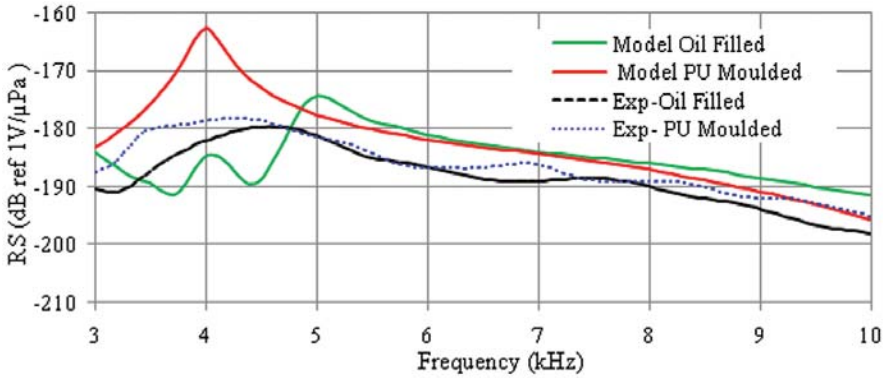

Fig. 12. Model and experimental results of RS in open tank for PU and oil filled transducers.

After the open tank experiments, measurements in the pressurised chamber is carried out upto 50 bar. During pressurisation, PU moulded transducer resonance frequency is reduced to 3828 Hz from 4535 Hz (*i.e.*, 25.5% reduction) when the pressure is increased from 10 to 20 bar but thereafter it remained steady when the pressure is increased from 20 to 50 bar as shown in Fig. 13.

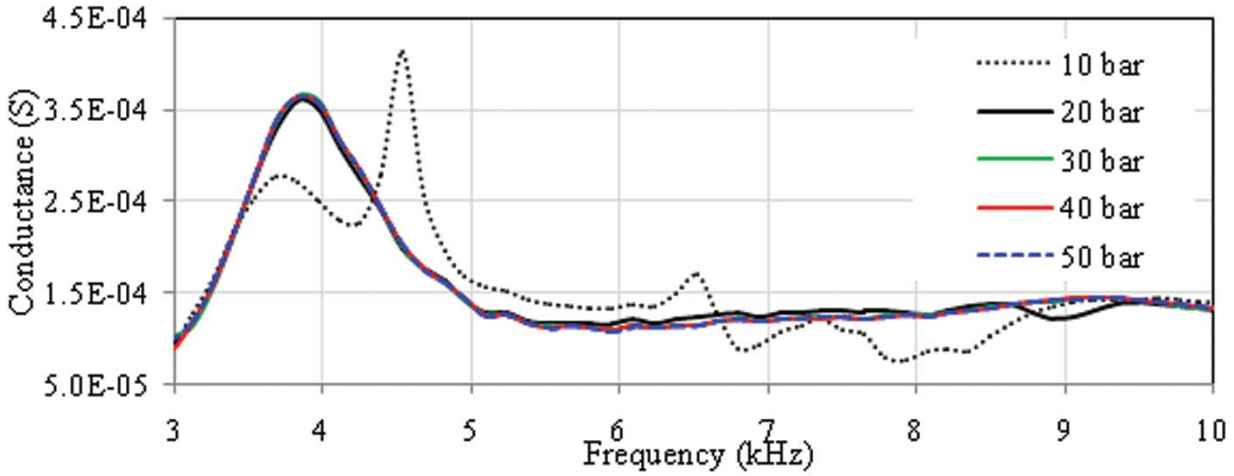

Fig. 13. Effect of pressure on resonance frequency for PU moulded transducer.

Reduction in resonance frequency is observed for oil filled transducer also when the pressure is increased from 10 to 20 bar. The frequency changed to 3909 Hz from 4272 Hz but it is significantly less at about 8.5% (Figure 14). Beyond 20 bar the change in resonance is not significant for oil filled transducer also.

The measured TVR under pressure for the PU moulded and oil filled transducers are shown in Figures 15 and 16. With increase in pressure from 10 to 20 bar there is a 3 dB reduction in TVR in the 3 to 4 kHz band for the PU moulded transducer but above 20 bar pressure the reduction is less than oned B. The TVR of PU moulded transducer is stable over the frequency band of 4 to 9 kHz when the pressure is increased from 20 to 50 bar.

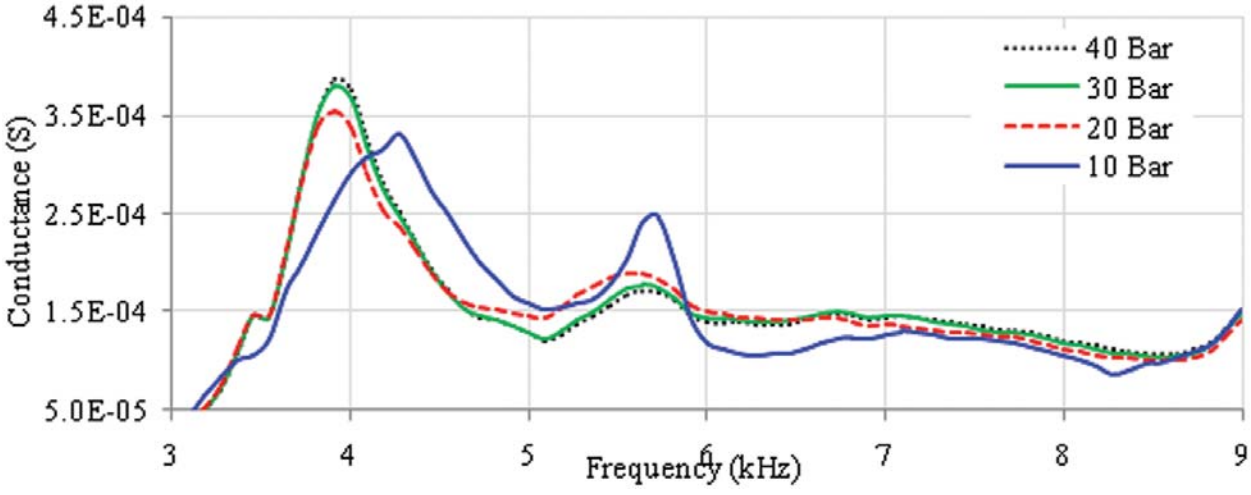

Fig. 14. Effect of pressure on resonance frequency of oil filled transducer.

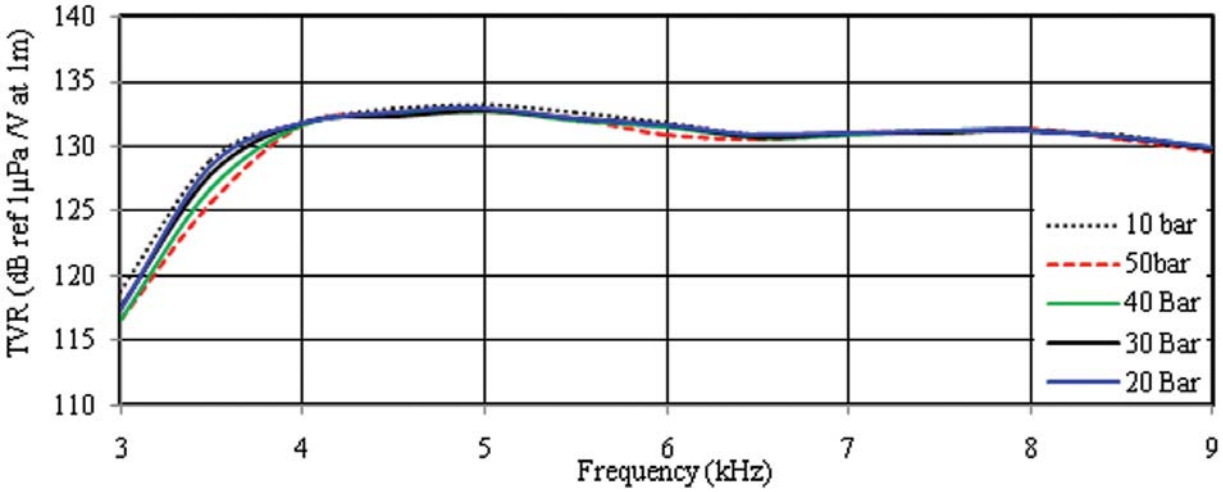

Fig. 15. Measured TVR of PU moulded transducer under 10 to 50 bar pressure.

For oil filled transducer also there is reduction in TVR with increase in pressure for frequencies below 3.5 kHz but above this frequency the TVR increases with pressure. When pressure is increased from 10 to 20 bar, the TVR increase is 1 to 3 dB in the band of 3.5 to 8 kHz. When the pressure is further increased from 20 bar to 40 bar, the change in TVR is not considerable.

Figure 17 shows the comparison of PU moulded and oil filled transducer at 40 bar pressure. The results indicate that the oil filled transducer has upto 3 dB advantage in the band of 3.5 to 8.0 kHz frequency, except around 5 kHz. However, the PU moulded transducer has a flatter response over the frequency band of 3.8 to 9 kHz. In conclusion, the tests indicate that, for deep sea application oil filled transducer has advantage but, if the depth of operation is less than 200 m then PU moulding is a cost effective and simple method of encapsulation.

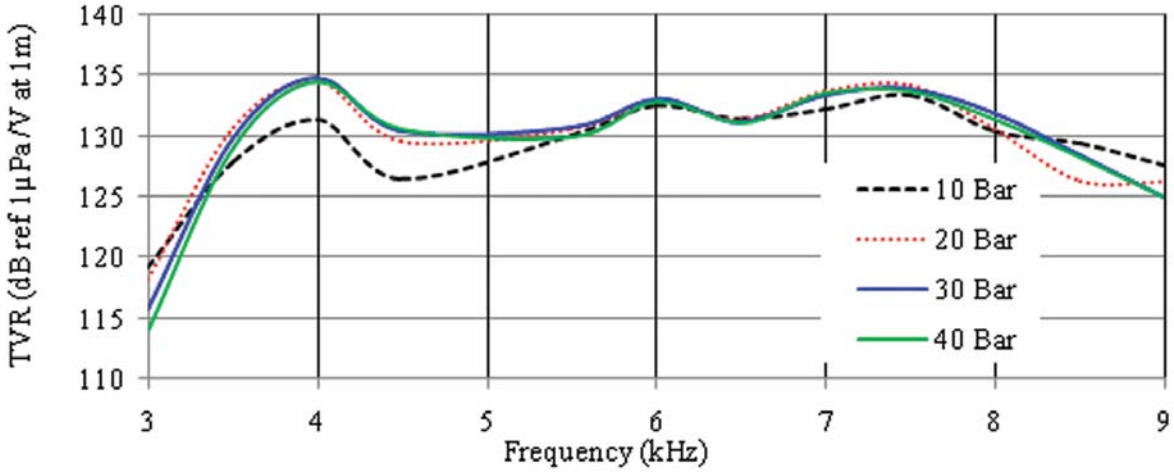

Fig. 16. Measured TVR of oil filled transducer under 10 to 40 bar pressure.

Subsequent to the acoustic measurement under pressure, the transducers are subjected to 90 bar for two hours to test the pressure with standing capability. Continuity, capacitance and insulation resistance of the transducers are checked at an interval of 10 bar till the maximum pressure of 90 bar. There was no significant change in these values for both the transducers which indicate the transducers can be safely operated upto 90 bar.

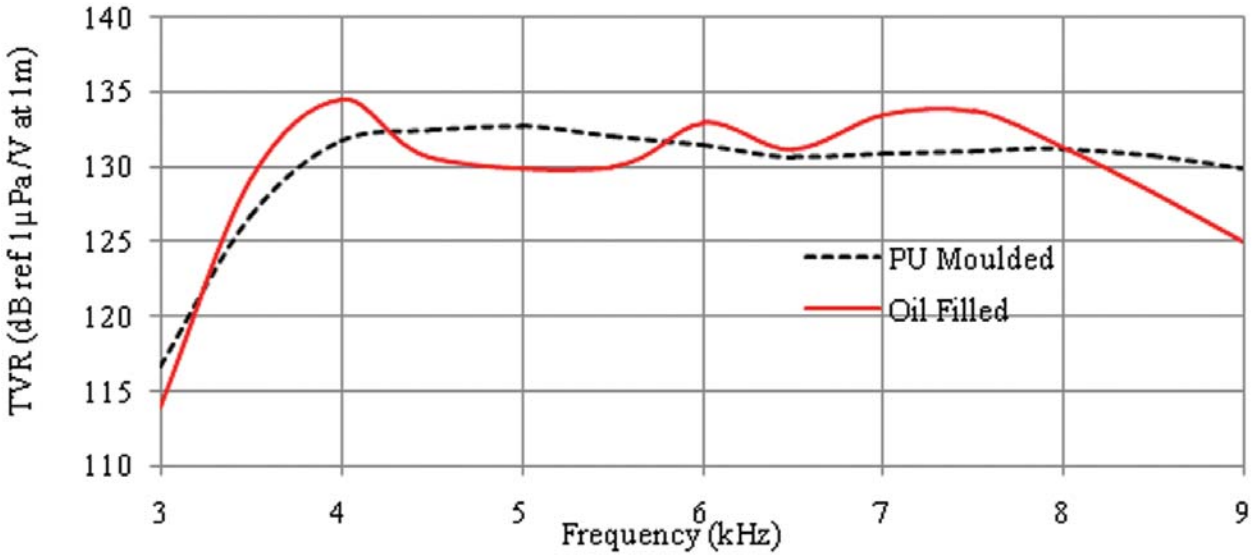

Fig. 17. Measured TVR of transducers at 40 bar pressure.

7. CONCLUSION

Free flooded PU moulded and oil filled transducers are modelled using ATILA and manufactured. Transducers manufactured are tested in an open acoustic tank and under pressure upto 50 bar to study the effect of depth on their acoustic performance. The studies indicate that the resonance frequency of oil filled transducer with rubber boot has lower resonance and at resonance has higher TVR compared to PU moulded transducer. For less than 200 m application, PU potting is better since the TVR values are higher for this transducer except around the resonance. For operational depth of 200 m and above, oil filled transducer has the advantage of about 3 dB higher TVR.

There is reduction in resonance frequency with pressure for both the transducers. For PU moulded transducer the resonance frequency is reduced by 25% and for oil filled transducer it is reduced by 8.5%, when the pressure is increased from 10 to 20 bar. Beyond 20 bar, resonance frequency remained stable for both type of transducers. The transducers are also subjected to 90 bar to test its pressure withstanding capability.

8. ACKNOWLEDGMENTS

Permission from Director, NPOL to publish the paper and support for manufacture and assembly of transducers from Mr. T.K. Vinod and Mr. E.R. Ratheesh are gratefully acknowledged.

9. REFERENCES

[1] W. J. HUGHES, 1998. Transducers, Underwater Acoustic, *Encyclopaedia of Applied Physic*s, **22**, 67- 84.

[2] A. LIPPER and J. BORDEN, 2012. Urethane Transducer Encapsulation versus Oil Filled Boot Encapsulation of Piezoelectric Transducers, *IEEE Oceans*, pp 1-4.

[3] N. RENNA, 1972. Underwater acoustic projector. US Patent 3706967.

[4] M.R. SUBASH CHANDRABOSE and D. D. EBENEZER, 2014. Free flooded segmented ring transducers for deep sea applications, *J.Acoust. Soc. Ind*. **41**(3), 119-124.

[5] T. H MEHNERT, 1972. Handbook of fluid filled depth pressure compensated systems for deep ocean applications. Naval Ship Research and development Centre, Annapolis Laboratory, Maryland, USA.

[6] M.R. SUBASH CHANDRA BOSE and D. D. EBENEZER, 2012. Design curves for free-flooded deep-submergence ring transducers in annular fill-fluids, *Proceedings of the National Symposium on Acoustics, NSA* pp.234-240.

[7] ATILA user's manual, 1997. Version 5.1.1, Institute Superieur d 'Eletronique du Nord, Acoustic Laboratory, LILLE CEDEX, France.

[8] http://aldax.com.au/msds_tds/tds/Easycast.pdf

[9] http://drdo.gov.in/drdo/labs/NPOL/English/index.jsp?pg=facility.jsp

Journal of Acoustical Society of India : Vol. 43, No. 4, 2016 (pp. 186-193)

Distributed feed-back fiber laser hydrophone with metallic packaging suitable for thin-linetowed array sonar applications: preliminary results

Vivek K, R Rajesh*, C.V. Sreehari, S. Sham Kumar, T.V. Praveen, Shan Victor Pereira, T. Santhanakrishnan, R.L. Awasthi and K.P.B. Moosad
Naval Physical and Oceanographic Laboratory (NPOL), Thrikkakara, Kochi
e-mail: rajeshr@npol.drdo.in

[Received: 28-09-2016; Revised: 11-10-2016; Accepted: 17-10-2016]

ABSTRACT

Attractive features such as compact size and absence of electrical components or cablings at wet-end make Distributed Feed-Back Fiber Laser (DFB-FL) hydrophones suitable sensors for Thin Line Towed Array (TLTA) sonar systems. Coupling multiple fiber laser hydrophones of different emission wavelengths in a single lead fiber along with a single pump laser source allows efficient multiplexing, still maintaining the simplicity in array engineering. In this paper, we present the preliminary results obtained from an eight-element DFB-FL hydrophone array along with Dense Wavelength Division Multiplexing (DWDM), realized under laboratory conditions. Sensitivities of the hydrophones are found to be better than -150 dB ref. 1V / µPa in the frequency band 1 to 9 kHz.

1. INTRODUCTION

Underwater acoustic sensing using fiber optic hydrophones is an important area of research due to their advantages over conventional hydrophones[1,2]. The latest trend is to use Fiber Bragg Grating Laser (FBGL) hydrophones, either in a Distributed Bragg Reflector (DBR) configuration or in a Distributed Feed-Back (DFB) configuration[3,4]. Used along with highly sensitive optical interferometers, these systems result in miniature hydrophone arrays with sufficiently high sensitivities required for critical applications. Such compact arrays with their hydrophones being electrically passive, are expected to have wide applications in advanced surveillance sonar systems like sea-bed arrays, thin towed arrays and submarine flank arrays[5]. In recent years, considerable efforts have been devoted to the development of fiber optic hydrophones based on Distributed Feed-Back Fiber Lasers (DFB-FL).

For deep-sea applications, the sensitivity of hydrophones needs to be sufficiently high so as to detect the background acoustic noise of quiet ocean, *i.e.*, Deep Sea State Zero (DSS0), which is ~ 45 dB ref 1µPa at 1 kHz. The DFB-FL sensor is a promising option for underwater acoustic sensing due to its capability to sense very small strains in the sub-pico strain range[6]. When these lasers experience a longitudinal strain (ε_z), the pitch of the gratings varies and alters their emission wavelength which can be detected using suitable interferometric methods. Generally, a bare fiber laser cannot meet the stringent requirements of an underwater sensor array, due to their long, thin geometry, high axial stiffness and residual strain noises. Suitable packaging for the fiber lasers is necessary to enhance their acoustic sensitivity and also to avoid

residual strains due to molecular motion of water on thin fibers with very low mass. Different packaging schemes, each with its own advantage, have been attempted for DFB-FL hydrophones[7, 8].

In sonar technology, hydrophone arrays are designed to meet requirements such as array gain, directivity, distributed sensing and acoustic band selection. In the case of towed array sonar, hydrophones are assembled in a linear fashion inside a flexible hose of acoustically transparent material and towed behind the platforms using re-inforced tow cables[9-11]. Towed arrays facilitate large reduction of own-platform noise and hence improve the detection capability. Its long and linear geometry allows operation in low frequency bands and hence is highly useful in advanced sonar systems. However, towed array sonar technology, in general, is quite complex due to the requirement of sophisticated, and large-sized Winch and Handling System (WHS) for its deployment. The size (diameter) of the hydrophones dictates the size of the hose to be used, and in turn, the complexity of the WHS. This happens in the case of conventional arrays using large, PZT-based hydrophones, which are packed inside the hose along with the electronic circuitry for signal amplification and transmission to the sonar room. Introduction of compact fiber optic hydrophones makes the system much simpler and easier to handle. Thin towed array sonar, making use of fiber optic hydrophones, fitted onto platforms like submarines and AUVs has been reported in literature, nearly a decade ago[9]. The advantage of fiber laser hydrophone is that it is possible to pump multiple laser hydrophones of different wavelengths in series using a single pump source, in effect achieving a self-multiplexing Dense Wavelength Division Multiplexing (DWDM) sensor array. However, for realization of fiber laser hydrophone array, multiple DFB-FLs are to be coupled, preferably in a single lead fiber with a common pump laser source, which makes the task a little more complex.

In this paper, we present the preliminary results obtained from an eight-element array realized at NPOL, in a single lead fiber pumped with a 500 mW pump source. An eight channel DWDM with 400 GHz separation and a high sensitive low noise Mach-Zehnder interferometer with 50 m optical path difference were also used. Simultaneous phase demodulation was carried out from all eight channels using an optical phase demodulator. Sensitivity of the hydrophones was found to be -155 ± 5 dB ref. 1V / µPa for the frequency band 1000 - 9000Hz, the noise floor of all the sensors was found to be within ± 5 dB.

2. HYDROPHONE DESIGN

The bender-bar geometry adopted for the packaging of DFB-FL hydrophone and the fabricated structure are shown in Fig. 1 (a) and (b), respectively. The bender-bar mechanical packaging is developed in a pair of metal plates each having 1 mm thickness, 80 mm length and 8 mm width. A beam of 15 mm length and 1mm width was introduced on the upper metal plate with two hinge configurations at its ends having 0.5 mm depth and width. A recess was made on the bottom plate which enables the free movement of the beam and forms an air-backed cavity. A commercial DFB-FL with 55 mm length was used for realization of the hydrophone. The laser has an output power of about 50 µW for a pump power of 100 mW at 980 nm, and a line-width of ~100 kHz. Relative Intensity Noise (RIN) was less than -130 dB / Hz, in the frequency range 1 - 20 kHz.

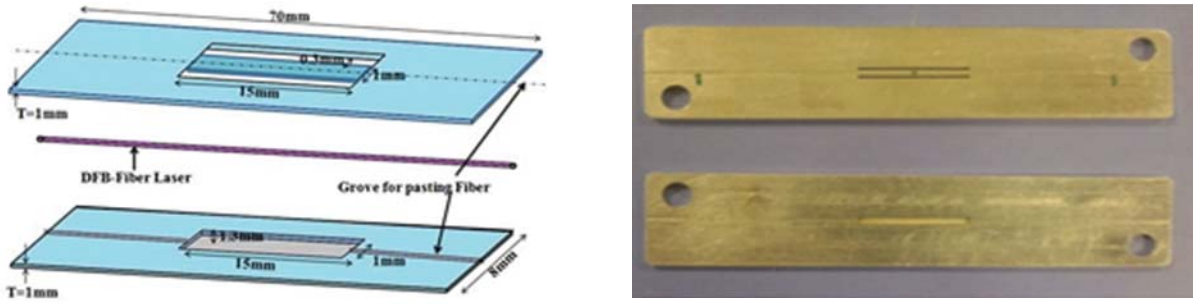

(a) (b)

Fig. 1. (a) Geometry of the bender-bar structure and (b) fabricated metal bender-bar structures.

In case of bare Fiber Bragg Grating or DFB -FL without any mechanical packaging, the shift in wavelength resulting from the axial strain developed by the external forces acting on them is governed by the relation[4].

$$\Delta\lambda_L = \lambda_L \xi_z \left[1 + \frac{n_{eff}^2}{2}\left[\nu(p_{11} + p_{12}) - p_{12}\right]\right] \quad (1)$$

where ξ_z is the axial strain, p_{11} and p_{12} are the photo-acoustic coefficients of the fiber material, ν and n_{eff} are the Poisson's ratio of the fiber material and effective refractive index of the grating. For a single mode fiber and a plane acoustic wave at normal incidence, the strain ξ_z can be related to the change in pressure ΔP through the relation

$$\Delta\lambda_L = \lambda_L \xi_z \left[1 + \frac{n_{eff}^2}{2}\left[\nu(p_{11} + p_{12}) - p_{12}\right]\right] \quad (2)$$

where E_{fib} is Young's Modulus of the fiber material and L is the grating length. Substituting equation (2) into (1) gives the shift in wavelength in terms of pressure as

$$\Delta\lambda_L = \lambda_L \frac{(1-2\nu)}{E_{fib}}\left[1 + \frac{n^2}{2}\left[\nu(p_{11} + p_{12}) - p_{12}\right]\right]\Delta P \quad (3)$$

From Eq. (3), for an FBGL with n_{eff} = 1.465, λL = 1550 nm, ν = 0.17, p_{11} = 0.121, p_{12} = 0.27, E_{fib} = 70 GPa, the pressure sensitivity of bare FBG is ~4pm / MPa. This sensitivity value is extremely small for the detection of DSS0 level (~ 100 µPa at 1 kHz) even with an efficient inter ferometric method. Therefore, suitable packaging which enhances the sensitivity to sufficient level is essential.

For the above bender-bar structure, the beam (along with the fiber laser) bends due to the acoustic pressure acting on it and the resulting strain ε, is expressed as[8]

$$\varepsilon = t \,/\, 2R(p) \quad (4)$$

(a)

(b)

(c)

Fig. 2. (a) Bender-bar hydrophone, (b) Delrin® mounting fixture and (c) Hydrophone, assembled with the mounting fixture

where, t and R are thickness and bend radius of the beam respectively. Correspondingly, the frequency shift due to the strain on the laser is given by,

$$\Delta f = f(1-\varrho_z)t \,/\, 2R(p) \tag{5}$$

where f is the frequency of the laser emission and e_z is the strain optic coefficient of the fiber. In the work by Foster *et al.*[8], silica wafer was used as the material and the two plates were ionic-bonded with each other after mounting the laser on the grooved portion along the length of the bender-bar. The ionic bonding ensures proper sealing between the plates and an excellent coupling of the fiber with the bender-bar. In our work, we used the bender-bar structures made using metals, Aluminium and Steel. A cylindrical mounting fixture was also used to mount the hydrophone inside the flexible hose. The fixture was in made of Delrin®. The bender-bar is isolated from the fixture using neoprene washers. The assembled bender-bar hydrophone, the Delrin® mount and the assembled unit are shown in Fig. 2(a), (b) and (c), respectively.

Provision was also made in the mounting fixture for passing a 1mm-thick Kevlar® thread for providing additional mechanical strength for the array. Further, the two O-rings around the structure firmly held the mounting structure and also isolated the vibration and shocks from the hose to the sensors.

3 ARRAY INTEGRATION

For the realization of DFB-FL hydrophone array, eight different DFB-FL hydrophones with packaging as described in the previous section are used. The emission wavelengths of the hydrophones are chosen based on ITU standard with 400 GHz separation and spliced in a single lead fiber with 60 cm spacing between hydrophones. The bender-bar hydrophone assembly is fitted inside a flexible Polyurethane (PU) tube of 32 mm outer diameter and 26 mm inner diameter. The array multiplexing scheme adopted is shown in Fig. 3.

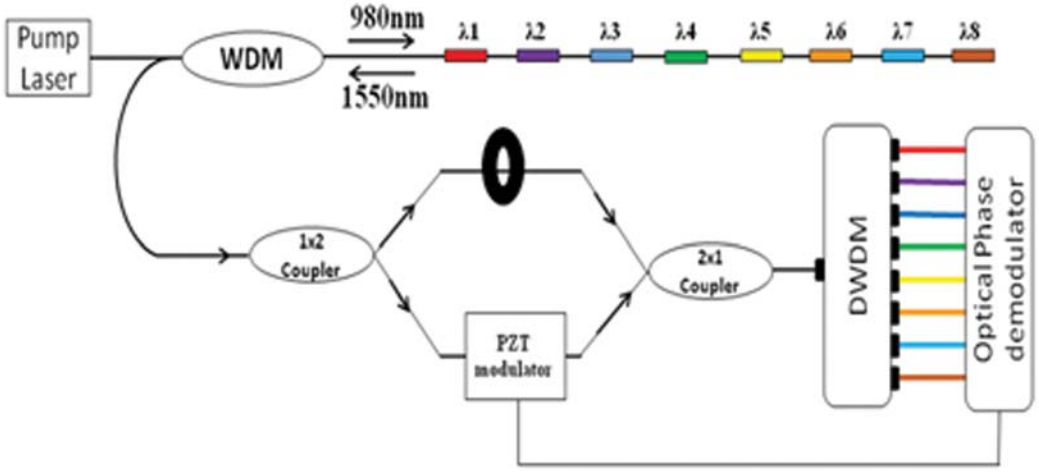

Fig. 3. The scheme for eight element array with DWDM concept

The array assembled inside a tube is shown in Fig. 4. As the lasers are of different wavelengths and also for reasons like splicing, repeatability in writing identical gratings and other unknowns, the efficiency of individual lasers are found to be not identical. Therefore, optimization is carried out in deciding their positions in the array so that almost identical and sufficient power for shot noise limited operation (preferably within 3 dB variation) can be obtained. Optimization is carried out by online monitoring of both emission and unused pump power during the splicing of the array.

All the fiber laser sensors were pumped by a common 980 nm, 500 mW pump source. A WDM coupler was used to separate the laser emissions along the pump side through the same lead fiber. An inline optical isolator suppresses the back-reflected pump laser and reduces the phase noise. A Mach-Zehnder

Fig. 4. Eight element array in 32 mm PU tube, sensor positions circled and enlarged

interferometer with 50m optical path difference and a PZT stretcher in its one arm for carrier phase modulation were employed for interrogation. The interferometer assembly was placed inside an anechoic chamber with vibration isolated chamber for avoiding ambient noise effects. The DWDM device separates out the channels by wavelength and are simultaneously demodulated using an optical phase demodulator (M/s Optiphase Model:OPD-4000)

4 PRELIMINARY RESULTS AND DISCUSSION

The acoustic sensitivities of the prototype bender-bar hydrophones are measured in a water tank in the frequency range of 1 to 9 kHz. Typical sensitivity responses for bender-bar hydrophones in two different metals *viz.* Aluminium and Steel are given in Fig. 5(a) and (b) respectively. In case of aluminium, the sensitivity varies from a maximum of -113 dB ref. V/µPa at 1.5 kHz to a minimum of -158 dB ref. V/µPa at

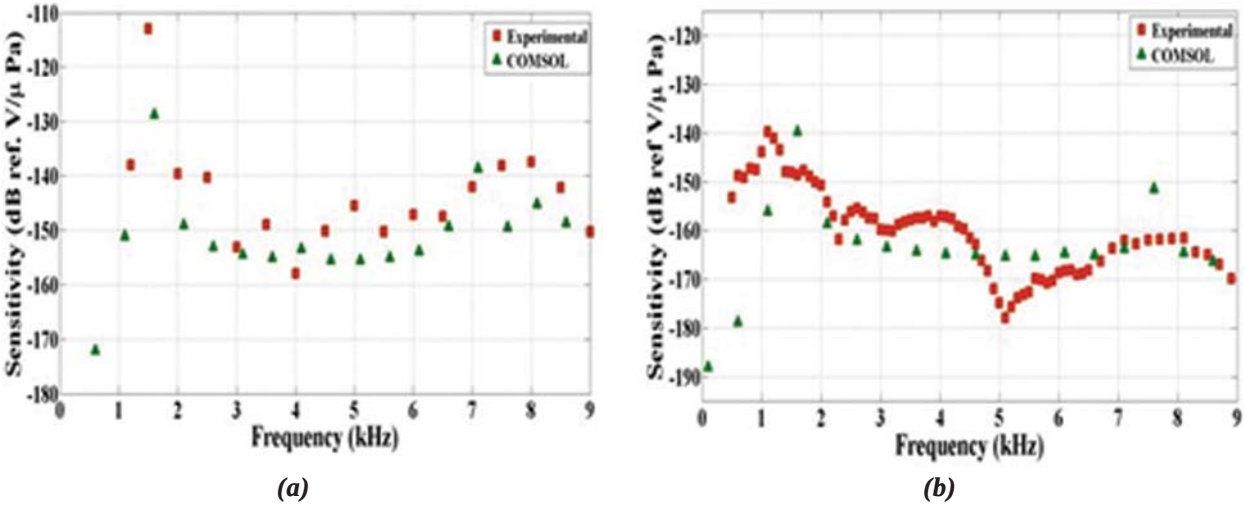

Fig. 5. (a) Frequency response of bender-bar hydrophone (a) in aluminium and (b) in steel

4 kHz in the measured range of 1 to 9 kHz. At the same time, for steel, the maximum sensitivity observed is -139 dB ref. V / µPa at 1.1 kHz and minimum is about -178 dB ref. V / µPa at 5.1 kHz. The results of Finite Element simulation obtained for the two cases using the FEM package COMSOL Multi-physics are also included in the same response plots. It is observed that the experimental and FEM results are matching fairly well. The reason for small deviations in experimental results may be due to the fact that DFB-FL was bonded on the bender-bar using polyimide adhesive tape while it was not considered in simulation. Both experimental and simulated results show a resonance peak at 1.6 kHz in frequency response of Aluminium bender-bar. The steel bender-bar also shows a resonance peak below 2 kHz in both experimental and simulated results. In order to analyze this, the free vibration modes of the hydrophones structure were carried out using COMSOL Multi-physics. The observed vibration modes are at the following frequencies: 1.6 kHz, 4.4 kHz, 6.3 kHz, 7.9 kHz, 8.7 kHz and 15.7 kHz, respectively in air. Generally, the bandwidth of the hydrophone is determined by the fundamental resonance frequency of the beam, was found to be at 15.7 kHz for the beam[12]. All other modes arise because of the plate vibration modes. For achieving flat frequency response, it is necessary to arrest the plate vibrations. Since the bender bar portion is linked with the plate, and the portion of the sensing laser grating is pasted also along plate, it will be difficult to completely remove the effects of plate vibrations. However, the plate effects and resonances can be reduced either by increasing the depth of the hinges and making bar vibrations as prominent one compared to that of plates or completely clamping the plate by attaching it with a proper rigid mass. Efforts are currently in progress towards this.

The position of each element in the array was optimized through various iterations by splicing them at different positions in the linear array while monitoring the output power online. The observed laser emissions from all the eight elements in the array with an Optical Spectrum Analyzer (OSA) (JDSU Model : OSA 500 M) under optimized condition is shown in Fig. 6. Under this condition, the powers from all the lasers were sufficient while pumping at about 430 mW and the power variation was found to be within ±3dB.

The underwater acoustic sensitivity of the individual hydrophones was measured by deploying the array at a depth of 10 m in a large water tank. The DFB-FL hydrophone array was insonified by a broadband projector (developed in-house) and a standard hydrophone (B&K Model No. 8305) was lowered at the same depth for the calibration of the sensor. Simultaneous demodulation was achieved with the eight

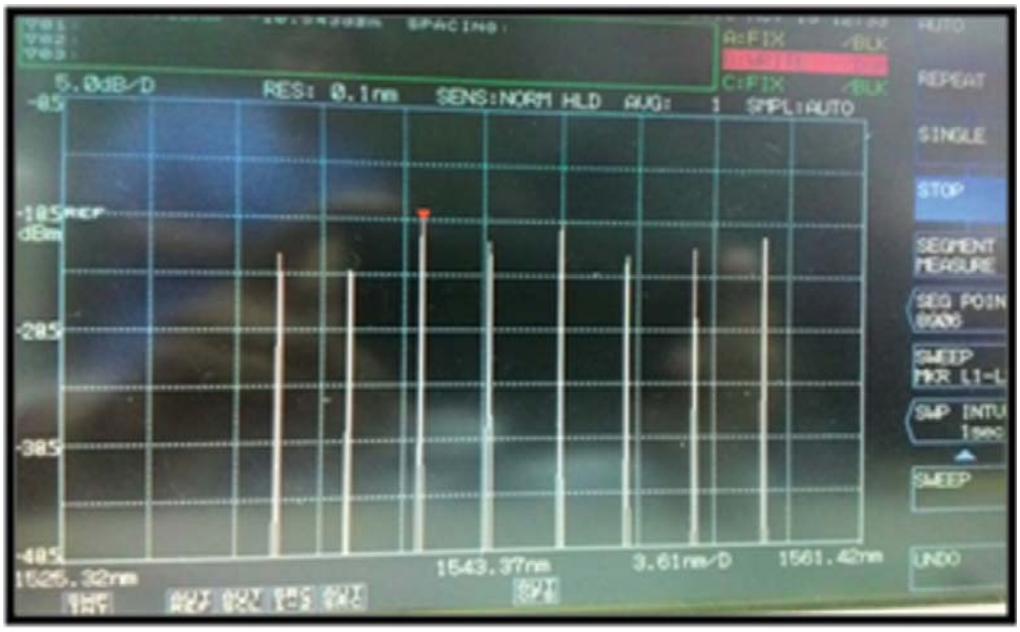

Fig. 6. The laser emissions from array as observed in OSA

channel optical phase demodulator. The observed noise spectrum is shown in Fig. 7. It was found that the noise is within 80-90 dBV / $\sqrt{Hz}$ for the frequency band 1-10 kHz, while using the interferometer with 50 m optical path difference.

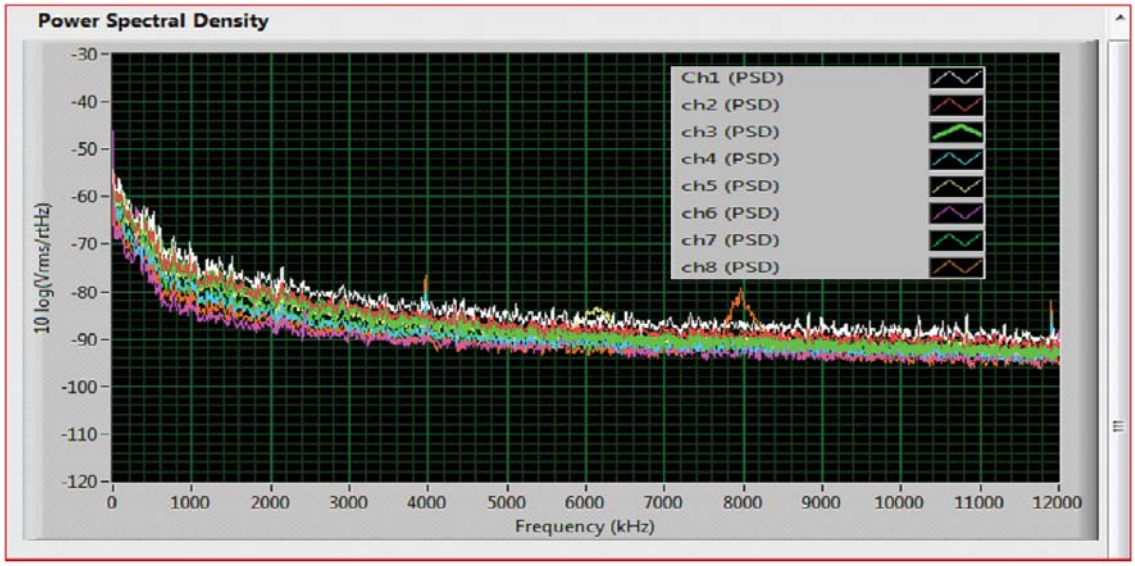

Fig. 7. Observed noise floor in each channel of the array

The time signal and the frequency spectrum of the array during the insonified condition at 5000Hz is shown in Fig. 8. The difference in peak level between sensors corresponds with their separation from the projector.

Fig. 8. Observed time signal from the array when insonified at 5000Hz

5. SUMMARY

An eight element hydrophone array with DFB-FL hydrophones was developed and preliminary tests were carried out in water. Using Mach-Zehnder interferometer with 50 m optical path difference, the noise floor observed was close to the Frequency Noise of the laser source. In case of Aluminum bender-bar hydrophones, the sensitivity was better than -150dB ref. 1V/µPa for the frequency band 1000-9000 Hz. In case of Steel bender-bar, sensitivity was better than -160 dB ref. 1V/µPa for frequencies up to ~4000 Hz. However, flat response was not achieved in both cases due to the plate vibrations. Efforts are in progress for obtaining flat response with this bender-bar packaging. Ruggedization for towing and smoothening of the sensor response along with noise measurements are being undertaken currently, to realize a field-deployable array.

6. ACKNOWLEDGEMENT

The authors acknowledge Director, NPOL and various other technical groups for the support received for accomplishing the work reported in this paper.

7. REFERENCES

[1] C.K. KIRKENDALL and A. DANDRIDGE, "Overview of high performance fibre-optic sensing", *J. Phys. D: Appl. Phys.* **37**, (2004) 197-216.

[2] G. WILD and S. HINCKLEY, "Acousto-Ultrasonic Optical Fiber Sensors: Overview and State-of-the-Art", *IEEE Sensors Journal*, **8**, (2008) 1184-1193.

[3] D.J. HILL, P.J. NASH, D.A. JACKSON, D.J. WEBB, S.F. O'NEILL, I. BENNION and L. ZHANG "A fiber laser hydrophone array", *Proc. SPIE* **3860**, (1999) 55-66.

[4] NICOLO BEVRINI, RICCARDO FALCIAI, ENRICO MACCIONI, MAURO MORGANTI, F. SORRENTIO and C. TRONO, "Developing fiber lasers with Bragg reflectors as deep sea hydrophones", *Annals of Geophysic*, **49**(6), (2006) 1157-1165.

[5] STEVEN GOODMAN, SCOTT FOSTER, JOHN VAN VELZEN and HEYSHAN MENDIS, "Field demonstration of a DFB fiber laser hydrophone seabed array in Jervis Bay Australia", *Proc. SPIE* 7503, 75034L (2009).

[6] K.P. KOO and A.D. KERSEY, "Bragg Grating based Laser Sensors Systems with interferometric Interrogation and Wavelength Division Multiplexing", *Journal of Light wave Technology*, **13**(7), (1995) 1243-1249.

[7] D.J. HILL, "A fiber laser hydrophone array", *SPIE, Conference on Fiber Optic Sensor Technology Applications*, **3860**, (1999) 55-66.

[8] S. FOSTER, A. TIKHOMIROV and J. VAN VELZEN, "Towards a high performance fiber laser hydrophone", *Journal of Lightwave Technology*, **29**, (2011) 1335-1342.

[9] C. KIRKENDALL, T. BAROCK, A. TVETEN, and A. DANDRIDGE, "Fiber Optic Towed Arrays", *NRL Review on Acoustics*, (2007) 121-123.

[10] FABIO SOUTO, "Fibre Optic Towed Array: The High Tech Compact Solution for Naval Warfare", *Proceedings of Acoustics - Victor Harbor*, (2013) 1-5.

[11] SCOTT FOSTER, ALEXEI TIKHOMIROV, MARK ENGLUND, HUGH INGLIS, GORAN EDVELL and MARK MILNES, "A 16 Channel Fibre Laser Sensor Array", *ACOFT/AOS2006 - Proceedings Melbourne, Australia*, (2006) 40-42.

[12] K. VIVEK, C.V. SREEHARI, SHAM KUMAR, PRAVEEN T V, KATHIRESAN M, R RAJESH and K. P. B. MOOSAD "Hydrophone using distributed feedback fiber laser in Bender bar configuration", CT 029, Proceedings of Sensors 2016 Conference at Hyderabad, India.

Journal of Acoustical Society of India : Vol. 43, No. 4, 2016 (pp. 194-199)

Design and development of low frequency barrel stave transducers for towed arrays

P. A. Nishamol*, Rijo Mathews Abraham, V. Vinothkrishnan and T.K. Vinod
Naval Physical and Oceanographic Laboratory, Thrikkakara, Kochi 682021, India
e-mail: p.a.nishamol@gmail.com

[Received: 21-09-2016; Revised: 10-10-2016; Accepted: 17-10-2016]

ABSTRACT

Acoustic design and development of a low frequency Barrel Stave Transducer for towed horizontal projector array is described. Finite element software package ATILA[1] is used to acoustically design the transducer. Important in-water performance parameters, such as resonance frequency at which the Transmitting Voltage Response (TVR) is maximum and the corresponding TVR value are presented. Effect of transducer structural variables, such as shell thickness, shell curvature and shell material, on these parameters is investigated. Several modeling studies have been carried out to optimize the shell material, dimensions, curvature of the shell. A few prototype transducers are developed, acoustically evaluated and results are compared.

1. INTRODUCTION

Barrel Stave Transducer (BST) is a Class I Flextensional Transducer (FT) that consists of a stack of axially polarized piezoelectric rings and a surrounding mechanical concave shell. The components of this transducer are shown in Fig. 1. The mechanical shell has slots along the axial z-direction forming staves in order to reduce the axial stiffness and thus decrease the resonance frequency of the transducer. Between adjacent staves, there are gaps that permit the staves to vibrate freely in flexure. The transducer has end plates on both ends and a stress rod. The stress rod passing through the centre of the transducer holds the end plates in place. Adjacent rings in the piezoceramic stack are polarized in opposite direction. Under an electric drive, at the first resonance frequency of the Transmitting Voltage Response (TVR) of the transducer, the piezoelectric stack vibrates in its thickness mode along the longitudinal axis of the transducer. With this piston motion of the driver, the endplates displace axially causing the staves to flex in the radial direction. Because the staves are curved, the relatively small driver displacements are transformed into larger stave displacements. The transducer has a rubber boot to isolate it from the external acoustic fluid. The advantages offered by this type of flextensional transducer include low resonance frequency, high power density, low weight, and low cost due to simplicity in its design and assembly. Comparatively small size and barrel shape of these transducers permit them to be kept inside a tube that in turn can be used as a Horizontal Projector Array (HPA) for towed arrays. Though for a horizontal receiver array,the optimal corresponding transmitter array geometry is a linear Vertical Projector Array (VPA), the deployment and recovery of the tow-body used to house the VPA requires a significant handling system. A practical alternative is a reelable horizontal projector array that can be stored, deployed, towed, and recovered in-line with the receiver array so that handling and ship-fit issues can be minimized.

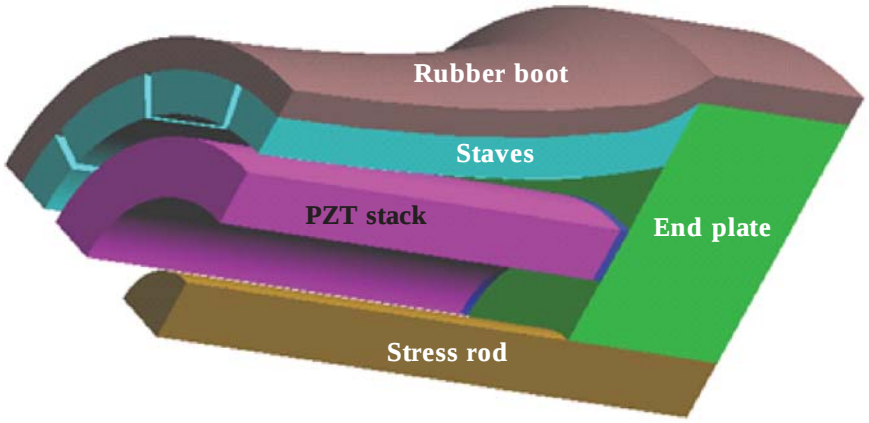

Fig. 1. 1/8th model of the Barrel stave transducer.

In this paper, the design and development of a low frequency, less than 3kHz, barrel-stave transducer is described. Transducer is designed using the finite element tool ATILA to reduce prototype fabrication times. Three dimensional finite element models of the transducers are developed in ATILA. The effect of structural and material parameters on the acoustic performance of the transducer is analyzed. The transducer dimensions are finalized so as to use it in an available towed array tube. The design is optimized with maximum TVR within the dimensional constraints. The analysis of Barrel stave transducers using finite element tools is reported in literature[2].

2. DESIGN AND ANALYSIS

A preliminary design is first made and analyzed using the FE package ATILA. The outer diameter and length of the transducer are fixed based on the diameter of the available towed array tube and the diameter of the winch on which the tube is to be wound. A stack of PZT 4 rings is used in the design. In the initial analysis, the shell is assumed to be without slots and hence the geometry was axisymmetric. Only $1/8^{th}$ of the transducer is to be modelled because of symmetry. The first longitudinal mode resonance frequency is computed. The axial slots are then introduced and it reduces the shell hoop stiffness and thus lowers the flexural resonance frequency of the shell. The radius of the external water medium is equal to λ of the minimum frequency analyzed so that the fluid medium is infinite. By arresting the normal displacements along the axial and radial planes, symmetry in both longitudinal and circumferential directions is established and the original 3D geometry thus reduces to $1/8^{th}$ cross- section as shown in Fig. 1. Polarization is defined in opposite direction on adjacent piezoceramic rings. FRP material is used to isolate the piezoceramic stack from the metallic ends. Nitrile rubber boot is used to isolate the shell from the external fluid. All volumes are meshed with structured hexahedral elements. The piezoelectric stack is electrically driven and the

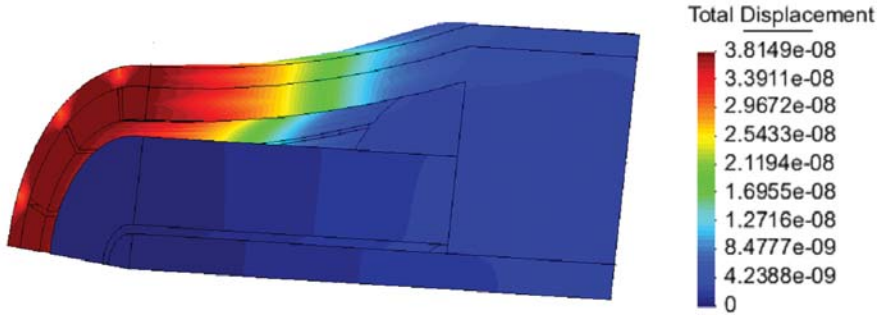

Fig. 2. Magnitude of the displacement in metre at the flexural mode resonance of BST

transducer radiates into the infinite external fluid space. Harmonic analysis is performed. The pressure field, displacement field, electric potential, electrical impedance, and electrical admittance are computed. After several parametric studies, an optimal design with circular profile has been arrived at for use in the present towed array systems available. The displacement pattern at the flexural resonance frequency of the optimized design is shown in Fig. 2. The displacement is maximum at the axial centre of the staves and is minimum towards the ends.

Effect of various structural parameters on resonance frequency and TVR of the transducer is reported in literature[3-4]. To study these effects, analyses are conducted with different shell and endplate materials and varying endplate and shell thickness. The analysis with different shell materialis carried out using Titanium, Aluminium, Aluminium-Bronze and Steel as the shell material. Computed TVR is plotted in Fig. 3. Here, the TVR and resonance frequency are normalized w.r.t. the TVR and resonance frequency of the Steel shell. It can be seen from Fig. 3 that the resonance frequency increases as the specific modulus of the material increases. Specific modulus is minimum for Brass and maximum for Steel. The lowest resonance frequency occurs for Brass, shown with a solid line, and the highest for Steel, shown in solid line with squares. Resonance frequencies of other materials lie in between these two in the above said order. Stiffness to weight ratio is minimum for Brass and thus increases the effective stave compliance and reduces the flexural resonance frequency to the lower side. Thickness of the shell is also varied to anlyze its effect on the resonance frequency. The resonance frequency increases as the shell wall thickness increases.

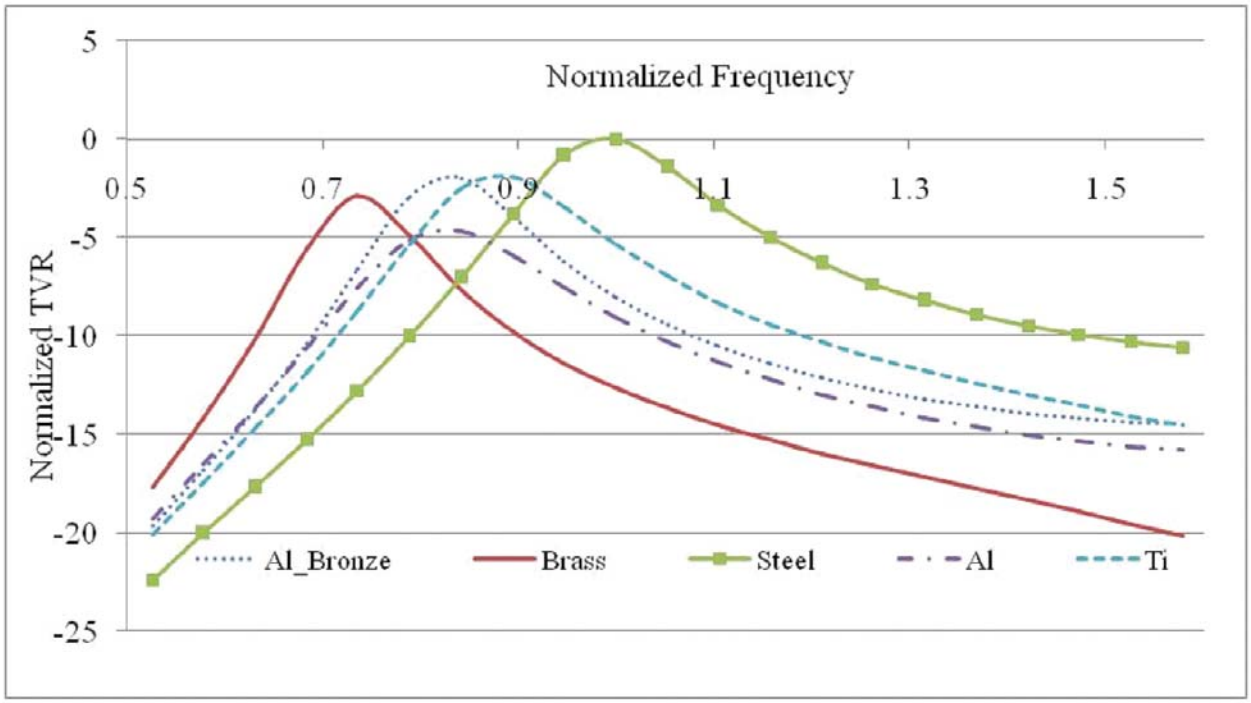

Fig. 3. Change in the normalized resonance frequency w.r.t. shell and endplate material

Effect of endplate thickness is also analyzed. The analysis is repeated with different end-plate materials. In all cases, it is found that when the end-plate thickness increases, the effective mass also increases and hence the resonance frequency decreases. It is also known from literature that the radius of curvature of the Barrel shaped shell has a significant effect on the resonance frequency and TVR of the transducer[4]. This is also studied by changing the geometry of the shell. Two options that are easy to machine are tried out on the same model; in one case the shell boundary is a part of an ellipse and in the other, it is a part of a circle.The results are plotted in Fig. 4. Here, TVR and resonance frequency are normalized w.r.t. that of the

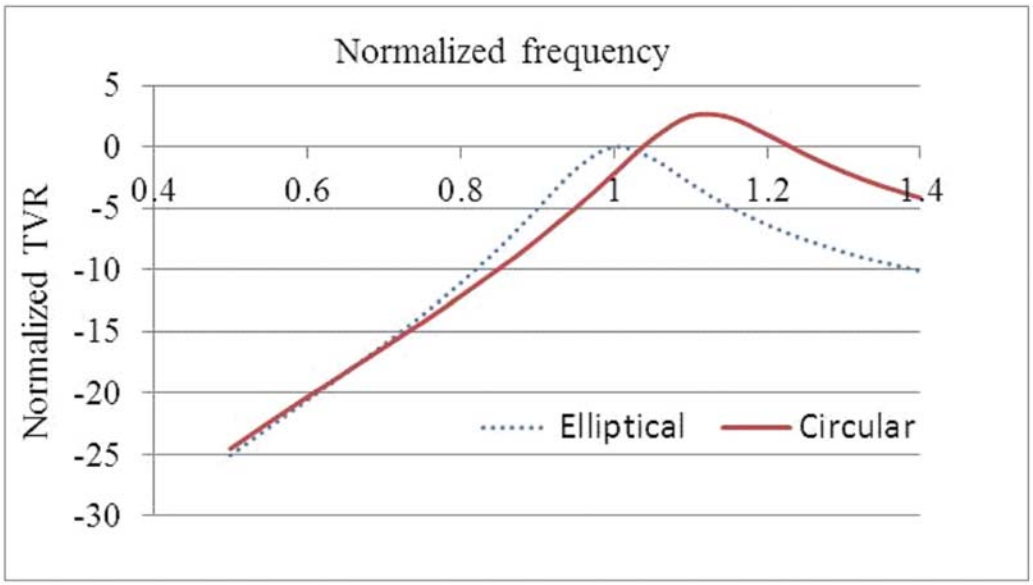

Fig. 4. Effect of circular and elliptical shell profile on TVR and resonance frequency

transducer with elliptical shell. It is observed that a brass shell with circular profile has nearly 3 dB more TVR than one with an elliptical profile. The resonance frequency is also higher for the transducer with circular profile. The solid line represents the predicted TVR of a Brass shell with circular profile and the dotted line represents that of a Brass shell with elliptical curvature.

3 DEVELOPMENT OF BARREL STAVE TRANSDUCER

A few prototypes of the optimized design are developed. The shell is manufactured using EDM wire cutting method. Shells are made up of three different materials, viz. Aluminium, Brass and Aluminium bronze.

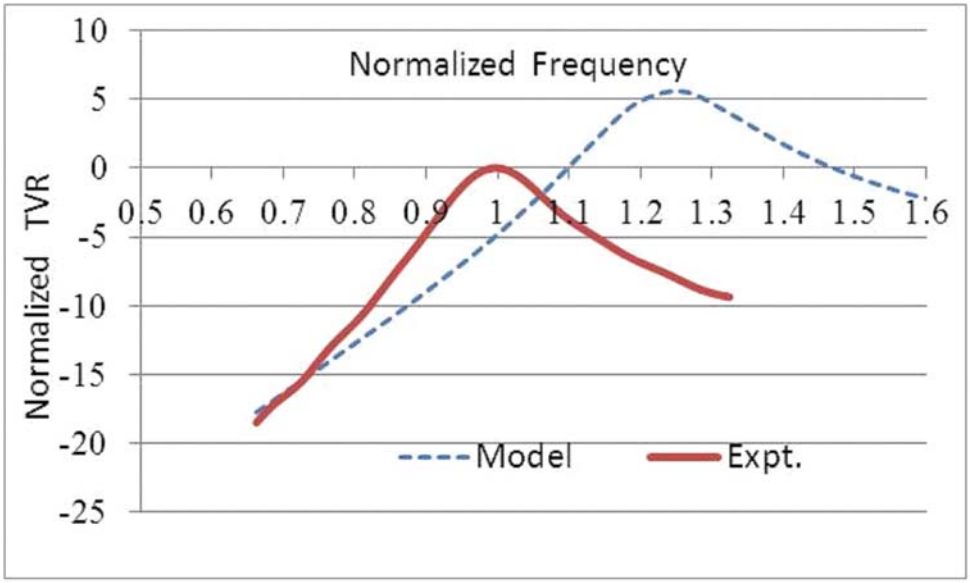

Fig. 5. Measured and Predicted TVR of the transducer

Nitrile rubber is used for encapsulation by post vulcanization bonding considering long duration exposure in oil environment inside the tube of horizontal projector array. Unlike other transducers, the piezoceramic stack used in BSTs is pre-stressed before assembly into the shell. This is done by means of a Beryllium Copper stress rod. The stress rod is tightening enough to prestress the stack. For assembling the transducer, the pre-stressed stack is inserted into the shell and fastened using the end caps of the shell. Then the ends of the shell are closed using PU moulding with terminals taken from one side. It is found that the Brass shell has minimum resonance frequency and maximum TVR and hence it is decided to proceed further with Brass shells. Because BSTs are to be used in towed arrays, the tuning coils also have to be inserted in the towed array tubes, filled with oil. Tuning coil was designed and encapsulated in rubber in such a way that the inside of the core does not get flooded with oil. The coil parameters were calculated from the measured underwater susceptance of the BST. The measured TVR of a prototype transducer with normalized frequency is shown in Fig. 5. Here, TVR and resonance frequency are normalized w. r. t. that of the experimental results. ATILA predicted TVR of the transducer is shown in the figure with a dashed line for comparison. Model predicted TVR is 6 dB more than the measured TVR. This difference is because of the fact that no losses are included in the model. But, in the actual prototype, all the materials have losses. There is 20% difference in the measured and model predicted resonance frequencies. In the FEM model, all the components of the transducer are integral and hence the joints are ideal as in Fig. 1. This is not achieved in the prototypes made. Efforts are on to make these differences minimal. Eventually, prototypes will be made with performances as good as that of the FEM model.

Measured fundamental flexural resonance frequencies can be matched with the FEM predicted results using several geometric and material approximations. Measured response levels can be achieved by using appropriate damping in the models. This is not attempted in the present analysis because the experimental results are satisfactory for the intended application. The change in resonance frequencies of a BST with depth is reported in literature[5]. As the depth increases resonance frequency increases quickly for an uncompensated transducer. The variation is at a slower rate for a projector with pressure compensation. To study the effect of depth in resonance frequency, one of the prototypes is subjected to various depths and a graph is plotted and is shown Fig. 6. It can be seen from Fig. 6 that the resonance frequency changes at slow rate from 10 m to 150 m. After 150 m, there is a rapid change.

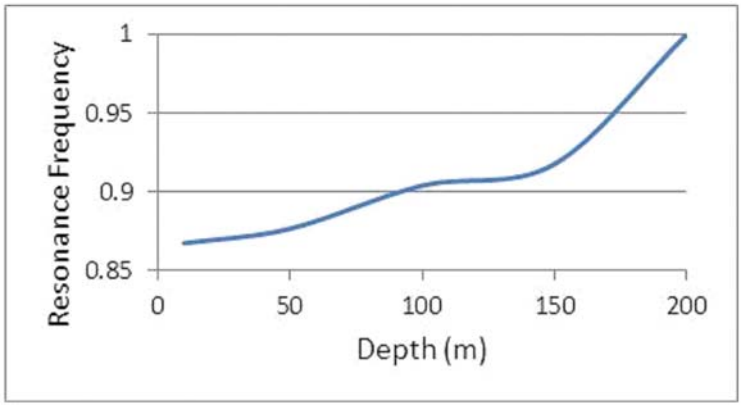

Fig. 6. Resonance Frequency as a function of depth

4 CONCLUSION

In this paper, the design and development of barrel-stave flextensional transducer is reported. Finite element package ATILA is used for the acoustical design of the transducer. Parametric studies are also conducted by using ATILA. The optimized design is prototyped and acoustically evaluated. FEM results are compared with experimental results.

5. ACKNOWLEDGEMENT

The helps rendered by Shri. M. Ajesh Kumar and Shri. Antony Jose in the design of the transducer; the effort and cooperation by Smt. Laly Joseph and Shri. P K Jayaprakasan in the design and development of tuning coil; by Shri E. R. Ratheesh in the assembly of the transducers are greatly acknowledged. We acknowledged with thanks the suggestions and guidance by Dr. R. Ramesh, Dr. D. Thomas, Dr. K P B Moosad, and Dr. D. D. Ebenezer. We are grateful to the keen interest and valuable guidance by Shri. M. R. Subash Chandrabose, Group Head, Transducer Group. The encouragement and facilities provided by Director, NPOL are gratefully acknowledged.

6. REFERENCES

[1] *ATILA user's manual.* Version 5.1.1, Institut Superieurd 'Eletronique du Nord, Acoustic Laboratory, LILLE CEDEX, France, (1997).

[2] R.A.G. FLEMING, M.KWIECINSKI, and D.F. JONES, Analysis of barrel-stave flextensional transducers using MAVART and ATILA finite element codes. *Canadian Acoustics,* **36**(2), (2008) 43-47.

[3] D.F. JONES and D.J. LEWIS. The effects of shell wall thickness and number of slots on the on the performance of the merchant slotted-shell Flextensional projector.Technical Memorandum 95/203, *DREA, Canada,* (1995).

[4] D.F. JONES and C.G. REITHMEIER.The effects of stave radius of curvature and end plate material on the performance of the Barrel stave Flextensional projector.Technical Memorandum 95/206, DREA, Canada, (1995).

[5] Y.R. BONIN and J. S. HUTTON. Increasing the depth capability of Barrel stave projectors. *Defence Research Establishment Atlantic,* (1968).

Journal of Acoustical Society of India : Vol. 43, No. 4, 2016 (pp. 200-207)

Very low frequency, compact, standingwave tube, hydrophone calibrating system

A.J. Sujatha, R. Ramesh* and D.D. Ebenezer
Naval Physical & Oceanographic Laboratory, Kochi-682021
e-mail: ramesh_rmani@hotmail.com

[Received: 22-09-2016; Revised: 10-10-2016; Accepted: 17-10-2016]

ABSTRACT

An improved method to calibrate hydrophones at very low frequencies in a small, water-filled, open chamber using standing waves is presented. The characteristics of the chamber are first determined using Finite Element Modelling (FEM), and then used to find appropriate locations in the chamber where the pressure field is uniform. The Sound Pressure Level (SPL) along the axis of the chamber estimated by modelling agrees well with the measured data in the frequency band (10 Hz - 4000 Hz). SPL is found to vary linearly with excitation voltage at high frequencies. A novel method is proposed in which the ambient noise is combined with the random noise signal generated by the projector to produce nearly constant SPL at low frequencies that is otherwise impossible to achieve using small projectors. In the present method, the Signal-to-Noise Ratio (SNR) of the measurement system is enhanced up to 20 dB below 200 Hz enabling accurate sensitivity measurements.This technique is demonstrated by measuring the receiving sensitivity of a few standard hydrophones at very low frequencies down to 10 Hz. The results are in good agreement with the reported values. Variations in sensitivity values are found to be less than ± 0.5 dB in the band 10 Hz to 4000 Hz for all the hydrophones studied.

1. INTRODUCTION

Performance of sonar systems depends largely on the ability of hydrophones to detect weakest signals arriving from underwater targets in the ocean[1]. The detection range of a passive sonar system is decided by the Minimum Detectable Level *(MDL)* of the receiver system which in turn is decided by the *SNR* at the output of the hydrophones. The *SNR* of a hydrophone depends on its receiving sensitivity and self noise. The receiving sensitivity is approximately constant far below its first resonance frequency. However, it drops sharply, *i.e.* 6 dB per octave, below a cut-off frequency that is decided by the RC time constant[2]. This means that the hydrophones and hence, the passive sonar system would become less and less effective below some limiting frequency. On the contrary, major part of the radiated noise of underwater targets lies in the low frequency region, typically of the order of few tens of Hz to few hundreds of Hz. Therefore, it is essential to characterise hydrophones used in sonar systems at very low frequencies.

Hydrophones are usually calibrated under free-field conditions in a laboratory water tank or in a large lake facility[3]. Such large water bodies allow sufficient spatial separation between the projector and the test hydrophone in order to satisfy the far-field criterion that is required to ensure approximately plane wave propagation during calibration. However, this condition is violated at low frequencies where the wave length of sound waves in water is much large. The dimensions of the tank set the low frequency limit of a measurement tank. For any practically feasible dimensions of laboratory tanks, typical low frequency limits lie in the range (1-2) kHz. For calibrating transducers below 1 kHz, one has to resort to alternative methods.

A few alternative methods of low frequency calibration are available. These methods make use of near field calibration techniques implemented in small chambers[3]. The chambers may be closed or open ended, but in any case, the dimensions of the chambers are much smaller than the acoustic wavelengths under consideration. The test hydrophone positioned in the chamber experiences uniform acoustic pressure generated by an appropriate mechanism. The main drawbacks in these methods are that they work under certain restrictions on the measurement conditions and they operate in a spot frequency or in a very narrow band. Measurements done using different techniques at various spot frequencies are to be combined for obtaining a calibration chart covering a reasonable frequency band. Any measurement technique that gives broad band calibration data of hydrophones would be handy for a sonar designer.

A broadband hydrophone calibrator that operates in the band (200 Hz - 4000 Hz) has been reported in literature[4]. This calibrator is an open-ended, fluid-filled rigid tube and generates standing wave pressure pattern. Hydrophones of finite sizes are calibrated using this method. The hydrophone calibrator developed by NRL operates in the band (25 Hz - 1000 Hz) and is designed to work in harsh environments such as on-board ships[5]. A few variants of hydrophone calibrators are commercially available[6-8]. However, no published literature is available in public domain on very low frequency hydrophone calibrators using open-ended chambers.

An attempt is made in the present work to develop and demonstrate a method to calibrate hydrophones using standing waves generated in an open-ended cylindrical chamber, in the frequency band (10 Hz - 4000 Hz). The calibrating system is modelled using finite element modelling code, ATILA[9]. The model results are validated by experimental studies. The new method proposed in this work is implemented in an experimental setup and demonstrated by calibrating a few standard hydrophones for which the data is available for verification. The details of the modelling and experimental studies are presented in this paper.

2. MEASUREMENT SYSTEM

The acoustic measurement system for calibrating hydrophones at low frequencies is shown in Fig.1. It consists of an open-ended rigid chamber of cylindrical cross section filled with a fluid. A piezoceramic projector is attached at the bottom plate of the closed end and driven by a transmitting system excited by the source signal generator through the Dynamic Signal Analyser (Agilent, Model 35670A) and a power amplifier (Instruments Inc., Model L2). Random noise signal in the frequency band (10 Hz - 4000 Hz) is transmitted through the projector. The hydrophone under calibration and a standard hydrophone (B&K, Models 8103 and 8104) are positioned adjacent to each other at a depth *h* from the surface of the fluid and

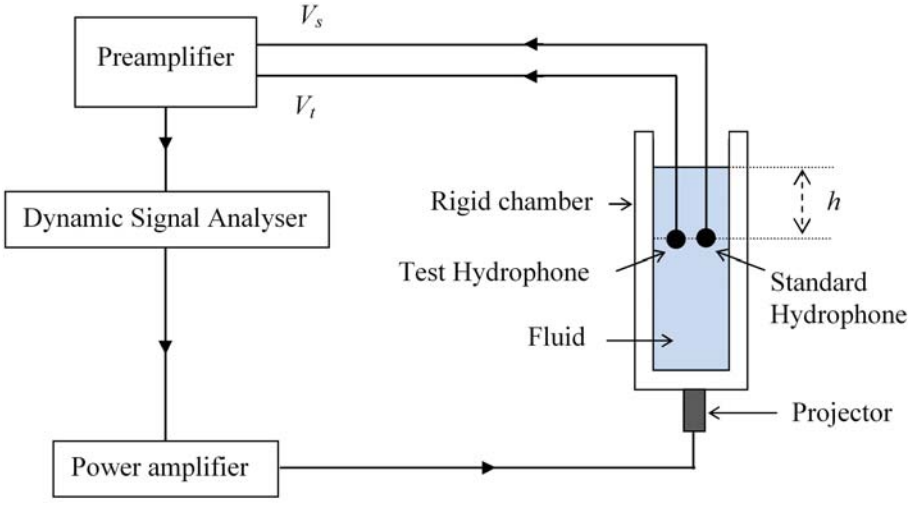

Fig. 1. Standing wave tube hydrophone calibrator system

close to the axis of the chamber. The output signals from the hydrophones are amplified using two channels of the preamplifier (B&K, Model Nexus2693). The gain of the preamplifier is set at 100 for both the channels. The amplified signals are fed to the Dynamic Signal Analyser for processing. The frequency response and the known sensitivity of the standard hydrophone are used to determine the sensitivity of the test hydrophone by comparison calibration method[3].

3. FINITE ELEMENT MODELLING

In order to understand the characteristics of the measurement system and to optimally use it for measuring acoustic parameters of hydrophones with minimum possible errors, it is important to initially characterise the measurement chamber. Numerical modelling is an effective tool for determining the characteristics of acoustic systems. Therefore, the measurement system shown in Fig.1 is modelled using finite element code, ATILA. Fig. 2 shows the finite element mesh of the critical part of the measurement systems, namely, the open-ended rigid chamber. The chamber is made up of stainless steel and filled with a suitable fluid, water or oil as required.The height, outer diameter and wall thickness of the chamber are 400 mm, 170 mm and 10 mm, respectively. A ring projector is fitted at the base of the chamber to generate the acoustic signal. The complete structure of the calibrating chamber is axisymmetric and therefore, analysed using 2-dimensional axi-symmetric model. Structured mesh with 8-noded HEXA elements are used. Harmonic analysis is carried out in the frequency band (10 Hz - 4000 Hz) with 100 points resolution.

The projector is driven with sinusoidal signals of 1V amplitude at each frequency in the band. The pressure field generated in the chamber forms a standing wave pattern with a pressure node at the water-air interface at the open end. The pressure field determined by the finite element analysis is used to find the best location in the chamber to position the hydrophones under calibration, in order to ensure that the hydrophones are exposed to maximum and uniform pressure amplitudes at all frequencies, and to improve the SNR ofthe measurement system.

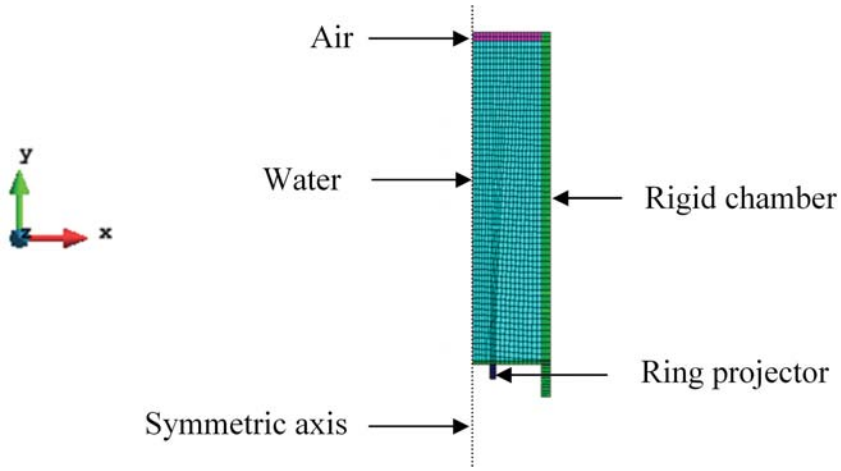

Fig. 2. Finite element model of the measurement chamber

4. RESULTS AND DISCUSSION

4.1 Finite element modelling results

Fig. 3 shows the electrical impedance spectrum determined across the input terminals of the projector fitted in the measurement chamber as predicted by FEM and compared with the measurement result. The loading effect of the measurement chamber on the projector modifies its original impedance pattern. A set of resonance peaks is observed at 216 Hz, 1089 Hz, 1960 Hz and 3718 Hz. It is seen from the figure that the model results, in general, agree with the experimental data. Small shift observed in some resonance

frequencies is attributed to the differences in material properties of various components of the chamber, used in finite element modelling.

Fig. 4 shows the normalised pressure distribution inside the measurement chamber at different frequenciesas predicted in FEM analysis. The pressure distribution is typical of a standing wave pattern in a tube with one-end open. The pressure field varies uniformly as the frequency is increased. The pressure amplitude remains constant along the radial direction upto about 3000 Hz and varies to a very small extent near the highest frequency, *i.e.,* 3718 Hz. The pressure distribution at two off-resonant frequencies, 2513 Hz and 3015 Hz are also shown in the figure to illustrate the pressure uniformity at all frequency regions including resonance and off resonance frequencies.The dotted line marked at a depth of 100 mm from the top surface indicates the ideal location of the hydrophone to be placed in the chamber for reliable measurements.

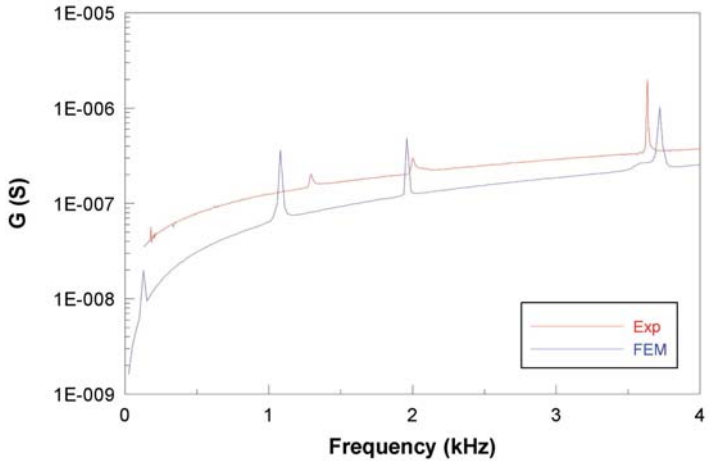

Fig. 3. Predicted and measured input electrical conductance spectrum of the measurement system.

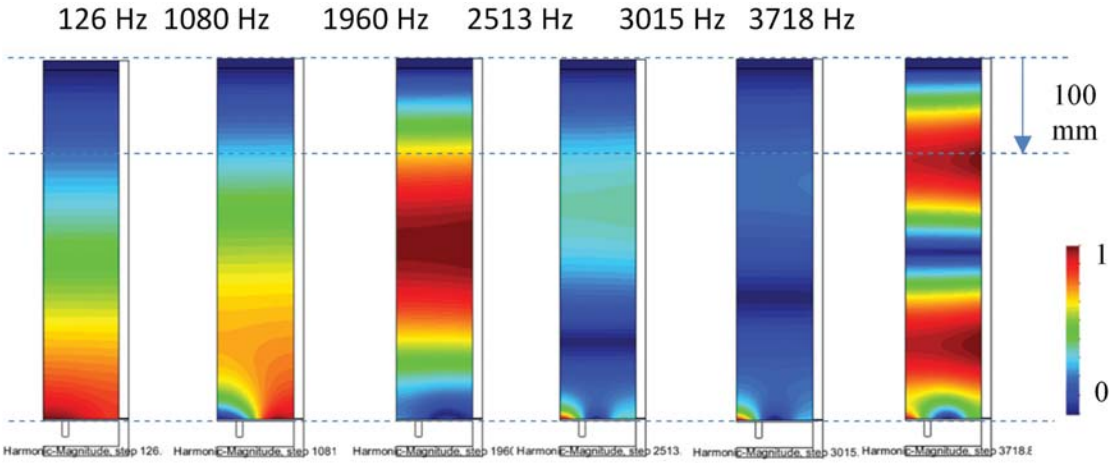

Fig. 4. Normalised pressure distribution in the measurement chamber at different frequencies

Graphical representations of pressure distribution in the measurement chamber are shown in Fig.5. The Sound Pressure Level (SPL) determined along the axis of the chamber at resonance frequencies are shown in Fig.5(a). SPL is nearly constant in most partof the chamber except at locations very close to the projector and at the free end of the chamber,for all frequencies except at 3719 Hz, where a pressure node is observed at the centre. It can be seen from the figure that the projector generates above 115 dB of SPL at a depth of

about 100 mm from the top surface at all frequencies studied. This is the best location in the chamber for positioning the hydrophones for calibration in order to achieve sufficient SNR and minimum measurement error. The optimum location is marked by dashed lines in Figs. 4 & 5. It can also be seen from the figures that SPL remains nearly constant and usable at axial distances varying upto $\pm$ 50 mm about the recommended position. This allows more tolerance in the length of the hydrophones that can be calibrated using this system.

Fig. 5(b) shows the pressure distribution along the radial direction of the chamber. The *SPL* remains constant over radial distances upto 70 mm at all frequencies studied. It is essential to maintain constant pressure in the plane perpendicular to the axis in order to use comparison calibration method where it is mandatory to simultaneously expose both the standard and the test hydrophones to equal pressure amplitudes[3]. Further, the uniform radial pressure amplitudes allow us great tolerances in the width of the hydrophones that can be calibrated using this system.

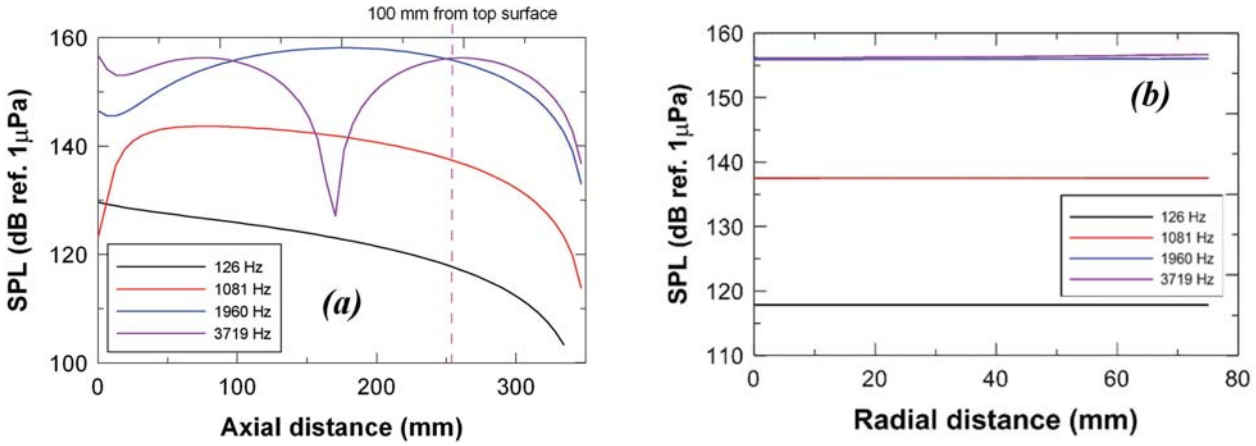

Fig. 5. (a) Axial and (b) Radial pressure distribution at different frequencies. Pressure node occurs at water-air interface at the top end of the chamber. The axial and radial distances are measured from the bottom and axis, respectively, of the chamber.

4.2 Measurements of calibrating system parameters

The appropriate location of the hydrophone *i.e.*, 100 mm from the surface,on the axis of the measurement chamber as determined by the finite element modelling is fixed in all subsequent measurements. The sound pressure level at this location is measured by exciting the projector fitted at the base of the chamber and recording the standard hydrophone output in the frequency band (10 Hz - 4000 Hz). Fig. 6(a) shows the variations in *SPL* in the measurement chamber with frequency at different excitation levels. A set of resonance peaks is observed in the band as seen in the conductance spectrum shown in Fig. 3. The *SPL* values increase with excitation voltage and is found to be above 110 dB in the band at the excitation voltage of about 2 V. This level is later found to be sufficient to achieve the required *SNR* of the measurement system. An important observation made from these plots is that the *SPL* remains constant as the frequency decreases below 1000 Hz. This phenomenon is contrary to the general behaviour of a typical projector response which decreases 12 dB/Octave below the first fundamental resonance[2]. In additions, a small increase in *SPL* is noticed at low frequencies for the lowest excitation voltage. This indicates that the pressure level generated by the projector is augmented by additional contributions from other sources. It has been found that the ambient noise, which is generally considered as unwanted, is responsible for this behaviour. SPL is linear with excitation voltage for frequencies above 1000 Hz and deviates from linearity at low frequencies as shown in Fig.6(b). The increase in *SPL* at low frequencies is contributed by the ambient noise.

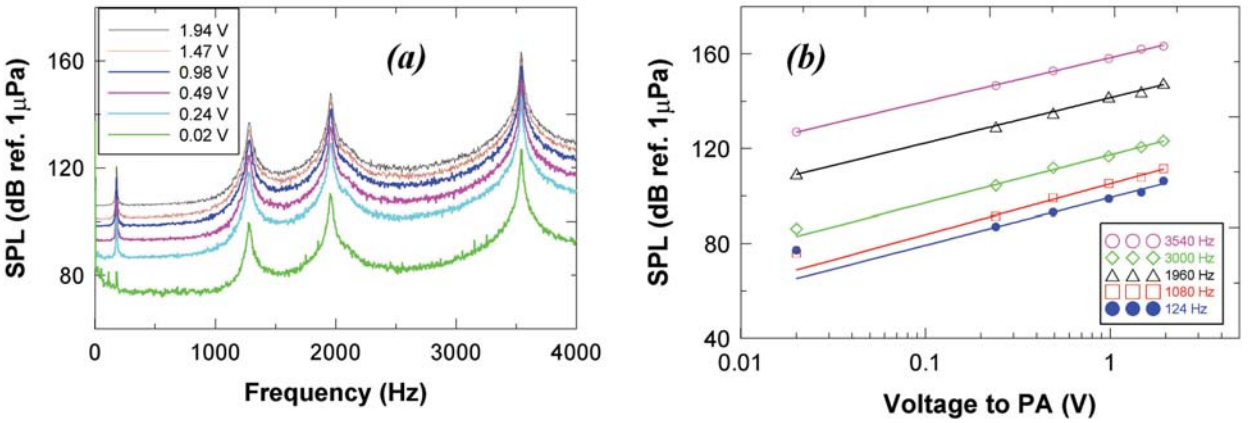

Fig. 6. (a) *SPL* and (b) linearitywith different excitation voltages, measured at a depth of 100 mm along the axis.

Therefore, the ambient noise in the system is measured using the same standard hydrophone. Fig. 7(a) shows the contribution of ambient noise to the sound pressure level of the measurement system. As seen in the figure, the pressure level is about 15 dB for frequencies above 500 Hz and it increases to about 35 dB for frequencies below 500 Hz down to 10 Hz. This effect is also seen in the linearity plot shown in Fig. 6(b).

In the absence of ambient noise, the *SPL* plot would be similar to that of the combination of projector and the measurement chamber. This is verified by subtracting the noise effect from the total *SPL* and the resultant plot is shown in Fig. 7(b). The measured plot is comparable to that predicted by finite element modelling, which takes into account only the response of the projector in combination with the measurement chamber, excluding ambient noise.

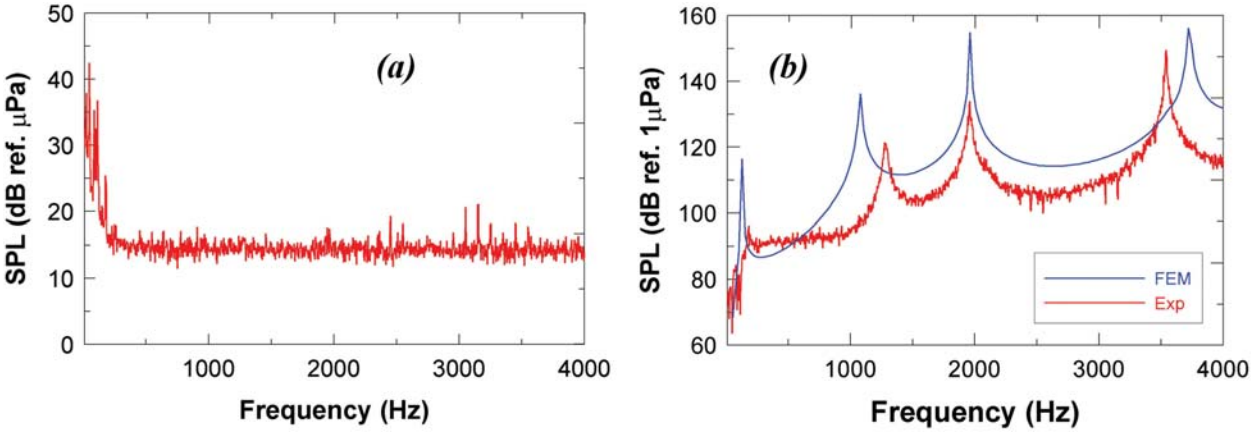

Fig. 7. (a) Contribution of ambient noise to SPL, measured at a depth of 100 mm along the axis of the measurement chamber and (b) Comparison of predicted and experimental SPL after subtracting the ambient noise.

4.3 Calibration of hydrophones

The measurement system is fully characterised as described in the previous sections and used to calibrate unknown hydrophones. In order to validate the calibrating system, three standard hydrophones, namely, B&K 8103, 8104 and 8105 are taken for the present studies. Their receiving sensitivities are determined

with reference to another standard hydrophone B&K 8100. Fig. 8(a) shows the receiving sensitivity of these three B&K hydrophones measured in the present calibrator in the frequency range (10 Hz - 4000 Hz). The dashed lines are the corresponding sensitivity values reported by the manufacturer. The sensitivity plots are found to be flat in the frequency range studied. The measured sensitivities are - (211.6 0.5) dB ref.1V / µPa for 8103, - (206.3 ± 0.5) dB ref.1V / µPa for 8104 and - (206.7 ± 0.5) dB ref.1V / µPa for 8105. These values agree well with that reported by the manufacturer and available in literature [10]. The maximum deviation in sensitivity values are found to be about ± 0.5 dB. This validates the present method of calibration. Calibration of hydrophones in the very low frequency region from 10 Hz to 200 Hz is an added feature in the present work.

It should also be noted that the *SNR* at frequencies above 1000 Hz is much improved than at low frequencies. SPL corresponding to this frequency is about 110 dB as seen in Fig.6. This indicates that the SPL values higher than 110 dB improves the measurement accuracy. However, the present system is capable of measuring the sensitivity even at very low frequencies because of additional improvements made in the receiver systems noise performance. Electrical noise in the system is greatly minimised by implementing proper electrical grounding methods[11]. The effect of proper electrical grounding technique on receiving sensitivity, for example, of B&K 8104 hydrophone is shown in Fig. 8(b). The receiving sensitivity measured with grounding shows significant improvement in SNR at low frequencies and close agreement with the reported values.

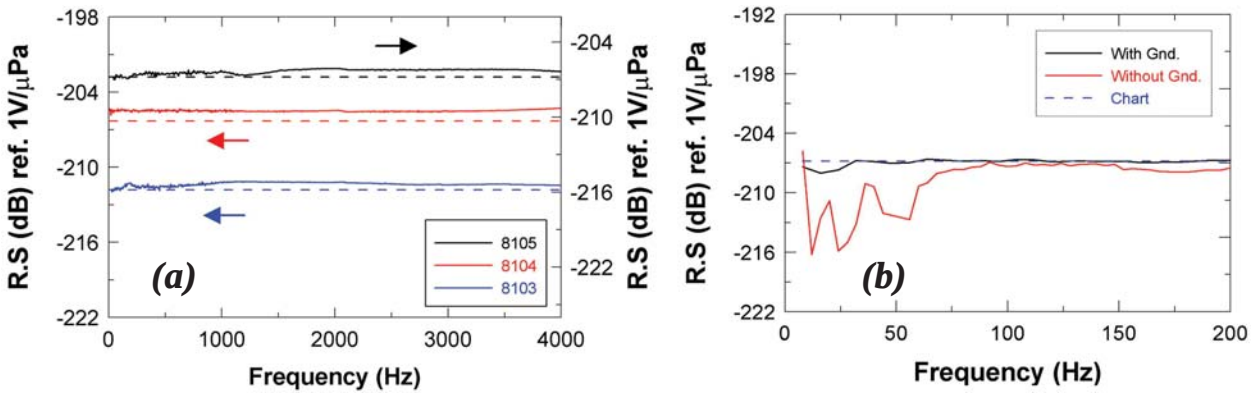

Fig. 8. (a) Receiving Sensitivity of standard hydrophones B&K 8103, 8104 and 8105 measured using the present system. The dashed lines are the corresponding calibration charts provided by the hydrophone manufacture and (b) Effect of proper grounding in enhancing the capability of very low frequency calibration.

5. CONCLUSIONS

The characteristics of a hydrophone calibrating system, that is a rigid, fluid-filled, open-ended chamber, are modelled and validated using experimental methods. Regions of uniform pressure field in the chamber are determined using FEM studies and used to position the hydrophones during calibration. It is found that a depth of about 100 mm from the top surface is the best location to place hydrophones. The characteristics of the measurement system, such as, electrical admittance spectrum and SPL in the frequency band (10 Hz - 4000 Hz) as determined in FEM and experimental studies agree well. An improved measurement technique is proposed to calibrate hydrophones at very low frequencies down to 10 Hz. An improvement in SNR upto 20 dB below 200 Hz is achieved, enabling accurate sensitivity measurements at very low frequencies. This technique is demonstrated by measuring the receiving sensitivity of a few standard hydrophones. The results are in good agreement with that reported by the manufacturer. Variations in sensitivity values are found to be less than ± 0.5 dB in the band (10 Hz - 4000 Hz) for all the hydrophones studied.

6. ACKNOWLEDGEMENT

The authors thank Director for providing facilitiesand permission to publish this paper.

7. REFERENCES

[1] R.J. URICK,1983, Principles of underwater sound, McGraw Hill, 3rd Ed., New York.

[2] C.H. SHERMAN and J.L. BUTLER, 2007, Transducers and arrays for underwater sound, Springer, New York.

[3] R.J. BOBBER,1988,Underwater electroacoustic measurements, Peninsula Publishing, Los Altos.

[4] D.D. EBENEZER, S. VASUDEVAN, A.J. SUJATHA and S. VASANTHA KUMARI, 2003. A low frequency, wideband, tabletop, hydrophone calibrator. Proc. National Symposium on Acoustics, NSA 2003-087.

[5] G.D. HUGUS and I.D. GROVES, 1974, Hydrophone calibrator for shipboard use, *J. Acous. Soc. Am.*, **56**(1), 70-74.

[6] D.T. DAKIN, J. BOSMA, J. DOROCICZ and N. BAILLY, Calibrating low frequency digital hydrophones, *1st Int. Conf. Exhibition on Underwater Acoustics*, pp. 1163-1168.

[7] *C100 Hydrophone Calibrator*, 2009, Underwater Science Research and Development Inc., USA.

[8] *Hydrophone field calibrator*, 2016, Geo Spectrum Technologies Inc., Canada.

[9] ATILA - FEM software for elastic, piezoelectric, magnetostrictive and electrostrictive structures radiating in a fluid, 2006, ISEN Recherche, Lille, France.

[10] *Introduction to underwater acoustics, Hydrophones - their characteristics and applications*, Bruel & Kjaer, Denmark.

[11] *Grounding and bonding electrical systems*, 2007, Engineers Educators Inc., USA.

Journal of Acoustical Society of India : Vol. 43, No. 4, 2016 (pp. 208-213)

Development of a ship sonar dome

Kurian Isac and Jineesh George
Naval Physical and Oceanographic Laboratory, Kochi
e-mail: kurian@npol.drdo.in

[Received: 26-09-2016; Revised: 10-10-2016; Accepted: 18-10-2016]

ABSTRACT

Sonar domes made of composite material are fast replacing the conventional domes made of metal owing to their better acoustic properties and manufacturability. The first indigenous development of sonar dome took place in early 2000s at Naval Physical and Oceanographic Laboratory, Kochi in association with Indian Institute of Technology Madras under a Naval Research Board project. Based on this development, a similar dome was recently manufactured for export to Myanmar. This paper describes the various steps involved in the development of the first hull mounted ship sonar dome made of composite material in India.

1. INTRODUCTION

A sonar dome is a streamlined, water tight enclosure that provides protection for one or more sonar transducers or arrays and associated equipment, while offering minimum interference to sound transmission and reception. In general, the sonar domes are curved, multi-layered and stiffened structures. The design of sonar dome is based on its type, operating frequency range, size and location of sonar transducers they

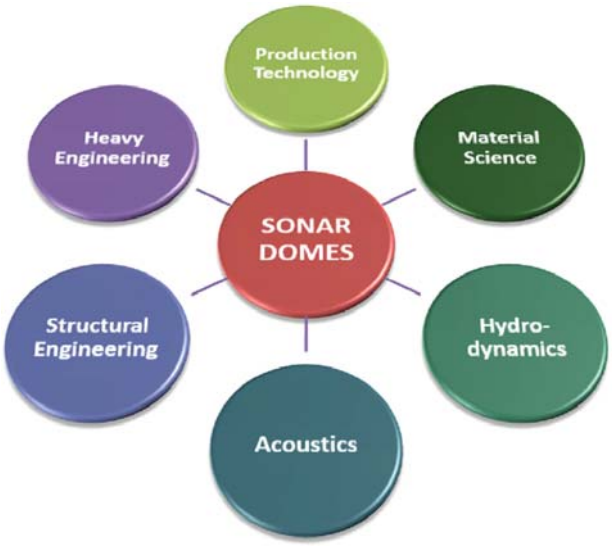

Fig. 1. Various technologies involved in the design and development of sonar domes.

cover. It should be strong enough to withstand the structural and hydrodynamic loads. Design and development domes is a complex task requiring expertise in various fields as illustrated in Fig. 1.

Older sonar domes were made of steel, which were replaced by titanium domes for better acoustic transparency. Naval Physical and Oceanographic Laboratory (NPOL), in association with M/s Larsen and Toubro Ltd., has developed and installed various types of titanium sonar domes for submarines. However, titanium is a very expensive material and has poor manufacturability. This has led to development of non-metallic composite domes, mainly made of rubber and composite materials. Since rubber is structurally weak, especially against concentrated loads, it is generally suitable for smaller domes. Meanwhile, the advances in composite material technology has made it the most widely used material for sonar domes[1]. The following sections describe the development of a ship sonar dome and the challenges involved in the development.

2. INDIGENOUS DEVELOPMENT OF A COMPOSITE SONAR DOME FOR SURFACE SHIPS

NPOL, in association with Composite Technology Centre of IIT Madras, Chennai developed two numbers of sonar domes for Indian naval ships fitted with hull mounted sonar systems under a Naval Research Board Project. This was a boat-hull shaped dome with the technical specifications as shown in Table. 1.

Table. 1: Technical details of the indigenously developed ship sonar dome

Type of Platform	**Surface Ship**
Sonar Type	Hull Mounted Array
Frequency Range	5 kHz to 11 kHz
View Angle	± 160
Acoustic Performance	Insertion Loss < 2 dB
Material	Polyester Isophthalic Resin
Fabrication Method	Vacuum Bag Moulding
Dimensions	Length : 3.8 m Width : 1.6 m Height : 1.55 m Thickness : 0.025 m
Weight	700 kgf
Structural loads	(a) Dynamic loads corresponding to a ship speed of 34 knots. (b) Buckling due to external hydrostatic pressure when the water inside the dome is drained out.

This dome was to be fitted to the bottom of the ship hull, close to midship location. The dome assembly consisted of the moulded sonar dome hull which was attached to the dome skirt flange in the ship hull using hull fairings.

The design of the dome was carried out to maximize the performance of the sonar array by reducing the effects of turbulence and protecting the sensitive transducers from wave slam, collisions etc. In the design of sonar dome, structural, hydrodynamic and acoustic aspects were considered. Structural constraints included the deformation of the structure under steady external flow, and accelerations and slamming loads. The structural design of the dome was carried out using Finite Element Analysis. The streamlined

profile already used for the existing HO 36 dome for minimum hydrodynamic resistance was followed for the new dome. The dome material and structure were selected for providing minimum acoustic signal loss and adequate mechanical strength to resist the static and dynamic loads arising from the ship motion. Before the final fabrication of the dome, a number of test panels and representative sections were made in order to verify the acoustic performance through Insertion Loss measurements in the acoustic tank at NPOL.

2.1 Material Selection

Glass fibre reinforced plastic (GRP) was selected for sonar domes because of its good acoustic impedance matching with water which results in minimum signal loss. GRP had other advantages as well, such as high strength and rigidity, low weight, corrosion resistance against seawater and easy mouldability.

Since the sonar dome had a thick cross section, a laminated construction was selected. To increase rigidity, glass fibre woven roving mat (WRM) was selected. However, chopped strand mat (CSM) layers were used in between the WRM for increasing the inter-laminar shear strength of laminate. The outermost and the innermost layers were selected to be of CSM in order to give the resin rich outer layers with good resistance to seawater. The mat density of CSM and WRM were finalized considering the acoustic aspects.

Isophthalic polyester resins were used as they were well proven for marine environment giving excellent resistance to water and durability. More commonly used epoxy resins were not selected because of high water absorption property. The gel coat and the outer resin coat of the final finish surface were selected to be Neopentyl glycol (NPG) based isophthalic resin. This resin system has excellent resistance to water. Surface mat was used in the resin coat and gel coat for improved moisture resistance. No fillers or pigments were used either in the lay-up resin or in the gel coat. An air release agent was used for reducing air bubbles in the lay-up resin. Fibre to resin ratio of 1:2 by weight for CSM lamina, and 1:1 by weight for WRM lamina were chosen as they were the optimum ratios for hand lay-up.

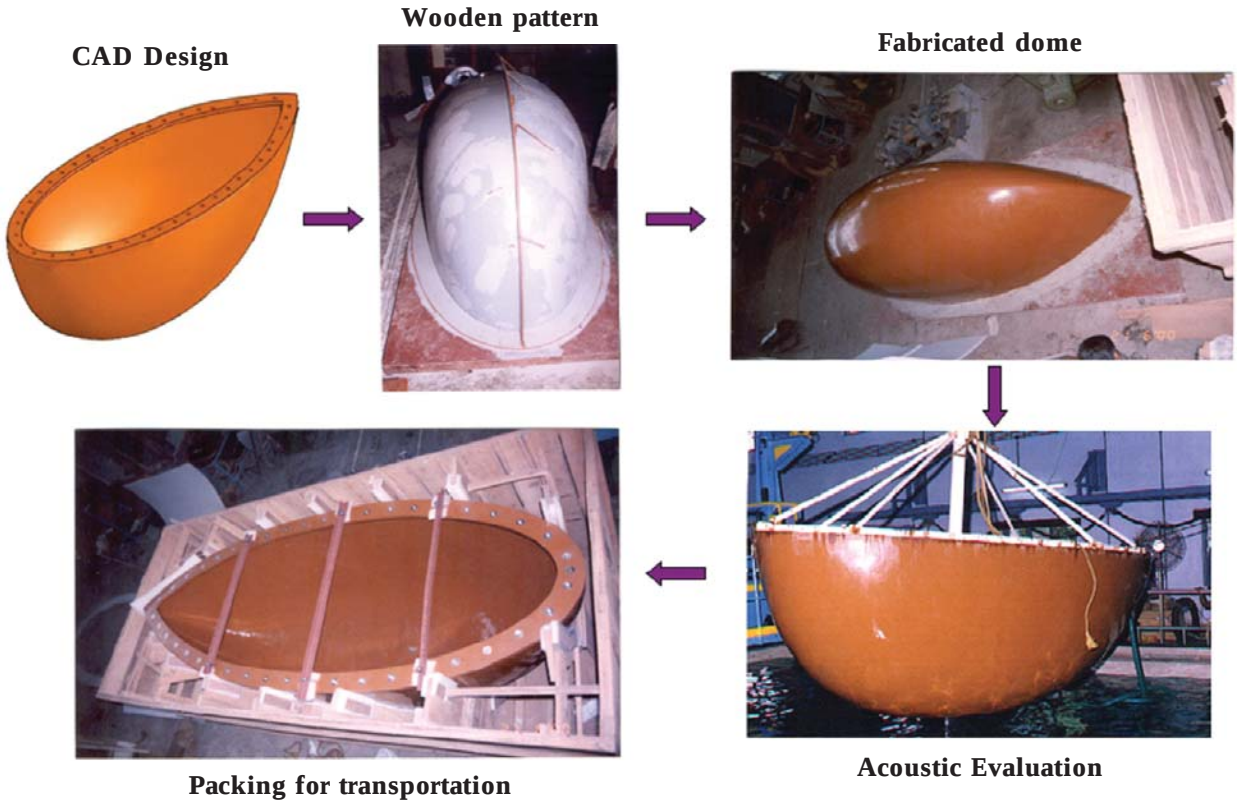

Fig. 2. Various steps involved in the development of the sonar dome

2.2 Manufacturing Process

Fig. 2 shows various steps in the development of the sonar dome. The design was frozen for fabrication after the experimental and computer aided analysis results proved that the shell structure synthesized could give the required performance under a wide range of frequencies and was safe under various load conditions. In order to create a void free laminate, vacuum bag method of fabrication was chosen. In this process, the glass fibre laminates were made by the wet lay-up process. The lay-up before gelation was subjected to vacuum by enclosing it using a butyl rubber sheet and sealing it all round the laminated shell. Over the wet lay-up, a perforated peel ply was placed which allows the excess resin and air bubbles to pass through under vacuum. Over the perforated sheet, a bleeder layer of spongy material like jute felt or jute cloth was used below the vacuum bag, which provided the passage for the air to escape and helped to absorb the excess resin squeezed out from the laminate. The vacuum bagging was done for every two layers of lay-up.

In order to study the optimum vacuum level and the duration for which the vacuum was to be applied, studies were carried out on a flat laminate laid over a vacuum bag table. Studies were conducted for different pressures acting for different durations. It was found that a high vacuum applied for a longer duration caused vapourisation of styrene, while the application of low vacuum caused air bubbles. Therefore, by repeated trials, the optimum pressure and duration were selected as 450 mm of mercury vacuum for 3 minutes for a two-layer laminate. The addition of air release agent to the resin mix also helped to minimize the air voids in the final laminates.

The vacuum was applied on each half of the sonar dome simultaneously since the duration for laying both halves of the dome is long and gelation could occur well before the vacuum application could be completed. The vacuum bag was made for the full dome and the vacuum seal was provided along the flanges at the top edge of the mould.

An autoclave cum vacuum bag facility with a large capacity vacuum pump was developed at the Composite Technology Centre of IIT Madras. A butyl rubber bag was specially made by a local manufacturer in 2 m × 2 m size and was joined for the entire dome by vulcanizing along the joints to make the full bag. An air-conditioned fabrication shop was created for carrying out the lay-up without any loss of styrene and under controlled humidity and temperature.

Fabrication of the sonar dome involved nine stages of operation as described below:

(i) Preparation of a pattern made of a framework of wooden planks. The surface was finished with nitro-cellulose putty.

(ii) Preparation of the FRP mould made of glass fibre reinforced vinyl ester resin. The FRP lay-up of the dome mould was made under ambient conditions and with slow curing to minimize shrinkage. It was made in 2 halves and was bolted together along the joint at the keel. A heavy steel stiffener framework was provided for additional rigidity.

(iii) After releasing the mould, the inner profile of the mould was checked using aluminium templates made for different cross sections at 0.5 m interval along the length.

(iv) A flat mould was made which could be attached to the dome mould on its top flange which served as the mould surface for the inward projecting flange.

(v) Reinforcement mats were cut using standard templates made for each layer or ply of the dome wall. The resins required for each such mat was separately made and used for that mat alone. This process ensured the correct fibre to resin ratio.

(vi) After the lay-up of two layers of mat, vacuum bagging was done to drive out the voids and volatiles present in the wet laminate.

(vii) By repeating the lay-up process the entire laminate structure was built-up within the mould. Metallic inserts for bolting the dome to the hull were also placed while moulding.

(viii) After the complete lay-up, the top surface was finished with surface grinding and resin coating. The inner profile was checked using specially made templates in order to verify the geometry.

(ix) The finished sonar dome while it was in the mould was post cured by enclosing the mould top with a flat panel and pumping in hot air. The air temperature was maintained at 80°C and the curing was carried out for 8 hours continuously.

3. ACCEPTANCE TESTS AND EVALUATION

The fabricated dome was subjected to the following acceptance tests :

(a) Profile Accuracy Measurement : The accuracy of the dome inner and outer profiles were measured after leaving the dome for a month under natural environment permitting it to undergo any possible shrinkages. The dome profile was then checked using master templates and were found to be within specified limits.

(b) Ultrasonic Evaluation : Ultrasonic A scan was used for measuring the shell thickness as well as to detect any flaws present in the shell wall. A standard test laminate having the thickness same as that of the shell which was prepared for the acoustic measurement was used as a reference medium for calibrating the ultrasonic A scan. After extensive measurements using the ultrasonic scan equipment, no detectable flaw was found in the laminate.

(c) Acoustic Performance Evaluation : Transmission loss measurements of the sonar dome were conducted by the free-field method. The sonar dome was evaluated for its acoustic transparency in the frequency range of 5 kHz to 11 kHz in the acoustic tank at naval base. The dome was lowered to a depth of 4 m and then mounted onto a heavy duty turn table using suitable frames. A standard hydrophone was suspended inside the dome and an acoustic wave was transmitted using a projector kept at a distance of 7 m. The insertion loss (IL) was calculated from the hydrophone output with and without the dome as[2].

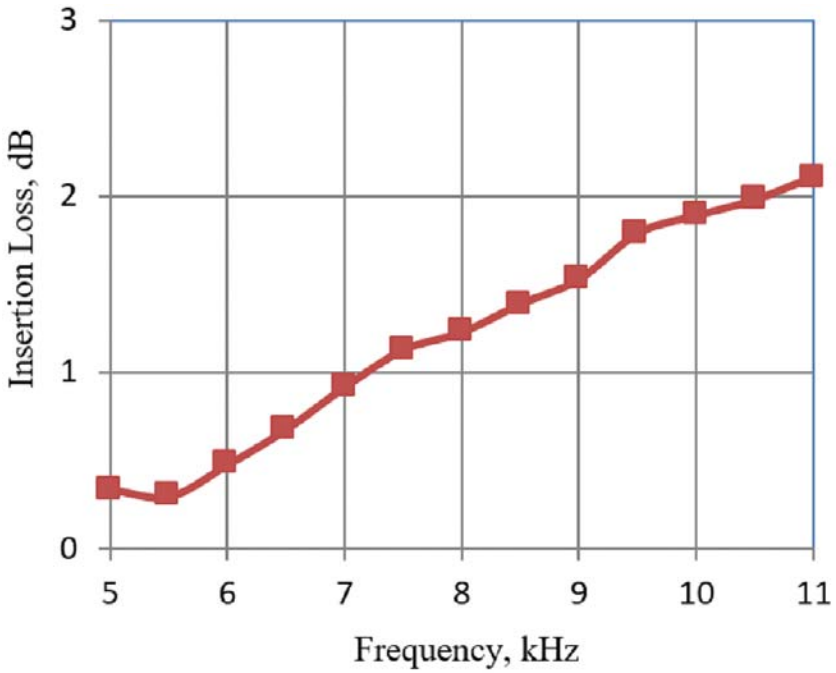

Fig. 3 Insertion Loss of the dome for a particular angle of incidence. Similar results were obtained for other locations around the dome.

$$IL = 20 \log \frac{\text{Incident sound pressure}}{\text{Transmitted sound pressure}} \quad (1)$$

The result of the acoustic evaluation of the composite sonar dome is shown in Fig. 3. Installation trials of this dome was carried out in March 2005 and it is currently in service onboard a naval vessel. Three numbers of similar domes with certain improvements were developed in 2013 for installation onboard Myanmar Navy ships.

4. CONCLUSION

The composite domes, owing to their superior flow noise suppression and better acoustic transparency, are replacing the metallic domes. This paper described the development of the first composite sonar dome made in India. Two numbers of hull mounted sonar domes were manufactured using Vacuum Bag Moulding technique under this project. One of the two domes made under this project is in active service onboard a naval platform. Successful completion of this project led to the inception of many other sonar dome development projects for submarines and surface ships.

5. ACKNOWLEDGEMENT

Contribution and guidance by Dr. J Narayana Das, Former Chief Controller for Research & Development Defence Research and Development Organisation and Prof (Retd.). N.G. Nair from Indian Institute of Technology Madras is gratefully acknowledged. The later sonar dome development projects were carried under the guidance of Dr. D.D. Ebenezer of Naval Physical and Oceanographic Laboratory. The authors wish to thank Director, NPOL for granting permission to publish this paper.

6. REFERENCES

[1] T.G. BELL, 2010. *Probing the Ocean for Submarines: A History of the AN/SQS-26 Long Range, Echo-Ranging Sonar, 2nd Edition*. Naval Sea Systems Command Report of Project No AC31151.

[2] Q. LIU and J.Y.GUIGNE, 1996. Acoustic Properties of Sonar Dome Materials,Defense Research Establishment Atlantic Canada Contractor Report No. CR/96/420.

Journal of Acoustical Society of India : Vol. 43, No. 4, 2016 (pp. 214-223)

Recent trends in power amplifiers for sonar projectors

V.N. Panchalai and N. Sivakumar
Naval Physical and Oceanographic Laboratory, Thrikkakara, Kochi
e-mail: panchalai@gmail.com

[Received: 01-02-2016; Revised: 29-09-2016; Accepted: 19-10-2016]

ABSTRACT

Sonar Power Amplifiers (SPAs) are required to drive high impedance complex loads in pulsed mode. The important parameters of interest are bandwidth, power output, efficiency and Total Harmonic Distortion (THD). Switch Mode Power Amplifiers (SMPAs) are preferred over Linear Power Amplifiers (LPAs) at low frequencies. However, at high frequencies, it is difficult to design a SMPA that satisfies THD requirements. Hence LPA is preferred for high frequency operation. Multilevel converters as power amplifiers can replace LPAs at high frequencies as they have better efficiency. A few converter topologies that are suitable for SPA, which can deliver a selectable constant power over a finite bandwidth to drive a sonar acoustic projector with frequency-dependent impedance is explained.

1. INTRODUCTION

Active Sonars are used to transmit acoustic pulses of various types such as Continuous wave (CW), Linear Frequency Modulation (LFM), Hyperbolic Frequency Modulation (HFM) and Pseudo Random Noise (PRN)[1]. A typical active sonar transmitter consists of sonar signal generation circuit, Power Amplifier (PA), power supply and electro acoustic transducer array. The acoustic Source Level delivered by an electro-acoustic transducer underwater, SL is expressed as[2, 3]

$$SL = 170.8 + 10\log_{10}P_e + 10\log_{10}(\eta) + DI \quad (1)$$

where, DI is the Directivity Index, P_e is the Electrical Power applied to the transducer and η is the conversion efficiency. The Electrical Power P_e is higher than the Acoustic Power $P_a = \eta P_e$, due to the electro acoustic conversion efficiency of the transducer (η).

The underwater acoustic transducer offers resistive load at resonance frequency (F_r), becomes capacitive for frequency less than Fr and inductive between F_r and F_{ar} where F_{ar} is anti-resonance frequency. The impedance of the transducer may vary with input power, especially at higher power levels[4, 5]. A well designed PA is expected to deliver different power levels (selected by the operator) to a transducer with frequency-dependent impedance even when the power supply to it is not constant with time. The impedance of underwater transducer is usually high and hundreds of volts are often required at the output of the PA in order to transmit high power[3]. The equivalent circuit of underwater projector includes reactive elements[6, 7] as shown in Fig. 1.

The power amplifiers which deliver constant power (selectable by operator) to frequency dependent transducer load are need of the day and a few topologies that satisfy the requirements are explained in subsequent sections.

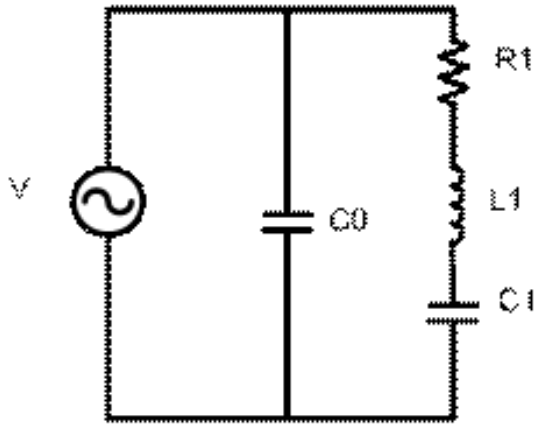

Fig. 1. Electrical equivalent circuit of a transducer with single resonance

2. POWER AMPLIFIERS FOR SONAR APPLICATIONS

A typical sonar transmitter system is shown in Fig. 2. It uses either LPA or SMPA as power amplifier which is normally powered by a Switch Mode Power Supply (SMPS). In LPA, the power devices are operated in linear region and large power is wasted as heat during operation. In SMPA, the power devices are operated either in 'ON' or 'OFF' state. During 'ON' state, the voltages across the devices are low, so the device's power consumption is low. On the other hand during the 'OFF' state, there will be no current flow through the devices; and thus, here also the power consumption will be low

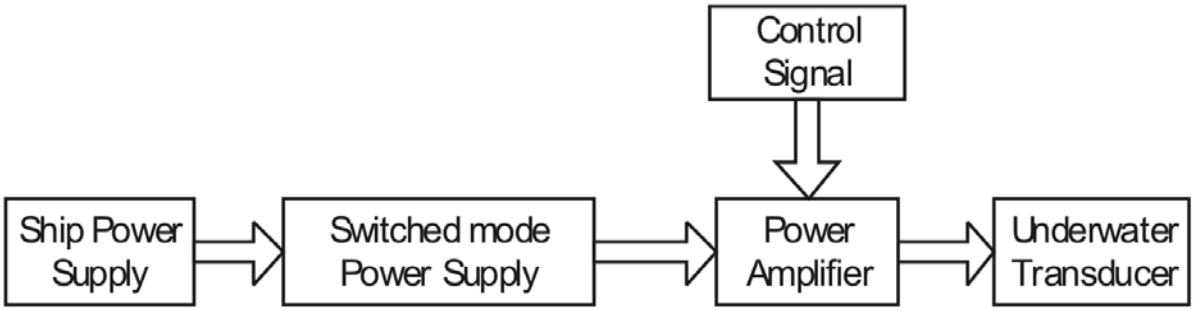

Fig. 2. Block schematic of an active sonar transmitter system

2.1 Linear Power Amplifiers (LPAs)

The most commonly used linear power amplifiers are class A, B, AB and C. The class- A power amplifiers are highly linear type. The power devices used in this type are operated in the active region of its characteristic curve and the conduction angle is 360°. The major disadvantage of this class is its efficiency which is less than 30% and hence the system is bulky. The conduction angle of class-B type power amplifier is 180° and the efficiency is around 78%. But this class suffers from cross over distortion. The class AB is the combination class A and B and hence has the advantages of both. The conduction angle is between 180° and 360°. The class C is the most efficient linear power amplifier. But it is a tuned power amplifier with conduction angle less than 180° and poor bandwidth[8].

2.2 Switch Mode Power Amplifiers (SMPA)

There are two major classes of SMPA namely class-D and class-S. In class-D power amplifier, the sonar signal is modulated with a high frequency carrier wave and the output which is the Pulse Width Modulated (PWM) signal, is used to drive the semiconductor devices, whereas fundamental frequency switching is used in class-S power amplifier. The switching frequency of class-D PA is very high compared to class-S; hence the switching losses are more, but require smaller filter components at the output[9]. The usage of class-D SMPA is limited to frequencies less than 10 kHz and the class- S SMPA is preferred at higher frequencies.

3. RECENT TRENDS AND TOPOLOGIES IN SONAR POWER AMPLIFIER DESIGN

Over the years, the SPAs have seen many advancements from general open loop LPAs to feedback controlled SMPAs. Every topology has got its own advantages and disadvantages. The selection of topology depends on the requirements such as frequency of operation, linearity and maximum power required. Low frequency medium power applications use class-D SMPA with SMPS. For high power applications, multilevel class-D SMPA is preferred instead of simple centre tapped or full bridge topology.

3.1 Class-D SMPA with custom made SMPS

A topology which can be used up-to a frequency of 10 kHz and power levels less than 5 kW is shown in Fig. 3. It is a processor controlled AC-DC converter fed class-D SMPA. Based on the sonar signal information, Sine Pulse Width Modulated (SPWM) signals are generated digitally to drive semiconductor devices in Controlled Full Bridge (CFB) at SMPA[10].

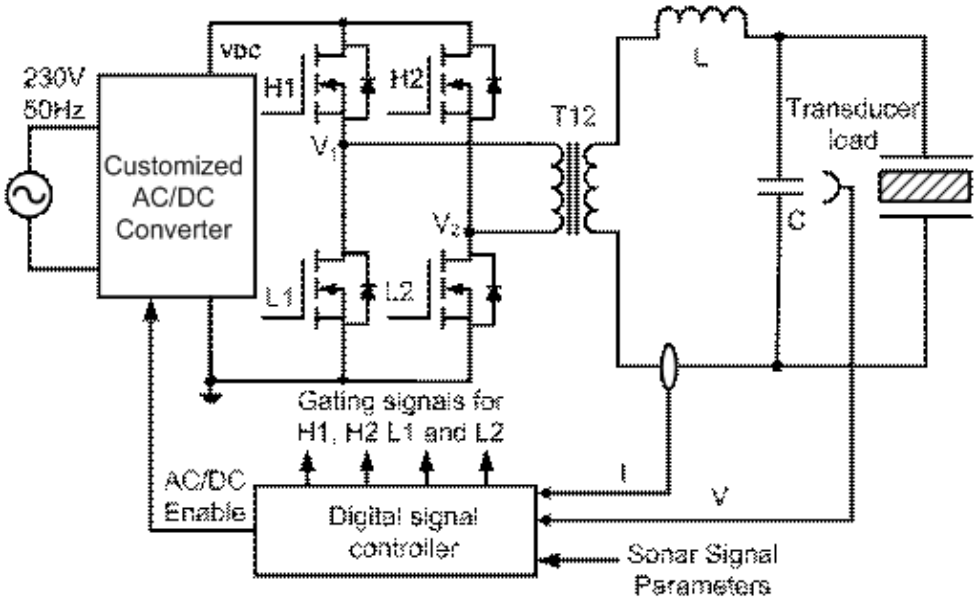

Fig. 3. Processor based feedback controlled SPA

Typical SPWM gating pulses for the devices H1 and H2 of CFB in SMPA are shown in Fig. 4. The output of CFB (*i.e.* V_1-V_2) is uni-polar SPWM signal whose amplitude is proportional to V_{DC} and the pulse widths are proportional to the amplitude of sonar signal. The step-up transformer boosts the voltage $V_1 - V_2$ and provides isolation. The output of the transformer is passed through a power filter which removes the harmonics before connecting to the transducer load.

If the output of the PA across the transducer load is V_o, then the power delivered is $\frac{V_o^2}{Z}$ where, Z is the impedance of the transducer load. The output voltage V_o in CFB of SMPA can be expressed as

$$V_o = m_a V_{DC} N_P \quad (2)$$

where m_a is modulation index (modulation index is the ratio of amplitude of sonar signal to amplitude of carrier wave), V_{DC} is the output of AC – DC converter *i.e.* the DC supply for the CFB and N_p is the turns ratio of the step up transformer.

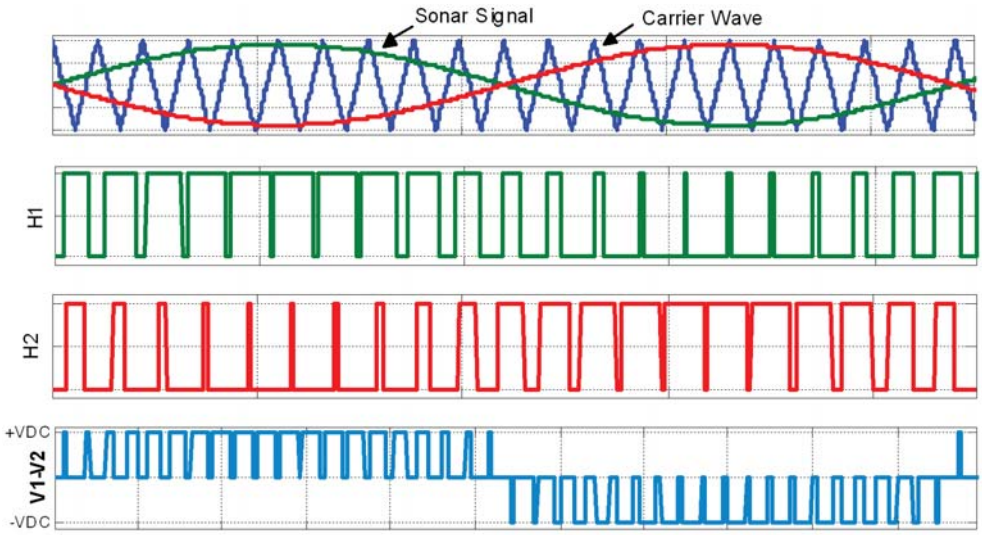

Fig. 4. Gating pulses for class-D SMPA for unipolar SPWM

From the equation 2, it is clear that the output power can be controlled by either m_a or by V_{DC}. The control through m_a requires comparison of required power with delivered power to generate SPWM as control parameter while V_{DC} is kept constant. The power delivered is estimated from the sensed values of output voltage, current and the phase angle between them. The calculation of phase angle for variable frequency signal pulses such as LFM and HFM is difficult especially at high frequency. The implementation of control algorithm needs high speed processors and extra memory.

The control of output power by means of V_{DC} needs a variable AC-DC converter while m_a is kept constant. A typical variable output AC-DC converter that delivers a controlled power is given in Fig. 5. The gate

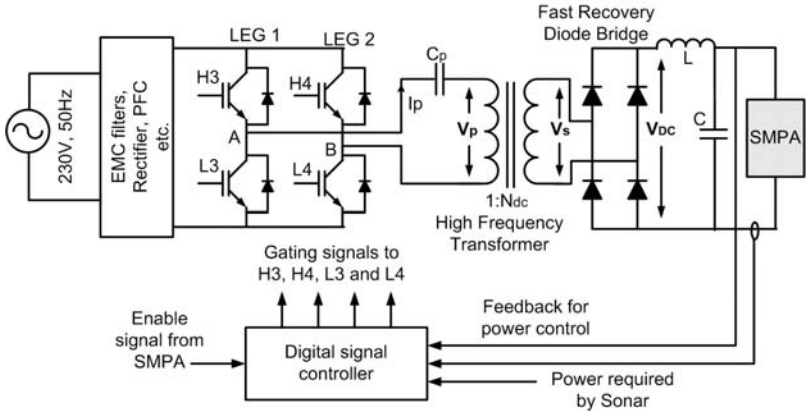

Fig. 5. Processor controlled AC-DC converter

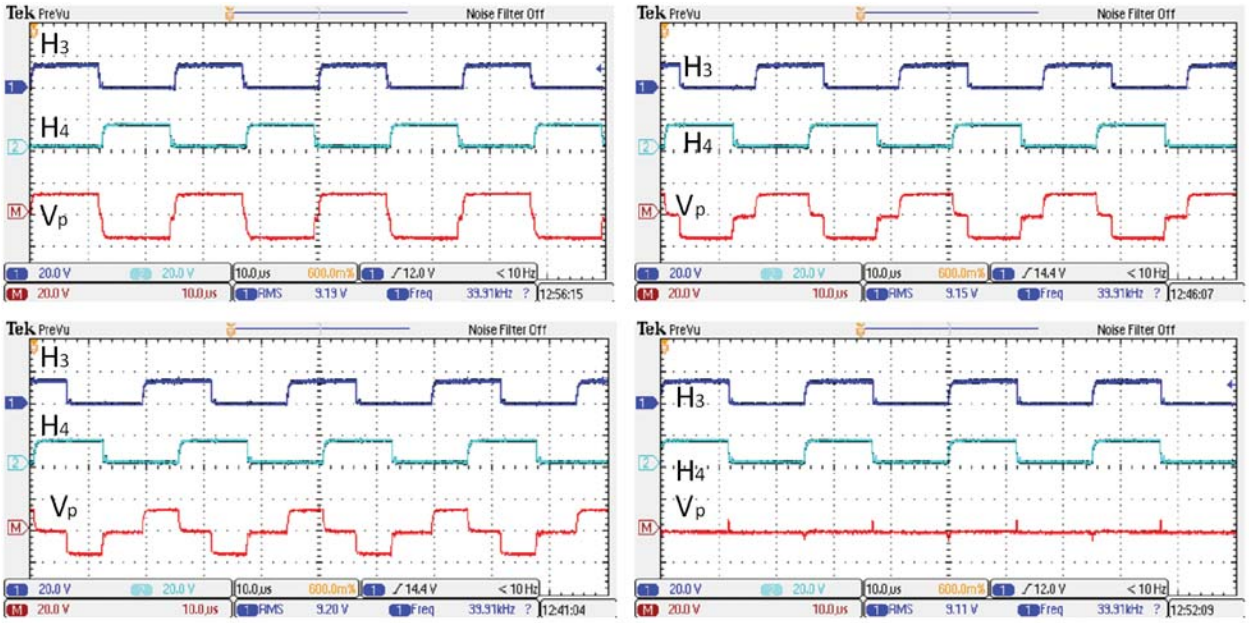

Fig. 6. Gate drive signals for CFB of AC-DC converter for different values phase shifts

drive signals for CFB are generated using digital controller based on Phase Shift Modulation (PSM) technique. The gating signals for H3 and H4 and primary voltage V_p for different phase shift values are given in Fig. 6. The advantage of PSM is that the soft switching can be implemented effectively to improve the efficiency of AC-DC converter. The power devices used in the system are switched in equal duration and hence the stresses on the devices are equal. Voltage mode control of full bridge DC-DC converter has been well explained in many papers[11-13] and it uses gain scheduling to implement power control for the present application[14].

Fig. 7(a) shows the experimental voltage and the current waveform of the system, when connected to a transducer load. Fig. 7(b) shows the amplitude plots of voltage, current, impedance of transducer and active power delivered for a variable frequency signal. It can be observed that the power delivered is maintained constant when the impedance is varying.

Advantages of the AC-DC fed SMPA are that

i. The power delivered to the transducer is controlled by controlling VDC / m_a or by both and hence the dynamic range of the system is more.

ii. By driving SMPA with higher modulation index (m_a) signals and employing processor controlled AC-DC converter, the THD of the output waveforms can be reduced.

iii. As per operator selection, constant power output over a desired band is possible

iv. Since processors are used for signal generation and control loop implementation, up-gradation does not require any hardware change.

There are few drawbacks in this topology which is due to class D SMPA.

i. The sonar operating frequency is generally in kilo hertz range and hence the frequency of SPWM signal is greater than100 kHz, which is near maximum operating frequency of semiconductor power devices. This puts limitation on usage of class-D power amplifier at higher sonar operating frequency.

ii. The power filter that follows the full bridge circuit needs to be designed properly which may otherwise increase the THD of the output waveform.

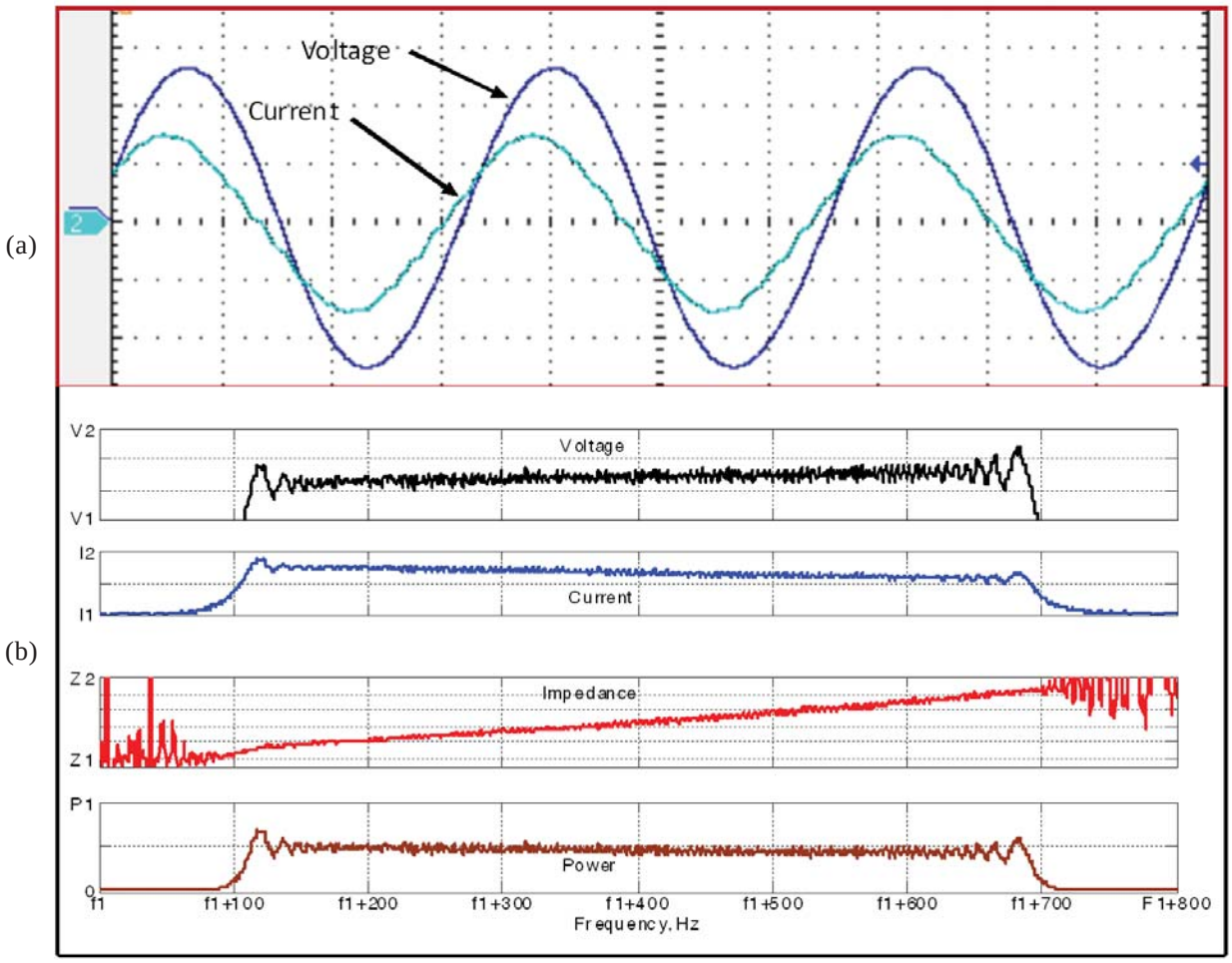

Fig. 7 (a). Experimental Load Voltage and Current waveforms &
7(b). Load Voltage, Current, Impedance and power delivered for variable frequency pulse

iii. The switching transients of power circuit generate electromagnetic interference (EMI), and it needs to be suppressed.

3.2 Class-S SMPA with custom made SMPS

The topology which is useful at frequencies greater than 10 kHz and power more than 5 kW is shown in Fig. 8(a). It is a programmable AC-DC converter fed multilevel SMPA.

The multi-level SMPA shown here uses single DC source (V_{DC}) for the two CFBs whose outputs are connected with primaries of two isolation transformers. The secondary of the isolation transformers are connected in series to achieve a five level output[15]. The system uses a digital controller for generating gating pulses of the devices S1 to S8. The sonar signal is compared with DC voltage (this voltage is derived from number of levels in the staircase waveform) of different values to generate the gating signals as shown in Fig. 8(b). Experimental five level output waveform is shown in Fig. 8(c) and the efficiency of the system at different power levels selected is shown in Fig. 8(d). The control of output power is achieved by controlling AC-DC converter output voltage V_{DC}. The quality of output waveform can be improved by increasing the number of levels. It requires increased number of CFB, isolation transformers and more gating pulses which increase the complexity of the circuit.

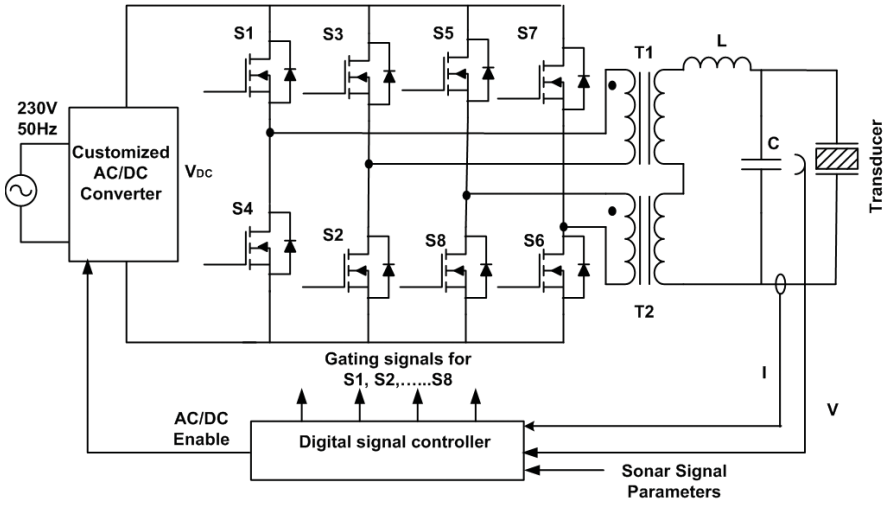

(a) AC-DC converter fed multi-level converter

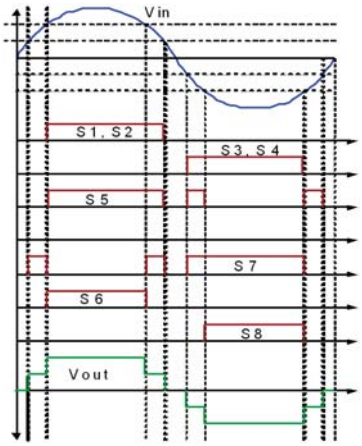

(b) Gating signals for multilevel converter

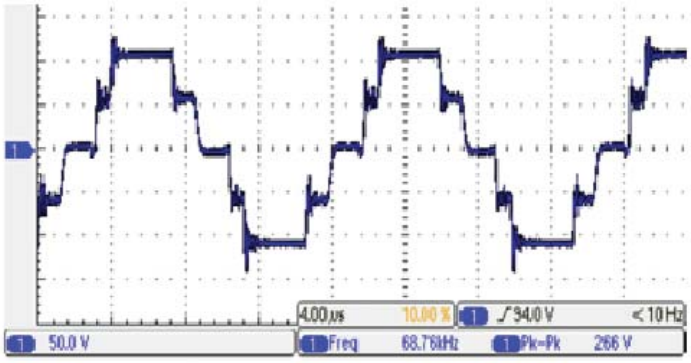

(c) Experimental output voltage waveform

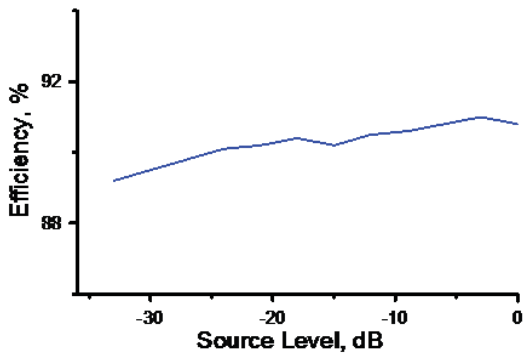

(d) Efficiency at different loads

Fig. 8 Schematic of AC-DC converter fed Multilevel SMPA, Gating signals for the devices, experimental output voltage and Efficiency curve at different Source Levels

Another multi-level topology which can be used for high frequency and high power application is shown in Fig. 9. It uses two CFBs (one leg is used as shared leg) and three isolation transformers to achieve seven level output at SMPA stage[16]. The generation of gating pulses is complex compared to previous topology. But the advantage of this topology is that it uses less number of devices and it can be easily configured to use with class-D, class-S and hybrid switching. The gating pulses for the devices are shown in Fig. 9 (b). The output voltage of the converter depends on the turn's ratio of the isolation transformer. Efficiencies at different DC supply voltage across three different loads are shown in Fig. 9(c) and the shape of the waveform before power filter (V_{01}) and the load voltage (V_{02}) is shown in Fig. 9(d). The control of output power is achieved by controlling the supply voltage V_{DC}.

4. CONCLUSION

The recent trend in the design of SPA aims at the provision of a selectable constant power output over a bandwidth of interest across a frequency dependent transducer load. The class-D SMPA powered by a

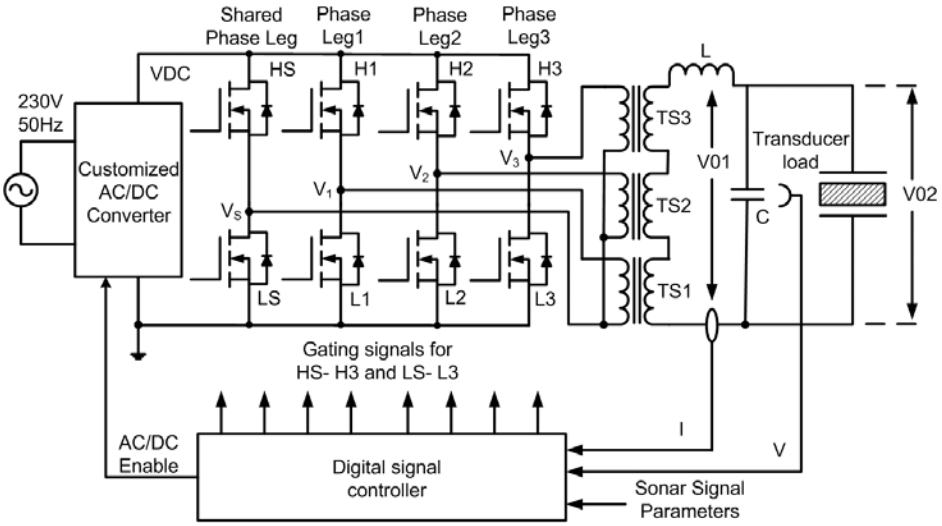

(a) Schematic of Multilevel shared leg SMPA

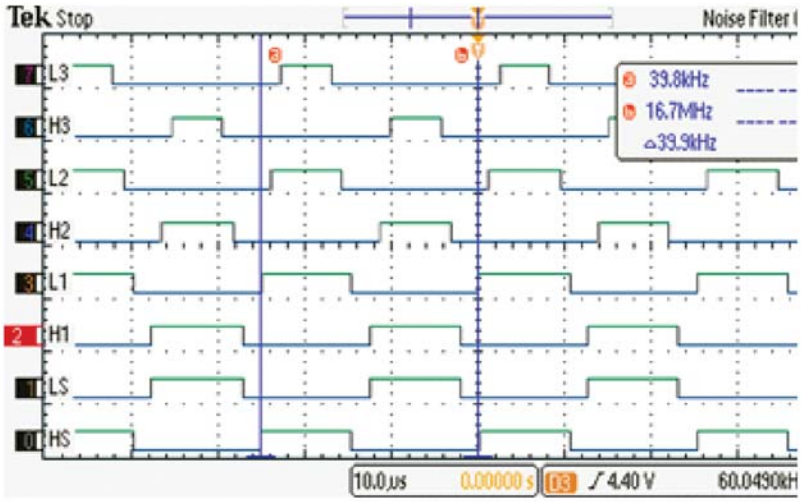

(b) Gating signals of Multilevel shared leg SMPA

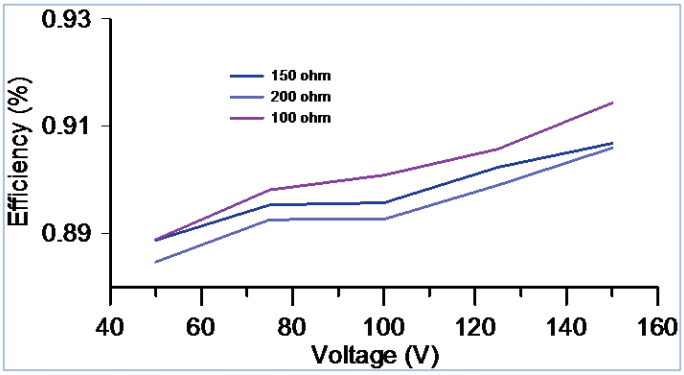

(c) Efficiency for different DC supply with three different loads

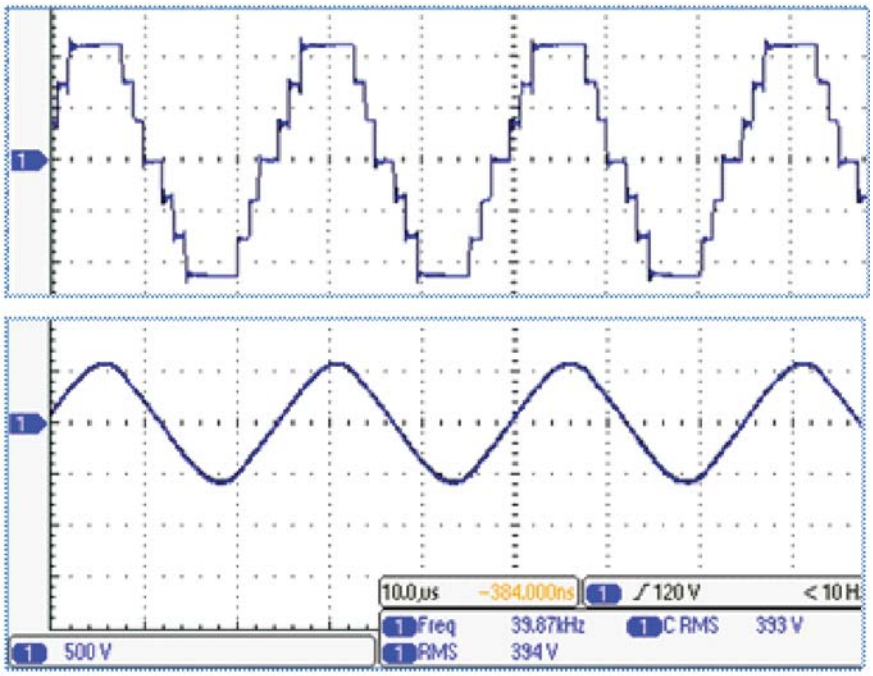

(d) 7 level output voltage (V_{01}) and load voltage (V_{02})

Fig. 9. Schematic of shared leg Multilevel SMPA with custom made AC-DC converter, gating signals for the devices in the system, efficiency plots and experimental output waveforms.

programmable AC-DC converter gives better performance at frequencies less than 10 kHz and power less than 5 kW applications. Multi-level converters can be configured to use as SPA at higher frequencies, where LPAs are widely used at present. Multilevel SMPA powered by a programmable AC-DC converter can be used for high power applications. The designer need to choose the appropriate class of power amplifier with suitable topology based on the requirement.

5. REFERENCES

[1] A. A. WINDER, 1975. Sonar System Technology, I*EEE Transactions on Sonics and Ultrasonics*, **22**(5), 291-331.

[2] A. D WAITE, 2002. *Sonar for practicing Engineers*, Wiley Publications.

[3] R. COATES and SCICHE, 2003. *The Sonar Course*, Seiche Technical Education.

[4] K. AGBOSSOU, J. DION, S. CARIGNAN, M. ABDELKRIM and A. CHERITI, 2000. Class D Amplifier for a Power Piezoelectric Load. *IEEE Transactions on Ultrasonics, Ferroelectrics, and Frequency Control*, **47**(4), 1036-1041.

[5] N. GHASEMI, F. ZARE, P. DAVARI, C. LANGTON, P. WEBER and A. GHOSH, 2012. Power Electronic Converters for High Power Ultrasound Transducers, *Proc. of ICIEA*., pp. 647-652.

[6] D. STANSFIELD, 1990. *Underwater Electro-acoustic Transducers*, Bath University Press.

[7] R. RAMESH, S. S. PILLAI, P. ABRAHAM and D. D. EBENEZER, 2009. Characteristics of Broadband Underwater Transducers Integrated with Tuning Coils and Cable. *Proceedings of SYMPOL*, pp. 33-138.

[8] T. L. FLOYD, 2005. *Electronic devices*, Prentice Hall, USA.

[9] N. MOHAN, T. M. UNDELAND and W. P. ROBBINS, 2010. *Power Electronics-Converters, Applications and Design*. John Wiley & Sons Inc., 200-217.

[10] V.N. PANCHALAI, B. P. CHACKO and N. SIVAKUMAR, 2016. Digitally controlled power amplifier for underwater electro acoustic transducers. *IEEE, International conference on Signal Processing and Integrated Networks* (SPIN), pp. 306-311.

[11] G. LIM, S.H. LIM and S.K. CHUNG, 2007. Digital control of phase-shifted full bridge PWM converter. *Proceedings of 7th Int. Conf. Power Electronics*, pp. 772-777

[12] H. CHO, H.W. SEONG, S.M. JUNG, J.S. PARK, G.W. MOON and M.J. YOUN, 2010. Implementation of digitally controlled phase shift full bridge converter for server power supply. *Proc. IEEE Energy Conversion Congress and Expo,* pp. 802-809.

[13] P. F. KOCYBIK and K.N. BATESON, 1995. Digital control of a ZVS full-bridge dc-dc converter. *IEEE, Proc. 10th Annual Applied Power Electronics Conf. and Expo*, pp. 687-693.

[14] N. GEORGE, V. N. PANCHALAI and E. SEBASTIAN, 2014. Digital Feedback Control of a Full-Bridge DC-DC Converter with Input Voltage Based Gain Scheduling' *IEEE, International Conference on Advances in Computing and Communications*, pp. 347-351.

[15] ANAND SREEKUMAR, V. N. PANCHALAI, B. P. CHACKO and P. THEKKATH, 2015. Multilevel converter for excitation of underwater transducers. *IEEE, International Conference on Advances in Computing, Communications and Informatics* (ICACCI), pp. 651-655.

[16] B. P. CHACKO, V. N. PANCHALAI and N. SIVAKUMAR, 2015. Multilevel digital sonar power amplifier with modified uni-polar SPWM. *IEEE International Conference on Advances in Computing, Communications and Informatics* (ICACCI), pp. 121-125.

Journal of Acoustical Society of India : Vol. 43, No. 4, 2016 (pp. 224-231)

Acoustic target tracking with a distributed bearing only measurement sensor field

P. Murali Krishna[1], Febi Ibrahim[1] and Lakshmi K. Raju[2]
[1]Naval Physical and Oceanographic Laboratory, Kochi, India
[2]School of Engineering, Kochi University of Science and Technology, Kochi, India
e-mail: muralikrishna@npol.drdo.in

[Received: 28-09-2016; Revised: 06-10-2016; Accepted: 13-10-2016]

ABSTRACT

In this paper, we analytically model a passive acoustic target tracking scenario with a distributed sensor field. Each sensor in the sensor field measures the relative bearing of the target with respect to a pre designated reference direction. The objective of this study is to study the performance of localization of the target and its subsequent tracking with bearing only measurements. The algorithm proposed for the sensor measurement fusion and subsequent tracking is the extended Kalman filter. The performance of the algorithm is evaluated through numerical simulations involving various scenarios. The algorithm performance as a function of sensor configuration, measurement noise and target track dynamics is reported in this paper.

1. INTRODUCTION

Tracking of a moving target has attracted considerable interest in both military and civilian applications. In this paper we investigate a method to track the target by using relative bearing measurements using a distributed sensor field[1]. The target of interest is assumed to radiate an acoustic signal whose direction of arrival is estimated independently at each sensor. The sensors themselves are modelled as independent with uncorrelated measurement errors which are deployed in an area of interest in any specific geometrical pattern. We assume that the positions of the sensors are known. These independent bearing measurements and sensor position information are used to localize and track the acoustic source. The extended Kalman filter (EKF) algorithm is used for sensor fusion based on the bearing measurements made at each sensor[2]. The paper is organized as follows.

In Section 2, the analytical model used in the study is described in detail. This will help to formalize the sensor fusion technique namely the EKF technique which is mentioned in section 3. The simulation results of the algorithm are presented in section 4. We conclude the paper in section 5 with a summary of the results and an overview of future extension of the work.

2. ANALYTICAL MODEL FOR DISTRIBUTED BEARING ONLY SENSOR FIELD MEASUREMENTS

The mathematical model for the distributed bearing measurement sensor field can be derived as follows. Consider a rectangular grid in the (X-Y) plane with a reference origin. Let there be N sensors which are

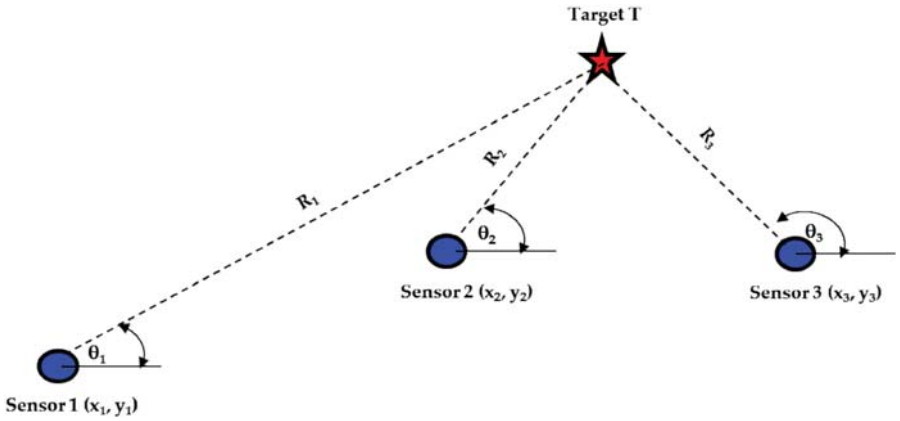

Fig. 1. Bearing only Measurement Sensor Field

distributed at locations (x_i, y_i), (i=1,…,N). Let the target be located at coordinates (x_T, y_T) and let R_i and θ_i be the distance and relative bearing between the target and theithsensor.

From the geometry depicted in Figure 1, we can write

$$x_T = x_i + R_i \cos \theta_i \quad (1)$$

$$y_T = y_i + R_i \sin \theta_i \quad (2)$$

In a practical sensor deployment scenario, typical geometrical configurations depicted in Figure 2 may be used[3]. The target is assumed to be within the sensor field.

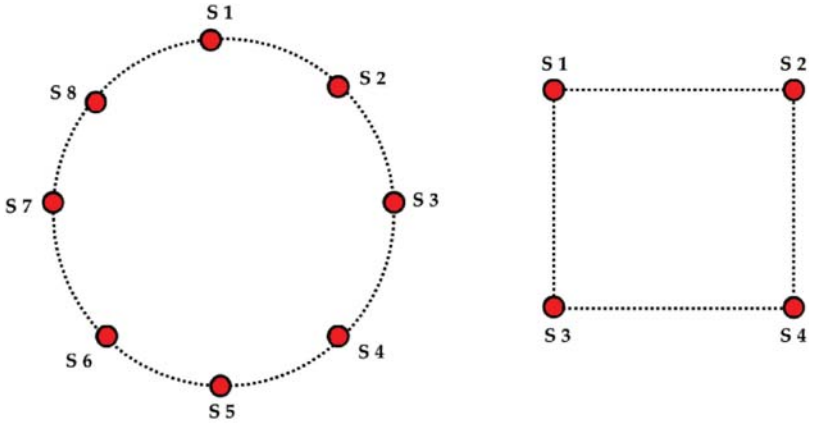

Fig. 2. Typical Sensor Deployment Geometry

3 EXTENDED KALMAN FILTER BASED SENSOR FUSION

We convert the target position estimation and tracking problem into one of a recursive state estimation. The recursive state estimation problem is solved by using a Kalman filter[4]. The Kalman filter is an optimal recursive processing algorithm that is used for sensor fusion. A useful feature of the Kalman filter is that it combines the currently available measurements and the prior knowledge about the system to estimate the underlying state in a minimum mean square error sense[5]. An extended Kalman filter is used when the process to be estimated and (or) the measurement relationship to the process is non-linear. The extended Kalman filter linearizes the non-linear functions by using the first order terms of Taylor's series approximations[6]. We are not deriving the EKF relations in this paper since the theory is well known and standard references are widely available for the same.

The state vector for the problem is given by the position and velocity coordinates of the target[7,8]. The target is assumed to move with uniform velocity in the x and y directions. The state vector for the target at the k^{th} instant is given by

$$X_k = [x_k y_k \dot{x}_k \dot{y}_k]^T \tag{3}$$

where (x_k, y_k) is the position coordinate of the source, $\dot{x}_k$ is the velocity of source in x direction and $\dot{y}_k$ is the velocity of source in y direction at k^{th} instant. The corresponding state transition equation is given by

$$X_k = FX_{(k-1)} + W_{(k-1)} \tag{4}$$

In equation (4), F is the state transition matrix given by

$$F = \begin{bmatrix} 1 & 0 & dt & 0 \\ 0 & 1 & 0 & dt \\ 0 & 0 & 1 & 0 \\ 0 & 0 & 0 & 1 \end{bmatrix} \tag{5}$$

where W_k is the process measurement noise with covariance matrix Q_k and dt is the time interval between the measurements. The measurements are given by the bearing angles at each sensor given by the relation

$$Y_k = \begin{bmatrix} \theta_1 \\ \theta_2 \\ \vdots \\ \theta_N \end{bmatrix} \quad H(X_k) + V_k = \begin{bmatrix} tan^{-1}\left(\frac{y_k - y_1}{x_k - x_1}\right) + v_k^1 \\ tan^{-1}\left(\frac{y_k - y_2}{x_k - x_2}\right) + v_k^2 \\ \vdots \\ tan^{-1}\left(\frac{y_k - y_N}{x_k - x_N}\right) + v_k^N \end{bmatrix} \tag{6}$$

The term V_k represent the measurement noise with covariance matrix R_k. The measurement noise terms $v^n{}_k$ are assumed to independent identically distributed Gaussian random variables. The coordinates (x_1, y_1) to (x_N, y_N) are the locations of the N angle measurement sensors. It can be seen that the measurement function H(.) is nonlinear and the Jacobian of H has to be computed for applying the EKF algorithm for target localization and tracking. For finding the Jacobian, the partial derivatives

$$\frac{\partial H^i}{\partial x_k}, \frac{\partial H^i}{\partial y_k}, \frac{\partial H^i}{\partial \dot{x}_k}, \frac{\partial H^i}{\partial \dot{y}_k} \quad \forall\ i \in \{1, 2 \ldots N\} \tag{7}$$

are to be computed. On evaluating the individual partial derivatives by using the chain rule for evaluating the derivative, we obtain

$$\frac{\partial H^i}{\partial x_k} = \frac{\partial\left(arctan\left(\frac{y_k - y_i}{x_k - x_i}\right)\right)}{\partial x_k} = -\frac{(y_k - y_i)}{(x_k - x_i)^2 + (y_k - y_i)^2} \tag{8}$$

$$\frac{\partial H^i}{\partial y_k} = \frac{\partial\left(arctan\left(\frac{y_k - y_i}{x_k - x_i}\right)\right)}{\partial y_k} = \frac{(x_k - x_i)}{(x_k - x_i)^2 + (y_k - y_i)^2} \tag{9}$$

$$\frac{\partial H^i}{\partial \dot{x}_k} = 0 \tag{10}$$

$$\frac{\partial H^i}{\partial \dot{y}_k} = 0 \tag{11}$$

The Jacobian of H is evaluated to obtain

$$J_H = \begin{bmatrix} -\dfrac{(y_k - y_1)}{(x_k - x_1)^2 + (y_k - y_1)^2} & \dfrac{(x_k - x_1)}{(x_k - x_1)^2 + (y_k - y_1)^2} & 0 \\ \vdots & \vdots & \vdots \\ -\dfrac{(y_k - y_N)}{(x_k - x_N)^2 + (y_k - y_N)^2} & \dfrac{(x_k - x_N)}{(x_k - x_N)^2 + (y_k - y_N)^2} & 0 \end{bmatrix} \tag{12}$$

The bearing measurements from the sensors at instant k is

$$Y_{meas} = \begin{bmatrix} \theta_k^1 & \ldots\ldots & \theta_k^N \end{bmatrix}^T \tag{13}$$

The state vector is updated as

$$X_k = \hat{X}_{\bar{k}} + K\left(Y_{meas} - Y_k\right) \tag{14}$$

where $\hat{X}_{\bar{k}}$ is the apriori state estimate (before the measurement was available) and K is the Kalman gain computed as[6]

$$K = \frac{P_k^- J_H(X_k)}{J_H(X_k) P_k^- J_H(X_k) + R_{\{k\}}} \tag{15}$$

with $P_{\bar{k}}$ being the prior covariance matrix. The covariance matrix is updated as[6]

$$P_k = P_k^- - K\left(J_H * P_k^- * J_H^T + R_{\{k\}}\right) K^T \tag{16}$$

4 SIMULATION RESULTS

In this section, we present the results of simulations. In the first case, we present the result in which an acoustic source is moving with a constant velocity from point (0, 0) to point (100, 100) on a straight path. There are four bearing measurement sensors positioned at the vertices of a quadrilateral which report the bearings to the fusion center. Based on the measurements, the EKF algorithm is able to localize and track the target movement. It is assumed that the bearing measurements are corrupted by zero mean Gaussian noise of standard deviation 2.23 degrees. Figure 3 illustrates the simulation results obtained with fixed sensor locations at coordinates (-10, 10), (-10, 110), (110, 110) and (110, -10).

Figure 4 illustrates the simulation results when the sensors are randomly located rather than being on the vertices of a quadrilateral. The coordinates of the sensors are randomly chosen from a uniform distribution in the interval [-100, 100]. It is seen that there is a slight delay in the convergence of the target track when compared to the earlier case. In a similar manner we also evaluated the behaviour of the algorithm with different initial conditions and concluded that there is no dependence on the choice of the initial condition. The EKF algorithm converges to the actual target track irrespective of the choice of the initial conditions or the sensor geometry.

However when one pair of sensors becomes collinear to the target, the algorithm diverges due to the non-observable nature of the measurement parameter. The divergence in such a case can be avoided by ignoring the bearing measurements from the corresponding sensors before fusion by the EKF. Figure 5 illustrate the

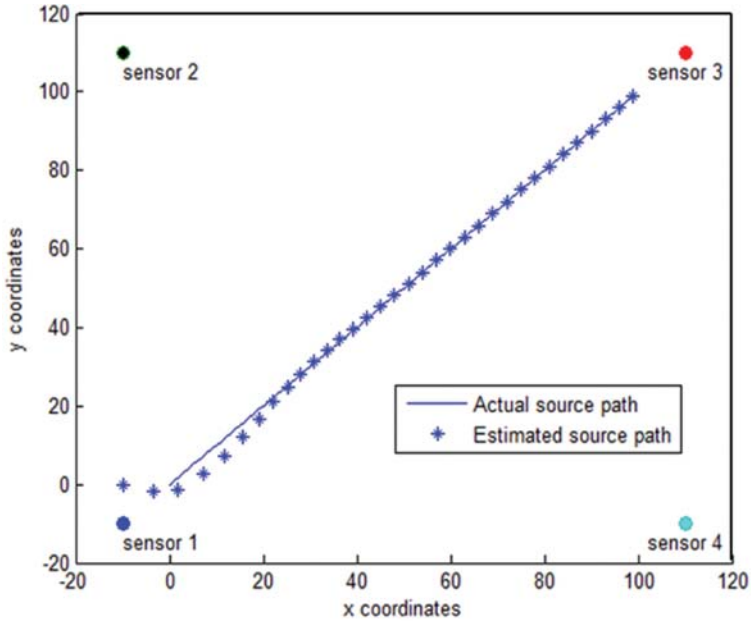

Fig. 3. Simulation Results:Linear Trajectory with Prefixed Sensor Positions

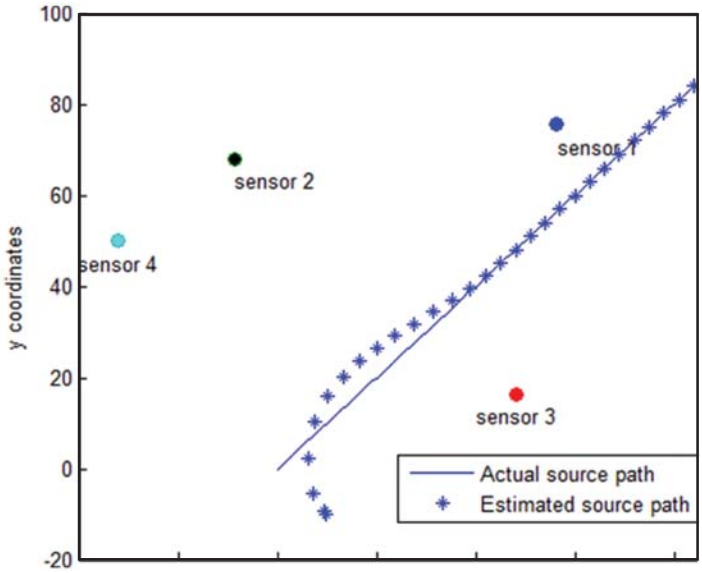

Fig. 4. Simulation Results: Linear Trajectory with Random Fixed Sensor Positions.

variation in the tracking performance as a function of the noise in the bearing measurements. To simulate the same, we have considered a case where the target trajectory is linear as described earlier and the individual bearing sensors are corrupted with noise having different standard deviations. The noise is assumed to be a Gaussian distribution with zero mean and standard deviations as indicated.

It is seen from the simulation results that the distributed tracking algorithm is able to converge for the varying levels of noise in the bearing measurements. There will be an initial transient phase in the tracking history where the estimation error will be likely increase. With the availability of more samples, the recursive estimator will converge as indicated in Figure 5. To understand the effect of target dynamics, we have also

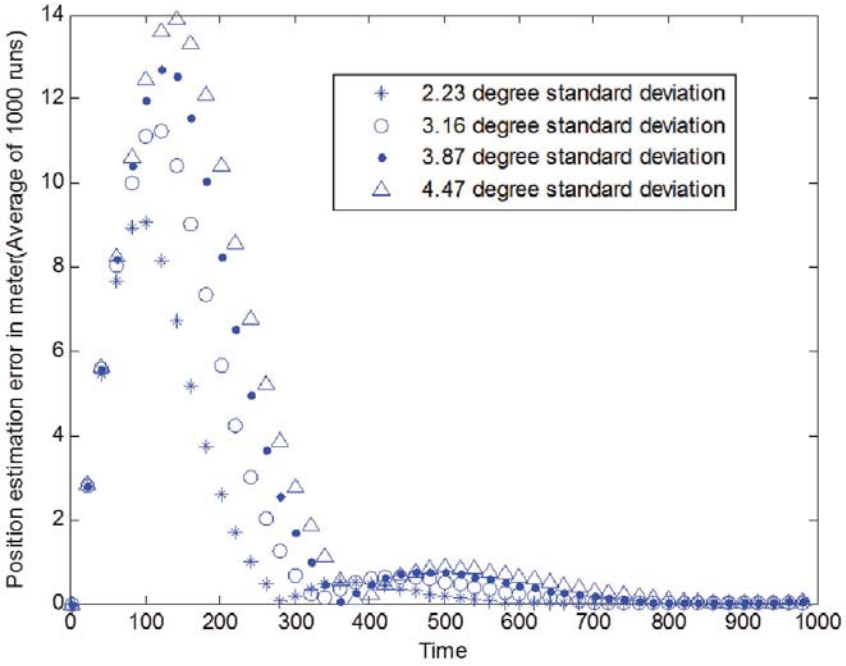

Fig. 5. Tracking Performance with Respect to Bearing Measurement Noise

simulated a scenario in which the target maneuvers sharply at right angles during the path. This case is presented in Figure 6 with sensor coordinates similar to Figure 3. It can be observed from the simulation results that the EKF algorithm has been able to localize and track the target trajectory with time varying dynamics. This result has verified the efficacy of the proposed method in tracking targets which have greater maneuverability with independent sensors. It is observed from the simulation result that there is an initial transient behavior for the tracking algorithm during the target maneuvers which stabilizes as the target reaches the geometric center of the sensor distribution. The target observability improves as it reaches the center of the sensor field and this is replicated in improvement in the tracking performance. The same results are observed with the random sensor deployment case also.

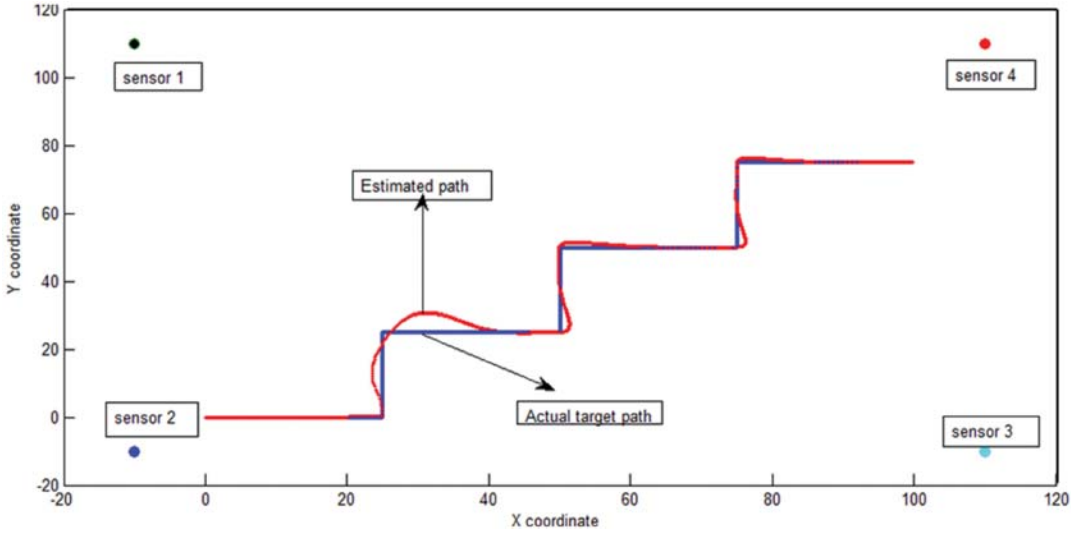

Fig. 6. Tracking Performance with Dynamic Target Trajectory.

As a final case, we consider the situation where each of the sensor executes a two dimensional random walk. This is similar to situations where the sensors might change their position due to drift / random movement in the environment due to various factors like ocean currents, wind *etc*. The results are depicted in Figure 7 where the standard deviation of the random walk parameter is taken as 1m in both *x* and *y* directions.

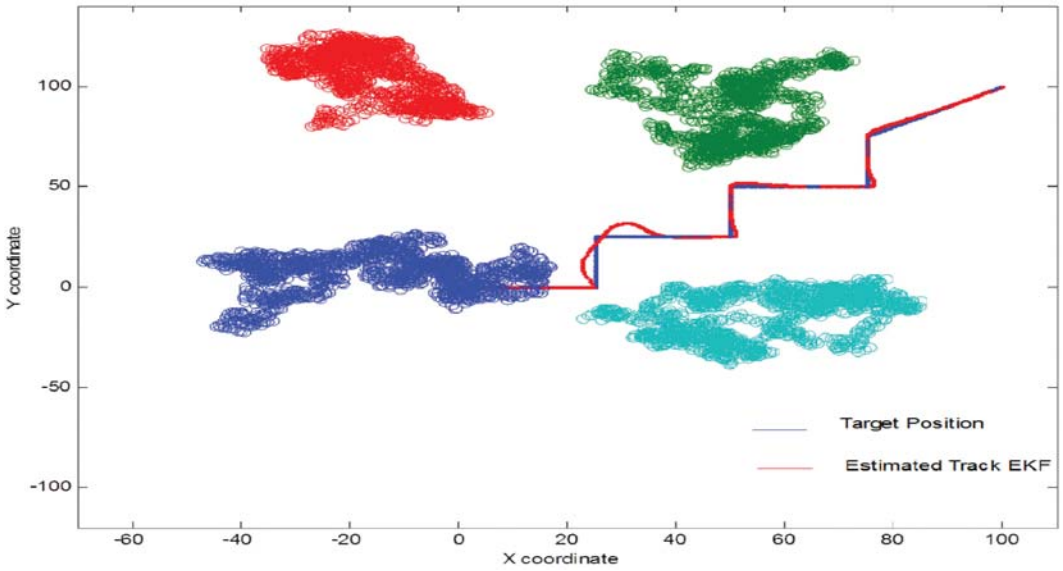

Fig. 7. Tracking Performance with Randomly Varying Sensor Position.

The results in Figure 7 indicate that the sensor perturbation does not affect the tracking performance of the algorithm. The initial transient behaviour is also more or less preserved. In order to illustrate the usefulness of the tracking algorithm, the variation of the tracking error in position for the perturbed sensor simulations is displayed in Figure 8. The tracking error is computed as the Euclidean distance between the estimated target position and the actual target position. In Figure 7, there are a total of six positions where the target course is changed in the course of the tracking simulation. The tracking error also exhibits transient behaviour at these six locations before converging to the steady state value.

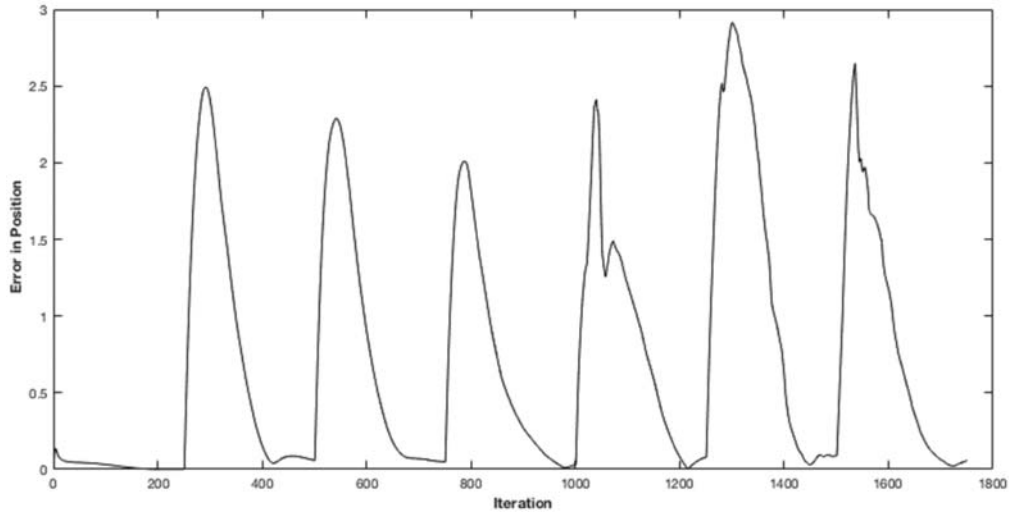

Fig. 8. Variation in Position Error with Dynamic Target Trajectory

From the results in tracking error performance, it is seen that the position error converges each time after the perturbation caused by the target manoeuvre. It can be concluded that the target tracking performance with distributed bearing sensors is consistently convergent.

5. CONCLUSIONS

In this paper, we have investigated the feasibility of distributed target localization and tracking of a target based on a sensor field of bearing only measurement sensors. It has been verified through simulations that such a technique can work with sensor fusion algorithm implemented by an extended Kalman filter. The effect of the measurement noise, the sensor geometry and target dynamics on the performance of the algorithm were also verified. The future work in this area includes the investigation on alternate nonlinear filtering and estimation techniques similar to the ones mentioned in[9] for distributed sensing and information fusion. The analytical treatment of the random walk sensor perturbation model and the analysis of a distributed sensor network in active mode of operation is also a possible area of theoretical work.

6. ACKNOWLEDGEMENT

The authors would like to acknowledge with gratitude the support given to this work by Sri. S. K. Shenoy, Director NPOL. We would like to thank Dr. D.D. Ebenezer, Associate Director, NPOL and the reviewers for their suggestions. The help and support of the HRD cell of NPOL for availing speedy sanction for publishing this work is also acknowledged.

7. REFERENCES

[1] A. FARINA, 1999. Target Tracking with Bearings Only Measurements. Signal Processing **78**, 61-78.

[2] K. SPINGARN, 1987. Passive Position Location Estimation Using the Extended Kalman Filter. *IEEE Transactionson Aerospace and Electronic Systems*, **23**, 558-567.

[3] CHUN YANG, ERIK BLASCH and IVAN KADAR, 2009. Geometric Factors in Target Positioning and Tracking. *12th International Conference on Information Fusion*. 85-92

[4] Y. BAR-SHALOM and X.R. LI, 1993. Estimation and Tracking: Principles,Techniques, and Software, Artech House, Norwood.

[5] R. FARAGHER, 2012. Understanding the Basis of the Kalman Filter via a Simple and Intuitive Derivation. *IEEE Signal Processing Magazine*, 29(5), 128-32

[6] P. S. MAYBECK, 1982. Stochastic Models, Estimation and Control, Academic Press, New York.

[7] D.J.TORREIERI, 1984. Statistical Theory of Passive Location Systems. *IEEE Trans.Aero and Electronic Systems,* **20**(2), 183-198.

[8] M.GAVISH and A.J.WEISS, 1992. Performance Analysis of Bearing only Target Location Algorithms. *IEEE Transactions on Aerospace and Electronic Systems*, **28**(3), 817-828.

[9] A. DOUCET, J.F.G DE FREITAS and N.J.GORDON, 2001. Sequential Monte Carlo Methods in Practice, Springer Verlag, New York

Journal of Acoustical Society of India : Vol. 43, No. 4, 2016 (pp. 232-238)

A cyclic feature based detector for intercept sonar signal processing

Febi Ibrahim and R. Pradeepa
Naval Physical and Oceanographic Laboratory, Kochi 682021, India
e-mail: febi@npol.drdo.in

[Received: 29-09-2016; Revised: 05-10-2016; Accepted: 13-10-2016]

ABSTRACT

Intercept sonar systems are used to detect the active transmissions of a target and estimate the parameters of the detected active transmissions. Traditional approaches for the detection of unknown pulsed signals, as in the case of intercept sonar, are based on energy detectors. The drawback of energy detector based methods is that they do not differentiate between modulated signals, noise and interference. Intercept signals are typically modulated. Hence they could be more appropriately modelled as cyclostationary signals. The objective of this work is to study the applicability of cyclostationarity based signal processing for intercept sonar detection and estimation problem. In this paper, a cyclic feature based detector is designed and analysed for the detection of various pulsed sonar signals. The cyclic feature used here is the frequency smoothed spectral correlation density estimate of the received signal. The benchmarking is done by comparing the Receiver Operating Characteristic (ROC) of the proposed detector with that of Channelized Radiometer (CR), a popular energy measurement based detector. The simulation results show the improved detection performance of the cyclic feature based detector compared to CR detector.

1. INTRODUCTION

The fundamental objective of intercept sonar is to detect a target using its active transmissions for detection or homing. These systems operate in passive mode. The intercept sonar provides early warning to the sonar operator. This is possible since the signal received by the intercept sonar undergoes only a one way propagation loss. Intercept sonars are also useful for detection of homing signals from torpedoes. Efficient detection and estimation algorithms are required to meet the functional objectives of intercept sonar.

Traditional approaches to detection and estimation processing in intercept sonar are based on energy measurements. These methods are collectively called as *radiometric* techniques. The most commonly used and popular energy detector is the FFT filter bank energy detection scheme also known as *Channelized Radiometer*[1,2]. The drawback of energy detector based methods is that they do not differentiate between modulated signals, noise and interference. Intercept signals are typically modulated. Hence they could be more appropriately modelled as cyclostationary random processes[3]. Cyclostationarity based detectors rely on the structural properties of the signal[4]. Therefore the applicability of cyclostationarity based detector and estimator for intercept sonar signal processing is explored in this paper.

The detection problem in intercept sonar is similar to the spectrum sensing problem in cognitive radio system. A cognitive radio system provides opportunistic spectrum access to the secondary users in the

absence of the primary users through the process of spectrum sensing. Cyclic feature detection based on the cyclostationary property of the signal is used extensively in cognitive radio spectrum sensing[5]. In intercept sonar also the role of the signal processor is to identify the presence of the active transmission of the opponent passively and hence provide early warning. Therefore we consider the development of a cyclic feature based detector for intercept sonar.

The main contribution of this paper is that cyclostationary property of various sonar signals is observed and a suitable method for estimating the cyclic feature of the pulsed signal is identified. A cyclic feature based detector implementation is proposed. Simulation results show that the detector outperforms the CR detector.

In the next section, the system model is explained. In section 3, a brief description of CR detector and its realization for real world scenario is provided. In section 4 a brief description of cyclostationary signal processing is given. In section 5 the design of detector based on cyclic feature is presented. Simulation results and conclusion are given in section 6 and 7 respectively.

2. SYSTEM MODEL

Let X_k be the observation made at the intercept sonar at time index k. Here X_k will be the output time series of a beam data after spatial filtering. The samples X_k, $k \geq 1$ are independent and identically distributed (IID) under hypothesis H_0. The observations are drawn either from a distribution that belongs to hypothesis H_0 (target absent) or from a distribution that belongs to hypothesis H_1 (target present). Thus,

$$H_0 : X_k = N_k,\ k = 0, 1, \ldots, N-1$$
$$H_1 : X_k = S_k + N_k,\ k = 0, 1, \ldots, N-1 \quad (1)$$

where S_k is the active transmission from the target and N_k is the observation noise at the intercept sonar receiver at time index k. Let N be the number of observations (can be fixed depending on the maximum expected pulse length) used to make a decision (target present or absent) at the intercept sonar.

The objective of the intercept sonar processing system is to determine whether H_0 or H_1 is true. The intercept signal S_k is a modulated signal but has traditionally been modeled as a stationary random process. S_k could be more appropriately modeled as cyclostationary. The cyclic feature of S_k will be unique for different modulation types. The objective is to determine the best approach (stationary or cyclostationary) for detection and estimation purposes. The intercept signal S_k can be any active transmission from a target and the most commonly used signals are *pulsed continuous wave* (PCW) and *pulsed linear frequency modulation* (PLFM). The expressions for PCW and PLFM are

$$S_k = \cos(2\pi f_c\, kT_s),\ k = 0, 1, \ldots, N-1, \quad (2)$$

and

$$S_k = \cos[2\pi(f_c kT_s + 0.5\, mk^2\, T_s^2)],\ k = 0, 1, \ldots, N-1, \quad (3)$$

respectively, where T_s is the sampling time, f_c is the carrier frequency, and m is the sweep rate.

3 CHANNELIZED RADIOMETER

The input signal for intercept sonar is the active transmission of a target which is an unknown pulsed signal and the Generalized Likelihood Ratio Test (GLRT) based detector is energy detector. The most popular energy detector is the Channelized Radiometer (CR)[1]. The CR detector integrates the energy contained in the frequency band of interest to the sonar[2]. The operation of the channelized radiometer is as follows. The data is segmented into overlapping blocks of fixed size and the FFT is computed. The FFT output is magnitude squared and exponentially averaged[6]. The averaged output is peak picked across FFT bins and normalized using Split Two Pass Mean (STPM) normalization algorithm[7]. STPM algorithm normalizes the ambient noise in the real world scenario. The peak of the normalized energy output is the test statistic or decision statistic. The decision statistic is compared with a threshold, which is computed for the desired P_{FA} to make a decision whether only noise or noise plus unknown active transmissions from targets are present. The block diagram of the channelized radiometer is given in Fig. 1.

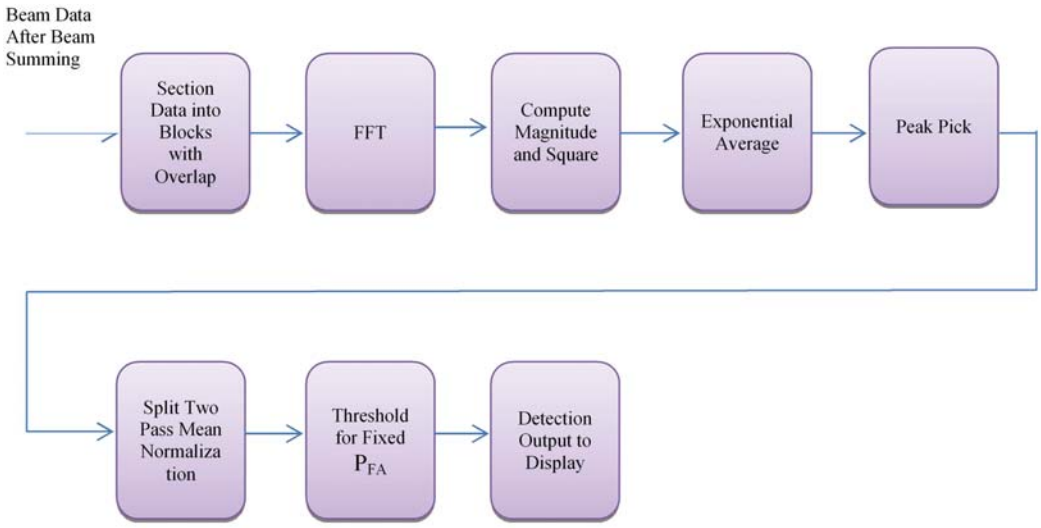

Fig. 1. Block diagram of CR detector for implementation.

The standard methods of interception based on energy measurement collectively called as *radiometric* techniques are susceptible to changing noise background and interferences. These methods do not consider the structure of modulated signals which is the case for intercept sonar input signals. The modulated signals typically involve one or more periodicities due to the sine wave carriers. This structure of modulated signal is exploited in a detector based on cyclostationarity[8].

4 CYCLOSTATIONARY SIGNAL PROCESSING

Cyclic Spectrum: A process *x(t)* is almost cyclostationary in the wide sense, if its Cyclic Autocorrelation Function (CAF), $R_x^{\alpha}(\tau)$, is not zero for some nonzero frequency α, called the cyclic frequency[3]. The CAF is defined as,

$$R_x^{\alpha}(\tau) = lim_{T\to\infty} \frac{1}{T}\int_{-T/2}^{T/2} R_x(t + \frac{\tau}{2}, t - \frac{\tau}{2}) e^{-j2\pi\alpha t} dt, \tag{4}$$

where $R_x(t + \frac{\tau}{2}, t - \frac{\tau}{2})$ is the autocorrelation function. If the process *x(t)* is cycloergodic (assumed henceforth) the CAF is,

$$R_x^{\alpha}(\tau) = lim_{T\to\infty} \frac{1}{T}\int_{-\frac{T}{2}}^{\frac{T}{2}} x\left(t + \frac{\tau}{2}\right) x^*\left(t - \frac{\tau}{2}\right) e^{-j2\pi\alpha t} dt. \tag{5}$$

The Fourier transform of the CAF is called the Cyclic Spectrum, defined as,

$$S_x^{\alpha}(f) \triangleq \int_{-\infty}^{+\infty} R_x^{\alpha}(\tau) e^{-j2\pi f\tau} d\tau. \tag{6}$$

Measurement of Spectral Correlation Density (SCD) Function : The interpretation of cyclic spectrum as a SCD function arises from the fact that it is obtainable from the operations (limit of spectrally smoothed products of spectral components) described by the expression,[9]

$$S_x^{\alpha}(f) = lim_{\Delta f\to 0} lim_{\Delta t\to\infty} \frac{1}{\Delta f}\int_{f-\frac{\Delta f}{2}}^{f+\frac{\Delta f}{2}} \frac{1}{\Delta t} X_{\Delta t}(t, \upsilon + \frac{\alpha}{2}) X_{\Delta t}^*(t, \upsilon - \frac{\alpha}{2}) d\upsilon \tag{7}$$

where $X_{\Delta t}$ is the Fourier transform of a segment of $x(t)$ of length Δt and Δf is the width of the spectral smoothing interval.

Frequency Smoothing Method for Estimating SCD : The signal of interest to intercept sonar is the active transmissions of target. These signals are typically pulsed. The signal block length N, which is used for processing should contain the entire transmitted pulse inorder to estimate the signal's cyclic feature correctly.The estimation of SCD using discrete-frequency smoothing method is done by the following expression,

$$S_x^{\alpha}(t,f)_{\Delta f} = \frac{1}{M}\sum_{\upsilon=\frac{M-1}{2}}^{\frac{M-1}{2}} \frac{1}{\Delta t} X_{\Delta t}(t, f+\upsilon F_s+\frac{\alpha}{2}) X_{\Delta t}^{*}(t, f+\upsilon F_s-\frac{\alpha}{2}) \tag{8}$$

where

$$X_{\Delta t}(t,f) \triangleq \sum_{k=0}^{N-1} x(t-kT_s) e^{-j2\pi f(t-kT_s)},$$

which is the output of a sliding DFT. Δt is the duration of the data segment which contains N number of time samples. Ideally, when the input signal is pulsed transmission, Δt should be chosen as the pulse length or if pulse length is unknown as in the case of intercept sonar Δt can be made equal to the maximum pulse width expected. $\Delta f = MF_s$ is the width of the spectral smoothening interval, M is the number of frequency samples used for spectral smoothening and $F_s = \frac{1}{NT_s}$ is the frequency sampling increment. T_s is the time sampling increment. The SCD of a LFM pulse with carrier frequency f_c=6 kHz and bandwidth = 500 Hz is given in Fig. 2. From Fig. 2 it can be seen that the peaks along the cycle frequency α=0 axis is the *power spectral density* (PSD) of the waveform and the peaks along the α axis occurs at twice the carrier frequency.

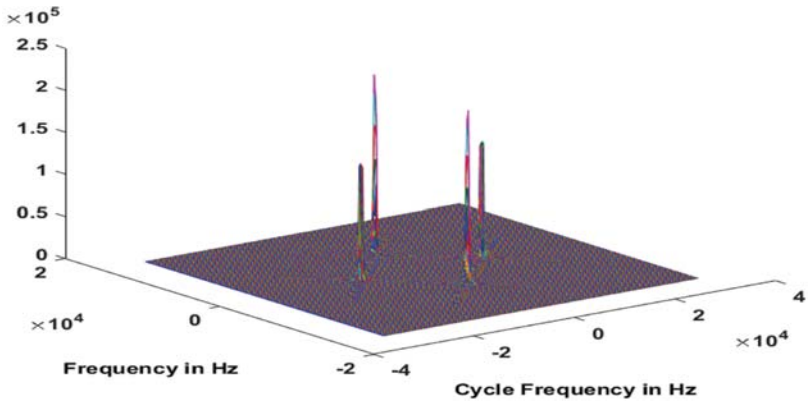

Fig. 2. SCD for pulsed LFM using frequency smoothening.

5. CYCLIC FEATURE BASED DETECTOR

The estimate of the SCD of the received signal can be mapped from the $f \sim \alpha$ bifrequency plane to the α axis through the following expression,

$$I_x(\alpha) = max_f \left| S_{x_{\Delta t}}^{\alpha}(t,f)_{\Delta f} \right|. \tag{9}$$

$I_x(\alpha)$ can be regarded as the SCD of a signal at the cycle frequency domain and is called the Cycle Frequency Domain Profile (CDP). The CDP is a cyclic feature of the modulation contained in the signal. The CDP of a

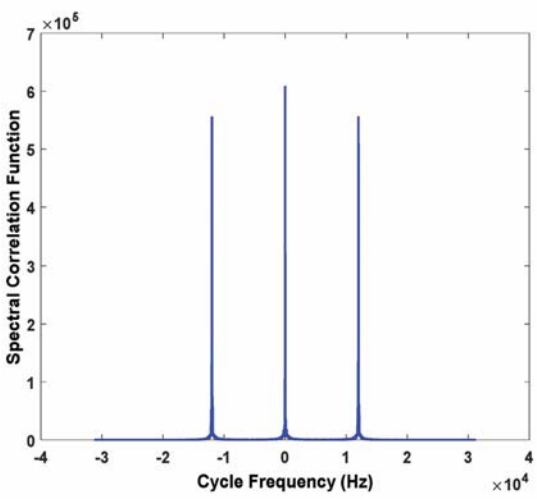

Fig. 3. CDP for pulsed CW.

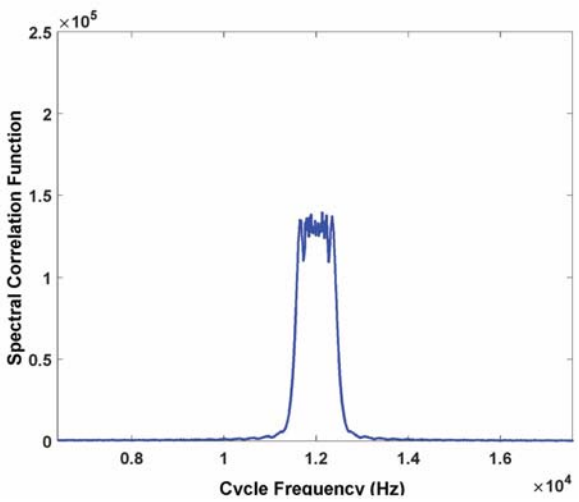

Fig. 4. . CDP for pulsed LFM.

Pulsed Continuous Wave (PCW) and Linear Frequency Modulated (LFM) signal are given in the Fig. 3 and Fig. 4 respectively.

The PCW signal has a significant cycle frequency at $\alpha_0 = 2f_c$, where f_c is the carrier frequency. For the pulsed LFM signal the cycle frequencies extend over twice the signal bandwidth. From Fig. 4 it can be seen that the cycle frequency peaks from 11.5 kHz to 12.5 kHz since the bandwidth of the LFM pulse used for simulation is 500 Hz and f_c is 6 kHz. The type of modulation, carrier frequency and signal bandwidth can be estimated easily from the CDP.

The most significant cycle frequency is used for making a decision. The decision metric of the cyclic feature based detector is obtained by,

$$T = max_{\alpha} I_x(\alpha). \tag{10}$$

The decision rule is given by,

$$T \geq \gamma, \text{ Decide } H_1,$$
$$T < \gamma, \text{ Decide } H_0,$$

where γ is the threshold fixed to achieve the desired P_{FA}. The noise is assumed to be Gaussian distributed. The received signal is normalized by subtracting the sample mean and dividing with the sample standard deviation. The resulting noise will be standard Gaussian.

Using Monte Carlo simulation the Probability Density Function (pdf) of the noise at the output of the cyclic feature based detector can be estimated. From this pdf the threshold γ required for achieving the desired P_{FA} can be obtained.

In real world situations, the received signal is normalized by its empirical power estimate. This is similar to passing the signal through an *Automatic Gain Controller* (AGC), which is tuned such that its output is normalized to unit power.

6. SIMULATION RESULTS

In this section the results of Monte Carlo simulation of two detectors - CR and cyclic feature detector are presented. The detectors are compared by generating ROC. In order to compute ROC the probability of detection P_D is obtained for different Signal to Noise Ratios (SNR) by fixing a desired P_{FA}. The P_D is computed by generating many sample paths of the received signal for an intercept sonar such that sufficient samples of detection statistics are obtained. The generated detection statistics are compared with the threshold which corresponds to the set P_{FA}.

The P_{FA} is fixed as 0.01and the corresponding threshold is obtained. The signal considered for computing ROC is pulsed LFM with f_c = 6 kHz and 500 Hz bandwidth. A data segment with N = 2048 samples is used. The width of the spectral smoothing interval M is chosen as 10. In Fig. 5, the ROC of the cyclic feature detector and CR detector are plotted. In the simulations cyclic feature detector was found to perform better than CR.

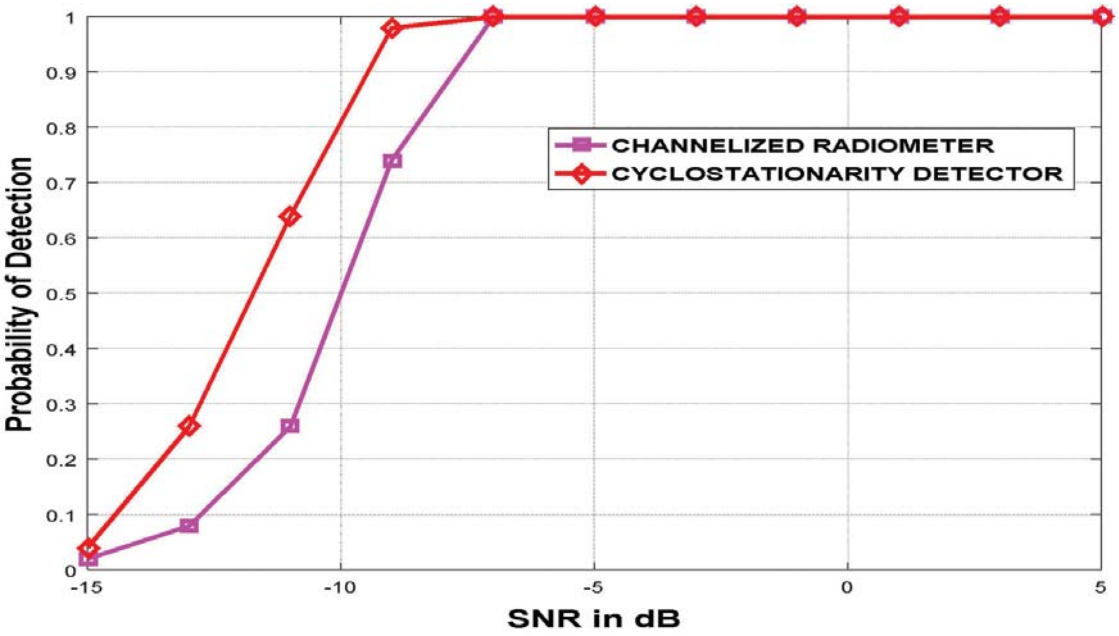

Fig. 5. ROC.

The proposed detector was tested on the captured field trial database and the detector outperformed the CR detector. The CDP of an intercepted pulse in the database is shown in Fig. 6. From Fig. 6 it can be seen that the intercepted signal is an LFM pulse.

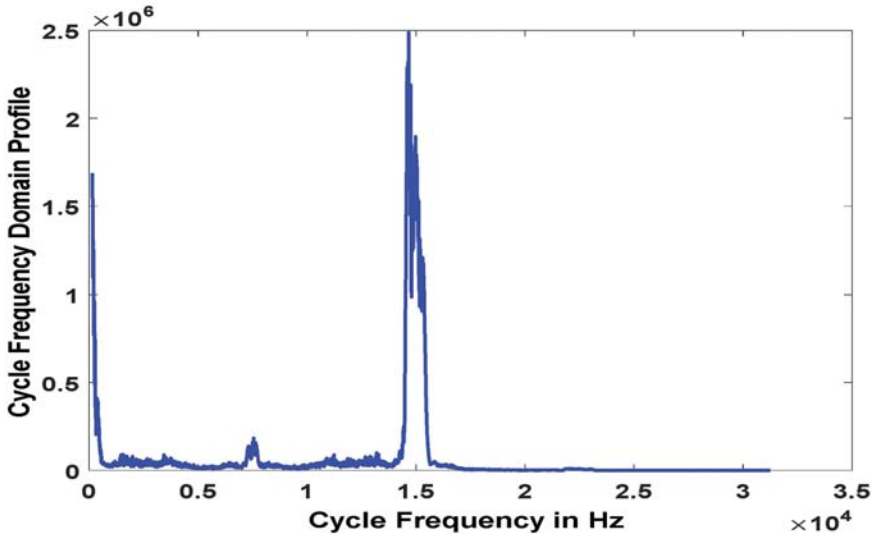

Fig. 6. CDP of intercepted pulse.

7. CONCLUSIONS

The problem of detecting the active transmissions of a target in intercept sonar using a cyclic feature detector is considered. The proposed detector exploits the cyclostationary nature of the received signal in intercept sonar. In the simulation study the performance of the cyclic feature detector was compared with the CR detector. The ROCs for different SNR were plotted using Monte Carlo simulations. The proposed detector was tested on the data collected in the field trials and was seen to outperform CR detector. The drawbacks of the cyclic feature detector compared to CR detector are higher computational and memory requirements, but with the advent of high speed digital signal processors the proposed detector is a strong candidate for intercept sonar detection processing.

8. ACKNOWLEDGEMENT

The authors would like to acknowledge with gratitude the support given to this work by Director NPOL.

9. REFERENCES

[1] J. J. LEHTOMAKI, 2005. CFAR Strategies for Channelized Radiometer. *IEEE Signal Processing Letters*. **12**(1), 13-16.

[2] A.V. KANTAK, 1993. Frequency-Hopping Signal Detection Using Partial Band Coverage. *IEEE Transactions on Aerospace and Electronic Systems.* **29**(2), 540-553.

[3] W.A. GARDNER, 1990. Introduction to Random Processes with Applications to Signals and Systems, McGraw-Hill, New York.

[4] E. AXELL, 2012. Spectrum Sensing for Cognitive Radio: State-of-the-Art and Recent Advances. *IEEE Signal Processing Magazine*. **29**(3), 101-116.

[5] B. RAMKUMAR, 2009.Automatic Modulation Classification for Cognitive Radios Using Cyclic Feature Detection. *IEEE Circuits and Systems Magazine*. **9**(2), 27-45.

[6] R.G. LYONS, 2012. *Understanding Digital Signal Processing*. Pearson, India.

[7] R.O. NIELSON,1991. *Sonar Signal Processing.* Artech House Publishers, Norwood, US.

[8] W.A. GARDNER, 1991. Exploitation of Spectral Redundancy in Cyclostationary Signals. *IEEE Signal Processing Magazine.* **8**(2), 14-36.

[9] W.A. GARDNER, 1986. Measurement of Spectral Correlation. *IEEE Transactions on ASSP*. **34**(5), 1111-1123.

Journal of Acoustical Society of India : Vol. 43, No. 4, 2016 (pp. 239-246)

Sonar target tracking using suboptimal joint probabilistic data association

Anila John, Sarath Gopi and E.N. Sreedavy
Naval Physical and Oceanographic Laboratory, Kochi
e-mail: anilajohn@npol.drdo.in

[Received: 26-09-2016; Revised: 14-10-2016; Accepted: 19-10-2016]

ABSTRACT

Simultaneous tracking of multiple sonar targets is often required in the dense environment of present day underwater surveillance scenario. In this paper we consider tracking of active sonar targets. The inputs to the tracking system are the range and bearing measurements of the detected targets. Heavy clutter and high false alarm rate renders the measurement origins uncertain. This makes it necessary to have efficient data association schemes augmented with tracking algorithms for auto tracking of targets. A computationally efficient and hence implementable solution for this problem is sought in this paper. Probabilistic Data Association (PDA) techniques have been widely used for tracking applications. A variant of PDA, Joint Probabilistic Data Association Filter (JPDAF) is an algorithm for multi-target tracking. However, JPDAF is computationally intractable. We have implemented the Suboptimal Joint Probabilistic Data Association Filter for tracking of active sonar targets and performance was evaluated. The algorithm was evaluated in the underwater test facility UARF of NPOL.

1. INTRODUCTION

Systems such as Harbour Protection Surveillance Sonar are used round the clock and it is better to use automatic methods than rely on operator intervention. Automatic detection and tracking requires association of the present locations of the targets to the existing tracks to update the track. Many different data association techniques are used in multiple target tracking systems ranging from the simple nearest neighbour approach to the very complex Multiple Hypothesis Tracker (MHT). The performances of the simpler techniques degrade in clutter. The more complex MHT provides a large number of hypotheses to be maintained, which requires extensive computational resources. Because of these difficulties, recursive algorithms having smaller computational requirements were developed. These techniques are based on Probabilistic Data Association (PDA), which uses a weighted average of all the measurements falling inside a track's gating region at the current time to update the track state.

Bar-Shalom and Tse developed the first PDA algorithm, called the Probabilistic Data Association Filter (PDAF), to track a single target in clutter[1]. The PDAF was then extended to the multi target case by Bar - Shalom, resulting in the Joint Probabilistic Data Association Filter[2]. The suboptimal JPDAF is a suboptimal but computationally tractable implementation of JPDAF[3].

2. PROBABILISTIC DATA ASSOCIATION FILTER (PDAF)

The standard discrete linear model[4] in tracking is given by the state equation

$$x_{k+1} = F\, x_k + v_k \tag{1}$$

and measurement equation

$$z_k = H\, x_k + w_k \tag{2}$$

x_k is the target state vector at k^{th} time index and consists of the position and velocity of the target. F is the state transition matrix which models the change in the state of the target over time. v_k is the process noise arising due to inaccuracy in our system model. In Eqn. (2), z_k represents the target measurements, which consists of the range and bearing of the target and H is the measurement matrix which connects the target state and the measurement. The measurement noise is represented as w. The process and measurement noises are assumed independent, white, and Gaussian with covariance matrices

$$E(v_k\, v_k^{\,T}) = Q_k \tag{3}$$

$$E(w_k\, w_k^{\,T}) = R_k \tag{4}$$

In Multi Target Tracking (MTT) systems, the value of the measurement in the present time scan is predicted using the system model in Eqns (1) and (2) and a validation region is constructed around the predicted measurement for each track. Due to the random noise in the measurement process, the actual measurement and the predicted measurement do not coincide. The validation region is that region about the predicted measurement, where actual target originated measurement is likely to be found with a specified probability. A measurement z will be in the validation region of track with state vector x_k, if , $\left(z - \hat{z}\right)^T R_k^{-1} \left(z - \hat{z}\right) \leq g^2$ where $\hat{z}$ is the predicted measurement using Eqns (1) and (2) and g is constant determined from χ^2 table[2] for the gate probability PG. PG is a predetermined value which is usually chosen to be greater than 0.95. If a measurement falls inside the validation region, it becomes a candidate for association to the track. Otherwise it is not considered as an association candidate. Once the validated measurements are calculated, multi target tracking is done using Joint Probabilistic Data Association Filter (JPDAF). JPDAF is built upon the probabilistic data association filter which is used for single target tracking.

The PDAF is a Bayesian approach that computes the probability that a measurement in a track's validation region is the correct measurement or not. These probabilities are called *association probabilities.* All the valid measurements and their corresponding association probabilities are used in a state estimator (see Eqn. 9) in the PDAF to update the target state. The PDAF assumes that

1. a single target is present.
2. a track exists for the target (*i.e.* the track has been initialised).
3. at most one of the measurements is target originated
4. any other validated measurement is a clutter detection
5. the non-target originated measurements are modelled as random interference.

The PDAF algorithm is briefly outlined below. For m measurements falling inside the validation region at time t_k, the probability that the j^{th} validated measurement $z_j\,(k)$ is target originated, denoted β_j, is

$$\beta j = \frac{e_j}{b + \sum_{l=1}^{m} e_l} \quad j = 1, \ldots, m \tag{5}$$

while the probability that none of the measurements is target originated, denoted β_0, is

$$\beta_0 = \frac{b}{b + \sum_{l=1}^{m} e_l} \quad j = 1, \ldots, m \tag{6}$$

The term e_j is given by

$$e_j = exp\{-0.5\nu_j^T(k)S^{-1}(k)\nu_j(k)\} \tag{7}$$

where $\nu_j(k)$ is the residual for the j^{th} validated measurement and $S(k)$ is the residual covariance for the measurements. All the measurement residuals are assumed to have the same covariance. The term b is given by

$$b = \lambda\sqrt{det2\pi S(k)}\frac{1-P_D P_G}{P_D} \tag{8}$$

where P_D is the probability of detection.
The state in the PDAF is updated using all of the validated measurements. The updated state is given by

$$\hat{x}_{k/k} = \hat{x}_{k/k-1} + K(k)v(k) \tag{9}$$

where $\hat{x}_{k/k-1}$ is the predicted state using k-1 measurements and $\hat{x}_{k/k}$ is the updated state using all k measurements, $K(k)$ is the Kalman gain, and $\nu(k)$ is the combined residual, which is given by

$$v(k)=\sum_{j=1}^{m}\beta_j v_j(k) \tag{10}$$

where the residual for the j^{th} validated measurement $\nu_j(k)$ is,

$$\nu_j(k) = z_j(k) - H\hat{x}_{k/k-1} \tag{11}$$

The updated covariance is given by

$$P(k/k) = \beta_0 P(k/k-1) + (1-\beta_0)P^c(k) + \tilde{P}(k) \tag{12}$$

where

$$P^c(k)=P(k/k-1) - K(k)S(k)K^T(k) \tag{13}$$

and

$$\tilde{P}(k)=K(k)\left[\sum_{j=1}^{m}\beta_j v_j(k)v_j^T(k) - v(k)v^T(k)\right]K^T(k) \tag{14}$$

The PDAF assumes that a target track exists and a track is neither formed nor deleted. Therefore, separate logic has to be incorporated with PDAF for initiation and termination of target tracks.

3 JOINT PROBABILISTIC DATA ASSOCIATION FILTER (JPDAF)

The JPDAF is the extension of the PDAF to the multi-target case[2]. The JPDAF is the same as the PDAF except for the computation of the association probabilities. The measurement-to-track association probabilities are computed jointly across all targets and all validated measurements. JPDAF assumes that

1. there is a known number of targets with existing tracks (*i.e.* all the tracks have been initialised)
2. a target can generate at most one measurement per scan
3. a measurement could have originated from utmost one target
4. the non-target originated measurements are modelled as random interference.

The JPDAF first enumerates all feasible joint association events θ in the current scan. A feasible joint association event is a set of non-conflicting measurement-track pairs. This means that a feasible joint event is one in which a measurement is considered to be originated from only one target, and at most one measurement originates from a target. Any number of measurements can originate from clutter. Consider the conflicting association situation illustrated in figure 2. Here measurement M_2 falls in the validation region of both targets T_1 and T_2. But we will consider only those association events in which M_2 is attached to either T_1 or T_2 or not both.

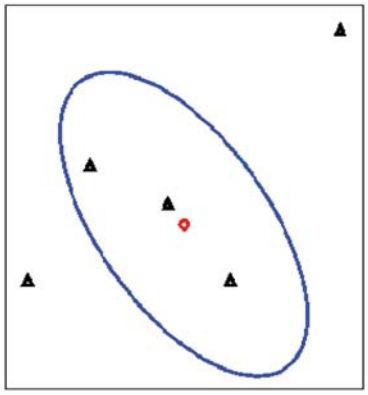

Fig. 1. Validation region for a single target with measurements of uncertain origin

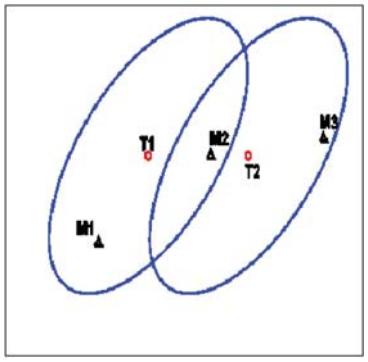

Fig. 2. Validation region for two targets with measurements of uncertain origin

Table 1 lists the eight feasible joint association events θ for figure 2. The $\theta_{t,j}$' s are the single events making up a joint event θ. Here, $\theta_{t,j}$ denotes the single event that measurement $j(j = 1, ..., m)$ originated from target $t(t = 0, ..., N)$, where m is the total number of measurements in the current scan, N is the total number of targets.$t = 0$ indicates that the measurement is a clutter detection. For example, in Fig. 2 and Table 1, $m = 3$, $N = 2$; the joint event $\theta = 7$ is made up of $\theta_{1,1}$ (T_1 originates M_1), $\theta_{0,2}$ (M_2 originates from clutter), and $\theta_{2,3}$ (T_2 originates M_3). The binary target indicator δ_t for target t, $(t = 1, ..., N)$ has a value 1, if a measurement is assigned to target t in θ, and it is 0 otherwise. The binary measurement association indicator τ_j for measurement j has a value 1, if measurement j is assigned to a target $t(t = 1, ..., N)$ in θ, and it is 0 otherwise. The quantity φ is the number of measurements originating from clutter in θ.

Table 1. Feasible Joint Association Events.

θ	Events	δ_1	δ_2	τ_1	τ_2	τ_3	φ
1.	$\theta_{0,1}$,$\theta_{0,2}$,$\theta_{0,3}$	0	0	0	0	0	3
2.	$\theta_{1,1}$, $\theta_{0,2}$, $\theta_{0,3}$	1	0	1	0	0	2
3.	$\theta_{0,1}$, $\theta_{1,2}$, $\theta_{0,3}$	1	0	0	1	0	2
4.	$\theta_{0,1}$, $\theta_{2,2}$, $\theta_{0,3}$	0	1	0	1	0	2
5.	$\theta_{0,1}$, $\theta_{0,2}$, $\theta_{2,3}$	0	1	0	0	1	2
6.	$\theta_{1,1}$, $\theta_{2,2}$, $\theta_{0,3}$	1	1	1	1	0	1
7.	$\theta_{1,1}$, $\theta_{0,2}$, $\theta_{2,3}$	1	1	1	0	1	1
8.	$\theta_{0,1}$, $\theta_{1,2}$, $\theta_{2,3}$	1	1	0	1	1	1

The number of clutter detections is modelled by a Poisson distribution. The joint association event probabilities, denoted $Pr\left(\theta/z_1^k\right)$ are given by $Pr\left(\theta/z_1^k\right) = \frac{\gamma(\theta)}{c}$, where

$$\gamma(\theta) = \lambda^{\varphi} \Pi_{(j=1)}^{m}(\lambda_{t,j})\tau_j \Pi_{(t=1)}^{N}\left\{(P_D^t)^{\delta_t}(1\text{-}P_D^t)^{(1-\delta_t)}\right\}, \tag{15}$$

and c the normalisation constant, $c = \sum_{\theta}\gamma(\theta).z_1^k$ is the set of all measurements from the initial time to the current time, λ is the spatial density of the clutter and P_D is the probability of detection for the target t. If the measurement j is assigned to the track t_j in an event $\theta_{t,j}$, the Gaussian likelihood $\Lambda_{t,j}$ of associating measurement j to t is

$$\Lambda_{t,j} = \frac{1}{\sqrt{det(2\pi S_{t,j})}} exp\left\{-0.5 v_{t,j}^T(k) S^{-1}(k) v_{t,j}(k)\right\} \tag{16}$$

where $v_{t,j}$ is the residual for track t_j and measurement j, and $S_{t,j}$ is the residual covariance.

The marginal probability of the measurement j originating from target tj, denoted $\beta_{t,j}$, is obtained by summing over all feasible joint events θ in which the single events $\theta_{t,j}$ occurs, and it is given by

$$\beta_{t,j} = Pr(\theta_{t,j}/z_1^k) = \sum_{\theta:\theta_{t,j}\in\theta} Pr(\theta/z_1^k) \tag{17}$$

Once the marginal association probabilities $\beta_{t,j}$ are computed, they are used in Eqns. (9) and (10) to update the state for target t.

4 SUBOPTIMAL JOINT PROBABILISTIC DATA ASSOCIATION (SJPDAF)

Implementation of JPDAF is computational complex due to the selection of feasible joint events θ which has combinatorial complexity. Therefore, for implementation purpose, a suboptimal version of JPDAF called Suboptimal JPDAF (SJPDAF) was used in simulations. SJPDAF introduces the concept of *partial joint events*. A partial joint event considers at most two track-measurement pairs, *i.e.* the association probabilities are calculated based on at most two single events. This prevents the exponential increase in the number of events. Hence it offers a computationally tractable solution for data association and tracking.

For each track t, let A_t be the set of measurements validated by t and for each measurement j, let C_j be the set of all tracks which validate measurement j. Now for a track t let L_t be the union of all C_j such that j belongs to A_t, such that $L_t = U_{j\in A_t} C_j - \{t\}$. The association probability $\beta_{t,j}$ for a track t and measurement j is calculated as

$$\beta_{t.j} = \frac{D_{t,j}}{B + \sum_{l\in A_t} D_{tl}} \quad \text{where D(t, j)} = \begin{matrix} \Lambda_{tj} \\ \Lambda_{tj}\sum_{s\in L_t}\max_{k\in A_s, k\neq j}\{\Lambda_{sk}\} \end{matrix} \begin{matrix} if\ L_t = \phi \\ if\ L_t \neq \phi \end{matrix} \tag{18}$$

Here B is a bias to account for clutter density.

5. SIMULATION RESULT

The SJPDA algorithm preceded with an auto track initiation algorithm for generating target tracks was implemented in Lab View and performance was evaluated. A matched filter output is the input given to the tracking system. At each time instant, measurements are found out by detection using a Cell Averaging Constant False Alarm Rate (CACFAR) processor that adaptively sets the threshold based on local information of total power. The threshold in the CACFAR detector is set on a cell by cell basis using estimated noise power by processing a group of reference cells surrounding the cell under investigation. New tracks are initiated from the detected measurements using an M/N logic track initiator[5].

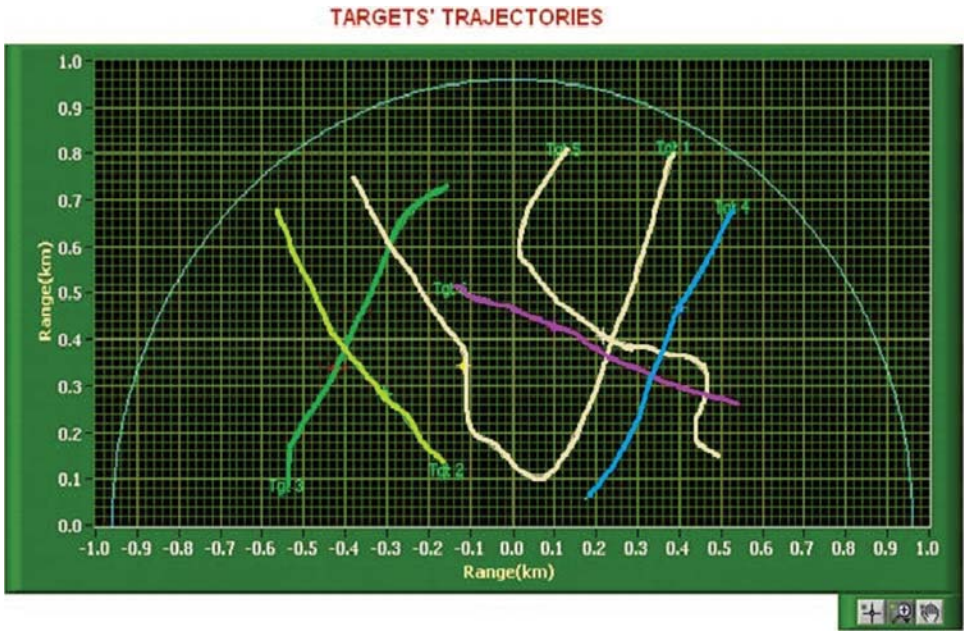

Fig. 3. Simulated Targets

The algorithm was tested for scenarios containing trajectories of up to six simultaneous targets. Target scenarios were generated using Lab View software. The targets were simulated in such a way that two targets crossed each other. Clutter was simulated by generating almost stationary strong targets which appears intermittently according to Bernoulli distribution with probability of appearance greater than 0.9. The position of the clutters changes in a small area uniformly. Figure 3 shows a planar plot of the simulated

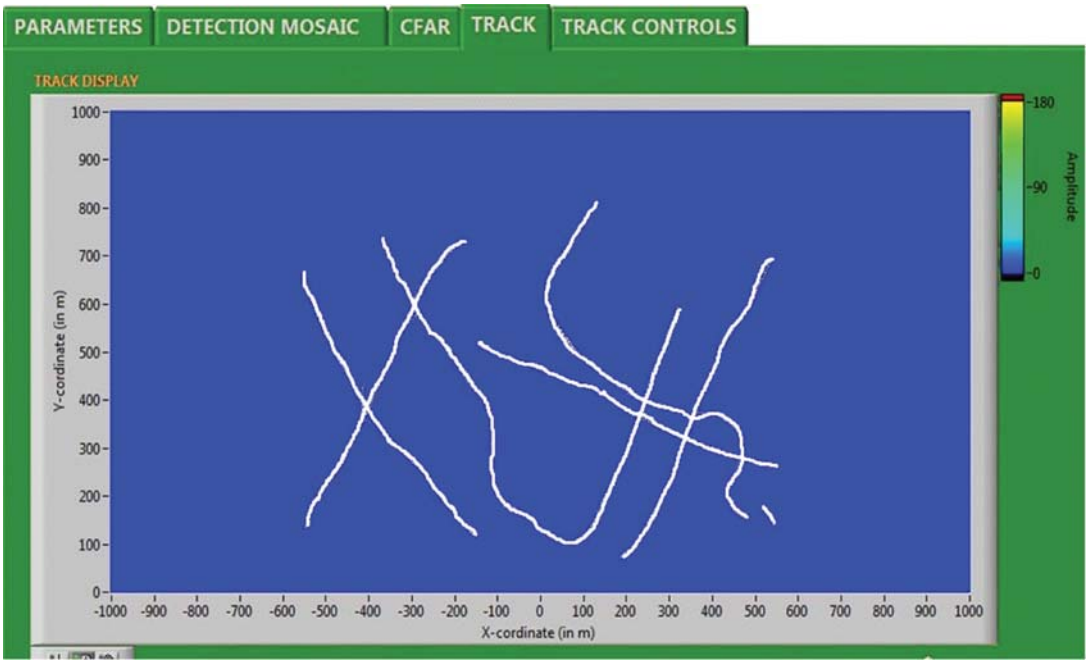

Fig. 4. Output of JPDAF tracker

trajectories. The axes represent the *x* and *y* position of the targets. The algorithm was able to automatically initiate all the targets and was tracked by the SJPDAF algorithm. Figure 4 shows the output of JPDAF tracker.

The algorithm was tested in the field as part of an auto contact designation and tracking system in the UARF test facility of NPOL. A single target was deployed in a cluttered environment. The output of the tracker is given in the table (see Table 2). The actual values of the range and bearing of the target is not readily available. So it was hand-picked from the detection image. The target was towed at a speed of approximately 1 knots and -120 degree course. These approximate values of range, bearing, course and speed values are compared with that of the tracker output. The error in range is 1.56% and that in speed is 12.22%. A bearing error of 0.95 degree and a course error 16.5 degree also was achieved.

Table 2: Experimental Results of Auto Tracking Algorithm

Actual Values (approximate)				Tracker Output			
Range(mts)	True Brg(deg)	Speed(m/s)	Course(deg)	Range(mts)	True Brg(deg)	Speed(m/s)	Course(deg)
73	42	0.50	-120.00	73.50	41.25	0.5187	-98.307
72	41	0.50	-120.00	73.40	41.13	0.4974	-101.09
70	40	0.50	-120.00	69.55	39.91	0.4568	-101.06
69	39	0.50	-120.00	68.70	39.03	0.4117	-129.35
67	39	0.50	-120.00	66.45	37.86	0.4262	-135.98
62	40	0.50	-120.00	63.25	40.64	0.4103	-136.77
60	39	0.50	-120.00	62.10	37.67	0.3827	-131.14
59	39	0.50	-120.00	58.45	38.57	0.3762	-132.9
58	39	0.50	-120.00	59.00	40.13	0.3751	-135.3
56	39	0.50	-120.00	55.15	38.41	0.3837	-138.04
55	39	0.50	-120.00	55.70	40.43	0.3719	-139.36
53	37	0.50	-120.00	53.65	38.33	0.393	-107.99

6. CONCLUSIONS

The JPDAF was seen to perform efficiently in multi-target tracking for closely spaced targets. It gives much better performance than simpler data association techniques and is lesser computationally intensive than MHT. But it was seen that computational requirements increase extensively as the number of tracks increases. The algorithm has been implemented in actual sonar systems and was seen to perform well in sea trials.

7. ACKNOWLEDGEMENT

We would like to thank Director, NPOL for giving permission to undertake this work and also for the support given by him in pursuing this work. We would like to thank Group Head, Signal Processing Algorithms Group for the unstinted support provided throughout.

We would also like to thank all the SPA group members for their generous support and valuable suggestions in the course of this work.

8. REFERENCES

[1] Y.BAR-SHALOM. and E. TSE., 1975. Tracking in a Cluttered Environment with Probabilistic Data Association. *Automatica.* **11**, 451-460.

[2] Y.BAR-SHALOM. and W.D. BLAIR, 2000. *Multitarget - Multisensor Tracking: Applications and Advances,* Artech House, London, **3**.

[3] J.A. ROECKER. and G. PHILLIS., 1993. Suboptimal Joint Probabilistic Data Association. *IEEE Transactions on Aerospace and Electronic Systems,* **29**(2),510-517.

[4] Y.BAR-SHALOM., X. R. LI. and T KIRUBAKARAN, 2001. *Estimation with Applications to Tracking and Navigation,* John Wiley & Sons, Inc.

[5] SARATH GOPI, ANILA JOHN, P MURALI KRISHNA and E.N. SREEDAVY, 2012. Diver Detection Sonar Simulator, DRDO / NPOL / SPA / 11 / 2012.

INFORMATION FOR AUTHORS

ARTICLES

The Journal of Acoustical Society of India (JASI) is a refereed publication published quarterly by the Acoustical Society of India (ASI). JASI includes refereed articles, technical notes, letters-to-the-editor, book review and announcements of general interest to readers.

Articles may be theoretical or experimental in nature. But those which combine theoretical and experimental approaches to solve acoustics problems are particularly welcome. Technical notes, letters-to-the-editor and announcements may also be submitted. Articles must not have been published previously in other engineering or scientific journals. Articles in the following are particularly encouraged: applied acoustics, acoustical materials, active noise & vibration control, bioacoustics, communication acoustics including speech, computational acoustics, electro-acoustics and audio engineering, environmental acoustics, musical acoustics, non-linear acoustics, noise, physical acoustics, physiological and psychological acoustics, quieter technologies, room and building acoustics, structural acoustics and vibration, ultrasonics, underwater acoustics.

Authors whose articles are accepted for publication must transfer copyright of their articles to the ASI. This transfer involves publication only and does not in any way alter the author's traditional right regarding his/her articles.

PREPARATION OF MANUSCRIPTS

All manuscripts are refereed by at least two referees and are reviewed by the Publication Committee (all editors) before acceptance. Manuscripts of articles and technical notes should be submitted for review electronically to the Chief Editor by e-mail or by express mail on a disc. JASI maintains a high standard in the reviewing process and only accept papers of high quality. On acceptance, revised articles of all authors should be submitted to the Chief Editor by e-mail or by express mail.

Text of the manuscript should be double-spaced on A4 size paper, subdivided by main headings-typed in upper and lower case flush centre, with one line of space above and below and sub-headings within a section-typed in upper and lower case understood, flush left, followed by a period. Sub-sub headings should be italic. Articles should be written so that readers in different fields of acoustics can understand them easily. Manuscripts are only published if not normally exceeding twenty double-spaced text pages. If figures and illustrations are included then normally they should be restricted to no more than twelve-fifteen.

The first page of manuscripts should include on separate lines, the title of article, the names, of authors, affiliations and mailing addresses of authors in upper and lowers case. Do not include the author's title, position or degrees. Give an adequate post office address including pin or other postal code and the name of the city. An abstract of not more than 200 words should be included with each article. References should be numbered consecutively throughout the article with the number appearing as a superscript at the end of the sentence unless such placement causes ambiguity. The references should be grouped together, double spaced at the end of the article on a separate page. Footnotes are discouraged. Abbreviations and special terms must be defined if used.

EQUATIONS

Mathematical expressions should be typewritten as completely as possible. Equation should be numbered consecutively throughout the body of the article at the right hand margin in parentheses. Use letters and numbers for any equations in an appendix: Appendix A: (A1, (A2), etc. Equation numbers in the running text should be enclosed in parentheses, i.e., Eq. (1), Eqs. (1a) and (2a). Figures should be referred to as Fig. 1, Fig. 2, etc. Reference to table is in full: Table 1, Table 2, etc. Metric units should be used: the preferred from of metric unit is the System International (SI).

REFERENCES

The order and style of information differs slightly between periodical and book references and between published and unpublished references, depending on the available publication entries. A few examples are shown below.

Periodicals:

[1] S.R. Pride and M.W. Haartsen, 1996. Electroseismic wave properties, *J. Acoust. Soc. Am.*, **100** (3), 1301-1315.
[2] S.-H. Kim and I. Lee, 1996. Aeroelastic analysis of a flexible airfoil with free play non-linearity, *J. Sound Vib.*, **193** (4), 823-846.

Books:

[1] E.S. Skudzryk, 1968. *Simple and Comlex Vibratory Systems*, the Pennsylvania State University Press, London.
[2] E.H. Dowell, 1975. *Aeroelasticity of plates and shells*, Nordhoff, Leyden.

Others:

[1] J.N. Yang and A. Akbarpour, 1987. Technical Report NCEER-87-0007, Instantaneous Optimal Control Law For Tall Buildings Under Seismic Excitations.

SUMISSIONS

All materials from authors should be submitted in electronic form to the JASI Chief Editor: B. Chakraborty, CSIR - National Institute of Oceanography, Dona Paula, Goa-403 004, Tel: +91.832.2450.318, Fax: +91.832.2450.602,(e-mail: bishwajit@nio.org) For the item to be published in a given issue of a journal, the manuscript must reach the Chief Editor at least twelve week before the publication date.

SUMISSION OF ACCEPTED MANUSCRIPT

On acceptance, revised articles should be submitted in electronic form to the JASI Chief Editor (bishwajit@nio.org)